TURBOCHARGING

THE INTERNAL COMBUSTION ENGINE

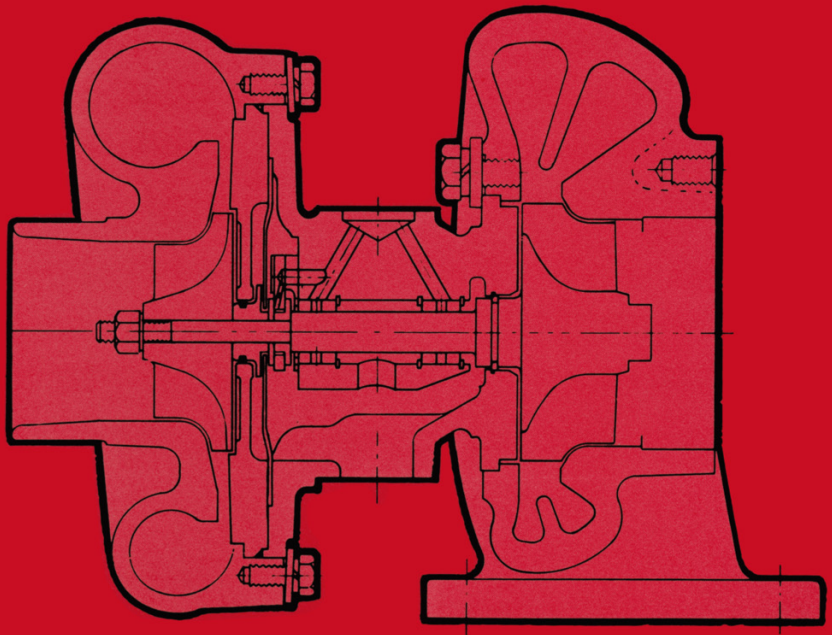

N. Watson and M.S. Janota

Turbocharging the Internal Combustion Engine

Turbocharging the Internal Combustion Engine

N. Watson

Reader in Mechanical Engineering,
Imperial College, London

the late M. S. Janota

Professor of Mechanical Engineering,
Queen Mary College, London

palgrave
macmillan

Softcover reprint of the hardcover 1st edition 1982

First published 1982 by
THE MACMILLAN PRESS LTD
London and Basingstoke
Companies and representatives
throughout the world

Typeset in 10/11 Times by
MULTIPLEX techniques ltd., Orpington, Kent

ISBN 978-1-349-04026-1 ISBN 978-1-349-04024-7 (eBook)
DOI 10.1007/978-1-349-04024-7

Contents

Preface

The turbocharger was invented a surprisingly long time ago but only relatively recently has it been an accepted component on all but very small diesel engines. After several false starts they are now also being used on petrol engines. Unlike most other components of an engine, the turbocharger can radically transform the performance of the engine and is therefore very much a critical component. As a result more engineers need to understand how and why it does what it does.

The characteristics of turbomachines are fundamentally different from those of reciprocating machines, hence the combination of turbocharger and engine has many complex characteristics. Yet engineers with diesel or petrol engine experience have little knowledge of turbomachines, and vice versa, and are therefore not well equipped to optimise the combination. This book is an attempt to help these engineers by explaining the principles of turbocharging, with special emphasis on the interactions between engine and turbocharger. Many examples of the current practice of turbocharging are also given to explain how the principles can be used to advantage. Although examples relating to large industrial and marine engines are not omitted, preference has deliberately been given to examples of practice on automotive (truck-type) diesel engines for several reasons. Firstly turbocharging is longer established on marine and industrial engines and hence the principles are better known in that industry. Secondly engine designers, development engineers and users who are new to turbocharging are mainly involved with truck and passenger car diesel engines.

The application of turbocharging to passenger car petrol engines has many unique features and therefore a special chapter has been devoted to this subject.

The authors, as academics, are firmly convinced that an understanding of the basic theory underlying a subject will lead the engineer to make wiser decisions. It is common practice to present this theory to students through mathematics, as the language of the engineer. This book is aimed at both the student and the practising engineer and the authors have recognised that the latter finds a mathematical approach tedious. As far as possible therefore explanations of principles have been presented in words and not through mathematics, so that the book is more readable than it would otherwise be. However, the techniques of analysis, mathematics and computer-aided design are now so useful to the

engine designer that they should not be ignored. The mathematical representation of turbocharged engines has therefore been treated in a chapter of its own at the end of the book (chapter 15).

The organisation of the book is based on the premise that most readers will know more about engines than turbomachines. Following a brief over-all introduction to turbocharging, chapters 2 to 5 are devoted to the construction of turbochargers and the principles of radial compressors and radial and axial turbines, with reference to the turbocharger application (axial compressors are not used on turbochargers, being more suited for larger and more expensive gas turbines). Some readers may wish to omit the detailed description of flow processes in the turbomachines. Chapters 6 to 9 are concerned with turbocharging systems and the best methods of utilising exhaust gas energy via the turbocharger. Chapter 10 describes the critical task of matching the turbomachine to the engine to achieve optimum performance of the combination for all the common applications. Chapters 11, 12, 13 and 14 are concerned with factors specific to or important in certain applications such as high-output turbocharging, transient performance, applications to petrol engines and the effect of turbocharging on exhaust emissions. The final chapter (15) has been mentioned above.

The authors are indebted to a large number of individuals, companies and organisations who have helped them in the preparation of this book. In particular, thanks are due to Professor F.J. Wallace, B.E. Walsham, I.W. Goodlet, E. Meier, Dr M. Marzouk, past and present students, Garrett-AiResearch, Holset Engineering Co. Ltd, Brown Boveri et Cie and Napier Turbochargers.

Mrs U. Harris, Mrs S. Boyle and Mrs M. Parsons have stoically retyped and redrawn as the authors have changed the manuscript.

Finally the authors are grateful to I.Mech.E., SAE, ASME, VDI, CIMAC, FISITA, MTZ, Butterworths, and Longman for permission to reproduce many of the illustrations used in the book.

N. WATSON
M. S. JANOTA

Marian Janota died shortly before the publication of this book. We had completed every stage in preparing the book but sadly he did not see the final bound volume.

N. WATSON
February 1982

Acknowledgements

The authors wish to make acknowledgement to the following publishers for permission to reproduce figures from the texts indicated below

Longman Group Ltd

Gas Turbine Theory, by H. Cohen, G.F.C. Rogers and H.I.H. Saravanamuttoo.

Springer Verlag

Supercharging of Internal Combustion Engines by K. Zinner.

G.T. Foulis

Gas Flow in the Internal Combustion Engine by W.J.D Annand and G.E. Roe.

In addition a number of figures from papers by the authors and other authors have been reproduced by permission of ASME, *Brown Boveri Review*, CIMAC, *Diesel & Gas Turbine Progress*, I.Mech.E., *MTZ*, SAE and *VDI*.

Nomenclature

a	sonic velocity	m/s
a'	non-dimensional sonic velocity, a/a_{ref}	–
A	area	m^2
ABDC	above bottom dead centre	–
ADR	air delivery ratio	–
AFR	air/fuel ratio	–
AR	area ratio	–
AS	aspect ratio	–
b	width	m
B	cylinder bore	m
BBDC	below bottom dead centre	–
BDC	bottom dead centre	–
BMEP	brake mean effective pressure	bar
BS	brake specific value	–
BSAC	brake specific air consumption	g/kW h
BSFC	brake specific fuel consumption	g/kW h
c_p	specific heat at constant pressure	kJ/kg K
c_v	specific heat at constant volume	kJ/kg K
C	velocity	m/s
C'	non-dimensional velocity, C/a_{ref}	–
Cd	discharge coefficient	–
Ch	enthalpy loss coefficient	–
C_{LF}	lift coefficient, per unit length	–
CP, CPR	pressure recovery coefficient	–
CPL	pressure loss coefficient	–
CR	compression ratio	–
CTQ	torque coefficient	–
D	diameter	m
Df	diffusion factor	–
DI	direct injection diesel engine	–
DS	specific diameter	–
E	energy	kJ
EC	exhaust port or valve closes	°
EO	exhaust port or valve opens	°

ER	expansion ratio	–
EVC	exhaust valve closes	°
EVO	exhaust valve opens	°
f	frequency; friction factor; function; burnt fuel/air ratio	Hz; –
F	equivalence ratio; force	–; kN
FB	fuel burnt	–
FBR	fuel burning rate	–
FL	frictional loss as torque	N m
FMEP	frictional loss as loss of mean effective pressure	bar
FP	fuel prepared	kg
FR	fuel reacted	kg
h	height; specific enthalpy	m; kJ/kg
HD	pressure head	m^2/s^2
hf	humidity factor	–
HSU	Hartridge smoke units	–
HP	high pressure	–
ht	heat transfer coefficient	kW/m^2 K
i	incidence angle; control volume number	°; –
I	section modulus (inertia)	kg m^2
IC	inlet port or valve closes	°
ID	ignition delay	°
IDI	indirect injection diesel engine	–
IMEP	indicated mean effective pressure	bar
IO	inlet port or valve opens	°
IVC	inlet valve closure	–
k	conductivity; constant	kW/m K; –
K	general constant	–
KE	kinetic energy	J
l	length, chord	m
L	losses	–
LF	lift force	kN
LP	low pressure	–
LT	load torque	N m
m	mass	kg
$\dot{m}$	mass flow rate	kg/s
M	Mach number	
MBT	maximum brake torque	–
MR	Mach number ratio	–
n	number	–
N	rotational speed	rev/min
NA	naturally aspirated	–
ND	specific diameter	–
NS	specific speed	–
Nu	Nusselt number	–
P	pressure	bar
PE	potential energy	J
PP	partial pressure	bar

ppm	parts per million (concentration)	–
Pr	Prandtl number	–
PR	pressure ratio	–
Q	heat transfer	kJ
$\dot{Q}$	heat transfer rate	kW
r	radius	m
R	gas constant	kJ/kg K
Re	Reynolds number	–
RN	degree of reaction	–
RPM	revolutions per minute	min^{-1}
s	specific entropy	kJ/kg K
sp	circumferential spacing (pitch)	m
t	time	s
t'	non-dimensional time, ta_{ref}/l_{ref}	–
T	temperature	K
TC	turbocharged	–
TDC	top dead centre	–
th	thickness	m
TQ	torque	N m
u	specific internal energy	kJ/kg
U	rotor tip speed	m/s
v	specific volume	m^3/kg
V	volume	m^3
$\dot{V}$	volumetric flow rate	m^3/s
vo	valve opening period	°
W	work done; velocity relative to blade	kJ; m/s
$\dot{W}$	power	kW
x	distance; relative change in rack movement	m
x'	non-dimensional distance, x/l_{ref}	–
y	relative change in speed	m/s
z	number of nozzles or vanes	–
Z	number of blades	–
α	angle	°
β	backsweep angle; phase proportionality factor; Riemann parameter	°; –
γ	c_p/c_v	–
Δ	increment	–
ϵ	effective impeller exit area ratio; arc of admission; effectiveness; emissivity	–; °; –; –
η	efficiency	–
θ	angle	°
λ	Riemann parameter	–
Λ	r_{hub}/r_{tip}	–
μ	dynamic viscosity; energy transfer coefficient	kg/m s; kg m/s
ν	Poisson's ratio; kinematic viscocity	–; m^2/s^2
ρ	density	kg/m^3
σ	compressor slip factor; Stephan-Boltzmann constant; stress	–; $kW/m^2\ K^4$; kN/m^2

ϕ	angle; relative humidity	°; –
ψ	azimuth angle; blade loading coefficient	°; –
ω	angular velocity	rad/s

Subscripts

a	axial; air; ambient	n	nozzle
alt	altitude	NOM	nominal
an	anemometer	p	exhaust pipe; polytropic
APP	apparent	*p*	pressure
b	blade; backsweep	P	profile
bu	bursting	pis	piston
c	compressor; centrifugal	q	casing (exit)
carb	carburettor	r	radial; root
cl, C	clearance	R	rotor
com	combustion	ref	reference
cool	coolant	rel	relative
cyl	cylinder	s	isentropic
dif	diffuser	S	secondary
e	engine; trailing edge	ss	isentropic throughout
es	end of sector	sf	surface
ex	exhaust	sh	shroud
f	fuel	st	stalled
fb	fuel burnt	sto	stoichiometric
for	formation	svp	saturated vapour pressure
fr	friction	sw	swept
g	gas	t	turbine; tip
gb	gas bending	tc	turbocharger
ge	gas exchange	th	throat
h	hoop; hub	tot	total
ht	heat transfer	TS	total to static
i	instantaneous	TT	total to total
ic	inlet casing	u	unburnt fuel
imp	impeller	ult	ultimate
ind	indicated	*v*	volume
j	control volume port	vol	volumetric
k	casing (inlet)	w	water, windage
l	load	z	start of compression
m	manifold; mean	*	naturally aspirated
max	maximum	0	stagnation
min	minimum	θ	tangential
mot	motored	ω	whirl

1

Introduction to Turbocharging and Turbochargers

1.1 Supercharging

Supercharging can be defined as the introduction of air (or air/fuel mixture) into an engine cylinder at a density greater than ambient. This allows a proportional increase in the fuel that can be burned and hence raises the potential power output. The principal objective is to increase power output, not to improve efficiency, although the efficiency may benefit. The effect of supercharging on power output can be seen from a cylinder pressure/volume (P-V) diagram. Figure 1.1 shows an ideal naturally aspirated dual-combustion cycle. Point 1 denotes the beginning of the compression stroke when the piston is at bottom dead centre (BDC). Process 1-2 is the compression stroke. 2-3 is the part of the combustion process occurring (instantaneously) at constant volume (top dead centre, TDC). 3-4 is the remaining part of the combustion process occurring at constant pressure while the piston is moving along the cylinder. 4-5 is the continuation of the expansion process following the end of combustion. At point 5 the

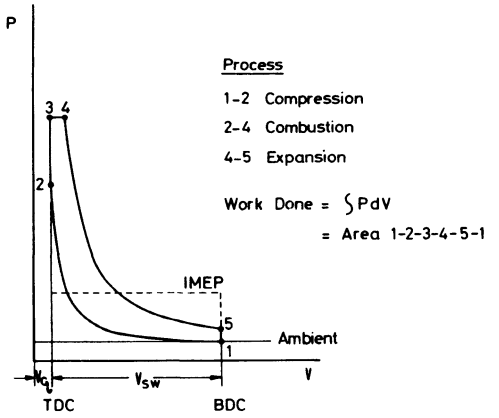

Figure 1.1 *Ideal dual-combustion (limited pressure) air standard cycle; Naturally aspirated engine*

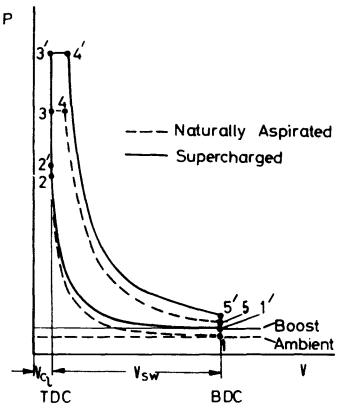

Figure 1.2 *Comparison of supercharged and naturally aspirated air standard dual-combustion cycles having the same compression ratio*

exhaust valve opens, allowing some exhaust gas to leave the cylinder and the pressure to fall back to the ambient level. The intake and exhaust processes are not shown.

Useful work is obtained during processes 3-4-5 since the pressure acting on the piston is aiding its outward motion. This is the power stroke. Against this must be set the work required to compress the gas in the cylinder, process 1-2. The work done (W) may be calculated from the integral

$$W = \int P \, dV \tag{1.1}$$

It follows that the net work output (expansion work minus compression work) is given by the area inside the diagram, area 1-2-3-4-5-1. This is the work output per complete cycle. The process described above takes one revolution of the crankshaft (four-stroke engine). The intake and exhaust processes occupy a second revolution. Useful power is therefore obtained every second revolution of the crankshaft. It follows that the area inside the diagram multiplied by half the engine speed gives the power output of a four-stroke engine.

Figure 1.2 compares the naturally aspirated and supercharged ideal cycles. The supercharged cycle starts at a higher pressure (and density) point 1′. Extra fuel can be burned between 2′-4′ because more air is available (the same volume, but a higher density). Two things are clear: the supercharged engine has a greater power output (see diagram area) and a much higher maximum pressure. Unless the engine is designed to be supercharged, the high maximum pressure may not be acceptable – the engine may not withstand the stresses involved. By reducing the compression ratio the clearance volume (V_{c1}) is increased and maximum pressure will be reduced. If the compression ratio is suitably chosen, the maximum pressure in the supercharged engine can equal that of the naturally aspirated engine (figure 1.3); the power output of the supercharged engine remains greater than that of the naturally aspirated engine.

In considering the power output as the product of the area of the P-V diagram and the cyclic operating speed, the fact that not all of this power can be trans-

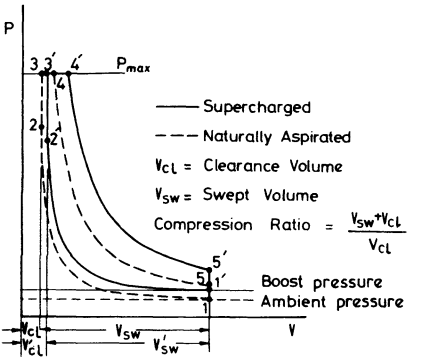

Figure 1.3 *Comparison of supercharged and naturally aspirated air standard dual-combustion cycle having the same maximum pressure but different compression ratios*

mitted to the output shaft of the engine has been ignored. Some will be lost as friction, in the bearings, at the piston rings, etc., and some will be required to drive the valve gear, oil and water pumps. This must be debited from the 'indicated' power of the *P–V* diagram. Furthermore in order to obtain high density air at point 1′, work must be done to compress ambient air up to the boost pressure at that point. A compressor can be driven from the crankshaft of the engine (figure 1.4). This is a conventional mechanically driven supercharger. In addition to the frictional losses the power required to drive this compressor must be debited from the indicated power (*P–V* diagram) output. Fortunately, when fitting a mechanically driven supercharger to an engine it is easy to ensure that the indicated power output rises sufficiently to more than compensate for the power requirement of the supercharger and any additional frictional losses.

The ideal dual-combustion four-stroke cycle has been used to illustrate the power gain of the supercharged engine. A similar argument can be put forward for the ideal two-stroke engine cycle and for real petrol and diesel engines.

The mechanically driven supercharger is not the only method of supercharging. This type of supercharger has been successfully used many times in the past, particularly on piston aircraft engines, but it is not in common use today. This book is exclusively concerned with quite a different method—turbocharging—but the basic objective of increasing the power output of a given size of engine remains unaltered.

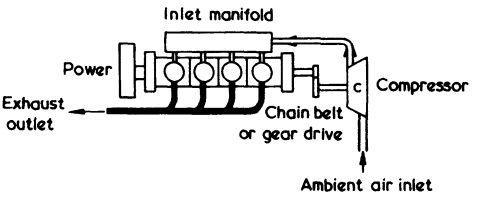

Figure 1.4 *Typical arrangement of an engine fitted with a mechanically driven supercharger*

1.2 Turbocharging

Since 1945, the power output of diesel engines has rapidly increased as a result of developments in turbocharging. This is particularly true of the engines used for ship and rail propulsion and industrial generating sets.

Figure 1.5 shows this trend for four and two-stroke engines. The BMEP (brake mean effective pressure) is a measure of the work output for a given swept volume or cylinder capacity. The indicated mean effective pressure (IMEP) is the average pressure obtained by dividing the indicator diagram (area 1-2-3-4-5-1 in the ideal case, see figure 1.1) by the swept volume of the cylinder (V_{sw}). The brake mean effective pressure is the equivalent of IMEP at the engine output shaft, IMEP reduced by friction, etc.

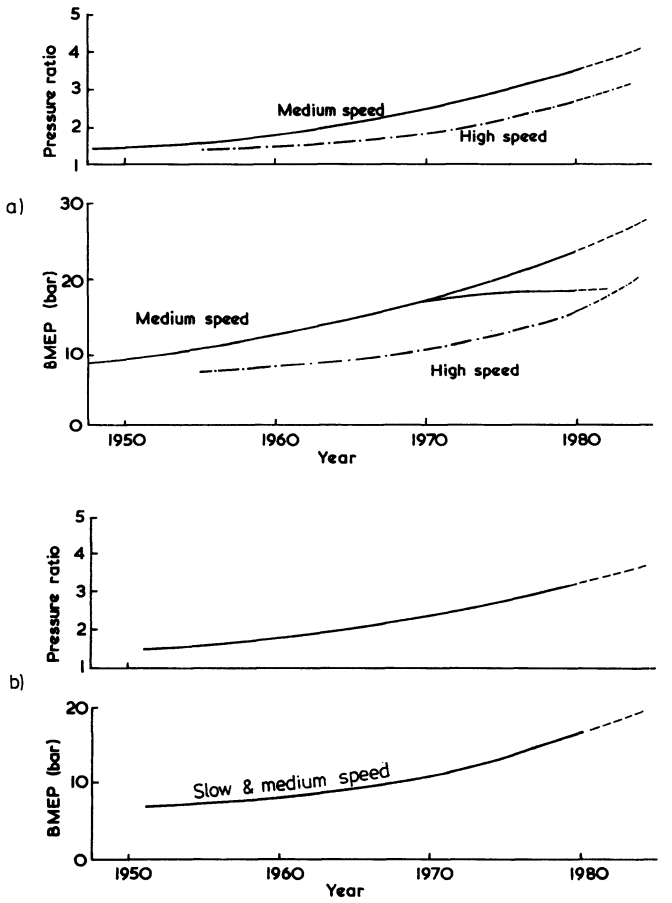

Figure 1.5 (a) *Four-stroke diesel engine: increase in BMEP and compressor pressure ratio.* (b) *Two-stroke diesel engine: increase in BMEP and compressor pressure ratio*

Figure 1.5 shows that the average BMEP of some types of engines has tripled since 1945. Figure 1.5a shows that the commercial ratings of medium-speed four-stroke diesel engines increased rapidly in the last 30 years, approaching 20 bar (290 lbf/in.^{2}) at present. The combined effects of legislation regarding power/weight ratio, pollutant emission, economic constraints and the need to conserve liquid fuel resources, have led to increasing use of turbochargers on vehicle diesel engines. In consequence, an increase in the rating of these engines has been evident recently and is expected to continue.

If these trends are extrapolated to the future, one might expect ratings of some engines to exceed 27.5 bar (400 lbf/in.^{2}) in the 1990s. Already experimental engines have run at this rating, and higher ratings, with no absolute limitation in performance or thermal loading. However, most current turbocharger compressors are limited to a maximum useful pressure ratio of 3.5, by aerodynamic and stress considerations. This has caused the trends of increased BMEP to diverge. Some manufacturers, retaining the standard type of turbocharger, have given more attention to improved reliability without appreciable increase in rating. Others are exploring higher ratings using two-stage turbocharging or more sophisticated single stage systems.

The trend of increasing BMEP developed by slow and medium-speed two-stroke diesel engines over the past 30 years, has been similar to that of four-stroke engines (figure 1.5b). Again experimental work has revealed no fundamental reason why this trend should not continue beyond the typical figure of 14 bar (200 lbf/in.^{2}) BMEP current in 1980. Fortunately, the pressure ratio developed by current turbochargers is sufficient to meet the immediate needs of most two-stroke engines, although two-stage systems are being considered for large marine two-stroke engines.

Turbocharging is a specific method of supercharging. An attempt is made to use the energy of the hot exhaust gas of the engine to drive the supercharging compressor. The user is not getting something for nothing, but is merely using energy that would normally go to waste; however, it is clear that it is no longer necessary to debit the power requirement of the compressor from the indicated power of the engine.

The ideal available exhaust energy is shown in figure 1.6. The energy consists of the 'blow-down' energy after reversible adiabatic expansion from condition 1 (where the exhaust valve opens) to ambient pressure at point 2, area 1-2-3, and the work done by the piston in displacing remaining exhaust gas, area 3-4-5-6, in the case of the four-stroke engine.

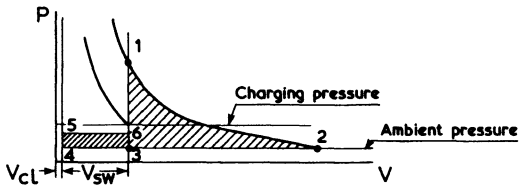

Figure 1.6 *Work available from ideal exhaust process*

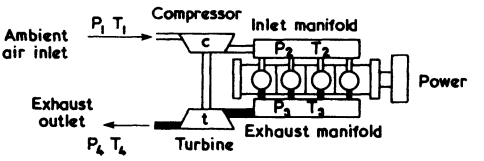

Figure 1.7 *Typical arrangement of a turbocharged engine operating with the constant pressure system. The compressor and turbine form a self-contained unit: the turbocharger*

The first attempts to use exhaust gas energy to drive a supercharging compressor were proposed by Büchi [1] as long ago as 1909. However, it was many years before Büchi achieved success (around 1925). He used the exhaust gas to drive a turbine which in turn drove the supercharging compressor (figure 1.7). The compressor and turbine were a self-contained unit (the turbocharger) with no mechanical linkage to the engine other than ducting for the compressed air and exhaust gas. The turbocharger, in principle, remains the same today.

It might be thought that the back pressure created by the turbine would hinder the exhaust process from the cylinders and hence reduce the potential gain in power output. However, provided that the turbocharger is efficient enough to raise the boost pressure above the exhaust pressure of the engine, the intake and exhaust process will benefit. Paradoxically it was the advent of the aircraft gas turbine in the 1940s that enabled major strides to be made in turbocharging. Both the gas turbine and the turbocharger required turbine blade materials that would withstand high stresses at very high temperatures. These materials were developed for aircraft gas turbines and were then used in turbochargers. It was primarily the development of the materials, and more efficient compressors and turbines, that permitted the trends shown in figure 1.5 to occur.

1.2.1 Constant Pressure Turbocharging

Büchi's early (unsuccessful) attempts at turbocharging utilised the constant pressure system (figure 1.7) with a multi-cylinder four-stroke diesel engine. The exhaust manifolds from all cylinders were connected to a common large chamber. This led to a single turbocharger turbine. A reciprocating engine is inherently an unsteady flow device, each cylinder exhausting in turn at intervals during the cycle. Turbines can be designed to accept such an unsteady flow, but they operate more efficiently under steady flow conditions. Thus the combination of engine and turbine is a difficult one. Büchi used a large chamber to damp out the fluctuating gas flow from the cylinders so that the flow to the turbine was essentially steady (constant pressure). Büchi's turbocharger was not efficient enough to maintain a reasonable boost pressure, but many engines today operate successfully with the constant pressure system.

Figure 1.8 shows a specific enthalpy/specific entropy (h-s) diagram for the constant pressure turbocharging process. It is relatively simple to calculate whether the turbocharger will run as a self-supporting unit producing a specified boost

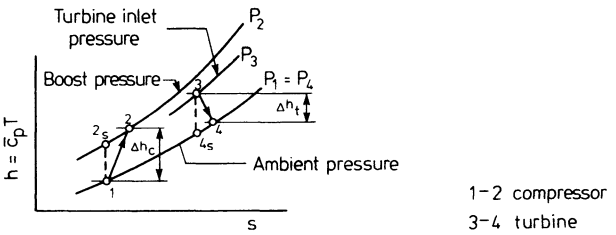

Figure 1.8 *Constant pressure turbocharging*

pressure under the constant pressure system, by considering the energy balance between turbine power (process 3-4, figure 1.8) and compressor power (process 1-2, figure 1.8).

The calculation is presented in chapter 6, but figure 1.9 shows a typical set of results. When turbocharging, it is desirable to achieve a small positive pressure difference between intake and exhaust manifold ($P_2 - P_3$, figure 1.8), or a pressure ratio (P_2/P_3) greater than unity. Figure 1.9 shows that a reasonably high turbocharger efficiency and turbine inlet temperature are required to achieve this (for example, 45% efficiency and 500 °C for a pressure ratio of 2:1).

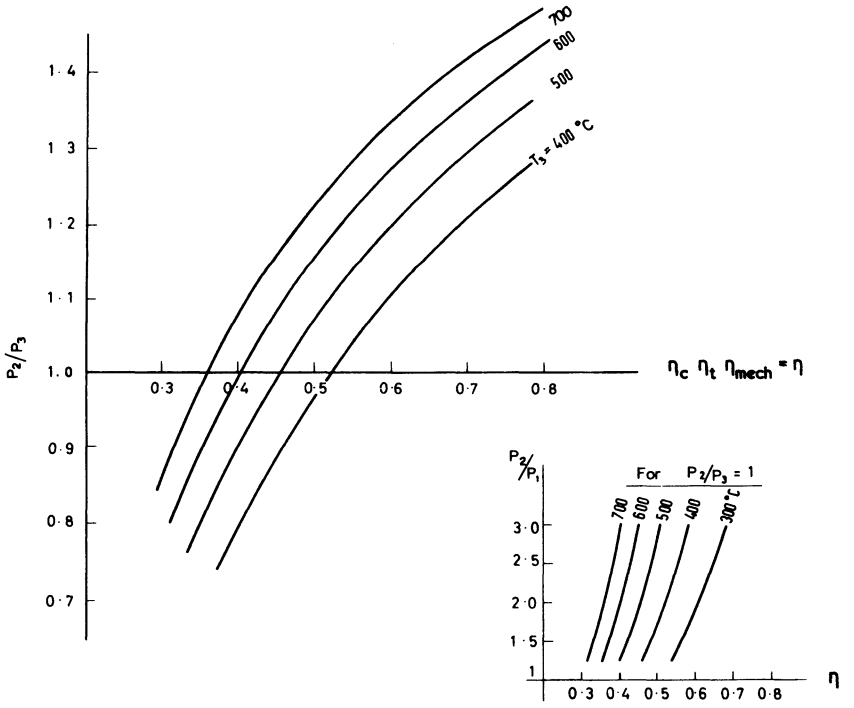

Figure 1.9 *Effect of over-all turbocharger efficiency on the pressure drop between inlet and exhaust manifolds (constant pressure system) for* $P_2/P_1 = 2$

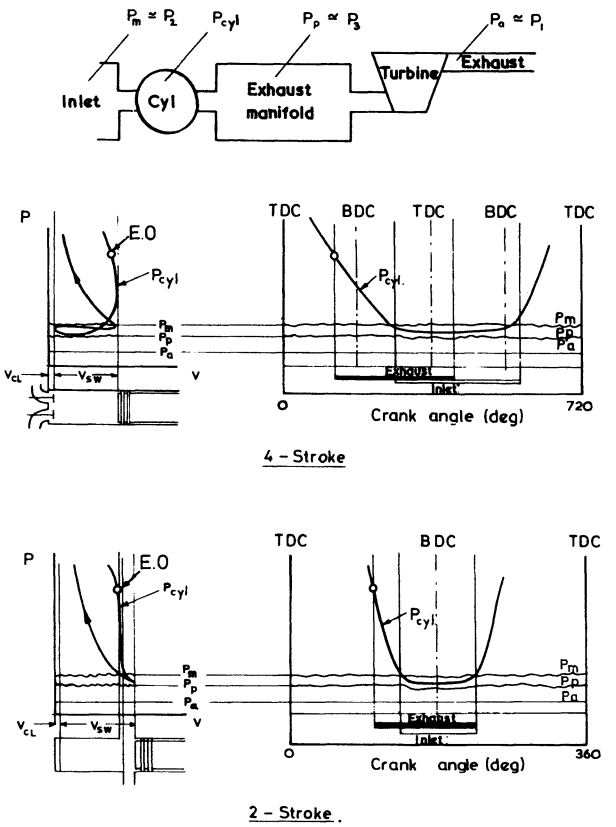

Figure 1.10 *Constant pressure system*

Figure 1.10 (top and middle) shows the principle of constant pressure turbocharging, by means of the cylinder and exhaust pressure diagrams for a single cylinder. The large volume of the exhaust manifold ensures that its pressure (P_p) remains substantially constant. During the exhaust process, the cylinder pressure (P_{cyl}) drops to almost equal the exhaust manifold pressure. With a sufficiently high turbocharger efficiency, the inlet manifold pressure (P_m), slightly exceeds the exhaust manifold pressure. Thus during the period when inlet and exhaust valves are both slightly open (valve overlap), some fresh air flows through the cylinder.

1.2.2 Pulse System Turbocharging

A disadvantage of the constant pressure system is that it does not fully utilise the high kinetic energy of the gases leaving the exhaust valves or ports. As the gas blows down from a relatively high pressure in the cylinder through the small area

of the partly opened exhaust valve, the discharge velocity is high. This high-velocity gas enters the relatively large volume of low-velocity gas in the damping chamber. The frictional losses inherent in this mixing process ensure that not all of the velocity is converted into a pressure rise in the damping chamber.

Büchi developed the pulse system to try to improve the transmission of energy from the cylinders to the turbine. The principle can be explained with reference to a single-cylinder engine (figure 1.11) fitted with a single turbocharger (although it would not normally be sensible to turbocharge such an engine). A short narrow pipe ensures that some of the kinetic energy of the gas leaving the exhaust port is maintained and not destroyed in a sudden expansion. The kinetic energy is partially transmitted to the turbine (with sonic velocity) in the form of a pressure wave. Figure 1.11 also shows a typical pressure/time diagram in the cylinder and in the pipe. Compared with the constant pressure system (figure 1.10), the exhaust manifold pressure is no longer constant.

By improving the transmission of energy from the cylinder to the turbine the energy available at the turbine is increased. However, this is of little benefit

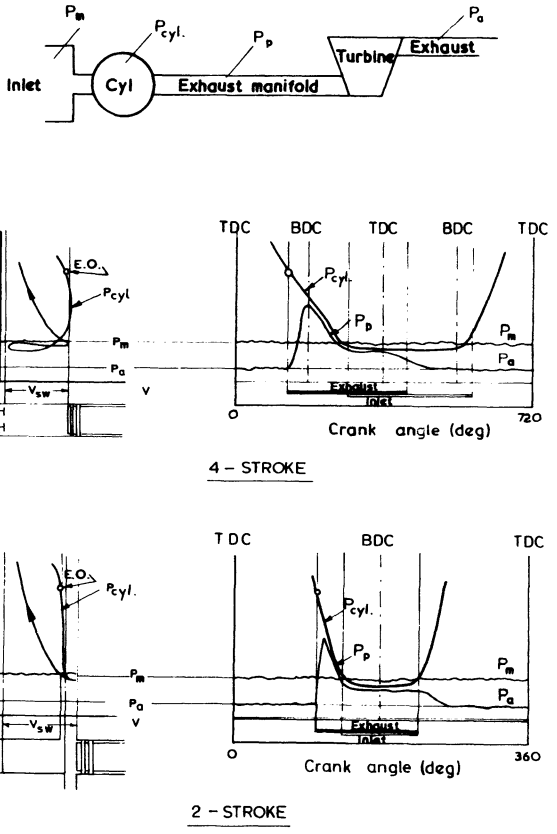

Figure 1.11 *Pulse system*

unless the energy can be usefully recovered in the turbine. Consider the pressure diagram in the exhaust pipe (figure 1.11). It is clear that the gas flow into the turbine is highly unsteady and will in fact be zero for much of the time. When the pressure wave arrives at the turbine entry, the turbine will tend to accelerate. When the pressure wave decays, the turbine will tend to decelerate due to the power absorption of the compressor. It is difficult to design a turbine that will operate efficiently under these conditions and hence the utilisation of the exhaust energy is poor. In this case the pulse system has increased the available energy at the turbine, but has reduced the efficiency of its conversion into compressor work. For the system to work well, attempts must be made to reduce the flow unsteadiness at the turbine entry.

It is possible to reduce flow unsteadiness by connecting the narrow exhaust pipes from several cylinders to a common turbine. The pulses from the additional cylinders can help fill in the voids in the pressure diagram (P_p) shown in figure 1.11. For example, if the firing intervals of the cylinders of a three-cylinder engine are phased at 240° in the 720° complete operating four-stroke cycle, and their exhaust valves are open for 250°, then the exhaust pipes from all three cylinders may be connected together. Their exhaust pulses will follow each other sequentially, with only 10° periods when the end of an exhaust process from one cylinder might influence the beginning of the exhaust process from another cylinder. If all the cylinders of a six-cylinder engine were connected to a common exhaust pipe, the exhaust processes would overlap in time. The high-pressure blow-down pulse from the early part of one exhaust process would interfere with the lower-pressure part of the exhaust process, from the previously firing cylinder. Certain cylinders whose exhaust processes are suitably separated in time must be grouped together. This usually means that more than one group is required (figure 1.12). It follows that more than one turbine or a multi-entry turbine is also required.

With careful choice of cylinders grouped together in a common manifold, combined with a good exhaust design, it is possible to obtain reasonably high turbine operating efficiencies (although rarely as high as results from the constant pressure system). The combination of increased energy available at the turbine plus a reasonable turbine efficiency (obtained in part from designing a turbine to accept unsteady flow) results in the pulse system being more commonly used than the constant pressure system. This is true even though not all of the 'pulse' energy is lost in the constant pressure system. The complex pressure wave system in the exhaust manifold of a pulse turbocharged engine results in quite a difficult design problem on some engines. The subject is discussed in detail in chapter 7.

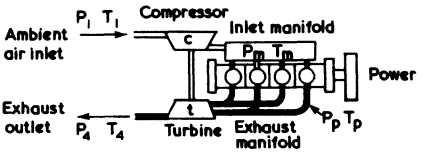

Figure 1.12 *Typical arrangement of a turbocharged engine operating with the pulse system. Two-entry turbine inlet casing*

1.3 Turbocharging the Two-stroke Engine

The four-stroke engine has a distinct intake stroke during which the piston moves away from the cylinder head, drawing fresh charge into the cylinder. The engine is self-aspirating. The two-stroke engine has no complete suction stroke. In fact, when the inlet port (or valve) is open, the piston is moving to reduce cylinder volume, tending to oppose any attempt to fill the cylinder with fresh charge. The two-stroke engine is not self-aspirating and requires some form of compressor to force fresh charge into the cylinder. Although a compressor is used, this need not necessarily be a supercharger, since the pressure in the cylinder at the end of the intake stroke may be little above ambient. It is of course possible to devise a system in which the compressor acts as a supercharger at the same time. The four-stroke engine also has a distinct exhaust stroke during which the piston moves towards the cylinder head, driving the exhaust gases out of the cylinder. Again the two-stroke engine has no such positive exhaust expulsion. Similarly to the four-stroke engine, much, but not all of the exhaust gas leaves of its own accord due to the exhaust valve (or port) opening while the cylinder pressure exceeds that in the exhaust manifold. This gas simply expands out into the exhaust manifold. The remaining exhaust gases fill the cylinder at roughly exhaust manifold pressure; it is this gas that the piston of the four-stroke engine pushes out during the exhaust stroke. Because the two-stroke engine is not self-exhausting the fresh inlet charge driven in by the compressor is used to help force out residual exhaust gases. This process (called scavenging) is the key to successful operation of an efficient two-stroke engine.

Supercharging (mechanically) the two-stroke engine is relatively simple—a compressor designed to produce a higher pressure ratio is used. However, during the scavenging process both inlet and exhaust ports are open (to allow the fresh charge to expel the residual exhaust gas). The port timing must be adjusted so that only a relatively small quantity of fresh charge mixes and escapes with the exhaust gas. Two-stroke engines are very sensitive to the design of their exhaust system, since any residual pressure may impair the vital scavenging process. It follows that care must be taken when turbocharging a two-stroke engine, since the exhaust turbine inherently increases pressure in the exhaust manifold. Provided that the system is designed so that the boost pressure exceeds the exhaust pressure (by a suitable margin) during the scavenging process, the engine will operate well. If the constant pressure turbocharging system is used this is largely a matter of having a sufficiently high turbocharger efficiency. But the system is hindered by the low exhaust temperature of the two-stroke, thus an auxiliary compressor is used if the turbine energy is not sufficient to generate the boost required. This has the added advantage of enabling the engine to start more easily, since a turbocharger obviously provides no boost pressure before combustion begins.

The two-stroke engine can run quite successfully with a pulse exhaust system provided that the exhaust manifold design is such that positive pressure waves do not arrive at the exhaust port at a critical phase in the scavenging process. It is necessary to keep the exhaust pressure low for most of this process. Some rise in pressure when scavenging is nearly complete can help increase that trapped mass of fresh charge in the cylinder, which is desirable. There is considerable

scope for ingenuity in the design of the exhaust system but a requirement to operate over a large speed range may prove to be a limitation. Again, pulse turbocharged two-stroke engines are sometimes fitted with auxiliary fans or compressors to aid scavenging at low speeds. Two-stroke engines running without an auxiliary compressor are usually started from compressed air bottles.

1.4 Charge Cooling

Compression of a gas in an adiabatic compressor is accompanied by a temperature rise. This temperature rise will depend on the pressure ratio and the efficiency of the compressor. Anything that helps reduce the inlet manifold air temperature will increase the density of the air and consequently increase the mass of air in the cylinders. It follows that reducing this temperature will enable more fuel to be burnt and the power output to increase.

Since the compressor delivery temperature (T_2) is greater than the ambient temperature it is possible to use a simple heat exchanger to reduce T_2. This could be an air-to-air or an air-to-water system (running from the water-cooling system of the engine for example). Since the charge cooler is fitted between the compressor and engine, the installation is often called an intercooler, or sometimes an aftercooler (figure 1.13).

The performance of a charge cooler is measured by its effectiveness (ϵ), which is the temperature drop of the air being cooled divided by the maximum possible temperature drop (the inlet temperature of the warm air, T_{2a}, minus the inlet temperature of the cooling water T_W, see figure 1.13). Thus

$$\epsilon = (T_{2a} - T_{2b})/(T_{2a} - T_W) \tag{1.2}$$

Unfortunately the flow of gas through the complex passage of the cooler results in some pressure loss, although this is usually small. The gain in density due to the temperature reduction should substantially exceed the loss due to the pressure drop (ΔP_{cool}, figure 1.14).

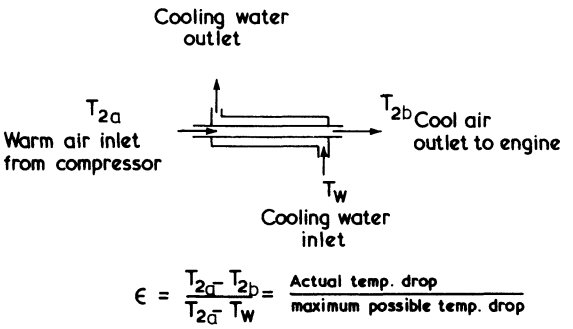

Figure 1.13 *Aftercooler effectiveness*

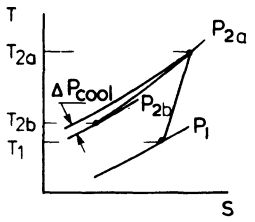

Figure 1.14 *Pressure loss in a charge air cooler*

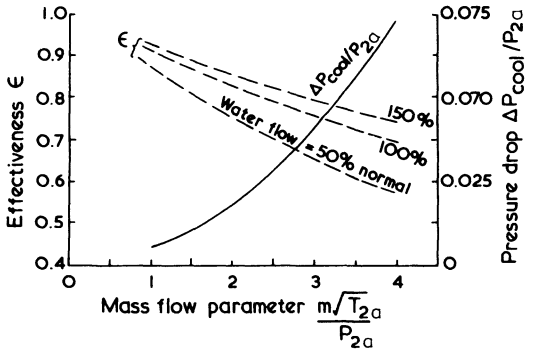

Figure 1.15 *Charge air-to-water aftercooler performance*

Typical performance (effectiveness and pressure drop against mass flow rate) of an air-to-water aftercooler is shown in figure 1.15. The effectiveness will vary with the mass flow rate of the charge air and the cooling water.

1.5 Compound Engines

The conventional turbocharged engine is characterised by the lack of any mechanical linkage between the turbocharger shaft and the crankshaft of the engine. The turbocharger is a free-running unit, which receives and transmits energy via the exhaust gas and compressor delivery air flow respectively. Compressor power requirement inherently balances the power output of the turbine, and if for any reason the balance is disturbed the turbocharger will adjust its speed until balance is achieved. No net power is extracted from the turbocharger shaft. However, there are attractions in a system in which the turbocharger shaft and engine crankshaft are linked, allowing power transmission between the two. The turbocharger relies on exhaust gas energy to provide supercharging boost pressure to the engine. Under some circumstances this energy, due to low turbocharger system efficiency, is not enough to provide a reasonable level of boost (typically at low engine speed particularly on two-stroke engines). In this situation it might be useful to help drive the turbocharger compressor from the crankshaft (similar,

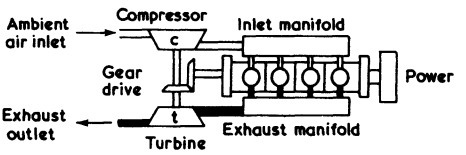

Figure 1.16 *Turbo-compound engine arrangement*

in part, to a conventional mechanically driven supercharger). This raises the boost pressure and hence the power output at low speed. The linkage between engine and turbocharger might be via a gear drive (figure 1.16). Such an engine would undoubtedly have an attractive low-speed torque output, but there are two disadvantages.

(1) Typical rotational speeds of engine and turbochargers differ by at least one order of magnitude. A high gear ratio is required which, at the turbocharger end, might involve gears running at between 20 000 and 80 000 rev/min (depending on engine size). The reliability and efficiency of such a gear drive is questionable.

(2) At high engine speeds and loads the power output of the turbocharger turbine is usually quite adequate (often it is more than required). When running as a free unit the turbocharger speed will therefore rise more rapidly than engine speed. If a fixed gear train connects the two, the turbocharger will be restrained, and although some useful power will be transmitted to the engine, the relatively low rotational speed of the turbine limits the benefit obtained. A solution to this problem is to use a variable gear ratio between the two, but this introduces obvious mechanical difficulties, although it has been attempted (for example, Napier Nomad aircraft engine).

Engines in which the turbocharger and crankshaft are linked are termed compound engines. The final power output is taken from the crankshaft in the normal way. The attractive power output and torque characteristics of these engines still encourage some manufacturers to pursue them, but they have not yet achieved commercial success, primarily due to their complexity. Figure 1.17 shows an approximate calculated power output of a theoretical compound engine and how it increases with pressure ratio. The turbine power output exceeds the power requirement of the compressor resulting in a positive work transfer from the turbine to the crankshaft. Thus the difference between the turbine output and compressor input powers may be added to the engine output curve giving the net power output shown.

1.6 Gas-generator Power Plant

The estimated performance curve for the compound engine in figure 1.17 shows that at a pressure ratio of 7.6:1, the engine power output alone balances the requirements of the compressor. At this condition it is possible to envisage an

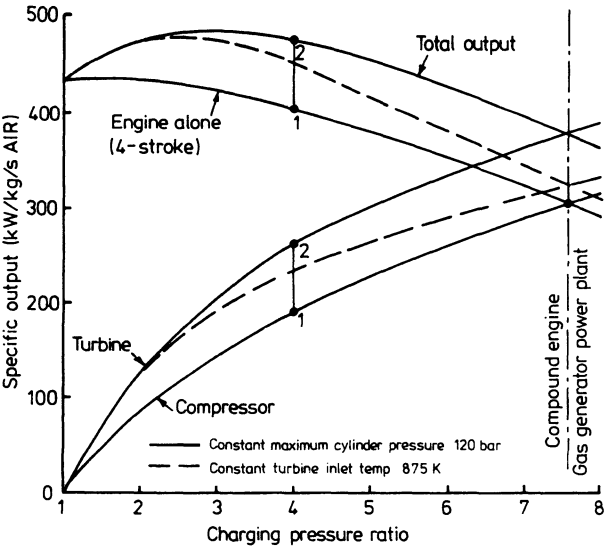

Figure 1.17 *Turbocharged, compound and gas-generator power plant. Turbine efficiency* $\eta_t = 0.8$*; compressor efficiency including transmission losses* $\eta_c \times \eta_{mech} = 0.75$

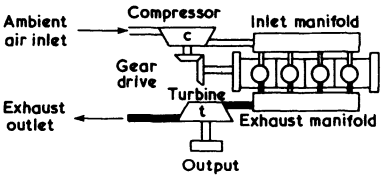

Figure 1.18 *Gas-generator power plant*

alternative engine, mechanically driving a compressor with no net crankshaft power output. The turbine would not be connected to the compressor, but its power output would be harnessed directly, replacing the engine as the power source (figure 1.18). The engine and compressor combination alone would form a self-supporting gas-generator (that is, generate a high-energy exhaust gas flow). The turbine converts this to useful power output. Engines have been built using this principle, some of the free-piston type, but again, they have not been commercially successful.

1.7 Turbocharging the Spark-ignition Engine

Today turbocharged diesel engines are common but turbocharged petrol engines are rare. There are sound reasons, both technical and economic for this situ-

ation. The principal reasons stem from the difference between the combustion systems of petrol and diesel engines. The petrol engine uses a carburettor or fuel-injection system to mix air and fuel in the inlet manifold so that a homogeneous mixture is compressed in the cylinder. A spark is used to control the initiation of combustion which then spreads throughout the mixture. It follows that the mixture temperature during compression must be kept below the self-ignition temperature of the fuel. Once combustion has started it takes time for the flame front to move across the combustion chamber burning the fuel. During this time, the unburnt 'end-gas' (furthest from the spark-plug, figure 1.19) is heated by further compression and radiation from the flame front. If it reaches the self-ignition temperature before the flame front arrives, a large quantity of mixture may burn extremely rapidly producing severe pressure waves in the combustion chamber. This situation is commonly referred to as 'knock' and may result in severe cylinder head and piston damage. It follows that the compression ratio of the engine must be low enough to prevent knock from occurring.

In the diesel engine cylinder, air alone is compressed. Fuel is sprayed directly into the combustion chamber from an injector only when combustion is required. This fuel self-ignites and in contrast it follows that in a diesel engine the compression ratio must be high enough for the air temperature on compression to exceed the self-ignition temperature of the fuel. Because injection takes time, only some of the fuel is in the combustion chamber when ignition starts, and since much of this fuel has not fully vaporised or mixed with the air the initial rate of combustion is not as damaging as the knocking situation in a petrol engine.

The maximum compression ratio of the petrol engine, but not the diesel engine, is therefore limited by the ignition properties of the fuel. The minimum compression ratio is limited by the resulting low efficiency. Turbocharging (or mechanical supercharging) results in not only a higher boost pressure, but a

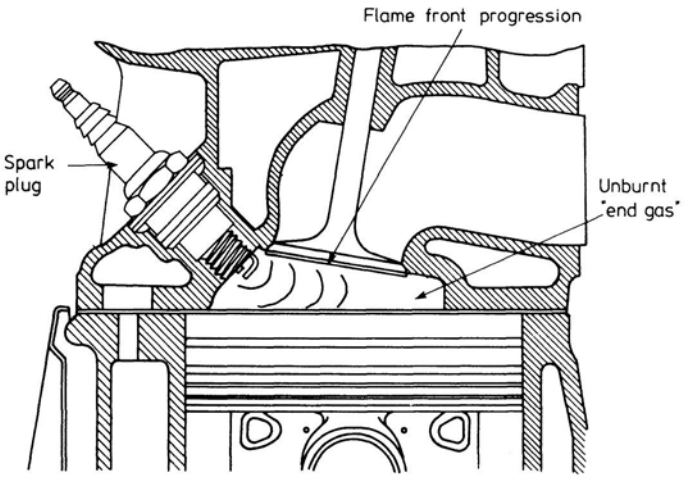

Figure 1.19 *'End-gas' in a petrol engine combustion chamber*

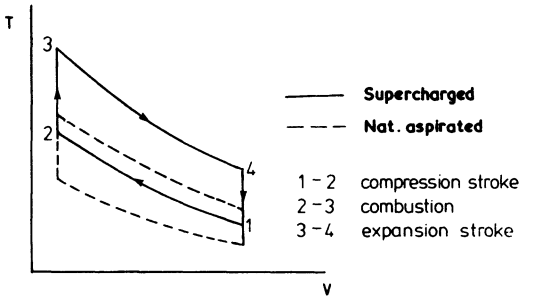

Figure 1.20 *Temperature/volume diagram for naturally aspirated and supercharged petrol engines*

higher temperature. Unless the compression ratio of a petrol engine is reduced (figure 1.20) the temperature at the end of the compression stroke will be too high and the engine will knock (the engine may remain knock free under mild boost–but only because the manufacturer has left a sufficient safe knock-free margin, or a fuel of higher self-ignition temperature/octane number has been used, or ignition timing has been retarded). Thus the potential power output of a turbocharged petrol engine is limited. The diesel engine has no such limitation and can therefore use a much higher boost pressure.

Petrol engines cost substantially less to produce than diesel engines of equivalent power output. The cost of the turbocharger on a diesel engine is more than offset by the reduced engine size required for a specified power output (with the exception of very small engines). This situation will rarely occur in the case of a petrol engine. As a result this book concentrates on diesel engines; however, chapter 13 is devoted to the special problems of turbocharging petrol engines.

1.8 Engine Efficiency

The principal objective of turbocharging is to increase the power output per volume and cost of the engine. A turbocharger is used in preference to a mechanically driven supercharger so that this benefit may be obtained without loss of efficiency. The fact that the turbocharger increases the mass of air in the cylinder and consequently allows more fuel to be burnt, says nothing about efficiency. In practice, it is usually possible to improve engine efficiency by a small but worthwhile amount. Consider a naturally aspirated engine and a similar turbocharged engine having double the indicated power output (double the work per cycle at the piston). Frictional losses are speed rather than load dependent, therefore the relative difference between the indicated and brake (flywheel) power output of the two engines will be small. Thus if frictional losses are subtracted from the indicated power outputs of the two engines, it will be evident that the turbocharged engine produces more than twice the net power output of the naturally aspirated engine. Yet it consumes double the quantity of fuel, hence its overall efficiency is superior.

In addition, if the turbocharging system enables the intake system pressure to

exceed that in the exhaust pipe, piston pumping during the intake and exhaust processes may be turned from a debit into a small but significant work bonus.

The above is a much simplified analysis, but the principle is valid. Further factors which influence efficiency will become apparent in the later chapters of this book.

Reference

1. A. Büchi, Über Brennkraftmeschinen, *Z. Gasturbinenewesen* (1969)

Further Reading

1. H. List, *Der Ladungswechsel der Verbrennungs Kraftmachine* (Springer Verlag, Vienna, 1950)
2. C. C. Pounder, *Diesel Engine Principles and Practice*, 2nd ed. (Newnes, 1962)
3. P. H. Schwitzer, *Scavenging of Two-stroke Diesel Engines* (Macmillan, New York, 1949)
4. C. F. Taylor and E. S. Taylor, *The Internal Combustion Engine*, 2nd ed. (International Textbook Company, 1961)
5. E. T. Vincent, *Supercharging the Internal Combustion Engine* (McGraw-Hill, 1948)
6. K. Zinner, *Aufladung von Verbrennungs-motoren* (Spring Verlag, Berlin 1975)

2

Turbochargers

2.1 Introduction

Various types of exhaust-driven turbochargers have been designed for supercharging reciprocating internal combustion engines. A turbocharger consists basically of a compressor and a turbine coupled on a common shaft. The exhaust gases from the engine are directed by the turbine inlet casing on to the blades of the turbine and subsequently discharged to atmosphere through a turbine outlet casing. The exhaust gases are utilised in the turbine to drive the compressor, which compresses the air and directs it to the engine induction manifold, to supply the engine cylinders with air of higher density than is available to a naturally aspirated engine. There exist a number of different types of compressors and turbines (or expanders), but few of these are ideally suitable to form the basis of an exhaust-gas driven supercharging system. The combination of a single-stage centrifugal compressor and a single-stage axial flow or radial flow turbine is almost universally used in turbochargers. The former type with the axial flow turbine is used for most of the medium and large size engines suitable for rail traction, industrial and marine purposes and the latter type with the radial flow turbine for small engines of the automotive (truck and automobile) type. A detailed analysis of centrifugal compressors, axial and radial flow turbines has been deferred to chapters 3, 4 and 5. This chapter is concerned with the specific requirement placed on a compressor-turbine for turbocharger use; the methods of comparing types and performance; and description and comments on typical turbochargers.

2.2 Turbomachines

Consider the basic requirements of the gas expander for a turbocharger. Its size must be small but its mass flow rate must be high. It must withstand a very high inlet temperature, be efficient over a wide mass flow range and be very reliable. Only axial and radial flow turbines meet these requirements. A positive displacement expander would require a swept volume considerably larger than the engine to which it would be coupled. The same applies to the compressor. Turbomachines are ideally suited for high mass flow rates at relatively low pressure

ratios. This is achieved by using high rotational speeds. In consequence, the turbine must be joined to a compressor which operates at similarly high speeds.

Turbocharger compressors are almost universally of the radial outflow type (that is, centrifugal) - see figure 2.1a. A single-stage subsonic centrifugal compressor can be designed to operate at any pressure ratio up to about 3.5:1 with reasonable efficiency and good reliability, with heat-resistant aluminium alloys. This pressure ratio limit is within the requirements of the majority of turbocharged engines at present, except for some special applications (for example, military), although current trends for industrial engines indicate a further increase up to 4.5:1 in the 1980s. At higher pressure ratios gas velocities will exceed the speed

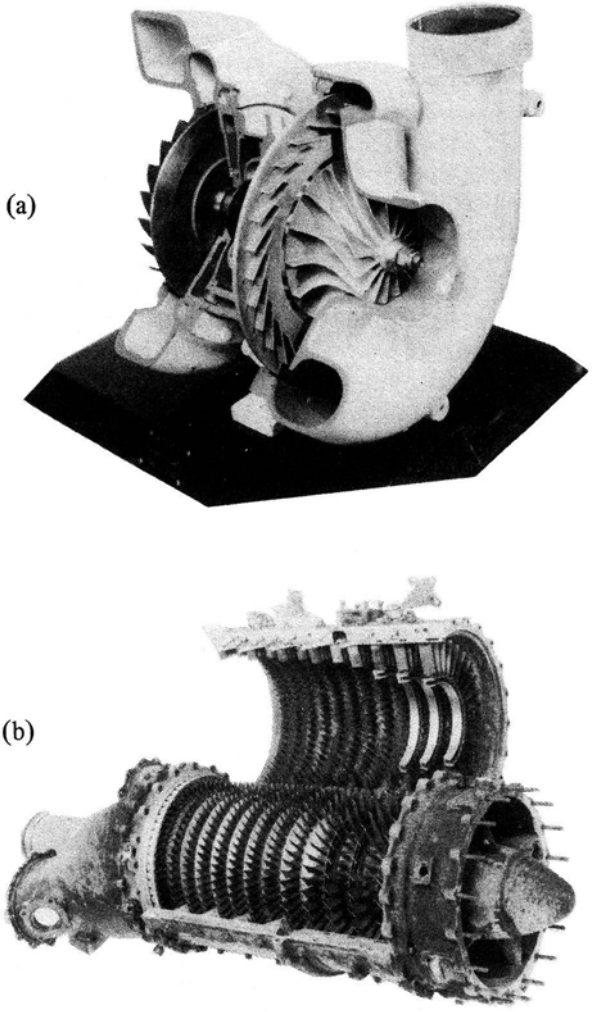

Figure 2.1 (a) *Centrifugal compressor;* (b) *axial flow compressor (Napier)*

of sound, and shock waves will impair efficiency. Single-stage supersonic centrifugal compressors have been developed and built for gas turbines, but the operational flow range is narrow, and the use of exotic materials (such as titanium) for the impeller makes them too expensive to be normally used as a turbocharger component. However, a considerable effort has been made to develop a reliable high-pressure ratio (up to 4.5:1) centrifugal compressor with wide range and high efficiency (Brown Boveri [1], MAN [2], Elliot [3]). Axial flow compressors (figure 2.1b) operate more efficiently than the radial flow type, but have a smaller operating range. Pressure ratios up to 12:1 can be achieved by multi-staging. However, the axial flow compressor is more expensive, heavier, longer (in construction) and less robust than a single-stage radial flow compressor for the same pressure ratio. Thus axial flow compressors have rarely been used in commercially available turbochargers.

Turbines may be radial, axial or mixed flow type, the first mentioned being fitted to small turbochargers, the second to larger units. Undoubtedly the single-stage radial inflow (centripetal) turbine (figure 2.2) is simpler and cheaper to manufacture than an axial flow turbine (figure 2.3), if the impeller can be cast. Unfortunately it has proved difficult to obtain sound large castings with high-temperature alloys, which is one reason why large turbochargers have exclusively axial flow turbines. Axial flow turbines become less efficient as size is reduced, when compared with the radial flow turbine, due to very short blades and narrow flow passages resulting in high boundary layer blockage. This is another reason why radial flow turbines perform satisfactorily and are widely used in small turbochargers (figure 2.4). Another factor working against large centripetal turbines is the problem of heat transfer out of the rotor. It is considerably easier

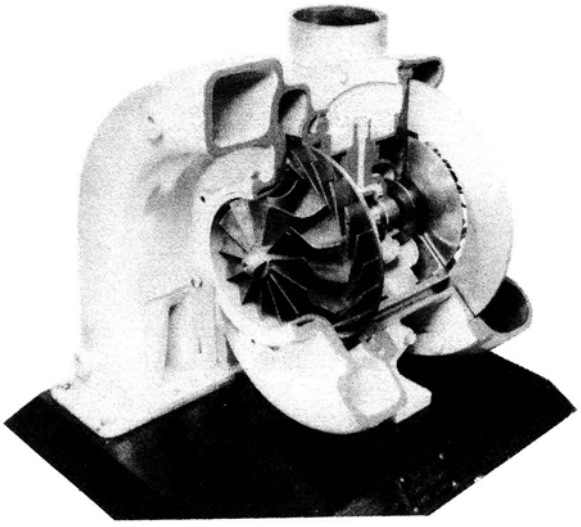

Figure 2.2 *Radial flow turbine (Napier)*

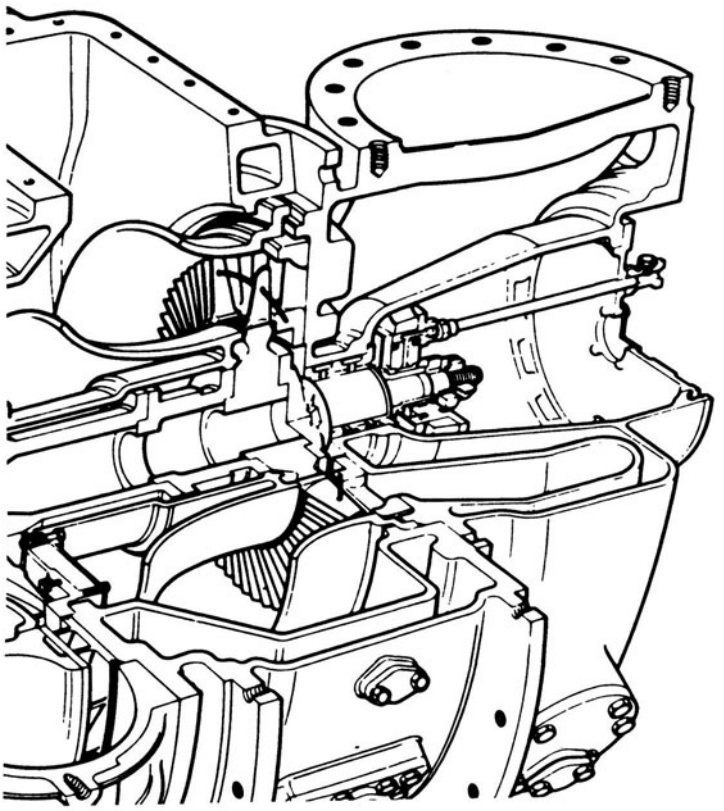

Figure 2.3 *Axial flow turbine (Napier)*

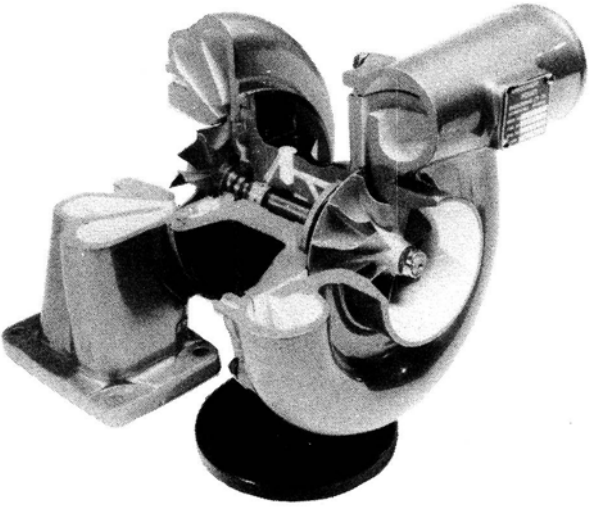

Figure 2.4 *Small turbocharger (Holset)*

to arrange a suitable cooling flow path and uniform metal temperature distribution along the blade in an axial machine than in a radial flow type.

2.3 Total and Static Pressure and Temperature

The static pressure (P_1) of a fluid flowing in a duct is that measured at the surface of the wall. The total or stagnation pressure (P_{01}) is the pressure that will be measured in the stream if the fluid were brought to rest isentropically (see figure 2.5). Thus

$$P_{01} = P_1 \left(\frac{T_{01}}{T_1}\right)^{\gamma/(\gamma-1)} \tag{2.1}$$

Similarly the static temperature (T_1) is the free stream temperature and the total (or stagnation) temperature (T_{01}) is the temperature that will be measured if the gas were brought to rest. For a perfect gas it can be shown that

$$T_{01} = T_1 + \tfrac{1}{2}\frac{C_1^2}{c_p} \tag{2.2}$$

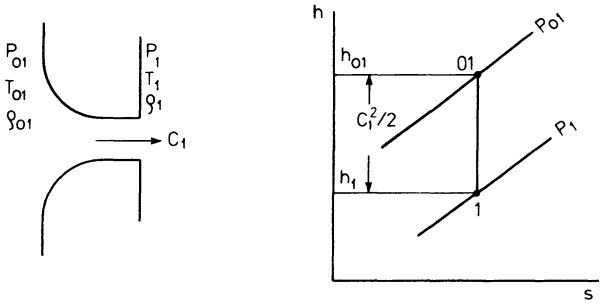

Figure 2.5 *Relationship between total and static conditions*

2.4 Compressor and Turbine Efficiencies

The work output from (or input to) a turbomachine can be found from the first law of thermodynamics. From this law the steady-flow energy equation may be derived.

$$\dot{Q} - \dot{W} = \dot{m}\,[(h_2 + \mathrm{KE}_2 + \mathrm{PE}_2) - (h_1 + \mathrm{KE}_1 + \mathrm{PE}_1)]$$

where $\dot{Q}$ = heat transfer rate to the system

$\dot{W}$ = work transfer rate from the system

$\dot{m}$ = mass flow rate

h = specific enthalpy

KE = specific kinetic energy

PE = specific potential energy

subscript 1 = inlet; subscript 2 = outlet

Denoting stagnation enthalpy h_0 as

$$h_0 = h + \text{KE}$$

and neglecting any change in potential energy, then

$$\dot{Q} - \dot{W} = \dot{m}(h_{02} - h_{01})$$

It is customary to neglect heat transfer from turbomachines since this is usually small, and clearly difficult to measure. Thus

$$-\dot{W} = \dot{m}(h_{02} - h_{01}) \tag{2.3}$$

(Note: $-\dot{W}$ is a result of the sign convention denoting work transfer from the system as positive.)

Both air and exhaust gas from an engine are considered perfect or semi-perfect gases. They obey the equation of state

$$Pv = RT$$

where R is the gas constant. Specific heat capacities are defined as

$$c_p \equiv \left(\frac{\partial h}{\partial T}\right)_p \text{ and } c_v \equiv \left(\frac{\partial u}{\partial T}\right)_v$$

where c_p = specific heat capacity at constant pressure

c_v = specific heat capacity at constant volume

u = specific internal energy

For a perfect gas it can be shown that c_p and c_v are constant. For a semi-perfect gas they are functions of temperature only. It follows that

$$c_p = \frac{\mathrm{d}h}{\mathrm{d}T} \text{ and } c_v = \frac{\mathrm{d}u}{\mathrm{d}T}$$

Thus $\mathrm{d}h = c_p\,\mathrm{d}T$, and for a perfect gas equation equation 2.3 becomes

$$-\dot{W} = \dot{m}\,c_p\,(T_{02} - T_{01}) \tag{2.4}$$

where the subscript 0 denotes stagnation (or 'total') conditions.

The second law of thermodynamics tells us that the property specific entropy (s) is related to heat transfer, and for a reversible process

$$\mathrm{d}s = \frac{\mathrm{d}Q}{T}$$

and for an irreversible process

$$ds > \frac{dQ}{T}$$

Thus for an adiabatic process the entropy is unchanged if the process is reversible (isentropic process) and rises if the process is irreversible.

2.4.1 Compressor Isentropic Efficiency

One definition for the efficiency of a compressor might be the work required for ideal adiabatic compression divided by the actual work required to achieve the same pressure ratio. From the second law of thermodynamics it is clear that this definition is equivalent to

$$\eta_c = \frac{\text{isentropic work}}{\text{actual work}} \tag{2.5}$$

Hence η_c is called the isentropic efficiency (figure 2.6). From equations 2.3 and 2.4

$$\eta_{cTT} = \frac{h_{02_s} - h_{01}}{h_{02} - h_{01}} \tag{2.6}$$

and for a perfect gas c_p = constant therefore

$$\eta_{cTT} = \frac{T_{02_s} - T_{01}}{T_{02} - T_{01}} \tag{2.7}$$

The expressions are for 'total to total' isentropic efficiency, henceforth denoted by η_{cTT}.

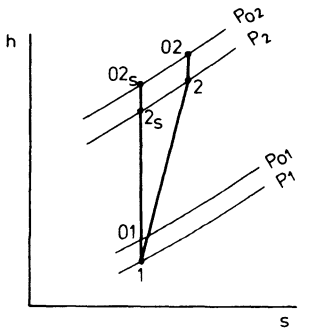

Figure 2.6 *h–s diagram for a compressor*

For isentropic compression, pressure and temperature are related by the expression

$$\frac{P_{02}}{P_{01}} = \left(\frac{T_{02_S}}{T_{01}}\right)^{\gamma/(\gamma-1)} \tag{2.8}$$

where $\gamma = c_p/c_v$. Hence equation 2.7 becomes

$$\eta_{cTT} = \frac{T_{01}\,[(T_{02_S}/T_{01})-1]}{T_{02}-T_{01}} = \frac{T_{01}\,[(P_{02}/P_{01})^{(\gamma-1)/\gamma}-1]}{T_{02}-T_{01}} \tag{2.9}$$

or

$$\eta_{cTT} = \frac{(P_{02}/P_{01})^{(\gamma-1)/\gamma}-1}{(T_{02}/T_{01})-1} \tag{2.10}$$

An evaluation of efficiency based on equation 2.10 assumes that all the kinetic energy at station 2 can be used. This is not unrealistic in the case of a compressor for a gas turbine since the velocity at the compressor delivery is maintained at the entry to the combustion chamber. However, the compressor of a turbocharger must supply air via a relatively large inlet manifold to the cylinders. Hence the engine will only 'feel' the static pressure at compressor delivery and is unlikely to benefit from the kinetic energy at station 2. Thus a turbocharger compressor should be designed for high kinetic to potential energy conversion before the exit duct.

Since the engine benefits little from the kinetic energy of the air leaving the compressor, a more realistic definition of compressor efficiency is based on static delivery temperature

$$\eta_{cTS} = \frac{h_{2_S}-h_{01}}{h_{02}-h_{01}}$$

and

$$\eta_{cTS} = \frac{T_{2_S}-T_{01}}{T_{02}-T_{01}} = \frac{(P_2/P_{01})^{(\gamma-1)/\gamma}-1}{\left(\frac{T_{02}}{T_{01}}-1\right)} \tag{2.11}$$

where subscript TS denotes 'total to static'.

Unfortunately many manufacturers quote total to total efficiencies for turbocharger compressors (since the values are a few percentage points higher than total to static values). Even worse, some quote total to total efficiencies without declaring on what basis the efficiency value is calculated.

2.4.2 Compressor Polytropic Efficiency

The concept of polytropic efficiency is usually used on axial compressors since in essence it is a 'small stage' efficiency. It is the limiting value of isentropic

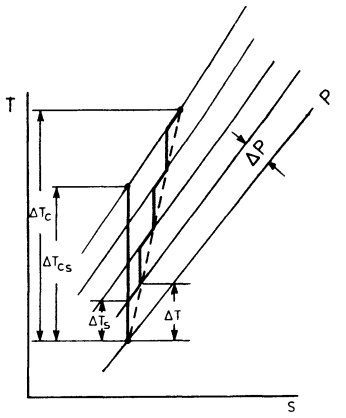

Figure 2.7 *T-s diagram for multi-stage compressor*

efficiency as the pressure ratio approaches unity. Since in a number of publications on turbocharger centrifugal compressors reference is made to the polytropic efficiency as a mean efficiency for the whole compressor stage, it is important to understand the concept of polytropic efficiency. To avoid a multiplicity of subscripts, P and T are used instead of P_0 and T_0 (see figure 2.7) and subscript s denotes isentropic for a single-stage, c the complete compressor and cs isentropic for the complete compressor. From equation 2.10 the isentropic stage efficiency is given by

$$\eta_s = \frac{\left(\frac{P + \Delta P}{P}\right)^{(\gamma-1)/\gamma} - 1}{\Delta T/T}$$

Hence the small stage efficiency can be written as

$$\eta_s = \frac{\left(1 + \frac{dP}{P}\right)^{(\gamma-1)/\gamma} - 1}{dT/T} \tag{2.12}$$

Assuming that the isentropic efficiency of a single stage (η_s) remains constant through the compressor, then the over-all temperature rise across the compressor (ΔT_c) is given by

$$\Delta T_c = \Sigma \frac{\Delta T_s}{\eta_s} = \frac{1}{\eta_s} \Sigma \Delta T_s$$

Also $\Delta T_c = \Delta T_{cs}/\eta_c$, thus

$$\frac{\eta_s}{\eta_c} = \frac{\Sigma \Delta T_s}{\Delta T_{cs}}$$

Because the vertical distance between a pair of constant pressure lines in the T-s diagram increases as the entropy increases (figure 2.7) $\Sigma \Delta T_s > \Delta T_{cs}$ it follows that the over-all efficiency of a multi-stage compressor is lower than

that of each component stage, that is, $\eta_c < \eta_s$. The excess temperature rise above the isentropic value is passed on to the following stage which itself will suffer a corresponding excess temperature rise. Since polytropic efficiency is based on an infinitely small stage of compression, the over-all efficiency based on it will be dependent on the over-all pressure ratio, not on the number of stages. These considerations have led to the introduction of a polytropic efficiency η_{c_p} which is defined as the isentropic efficiency of an elemental stage in the process such that it is constant throughout the whole process.

From the definition of the small stage efficiency for the compression process

$$\eta_{c_p} = \frac{dT_s}{dT} = \text{constant} \tag{2.13}$$

For an isentropic process $P = kT^{\gamma/(\gamma-1)}$, hence

$$\frac{dP}{dT_s} = k\left(\frac{\gamma}{\gamma-1}\right)T^{[\gamma/(\gamma-1)-1]} = \left(\frac{\gamma}{\gamma-1}\right)\frac{P}{T}$$

or

$$dT_s = \frac{T}{P}\,dP\left(\frac{\gamma-1}{\gamma}\right)$$

Inserting into equation 2.13 gives

$$\eta_{c_p} = \frac{T}{dT}\frac{dP}{P}\left(\frac{\gamma-1}{\gamma}\right) \tag{2.14}$$

Integrating between inlet 1 and outlet 2, with η_{c_p} = constant by definition

$$\eta_{c_p} = \frac{\ln\,(P_2/P_1)^{(\gamma-1)/\gamma}}{\ln\,(T_2/T_1)} \tag{2.15}$$

This equation enables us to calculate the compressor polytropic efficiency η_{c_p} from measured values of P and T at inlet and outlet of a compressor. Equation 2.15 can also be written in the form

$$\frac{P_2}{P_1} = \left(\frac{T_2}{T_1}\right)^{\gamma\eta_{c_p}/(\gamma-1)}$$

If a polytropic process is represented by PV^n = constant, then

$$P = T^{n/(n-1)} \times \text{constant} \tag{2.16}$$

or in differential form

$$\frac{dP}{P} = \frac{dT}{T}\left(\frac{n}{n-1}\right) \tag{2.17}$$

Substituting equation 2.17 into equation 2.14 gives

$$\frac{n}{n-1} = \frac{\gamma}{\gamma-1}\eta_{c_p}$$

Thus

$$\frac{T_2}{T_1} = \left(\frac{P_2}{P_1}\right)^{(n-1)/n} = \left(\frac{P_2}{P_1}\right)^{(\gamma-1)/\gamma\eta_{cp}} \tag{2.18}$$

Finally the isentropic and polytropic efficiencies may be related as follows. Substituting equation 2.18 into equation 2.10

$$\eta_{cTT} = \frac{(P_{02}/P_{01})^{(\gamma-1)/\gamma} - 1}{(P_{02}/P_{01})^{(\gamma-1)/\gamma\eta_{cp}} - 1} \tag{2.19}$$

Variation of the compressor isentropic efficiency for $\gamma = 1.4$ and compressor pressure ratio for a fixed value of polytropic efficiency of 0.85 is shown in figure 2.8.

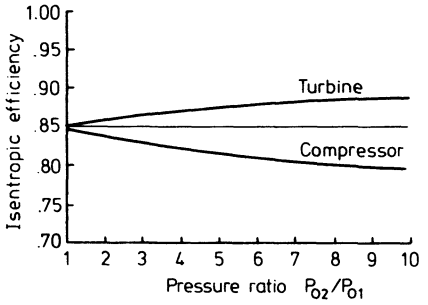

Figure 2.8 *Variation of compressor and turbine isentropic efficiency with pressure ratio (for a polytropic efficiency of 0.85)* [4]

2.4.3 Turbine Isentropic Efficiency

The isentropic efficiency of a turbine may be defined as the actual work output divided by that obtained from reversible adiabatic (isentropic) expansion between the same two pressures (figure 2.9).

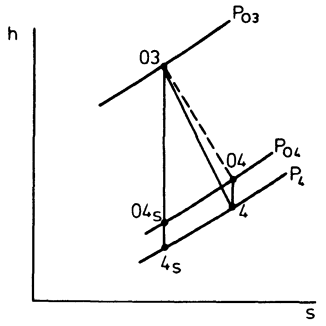

Figure 2.9 *h–s diagram for a turbine*

$$\eta_t = \frac{\text{actual work}}{\text{isentropic work}} \tag{2.20}$$

From equations 2.3 and 2.4

$$\eta_{t_{TT}} = \frac{h_{03} - h_{04}}{h_{03} - h_{04_s}} \tag{2.21}$$

and for a perfect gas (c_p = constant)

$$\eta_{t_{TT}} = \frac{T_{03} - T_{04}}{T_{03} - T_{04_s}} \tag{2.22}$$

where subscripts 3 and 4 represent turbine inlet and outlet respectively.

For isentropic expansion, pressure and temperature are related by

$$\frac{P_{03}}{P_{04}} = \left(\frac{T_{03}}{T_{04}}\right)^{\gamma/(\gamma-1)}$$

Hence equation 2.22 becomes

$$\eta_{t_{TT}} = \frac{T_{03} - T_{04}}{T_{03}\,[1 - (T_{04_s}/T_{03})]} = \frac{T_{03} - T_{04}}{T_{03}\,[1 - (P_{04}/P_{03})^{(\gamma-1)/\gamma}]} \tag{2.23}$$

or

$$\eta_{t_{TT}} = \frac{1 - (T_{04}/T_{03})}{1 - (P_{04}/P_{03})^{(\gamma-1)/\gamma}} \tag{2.24}$$

Clearly no use at all can be made of the kinetic energy leaving a turbocharger turbine; it goes to waste through the exhaust pipe. A more relevant isentropic efficiency could be based on static exit temperature. The total to static isentropic efficiency would be defined as the actual work output divided by isentropic expansion between the stagnation inlet and static outlet pressures.

$$\eta_{t_{TS}} = \frac{h_{03} - h_{04}}{h_{03} - h_{4_s}} = \frac{T_{03} - T_{04}}{T_{03} - T_{4_s}} = \frac{T_{03} - T_{04}}{T_{03}\,[1 - (P_4/P_{03})^{(\gamma-1)/\gamma}]} \tag{2.25}$$

and

$$\eta_{t_{TS}} = \frac{1 - (T_{04}/T_{03})}{1 - (P_4/P_{03})^{(\gamma-1)/\gamma}} \tag{2.26}$$

2.4.4 Turbine Polytropic Efficiency

The concept of polytropic efficiency is applied to axial multi-stage turbines in a

similar manner as it is to axial compressors. The polytropic (small stage) efficiency for a perfect gas is given by

$$\eta_{t_p} = \frac{-\,dT/T}{1 - \left(1 + \dfrac{dP}{P}\right)^{(\gamma-1)/\gamma}} \tag{2.27}$$

It can be shown from section 2.4.2 for the turbine polytropic efficiency that

$$\eta_{t_p} = \frac{dT}{dT_s} = \frac{dT}{T}\left(\frac{P}{dP}\right)\frac{\gamma}{\gamma - 1}$$

Integrating between inlet 3 and outlet 4 with η_{t_p} = constant by definition

$$\eta_{t_p} = \frac{\ln (T_3/T_4)^{\gamma/\gamma-1}}{\ln (P_3/P_4)} \tag{2.28}$$

This equation enables us to calculate the turbine polytropic efficiency η_{t_p} from measured values of P and T at inlet and outlet of a turbine.

Equation 2.28 can be written in the form

$$\frac{T_4}{T_3} = \left(\frac{P_4}{P_3}\right)^{\eta t_p (\gamma-1)/\gamma} \tag{2.29}$$

and the isentropic and polytropic efficiencies for the turbine may be related by substituting equation 2.29 into equation 2.24

$$\eta_{t_{TT}} = \frac{1 - (P_{04}/P_{03})^{\eta t_p (\gamma-1)/\gamma}}{1 - (P_{04}/P_{03})^{(\gamma-1)/\gamma}} \tag{2.30}$$

Variation of turbine isentropic efficiency with pressure ratio for $\gamma = 1.4$ and a polytropic efficiency of 0.85 is shown in figure 2.8.

2.5 Non-dimensional Representation of Compressor and Turbine Performance Characteristics

When studying the performance characteristics of turbomachinery it is a great help if results from different sources are directly comparable, even for machines of somewhat different size. It is fortunate that the behaviour of turbomachines can be illustrated using dimensionless parameters involving all relevant variables. We have already considered one dimensionless parameter: efficiency.

The mass flow rate ($\dot{m}$), the efficiency (η) and the temperature rise ($\Delta T_0 = T_{02} - T_{01}$) of a compressor can be expressed as functions of the independent variables: $\dot{m}$; η; $\Delta T_0 = f(P_{01}, P_{02}, T_{01}, N, D, R, \gamma, \mu)$, where N = rotational speed, D = diameter, R = gas constant, $\gamma = c_p/c_v$ and μ = dynamic viscosity. These can be reduced to a set of non-dimensional groups

$$\frac{\dot{m}\sqrt{(RT_{01})}}{P_{01}D^2}, \eta, \frac{\Delta T_0}{T_{01}} = f\left(\frac{ND}{\sqrt{(RT_{01})}}, \frac{P_{02}}{P_{01}}, \frac{\dot{m}}{\mu D}, \gamma\right)$$

Since turbochargers operate on a specific gas (air for the compressor, exhaust gas for the turbine), the values of R and γ are specified. Hence the non-dimensional groups become

$$\frac{\dot{m}\sqrt{(RT_{01})}}{P_{01}D^2}, \eta, \frac{\Delta T_0}{T_{01}} = f\left(\frac{ND}{\sqrt{(RT_{01})}}, \frac{P_{02}}{P_{01}}, \frac{\dot{m}}{\mu D}\right)$$

Fortunately the Reynolds number of the gas has little effect on the performance of the machine, and can usually be ignored. Hence

$$\frac{\dot{m}\sqrt{(RT_{01})}}{P_{01}D^2}, \eta, \frac{\Delta T_0}{T_{01}} = f\left(\frac{ND}{\sqrt{(RT_{01})}}, \frac{P_{02}}{P_{01}}\right)$$

A relationship between η, $\Delta T_0/T_{01}$ and P_{02}/P_{01} has already been established (equation 2.10), namely

$$\eta_{cTT} = \frac{(P_{02}/P_{01})^{(\gamma-1)/\gamma} - 1}{\Delta T_0/T_{01}}$$

For a particular machine the diameter (D) is constant and therefore may be ignored. Thus the complete performance of the compressor may be represented by the relationships (for a particular fluid, such as air)

$$\frac{\dot{m}\sqrt{T_{01}}}{P_{01}} \text{ and } \eta = f\left(\frac{N}{\sqrt{T_{01}}}, \frac{P_{02}}{P_{01}}\right)$$

or

$$\frac{\dot{m}\sqrt{T_{01}}}{P_{01}} \text{ and } \frac{\Delta T_0}{T_{01}} = f\left(\frac{N}{\sqrt{T_{01}}}, \frac{P_{02}}{P_{01}}\right)$$

By plotting P_{02}/P_{01} against the mass flow parameter $\dot{m}\sqrt{(T_{01})}/P_{01}$ for a series of values of $N/\sqrt{T_{01}}$, the complete performance of the machine is apparent. Lines of constant efficiency may be superimposed on this map. A typical compressor map is shown in figure 2.10. A detailed explanation is given in section 2.6. A similar performance map may be drawn for a turbine, although naturally the curves will appear very different.

A disadvantage of removing the length term (or diameter) D and gas constant R is that the mass flow and speed parameters are no longer dimensionless. The major advantage of the presentation is that it illustrates the performance, independent of the inlet conditions (pressure and temperature), and can therefore be used for that compressor, at any time and place.

As discussed in section 2.3, the temperatures and pressures need not, of course, be total (stagnation) values.

2.6 Performance Characteristics of Compressors, Turbines and Turbochargers

It is conventional, but not universal, to plot compressor characteristics in terms of pressure ratio against mass flow parameter ($\dot{m}\sqrt{(T_{01}/P_{01})}$ for lines of constant

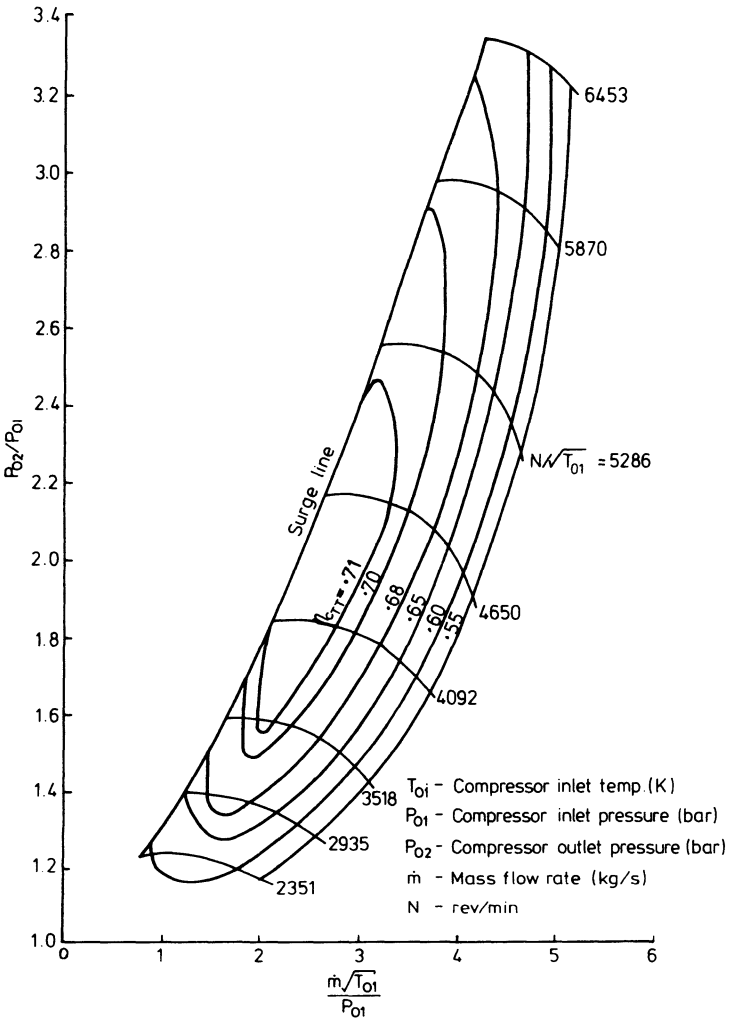

Figure 2.10 *Compressor characteristic*

speed parameter ($N/\sqrt{T_{01}}$) as in figure 2.10. In addition, contours of constant isentropic efficiency are superimposed. The important features of centrifugal and axial compressor characteristics are similar.

There are essentially three areas on a compressor map. The central area is the stable operating zone. This area is separated from the unstable area on its left by the surge line. A detailed explanation of the causes of surge has yet to be fully accepted, but it is clear that when the mass flow rate through a compressor is reduced while maintaining a constant pressure ratio, a point arises at which local flow reversal occurs in the boundary layers. This should result in low efficiency but not necessarily in instability. If the flow rate is further reduced, complete reversal occurs. This will relieve the adverse pressure gradient

until a new flow regime at a lower pressure ratio is established. The flow will then build up again to the initial condition and thus flow instability will continue at a fixed frequency. Surge is actually a more complex phenomenon than that described, but it is sufficient at this stage to realise that the compressor must not be asked to work in the area to the left of the surge line.

The area to the right of the compressor map is associated with very high gas velocity. It is the result of choking of the limiting flow area in the machine. Extra mass flow through the compressor can only be gained by higher speeds. This additional mass flow will certainly be limited by the ability of the diffuser area to accept the flow. When diffuser choking occurs, compressor speed may rise substantially with little increase in mass flow rate. The area of maximum efficiency naturally falls in the central stable operating zone. In practice it tends to lie in an area roughly parallel to the surge line with vaneless-type diffusers and very close to the surge line in the case of vaned-type diffusers (see chapter 3).

An axial flow turbine characteristic based on the same pressure ratio against mass flow parameters is shown in figure 2.11. The most evident feature is the way that the lines of constant speed parameter ($N/\sqrt{T_{03}}$) converge to a single line of almost constant mass flow parameter. This mass flow limit is caused by the gas reaching sonic velocity in the turbine stator nozzle blades or inlet casing. This choked flow will remain constant (unless the inlet temperature increases) regardless of the rotational speed of the turbine. At pressure ratios lower than that producing choked flow, the mass flow rate will be a function of turbine speed and hence a range of constant $N/\sqrt{T_{03}}$ lines is evident.

In the case of the radial flow turbine, due to the centrifugal field created by the rotor, there is a noticeable spread of constant speed parameters for choked flow conditions, as shown in figure 2.12.

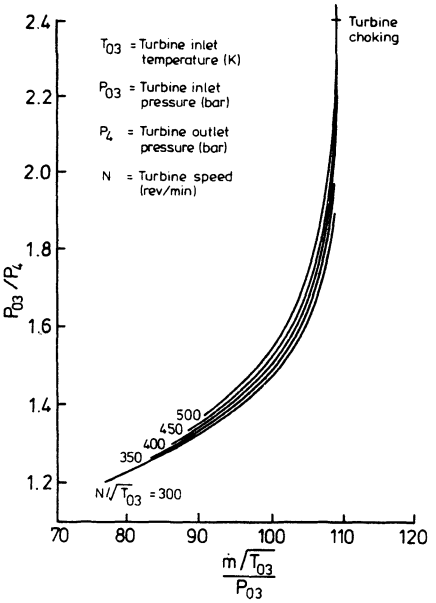

Figure 2.11 *Axial flow turbine characteristic*

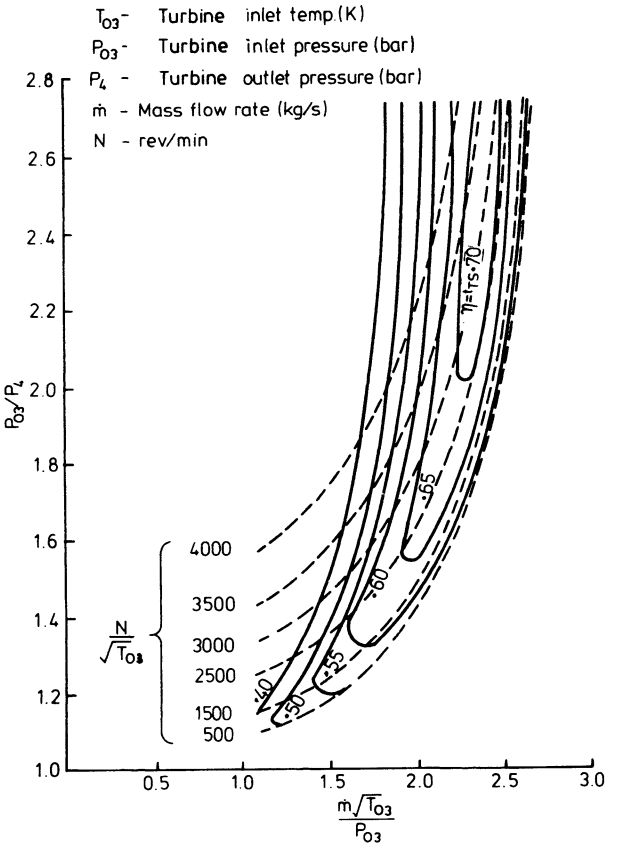

Figure 2.12 *Radial flow turbine characteristic*

Since the operational area of the turbine occupies such a restricted area on the pressure ratio/mass flow parameter map, it becomes simpler to present efficiency on a separate diagram. It is conventional to plot efficiency against velocity ratio (blade speed ratio). This is the blade speed (at its mean height) in the case of the axial flow turbine, or the wheel tip speed in the case of the radial flow turbine, divided by the velocity equivalent of the isentropic enthalpy drop across the turbine stage (see chapter 4). Lines of constant pressure ratio (total to total or total to static) or sometimes constant speed parameter ($N/\sqrt{T_{03}}$) are drawn on the map (figure 2.13). This method of representation is important in matching the compressor and the turbine wheel size to ensure operation of the turbine at optimum efficiency (at constant pressure operation). It is also used in the quasi-steady analysis for unsteady flow operation (pulse system). It is usual to include the turbocharger mechanical (bearing) losses in the turbine efficiency since it is difficult in practice to separate them.

For a given turbocharger it is possible to link the compressor and turbine

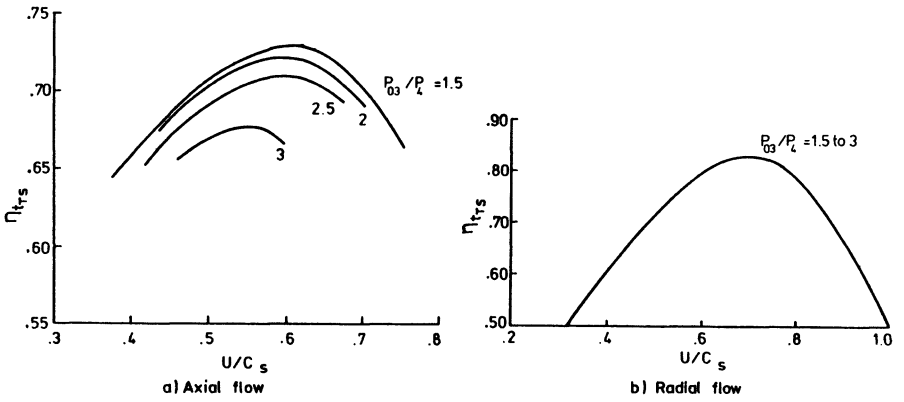

Figure 2.13 *Axial and radial flow turbine efficiency against blade speed ratio:* (a) *axial;* (b) *radial*

characteristics and plot on the compressor map the turbocharger equilibrium running lines, the so-called 'turbocharger characteristic'.

Since the compressor and turbine are on a common shaft, then

$$\frac{N}{\sqrt{T_{01}}} = \frac{N}{\sqrt{T_{03}}} \sqrt{\frac{T_{03}}{T_{01}}} \tag{2.31}$$

for $\dot{m}_c = \dot{m}_t = \dot{m}$

$$\frac{\dot{m}\sqrt{T_{01}}}{P_{01}} = \frac{\dot{m}\sqrt{T_{03}}}{P_{03}} \left(\frac{P_{03}}{P_{01}}\right) \sqrt{\frac{T_{01}}{T_{03}}} \tag{2.32}$$

and for equilibrium between compressor and turbine work

$$\left(\frac{T_{02} - T_{01}}{T_{01}}\right) c_{p_c} = \left(\frac{T_{03} - T_{04}}{T_{03}}\right) c_{p_t} \frac{T_{03}}{T_{01}}$$

hence

$$\left(\frac{P_{02}}{P_{01}}\right)^{(\gamma_c - 1)/\gamma_c} - 1 = \eta_c \eta_t \eta_{mech} \frac{c_{p_t}}{c_{p_c}} \left[1 - \left(\frac{P_4}{P_{03}}\right)^{(\gamma_c - 1)/\gamma_c}\right] \frac{T_{03}}{T_{01}} \tag{2.33}$$

Assuming that the turbine outlet pressure (P_4) equals the ambient pressure (P_{01}), the equilibrium running lines for constant T_{03}/T_{01} values as parameters can be estimated.

Figure 2.14 represents a typical turbocharger characteristic based on the compressor characteristic from figure 2.10 and the radial flow turbine characteristic from figure 2.12. The chain-dotted self-supporting running line represents the unique conditions for $P_{02} = P_{03}$ (that is, no pressure drop across the cylinders of the engine.) The area on the left of this line represents positive pressure drop across the cylinders and the area on the right of the line represents a negative pressure drop across the cylinder.

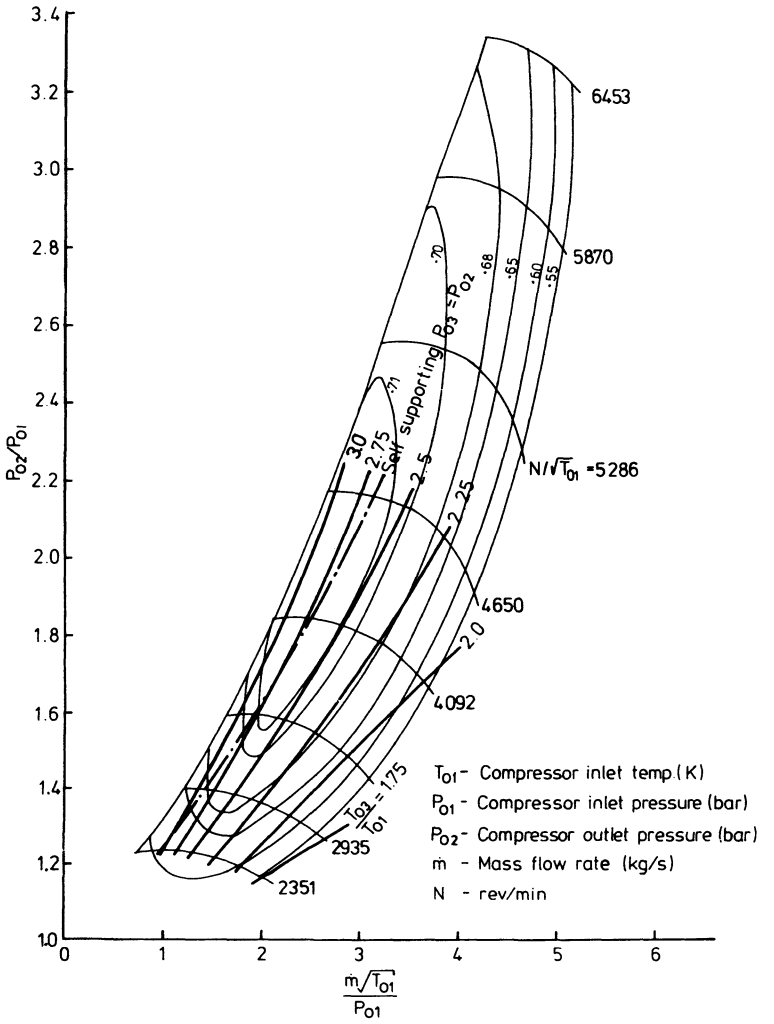

Figure 2.14 *Turbocharger characteristic*

It should be noted that the 'turbocharger characteristic' was derived on the basis of steady flow conditions and therefore it can only be used for constant pressure applications.

2.7 Turbochargers

In the early 1920s the first exhaust-gas turbochargers for diesel engines were of very simple design. They were large and heavy machines, built on their own bed-plates and installed on the floor beside the diesel engine. A typical sectional

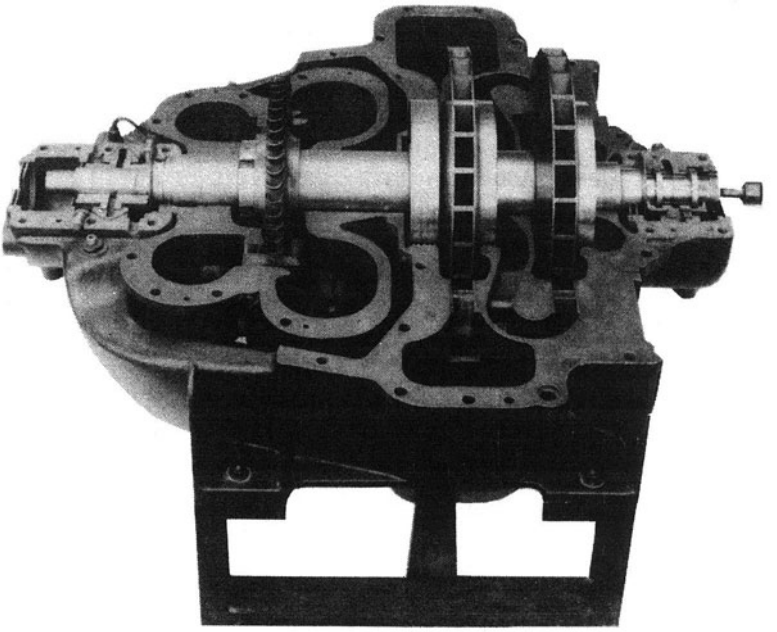

Figure 2.15 *One of the first Brown Boveri turbochargers*

view of one of the first Brown Boveri turbochargers is shown in figure 2.15. A single-stage axial flow turbine was used along with a two-stage radial flow compressor which was made with backward curved impeller vanes. Both of these were fitted on to a single shaft with outboard plain bearings mounted at the turbine and compressor ends. A pressure-compensating piston between the compressor and turbine was used to balance out the thrust load. The uncooled gas casings were covered with an insulating shield and the casings were horizontally divided to ease assembly. The pressure ratio normally attained with the two-stage compressors was of the order of 1.3:1.

Since the Second World War, great advances have been made in turbocharging the internal combustion engine. The continuous increase in engine output which demanded higher BMEP and hence higher boost pressures and efficiencies, has led to progressive development and evolution in the design and construction of the modern turbocharger, as have the use of heavy fuel, the requirement of faster response and reduced noise levels and the increasing spread of turbocharging to truck and passenger car engines. The major advances in fluid dynamic analysis made in gas turbine technology are now used in the design of the components of modern turbochargers. However, the turbocharger designer is faced with additional design requirements caused by the large range of mass flow rates, the non-steady character of the flow and cost considerations.

In general, the commercially available turbochargers can be subdivided into two principal groups: those primarily designed for use on automotive and truck engines, and those for use on medium-speed and low-speed diesel engines for

railway traction, electricity-generating sets, industrial and marine applications. The latter group may be further sub-divided into smaller units having radial inflow turbines and larger units with axial flow turbines. The difference between the two principal groups can be summed up as a contrast between small, simple and cheaply mass-produced units, and larger, more complex, expensive and reliable industrial or large marine units. Before analysing their design and construction the general design consideration for the layout of the single-stage turbocharger unit must first be discussed.

2.7.1 General Design Consideration

In the design and construction of turbochargers, the following important limiting criteria have to be taken into account: long service life, a high degree of safety, broad and efficient compressor and turbine characteristics, adaptability to different types of operation, and cost.

2.7.1.1 Compressor-Turbine Matching

The single-stage turbocharger consists of two basic components: the radial flow compressor and an axial or radial flow turbine mounted on a common shaft. Since most turbochargers are initially designed to operate under steady flow conditions, the basic principle is to match the impeller of the compressor to the turbine wheel to allow the turbine to operate at its peak efficiency (chapters 4 and 5). Thus a unique relationship can be derived between the compressor impeller tip diameter and the turbine wheel tip diameter, in the case of the radial flow turbine, and the impeller tip diameter and the turbine wheel mean blade height diameter, in the case of the axial flow turbine. From the compressor work transfer equation for a radial vaned impeller, the energy balance between compressor work and turbine work, and the definition of blade speed ratio, the following expression can be derived

$$\frac{D_c}{D_t} = \frac{1}{U/C_s} = \sqrt{\frac{\eta_t}{2\sigma}}$$

where D_c = compressor impeller tip diameter

D_t = turbine rotor tip diameter (radial flow) or rotor mean blade height diameter (axial flow)

σ = compressor slip factor (see chapter 3)

U/C_s = turbine blade speed ratio

Figure 2.16 shows the relationship between the D_c/D_t ratio and the U/C_s ratio for different values of turbine efficiency (η_t) (including mechanical efficiency) and compressor slip factor of 0.9 and 0.8. It can be seen from figure 2.16 that in the case of small automotive turbochargers incorporating compressor impellers with low vane numbers (slip factor approaching 0.8) and a radial flow

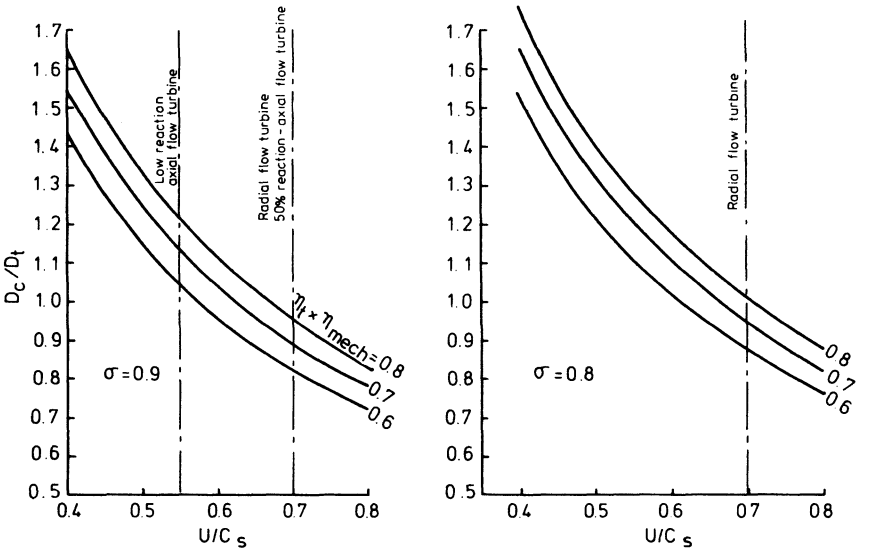

Figure 2.16 *Relationship between compressor impeller and turbine wheel diameters*

turbine of 0.7 isentropic efficiency, the compressor impeller tip diameter should be approximately the same as the tip diameter of the turbine wheel, if not slightly smaller. For the larger turbochargers incorporating low reaction axial flow turbines, the tip diameter of the compressor impeller should be about 20 per cent larger than the mean blade height diameter of the turbine wheel.

For non-steady flow applications (pulse system) the relationship between the compressor impeller tip and the turbine wheel diameter can be corrected by detailed analysis of known engine exhaust pressure diagrams applying a 'quasi-steady' approach and optimising for maximum energy extraction (chapter 15).

2.7.1.2 Bearing Configuration

There are four possible basic arrangements of bearing mounting in the turbocharger, as shown in figure 2.17

(a) the 'outboard' mounted bearings (one bearing outside the compressor impeller and one at the turbine wheel end);

(b) the 'inboard' mounted bearings (bearings located towards the centre of the shaft with the compressor impeller and turbine wheel overhanging at each end of the shaft);

(c) a mixture of one outboard and one inboard mounted bearings (normally the outboard bearing is in front of the compressor impeller and the inboard bearing between the compressor impeller and the turbine wheel);

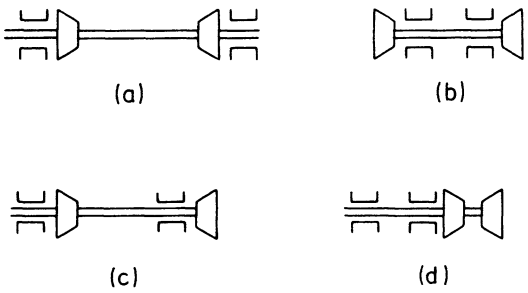

Figure 2.17 *Turbocharger bearing configurations*

(d) both bearings outboard mounted at one end of the shaft (normally at the inlet to the compressor, with a compressor impeller and turbine wheel unit overhanging).

The outboard bearing installation as shown in figure 2.18 provides the minimum radial load on the bearings due to the rotor imbalance. The shaft diameter at the bearings can also be kept small without serious problems arising at critical

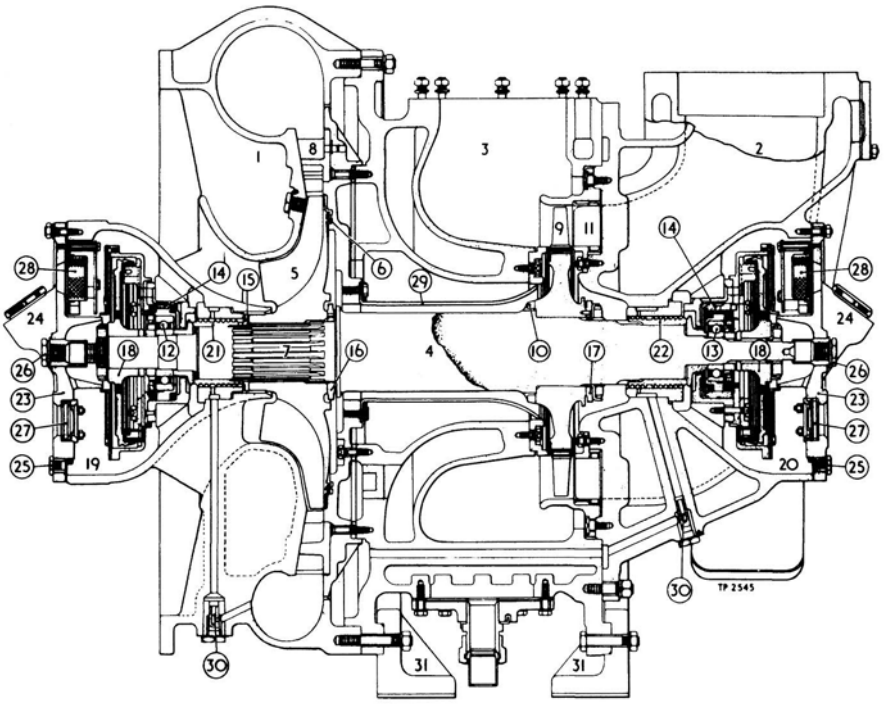

Figure 2.18 *Outboard mounted bearings (Napier)*

speeds. The installation provides very good access to the bearings, hence permitting good maintenance and easy replacement of the bearings. The arrangement is ideal for self-contained lubrication systems when using rolling-contact bearings. The turbine-end bearing can be effectively cooled by housing it in a water-cooled casing. This design layout is suitable for turbochargers with axial flow turbines and is very popular with manufacturers of medium and large-size turbochargers. Dynamically it gives very stable operation, provided the rotor speed is kept below the first critical speed of the rotating assembly. The introduction of resilient mountings in the bearing assembly to prevent 'brinelling' of the rolling bearings has been found to raise the fundamental first critical speed of the shaft by up to 50 per cent. This improvement, however, adds two critical speeds, which are a function of the spring mounting (a conical and barrel-type mode), but these occur at relatively low speeds and are completely damped by the effect of laminations fitted in the bearing assembly. From the aerodynamic point of view, the outboard bearing layout calls for a long inefficient 'U' shape air intake to the impeller eye with webs supporting the bearing housing which obstruct the flow into the inlet passages. Proximity of the supporting webs to the impeller eye can contribute to an increase in noise levels and cause impeller vane excitation. Usually outboard mounted bearings require a long shaft.

The demand and search for a very simple, light and cheap turbocharger for automotive applications led to the adoption of the inboard mounted bearing arrangement. Such an arrangement is ideally suited to turbochargers with a radial flow turbine as shown in figure 2.19. It permits the direct entry of air into the compressor impeller and gas to the turbine nozzles or wheel. It also provides a turbine exhaust layout convenient for a vehicle. The inboard mounted bearing installation reduces the number of components compared with the outboard mounted

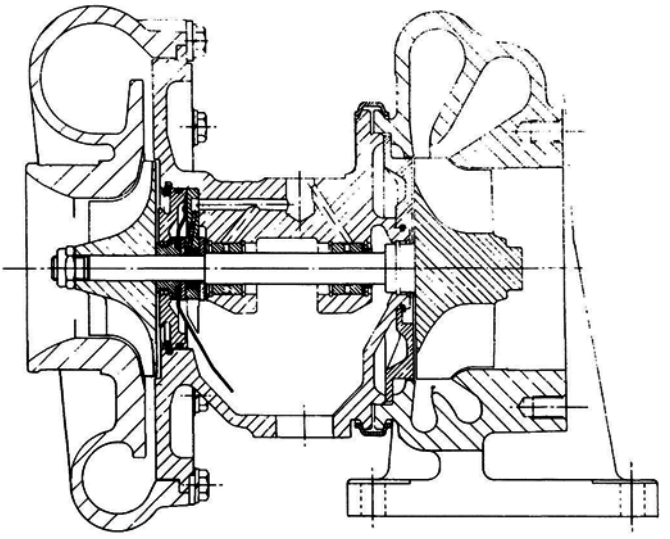

Figure 2.19 *Inboard mounted bearings (Holset)*

layout, and reduces length and weight. The result is a cheaper product. In its simplest form, it comprises an assembly of three casings joined together to house a centrifugal compressor and radial flow turbine. The centre casing houses two rotor shaft bearings or a 'single piece' bearing system and a lubrication oil inlet and drainage system. A great advantage of the inboard layout is that the turbocharger can be supplied either with air-cooled or water-cooled turbine and centre casings depending on whether more importance is attached to light weight or low surface temperature. The disadvantage of this layout is the inherently unstable running of the rotor assembly due to the short distance between the bearings and the heavy weight of the overhanging turbine wheel. It requires well-damped bearings and very careful balancing of the rotor assembly. Fully floating sleeve bearings and multi-lobe-type plain bearings have proved successful in these installations. The need for larger diameter bearings leads to higher friction losses in the bearings and therefore lower efficiency. The inboard bearings are less accessible for inspection or replacement. In this layout the lubricant supply usually comes from the engine circulation system.

The location of the turbine-end bearing between the compressor, impeller and turbine wheel in the third arrangement provides a simple gas flow path to and from the turbine. It also avoids the need for water-cooled turbine casings. Figure 2.20 shows a typical arrangement of the type with a rolling bearing between the turbine and compressor, and a ball bearing at the compressor end. Unfortunately this type of bearing mounting configuration incorporates many of the disadvantages of both the outboard and inboard type layouts and has only been used in rare cases.

The outboard bearing mounting at one end of the compressor impeller and turbine wheel assembly (preferably at the cool compressor intake as shown in figure 2.21) has been adopted by the De Laval Co. It provides a very simple and self-contained bearing housing assembly, with very good access to the bearings. The narrow shaft in relatively small bearings results in very stable and quiet running of the turbocharger above the critical speed of the rotating assembly. Care must be taken that the first critical speed of the rotating shaft is below the operating speed range of the turbocharger. This type of bearing mounting configuration is only suitable for turbochargers with centrifugal compressors and radial flow turbines. It leads to a very complex compressor impeller–turbine wheel unit which presents a difficult problem in preventing heat transfer from the turbine to the compressor.

2.7.1.3 Choice of Bearing and Lubrication System

There is a great diversity of views and opinions as to whether sleeve or rolling bearings are the most appropriate for turbochargers with outboard bearing mountings. Small and large turbochargers have been designed and are operating successfully with both types of bearing, except for the automotive type, where low-cost rolling bearings cannot meet the durability requirements at the very high speeds that are normal. The choice of bearing type depends on the nature of the application and the user's preference. The reasons for the popularity of rolling bearings are as follows.

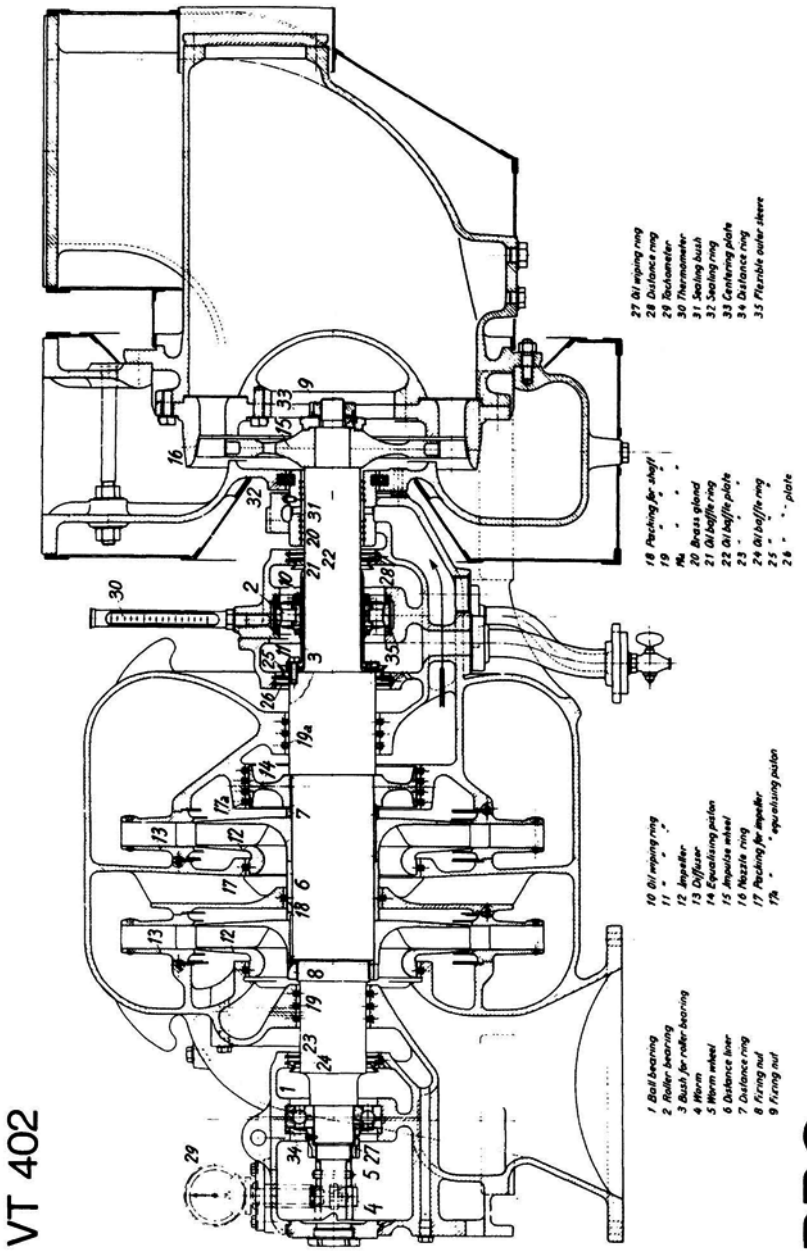

Figure 2.20 *One inboard and one outboard mounted bearing*

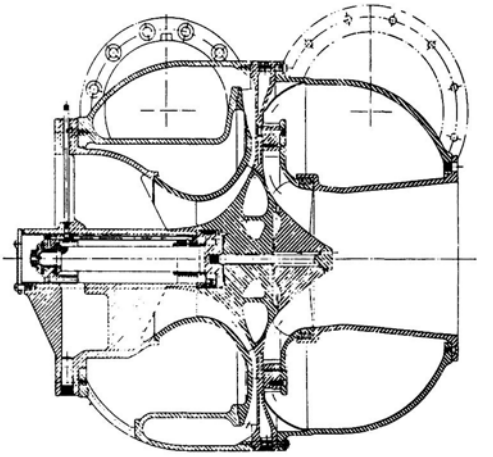

Figure 2.21 *Outboard mounted bearings at one end (De Jeval)*

(1) There are advantages in terms of engine performance deriving from small frictional power losses in the bearings, that is, when starting from cold, during acceleration; during operation at low engine speeds and loads where the exhaust energy level is very low, in particular in the case of two-stroke diesel engines without the assistance of auxiliary scavenge pumps.
(2) Rolling bearings can be very heavily overloaded for short periods.
(3) Insensitivity to lack of oil for short periods.
(4) A self-contained internal lubrication system.

The advantage of the self-contained lubrication system is that the operating reliability is independent of the lubrication system installed by the engine manufacturer. No additional costs are incurred and the turbocharger requires only simple maintenance. For low-pressure ratio operation of the turbocharger a steel disc partially immersed in an oil reservoir (as shown in figure 2.22) is quite

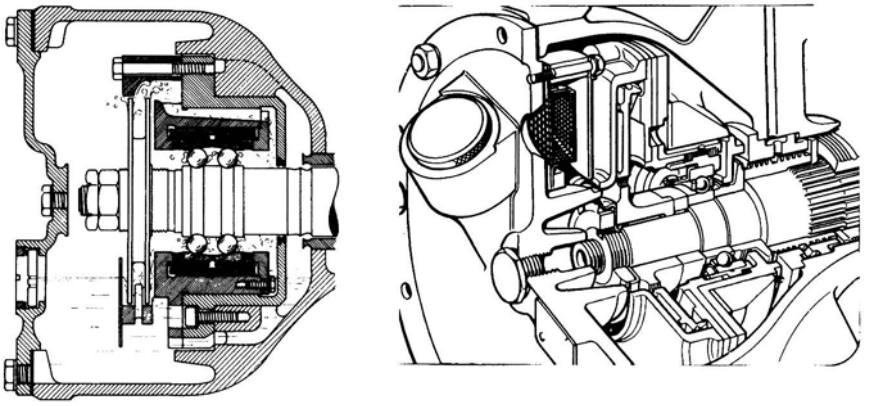

Figure 2.22 *Oil disc pump lubrication (Brown Boveri and Napier)*

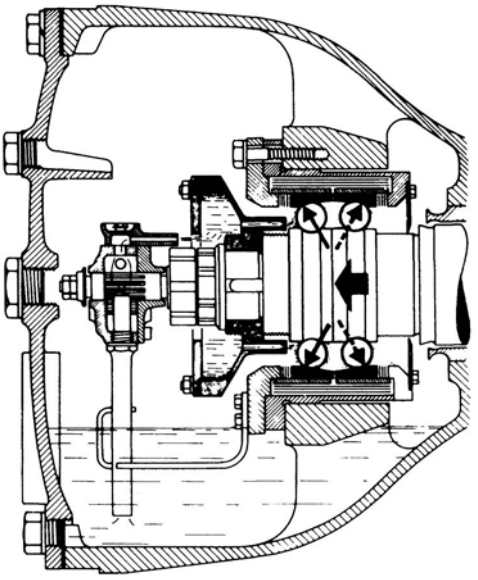

Figure 2.23 *Gear pump lubrication (Brown Boveri)*

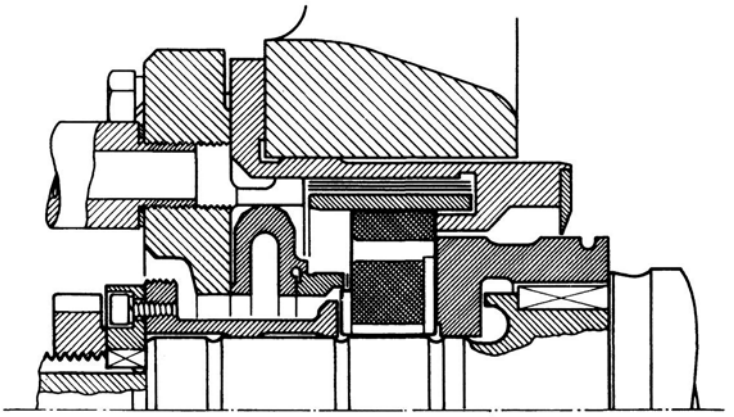

Figure 2.24 *Plain bearing mounting (Brown Boveri)*

adequate to pick up and deliver, via passages, lubricant to the bearings. At high pressure ratios, that is, at high speeds, oil has to be sprayed into the bearing. Figure 2.23 shows a rolling bearing assembly lubricated by a gear pump driven from the turbocharger shaft. The use of a separate oil supply allows an oil of lower viscosity than the lubricating oil of the engine to be used. This in turn further reduces the friction losses in the bearings.

Plain or sleeve bearings give an almost indefinite life, provided no foreign matter enters the lubricating system. They are capable of accepting larger out-of-balance loads and are insensitive to vibrations and shocks transmitted from outside. However, high oil pressure and larger oil flow rates are needed to provide adequate lubrication and cooling of plain bearings. This requires an independent external oil supply consisting of a high-pressure oil pump, oil filter and an oil cooler. These bearings also require priming after long periods of no operation, and adequate cooling at the turbine end after sudden stoppage, due to the heat flow from the turbine, particularly with the inboard bearing mounting arrangement. Lubrication of the bearings from the engine oil system is a cheap solution so long as the oil quality meets the requirements by filtration.

In marine applications sleeve bearings have a good reputation and are very often preferred to rolling bearings. In order to satisfy the various requirements, the tendency is to produce larger frame size turbochargers that can be supplied with either type of bearing, see figure 2.24.

As discussed above, the inboard bearing mounting calls for stable bearings with carefully tuned stiffness and damping characteristics. Plain bearings with circular bores are not suitable at low radial loads and high speeds due to instability, described as 'oil whip'. Bearings designed with multi-lobes (as shown in figure 2.25) have proved successful on some medium and large turbochargers.

Figure 2.25 *Multi-lobe bearing (MAN, Napier)*

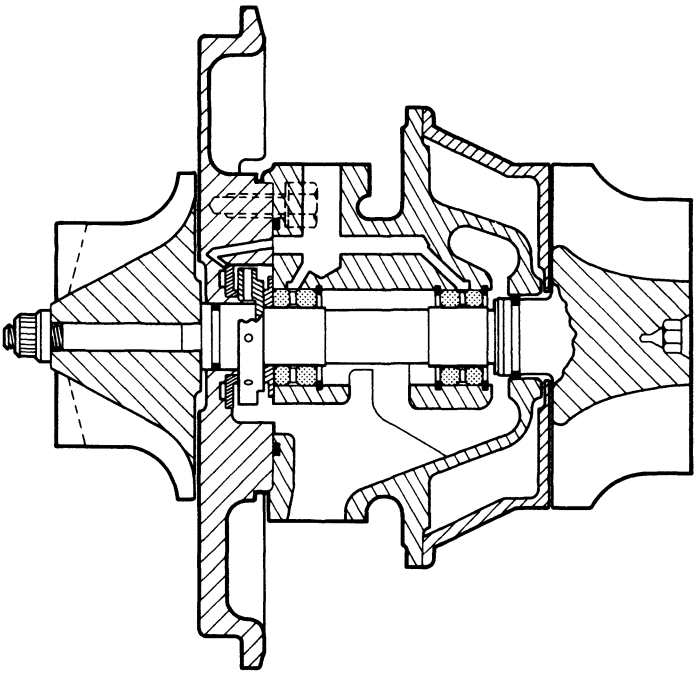

Figure 2.26 *Floating bush plain bearing mounting (Garrett)*

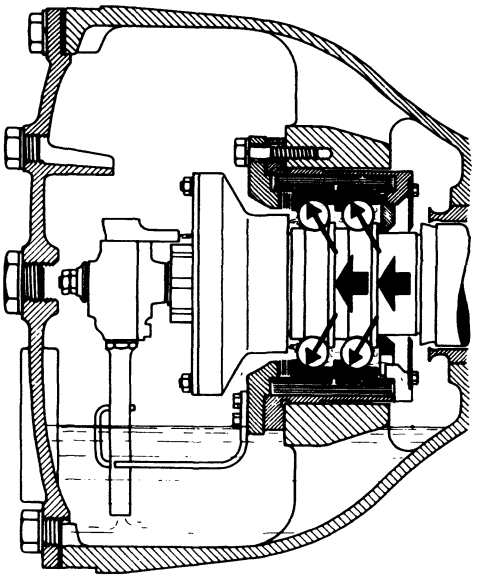

Figure 2.27 *Rolling bearing with auxiliary plain thrust bearing (Brown Boveri)*

Plain bearings in the form of rotating floating bushes are used almost exclusively in the small automotive-type turbocharger (figure 2.26) and in some medium-size turbochargers for railway traction and industrial application. The relative speeds between the rotating bearing surfaces are kept low, thus reducing friction losses. Increasing the number of oil films, due to the floating bush or bushes, provides a fractional frequency whirl which is better damped. It also provides better damping of the rotor critical frequency and larger effective bearing clearance permitting larger out-of-balance levels.

In the centrifugal compressor and radial flow turbine turbocharger design with back-to-back impeller and wheel layout, the axial thrust due to the impeller is balanced by the axial thrust acting in an opposite direction at the turbine wheel. For offdesign conditions, however, provision is made for two single thrust plates, located near the centre of the shaft, or for a plain thrust bearing designed to take the thrust loading in both directions, normally located inboard of the impeller but outboard of the journal bearing (figure 2.26).

Ball bearings have enough capacity to carry the thrust loading for moderate pressure ratio operation of the turbocharger. For high pressure ratios the tandem arrangement of angular-contact ball bearings is used to resist the high axial thrust with an auxilliary plain bearing for reverse thrust (figure 2.27). For turbochargers with sleeve bearings, axial thrust bearings with tapered land or tilting-pad-type

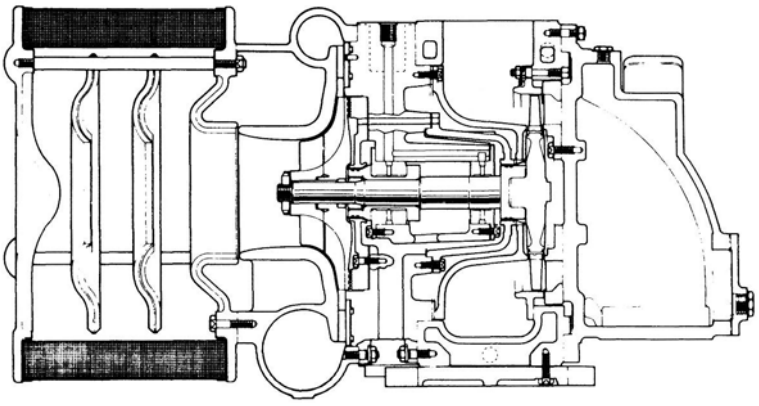

Figure 2.28 *Combined radial/axial bearing (Napier)*

bearings are used. These are designed to operate in both directions and are normally located at the cool compressor end (figure 2.28).

Another solution to resist the axial thrust in designs with axial flow turbines can be achieved by reversing the turbine so that the turbine inlet casing becomes the centre casing, as shown in figure 2.29.

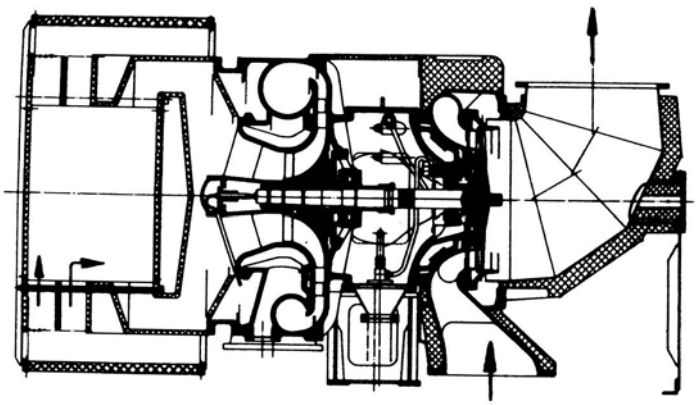

Figure 2.29 *Large turbocharger for marine application (ZA Series MAN)*

2.7.1.4 Silencing

With people becoming increasingly aware of excessive noise and the introduction of legislation to reduce it, considerable attention must be given, in the design of the turbocharger, to silencing. The axial or radial turbine emits comparatively little noise, but an intensive noise field is produced at the compressor end, particularly at the intake to the diffuser, as a result of the very uneven air velocity distribution at the impeller tip. The frequency of the imposed pressure disturbances is a product of the speed of the turbocharger and the number of impeller vanes. The noise so produced is transmitted to the environment by the air at the compressor inlet and outlet and also as solid-borne noise through the compressor casing (chapter 14).

Insulation of the compressor volute with sound-absorbing material (cladding mats) effectively reduces the solid-borne noise transmission. Insulated air inlet ducting takes care of the noise emitted from the compressor inlet. However, a large number of turbocharged engines draw their air from the engine room through a filter-silencer, and thus an effective silencer with minimum pressure losses is usually a turbocharger design requirement. The silencers operate on the principle of sound absorption. The sound waves originating at the compressor intake are reflected and reduced in intensity at the baffles and walls of a silencer lined with an absorbing material. Figure 2.30 illustrates the development of typical filter silencers from the very simple 'one baffle' type to the more complicated trumpet-shaped inlet ducts, and to the more efficient and more expensive radial plate or disc-type silencer developed by Brown Boveri, or the chamber-type silencer developed by MAN.

a)

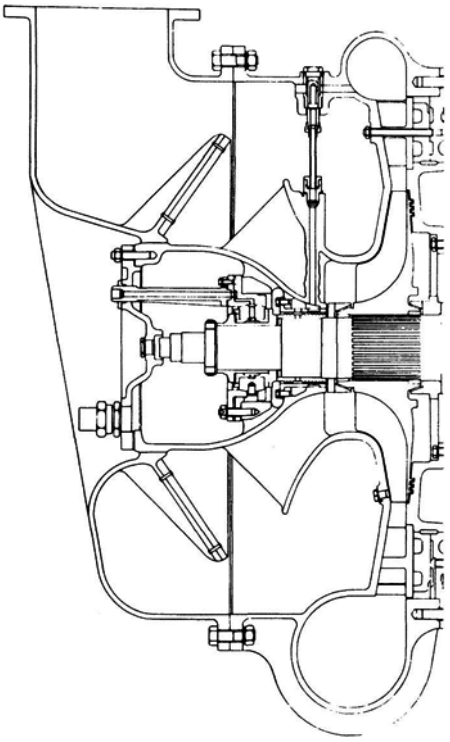

Figure 2.30 *Silencers:* (a) *baffle (Napier)*

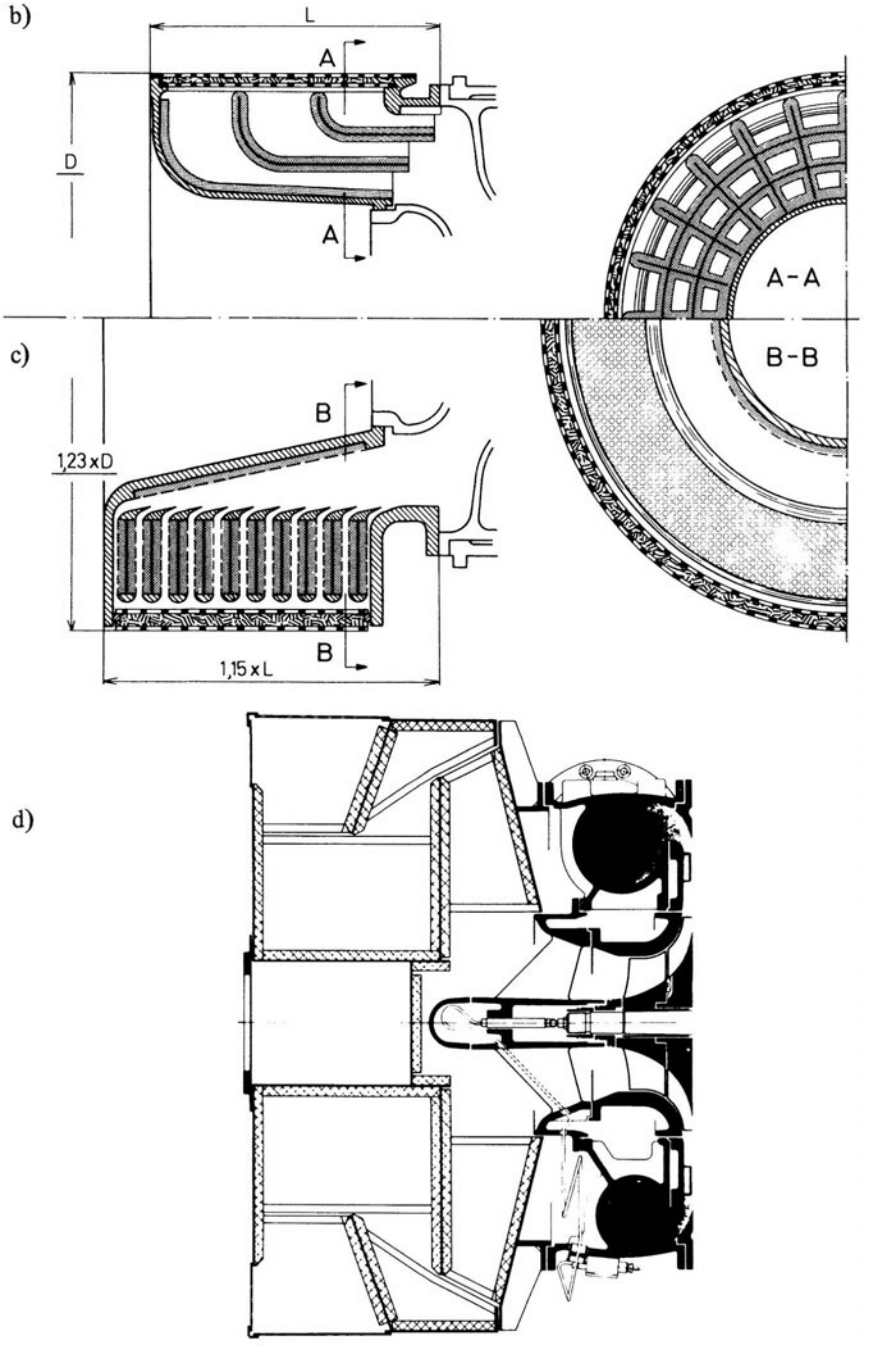

Figure 2.30 (b) *trumpet shape (Brown Boveri),* (c) *radial plate (Brown Boveri),* (d) *chamber (MAN)*

2.7.2 *Turbochargers for Automotive Diesel Engines*

Turbochargers are now widely used for truck engines, their outputs approaching passenger car engine values of 45 kW at one end of the power range and 600 kW at the other for special-purpose vehicles. The use of turbochargers on vehicle engines is relatively recent, but the rapid increase in power output demanded by the use of larger trucks and minimum power to weight ratio legislation, has speeded up their introduction. They are now also used on some petrol and diesel passenger cars.

The development of heat-resisting materials for gas turbine blades during and after the Second World War helped the development and use of turbochargers on industrial and marine engines. It was the perfection of precision casting techniques for high-temperature materials that allowed the development and use of turbochargers on small diesel engines.

Undoubtedly, the most important factor to consider in designing a turbocharger for truck engines is the initial cost. The design must substantially undercut the cost of producing a larger version of the engine capable of providing the same power. Even though truck engines operate at modest BMEP (~14 bar) and hence at lower boost pressure (up to 2.5:1), they work at much higher exhaust temperatures. They require good acceleration, high torque over a wide speed range and a high level of reliability and efficiency.

Clearly, to keep the costs of the turbocharger down the design must be as simple as possible. The simple inboard bearing mounting arrangement with a radial flow compressor and radial flow turbine on a single shaft is universal (see figure 2.31). The design with outboard bearings would be more complex to arrange and inevitably makes the design of inlet and exhaust casings more difficult.

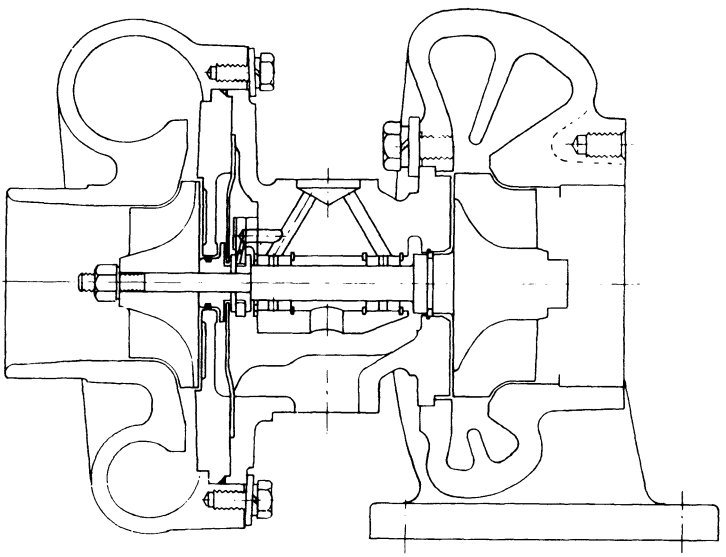

Figure 2.31 *Holset HIB turbocharger*

Since the required pressure ratio for most applications (at present) does not exceed 2.5:1, the compressor delivery temperature cannot be considered high. This poses no problem for an investment cast compressor impeller in aluminium (LM-16-WP or C-355T61). For special applications at high pressure ratios where impeller temperatures are high, the material is changed to K01 aluminium alloy. For much higher temperatures, for example, as in the second stage of a two-stage installation, investment castings of impellers in stainless steel have been used. In the past the compressor casing was produced by pressure die-casting. This has been superseded in some current models by the gravity die-casting method using LM-27-M aluminium. The only time aluminium is not used for the compressor casing is when the compressor impeller is not of aluminium alloy, and to contain the heavier impeller under burst conditions, cast iron casings are needed.

The turbine has a much harder life than the compressor with inlet temperatures as high as 1000 K when operating with diesel engines, and approaching nearly 1200 K in some petrol (gasoline) engine applications. High-temperature creep can be a problem, but the current turbine rotors made as investment castings in 713 C Inconel (a high nickel alloy) are safe to operate at up to 1300 K. The material is really too good for diesel engine turbochargers but since it is widely available (being used for gas turbine applications) it remains the most convenient material and is used in most automotive type turbochargers. Some turbine rotors are cast in GMR 235. Nevertheless, there is a constant search for a cheaper and lighter material (to aid transient response). Ceramics (silicon carbide and silicon nitride) appear very attractive for operation at high temperature and are a much lighter material than Inconel. However, the techniques involved in the manufacture of the rotors are not yet up to the production standards required for a commercial turbocharger. They are too brittle and their mounting to a shaft presents a number of problems. The turbine housing must be able to withstand the same high temperature as the wheel, but although it does not carry the same high stresses it should be strong enough to contain a turbine rotor burst. In addition, it must not scale readily. The turbine casings are normally sand or shell castings. The choice of materials is dependent on their application. S.G. iron (spheroidal graphite) is strong enough for diesel engine applications operating at temperatures up to 975 K, above which the material begins to scale. High-silicon S.G. iron is used for temperatures up to 1000 K. High-nickel cast iron (for example, Ni-resist D2 or 2B) resists scaling at temperatures above 1000 K, but is more prone to cracking from thermal cycling because of its higher expansion coefficient and the cost is inevitably higher. Nozzleless turbine inlet casings are used.

Many techniques have been used to connect the turbine rotor to its shaft, such as pressing, shrink fit, friction welding and electron beam welding. The latter two methods are the most common. It is possible to cast the turbine wheel and shaft in one, but machining may then be awkward. The compressor impeller is generally a loose or interference fit on the other end of the shaft. A self-locking nut holds the impeller tight against an abutment on the shaft. No splines or keys are provided. The friction force created is adequate to transmit the torque. The shaft is normally made of a high-carbon steel that allows induction hardening of journals (C1144 steel, EN 19C).

One of the early automotive turbochargers (Eberspaecher) incorporated ball

bearings in the design, but their short life and difficult access for replacement terminated their application in future designs. For low costs and simplicity of maintenance it is essential that the turbocharger uses the engine lubricating oil system for its bearings in preference to a separate system. At times, attempts have been made to use air bearings, but the bearing areas required are large. All automotive-size turbochargers made today use simple journal bearings running in oil from the lubrication system of the engine. The combination of high speeds and very light radial loads on the bearings, coupled with the relatively short distance between them and the heavy overhang at the turbine end, lead to extremely complex behaviour of the rotor-journal bearing system. The high operating speed dictates that the rotor normally runs through both the first and second critical speeds of the rotating assembly caused by the flexible characteristic of the bearings. The relatively massive turbine wheel and light compressor impeller produce an axial centroid, which may be positioned inside the turbine-end bearing, which leads to fractional frequency bearing whirl at the compressor-end bearing. Consequently, the problems faced in bearing design mainly concern the stability of the rotating assembly. Also important is heat removal at the turbine-end bearing due to additional heat transfer from the hot turbine wheel.

It is usual to use a fully floating sleeve bearing made of leaded bronze (SAE 67 Spec) with an added tin flashing, which is free to rotate at an intermediate speed. This speed is lower than that of the shaft, and is determined by bearing clearances, land lengths, diameters and oil viscosities. The outer film of oil imparts an additional degree of damping which helps maintain stability when running. The turbocharger must be able to run over a wide speed range with quite different oil viscosities and temperatures in different engines. As a result, bearing development has tended towards larger sleeve-to-housing clearances for improved stability. Typical tolerances on a small turbocharger bearing are of the order of 0.0075 mm on shaft and bearing sleeve bore, and 0.013 mm on bearing outer diameter and housing bore, making a total tolerance of 0.04 mm. The rather large bearing clearances ease the problem of oil filtration, and only necessitate filtration down to about 20 μm. This is quite easily met by current full flow paper engine oil filters.

The large area of bearing, relative to its loading, and the heat transfer from the hot turbine-end can result in an overheating problem unless a correspondingly large oil flow rate is used. Care must then be taken to ensure adequate drainage and this can cause difficulties if the engine manufacturer is not sufficiently aware of the problem. Bearing damage can result from cold starting after a long period of idleness or thermal soak on rapid shutdown. Axial thrust will vary in duration over the operating range of the engine, but fortunately the loadings are not excessive and a separate simple thrust assembly outboard of the bearing span is used. The thrust bearing can be either plain (flat surface) or a tapered land type, normally made of sintered leaded bronze. The tapered land thrust bearings provide a useful increase in load carrying capacity, allowing a smaller bearing to be used.

The power loss due to the bearings can be in the order of 2 to 7 per cent of turbine power (at maximum power), but more serious is the fact that this percentage increases as turbocharger speed decreases, significantly reducing the smoke-limited power output of the engine at low speeds.

The bearings normally run direct in the (honed) bore of the centre casing or

frame. The centre casing is invariably cast, usually in high-grade grey cast iron. The casing also contains the oil drain and holds the compressor and turbine casings (figure 2.31). For good oil drainage, the centre casing must remain close to the vertical position. The compressor and turbine casings are usually designed so that they can be freely rotated into a convenient angular position relative to the centre casing on assembly. This gives the engine designer more freedom in planning the exhaust and inlet pipework. The compressor housing shown in figure 2.19 is clamped by set screws, while the turbine housing is secured by a stainless steel V clamp. Usually, single and twin-entry turbine housings are available for reasons discussed in detail in chapter 5. It is almost universal for the turbocharger to be mounted on the engine via the turbine casing and not the central casing. The turbocharger is then solid with the exhaust manifold and may move with it as the manifold expands and contracts due to temperature changes, thus eliminating the need for a flexible exhaust system joint. It follows that the exhaust manifold must be strong enough (when hot) to withstand the weight of the whole turbocharger under conditions of high acceleration loading from engine vibration. The total weight of a small automotive turbocharger such as that shown in figure 2.31 is of the order of 10 kg. Since the turbine casing then holds the centre bearing casing they must be firmly connected together.

The oil seals on the shaft of the turbocharger are a difficult part of the over-all turbocharger design because of the combination of adverse pressure gradients under some conditions, the consequences of large bearing clearances, and the need to keep frictional losses to a minimum. The piston-ring-type seals shown in figure 2.32 are typical. The piston rings themselves are designed so that the radial wall pressure holds them tightly in the bore without axial movement or rotation. They act as a form of labyrinth seal in which the leakage between the piston ring and the sides and base of the groove in the shaft is kept small. In

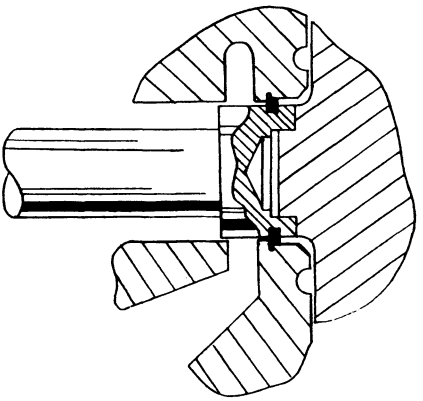

A single piston ring locates in a stepped bore bearing housing.

Figure 2.32 *Piston-ring-type oil seal (Holset)*

practice they will only work satisfactorily if care is taken to keep as much oil as possible away from them. They will leak if the oil drain from the turbocharger proves inadequate and a pool of oil builds up inside the housing. An oil shield is used at the compressor-end since it is here that under some running conditions a depression may exist at the back of the compressor housing (for example, high idling speed with a very dirty air filter) encouraging oil leakage. Some turbochargers are available with a carbon face seal at the compressor end, but this is usually only fitted when the turbocharger is to be used on a petrol engine with a throttle before the compressor. With this arrangement a vacuum exists in the compressor when the throttle plate is closed (see chapter 13). At the turbine end, the major gas leakage problem is from the turbine rotor into the bearing housing and then into the engine sump where it adds to engine blow-by.

Turbocharged automotive diesel engines are required to operate over a large speed and load range and therefore the turbine and compressor design is directed towards achieving reasonable efficiency over a wide range of mass flow rates, rather than high peak efficiency. Fortunately the requirement in terms of pressure ratio at present is moderate. To achieve a wide operating range the trend has been towards the use of vaneless, in preference to vaned, diffusers, particularly on the smaller machines. A small sacrifice in peak efficiency is more than compensated for by a wider area of high efficiency (figure 2.33) and reduced effect of dirt accumulation and lower noise level.

The design of the compressor impeller has to be a compromise between aerodynamic requirements, mechanical strength considerations and foundry capabilities. To achieve high mass flow and compressor efficiency, very thin and sharp impeller vanes are desirable, but to keep the levels of steady state and vibrating stresses low, a robust, thick-at-the-root vane is needed. The tip thickness of the impeller vanes (typically around 0.8 mm) is dictated by considerations of casting techniques and vane stiffness. This thickness limits the number of vanes that can sensibly be used without significantly reducing the inlet area available at the compressor eye. In consequence, the slip factor (see chapter 3) is usually rather

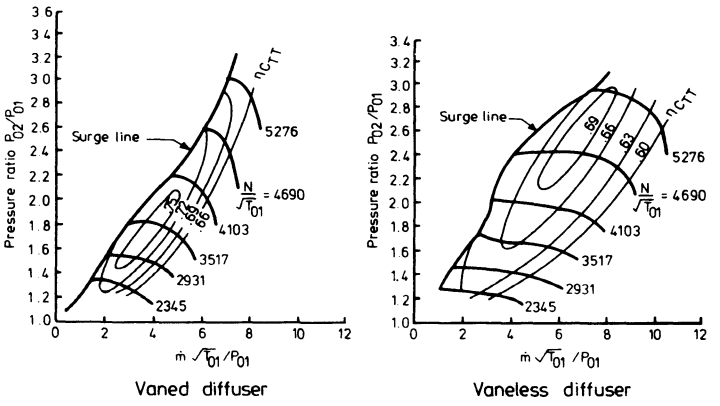

Figure 2.33 *Comparison of vaned and vaneless diffuser performance [5]*

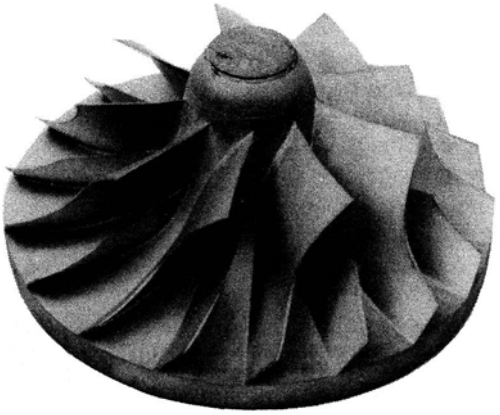

Figure 2.34 *Impeller with splitter vanes (Holset)*

low (typically around 0.82 for a 12-vaned and about 0.9 for a 18 to 20-vaned impeller). It is common practice to use splitter vanes (figure 2.34) that extend from part way through the inducer up to the impeller tip to aid flow control while minimising blockage at the eye. Gradual development of the impeller profile based on 'three-dimensional streamline curvature flow' and the 'jet/wake' concepts (see chapter 3) has led to the introduction of backswept impellers. This gives better control of the internal flow and reduces the flow distortion transmitted from the impeller to the diffuser, and combined with recent improvements in the surface finish of the casting, has resulted in even very small impellers having reasonable efficiencies. The mechanical design of the compressor impeller aims at a high blade vibration frequency and an adequate low-cycle fatigue life. Non-radial back-face designs of impeller have been introduced to reduce the back-face stress and avoid distortion at the impeller tip due to bending forces at high compressor pressure ratios.

Each basic design of turbocharger has been adapted to quite a large range of diesel engines. To cater for a wide difference in air flow requirements from one engine to another, a range of compressor impellers is available to fit the same basic unit. Although normally made from the same casting, the impeller eye diameter and the tip width would be chosen so as to optimise flow conditions for the required air flow rate and pressure ratio (figure 2.35).

Naturally a matching compressor housing must be supplied with each impeller and the total number of variants (or 'trims') available may exceed 10. However, since the impeller tip diameter is fixed for a given 'frame size' and the hub diameter at the impeller eye is determined by the shaft diameter, the resulting variation in passage shape causes a decrease in efficiency of the compressor the further the modified design departs from the original. This will therefore limit the mass flow range that can reasonably be covered by a single basic model (or 'frame size') of turbocharger.

The inward radial flow turbine is more tolerant of a wide mass flow range and a single wheel may be used with a large range of compressor impellers. Adjustment to the turbine flow is made by changes in the stator nozzle ring angle (and

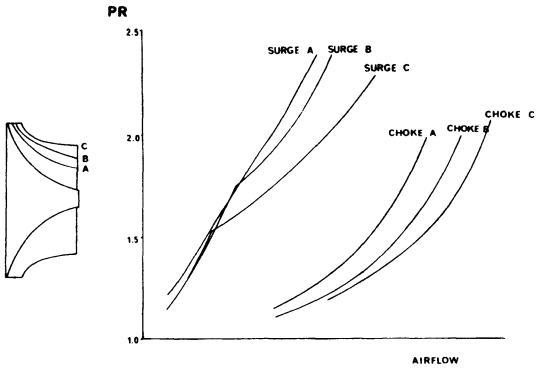

Figure 2.35 *Compressor trims, machined from one casting (Holset)*

hence in the throat area), wheel trim or the nozzleless housing (figure 2.36). Since the requirement is to have minimum unit cost while achieving a reasonable efficiency over a wide flow range, at relatively low expansion ratios, the trend has been towards the use of nozzleless housings. By reducing the cross-sectional area of the housing around the circumference of the turbine rotor, uniform inlet flow is obtained. If the cross-sectional area is scaled up or down (that is, if the throat area is changed) the mass flow characteristics (figure 2.36) can be controlled. The geometrical layout of the housing is usually such as to feed the exhaust gas into the rotor as if there is a vortex with its centre at the rotor centre, the aim being to give the gas a constant inlet angle and velocity around the periphery of the turbine rotor. The range of turbine housing areas available is usually about half that of the compressor options. However, since turbocharged automotive diesel engines invariably operate with the pulse system (chapter 7) an additional requirement is for single or twin-entry casings.

Single-entry casings have a single pipe (usually rectangular) entry to the volute. The twin-entry casings have two rectangular pipes, side by side, which split into two volutes so that each entry feeds a 180° sector of rotor entry (figure 2.37a) or two 360° sectors each assigned half of the tip width of the turbine wheel (figure 2.37b). In the latter case the dividing wall is usually stopped short some distance from the rotor tip to reduce blockage, and minimise the risk of thermal cracking. Circumferentially divided systems allow more interference between each branch of the engine exhaust system but tend to result in higher turbine efficiency when the flow rate is different at each entry, since there will always be substantial gas flow around the whole of the circumference of the turbine rotor. Pulsating flow entering a radially divided casing (180°, figure 2.37a) has an adverse effect on shaft dynamics and can easily result in no flow or a reversal of flow momentarily through some channels in the turbine wheel. (See chapter 4 for a more comprehensive description of the problem.)

The turbine rotor material has better fatigue characteristics than aluminium. However, the turbine wheel in its highest flow trim has a very high exducer tip/wheel tip radius ratio which results in highly stressed blades with a low natural

frequency. Much development work is required to ensure safe and long life operation in service.

The complete compressor impeller, shaft and turbine rotor assembly must form a well-balanced unit, since rotational speeds may reach 80 to 140 000 rev/min (depending on the size of the unit). To allow free interchangeability of parts

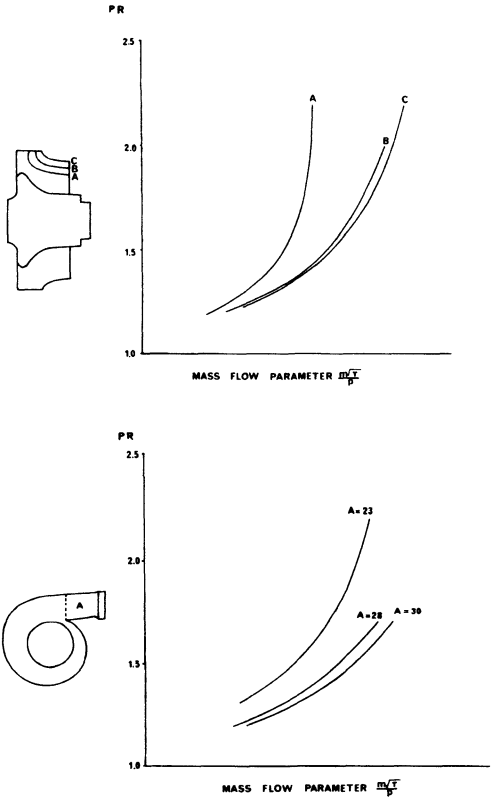

Figure 2.36 *Turbine trims (machined from one casting) and volutes (Holset)*

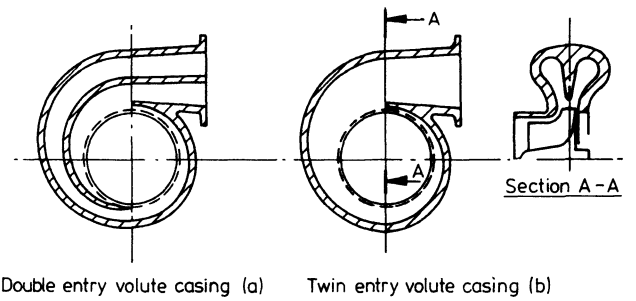

Figure 2.37 *Turbine housings:* (a) *double entry,* (b) *twin entry*

on assembly the compressor impeller and turbine wheel are balanced separately. Usually metal is removed from the front of the hub and the back face of the impeller or from the periphery of the impeller between blades (a typical balance limit for a small machine might be 0.75 g mm). By separate balancing, the impeller may be assembled on the shaft at any angular position relative to the turbine wheel. The small rotating components (washers, spacers, etc.) are usually sufficiently well balanced due to their machining technique. However, the complete rotor assembly is normally check-balanced after assembly by some manufacturers.

Small diesel engine turbochargers are now produced in large numbers at very low cost. This is largely due to their simplicity and the development of precision castings. To produce a turbocharger at low costs means that semi-mass-production techniques are used. Due to the large bearing clearances, the clearance between rotating parts and the housing must be kept proportionally greater than that adopted on larger-size turbochargers. Hence peak efficiencies are somewhat lower due to leakage and clearance losses. The use of cast impellers and turbine rotors inevitably means that there will be small variations in geometry between one machine and another of the same build. In consequence efficiency and mass flow rates can vary between nominally identical machines.

To make the product more adaptable some turbocharger manufacturers (Air Research, IHI and Schwitzer) provide special turbine casing designs combined with integral by-pass valves (wastegate, see chapter 10).

2.7.3 Industrial and Marine Turbochargers

This class of turbochargers covers industrial, rail traction and marine engines producing powers from around 200 kW upwards. In many applications more than one turbocharger is used. The duty of this type of engine is more arduous than that of the automotive type and it usually spends much more of its time near full load rather than at part load, and may be required to operate 24 hours a day. Furthermore, the consequences of a failure are usually more serious. For these reasons, although every attempt is made to keep the design simple, the primary objectives are a high degree of reliability, a high level of efficiency and versatility to cover a great range of engine sizes at acceptable costs. Since industrial diesel engines do not usually have to operate over such a wide speed range as an automotive unit, and since there is more incentive to operate with higher boost pressures, the turbochargers are designed to produce maximum efficiency at a higher pressure ratio level.

Before the Second World War, turbocharging was confined exclusively to the medium speed four-stroke industrial and marine engines covering a range of 400 to 4000 kW power outputs. The design of the turbochargers consisted mainly of single-stage centrifugal compressors coupled on a common shaft with a low-reaction (impulse) axial flow turbine. The outboard bearing mounting layout was preferred in Europe (Brown Boveri, Napier, Brush) and inboard bearing mounting in the United States (General Motors, Elliot, Alco) – see figure 2.38.

The success of turbocharging in the early 1950s led to the need to cover a widening range of engine outputs, and the production of a range of turbocharger sizes, all of the same basic design but scaled up and down in size. Difficulties

in maintaining high turbine efficiency on scaled down axial flow turbines, led to the introduction of the radial flow turbine to the bottom range of the industrial turbocharger sizes.

a)

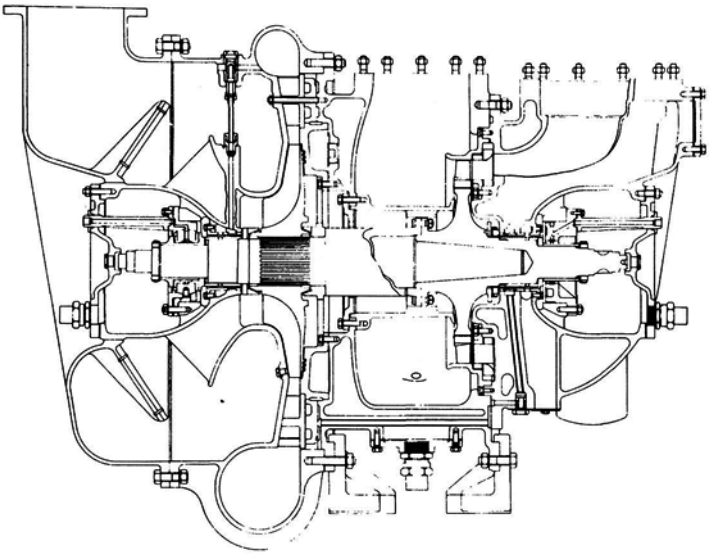

b)

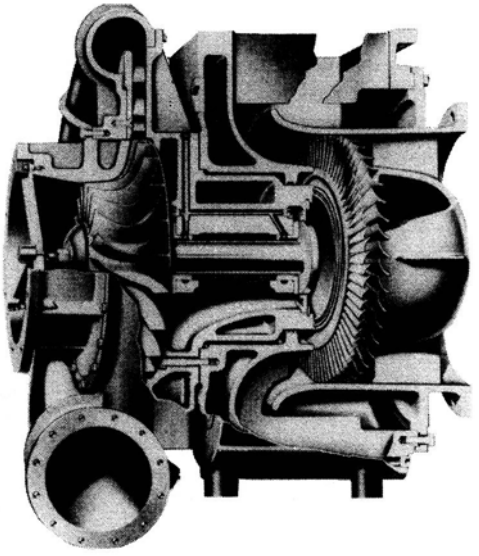

Figure 2.38 *Turbocharger with axial flow turbine:* (a) *Napier,* (b) *Elliott*

2.7.3.1 Designs with Radial Flow Turbines

Some turbochargers designed for diesel engines in the range 200 to 2000 kW tend to form a class of their own. Their basic design and arrangement are similar to those of the automotive unit, that is, radial flow compressors and turbines are used. But since they are larger and are made in much smaller numbers, production being by batch and not mass production, the cost of the turbocharger is greater. The radial flow turbines have nozzle rings to maintain a high isentropic efficiency (above 80 per cent) in small sizes. Vaned compressor diffusers are used for the same reason. Simple construction of the turbocharger and the use of cheap cast components enable a light, highly efficient and economical turbocharger to be made with good adaptability. Current precision casting techniques limit the size of radial flow turbine wheels, and the indications are that the economical limit at present is 300 mm in diameter. Within this range the small industrial turbochargers are proving to be more efficient in service than comparable designs with axial flow turbines on many engines. A further advantage of the radial flow turbine is its capacity to efficiently utilise expansion ratios exceeding 3:1 in a single stage.

The common design principle of overhung wheels on a shaft with the inboard plain bearings (floating bush) between the compressor and turbine, results in simple compressor and turbine housings with correspondingly low flow losses. Lubricating oil is usually taken from the engine supply and bearing clearances can be kept smaller, relative to shaft diameter, than those of the automotive type turbocharger. Consequently labyrinth-type oil seals can be used (see figures 2.39a and c).

a)

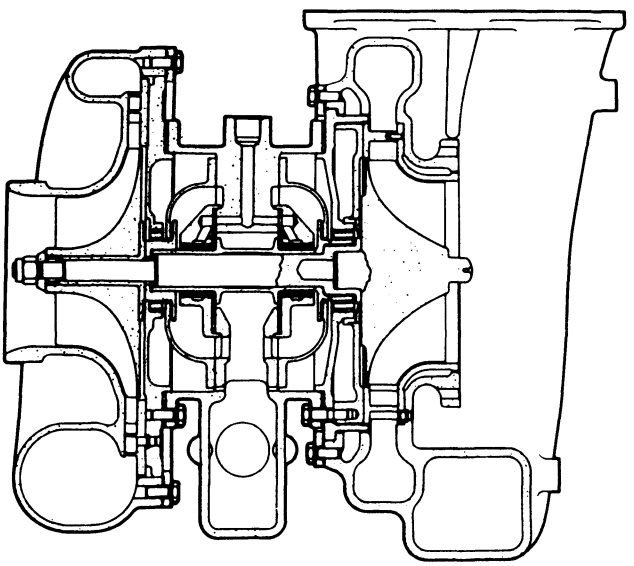

Figure 2.39 *Small industrial turbochargers:* (a) *Napier,*

Turbine housings can be supplied either water cooled or air cooled. The water-cooled versions are available for applications where the turbine casing must be kept cool for safety reasons, or where thermal radiation in a confined space causes problems (for example, locomotive or marine application). For non-water-cooled versions, installation is simpler, but bearings can become excessively hot unless some attempt is made at air cooling. The turbocharger shown in figure 2.39a uses a stream of bleed air from the compressor to cool the turbine hub and the bearing area. This air stream also helps prevent exhaust gas leaking

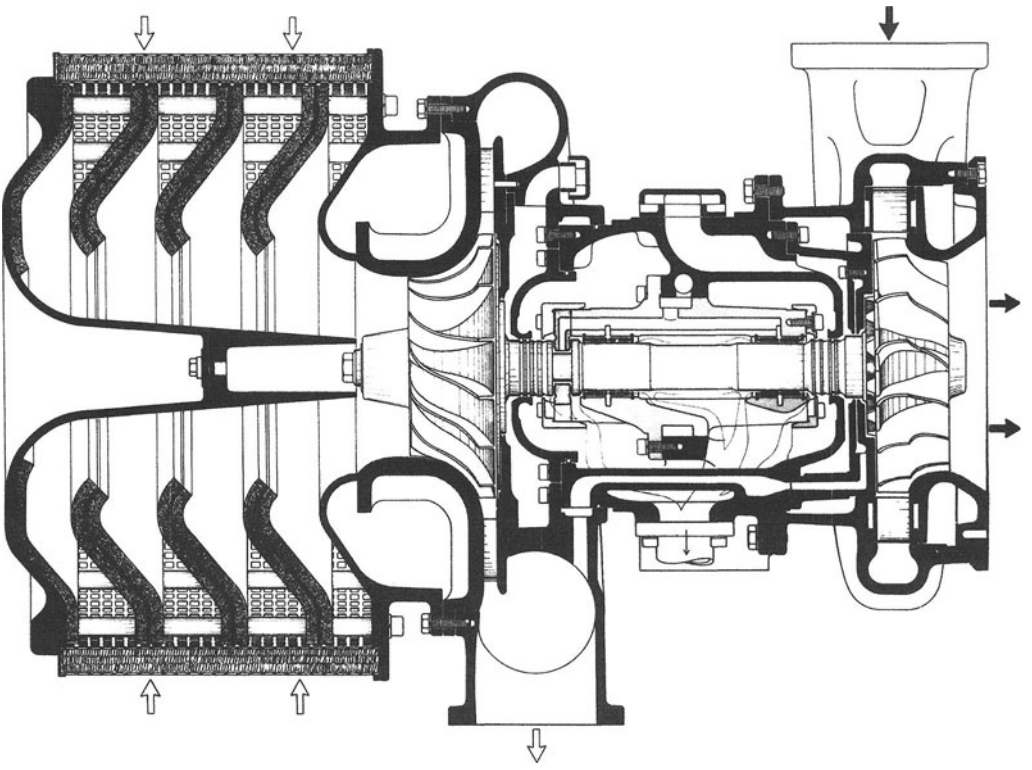

Figure 2.39 (b) *Brown Boveri,*

c)

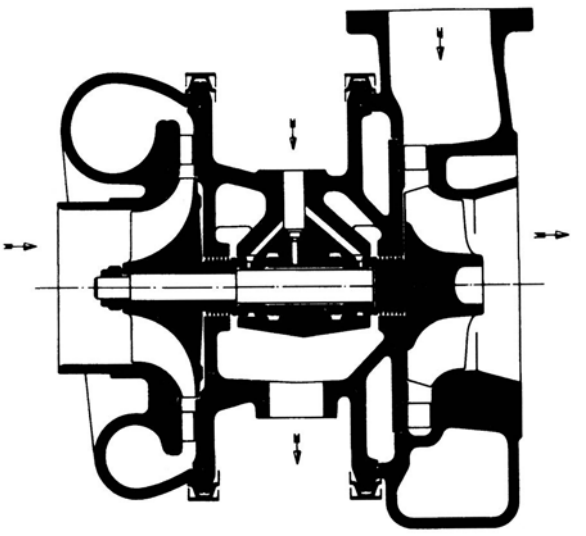

Figure 2.39 (c) *MAN*

down the back of the turbine wheel and reaching the bearing. Cooling air also passes around a partition plate between the turbine and the bearing area. By these means the bearing temperatures are kept low, preventing carbonisation of the lubricating oil. On the compressor side of the turbine housing, a thermal radiation shield may be used to reduce heat transfer to the remainder of the turbocharger.

Figure 2.39a shows a sectional view of the C-045/C Napier turbocharger. Three separate casings clamped together house a centrifugal compressor, bearing housing and a radial flow turbine, making up the turbocharger assembly. The main component of the turbocharger is a cast iron centre casing which houses two plain bearings, an inner sealed chamber for lubricating oil and an outer chamber ventilated to atmosphere. Sealing air is isolated from the lubricating oil to prevent pressurisation of the engine oil sump and to stop contamination of the engine oil by exhaust gases. The centre casing can be removed for service or exchange without disturbing the exhaust inlet and outlet connections. Attached to the centre casing, using a clamped arrangement, is the cast iron turbine inlet casing which is available in two or three entry configurations. It can be located in any radial position through 360° to suit the installation requirement. A turbine nozzle assembly is located adjacent to the turbine casing.

Also secured to the centre casing is the cast aluminium compressor outlet casing. This too, can be secured in any radial position through 360°. The rotor components are mounted on a common shaft. The steel rotor shaft is fitted with hard steel journals running in floating sleeve bearings. The axial thrust is taken on two thrust plates located near the centre of the rotor assembly. Nimocast 713 V is the material used for the turbine wheel and aluminium for the compressor impeller; both are precision cast. A range of compressor diffusers and turbine nozzles is available for matching of the turbocharger to the engine.

A similar bearing layout, but with the thrust surfaces outside the radial bearings, is shown in figure 2.39c, a sectional view of the 'NR' series of MAN turbochargers.

The Brown Boveri 'RR' series of turbochargers (see sectional view of the turbocharger – figure 2.39b) uses a separate assembly for the thrust bearing, located at the compressor end, similar to the automotive-type turbochargers. Piston-ring type air seals are used.

2.7.3.2 Designs with Axial Flow Turbines

This class of turbochargers is used to turbocharge two and four-stroke gas and diesel engines producing from 300 to 35000 kW or more. The size of the turbocharger required for the biggest marine diesel engines can be seen from figure 2.40. When installed on an engine (figure 2.41) this turbocharger will be transmitting up to 5000 kW from turbine to compressor.

The primary objectives in designing this type of turbocharger are high reliability, high turbocharger efficiency, plus a versatility to cover a great range of engine sizes. The axial flow turbine satisfies most of these requirements. In the larger size with a suitable exhaust diffuser the axial flow turbine can be designed with higher efficiencies than the radial flow type, approaching 88 per cent isentropic efficiency.

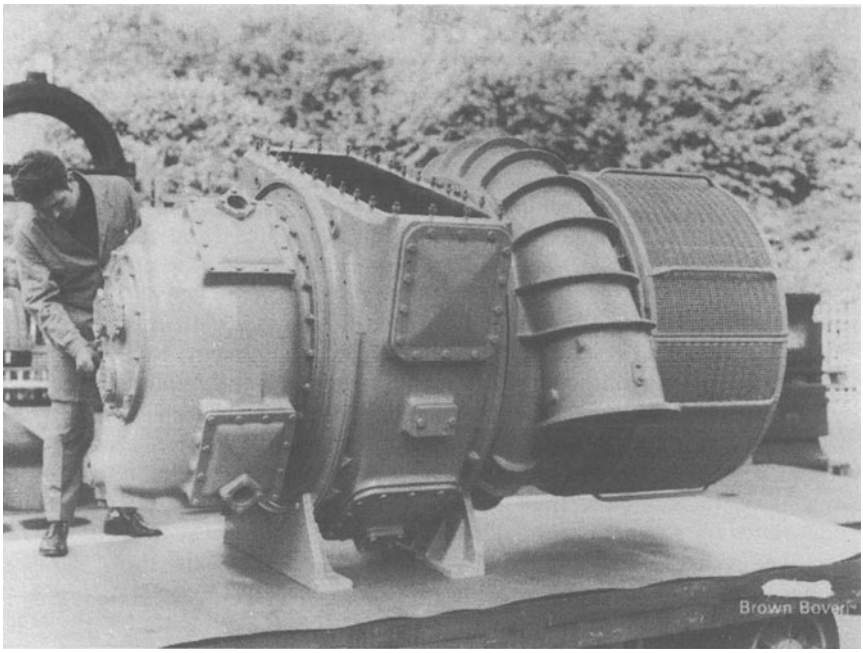

Figure 2.40 *Brown Boveri VTR 631 turbocharger*

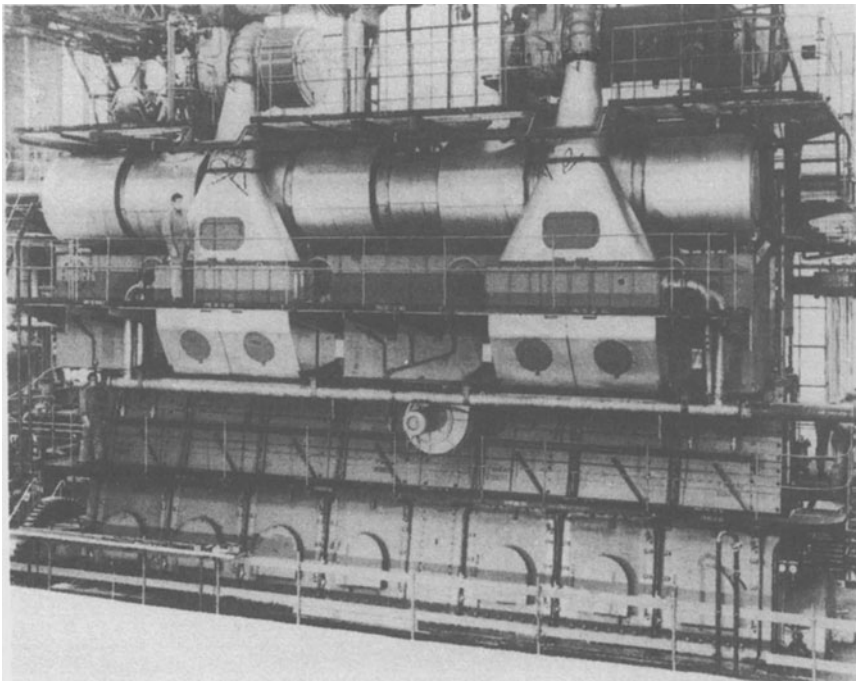

Figure 2.41 *7 RND 90 Sulzer diesel engine with two VTR 631 turbochargers*

Axial flow turbine rotor blades are exposed to a more uniform gas temperature along the blade and hence have a more favourable thermal stress distribution than in the case of a radial flow turbine wheel. Reducing the height of the turbine blades and changes in nozzle angle are used to obtain variations in turbine effective areas to provide a wide range of matching facilities.

However, the consequence of using an axial flow turbine is that the inlet and exhaust must be designed to turn the flow through 90°. It requires careful design and large radius bends to avoid serious flow losses. Both outboard and the inboard bearing mountings are common in the design of this type of turbocharger.

With the outboard bearing mounting, rolling bearings are used, as shown in figure 2.42. The major advantage with rolling bearings, as already stated, is reduced frictional losses, and this is particularly important when starting the engine, running at low load and during acceleration. One of the bearings is arranged to locate the shaft at the compressor-end and takes axial thrust while the other is housed so that it can move and take up the effects of differential thermal expansion between shaft and housings. A further advantage of the rolling bearing is that the heat generated by the bearings is low and a small self-contained oil system may be used. Since the two bearings are spaced well apart, a separate oil system and reservoir is provided at each end of the turbocharger, each unit with its own oil pump. The large frame sizes for marine application are designed

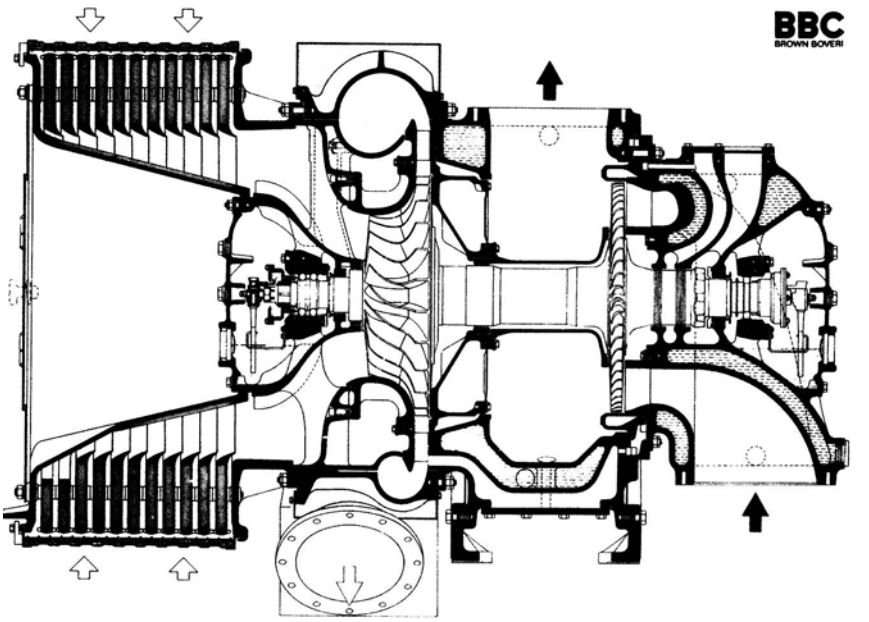

Figure 2.42 *Sectional view of VTR 454 (Brown Boveri)*

with plain bearings as in the Napier unit shown in figure 2.43, or provision is made for fitting both types of bearing (Napier NA, Brown Boveri VTR 320 to 750). Lubrication of the sleeve bearings may be provided from any suitable external oil system.

Normally four separate casings make up the assembly of this type of turbocharger. The water-cooled turbine outlet casing cast in high-grade iron forms the main structure to which all other sub-assemblies are secured. It incorporates the mounting feet which can be located in different positions around the casing. Bolted to the turbine outlet casing is the water-cooled turbine inlet casing incorporating the turbine-end bearing housing and oil reservoir. Single, two, three and four-entry gas inlet casings are available to cater for different engine installations. High-grade cast iron is also the material normally used. Between the turbine inlet and turbine outlet casing provision is made to fit a choice of turbine nozzle assemblies consisting of heat and corrosion-resistant steel blades cast into iron shroud rings. The compressor (inlet and outlet) casing is cast in sea-water resisting aluminium alloy. For high compressor ratios, the compressor outlet casing is made of cast iron (because of creep and the poor noise attenuation of aluminium alloys). This casing provides the delivery volute and the air inlet passage to the impeller, and also houses the compressor-end bearing. Assembled between the compressor casing and the turbine outlet casing is the compressor diffuser, made of aluminium.

When inboard bearings are used, these are normally plain and not roller type, and are usually lubricated from the engine oil system. Manufacturers of this

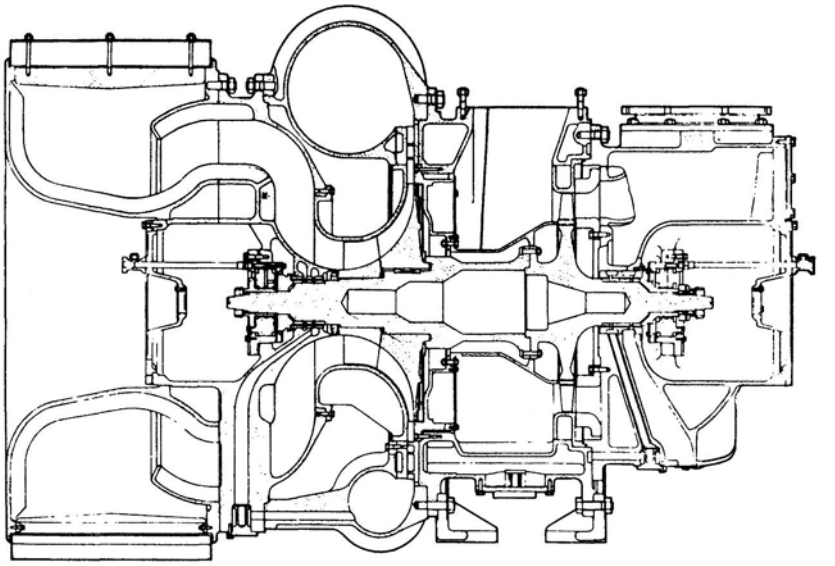

Figure 2.43 *Sectional view of S610 (Napier)*

type of turbocharger claim that the short rotor shaft assembly keeps the first fundamental critical shaft speed well outside the service speed of the unit and the reduced rotor shaft assembly inertia partly offsets the frictional bearing losses of the turbocharger during transient operation of the engine. Four separate casings make up the turbocharger assembly, the turbine outlet casing again being the main structure to which all other casings are bolted. Alternative configurations of water or air-cooled casings in axial or right-angle form are available. A special water-cooled centre or main casing (figures 2.28, 2.38 and 2.44) carrying the rotating assembly is inserted in some cases in cartridge form into the turbine outlet casing. This allows maintenance of the rotating assembly to be undertaken without disturbing the exhaust inlet and outlet and water connections to the engine.

In both turbocharger layouts (outboard or inboard bearings) the rotating assembly consists of a single-stage centrifugal compressor and a single-stage axial flow turbine. The compressor impeller is machined from an aluminium forging with a separate inducer made from a steel or aluminium casting or an aluminium forging. For high-pressure operation (above 3.5:1) impellers made of titanium are offered to secure very good reliability at high air temperature. The impeller is keyed and the inducer splined or keyed to the shaft; both are secured by a locking ring and nut. The use of a two-piece impeller not only simplifies production, but also can provide frictional blade damping between the inducer and impeller contact surfaces.

The turbine disc may be an integral part of the shaft (figure 2.42) or the shaft (figure 2.43) may be machined from a single forging. On some designs of medium size turbocharger the turbine disc is shrunk on or pressed on to the shaft.

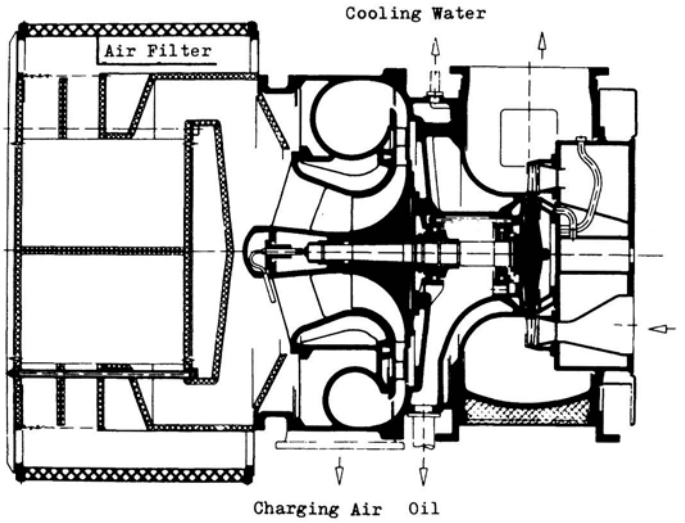

Figure 2.44 *Sectional view of NA (MAN)*

The turbine rotor blades are cast, forged or machined from solid high-creep-resistant steel (Nimonic 80 A or 90). To secure them to the disc, welded joints or 'fir-tree' roots are employed. The fir-tree root type fixing ensures a degree of vibration damping and allows free selection of the material for the turbine disc and the rotor blades; thus they are exclusively used for high-pressure rated turbochargers. Additional vibration damping is sometimes provided by wire-lacing the turbine blades.

Figure 2.29 shows an MAN turbocharger designed for large two-stroke engines. The normal arrangement of turbine inlet and exhaust casings and flow direction is reversed in order to improve the turbine exhaust flow path.

A decision affecting future turbocharger design is the point at which two-stage turbocharging is introduced. At present commercially available single-stage turbochargers, incorporating radial flow compressor impellers made of malleable aluminium alloys, have adequate safety in service against failure up to peripheral rotor speeds of 470 m/s. This corresponds to a boost pressure ratio limit of 4:1, adequate for engine ratings up to 25 bar BMEP for the four-stroke engine and 16.5 bar BMEP for the two-stroke engine. The highest effective pressures quoted today for the four-stroke engine in production approach 21 bar, (chapter 1). However, by drastically reducing the engine compression ratio, the boost pressure can be raised significantly, which allows for a higher engine BMEP without increasing the peak pressure in the cylinder (chapter 11). Development of centrifugal compressors up to 16:1 pressure ratio has been reported, but this is impracticable for turbocharger applications. Already, exotic materials like titanium have to be introduced in the manufacture of compressor impellers to allow safe operation up to a 4.5:1 compressor pressure ratio. Thus two-stage turbocharging seems to be the most technically viable method of providing boost pressure levels

a)

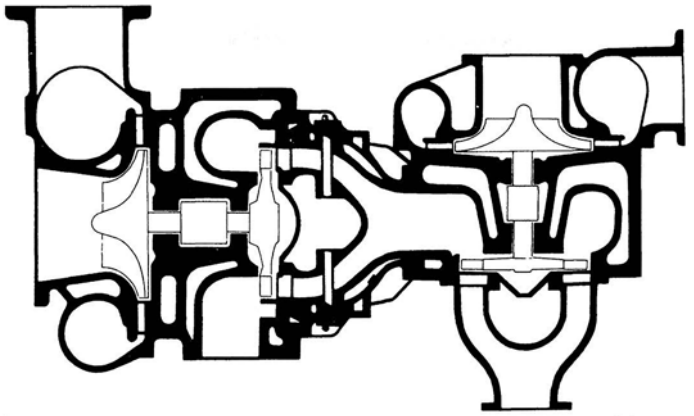

Cross-section of a Hispano Suiza two-stage turbocharging unit — left, the low pressure stage; right, the high pressure stage.

b)

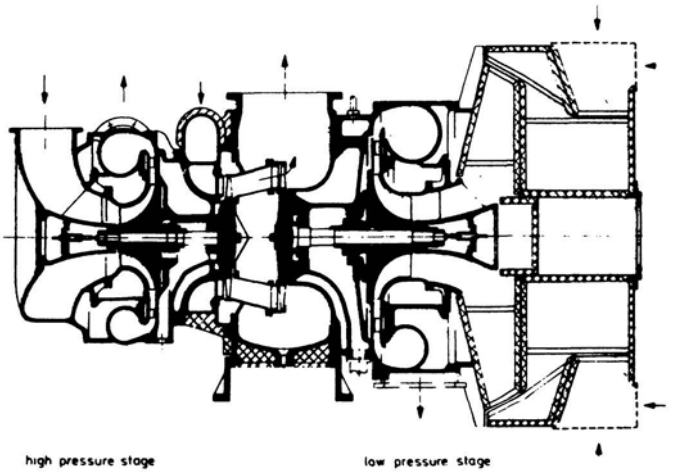

Figure 2.45 *Compact two-stage turbochargers – Hispano Suiza and MAN*

in the region of 4 to 7 bar. Further two-stage turbocharging with interstage and after-cooling offers significant thermodynamic advantages (high over-all turbocharger efficiency and low charging air temperatures – see chapter 11).

Development work on two-stage turbocharging also indicates that the use of two commercially available single-stage turbochargers, coupled in series, will not exceed the cost of a more compact but rigid two-stage single-shaft turbocharger. The flexibility in matching turbochargers, and their reliability achieved through many years of development, make series installation of two turbochargers attractive, in spite of a bulky installation (chapter 11). Thus the design methods used in single-stage turbochargers can be applied to two-stage turbocharging without any significant modification to the basic design. Hispano Suiza are manufacturing a compact two-stage turbocharger built from two standard

turbochargers as shown in figure 2.45a. MAN have tested one of their two-stage turbocharger prototypes on a medium-speed diesel engine rated at 30 bar BMEP. The sectional view of the turbocharger is shown in figure 2.45b.

References

1. H. Späti, VTR 4 – A new series of high performance turbochargers, *Brown Boveri Rev.*, **68** (May 1981)
2. D. Gorlich, MAN exhaust gas turbochargers to turbocharge high power diesel engines, *Turbocharging and Turbochargers, Proc. Inst. Mech. Engrs* (April 1978)
3. *Diesel and Gas Turbine Worldwide Catalog*, 46, Diesel and Gas Turbine Progress (1981)
4. H. Cohen, G. F. C. Rogers and H. I. H. Saravanamuttoo, *Gas Turbine Theory* (Longman, London, 1972)
5. W. E. Woollenweber, The turbocharger – a vital part of the engine intake and exhaust systems, *SAE 700534* (1970)

3

The Radial Flow Compressor

3.1 Introduction

Throughout the history of turbocharging, the type of compressors and turbines used have reflected the general state of the art, at any particular time, in the field of turbomachinery. The very first turbochargers (chapter 2) were built with radial flow single or two-stage compressors, incorporating backswept vaned shrouded impellers (figure 3.1a). Since the Second World War, due to great advances made in the development of the axial flow compressor, a few turbochargers have been built using multi-stage axial flow compressors, for experimental purposes. However, from an economic point of view their usage as turbocharger components is not attractive and has never reached the production stage.

With turbocharging to boost pressure levels above 2:1, the backswept vaned shrouded impellers disappeared because of strength limitations, and were replaced by unshrouded radial vaned impellers with axial inducers (figure 3.1b).

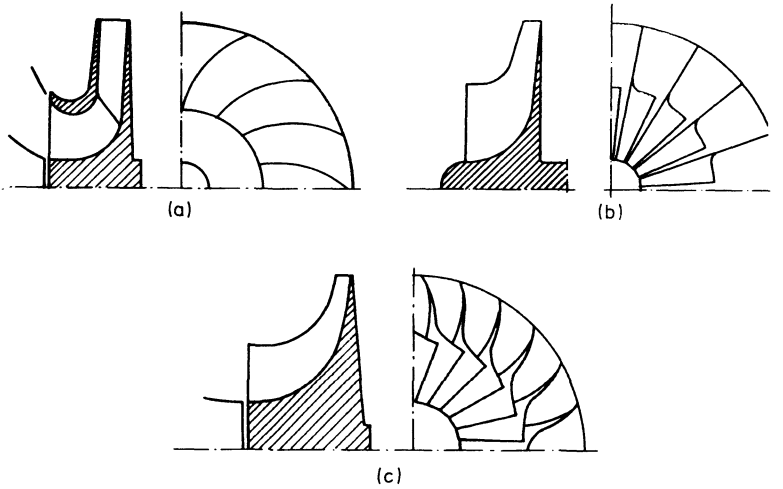

Figure 3.1 *Centrifugal compressor impellers*

In the 1970s, however, we have seen a demand for a further increase in boost pressure levels (above 3:1 pressure ratio), and a requirement for a wide efficient mass flow range. The latter has brought about the return of blade backsweep. The application of blade backsweep angles approaching 20 to 50° (at the tip of the impeller) and higher blade numbers (figure 3.1c), has led to significant improvements in impeller and stage performance levels in today's turbocharger compressors.

Research and development of profiled diffuser vanes has also contributed to further improvements in stage efficiency, stability and efficient operation at high pressure ratio and supersonic conditions.

3.2 Elementary Theory

The radial flow (centrifugal) compressor is made up from four basic components or sections

(1) a stationary inlet casing (in some applications provided with an air filter and noise reducing baffles);
(2) a rotating impeller;
(3) a stationary diffuser of the vaneless or vaned (preceded by a vaneless gap) type; and
(4) the collector or volute (figure 3.2).

Guide vanes have been fitted in the inlet casing of some compressors, principally to enable some control to be exercised over the flow characteristics (for example, lowering of the entry Mach number at the impeller eye or shift of the surge line by varying the vane angle).

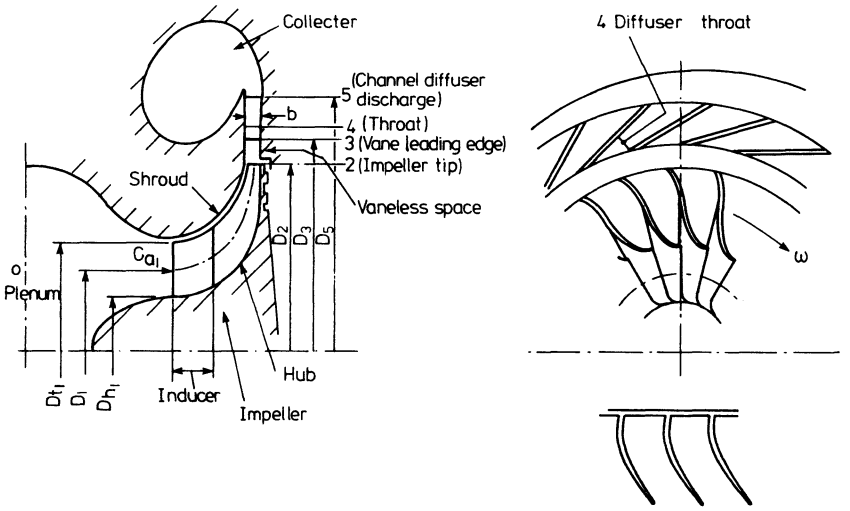

Figure 3.2 *Components of centrifugal compressor*

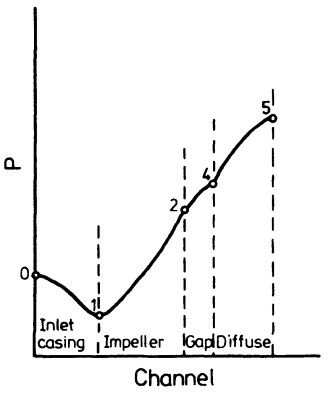

Figure 3.3 *Pressure rise across centrifugal compressor*

The contribution of each component of the compressor in producing the pressure rise in the stage is illustrated in figure 3.3. The inlet casing simply directs the airflow into the impeller eye, or inducer. Since the velocity of the air must increase as it approaches the eye, its static pressure will decrease accordingly. In the impeller the blades impart a swirling motion on the air, which leaves the impeller tip (its outer diameter) at high velocity. Work transfer takes place in the impeller and the static pressure of the air increases from the inducer to the impeller tip due to the centripetal acceleration. The purpose of the diffuser,

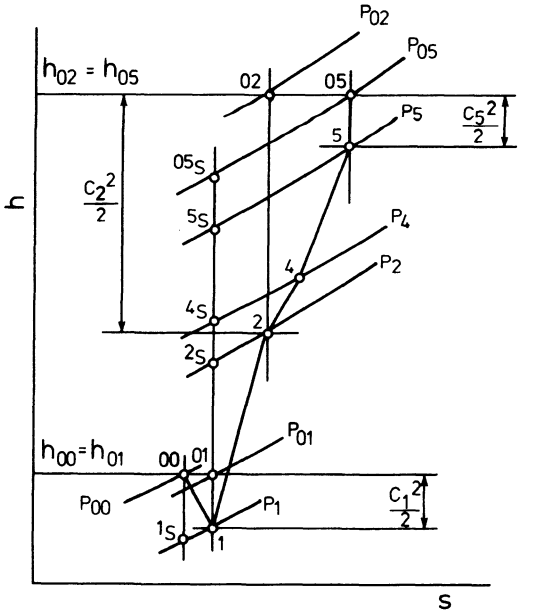

Figure 3.4 *h–s diagram for the centrifugal compressor stage*

whether vaneless or vaned, is to convert the high velocity of the air leaving the impeller into pressure by slowing it down carefully to an acceptable level (that is, to diffuse). The collector or volute collects the air from around the circumference of the diffuser and delivers it to single or multi-exit ducts. Sometimes a small amount of further diffusion may occur in the collector (hence it is called a volute) or through a short conical duct at the exit from the collector.

The process may be plotted on an enthalpy or temperature/entropy diagram, so that any departures from isentropic compression can be shown (figure 3.4). Station 01 represents ambient pressure of the air. Acceleration of the air in the inlet casing causes a pressure drop from P_{01} to P_1 (or P_{00} to P_1 when considering losses in the inlet casing), the change in enthalpy being equivalent to the increase kinetic energy ($C_1^2/2$). Isentropic compression to the delivery stagnation pressure P_{05s} is shown by the vertical line $01\text{-}05_s$. Energy transfer to the air takes place in the impeller and the process is indicated by the line 1-2. The corresponding insentropic process is shown by $1\text{-}2_s$. If the total kinetic energy of the air leaving the impeller ($C_2^2/2$) is converted to pressure (isentropically), the delivery pressure would be P_{02} (see point 02). Since the diffusion process is not accomplished isentropically (2-5), and some kinetic energy remains at diffuser exit (velocity C_5), the static delivery pressure at point 5 is P_5.

3.2.1 Velocity Triangles and Energy Transfer

The rotating part of the compressor, the impeller, is the only component of the stage where energy transfer occurs and in which the stagnation enthalpy rises, thus

$$h_{05} - h_{01} = h_{02} - h_{01} = \Delta h_{0c} \tag{3.1}$$

The specific energy transfer can be derived from the velocity triangles at inlet and outlet from the impeller. Considering the general case of the impeller with a pre-swirl axial inducer and backsweep blades, the velocity triangles at the entry (eye) and exit (tip) are shown in figure 3.5. The incoming air arrives at the impeller eye (inducer) at an absolute velocity C_1. Since the inlet velocity triangle at the eye hub will differ from that at the eye tip, it is the mean representative value which has to be considered, and this will occur at the eye diameter that divides the eye into two annuli of equal area

$$D_1^2 = \tfrac{1}{2}(D_{t1}^2 + D_{h1}^2)$$

At this diameter, the tangential velocity of the impeller U_1 is given by

$$U_1 = \frac{D_1}{2} \times \omega = \pi D_1 N$$

where N = rotational speed of the impeller.

The axial component of the absolute velocity C_1 of the air entering the inducer is C_{a1}, and the velocity relative to the inducer blade is W_1.

At the impeller tip the air leaves at an absolute velocity C_2 and a flow angle of α_2 from the tangential direction; its radial component is C_{r2}. The impeller tip speed is U_2, and the gas velocity relative to the rotor blades is W_2.

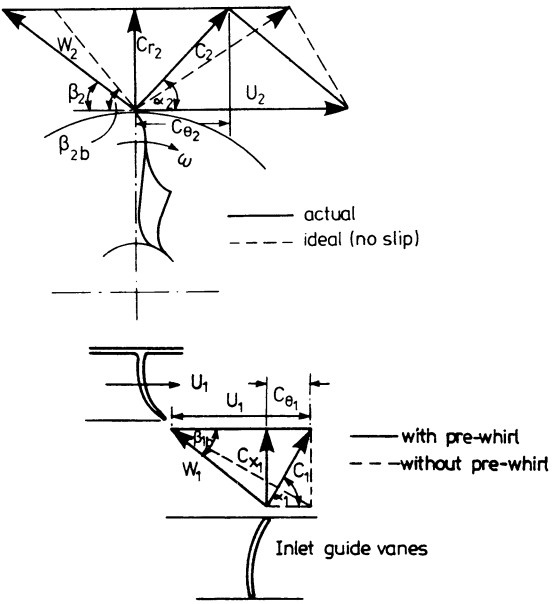

Figure 3.5 *Velocity triangles*

The rate of change of angular momentum will equal the sum of the moments of external forces (that is, the torque TQ). Since the angular momentum is the moment of linear momentum, the rate of change will be given by the product of mass flow rate, times radius, times tangential component of velocity (C_θ). Thus the torque is given by

$$TQ = \dot{m}(r_2 C_{\theta 2} - r_1 C_{\theta 1}) \tag{3.2}$$

The energy transfer is given by the product of torque and angular velocity (ω), given by the Euler equation

$$\dot{m}\Delta h_{0c} = -\dot{W} = \omega TQ = \dot{m}(U_2 C_{\theta 2} - U_1 C_{\theta 1}) \tag{3.3}$$

(*Note:* the negative sign arises from the sign convention established in chapter 2, namely that work input is negative.)

From the velocity triangle (figure 3.5) at impeller inlet or exit

$$(-)W^2 = C^2 + U^2 - 2UC_\theta \tag{3.4}$$

(the negative sign denoting a flow direction opposite to impeller rotation). Substituting this expression in equation 3.3 gives

$$-\dot{W} = \dot{m}\tfrac{1}{2}[(C_2^2 - C_1^2) + (U_2^2 - U_1^2) + (W_1^2 - W_2^2)] \tag{3.5}$$

This alternative form of the Euler equation throws light on the nature of the energy transfer and the mechanism of pressure rise in the compressor. The first term represents the change in absolute kinetic energy occurring in the impeller.

The second term represents the change of energy due to movement of the rotating air from one radius of rotation to another, that is, the centrifugal energy which raises the static pressure in the impeller. The third term represents the change in kinetic energy due to the change of the relative velocity, resulting in a further change of static pressure within the rotor.

Except for some isolated cases, the majority of turbocharger compressors are designed without stationary pre-whirl vanes and it is normal to assume that the air approaches the impeller without a tangential component of velocity. Thus equation 3.3 reduces to (with negative sign deleted henceforth)

$$\Delta h_{0c} = \frac{\dot{W}}{\dot{m}} = U_2 C_{\theta 2} \tag{3.6}$$

In an ideal radial vaned impeller, $C_{\theta 2}$ should equal U_2, thus

$$\frac{\dot{W}}{\dot{m}} = U_2^2 \tag{3.7}$$

The effect of the backsweep angle β_{2b} on the energy transfer can be shown as follows. From figure 3.5

$$C_{\theta 2} = U_2 - C_{r2} \cot \beta_{2b}$$

therefore

$$\frac{\dot{W}}{\dot{m}} = U_2^2 \left(1 - \frac{C_{r2}}{U_2} \cot \beta_{2b}\right) \tag{3.7a}$$

The energy transfer coefficient (μ) relates energy transfer to the energy achievable with a radial vaned impeller of the same diameter (tip speed U_2). Thus

$$\mu \equiv \frac{\dot{W}}{\dot{m} U_2^2} = \frac{C_{\theta 2}}{U_2} = \left(1 - \frac{C_{r2}}{U_2} \cot \beta_{2b}\right) \tag{3.8}$$

For the ideal radial vaned impeller with no backsweep, $\mu = 1$.

For a given value of β_{2b} there is a linear relationship between the energy transfer coefficient (μ) and the radial/tangential speed ratio (C_{r2}/U_2).

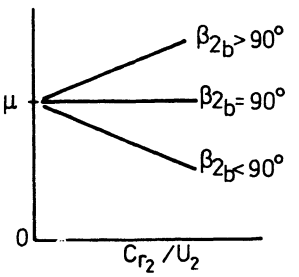

Figure 3.6 *Effect of β_{2b} and C_{r2}/U_2 on energy transfer [1]*

Figure 3.6 illustrates this relationship, indicating that for $\beta_{2b} < 90°$ (impeller with backsweep) the energy transfer falls for a given tip speed, and that reducing C_{r2}/U_2 for a given β_{2b} increases the energy transfer. The radial vaned impeller ($\beta_{2b} = 90°$)maintains a level characteristic, independent of C_{r2}/U_2.

3.2.2 Degree of Reaction

The degree of reaction (*RN*) of a centrifugal compressor may be defined as the energy transfer due to a change in static pressure in the rotor divided by the total energy transfer in the stage. From figure 3.4

$$RN = \frac{h_2 - h_1}{h_{05} - h_{01}} \tag{3.9}$$

For compressors with a higher impeller than diffuser efficiency there may be an advantage in designing for the maximum degree of reaction, in order to increase the conversion of energy to pressure in the impeller rather than the diffuser. This is achieved by optimising blade backsweep (β_{2b}) and the radial/tangential speed ratio (C_{r2}/U_2) as shown below.

If the inlet kinetic energy is neglected (it is usually very small) then it can be shown [1] that

$$RN = \frac{1 - (C_{r2}/U_2)^2 \operatorname{cosec}^2 \beta_{2b}}{2\,[1 - (C_{r2}/U_2) \cot \beta_{2b}]} \tag{3.10}$$

Equation 3.10 is plotted in figure 3.7. Reaction is a maximum when

$$C_{r2}/U_2 = (1 - \sin \beta_{2b}) \tan \beta_{2b} \tag{3.11}$$

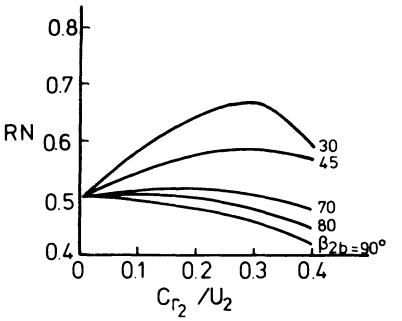

Figure 3.7 *Variation of RN with C_{r2}/U_2 [1]*

3.2.3 Radial Vaned Impeller (with No Inlet Pre-whirl)

With the radial vaned impeller (see figure 3.1b) ($\beta_{2b} = 90°$), the whirl or tangential component of the absolute air velocity leaving the impeller ($C_{\theta 2}$) should equal

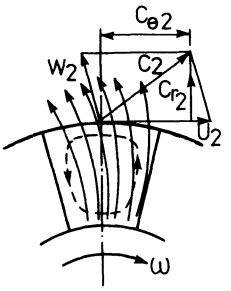

Figure 3.8 *Relative flow through radial vaned impeller*

the peripheral tip speed of the impeller. However, not all the air passes smoothly through the passage formed between the impeller blades and thus the tangential component of the absolute air velocity leaving the impeller tends to be less than the impeller tip speed (U_2) (figure 3.8).

The ratio between $C_{\theta 2}$ and U_2 in a radial vaned impeller is called the slip factor (σ), and is dependent on the number of impeller blades, the passage geometry, the impeller eye tip to impeller exit diameter ratio, and the mass flow rate (see section 3.3).

$$\sigma = \frac{C_{\theta 2}}{U_2} \quad \text{(with radial blades)}$$

Thus the specific energy transfer in the impeller becomes, using equation 3.6, is

$$\dot{W} = \dot{m}\sigma U_2^2 \tag{3.12}$$

It follows that the power required to drive the impeller is a function of mass flow rate and the square of the impeller tip speed, if pre-whirl or backsweep are not used.

3.2.4 Temperature Rise across the Compressor

The steady flow energy equation for a process from state 'a' to state 'b' can be written as

$$\dot{Q} - \dot{W} = \dot{m}\left[h_b - h_a + \frac{(C_b^2 - C_a^2)}{2}\right] \tag{3.13}$$

Since the stagnation enthalpy (h_0) is given by

$$h_0 = h + \frac{C^2}{2}$$

then

$$\dot{Q} - \dot{W} = \dot{m}(h_{0b} - h_{0a})$$

When applied to the compressor, with heat transfer neglected

$$-\dot{W} = \dot{m}(h_{02} - h_{01}) \tag{3.14}$$

Since no work is transferred in the diffuser and collector, the stagnation enthalpy remains constant therein, $h_{02} = h_{0s}$ hence

$$-\dot{W} = \dot{m}(h_{0s} - h_{01}) \tag{3.15}$$

Thus, from equations 3.3 and 3.14

$$-\dot{W} = \dot{m}(h_{0s} - h_{01}) = \dot{m}(U_2C_{\theta 2} - U_1C_{\theta 1}) \tag{3.15a}$$

or for the radial vaned impeller, with no pre-whirl

$$-\dot{W} = \dot{m}(h_{0s} - h_{01}) = \dot{m}U_2C_{\theta 2} = \dot{m}\sigma U_2^2 \tag{3.15b}$$

If the working fluid (air) may be considered as a perfect gas, then

$$h_{0s} - h_{01} = c_p(T_{0s} - T_{01}) = c_p\Delta T_{0c} \tag{3.16}$$

where ΔT_{0c} is the rise in stagnation temperature and c_p is the mean value of the specific heat capacity of air at constant pressure between T_{0s} and T_{01}.

Hence the temperature rise across the compressor is

$$\Delta T_{0c} = \frac{(U_2C_{\theta 2} - U_1C_{\theta 1})}{c_p} \tag{3.17a}$$

or for the radial vaned impeller

$$\Delta T_{0c} = \frac{\sigma U_2^2}{c_p} \tag{3.17b}$$

3.2.5 Isentropic Efficiency and Pressure Ratio

Using the definition of efficiency established in chapter 2 (equation 2.9) the compressor total to total isentropic efficiency becomes

$$\eta_{cTT} = \frac{T_{01}\left[(P_{0s}/P_{01})^{(\gamma-1)/\gamma} - 1\right]c_p}{(U_2C_{\theta 2} - U_1C_{\theta 1})} \tag{3.18a}$$

and for the radial vaned impeller

$$\eta_{cTT} = \frac{T_{01}\left[(P_{0s}/P_{01})^{(\gamma-1)/\gamma} - 1\right]c_p}{\sigma U_2^2} \tag{3.18b}$$

The pressure rise across the compressor is given (from equation 2.8) by

$$\frac{P_{0s}}{P_{01}} = \left[1 + \frac{\eta_{cTT}\Delta T_{0c}}{T_{01}}\right]^{\gamma/(\gamma-1)} \tag{3.19a}$$

and for the radial vaned impeller with no pre-whirl

$$\frac{P_{0s}}{P_{01}} = \left[1 + \frac{\eta_{cTT}\sigma U_2^2}{T_{01}c_p}\right]^{\gamma/(\gamma-1)} \tag{3.19b}$$

From equation 2.11 the compressor total to static isentropic efficiency is given by

$$\eta_{cTS} = \frac{T_{01}\left[(P_5/P_{01})^{(\gamma-1)/\gamma} - 1\right] c_p}{(U_2 C_{\theta 2} - U_1 C_{\theta 1})} \tag{3.20a}$$

and for the radial vaned impeller

$$\eta_{cTS} = \frac{T_{01}\left[(P_5/P_{01})^{(\gamma-1)/\gamma} - 1\right] c_p}{\sigma U_2^2} \tag{3.20b}$$

and the pressure rise across the compressor is

$$\frac{P_5}{P_{01}} = \left(1 + \frac{\eta_{cTS}\Delta T_{oc}}{T_{01}}\right)^{\gamma/(\gamma-1)} \tag{3.21a}$$

and for the radial vaned impeller

$$\frac{P_5}{P_{01}} = \left(1 + \frac{\eta_{cTS}\sigma U_2^2}{T_{01} c_p}\right)^{\gamma/(\gamma-1)} \tag{3.21b}$$

3.2.6 Specific Speed and Diameter

A simple guide to the expected performance and approximate geometry of a compressor for a given duty can be obtained from past compressor experimental test data, presented in terms of peak efficiency and geometry as a function of specific speed (*NS*) and specific diameter (*DS*).[2]

The volumetric flow rate passing through a turbomachine ($\dot{V}$) is proportional to a characteristic velocity (C) and the flow area (A). Since the area is proportional to the square of the inlet diameter (D) then

$$\dot{V} \propto CA \propto CD^2$$

In addition, the velocity term is proportional to the impeller tip speed, which is a product of diameter and rotational speed (N). Hence

$$\dot{V} \propto ND^3$$

The pressure head (HD) in terms of potential energy, developed by the compressor is proportional to the square of the impeller tip speed. Thus

$$(HD) \propto N^2 D^2$$

Comparing the volumetric flow rate and head with that of an optimum reference machine (subscript ref)

$$\frac{\dot{V}}{\dot{V}_{ref}} \propto \frac{ND^3}{N_{ref} D_{ref}^3}$$

and

$$\frac{(HD)}{(HD)_{ref}} \propto \frac{N^2 D^2}{N_{ref}^2 D_{ref}^2}$$

By arbitrarily assigning the value of unity to the flow rate and head of the reference machine, and solving for D,

$$D \propto \frac{V^{1/3} N_{\text{ref}}^{1/3}}{N^{1/3}} \times D_{\text{ref}} \propto \frac{(HD)^{1/2} N_{\text{ref}}}{N} D_{\text{ref}}$$

hence,

$$\left(\frac{N_{\text{ref}}}{N}\right)^{2/3} \propto \frac{\dot{V}^{1/3}}{(HD)^{1/2}}$$

$$NS = N_{\text{ref}} = \frac{N\dot{V}^{1/2}}{(HD)^{3/4}} \tag{3.22}$$

Specific speed (NS) is a dimensionless parameter which characterises the particular combination of flow rate, pressure head and diameter, and therefore shape of an impeller.

By solving for rotational speed, rather than diameter

$$N \propto \dot{V}\left(\frac{D_{\text{ref}}}{D}\right)^3 \propto (HD)^{1/2} \frac{D_{\text{ref}}}{D}$$

$$DS \equiv D_{\text{ref}} = \frac{D(HD)^{1/4}}{\dot{V}^{1/2}} \tag{3.23}$$

NS and DS are the rotational speed and rotor diameter of similar turbomachines producing unit head with unit flow rate. Although derived in the context of incompressible flow for water pumps and turbines, the specific speed and diameter concept can usefully be applied to low-pressure compressors and turbines.

Figure 3.9 compares compressor stage efficiency and specific speed for three

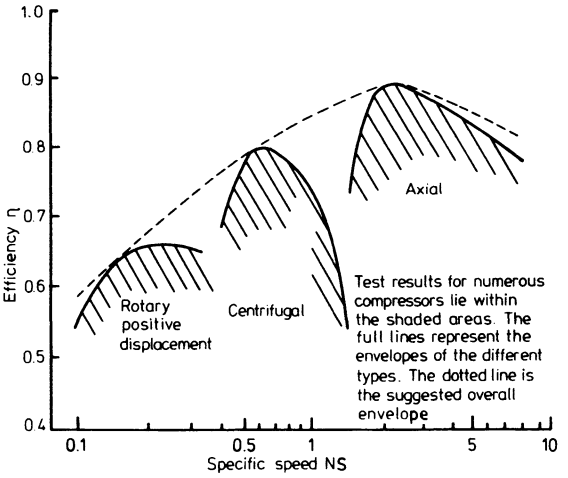

Figure 3.9 *Variation of compressor efficiency with specific speed NS [3]*

types of machine, indicating the range where a centrifugal compressor is appropriate for a particular application.

Balje [2] has claimed that the efficiency of any turbomachine may be described by four parameters: the Mach number, Reynolds number, specific speed and specific diameter. Thus, for chosen constant Mach number and Reynolds number, the compressor efficiency is a function of *NS* and *DS* as shown in figure 3.10, based on approximate loss analysis calculations. Although test results from many compressors do not fall on Balje's curve, the trends appear broadly correct,

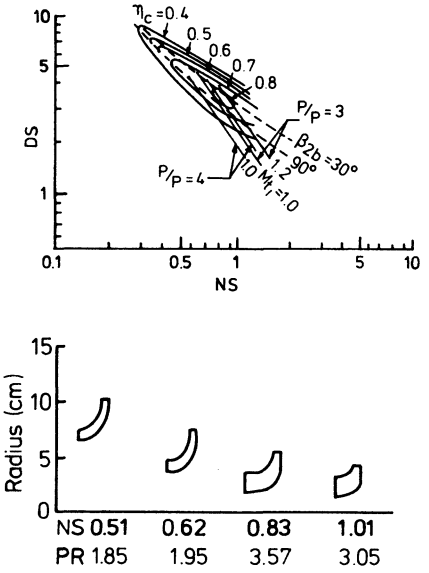

Figure 3.10 *Specific speed/specific diameter relationship [2]*

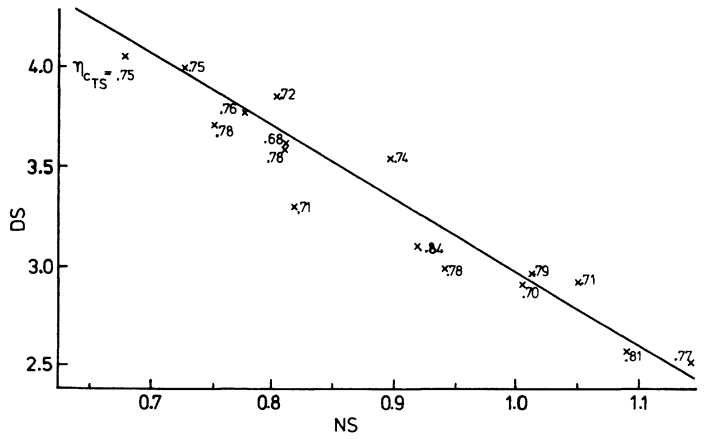

Figure 3.11 *NS against DS for typical small turbocharger compressor*

particularly for low-pressure compressors. It follows that a reasonably efficient machine can be built if the specific speed value lies in the range of 0.7 to 1 and the specific diameter in the range of 3 to 4. The impeller diameter and speed may then be established for a specific duty (flow rate and pressure ratio). Results from a number of small turbocharger compressors with radial vaned impellers are plotted on a *NS-DS* graph in figure 3.11 indicating the trend.

3.3 One-dimensional Flow Analysis Through the Radial Flow Compressor

In the early days of radial flow compressor development, the design and theoretical analysis was mainly based on the assumption that the air flow through the compressor may be considered one dimensional. Although the concept is incorrect, since the flow in the compressor is three dimensional, and further complicated due to flow separation and the appearance of shocks, it still provides the basis for the initial design of the components. The technique has been further refined over the years by the introduction of design parameters (or design criteria) gained from experimental data (section 3.4). Finally, the design can be modified with the help of three-dimensional flow analysis and the so-called 'jet/wake' approach to obtain optimum compressor performance (section 3.5).

With the aid of the moment of momentum equation, steady flow energy equation, continuity equation and thermodynamic equation of state, and the assumptions that the fluid is a perfect gas and the flow isentropic and one dimensional, it is possible, to estimate the representative state of the air (that is, pressure, temperature, velocity, Mach number) at any point in the compressor channels. This can be used to estimate the shape of compressor components (channel geometry) to produce desirable velocity or Mach number profiles from inlet to exit.

3.3.1 The Inlet Casing

The function of the inlet casing is to deliver air to the impeller eye with minimum loss and to provide a uniform velocity profile at the eye. Design of the inlet passage of a turbocharger compressor with inboard mounted bearings presents no problem. The inlet flange is axisymmetric and the inlet duct takes the form of a simple convergent nozzle. Since there is no energy transfer, the stagnation enthalpy remains constant. Hence from figure 3.4

$$T_1 = T_{01} - \frac{C_1^2}{2c_p} \tag{3.24}$$

and

$$P_1 = P_{01}\left(\frac{T_1}{T_{01}}\right)^{\gamma/(\gamma-1)} \tag{3.25}$$

With an air filter fitted to the compressor inlet casing a pressure drop will occur, which must be kept to a minimum. However, it should be accounted for in the flow analysis and prediction of compressor performance.

Significant losses can occur in inlet casings fitted with silencing baffles or turbochargers with outboard mounted bearings, where bearing housing support members cross the flow path. In these circumstances an 'inlet casing efficiency' (η_{ic}) may be used. Similar to the nozzle efficiency, the η_{ic} can be defined as

$$\eta_{ic} = \frac{h_{00} - h_1}{h_{00} - h_{1s}} \tag{3.26}$$

where $h_{00} - h_{1s}$ is the enthalpy change in isentropic expansion from P_{00} to P_1.

For a perfect gas assumption (c_p = constant) equation 3.26 becomes

$$\eta_{ic} = \frac{T_{00} - T_1}{T_{00} - T_{1s}} = \frac{T_{00} - T_1}{T_{00}\left[1 - (P_1/P_{00})^{(\gamma-1)/\gamma}\right]}$$

Since $T_{00} = T_{01}$, rearranging and using equation 3.24 gives

$$\frac{P_1}{P_{00}} = \left(1 - \frac{C_1^2}{2c_p\eta_{ic}T_{00}}\right)^{\gamma/(\gamma-1)}$$

From values of P_1 and $T_1 = T_{00} - (C_1^2/2c_p)$ the density at the impeller eye can be calculated

$$\rho_1 = \frac{P_1}{RT_1}$$

and hence the mass flow rate entering the impeller eye can be estimated

$$\dot{m} = \frac{\pi}{4}(D_{t1}^2 - D_{h1}^2)\, C_{a1}\rho_1 \tag{3.27}$$

where D_{t1} and D_{h1} are the impeller eye tip and eye hub diameters respectively, and C_{a1} is the axial component of the absolute velocity of the air entering the impeller eye. In the case of a swirl-free intake

$$C_{a1} = C_1$$

For compressor intakes, where the air must be turned from a radial to an axial direction, the air incidence angle at the impeller eye (inducer) has to be chosen carefully, due to variation in the axial velocity distribution caused by the free vortex flow effect in the bend of the inlet ducting.

3.3.2 The Impeller

Energy transfer occurs in the impeller of the compressor, hence there is an increase in stagnation enthalpy and pressure. To attain peak compressor efficiency great care must be taken to achieve very efficient diffusion processes in the impeller and the diffuser. Since the diffusion processes are related to the flow Mach number it is desirable to establish conditions which lead to a minimum

relative Mach number at the impeller inlet, and a minimum absolute Mach number at the impeller outlet.

3.3.2.1 The Inducer

The inducer, or entry section of the impeller, has a very pronounced effect on the impeller performance and hence on over-all compressor efficiency.

The eye hub diameter (D_{h1}) of the inducer is determined by a number of design considerations. If inboard bearings are used the minimum shaft and retaining nut diameter dictate the eye hub diameter. Turbochargers with outboard bearings require large eye hub diameters, dictated by the size of the shaft and bearing diameter. Inducer stress/vibration considerations, impeller manufacturing techniques and the number of blades selected also influence the choice of the eye hub diameter.

The tip of the inducer eye is the point where the highest inlet relative Mach number occurs, and therefore careful attention should be paid to the choice of the inducer eye tip diameter (D_{t1}).

With uniform axial velocity and no pre-whirl the relative velocity at the inducer eye tip is

$$W_{t1}^2 = C_{a1}^2 + U_{t1}^2$$

$$W_{t1} = \sqrt{[C_{a1}^2 + (\pi D_{t1} N)^2]}$$

where N = the rotational speed of the impeller.

The relative Mach number at the eye tip (M_{t1}) will be given by

$$M_{t1} = \frac{W_{t1}}{\sqrt{(\gamma R T_1)}} = \sqrt{\left[\frac{C_{a1}^2 + (\pi D_{t1} N)^2}{\gamma R T_1}\right]}$$

Using equation 3.27 the relative Mach number at inducer eye tip becomes

$$M_{t1} = \sqrt{\left\{\left[\frac{\dot{m}}{(\pi/4)(D_{t1}^2 - D_{h1}^2)P_1}\right]^2 \frac{RT_1}{\gamma} + \frac{(\pi D_{t1} N)^2}{\gamma R T_1}\right\}} \qquad (3.28)$$

For a given design mass flow rate and impeller speed, D_{t1} should be chosen so as to obtain a minimum relative Mach number (figure 3.12).

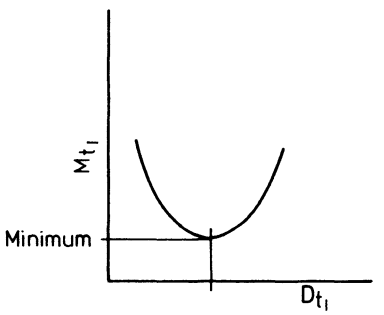

Figure 3.12 *Minimum relative Mach number at impeller eye tip*

To further reduce the relative Mach number (M_{t1}), pre-whirl (inlet guide vanes) may be used. However, the penalty will be a reduction in energy transfer in the impeller (see equation 3.3). Thus the technique is usually used only on high-pressure ratio compressors, where the inlet Mach number exceeds unity and shock waves reduce impeller efficiency. The use of inlet guide vanes has to be carefully evaluated for each application, since there is a trade-off between improved stage performance from the impeller and reduced stage performance from the diffuser. Use of variable inlet guide vanes enables the compressor flow characteristic to be altered and hence could ease engine-turbocharger matching (for example, during low-speed operation of highly supercharged engines).

3.3.2.2 The Impeller Channel

The relative velocity of the air in the impeller channels undergoes a rapid deceleration from the impeller eye through towards the impeller tip. In addition to the function of transferring energy to the air, the impeller should act as an efficient diffuser. A badly shaped channel will interfere with the diffusion processes, causing flow separation at the impeller walls, leading to high impeller losses. To obtain gradual deceleration of the flow in the channel, the geometry of the impeller channels (defined by blade shape and hub and shroud profiles) should be chosen to give a smooth change in the relative Mach number along the mean flow path (in the meridional plane – figure 3.13).

It has already been stated that the relative flow direction of the air leaving the impeller will not match that of the vanes. Consider the backswept impeller shown in figure 3.14, rotating clockwise. The body of air passing through the channel between the two blades has inertia and will resist the turning effect of the impeller. The air therefore tends to rotate relative to the impeller channel, but in the opposite direction. Near the tip this relative rotation causes the tangential component of absolute velocity ($C_{\theta 2}$) to be less than the value assuming

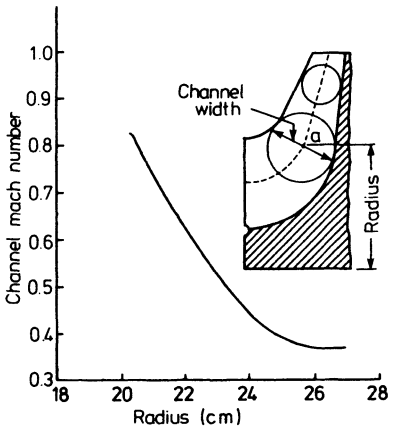

Figure 3.13 *Average channel relative Mach number*

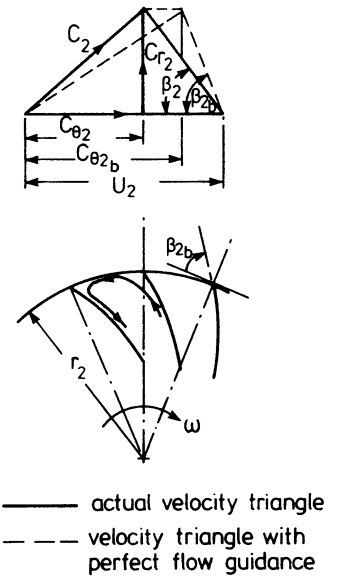

Figure 3.14 *Flow model for slip factor*

that the fluid leaves the impeller at the blade angle ($C_{\theta 2b}$, figure 3.14). The 'slip factor' defined as $C_{\theta 2}/C_{\theta 2b}$ is an empirical attempt to take some account of this phenomenon within the confines of a simple one-dimensional treatment of the flow. The greater the number of impeller blades, the more viscous drag from the blades reduces the effect of recirculation and the higher the slip factor becomes.

Many attempts have been made to predict the values for the slip factor. [1] Stanitz [4] applied the relaxation method of calculation and showed (for β_{2b} = 0 to 45°) that the slip factor depends mainly on blade spacing. For the radial vaned impeller ($\beta_{2b} = 90°$)

$$\sigma = 1 - \frac{0.63\pi}{Z} \approx 1 - \frac{2}{Z} \tag{3.29}$$

where Z = number of blades. A correlation of slip factors from many investigations has been published by Wiesner.[5] Figure 3.15 shows the variation of the slip factor with blade backsweep and impeller blade number.

All the expressions for slip factor produce constant values for a given impeller design, but evidence suggests that although they are useful at the design point, the values will also vary with flow rate.[6, 7]

The variation of slip factor with mass flow rate (at different rotational speeds) from an automotive diesel engine-type turbocharger with 12 radial blades (including 6 'splitter' blades) is shown in figure 3.16.

For a specified geometry of the impeller channel and an assumed slip factor variation with impeller radius, the temperature, static pressure, density and hence the mean relative velocity and relative Mach number, can be estimated at any point in the channel using one-dimensional theory. For example, for a

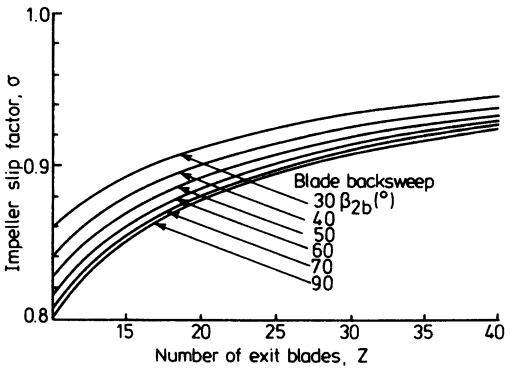

Figure 3.15 *Weisner slip factor correlation [5]*

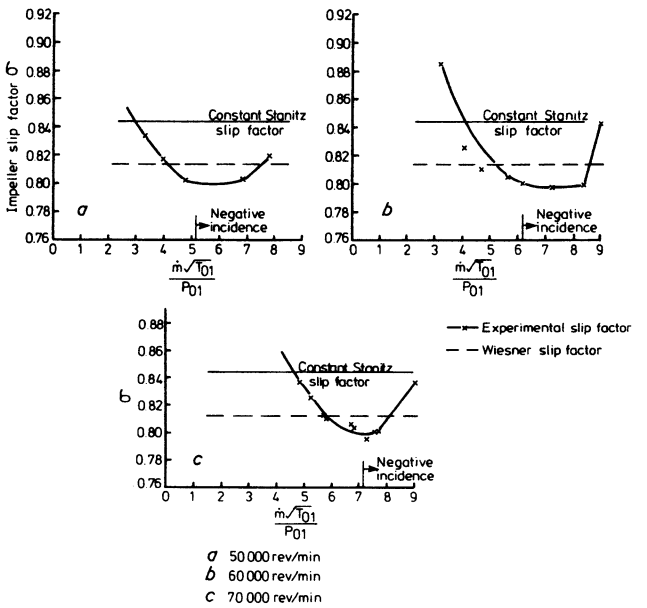

Figure 3.16 *Experimental slip factors [7]*

radial vaned impeller, an expression can be obtained for the total temperature rise ΔT_{1-a} from the impeller eye to point 'a' in the flow path using the steady flow energy equation (3.13).

$$-\dot{W}_a = \dot{m}\sigma_a U_a^2 = \dot{m}\left(\Delta h_{a-1} + \frac{C_1^2}{2}\right)$$

and

$$C_a = \sqrt{[(\sigma_a U_a)^2 + W_a^2]}$$

Equation 3.12 becomes

$$\dot{m}\sigma_a U_a^2 = \dot{m}\left[c_p \Delta T_{a-1} + \frac{(\sigma_a U_a)^2}{2} + \frac{W_a^2}{2} - \frac{C_1^2}{2} \right]$$

therefore

$$\Delta T_{a-1} = \frac{\sigma_a U_a^2}{c_p} - \frac{(\sigma_a U_a)^2 + W_a^2 - C_1^2}{2c_p} \tag{3.30}$$

The static pressure at station 'a' will be given by

$$P_a = P_1 \left(1 + \frac{\Delta T_{(a-1)s}}{T_1}\right)^{\gamma/(\gamma-1)} \tag{3.31}$$

where $\Delta T_{(a-1)s}$ is the temperature rise for isentropic compression between the static inlet pressure at impeller eye P_1 and channel pressure P_a at station 'a'. Assuming an average value for the impeller efficiency (η_{imp}), $\Delta T_{(a-1)s}$ can be calculated from

$$\Delta T_{(a-1)s} = \eta_{imp}\, \Delta T_{1-a}$$

The density of air at station 'a' can be calculated from the perfect gas relationship

$$\rho_a = \frac{P_a}{RT_a}$$

where $T_a = T_1 + \Delta T_{a-1}$. The mean channel relative velocity may then be estimated from the continuity equation

$$W_a = \frac{\dot{m}}{\rho_a A_a}$$

where A_a is the cross-sectional area of the channel at station 'a'. Solving these simultaneous equations gives W_a and T_a. The mean Mach number in the channel (M_a) is then given by

$$M_a = \frac{W_a}{\sqrt{(\gamma R T_a)}} \tag{3.32}$$

For a specified impeller geometry, the distribution of the relative Mach number along the meridional streamline of the impeller channel may be evaluated (figure 3.13). The hub and shroud profiles may then be altered to reduce the peak value of the relative Mach number and obtain a smooth curve. Thus an approximate impeller geometry can be designed, for gradual deceleration rates and pressure gradients along the channel. Towards the tip of the impeller, where the flow tends to be rather chaotic, slight acceleration of the flow proves to be beneficial.

In the early days of gas turbine design many efficient impellers were designed by the combination of the one-dimensional technique and an appreciation of the three-dimensional flow effect.

3.3.3 The Diffuser

The diffuser is a stationary component and is fitted directly around the impeller. The function of the diffuser is to convert the kinetic energy of the fluid leaving the impeller tip efficiently into static pressure. The influence of the diffuser on compressor efficiency is important, since approximately half of the fluid energy at the impeller tip is kinetic energy.

Centrifugal compressors are usually fitted with either a vaneless or a vaned diffuser. Virtually all vaned diffusers also use a small vaneless 'gap' to reduce fluid noise levels and decrease the Mach number at the entry to the vanes.

3.3.3.1 The Vaneless Diffuser

Vaneless diffusers usually have a constant width, normally set equal to the impeller tip width (figure 3.17). The gap width can be varied with radius, but the effect on diffusion is usually relatively small, although the boundary layer can be affected.

If the friction between the air and the diffuser wall is neglected, then the angular momentum of the air entering the diffuser will remain constant. Thus

$$C_{\theta 2} r_2 = C_{\theta a} r_a \tag{3.33}$$

where subscript 'a' denotes any section in the diffuser. From continuity

$$\dot{m} = C_{r2} \rho_2 A_2 = C_{ra} \rho_a A_a$$

For a radial vaneless diffuser of constant width b

$$A_2 = 2\pi r_2 b \quad \text{and} \quad A_a = 2\pi r_a b$$

hence

$$C_{r2} \rho_2 r_2 = C_{ra} \rho_a r_a \tag{3.34}$$

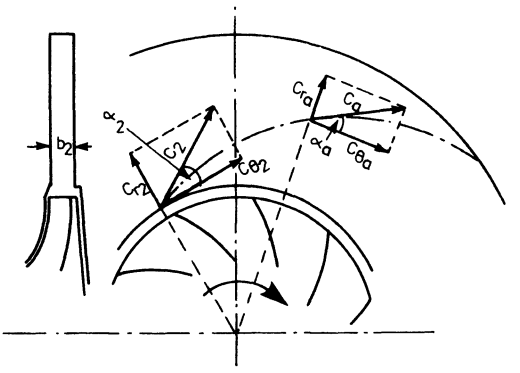

Figure 3.17 *Vaneless diffuser velocity diagrams*

The flow angle at entry (α_2) is given by

$$\tan \alpha_2 = \frac{C_{r2}}{C_{\theta 2}} = \frac{C_{r2}}{\sigma U_2}$$

The flow angle at section 'a' is given by

$$\tan \alpha_a = \frac{C_{ra}}{C_{\theta a}} = \frac{C_{r2} r_2 \rho_2 r_a}{C_{\theta 2} r_2 \rho_a r_a} = \frac{C_{r2} \rho_2}{C_{\theta 2} \rho_a} \tag{3.35}$$

that is

$$\tan \alpha_a = \text{constant} \times \rho_2 / \rho_a$$

Thus for isentropic incompressible flow in a diffuser of constant width, the moment of momentum and continuity equations indicate that the absolute air flow angle (α) is constant in the diffuser. The path the fluid follows is a logarithmic spiral.

A one-dimensional analysis yields the approximate state of the fluid at radius 'a' for compressible flow.

Since no work transfer takes place in the diffuser, the steady flow energy equation reduces to

$$h_a - h_2 = \frac{C_2^2 - C_a^2}{2} = c_p (T_a - T_2)$$

if heat transfer is neglected. Hence the actual temperature rise in the diffuser from the impeller tip to radius r_a is equal to

$$\Delta T_{a-2} = \frac{C_2^2 - C_a^2}{2c_p} = \frac{C_{\theta 2}^2 + C_{r2}^2}{2c_p} - \frac{C_{\theta a} + C_{ra}^2}{2c_p}$$

Assuming that angular momentum prevails, from equations 3.33 and 3.34

$$\Delta T_{a-2} = \frac{C_{\theta 2}^2 + C_{r2}^2}{2c_p} - \frac{C_{\theta 2}^2}{2c_p} \left(\frac{r_2}{r_a}\right)^2 - \frac{C_{r2}^2}{2c_p} \left(\frac{r_2}{r_a}\right)^2 \left(\frac{\rho_2}{\rho_a}\right)^2$$

therefore

$$\Delta T_{a-2} = \frac{C_{\theta 2}^2}{2c_p} \left[1 - \left(\frac{r_2}{r_a}\right)^2\right] + \frac{C_{r2}^2}{2c_p} \left[1 - \left(\frac{r_2}{r_a}\right)^2 \left(\frac{\rho_2}{\rho_a}\right)^2\right] \tag{3.36}$$

The static pressure at radius 'a' will be given by

$$P_a = P_2 \left(1 + \frac{\Delta T_{(a-2)s}}{T_2}\right)^{\gamma/(\gamma-1)}$$

where $\Delta T_{(a-2)s}$ is the static temperature rise during an isentropic pressure rise from P_2 to P_a, hence assuming an isentropic diffuser efficiency η_{dif}

$$\Delta T_{(a-2)s} = \Delta T_{a-2} \, \eta_{dif}$$

Thus

$$P_a = P_2 \left(1 + \frac{\eta_{dif} \Delta T_{a-2}}{T}\right)^{\gamma/(\gamma-1)} \tag{3.37}$$

and

$$T_a = T_2 + \Delta T_{a-2} \tag{3.38}$$

and

$$\rho_a = \frac{P_a}{RT_a} \tag{3.39}$$

Equations 3.36, 3.37 and 3.38 may be solved (by numerical methods) to find P_a, T_a and from equation 3.39 ρ_a can be calculated and the flow angle α_a estimated from equation 3.35.

The vaneless diffuser, which in its simplest form is defined by two parallel walls, is a much cheaper component to manufacture then a vaned diffuser and is widely used in automotive-type turbochargers because of the broad operating range it offers. It is also more tolerant to erosion and fouling. However, the diffusion rate in a radial vaneless diffuser is comparatively low, and a large diameter ratio, nearly twice the inlet diameter, is required if the outlet velocity is to be reduced to half the inlet velocity. In practice this will result in high losses due to viscous drag on the walls and a significantly lower pressure recovery than is found with vaned diffusers.

3.3.3.2 The Vaned Diffuser

In the vaned diffuser the diffusion rate is higher than that obtainable in a vaneless type, allowing a smaller outlet diameter to be used. A vaneless space precedes the vaned diffuser to help reduce flow unsteadiness and Mach number at the entry to the vanes. In a one-dimensional analysis, the 'gap' from the impeller tip to the vaned throat (see figure 3.18) can be treated in the same way as the vaneless diffuser. A theoretical throat area of the vaned diffuser can be found by determining the mean velocity and density for the mean throat radius. The throat area is that given by the continuity equation for logarithmic spiral diffusion at the radius considered. The actual throat area to be used should be 5 to 12 per cent greater than the theoretical area due to boundary layer blockage. [8, 9] The leading portion of the diffuser vane usually follows the corresponding logarithmic spiral path to the throat. From the throat, the diffuser channel is shaped to give a diffuser of an 'equivalent included cone angle' not exceeding 9° and an outlet to throat area ratio of about 2 to 3.5. Some designers prefer diffusers with a smaller number of vanes than the number of impeller vanes so that the flow is distributed more evenly from one diffuser channel to another. A small number of vanes reduces the area ratio (inlet throat to outlet) of the diffuser (consider removing the centre vane shown in figure 3.18). A larger outer diameter is required to restore the same area ratio. A large number of vanes reduces diffuser diameter ratio, but the operating range is considerably reduced.

There are a wide range of vaned diffuser designs. Most common for turbocharger applications are profiled blades and straight centreline vane-island types as shown in figure 3.19. The profiled blades vary from simple straight blades (figure 3.19a), through logarithmic spirals (figure 3.19b) to complex profiles

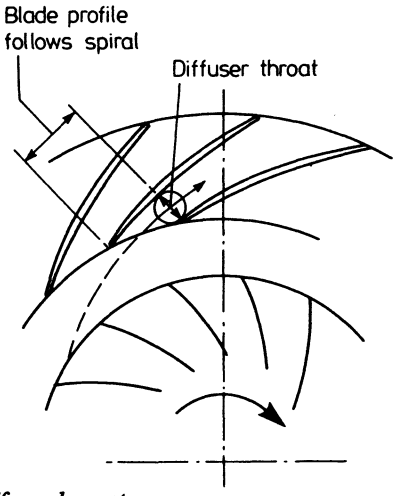

Figure 3.18 *Vaned diffuser layout*

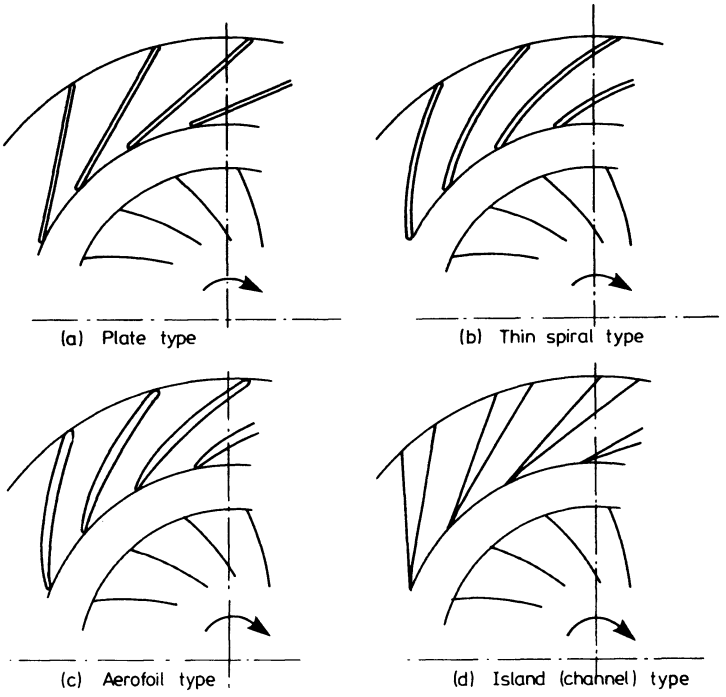

Figure 3.19 *Vaned diffuser types*

based on the results of axial compressor blade cascade tests (figure 3.19c). Channel diffusers (figure 3.19d) are usually used for operation at high Mach numbers and use the principle of straight line diffusion to reduce secondary losses, and to improve compressor stage efficiency.

The purpose of the vanes is to reduce the tangential component of velocity more rapidly than a vaneless space, thereby increasing the rate of diffusion and consequently reducing the length of the flow path required. Thus losses are reduced leading to more efficient diffusion. However, if the mass flow rate through the compressor varies at constant rotational speed, the gas angle at the impeller exit (α_2) will vary. This change will affect the incidence loss at the diffuser vane entry (figure 3.20) and will increase as the air flow angle departs from the vane entry angle. Thus the efficiency of the vaned diffuser, although higher than the vaneless type at its design flow, will degrade more rapidly as flow rate increases or decreases. Hence the efficient operating flow range of the vaned diffuser is limited.

For a simple one-dimensional theoretical treatment of the vaned diffuser, isentropic flow may be assumed along the passage from the throat to the exit and the pressure recovery estimated by using an isentropic diffuser efficiency or a friction loss coefficient, established experimentally.

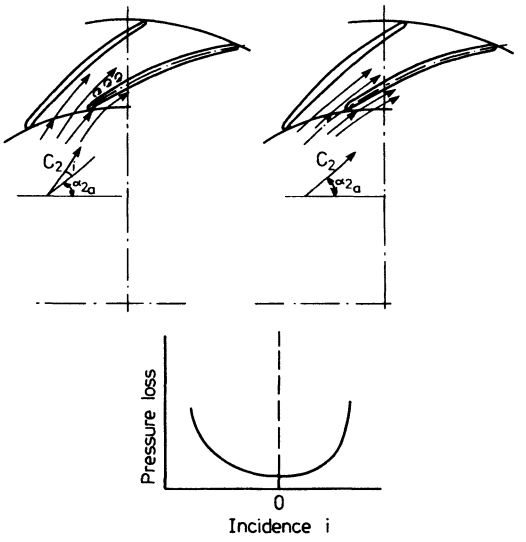

Figure 3.20 *Vaned diffuser incidence losses*

3.3.3.3 The Collector or Volute

The function of the collector or volute (scroll) is simply to collect the diffuser exit flow and to guide it as efficiently as possible to the exit pipe or manifold (sometimes via a conical diffuser to provide additional diffusion), without impeding the effectiveness of the diffuser. Only very mild diffusion can be

achieved in the volute if circumferential pressure distortions at the diffuser exit are to be avoided. If friction in the volute is neglected, then the design may be based on the assumption that the angular momentum of the flow remains constant. It follows that the tangential velocity times the radius is a constant

$$C_\theta \times r = \text{constant} = K$$

Considering the flow ($\dot{V}_\phi$) through an element in the volute at radius r (see figure 3.21) and angular position ϕ, then

$$d\dot{V}_\phi = l\, dr\, C_\theta = \frac{lK}{r} dr$$

It follows, that the total flow through the volute area at angular position ϕ is given by

$$\dot{V}_\phi = \left[\int_{r_{min}}^{r_{max}} \frac{lK}{r} dr \right]_\phi$$

and the total volume flow delivered is

$$\dot{V} = \frac{2\pi}{\phi} \left[\int_{r_{min}}^{r_{max}} \frac{lK}{r} dr \right]_\phi \tag{3.40}$$

assuming equal flow distribution from diffuser exit circumference ($\phi = 0$ to 2π). If A_ϕ is the cross-sectional area of the volute at ϕ and $\bar{r}$ is the radius at the centre of the area of the section

$$\int_{r_{min}}^{r_{max}} \frac{l\, dr}{r} \approx \frac{A_\phi}{\bar{r}}$$

and

$$\frac{A_\phi}{\bar{r}} = \dot{V} \frac{\phi}{2\pi} \frac{l}{K} \tag{3.41}$$

Equation 3.41 can be used to estimate the desired volute area as a function of ϕ. For a constant $\bar{r}$, the volute can be designed with a linear increase of volute cross-sectional area with circumferential angle ϕ from zero to the desired exit area.

Although volutes such as that shown in figure 3.21 are common on many

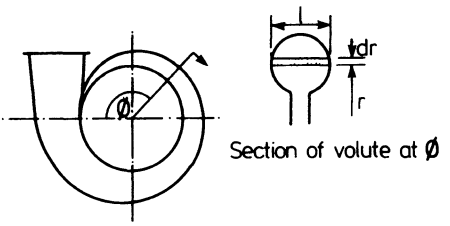

Figure 3.21 *Volute*

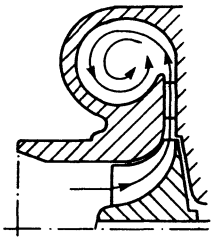

Figure 3.22 *Volute overhang design*

compressors, turbocharger compressors usually use the overhang design shown in figure 3.22, to reduce the over-all diameter of the compressor (usually the bulkiest part of the turbocharger). It has also been claimed that mixing losses at the entry are reduced since they only occur on one side of the diffuser exit.

3.4 One-dimensional flow Analysis with Energy Losses

The elementary theory described in section 3.3 is based on the concept of one-dimensional flow and a knowledge of the isentropic efficiencies of the compressor components (that is, intake, impeller, diffuser, and volute). A simple extension of this one-dimensional approach is to replace the over-all efficiency terms with semi-empirical expressions for the various losses in the system.

The energy losses that occur in the centrifugal compressor may be broadly divided into internal aerodynamic losses (wall friction, flow separation, mixing, secondary flow and shock losses), leakage loss and disc friction loss. Mechanical losses, such as bearing losses and mechanical seal losses due to friction, are additional losses which also occur, but these do not fall within the scope of this chapter.

3.4.1 Inlet Casing Losses

Inlet casing losses may be neglected on small automotive turbocharger compressors with inboard bearings, since the pressure loss through the air filter will dominate, and this should not be attributed to the compressor. However, various flow losses may occur on large turbocharger compressors with outboard bearings, due to poor velocity distribution, viscous drag on the struts that cross the flow path and heat transfer from the compressor casing. Figure 3.23 shows four stages in the development of a compressor inlet, with a gradual reduction in the strut area and improved velocity distribution at the compressor eye. The improvement resulted in a 6 per cent gain in compressor efficiency. Since designs of inlet casings vary a great deal, it is not convenient to attempt to predict the losses theoretically. It is much simpler to apply loss coefficients established from com-

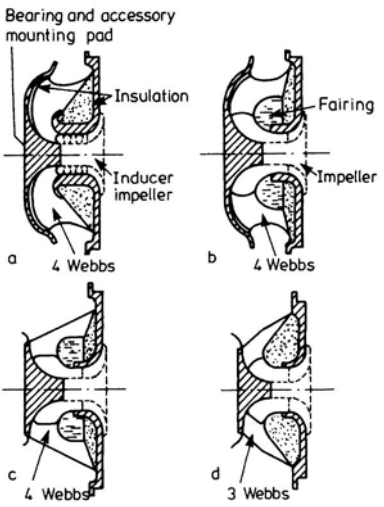

Figure 3.23 *Compressor intake development [10]*

pressors with intakes of very similar geometry. The enthalpy loss of the inlet casing can be expressed as

$$\Delta h_{0-1} = Ch_{0-1} \frac{C_1^2}{2\Delta h_0} \tag{3.42}$$

where Ch_{0-1} is the inlet enthalpy loss coefficient and can be as low as 0.05 for simple axial-type intakes, whereas the more complicated radial inlets with severe meridional contours can have loss coefficients up to 0.25.

Use of inlet guide vanes will inevitably result in some flow loss. The loss coefficient for inlet guide vanes ranges from 0.05 (for a simple plate at zero incidence) up to 0.3 or higher, depending on the shape of the vanes and swirl angle. [11] Although the inlet ducting and the inlet guide vanes are designed to minimise distortions of the flow at the leading edge of the impeller, some distortion is likely owing to geometric constraints and other factors. If possible, these distortions should be accounted for in the impeller design.

3.4.2 Impeller Losses

The function of the impeller is to achieve a high static pressure rise and efficient transfer of energy to the air. Dallenbach [12] divided losses in the impeller into

(1) surface viscous friction losses, modelled on a 'pipe friction' basis;

(2) diffusion and blade loading losses due to boundary layer growth, separation and mixing;

(3) blade incidence loss due to offdesign angles of the gas at the inducer (which is the major source of additional loss under offdesign conditions);

(4) 'shock' losses, associated with sonic flow at the inducer entry under high-pressure ratio operation;

(5) Recirculation losses due to backflow of air along the shroud from the impeller tip to the inducer and flow across the blade tip from the pressure to suction sides of the vanes, due to clearance;

(6) disc friction losses due to shearing of the air between the back face of the impeller and the adjacent stationary surface.

The impeller losses are usually expressed in terms of impeller enthalpy loss coefficients (Ch) related to the relative kinetic energy at the impeller inlet.

$$\Delta h_{1-2} = Ch_{1-2} \frac{W_{t1}^2}{2} \tag{3.43}$$

Although the extension of a one-dimensional analysis to include these loss coefficients has been developed with particular reference to design point operation, the inclusion of the incidence loss term may take some account of offdesign conditions. However, the values of experimental loss coefficients must be used with some caution. Not only will the absolute magnitude of the losses vary from one design to another, but so may their relative magnitudes. For example, clearance losses will be more significant in a small mass-produced compressor than in a larger batch-produced unit. Most manufacturers have established values of the relevant loss coefficients suitable for their own design size and type of compressor. It should also be noted that several designers do not divide the losses up as specified earlier, but frequently group them together, without distinguishing between, say, surface friction and diffusion losses.

Application of the energy and momentum equations to pipe flow with surface friction shows that the loss of useful energy due to friction is given by [1]

$$\Delta h = \tau \frac{4l}{\rho D} = 4f \frac{l}{D} \frac{W_1^2}{2} \tag{3.44}$$

or

$$\Delta h = Ch \frac{l}{D} \frac{W_1^2}{2} \tag{3.45}$$

where Ch = an empirical constant
f = friction factor (for the appropriate mean Reynolds number)
l = mean channel length
D = mean hydraulic channel diameter
W = mean relative velocity at inlet.

At the pressure ratios common on most automotive turbochargers, the diffusion and blade loading losses are usually not the dominant losses. It is therefore convenient to include these losses with the surface friction loss coefficient (Ch) (equation 3.45) being chosen to suit. An advantage of this approach is that it does not imply accurate knowledge of each loss, since in practice it is impossible to separate them experimentally.

Blade incidence losses take account of offdesign velocity triangles at the impeller eye (inducer) causing flow separation and are therefore zero at the design

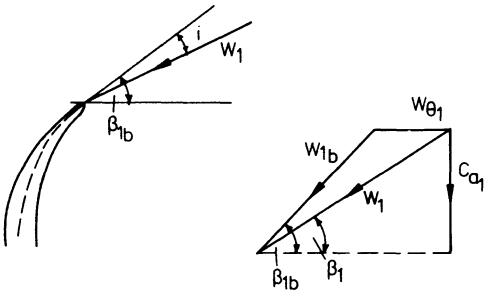

Figure 3.24 *Change in velocity in shock loss theory (NASA) [1]*

point. It is assumed that the fluid approaching a blade row with incidence instantaneously changes its direction at the blade inlet to comply with the blade inlet angle (from β_1 to β_{1b} figure 3.24). W_1 can be resolved into a component W_{1b} in the direction of β_{1b} and a component $W_{\theta 1}$ as shown in figure 3.24. A simple loss model is to assume that the kinetic energy associated with tangential component $W_{\theta 1}$ is destroyed as the fluid adapts to the blade direction. Thus the energy loss due to incidence is given by

$$\Delta h = \frac{W_{\theta 1}^2}{2} \tag{3.46}$$

Another simplified model for estimating the incidence loss has been reported by Whitfield and Wallace [13] and assumes that the gas flow just inside the blades has adapted to the blade angle via a constant pressure process. Figure 3.25 compares the loss coefficients predicted by both these methods for a small high-speed turbocharger compressor, indicating that the differences between them are small.

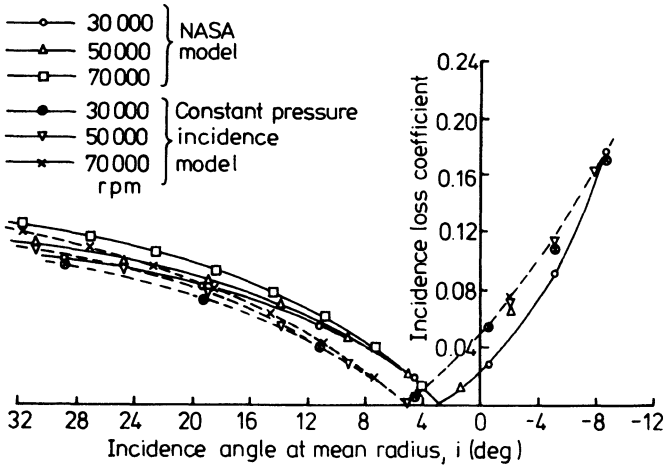

Figure 3.25 *Incidence loss coefficient against incidence angle*

Clearance losses will be a function of the clearance to passage width at the tip. Pampreen [15] showed that the stage efficiency loss increases with clearance, and can be expressed as

$$\Delta\eta_{cl} \approx 0.3(l_{cl}/b_2) \tag{3.47}$$

where l_{cl} = tip axial clearance
b_2 = impeller tip width.

The work input required to reprocess fluid that has been reinjected into the impeller due to pressure gradients existing in the impeller tip region (the impeller back flow loss) depends on the impeller exit Mach number, the exit swirl and the number and proximity of diffuser vanes to the impeller tip. Unfortunately, no theory or mathematical model exists at present to describe the backflow loss, which ideally should be regarded as another aerodynamic design parameter. Coppage *et al.* [16] recommend an empirical correlation for backflow loss

$$\Delta\eta = 0.02\,(C_{\theta 2}/C_{r2})^{1/2}\,Df^2U_2^2 \tag{3.48}$$

where Df is a diffusion factor. Dean and Young [8] suggest a backflow loss of 3 points of stage efficiency as typical. Disc friction losses may be evaluated from the expressions of Balje, [2] Dailey and Nece, [17] or Rodgers and Sapiro.[18]

3.4.3 Diffuser Losses

The loss due to viscous drag on the walls may be modelled by a simple one-dimensional approach with an approximate value of the coefficient of friction. [19, 20] In several early publications, the coefficient of friction was found to vary with radius. In particular, the value seemed to be very high at the entrance to the diffuser, but this was probably the result of ignoring the mixing losses at the impeller tip (section 3.5). If the entry losses are correctly accounted for, reasonable results can be obtained by using a constant value for the coefficient of friction. However, the approach is totally experimental and the value will depend on the size of the compressor, surface roughness and Reynolds number. Current practice is to use values for friction factor (f) between 0.005 and 0.01. [21]

Figure 3.26 illustrates the effect of the coefficient of friction on the diffuser performance under differing flow conditions. The loss in stage efficiency can become very large when the combination of a high tangential component of velocity at entry and a high coefficient of friction coexist. Such a situation might develop due to fouling of the diffuser with poor air filtration or operation in dirty surroundings. These results refer to a small automotive turbocharger with a radial vaneless diffuser.

If the area ratio of a parallel walled diffuser and its flow length are expressed as an equivalent cone angle of a conical diffuser, the result will often exceed the recommended diffusion angle of 8°. For this reason it is sometimes suggested that the diffuser width should reduce with increase in radius. However, experimental test data and theoretical predictions carried out by Watson and Ingham

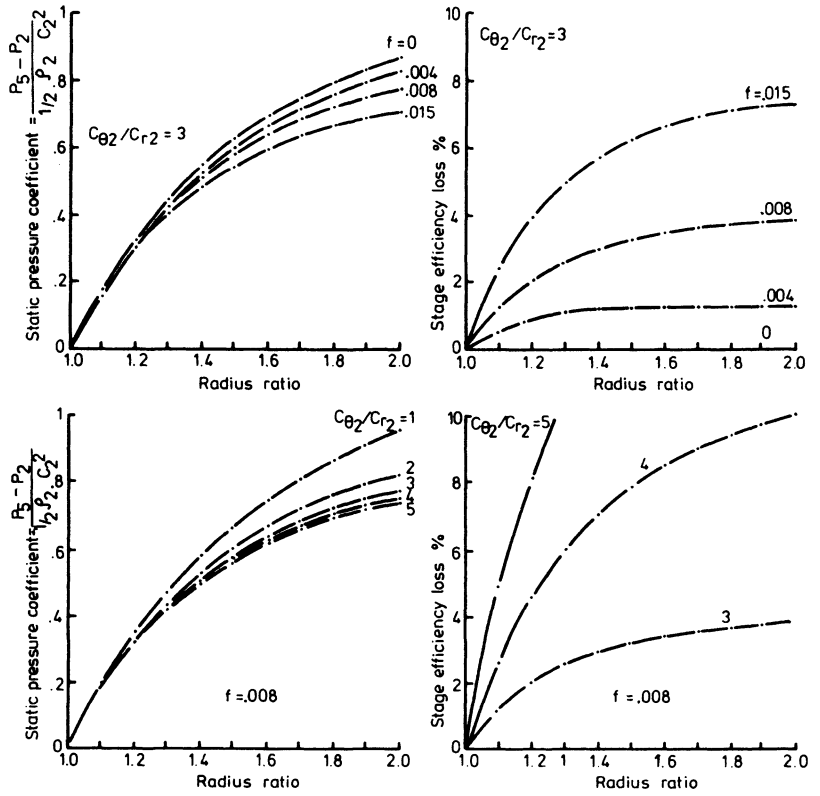

Figure 3.26 *The variation of static pressure and stage efficiency with flow angle and friction factor [19]*

[19] for different widths of parallel diffusers, or even diffusers with increasing width with increase in radius, indicate only marginal changes in pressure recovery.

Losses in vaned diffusers have been modelled using the same incidence loss and pipe friction approach as used in the impeller channel.

3.4.4 Collector Losses

The energy losses in the collector are primarily the result of kinetic energy at the diffuser exit being destroyed due to turbulent mixing as the flow enters the collector. The loss is often assumed to be about half of the kinetic energy leaving the diffuser.

Viscous friction losses at the walls of the scroll can be taken into account approximately. Brown and Bradshaw [22] and Eckert [9] have presented modified forms of equation 3.40 that take into account the effect of compressibility and friction. However, for collectors that are not excessively small,

friction losses and compressibility effects can usually be neglected. Further, as long as the kinetic energy at the outlet from the diffuser is small, there is no need for the diffuser to exactly match the collector.

3.5 Aerodynamic Phenomena and Design Parameters

The one-dimensional approaches described do not adequately highlight key aerodynamic phenomena taking place inside the compressor.

By developing simple flow models for these phenomena and determining the controlling variables for each process, backed by previous experimental data and optimisation studies, it is possible to establish guide lines, or 'design parameters' to aid the designer in minimising losses, thus providing high stage performance. It should be noted that in optimising the stage design, all components in that stage have to be considered simultaneously since the design parameters are interrelated.

The objective of the compressor is to impart high kinetic energy to the air and then decelerate it efficiently with a consequent rise in static pressure. With a viscous fluid, the losses in the impeller or diffuser channels are the result of friction at the walls and boundary layer separation.

As the flow progresses in a diffusing channel, the viscous shearing forces retard the flow near the wall and create a region of lower kinetic energy than the main flow (the boundary layer). If the kinetic energy is too low, the flow in the boundary layer is not able to progress into regions of higher pressure and an eddying region is formed (thickening of the boundary layer) leading to flow separation from the wall (figure 3.27). The kinetic energy in the vortices produced by the separation is lost by dissipation and the stagnating fluid blocks the passage, increasing the velocity in the main flow. The increased velocity raises the friction losses and, together with mixing losses, this leads to a reduction in useful pressure rise.

Thus to achieve high compressor performance, every effort should be made to maximise efficient diffusion in the two principal components, the impeller and the diffuser. The static pressure rise in the impeller is due to the combined effects of the 'centrifugal' pressure rise (largely to the Coriolis component of acceleration) and diffusion of the relative velocity. The centrifugal rise is independent of the flow conditions within the impeller and is attributable only to the change in radius and therefore angular velocity. However, diffusion of the

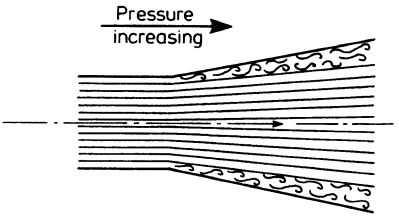

Figure 3.27 *Diffusing flow*

relative velocity in the impeller channels depends on the geometrical shape of the channels and the resulting flow conditions and has a profound effect on both impeller and stage efficiency.

An impeller diffusion parameter can be defined as the Mach number ratio (MR_{imp}) at inlet to outlet

$$MR_{imp} = M_{t1}/M_{rel_2} \tag{3.49}$$

where M_{t1} = the inlet relative Mach number at inducer tip

M_{rel_2} = the impeller exit relative Mach number.

and a diffuser pressure-recovery coefficient (CPR) as

$$CPR = \frac{P_5 - P_2}{P_{02} - P_2} \tag{3.50}$$

the ratio of static pressure rise across the diffuser divided by the inlet equivalent dynamic head.

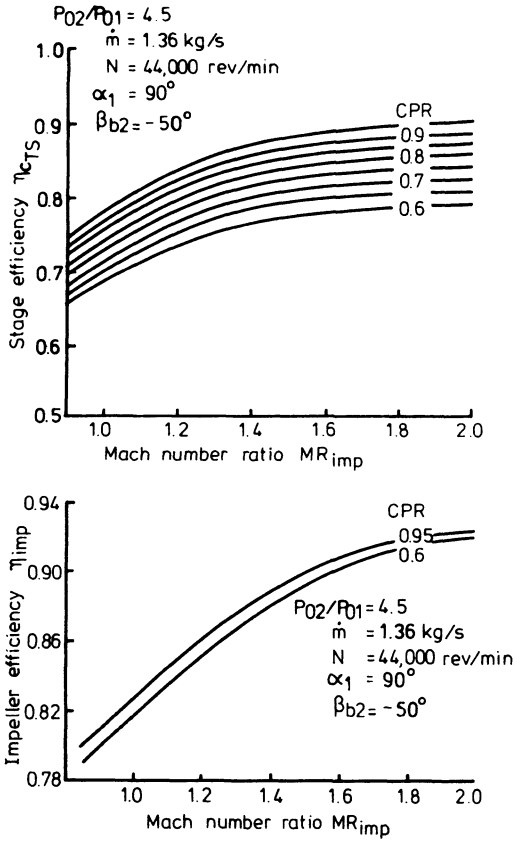

Figure 3.28 *Influence of impeller and diffuser recovery performance on impeller and stage efficiency [21]*

The degradation in stage efficiency due to inadequate diffusion in the diffuser can be expressed as

$$\Delta\eta \propto (1 - CPR) \left[\frac{C_2^2}{2(h_{02} - h_{01})} \right] \tag{3.51}$$

since the term in square brackets represents the kinetic energy at diffuser inlet, expressed as a fraction of the total stage energy input. Likewise, the degradation in stage efficiency due to inadequate diffusion in the impeller is given by

$$\Delta\eta \propto (1/MR_{imp}^2) \left[\frac{W_1^2}{2(h_{02} - h_{01})} \right] \tag{3.52}$$

where the term in square brackets again represents the kinetic energy available for diffusion at the compressor inlet, expressed as a fraction of the total stage energy input. Figure 3.28 shows the effect of the diffusion parameters on impeller and stage efficiency.

Small changes in the Mach number ratio (MR_{imp}) have a large effect on stage efficiency at low values of MR_{imp} with the effect diminishing at higher values. The improvement in stage efficiency with diffuser pressure recovery ratio is more uniform, about 0.1 increase in *CPR* gives 3 per cent point increase in stage efficiency.

3.5.1 Impeller

The impeller inducer plays an important role in determining the level of efficient diffusion which will be attained.

The leading edge of the inducer requires very careful design consideration. The flow arrives at the leading edge with a relative Mach number in the high subsonic or, in the case of pressure ratios above 3 or 4:1. the supersonic range (at the impeller tip). Further, the relative Mach number and incidence flow angle vary along the inducer leading edge from high values at the eye tip to much lower values at the eye hub. Consideration must be given to avoiding shock formation which can lead to boundary layer separation. Thus, approach Mach numbers exceeding 1.2 should be avoided at any section of the inducer. [23]

To achieve maximum diffusion, one strategy in designing the inducer is to diffuse the flow to the separation limit before the impeller passage turns towards the radial direction. This leads to long axial inducers.

To ensure low impeller losses the inducer eye is sized to minimise the relative eye tip Mach number as discussed under one-dimensional analysis. Further, the aim of inducer optimisation is not only to design for minimum Mach number at entry but also to ensure wide operating flow range. Therefore, the inducer eye hub to impeller eye tip ratio, the number of blades and the incidence angle (in the range from 5 to 8°) are chosen to avoid inducer stall (due to boundary layer separation) at low speeds, while simultaneously preventing premature inducer choke at high speeds. Figure 3.29 shows impeller efficiencies as a function of inducer tip flow angle and peripheral speed, indicating optimum efficiency for a 9° incidence angle.

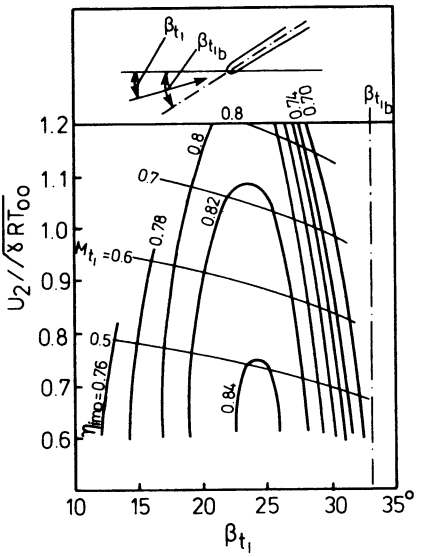

Figure 3.29 *Impeller efficiency against eye tip incidence angle [6]*

The inducer eye hub to impeller tip ratio has a relatively small effect on the relative inlet Mach number. Nevertheless, the eye hub diameter should be small to minimise inlet flow distortion with an open axial intake. The eye hub to impeller tip ratio for centrifugal compressors varies from 0.2 to 0.4, with the lower range for turbocharger compressors – the actual value being dependent on whether the bearings are inboard or outboard. Of course, the minimum is also dependent on the shaft diameter, dictated by stress and vibration considerations, and impeller casting or machining limitations. In addition, a compromise between a low eye hub to eye tip ratio and the required number of blades may be imposed by manufacturing limitations.

The choice of the eye tip to impeller tip ratio requires careful consideration, since it determines the shroud curvature of the impeller and hence influences the impeller diffusion capability. Experience indicates an optimum ratio around 0.5 for high pressure ratio operation (between 3:1 to 4:1). For moderate pressure ratios (below 2.5:1) values of eye tip to impeller tip ratios of 0.6 to 0.85 are used to maintain compactness of compressor design without serious degradation in compressor efficiency.

The post-inducer blading of the impeller is designed to direct the flow radially and to produce additional diffusion. However, secondary flows cause low-momentum fluids to accumulate on the blade suction and impeller shroud surfaces.

In the inducer, secondary flows are generated by blade channel curvature similar to the flow in curved pipes. Turning of the flow from the axial to radial direction generates secondary flows, which drive low-momentum fluid to the shroud making the boundary layer more prone to separation. Once the flow has separated on the shroud side, the separated flow region in the meridional plane

rapidly grows towards the hub surface and towards the impeller tip (see figure 3.30).

In the radial part of the impeller the inbalance between the local (blade-to-blade) pressure gradient sets up a secondary flow, which drives low-momentum fluid on to the blade suction side, creating a separation zone towards the impeller tip (figure 3.31). Separation in both the meridional plane and the blade-to-blade plane creates a 'wake' region at the impeller tip, of very low velocity fluid relative to the flow elsewhere. Thus a two-zone 'jet/wake' model has been pro-

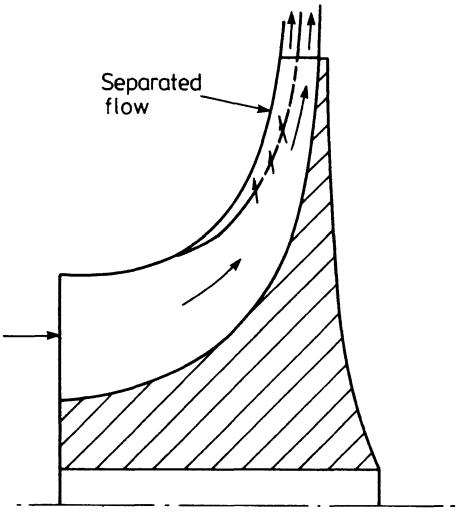

Figure 3.30 *Meridional plane, flow separation*

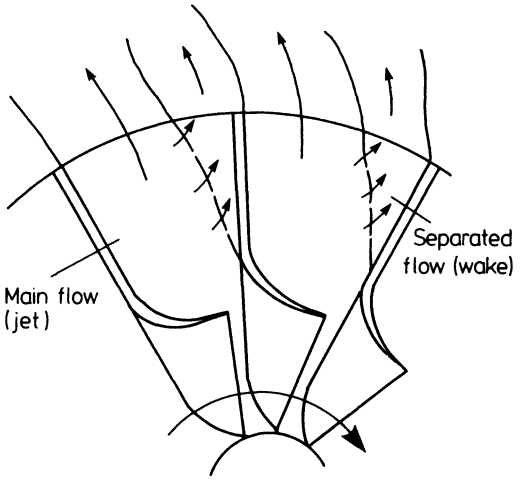

Figure 3.31 *Blade-to-blade flow separation*

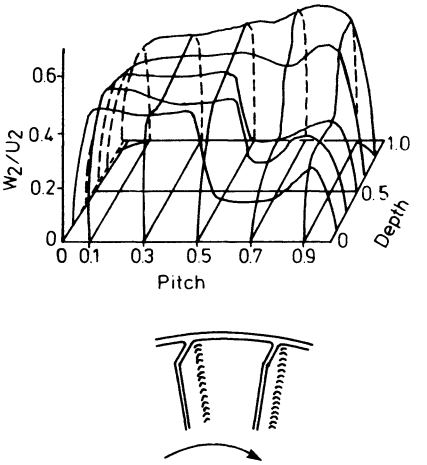

Figure 3.32 *Radial velocity distribution at impeller tip [25]*

posed [9, 24] which has subsequently been confirmed by experimental test data using hot wire anemometry and laser velocimetry measurements. [24, 25, 26]

Laser velocimetry measurements of the relative velocity distribution at a radially vaned impeller tip are shown in figure 3.32 and indicate that the 'wake' constitutes about 15 per cent of the mass flow and occupies approximately 35 per cent of the impeller tip exit area for this impeller at these test conditions.

This loss of kinetic energy, which is no longer available for diffusion, represents an internal flow irreversibility and hence reduces impeller performance. At the impeller exit the jet and wake slowly mix out to an axisymmetric flow. The loss associated with this mixing process can be treated as being analogous to a sudden expansion mixing loss in a duct. [8] Since the mixing loss is a function of how fully the exit area is filled with wake flow, the loss can be related to the diffusion parameter (MR_{imp}) and the kinetic energy at the impeller inlet. Expressed as an efficiency degradation this becomes

$$\Delta\eta \propto \frac{1}{(MR_{imp}{}^2)} \frac{W_1{}^2}{2\Delta h_{oc}} \tag{3.53}$$

3.5.2 Impeller Design Parameters

Over the years of development of the radial flow compressor, a number of design parameters affecting or describing the geometry of the impeller have been established to guide the designer. Two types of design parameter can be distinguished, aerodynamic and geometric.

Some of the *aerodynamic design parameters* have been discussed already: the inducer incidence angle, the impeller clearance (equation 3.47), the diffusion

parameter (equation 3.52) and the proportion of the through flow entrained into the impeller wake.

Since impeller efficiency depends to a great extent on its diffusion capability, it is important to maximise impeller diffusion. To achieve this some designers follow the simple rule of gradual deceleration of the meridional relative channel velocity (W) such that the impeller tip value (C_{r2}) is equal to the axial component of the inlet velocity at the impeller eye (that is, $C_{r2} = C_{a1}$).

Dean [8] has compared actual to ideal diffusion in numerous compressors and found that good performing impellers fall within quite a narrow band (figure 3.33). MR_{imp_s} is the inlet to outlet Mach number ratio of ideal isentropic flow filling the complete impeller passage and therefore reduces to the inlet to outlet area ratio in incompressible flow. The actual Mach number ratio (MR_{imp}, equation 3.53) is calculated from the relative Mach number at the eye tip and the exit relative Mach number in a jet occupying an assumed 70 to 80 per cent of the actual impeller exit area A_2 where

$$A_2 = \pi D_2 b_2 \sin \beta_{2b} - th_b Z b_2 \tag{3.54}$$

where th_b = average impeller blade thickness at the tip
Z = number of blades
b_2 = impeller tip width.

Thus figure 3.33 is a design guide for the diffusion achievable in good impellers.

An important aerodynamic design parameter is the impeller exit swirl $C_{\theta 2}/C_{r2}$. The choice of exit swirl influences both the impeller and diffuser geometry, since it will be shown that the impeller exit (hence diffuser inlet) axial depth is directly proportional to exit swirl. From the relationships

$$U_2 = \pi D_2 N$$

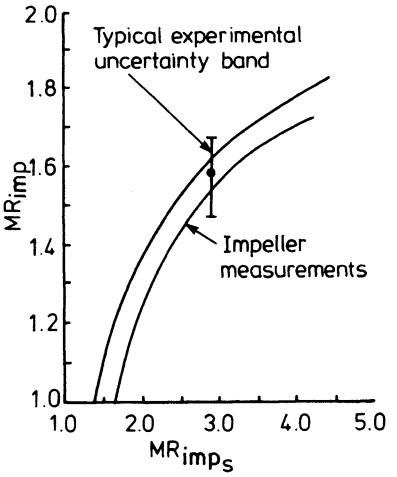

Figure 3.33 *Interpretation of impeller's* MR_{imp}/MR_{imp_s} *characteristic [8]*

and

$$\Delta T_{0c} = \frac{T_{00}}{\eta_{cTT}} \left[(P_{05}/P_{00})^{(\gamma-1)/\gamma} - 1 \right] = \frac{U_2 C_{\theta 2}}{c_p}$$

(from equations 3.15, 3.16, and 3.19) and the continuity equation (neglecting impeller blade thickness at the tip)

$$b_2 = \frac{\dot{m}}{\rho_2 C_{r2} \pi D_2} = \frac{\dot{m}N}{\rho_2 (C_{r2}/C_{\theta 2}) C_{\theta 2} U_2} = \frac{\dot{m}N}{\rho_2 \dfrac{C_{r2}}{C_{\theta 2}} \dfrac{c_p T_{00}}{\eta_{cTT}} [(P_{05}/P_{00})^{(\gamma-1)/\gamma} - 1]}$$

thus

$$b_2 = \frac{\dot{m}N \eta_{cTT} (\gamma - 1)}{T_{00} \gamma R \left[(P_{05}/P_{00})^{(\gamma-1)/\gamma} - 1 \right] \rho_2} \frac{C_{\theta 2}}{C_{r2}} \tag{3.55}$$

Normally the values for $C_{\theta 2}/C_{r2}$ are chosen between 2 and 3 for vaneless diffusers and between 3 and 4 for vaned diffusers.

Two important geometric design parameters are the exit blade backsweep angle (β_{2b}) and the number of impeller blades (Z).

The demand for high-efficiency turbocharger compressors with a wide mass flow range has led to the reintroduction of the blade backsweep in the impeller tip region.

Blade backsweep reduces the diffuser inlet kinetic energy ($C_2^2/2$), by reducing $C_{\theta 2}$. Since

$$\tfrac{1}{2} C_2^2 = \tfrac{1}{2} (C_{\theta 2}^2 + C_{r2}^2)$$

and from figure 3.34

$$C_{\theta 2} = U_2 - C_{r2} \cot \beta_2$$

This improves diffuser performance due to lower inlet losses and improved

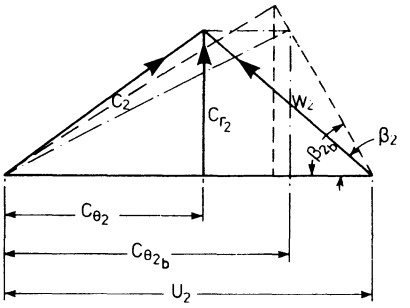

— — — velocity triangle with perfect flow guidance
— · — · — correction for sudden expansion
——— mixed-out velocity triangle

Figure 3.34 *Impeller (mixed-out) velocity triangle*

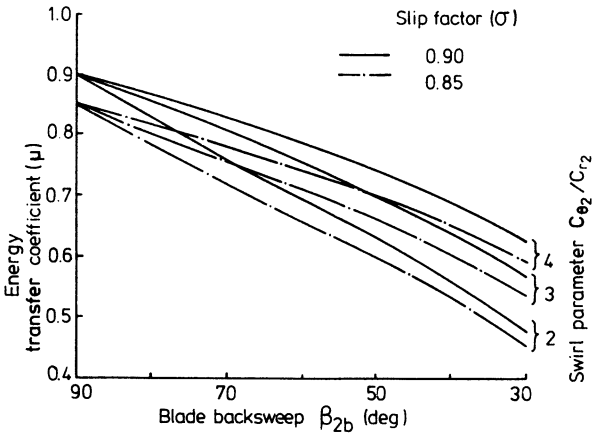

Figure 3.35 *Energy transfer coefficient as function of blade backsweep and swirl parameter [5]*

pressure recovery. The penalty is a reduction in the impeller energy transfer (equation 3.8), hence pressure ratio.

Figure 3.35 shows the fall off in energy transfer coefficient (μ) with increase in blade backsweep (β_{2b}). This must be compensated for by increasing impeller tip speed although this leads to higher impeller stresses. Backsweep also introduces additional blade root bending stresses near the impeller tip due to the centrifugal force acting perpendicular to the blade. Thus the degree of backsweep is a compromise between the performance advantages and mechanical disadvantages.

The choice of the number of blades (Z) is another important design parameter. A small number of blades leads to high pressure gradients (high 'blade loading') and boundary layer separation in the impeller channels. A large number of blades increases the value of the slip factor but leads to higher surface frictional losses. The number of impeller blades is normally chosen on the basis of providing adequate blade-to-blade loading control in the post-inducer portion. However, the optimum number of blades may be restricted due to inducer entry blockage and/or manufacturing limitations. For example, a small automotive turbocharger impeller is limited in its number of inducer blades due to casting requirements. However the problem can be solved by using splitter blades, and so avoiding inducer blockage problems, while allowing a sufficient number of exit blades to provide the desired blade loading control and high slip factor.

3.5.3 Diffuser

The fluid flow pattern existing in the region between the impeller tip and the entry to the vaneless or vaned diffuser is very complex. Since the flow losses in the diffuser are partly affected by the diffuser entry conditions (which is the

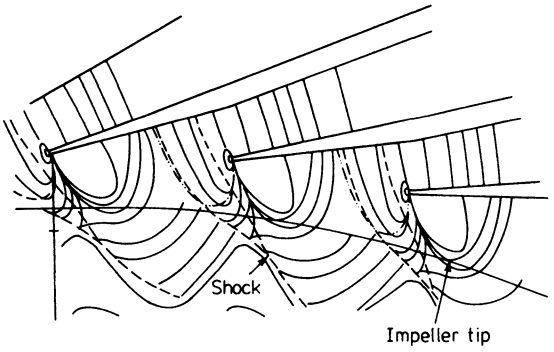

Figure 3.36 *Isobarics of measured pressure field of vaned diffuser entry [8]*

result of the undesirable velocity distribution leaving the impeller) it is important to separate this effect.

The velocity leaving an impeller channel will be higher on the pressure side of the blade than on the suction side, and higher on the impeller back (hub) than on the shroud side, due to recirculation and flow separation effects (figure 3.32). As the impeller rotates, the radial components of velocity entering the diffuser will be varying from that at the suction side of the blade to that of the pressure side and from the shroud to the impeller back. It follows that the flow entering the diffuser is highly unsteady, and non-uniform. Further, at sufficiently high pressure ratios the flow will be highly swirling, transonic and turbulent with shock waves (vaned diffusers), and boundary layer separation effects will be significant.

Figure 3.36 presents isobars from pressure field measurements at a vaned diffuser entry of a high pressure ratio compressor.

3.5.3.1 Vaneless Diffuser

The vaneless diffuser, which in its simplest form is defined by two parallel walls, is widely used in turbochargers due to the broad operating range, low cost and good tolerance to erosion and fouling. Its disadvantage, however, is much lower pressure recovery compared with a vaned diffuser of the same diameter.

The flow losses in the vaneless diffuser are due to the entry effects and viscous drag on the walls. The high and low velocity areas at the exit from the impeller tend to mix out as the air flow progresses through the diffuser. This process is accompanied by a pressure or efficiency loss (equation 3.53). Johnston and Dean [21] considered the high and low-velocity areas as a uniform jet and wake area both of constant velocity, as shown in figure 3.37. By proposing a sudden expansion at an impeller exit control volume, the resultant pressure loss was calculated, assuming zero velocity in the wake. Figure 3.38, calculated on this basis, shows the loss in over-all stage efficiency expressed as a fraction of the total passage area filled by the wake. Clearly, if the wake fills more than 40 per

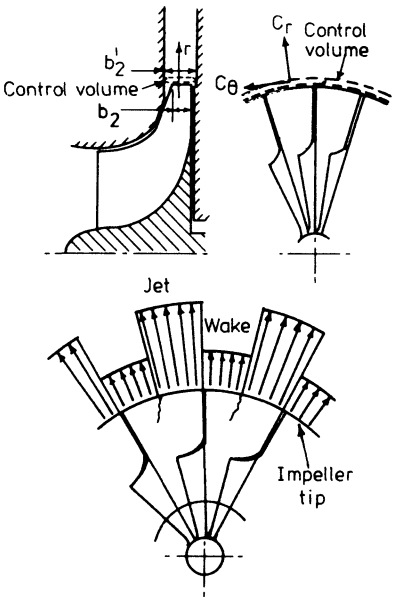

Figure 3.37 *Sudden expansion analysis: control volume and jet/wake flow pattern [19]*

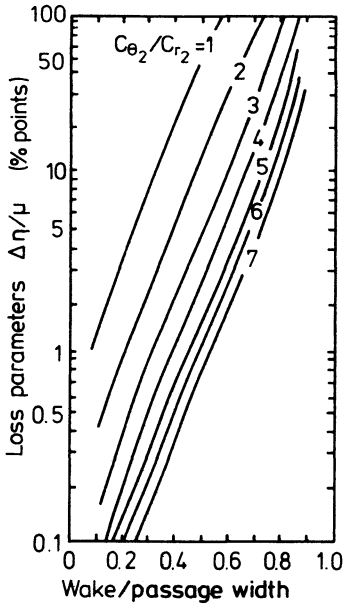

Figure 3.38 *Impeller discharge mixing loss for incompressible flow [21]*

cent of the passage, the loss becomes significantly large. This can occur if the impeller is poorly designed with a small number of impeller blades and if early boundary layer separation occurs in the impeller passage.

The flow conditions leaving the control volume of the sudden expansion model (the mixed-out data), can be considered as the entry conditions for steady flow treatment of the vaneless diffuser.

Eckert [9] provides a correction formula for the estimation of the slip factor for the mixed-out flow conditions at the impeller exit.

$$\sigma = \frac{1}{1 + \pi/\{(1-\epsilon)2Z\left(1 - \frac{D_{t1}}{D_2}\right)\sin\beta_{2b}\}} \tag{3.56}$$

where $\epsilon = 0.2$ for backsweep-type impellers and 0.3 for radial vaned impellers.

3.5.3.2 Diffuser Design Parameters

Four important design parameters can be identified when designing radial vaneless diffusers: the area ratio (radius ratio with parallel walls), the inlet swirl parameter ($C_{\theta 2}/C_{r2}$), the inlet mach number (M_2) and a friction width parameter (fr_2/b_2) where f is the wall friction factor. The optimum design can be achieved by minimising M_2 and the friction width parameter, and maximising area ratio. The loss due to viscous drag on the walls may be modelled by a simple one-dimensional approach with an approximate value of the coefficient of friction, as described in section 3.4.

Dean and Young [8] have shown that an optimum value of $C_{\theta 2}/C_{r2} = 2$ exists for incompressible flow.

Fluid flow in radial vaneless diffuser has a strong influence on compressor surge. Jansen [27] investigated the onset of rotating stall in a vaneless diffuser, while Senoo and Kinoshita [28] considered boundary layer flow reversal. Both found that stable vaneless diffuser operation could be maintained if the mixed-out swirl parameter ($C_{\theta 2}/C_{r2}$) did not exceed 4.

Large mass flow range (choke/surge) has been obtained by reducing vaneless diffuser width from diffuser inlet to discharge, to progressively reduce $C_{\theta 2}/C_{r2}$, but design point performance deteriorates due to the increase in absolute velocities.

Vaned Diffusers

Vaned diffusers are used for turbocharger compressors when high pressure ratio and stage efficiency are required. They offer a 2 to 7 per cent points increase [29] in efficiency compared with vaneless diffusers, but exhibit a much lower flow range.

Like vaneless diffusers, the entry conditions have a strong effect on the pressure recovery of the vaned diffuser.

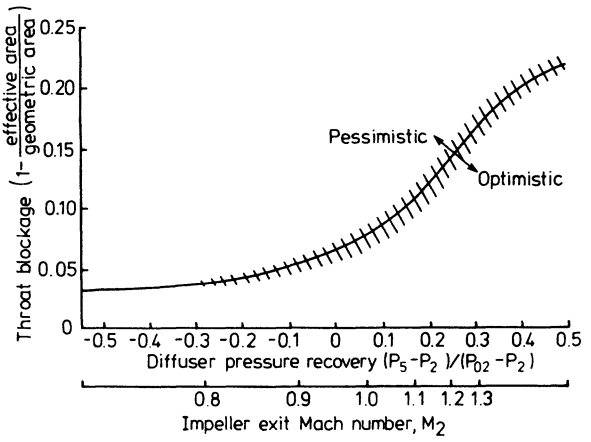

Figure 3.39 *Diffuser throat blockage against pressure rise coefficient, from impeller tip to diffuser throat [8]*

The flow in the semi-vaneless space between the impeller exit and diffuser throat is highly unsteady. Because true modelling of the flow presents great difficulties, an alternative approach [29] is to use empirical relationships and assume pseudo-potential flow from the impeller exit (mixed-out) state to the diffuser throat. A number of diffuser parameters such as throat blockage (effective throat area/geometric throat area), diffuser stagnation pressure loss [$(P_{02} - P_{05})/(P_{02} - P_2)$, varying from 0 to 0.15] and diffuser inlet pressure recovery coefficient [$CPR_{2-5} = (P_5 - P_2)/(P_{02} - P_2)$] have been established to guide the designer.

A simple correlation, suggested by Kenny [30] between throat blockage, diffuser pressure recovery coefficient and impeller exit Mach number is shown in figure 3.39 for an assumed diffuser throat Mach number $M_4 = 0.95$.

The diffuser throat conditions are normally estimated by first selecting the throat Mach number (M_4) to meet the required mass flow rate or to maximise the diffuser recovery. The actual geometric diffuser throat size can be estimated from the required mass flow rate, fluid conditions at the throat and blockage taken from figure 3.39.

A number of different types of vaned diffuser have been designed for centrifugal compressors (figure 3.19). A detailed study and design guidance for efficient, straight centre-line (vane-island) diffusers for high-pressure operation (above 5:1) is given by Sovran and Klomp [31], Runstadler and Dolan [32] and Dean and Young. [8] They found that the important parameters governing the performance of the diffuser are the throat blockage, the diffuser area ratio (outlet to inlet), Mach number (M_4) and the diffuser throat aspect ratio AS_4 = (width/depth at throat). Figure 3.40 shows the influence of the throat blockage and aspect ratio on the over-all diffuser pressure recovery for a throat Mach number $M_4 = 1.0$, indicating an optimum aspect ratio $AS_4 = 1$.

Experimental data, based on flow tests with uniform inlet conditions (figure 3.41), indicate that the optimum straight centreline diffuser configuration

corresponds to an area ratio of 3.5 and cone angle of 8°. Figure 3.42 shows an optimum value of 0.06 for the throat blockage. At high Mach numbers Sagi and Johnston [33] have shown, that the straight centreline diffusers perform much better than the curved types as illustrated in figure 3.43. The inferior performance

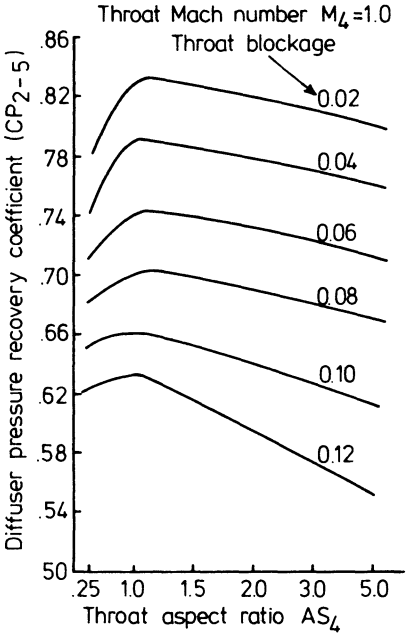

Figure 3.40 *Maximum pressure recovery of straight centreline, two-dimensional diffusers against throat aspect ratio and blockage [8]*

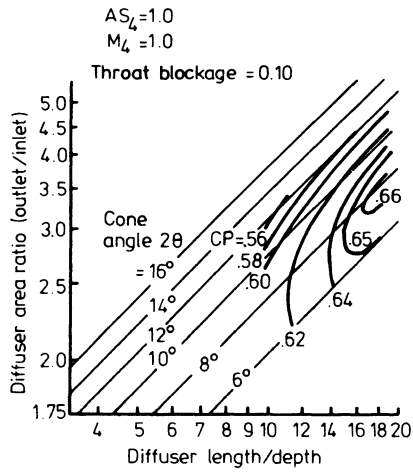

Figure 3.41 *Straight channel, two-dimensional diffuser performance [8]*

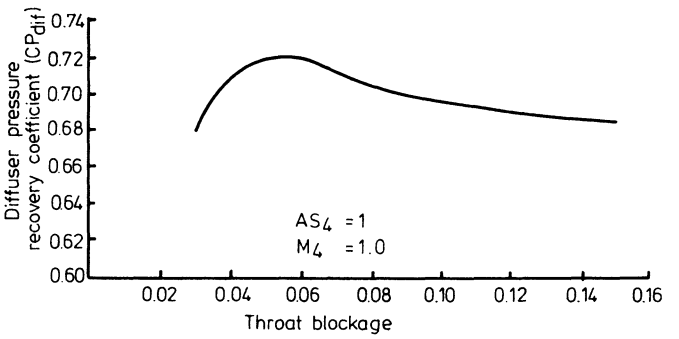

Figure 3.42 *Total diffuser pressure recovery against blockage [8]*

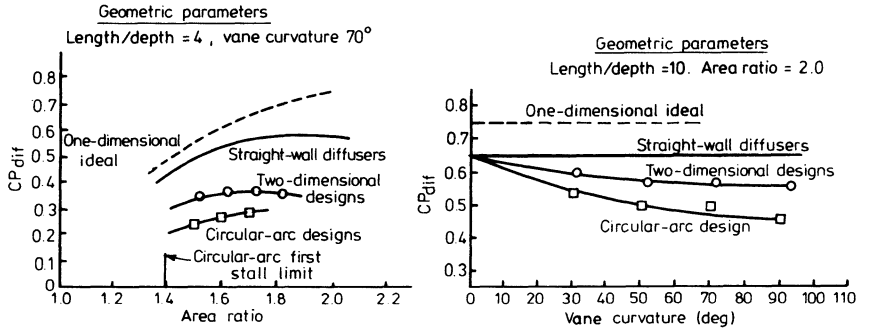

Figure 3.43 *Comparison of curved and straight centreline channel diffusers [29]*

of the curved vane diffuser can be explained by the presence of normal pressure gradients and secondary flow effects due to blade curvature.

Studies of two-dimensional curved vane diffusers (thin spiral and airfoil cascade) designed using data from axial flow compressor cascade tests are reported by Rodgers [34] and Pampreen. [35] The profile of the axial blade is modified into part of a circular cascade by using conformal transformation (figure 3.44). Although the method of transformation cannot strictly be justified for compressible flow, the method has been successfully used for turbochargers with moderate pressure ratios. The correlation of loss data for an axial cascade and the airfoil diffuser obtained by transformation is shown in figure 3.45. Figure 3.46 compares the performance of the thin spiral and aerofoil cascade vaned diffusers, showing better efficiency and pressure recovery with the latter. The thin spiral vane diffuser also has a smaller stall-free range at higher Mach number due to the rather long blade guide at the inlet to the throat.

As important as the basic losses in the diffuser channel at the design point are the losses resulting from the changes in the incidence angle as the mass flow

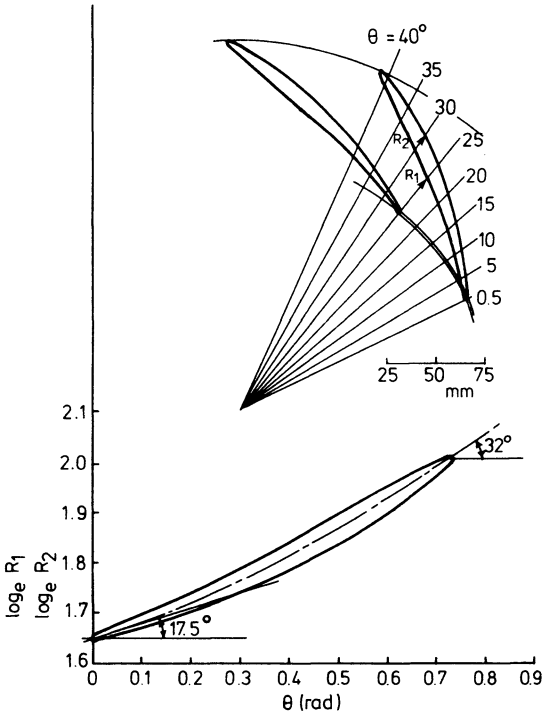

Figure 3.44 *Radial diffuser transformation [34]*

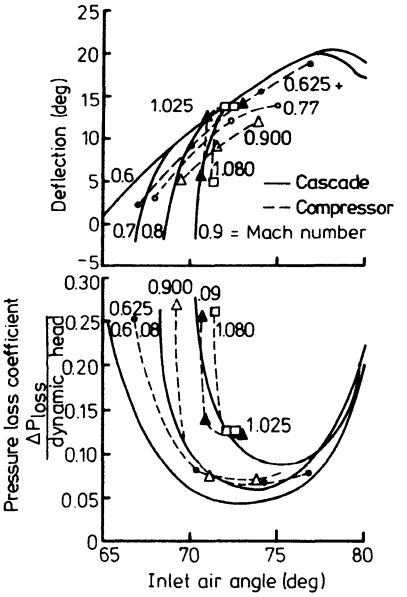

Figure 3.45 *Airfoil diffuser characteristics: compressor against cascade tests [36]*

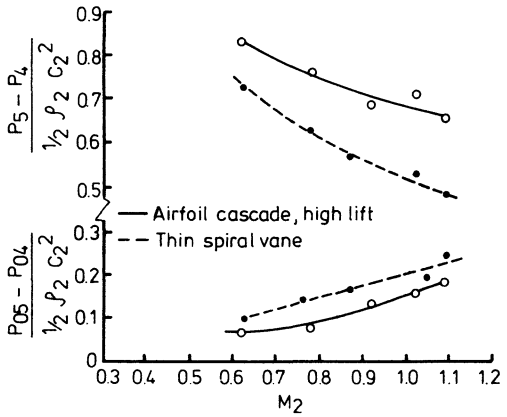

Figure 3.46 *Performance of thin vane and airfoil cascade diffusers [36]*

rate alters (that is, offdesign conditions). The high losses that result are shown in figure 3.45.

For example, at a relatively low diffuser inlet Mach number (0.6), a 5° change in gas angle, above or below the optimum, more than doubles the flow losses. At higher pressure ratios, corresponding to a Mach number greater than 1.0, the vaned diffuser becomes even more sensitive to changes in mass flow rate, and exhibits larger pressure losses for the same incidence angles.

3.6 Three-dimensional Flow Models

The one-dimensional approach to the design of a centrifugal compressor is a useful but limited technique. The actual flow in the impeller and diffuser, as already described, is extremely complex and is not properly understood today, although progress is being made. However, useful attempts have been made to predict what is happening to the flow inside impellers and diffusers.

Although the flow pattern is three-dimensional, the common technique is to reduce it to two two-dimensional analyses. A quasi-three-dimensional picture can be assembled by combining the two solutions.

These techniques usually neglect the direct effects of viscosity and time-dependent flows. Although some attempt can be made to account for irreversibilities, the technique will not give the true flow pattern occurring right through the compressor. However, provided that their limitations are well understood, the methods do provide useful information beyond that available from the simple one-dimensional analysis.

3.6.1 Flow in the Impeller

A quasi-three-dimensional flow picture may be assembled from the axisymmetric hub-to-shroud (meridional) analysis combined with a blade-to-blade solution as

shown in figures 3.47, 3.48 and 3.49. In practice, the hub-to-shroud analysis is sometimes used alone, since changes in the relative velocity are considerably greater in this plane and hence it is the more informative of the two analyses. The basis of the three-dimensional flow solutions was pioneered by NACA in the 1950s although it was largely based on the streamline curvature principles developed by Stodola [37] in 1927. Although the basic vector equations for inviscid relative flow in a rotating system are well known, extraction of the component equations, specification of the boundary conditions and the numerical computation are complex. The details of the mathematical computation are beyond the scope of this book and the reader is referred to references 4, 12, 37 and 38.

The basis of the hub-to-shroud solution is to estimate the positions of the streamline (figure 3.50) by two orthogonal parameters (m and n), which are functions of axial distance (x), radius (r) and slope of curvature (θ). When the impeller rotates, these streamlines form surfaces, which completely contain a

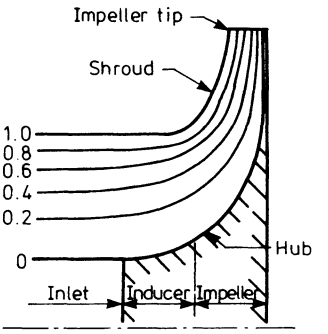

Figure 3.47 *Streamlines in meridional plane for 'axial-symmetry' solutions*

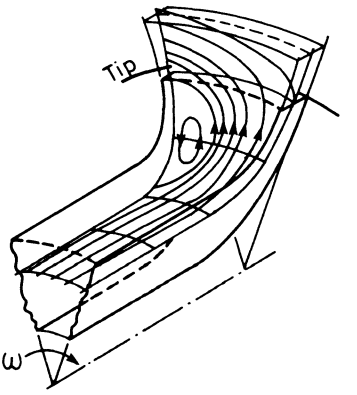

Figure 3.48 *Relative streamlines in 'blade-to-blade' solution*

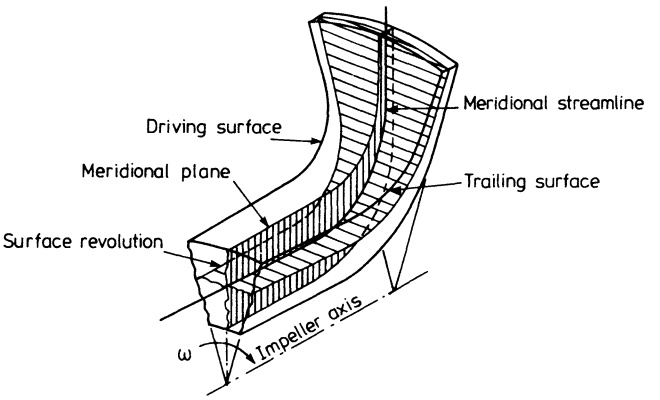

Figure 3.49 *Quasi-three-dimensional flow*

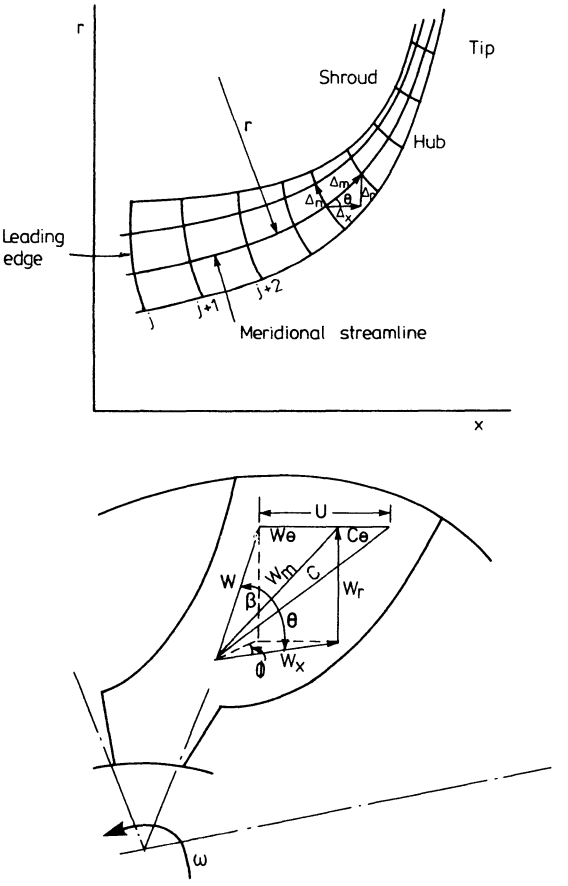

Figure 3.50 *Streamline curvature prediction*

section of the total flow. The continuity equation can then be satisfied by the conditions that the mass flow rate through annular passages or streamtubes is constant. The equations of motion are expressed in terms of m and n, and a solution is obtained by using the estimated streamlines and iterating to find closer values.

Typical flow profiles are shown in figure 3.51 (hub-to-shroud) and figure 3.52 (blade-to-blade) for a radial vaned impeller.

A review of the application of the NACA work to compressor design is given by Kramer *et al.* [39]

This quasi-three-dimensional flow analysis applies only to the inviscid flow (that is, to the flow outside the boundary layer). Attempts have been made to take account of boundary layer effects, in the analysis by Dallenbach [12] and Balje. [2] The presence of a stable boundary layer can be considered by specifying an assumed flow blockage distribution and an energy loss, usually accounted for as a viscous friction loss. However, a far more significant loss, particularly at offdesign conditions, occurs when the boundary layer separates, and it is this loss that is difficult to predict. Dallenbach proposed a much simplified model based on a two-dimensional boundary model with a separation criterion. However, the theoretical analysis should not be applied to the radial part of the impeller where an adverse pressure gradient exists. Balje attempted to predict the boundary layer thickness and separation in the presence of an adverse pressure gradient, but the work was not wholly successful since major simplifications were necess-

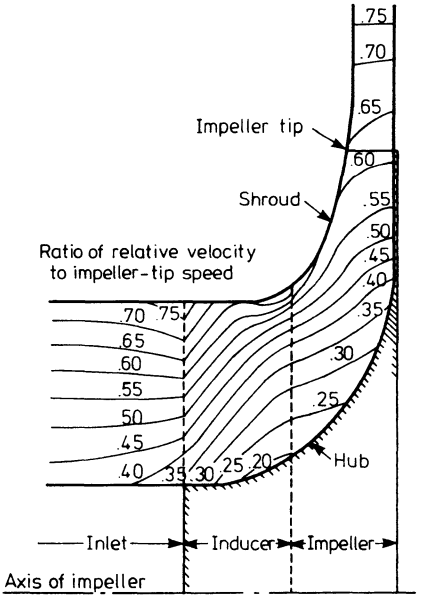

Figure 3.51 *Lines of constant relative velocity in meridional plane for axial-symmetry solution: incompressible flow [4]*

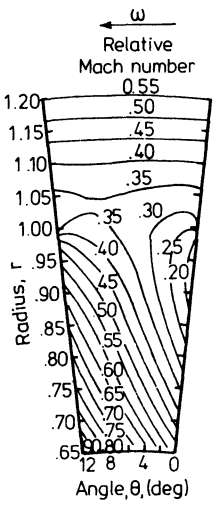

Figure 3.52 *Lines of constant relative Mach numbers for flow in 'blade-to-blade' solution [4]*

ary. Thus potential flow analysis should only be applied to predict predominant trends rather than establishing accurate numerical values. [2]

The jet/wake flow model illustrates shortcomings of the inviscid potential flow method since the relative velocity distribution from blade to blade at the impeller tip is opposite to that expected or measured.

The quasi-three-dimensional models used in conjunction with a blockage factor can realistically model the flow up to the point of boundary layer separation. Secondly, and perhaps more important, the methods can be used to establish a relative velocity profile along the channel at the hub and shroud on the suction and pressure sides of the impeller blades. Although these velocity profiles are only valid up to the point of boundary layer separation, they can indicate that a large deceleration of flow or a very high local velocity could be the cause of boundary layer separation. The diagrams can therefore be useful in tidying up the passage shape to produce relative velocity profiles that avoid excessive deceleration. Although the diagrams are presented in coordinates of relative velocity or relative Mach number against meridional passage length, they are often referred to as blade loading diagrams, since the pressure distribution on the blades is related to the relative velocity.

Figure 3.53 shows some possible blade loading diagrams for a radial vaned impeller. It is reasonable to assume that separation of the boundary layer is most likely to occur on the suction side of the blade on the shroud.

In figure 3.53a the average relative velocity decreases linearly from impeller eye to impeller tip, but this results in a high peak relative velocity on the suction side at the shroud in the inducer portion, where separation is likely to occur.

This can be reduced by modifying the channel (figure 3.53b) to provide at first a rapid deceleration of the average relative velocity in the inducer. However, this results in an excessively rapid deceleration and reacceleration of the flow

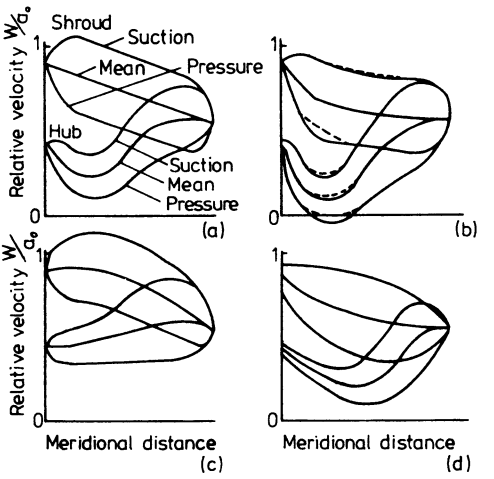

Figure 3.53 *Possible impeller blade loading distribution at shroud and hub of radial vaned impellers [12]*

at the hub, causing the boundary layer to thicken and probably separate. Figure 3.53d shows an 'ideal' diffusion and loading distribution. A moderate deceleration of the average velocity at the shroud leads to gradual deceleration on the suction side and still tolerable deceleration on the pressure side. Similarly, on the hub side there is a gradual change over from diffusion to reacceleration avoiding the occurrence of flow reversal. In principle, the approach is to rapidly decelerate the flow in the inducer portion where the boundary layers are thin, with loading and diffusion easing off in the radial part of the impeller where the boundary layers are thick or separated. This often leads to impellers with long inducers and rapid blade-turning at the downstream portion of the inducer. Blade back-sweep is used to reduce the large blade-to-blade loading in the radial position of the impeller. Very little work has been published on potential flow analysis including the jet/wake model. Figure 3.54 shows the predicted relative Mach

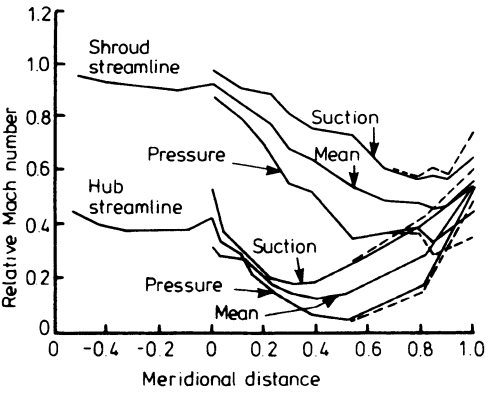

Figure 3.54 *Predicted relative Mach number distributions with jet/wake model [29]*

number distributions based on the assumption that, in the jet/wake model, the wake is treated as an additional blockage.

3.6.2 Flow in the Vaneless Diffuser

Although attempts have been made to analyse three-dimensional flow in the diffuser, none has yet been completely successful.

The combination of three-dimensional boundary layers and the unsteady inlet flow resulting from jet/wake flow at the impeller exit, produces an unsteady flow that is extremely difficult to model. Figure 3.55 illustrates the radial velocity distribution entering the vaneless diffuser of a small automotive turbocharger running at its design speed of 70 000 rev/min. The impeller passage width (blade-to-blade) at the tip has been indicated to highlight the low and high velocity regions.

Recorded mean velocity and flow angle profiles (figure 3.56) clearly show that the flow is far from one-dimensional. It is also apparent that the flow is

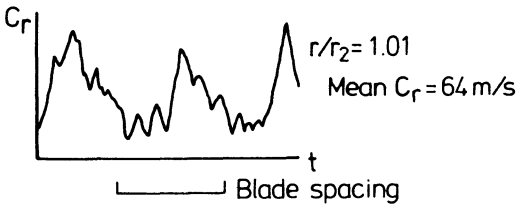

Figure 3.55 *Typical transient velocity traces at diffuser entry*

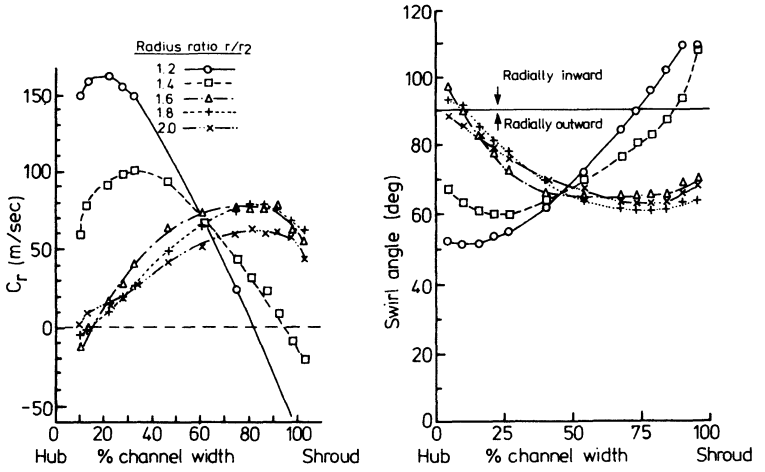

Figure 3.56 *Impeller discharge velocity survey, across passage depth at various radial positions [40]*

highly skewed and has actually separated and reversed on the shroud side at low radius ratios and stagnated on the hub side at high radius ratios. When the mass flow rate through the compressor is reduced, the flow angle of the air leaving the impeller will reduce, since the radial component of velocity reduces. This aggravates the flow reversal shown in figure 3.56 and is a contributory cause of surge in radial flow compressors with vaneless diffusers, limiting the flow range.

3.6.3 Flow in the Vaned Diffuser

Simplified vane-to-vane analysis, derived from impeller flow theory, may be applied to the vaned diffuser channel together with an approximate allowance for boundary layer growth. Emerson and Horlock [41] describe a method of adapting Stanitz blade-to-blade analysis [4] for this purpose. Nevertheless, the variation of velocity from vane-to-vane must be specified or assumed. In practice it has been observed that significant secondary flows develop along the sidewalls of the thin spiral and flat-plate-type diffusers, that cannot be predicted with this technique. Since, in general, the theoretical models cannot handle the highly complex three-dimensional time-dependent viscous flow at the diffuser entry, the designer is forced to use the one-dimensional approach and design parameters based on experimental development work.

3.7 Compressor Characteristics and Flow Range

The performance of the radial flow compressor is defined by curves showing the relationship between pressure ratio, isentropic compressor efficiency and pseudo-non-dimensional mass flow rate and speed (chapter 2).

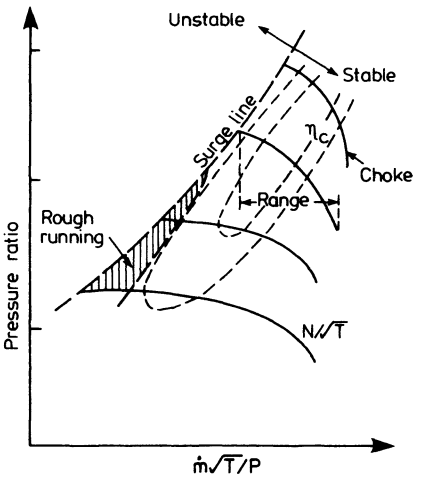

Figure 3.57 *Typical compressor characteristic*

A typical compressor characteristic, showing constant speed parameters ($N/\sqrt{T}$) and isentropic efficiency against the mass flow rate parameter ($\dot{m}\sqrt{T}/P$) and compression ratio is given in figure 3.57. In chapter 2, the important operating area on the compressor map was presented as the stable operating zone separated from the unstable area on the left by the surge line and on the right by the choke conditions. In the specific application of the compressor to a turbocharger, in particular for truck or automotive-type engines requiring a wide range of operation, the achievement of a wide flow range between surge and choke is as important as high efficiency.

Compressor flow range is commonly defined as the differences between the surge and choke line at a given speed, expressed as a percentage of the maximum flow rate (choke).

Before discussing surge and choke in more detail it is constructive to understand the shape of the constant speed line. If a compressor with a radial vaned impeller is run at constant speed and the mass flow rate through it is controlled by means of a delivery valve, the shape of the constant speed parameter ($N/\sqrt{T}$) on the pressure ratio/mass flow rate curve might be expected to be that shown in figure 3.58. This shape can be understood from the rather simplified but realistic analysis as shown in figure 3.58. The specific energy transfer will remain roughly constant as mass flow rate increases or reduces, since it is a function of tip speed and slip factor (equation 3.12). Frictional losses in the impeller and diffuser passages must increase with mass flow rate due to increased velocities. The other principal loss will be due to incidence effects as the air flow angle at the impeller eye and diffuser inlet deviates from the blade angle. Incidence loss will be least at the design point, but will increase quite rapidly as the mass flow rate (and hence flow angle) increases or decreases. If the incidence and frictional losses are both subtracted from the energy input, the curve shown in figure 3.58 is obtained. The point at which the energy transfer is greatest will occur at a mass flow rate somewhat less than might be expected from the incidence analysis above. In practice, surge prevents most of the curve between A and C being obtained. Point A represents a steady condition for zero mass flow rate at a pressure ratio generated by centrifugal force.

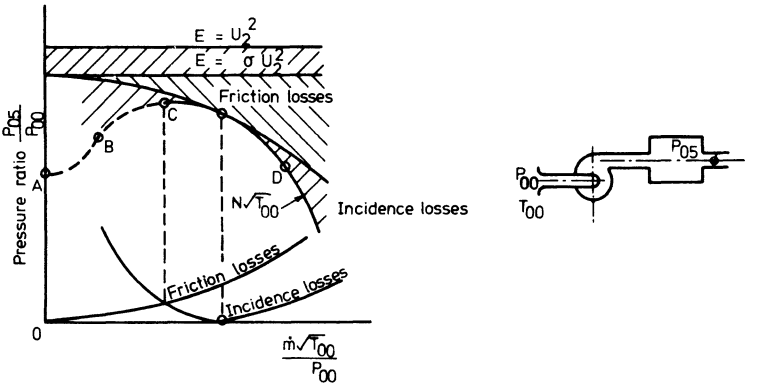

Figure 3.58 *Derivation of the shape of the constant speed line*

3.7.1 Compressor Instability

In a diffusing flow, or flow across an aerofoil, there is the possibility that the flow at the wall (the boundary layer) is retarded so severely that it can no longer follow the wall surface. In other words, the kinetic energy in the boundary layer is not sufficient to overcome the adverse pressure gradient leading to flow separation at the wall, described as a local stall. Similarly the effect of secondary flows, for example, in bend ducts, can cause flow separation (stall) leading to flow instability interfering with the diffusion process.

The instabilities occurring in the centrifugal compressor can be identified as (1) the component stall, (2) stage instability or stage stall and (3) system instability described as surge.

When the mass flow rate through the compressor is gradually reduced at constant speed, a breakdown in the flow process occurs leading to instability. At the inducer inlet, as the mass flow rate decreases, the axial component of the absolute velocity decreases, thus increasing the incidence angle of the air approacing the leading edge of the inducer. Beyond a critical incidence angle the flow can no longer adhere to the suction side of the inducer blade (figure 3.59). Flow separation from the surface creates a stall condition subsequently encouraging reversal of flow. Inducer stall may contribute to surge, particularly at high pressure ratios, but can exist at a nominally stable operating condition.

If there is non-uniformity in the approach flow to the inducer or in the geometry of the channels between the inducer blades, breakdown in the flow in one channel (for example 'b', figure 3.60) causes air to be deflected in such a way that channel 'a' receives fluid at an increased incidence angle. Channel 'a' then stalls, causing reduction of incidence angle to channel 'b' restoring normal flow. Thus the stall passes from one channel to the next channel. This rotating stall may or may not lead to stage instability, but can introduce aerodynamically induced vibrations resulting in increased noise level.

The flow separation occurring on the suction side of the blade in the radial portion of the impeller (figures 3.30 and 3.31) leading to the formation of a

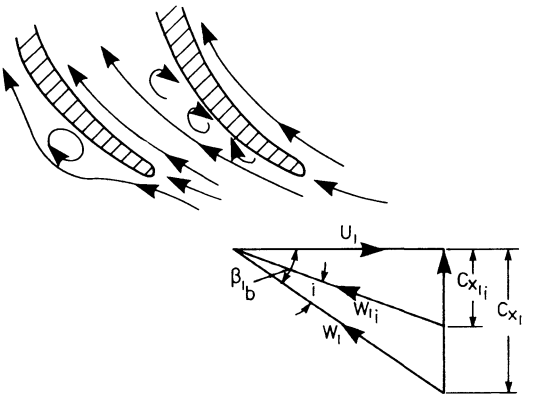

Figure 3.59 *Flow separation in the inducer*

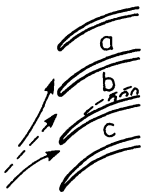

Figure 3.60 *Rotating stall schematic*

wake, can be described as impeller stall. Use of high blade backsweep can reduce the wake region and provide more stable operation of the diffuser.

The most common separation of flow in the vaneless diffuser is caused by the local reversal of flow normally occurring on the shroud side of the diffuser wall (figure 3.56) and is very much influenced by the flow leaving the impeller. To conserve angular momentum, the flow in a parallel walled vaneless diffuser tries to maintain a constant flow angle (equation 3.35). However, due to compressibility and viscosity effects the streamlines close to the wall have less kinetic energy and follow a path of much reduced spiral angle until eventually they are swept back towards the impeller. This backflow is a diffuser stall, which may be sufficient to trigger stage stall, but can be avoided by choosing larger impeller exit flow angles (that is, $C_{\theta 2}/C_{r2}$ less than 4). However, efforts to hold a reasonable impeller exit flow angle inevitably result in a very narrow tip width and high associated losses. Hence efficiency is traded for stable flow range. A high slip factor will reduce tip speed at a given pressure ratio which is an incentive to use a large number of impeller blades. However, the blockage effect at the impeller eye and manufacturing techniques limit the number of blades, especially on small impellers.

It becomes more difficult to obtain a wide flow range at high pressure ratios since the impeller tip speed increases. At compressor pressure ratios above 4:1, the flow leaving the impeller becomes supersonic, losses can increase and the flow range narrows substantially. Fortunately, the vaneless diffuser can maintain shock-free diffusion with a supersonic inlet velocity (due to symmetry, the shock could only exist in a circular ring, yet the velocity normal to the expected shock, remains subsonic) and it is therefore often used to diffuse a supersonic flow so that it enters the following vaned diffuser subsonically. A vaneless diffuser could be used alone at high pressure ratios, but the flow path required would result in an excessively large outer diameter and high frictional losses. Similar to inducer stall, vaned diffuser stall occurs when the air incidence angle at the diffuser vane inlet reaches a critical value. Also disruption of the flow at entry to the diffuser due to the non-uniformity of the flow leaving the impeller can induce rotating stall of the diffuser. If the number of diffuser vanes is less than the number of impeller blades, the effect that non-uniform flow leaving the impeller has on the diffuser is reduced and hence the flow range should improve. It is also the suction side of the leading edge of the diffuser vane that principally effects instability and some local contouring to alter the static pressure gradient can influence stability.

Normally the compressor can operate quite stably, although some of its components may be in a mode of stall. However, there comes a point, when operating at constant speed with ever-reduced mass flow rates, that causes a critical component or a combination of a number of components to stall, introducing a strong reversal of flow. The stage cannot continue to operate stably and the phenomenon is described as stage stall.

When the disturbance (stage stall) becomes periodic and grows to a large magnitude, the system (comprising the compressor and installation) can become self-exciting. This phenomenon is then a system instability described as surge.

In other words, surge is a self-excitation of a dynamic system with the stall of the stage as the driving force. During surging a noisy and often violent flow process can occur causing cyclic periods of backflow through the whole compressor. Operation in surge not only drastically reduces the performance of the compressor but can damage the compressor and its installation.

The surge frequency and amplitude are dictated by the size of the volumes of the installation before and after the compressor, their flow characteristics and compressor speed.

Surge tends to occur where the constant speed parameter (plotted on the pressure ratio against mass flow rate curve) becomes horizontal

$$\frac{dPR}{d\dot{m}} = 0$$

as indicated by point C in figure 3.58. Consider a compressor connected between two constant pressure reservoirs with a delivery valve and operating at point D on the negative slope of the speed parameter (figure 3.58). Now imagine a sudden disturbance occurs, such as a sudden partial closure of the delivery valve temporarily reducing the flow. This results in an increase in the delivery pressure from the compressor and a reduction in compressor flow. The former encourages a larger mass flow rate through the delivery valve, reducing compressor delivery pressure and increasing compressor flow. This is therefore self-compensating and an inherently stable system. However, if the compressor were operating at point C, a reduction in mass flow rate would result in reduced compressor delivery pressure reducing flow through the delivery valve, moving the operating point further and further to the left. Eventually the mass flow reduction will be so great that the pressure upstream of the delivery valve (for example, inlet manifold of an engine) falls below the compressor delivery pressure (whose minimum is governed by the centrifugal pressure rise at zero flow). Mass flow will then increase until the system is drawn back to operating point C, and the whole cycle will repeat. This analysis implies that surge will occur when the slope of the constant speed parameter curve is positive (that is, to the left of point C), but this is not necessarily so. For example, if the flow characteristic of the throttling system has a slope which is greater than the positive slope of the compressor speed parameter (figure 5.61) then as mass flow rate is reduced, the fall-off in compressor delivery pressure is less than that of the system and hence the flow system stabilises immediately. Surge would occur only at a point when the positive slope of the speed parameter exceeds that of the delivery system. Usually the flow characteristic of the inlet manifold system has only a small positive slope, hence surge occurs when the slope of the compressor speed

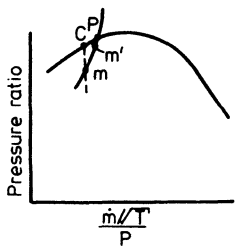

Figure 3.61 *Effect of slope of throttle characteristic [1]*

characteristic is zero or slightly positive (with vaneless diffusers) or slightly negative (with vaned diffusers), due to their smaller flow range.

Blade backsweep influences the shape of the speed characteristic and therefore the surge margin. Equation 3.7a shows that the specific energy transfer increases as radial velocity (C_{r2}), and hence mass flow rate, reduce, provided that $\beta_2 < 90°$. Thus backsweep forces pressure ratio to increase as mass flow reduces, relative to a purely radial impeller, moving the surge point to a lower flow rate. This is a much simplified analysis of surge but it does show that the surge line is governed by compressor and inlet system phenomena.

When the turbocharger compressor is connected to an engine inlet manifold, the volume of the manifold is often not sufficient to damp out the pressure fluctuations arising from periodic suction strokes of the pistons. As a result, even though the mean mass flow rate might lie to the right of a surge line obtained under steady flow compressor calibration tests, the minimum mass flow rate (at the peak of the pulse) may cause surge to develop. Thus fluctuating pressure in the receiver can cause the surge line to shift towards larger mass flow rates (to the right).

The quantitative influence of the pulsating back pressure on the compressor surge was investigated on an experimental compressor by Jenny. [42] By introducing sinusoidal pressure pulsations of variable amplitude (ΔP) and frequency ($f = 1/\Delta t$) the test showed that the compressor surge occurred at larger mass flow rates than with constant back pressure. Figure 3.62 indicates an increasing

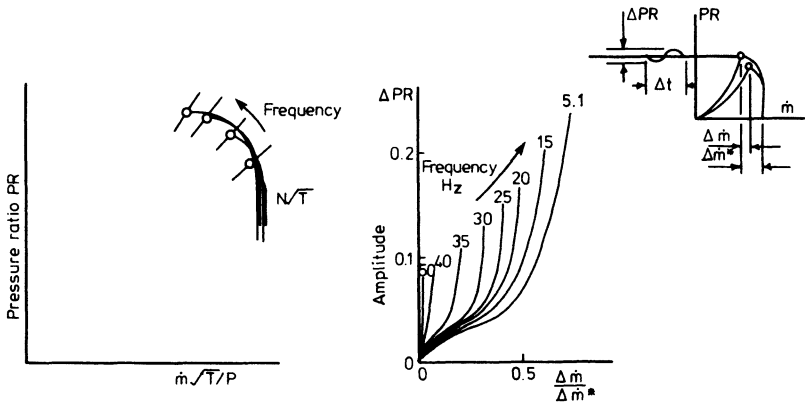

Figure 3.62 *Effect of unstable conditions in the receiver on surge point [42]*

shift of the surge point towards larger mass flows with reduction in pulse frequency and increase in pressure amplitude. This implies that for engines with a small number of cylinders and low rotational speeds (large marine engines) larger safety margins from surge (recorded under steady flow conditions) have to be used.

When two or more turbochargers are connected to a common inlet manifold, there is a danger of one compressor pushing the other into surge due to variation in energy supplied to the turbines or small differences in their compressor speed characteristics. For this reason the inlet manifolds on engines with multi-turbocharger installations are sometimes kept separate.

3.7.2 Choking

The other limit to the flow range is due to choking, when the flow reaches the velocity of sound at some cross-section. In centrifugal compressors choking normally occurs at the throat of the impeller eye (inducer) or at the entry to a vaneless diffuser or at the throat of a vaned diffuser. When choking occurs at the impeller eye it is the relative velocity (W_1) which equals the speed of sound. Assuming one-dimensional isentropic flow, Dixon [43] derived the relationship for choking mass flow rate for a swirl-free impeller as

$$\dot{m} = A_1 \rho_{01} a_{01} \left[\frac{2 + (\gamma - 1)\, U_1^2 / a_{01}^2}{\gamma + 1} \right]^{(\gamma+1)/2(\gamma-1)} \tag{3.57}$$

(where $\rho_{01} = P_{01}/(RT_{01})$ is the inlet stagnation density

$a_{01} = \sqrt{(\gamma R T_{01})}$ is the inlet stagnation sonic velocity

A_1 = effective inducer inlet throat area

showing that it is dependent on blade speed. Thus the impeller can accept a greater limiting mass flow rate at higher rotational speeds.

If choking occurs in a stationary component, for example in the throat of a vaned diffuser, then the mass flow rate is a product of the effective diffuser throat area, throat density and local sonic velocity

$$\dot{m} = A_4 \rho_4 a_4 = A_4 \frac{P_{04}}{\sqrt{T_{04}}} \sqrt{\left[\frac{\gamma}{R} \left(\frac{2}{\gamma + 1} \right)^{(\gamma+1)/(\gamma-1)} \right]} \tag{3.58}$$

Since the diffuser inlet pressure (P_2) and temperature (T_2) are a function of impeller tip speed, it can be shown that the choking flow in the diffuser throat is also impeller tip speed dependent, [43] namely

$$\dot{m} = A_4 \rho_{01} a_{01} \frac{[1 + (\gamma - 1)\, \eta_{\text{imp}} \sigma U_2^2 / a_{01}^2]}{[1 + (\gamma - 1) \sigma U_2^2 / a_{01}^2]^{\frac{1}{2}}} \left(\frac{2}{\gamma + 1} \right)^{(\gamma+1)/2(\gamma-1)} \tag{3.59}$$

Figure 3.63 indicates that the choking mass flow rate at the diffuser increases less rapidly with rotational speed (U_2) than the choking mass flow rate of the inducer. In order to choke the vaneless diffuser the radial component of the

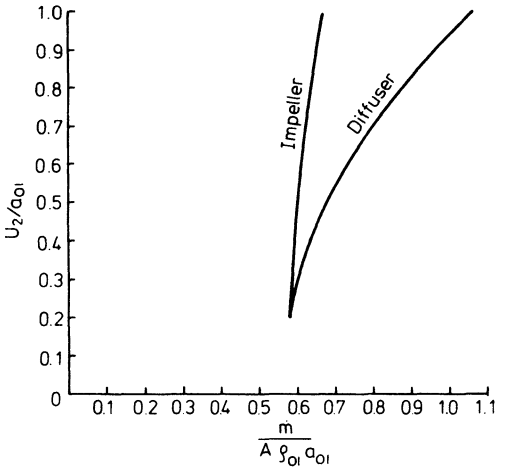

Figure 3.63 *Choking mass flow rate for impeller and diffuser*

absolute velocity entering the diffuser must reach sonic velocity. If the flow stagnation conditions are known at the inlet of the vaneless diffuser, then simple one-dimensional flow calculations can predict the choked vaneless diffuser mass flow rate.

3.7.3 Flow Range and Variable Geometry

An important factor that effects flow range of the centrifugal compressor is the choice of diffuser – vaneless or vaned – and the operating pressure level. The flow range of a vaned diffuser is narrower than that of a vaneless diffuser as shown in figure 3.64. This is mainly attributable to diffuser vane stalling when the air entry angle departs significantly from its design value.

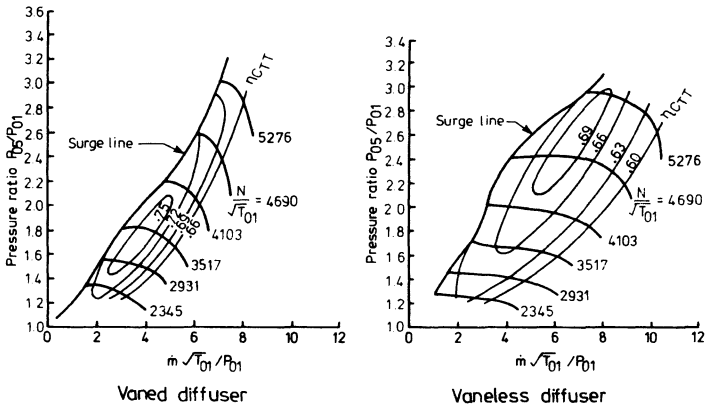

Figure 3.64 *Vaneless and vaned diffuser compressor characteristics [44]*

Since the choke line of the vaneless diffuser is limited by the impeller tip exit area, the only remaining way of extending flow range is to move the surge line to the left on the compressor map (towards smaller mass flow rates). Rapid reduction of vaneless diffuser width increases the radial component of the absolute velocity, delaying stall. This influences the mass flow rate at surge and at choke, but usually the effect of the former exceeds that of the latter. A more uniform flow distribution at the impeller exit can also improve stable operation of the diffuser. Blade backsweep may delay separation of the flow on the critical suction side of the impeller blade passage and hence raise compressor efficiency and produce a larger compressor mass flow range.

Variable geometry is another way of increasing the flow range of the centrifugal compressor. Pre-whirl vanes or diffuser vanes, whose angles can be altered while the compressor is running can both be used to increase flow range.

Variable inlet guide vanes present a simple solution to increasing flow range by varying the air incidence angle at the inducer inlet (figure 3.65). However, the negative inlet swirl reduces the work input, and a higher impeller tip speed is required for a given pressure ratio. Reduction of inlet Mach number at the impeller eye, with variable inlet guide vanes, improves impeller efficiency but this is partially offset by increased diffuser losses due to higher diffuser inlet Mach number.

Although more complex to arrange in practice, variable angle diffuser vanes are another method of approach, since it is the diffuser that usually limits the flow range. By adjusting the vane angle the surge and choke line of the compressor can be moved over a large mass flow range (figure 3.66).

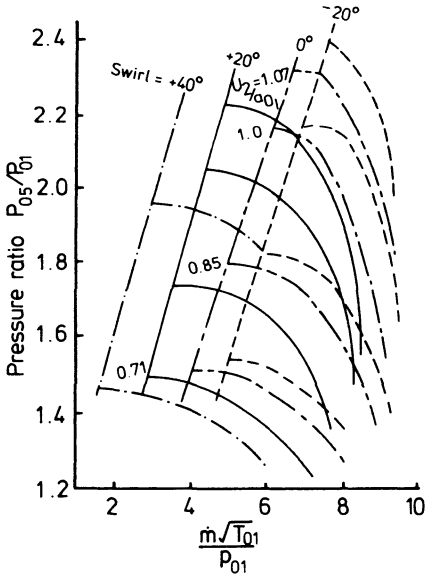

Figure 3.65 *Compressor characteristics with variable inlet guide vanes (vaneless diffuser) [45]*

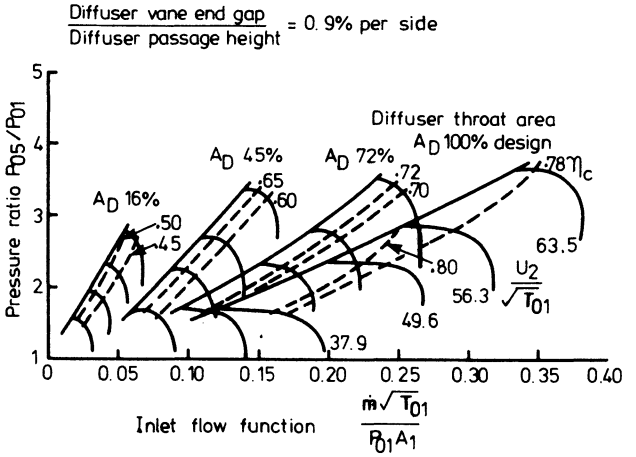

Figure 3.66 *Compressor characteristics with variable diffuser vanes [46]*

Use of variable geometry does introduce a complication in compressor design and manufacture since in addition to the movable compressor components themselves a control mechanism is required.

3.7.4 Compressor Trimming

From the economic point of view it is desirable to produce a single turbocharger unit that can cover a wide range of engine sizes and hence a large range of mass flow rates. To adapt a basic design of compressor to cover a large mass flow range involves changing the effective choking areas of the impeller and diffuser. There are four principal ways in which this is done

(1) varying the angle of the inlet guide vanes (provided guide vanes are fitted), figure 3.67a;

(2) narrowing the flow passage depth from compressor inlet to discharge by means of appropriate streamline cut, figure 3.67b;

(3) varying the inlet angle of the diffuser vanes, figure 3.67c;

(4) radial cropping of the diffuser vanes, figure 3.67d.

Method 2 is a very popular system conveniently adopted for the small automotive-type turbochargers. The effect of the flow cut is to shift the compressor surge and choke line to lower mass flow rates without appreciable loss in efficiency. Normally the compressor is cast with the passage depth oversize to allow machining for at least three impeller sizes and corresponding compressor casings. It should be noted that for a severe cut, clearance penalties and friction effects are increased and over-all stage performance is diminished.

Method 3 is very common with industrial and marine engine turbochargers

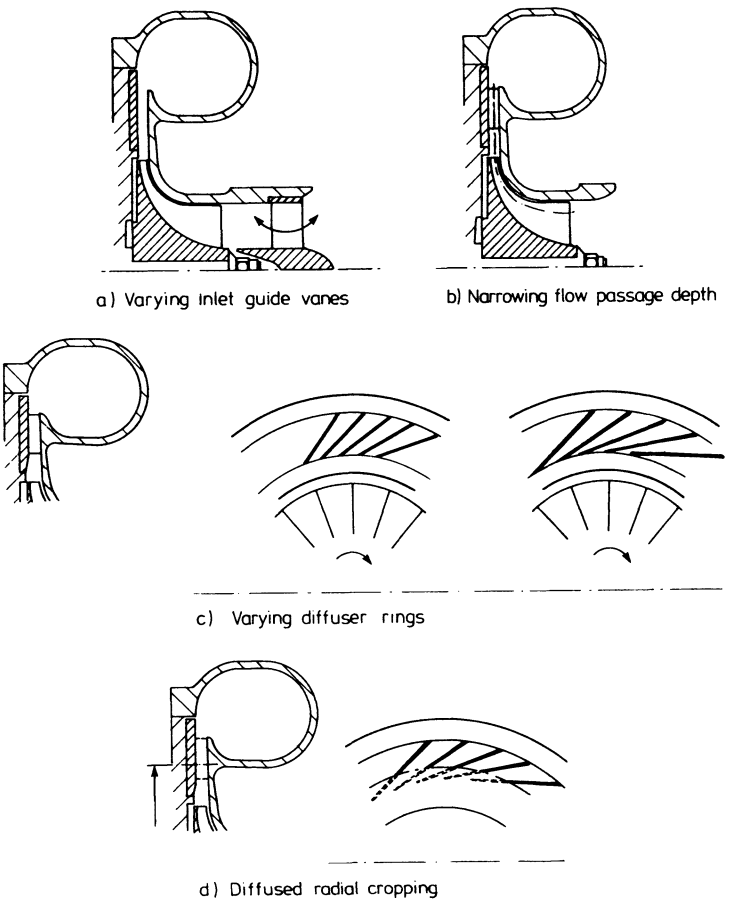

Figure 3.67 *Compressor trims, with a vaned diffuser*

fitted with vaned diffusers, and provides a considerable matching range without an appreciable penalty in efficiency, within the choking limits of the impeller.

Method 4 is a more economical approach than method 3, reducing the number of basic diffuser rings for matching and is very suitable for plate-type diffusers. However, inefficiency is introduced by mismatching the diffuser vane incidence angle with changes in diffuser throat area.

Changes in impeller diffusers, and associated casings, are commonly called 'trim' or 'build' changes within a certain turbocharger 'frame size'.

3.8 Impeller Stresses and Blade Vibrations

The design of the compressor impeller is not only governed by aerodynamic considerations, but also by stress levels and properties of the material used. The

trends towards higher stage pressure ratios and use of blade backsweep lead to higher impeller exit air temperatures and higher impeller tip speeds respectively, hence to highly stressed impellers. Thus the maximum speed of the compressor will be governed by the stress both in the impeller disc and blades and vibration problems.

3.8.1 Impeller Disc and Blade Stresses

One of the comparatively simple ways of estimating stresses in impellers is based on the method due to Donath (see Adams [47]). The assumption is made that the stress at any point in the disc is the algebraic sum of the stresses induced by internal centrifugal loading, and the load due to the temperature gradient from impeller hub bore to tip. The disc is divided into a succession of thin hollow cylinders and the blade elements corresponding to those cylinders are assumed to act as separate loading blocks.

Since the temperature-induced stresses are relatively small in relation to rotation-induced stresses, even at pressure ratios up to 8:1, it is reasonable to ignore stresses due to temperature distribution. [47]

Considering the elemental segment of the impeller as a uniform hollow cylinder, then at the inner radius the radial stress due to centrifugal loading is equal to [47]

$$\sigma_r = \frac{K_1}{2} - \frac{K_2}{r^2} - \frac{3+\nu}{8}\rho r^2\omega^2 \tag{3.60}$$

and the tangential (hoop) stress

$$\sigma_\theta = \frac{K_1}{2} - \frac{K_2}{r^2} - \frac{1+3\nu}{8}\rho r^2\omega^2 \tag{3.61}$$

where K_1 and K_2 are constants ω = rotational speed. ν = Poisson's ratio

The material density (ρ) must be artificially increased to simulate the additional loading of the blade.

This simple stress analysis of the whole impeller indicates that the maximum stress is the tangential component and that it occurs in the centre or bore of the disc.

Based on equation 3.61, Osborne [29] quotes the bore stress of well-optimised impeller geometries as

$$\sigma_{\theta\ \text{bore}} = (0.75 \text{ to } 1)\frac{3+\nu}{8}\rho U_2^2 \tag{3.62}$$

A more elaborate hollow cylinder disc theory, considering that the radial displacement of any point in the blades is the same as that for the disc at the same radius, is described by Adams. [47] Figure 3.68 illustrates typical radial and tangential stress distribution for a radial vaned impeller.

For backswept impellers an approximate estimate for the bending stress at

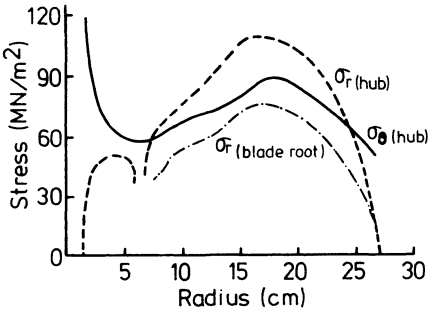

Figure 3.68 *Stresses in impeller and blades [47]*

the blade root near the impeller tip can be obtained using a cantilever beam analogy (as quoted by Osborne [29])

$$\sigma = \frac{6f(th)b_2^2 \sin \beta_{2b}}{th_{sh}} \rho r_2^2 \omega^2 \tag{3.63}$$

where $f(th)$ is a function of thickness distribution. For a linear increase in thickness with distance (hub to shroud)

$$f(th) = \left[(th_{sh}/th_h)/3 - \frac{1}{6} \right] (th_{sh}/th_h) \tag{3.64}$$

where th_{sh} = blade thickness at shroud
th_h = blade thickness at hub.

Experience gained from bursting tests of discs, impellers and turbine rotors indicates that the maximum disc stresses estimated from elasticity theory do not always represent the limiting criteria. As the speed of the impeller increases and the maximum stresses in the disc exceed the yield or proof stress of the material, plastic deformation takes place, relieving local stresses, leading to a more uniform stress distribution across the disc. Finally bursting of the disc occurs, when the tangential stress at any point in the disc reaches the ultimate tensile stress of the material.

A 'bursting speed' criterion based on the plastic deformation theory is very often used to estimate the safe maximum rotational speed of the impeller. Assuming that the impeller bursts into two equal halves (figure 3.69), the centrifugal force due to rotation of the impeller half is given by

$$F = 2\omega_{bu}^2 \int_{r_1}^{r_2} \rho r^2 th \, dr \tag{3.65}$$

where ω_{bu} = bursting angular velocity of the impeller
th = disc thickness.

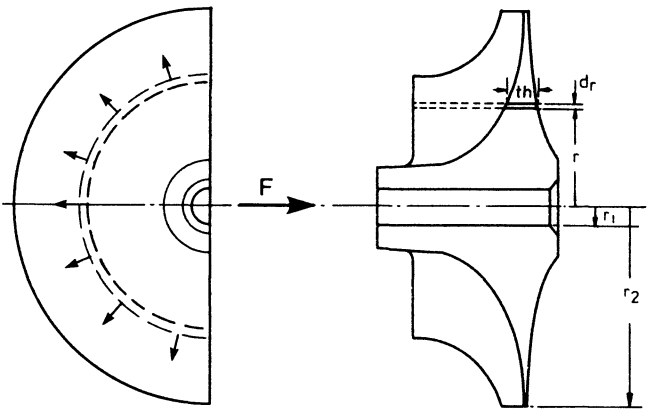

Figure 3.69 *Estimation of 'bursting speed' coefficient*

Considering now the maximum bursting force to be

$$F_{bu} = \sigma_{ult} \times A \tag{3.66}$$

where σ_{ult} = ultimate tensile stress of the material
A = cross-sectional area of the impeller disc.

The bursting safety factor is defined as N_{bu}/N. Combining equation 3.65 and 3.66 gives

$$\frac{N_{bu}}{N} = \frac{\omega_{bu}}{\omega} = \left\{ \frac{1}{\omega} \sqrt{\frac{\sigma_{ult} A}{2\int_{r_1}^{r_2} \rho r^2 th \, dr}} \right\} \tag{3.67}$$

For aluminium impellers the safety factor is chosen between 1.8 and 2.2.

The complex geometry of the impeller and the discontinuous nature of the blade loading can cause large bending stresses in the disc and blade itself which require a much more elaborate three-dimensional stress analysis. The 'finite element' stress analysis method based on plane triangular shell elements [49] is a very powerful and popular method of predicting stresses in complicated impeller designs, and establishing blade vibration modes. Details of the method and computation programs are too lengthy to be presented in this book and the reader is referred to Came [48] and Bell and Benhain. [50]

3.8.2 Impeller Disc and Blade Vibrations

Turbocharger compressor impellers, in common with other types of high-speed turbomachinery, are susceptible to vibration which can lead to fatigue failure. Impeller blades can vibrate relative to the disc (pure blade vibration) or together with the disc if the disc is very thin. Since turbocharger impellers are normally

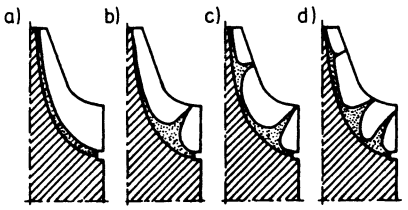

Figure 3.70 *Blade vibration modes [47]*

designed with robust discs (strong back-plates) it is quite safe to consider only the impeller blade vibration characteristic and to avoid operation of the turbocharger at excitation frequencies. Vibrations in the impeller blades are induced at the impeller eye when the blades pass through the wakes of inlet casing webs (if fitted) and at the impeller tip if the blades pass through disturbances projected back from the leading edges of the diffuser vanes. In addition impeller blade vibrations can be induced by the rotor speed passing through a multiple of the blade natural frequency.

Time-averaged laser holography [51, 52] is used to identify model shapes. Typical patterns for different natural frequencies of the blades are shown in figure 3.70. Experience has shown that only the first fundamental 'flap' mode (figure 3.70a) and second fundamental mode (figure 3.70b) are of importance.

As already mentioned, the finite element method is used in theoretical modal frequency analysis of impeller blades, since this method has the advantage of providing quantitative information on stress distribution.

One of the techniques used to avoid blade vibration problems at the design stage is stiffening of the blades at the root, or by changing the blade thickness distribution with height. Another method is to make the inducer separate from the impeller and assemble them together to provide friction damping between the contacting blade surfaces.

In isolated cases wire-lacing (a wire fed through holes in the impeller blades) has been used to damp vibrations but with a resultant degradation in aerodynamic performance.

3.9 Design of a Single-stage Radial Flow Compressor

The application and operating conditions of the turbocharger have considerable influence on the design of the compressor. The primary design objective for industrial and marine engine turbochargers is high compressor pressure ratio and maximum efficiency. For the small automotive-type turbocharger more attention is given to wide mass flow range at relatively moderate pressure ratios with emphasis on compactness, low cost and good acceleration characteristics – that is, to keep dimensions, weight and inertia small.

Since the turbocharger compressor, as distinct from a gas turbine compressor, is required to operate over a wide range of pressure ratios and mass flow rates and be adaptable to modifications (trims) to cover a whole range of options for

a given frame size, the selection of a specific design point is not critical. However, it is necessary to select a representative design point on the compressor map to establish the aerodynamic and mechanical design criteria and velocity diagrams.

The first requirement in the compressor design is to carry out preliminary optimisation studies with the aid of the one-dimensional flow analysis with loss coefficients to establish the desired compressor configuration and over-all geometric shape. For fixed design parameters – that is, compressor pressure ratio, mass flow rate, impeller eye hub/impeller tip diameter ratio (from mechanical considerations), assumed stage and impeller efficiency and diffuser configuration – the variable design parameters such as rotational speed, impeller eye tip diameter, blade backsweep, wake mass flow fraction, swirl parameter, slip factor and number of blades are varied parametrically over a probable range to yield an optimum stage efficiency.

Since the turbocharger has no mechanical linkage with the engine and therefore is a self-supporting free-running unit, the compressor rotational speed can be chosen from a compromise between potential maximum efficiency, inertia and over-all diameter and match with the turbine.

The first step in detailed impeller design involves an inducer inlet optimisation study with the objective of determining the minimum relative Mach number at the impeller eye tip. For different rotational speeds of the impeller (or for convenience, specific speeds, since pressure ratio and mass flow rate are kept constant) there is a minimum relative Mach number (M_{t1}). It should be noted that its value increases as specific speed increases and values exceeding unity should be avoided (to reduce impeller losses) if possible.

The impeller tip diameter is calculated from the impeller tip speed and rotational speed of the compressor, determined from the specific speed. Since the impeller tip speed is a function of compressor pressure ratio, compressor isentropic stage efficiency and energy input coefficient, which in turn is related to the slip factor, swirl parameter and blade backsweep, the optimisation study is carried out in the first place for nominally assumed constant values of the last three parameters.

The swirl parameter depends on the choice of the type of diffuser (vaneless or vaned). Blade backsweep improves stage efficiency and stage stability but increases impeller over-all diameter, hence it increases impeller weight, moment of inertia and blade root bending stresses. Thus the choice of degree of backsweep is a compromise between efficiency and flow range against mechanical and acceleration characteristics.

The impeller tip width is estimated from the continuity equation (at the mixed-out state) using the assumed values for swirl parameter and energy input coefficient.

The static pressure and temperature at the impeller tip are estimated using one-dimensional compressible flow relationships and assuming stage and impeller isentropic efficiencies.

The impeller exit conditions are then used as the input data for the diffuser calculations. In the case of vaneless diffusers, attention is focused on the choice of swirl parameter to ensure a large stable mass flow range. With a vaned diffuser, care is taken that the vaneless gap is deep enough to avoid noise and for the vane entry Mach number to be below unity. Throat blockage, throat aspect ratio and

diffusion area ratio are all affected by the choice of the number of diffuser vanes.

By estimating individual stage efficiency decrements (section 3.4) the isentropic stage and impeller efficiencies can be calculated. Thus the optimum rotational speed of the compressor can be established for a number of nominally fixed parameters (backsweep, swirl parameter, wake mass flow fraction, etc.).

For the selected rotational speed of the impeller a further analysis is carried out to optimise the previously nominally fixed parameters. Also further reference can be made to stress, inertia and cost constraints. After establishing the principal design parameters and over-all geometric dimensions of the compressor from the one-dimensional optimisation study, the next stage is to define the three-dimensional blade geometry of the impeller. The inducer leading edge blade angles are selected by adding incidence angles to the calculated relative inlet gas angles. These incidence angles (at eye hub and eye tip) are normally estimated using well-proven axial compressor technology.

In the construction of the blade shape, radial blade fibres are normally used to avoid bending stresses at the impeller blade root. With this geometry the shape of the blade centre surface is constructed of straight lines passing through the axis of rotation and intersecting at a series of axial positions along a reference camber line in a plane parallel to the axis of rotation (figure 3.71). The shape of the blading and flow passage is then checked by using the quasi-three-dimensional

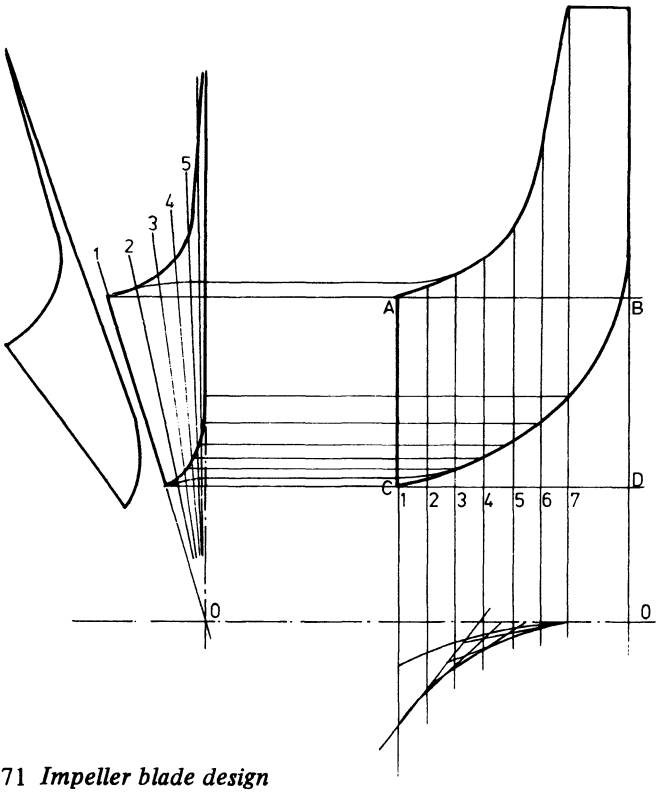

Figure 3.71 *Impeller blade design*

flow analysis, and the blade shape is modified, or the number of blades increased to obtain reasonable blade loading.

After concluding the aerodynamic design for the impeller blades the final task for the impeller designer is stress analysis of the impeller and blade vibration checks to avoid a resonance excitation.

References

1. T. B. Ferguson, *The Centrifugal Compressor Stage* (Butterworths, 1963)
2. O. E. Balje, Compressor and pump performance and matching of turbo-components, *J. Engng. Power* (January 1962)
3. D. G. Shepherd, *Principles of Turbomachinery* (Macmillan, New York, 1956)
4. J. D. Stanitz, Some theoretical aerodynamic investigations of impellers in radial and mixed-flow centrifugal compressors, *Trans. ASME*, **74** (1952) 473
5. F. J. Wiesner, A review of slip factors for centrifugal impellers, *ASME Publication 66-WA-FE-18* (1966)
6. U. Linsi, Experiments on the radial compressor of turbochargers, CIMAC Congress, London 1965
7. A. Whitfield, Slip factor of a centrifugal compressor and its variation with flow rate, *Proc. Inst. Mech, Engrs*, **188**, No.32/74 (1974)
8. R. C. Dean and L. R. Young, The fluid dynamic design of advanced centrifugal compressor, Fluid Dynamics Institute, Dartmouth College, Hanover, USA (1976)
9. B. Eckert, *Axialkompressoren und Radialkompressoren* (Springer Verlag, 1953)
10. G. A. Ball, A. J. Bell and L. B. Mann, The Development of the Chrysler Automotive Centrifugal Compressor, *SAE Technical Progress Series*, vol.3 (1961)
11. R. E. Morris and D. P. Kenny, High pressure ratio centrifugal compressor for small gas turbine engines, AGARD, *Helicopter propulsion systems* (Ottawa, June 1968)
12. F. Dallenbach, The aerodynamic design and performance of centrifugal and mixed-flow compressors, *SAE Technical Progress Series*, vol.3, pp. 2–30 (196)
13. A. Whitfield and F. J. Wallace, Performance prediction for automotive turbocharger compressors, *Proc. Inst. Mech. Engrs*, **189** (1975) 59
14. S. M. Futral and C. A. Wasserbauer, Off-design performance prediction with experimental verification for a radial inflow turbine, *NACA TN D-2621* (1965)
15. R. C. Pampreen, Small turbomachinery compressor and fan aerodynamics, *ASME Publication 73-GT-6* (1973)
16. J. E. Coppage *et al.*, Study of supersonic radial compressors for refrigeration and pressurization systems, *WADC Technical Report 55-257*, Astia Document No. AD 110467 (1956)
17. J. W. Daily and R. E. Nece, Chamber dimension effects on induced flow and frictional resistence of enclosed rotating discs, *Trans. ASME J. Basic Engng.*, **82** (1960)
18. C. Rodgers and L. Sapiro, Design considerations for high pressure-ratio centrifugal compressor, *ASME Paper 72-GT-91* (1972)

19. N. Watson and D. R. Ingham, Compressible flow in a radial vaneless diffuser, Conference on internal flows, University of Salford, Paper 8 (1971)
20. J. D. Stanitz, One dimensional compressible flow in vaneless diffusers of radial-and mixed-flow centrifugal compressors, including effects of friction, heat transfer and area change, *NACA TN 2610*, (Lewis Flight Propulsion Lab., 1952)
21. J. P. Johnston and R. C. Dean, Losses in vaneless diffusers on centrifugal compressors and pumps, *Trans. ASME J. Engng Power*, **88**, No.1 (1966)
22. W. B. Brown and B. R. Bradshaw, Design and performance of family of diffusing scrolls with mixed-flow impeller and vaneless diffuser, *NACA Report 936* (1949)
23. D. W. Holder, The transonic flow past two-dimensional aerofoils, *J. R. Aero. Soc.*, **68** (August 1964)
24. R. C. Dean, On the unresolved fluid dynamics of the centrifugal compressor; Advanced centrifugal compressors, *ASME 77-149815* (1971)
25. D. Eckardt, Detailed flow investigations within a high-speed centrifugal compressor impeller, *Trans. ASME, Jl Fluid Engng.*, (September 1976)
26. M. W. Johnson and J. Moore, The development of wake flow in a centrifugal compressor performance, *ASME Publication 78-GT-149* (1978)
27. W. Jansen, Rotating stall in a radial vaneless diffuser, *Trans. ASME, J. Basic Engng*, (December 1974)
28. Y. Senoo and Y. Kinoshita, Influence of inlet flow conditions and geometries of centrifugal vaneless diffusers on critical flow angle for reverse flow, *Trans. ASME*, **99** (March 1977)
29. C. Osborne, Turbocharging the internal combustion engine, Fluid Dynamics Institute, Short Course No.79-1, Dartmouth College, Hanover, USA (1979)
30. D. P. Kenny, A comparison of the predicted and measured performance of high pressure ratio centrifugal compressor diffusers, *ASME Publication 72-GT-54* (1954)
31. G. Sovran and E. D. Klomp, Experimentally determined optimum geometries and rectilinear diffusers with rectangular conical or annular cross section, in *Fluid Mechanics of Internal Flow* (Elsevier, Amsterdam, 1967)
32. P. W. Runstadler and F. X. Dolan, Further data on the pressure recovery performance straight-channel, plane-divergence diffusers at high subsonic Mach numbers, *ASME Publication 73-FE-5* (1973)
33. C. J. Sagi and J. P. Johnston, The design and performance of two-dimensional, curved diffusers, *ASME Publication 67-FE-6* (1967)
34. C. Rodgers, Radial compressor performance, SAE Progress in Technology Series, Centrifugal compressors 1-62 (April 1964)
35. R. C. Pampreen, The use of cascade technology in centrifugal compressor vaned diffuser design, *ASME Publication 72-GT-39* (1972)
36. V. J. Smith, A review of the design practice and technology of radial compressor diffusers, *ASME Publication 70-GT-116* (1970)
37. A. Stodola, *Steam and Gas Turbines* (McGraw-Hill, New York, 1927)
38. J. H. G. Howard and C. Osborne, A centrifugal compressor flow analysis employing a jet/wake passage flow model, *ASME Publication 76-FE-21* (1976)
39. J. J. Kramer, W. M. Osborne and J. T. Hamrick, Design and test of mixed flow and centrifugal impellers, *Trans. ASME*, Series A 82 (1960) 127
40. D. Japikse and J. Goebel, Turbocharger compressor performance and critical flow field measurements, *SAE 790315*, Turbochargers and Turbocharged Engines, SP442 (1979)

41. F. Emerson and J. Horlock, The design of diffusers for centrifugal compressors, *ASME paper 66-WA/GT-9* (1966)
42. E. Jenny, Über instationäre Vorgänge in Radial-Verdichtern, insbesondere in Aufladegruppen von Verbrennungsmotoren, *Schweiz. Bauztg*, **79** (1961) (46) 812-17
43. S. L. Dixon, *Fluid Mechanics, Thermodynamics of Turbomachinery*, 3rd ed. (Pergamon, Oxford, 1978)
44. W. E. Woollenweber, The turbocharger, a vital part of the engine intake and exhaust systems, *SAE 700534* (1970)
45. F. J. Wallace, A. Whitfield and R. Atkey, Experimental and theoretical performance of a radial flow turbocharger compressor with inlet prewhirl, *Proc. mech. Engrs*, **189**, No.43/75 (1975)
46. C. Rodgers, Variable geometry gas turbine radial compressor, *ASME Publication 68-GT-63* (1968)
47. A. T. Adams, *Elements of Internal Combustion Turbines Theory* (Cambridge University Press, 1949)
48. P. M. Came, The development application and experimental evaluation of a design procedure for centrifugal compressors, *Proc. Inst. mech. Engrs*, **192.**, No.5 (1978)
49. O. C. Zienkiewicz, *The Finite Element Method in Engineering Science* (McGraw-Hill, 1971)
50. R. Bell and P. P. Benhain, Theoretical and experimental stress analysis of centrifugal fan impellers, *J. Strain Analysis*, **13**, No.3 (1978)
51. R. C. Sampson, Holographic-interferometry applications in experimental mechanics, SESA Fall Meeting, Houston, Texas (October 1969)
52. L. F. Ellison and J. M. Partridge, Vane vibration in radial flow turbochargers, turbocharging and turbochargers, *Proc. Inst. Mech. Engrs.* (April 1978)

4

The Radial Flow Turbine

4.1 Introduction

There are two basic types of turbine suitable and used at present in turbochargers, the radial flow and the axial flow. The radial flow turbine is mainly used for small automotive or truck turbochargers; the axial type is commonly used for the large turbochargers applied to medium-speed stationary and railway traction engines and large marine engines.

The radial flow turbine is similar in appearance to the centrifugal compressor, but with the flow in the inward direction and nozzle vanes replacing the diffuser vanes. Historically, the radial flow turbine had a late start in the field of turbocharging and has been primarily developed for use in the small-size inexpensive automotive turbocharger. Its great advantage is that it maintains a relatively high efficiency when reduced to very small sizes. It can efficiently handle a high expansion ratio (approaching 4:1) and is also more robust and cheaper to manufacture than an axial turbine. Although well established in the automotive field, its use in larger turbochargers is at present limited by manufacturing techniques.

4.2 Elementary Theory

The turbocharger turbine is required to accept quite unfavourable inlet conditions if the pulse turbocharging system is used. The inlet might be divided into two or three separate sectors, each containing highly pulsating flow. It is indeed fortunate that the turbine is able to accept these conditions without a complete deterioration of its performance.

The radial inflow turbine consists of a scroll or inlet casing (figure 4.1), a set of inlet nozzles (sometimes omitted) followed by a short vaneless gap and the turbine wheel itself. Most small turbocharger turbines use a nozzleless casing to improve flow range at some penalty in peak efficiency, but also reducing cost. However, considering the more conventional type with nozzles, the function of the inlet casing is purely to deliver a uniform flow of inlet gas to the nozzle entries. The nozzles accelerate the flow, reducing pressure and increasing kinetic energy. A short vaneless space prevents the rotor and blades from touching and allows wakes coming off the trailing edge of the nozzle blades to mix out. Energy transfer occurs solely in the impeller, which should be designed for minimum kinetic energy at the exit.

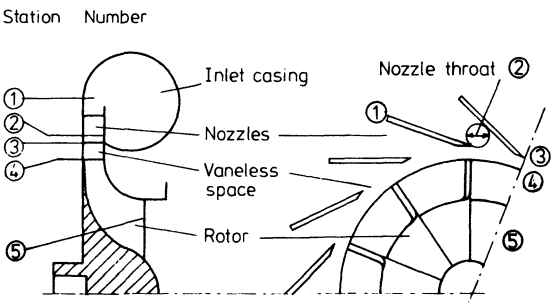

Figure 4.1 *Components of a radial flow turbine*

The flow process through the turbine may be plotted on a temperature or enthalpy/entropy diagram (figure 4.2). Station 01 refers to stagnation conditions at entry to the casing. The gas will already have a significant velocity (C_1) hence the stagnation pressure is P_{01}. The inlet nozzles accelerate the flow from station 1 to 2. If this process were isentropic, the end point would be 2_s. Energy transfer occurs in the rotor, between stations 4 and 5 (4 and 5_s if isentropic) down to the exit pressure (P_5). The stagnation pressure (P_{05}) will be higher than P_5 since the exit velocity (C_5) will remain significant. Station 3 is the nozzle exit.

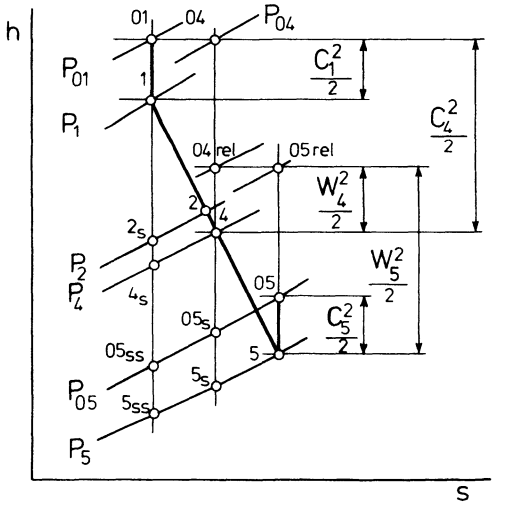

Figure 4.2 *h–s diagram for a turbine stage*

4.2.1 Velocity Triangles and Energy Transfer

The specific energy transfer in the rotor can be derived from the velocity triangles at inlet and outlet (figure 4.3). The absolute gas velocity entering the rotor is C_4, at an angle α_4; its radial component is C_{r4}. Since the rotor tip speed is U_4, the gas velocity relative to the rotor blades is W_4. At rotor exit the relative velocity

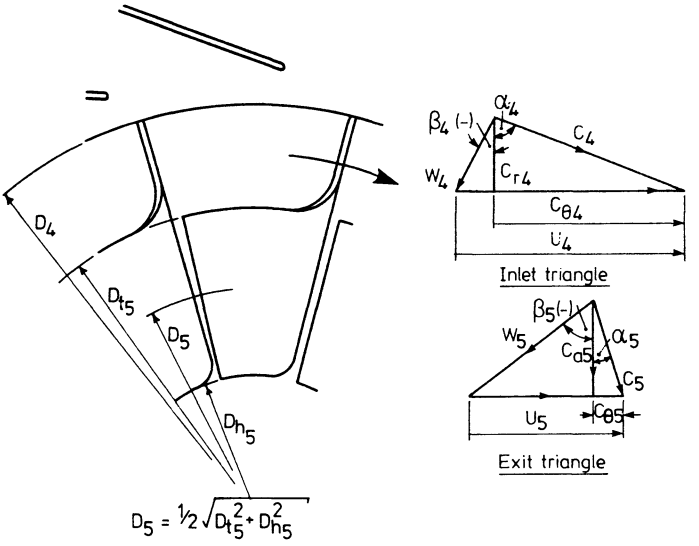

Figure 4.3 *Velocity triangles for a radial flow turbine*

will be W_5 at the blade angle β_5. Due to the blade speed U_5, the absolute exit velocity will be C_5, at angle α_5. The rate of change of angular momentum will equal the sum of the moments of external forces (that is, the torque TQ). Since angular momentum is the moment of linear momentum, the rate of change will be given by the product of mass flow rate times radius times velocity. Thus the torque becomes

$$TQ = \dot{m}(r_4 C_{\theta 4} - r_5 C_{\theta 5}) \tag{4.1}$$

The energy transfer will be given by the product of torque and angular velocity (ω), hence

$$\dot{W} = \omega TQ = \dot{m}(U_4 C_{\theta 4} - U_5 C_{\theta 5}) \tag{4.2}$$

In practice, since it is desirable to minimise the kinetic energy at the exit, it is usually arranged that the tangential component of the absolute exit velocity ($C_{\theta 5}$) is zero. Hence equation 4.2 becomes

$$\dot{W} = \dot{m} U_4 C_{\theta 4} \tag{4.3}$$

4.2.2. Temperature Drop across the Turbine

The steady flow energy equation for a process from state 'a' to 'b' can be written as

$$\dot{Q} - \dot{W} = \dot{m}\left[h_a - h_b + \frac{C_b^2 - C_a^2}{2}\right]$$

When applied to a turbine, rewritten in terms of stagnation enthalpy (h_0) with heat transfer neglected

$$\dot{W} = \dot{m}(h_{0a} - h_{0b})$$

Since no work is done in the inlet casing and nozzles, the stagnation enthalpy remains constant

$$h_{01} = h_{04} \tag{4.4}$$

For the turbine rotor

$$\dot{W} = \dot{m}(h_{04} - h_{05}) \tag{4.5}$$

that is, the specific power output is equal to the drop in stagnation enthalpy (in the absence of external friction in the bearings, etc.).

If the working fluid (the exhaust gas of the engine) may be considered as a perfect gas, then

$$h_{04} - h_{05} = c_p(T_{04} - T_{05}) \tag{4.6}$$

Since the rate of doing work (energy transfer) has already been established (equation 4.2), it follows that

$$\dot{W} = \dot{m}c_p(T_{04} - T_{05})$$

and

$$T_{04} - T_{05} = \frac{U_4C_{\theta 4} - U_5C_{\theta 5}}{c_p} \tag{4.7}$$

In the absence of swirl at the rotor exit

$$T_{04} - T_{05} = \frac{U_4C_{\theta 4}}{c_p} = \Delta T_{0t} \tag{4.8}$$

If the working fluid is assumed to be a semi-perfect, rather than a perfect gas (that is, $Pv = RT$ and $c_p = \mathrm{d}h/\mathrm{d}T$ but R and c_p are both functions of temperature), the value of c_p must be the mean value between that at temperatures T_4 and T_5.

4.2.3 Isentropic Efficiency and Expansion Ratio

The isentropic efficiency of the turbine, on a total-to-total basis, is given by equation 2.20. Using the notation of figure 4.2

$$\eta_{tTT} = \frac{h_{01} - h_{05}}{h_{01} - h_{05\,ss}} \approx \frac{T_{01} - T_{05}}{T_{01} - T_{05\,ss}} = \frac{1 - (T_{05}/T_{01})}{1 - (P_{05}/P_{01})^{(\gamma-1)/\gamma}} \tag{4.9}$$

giving

$$\frac{P_{01}}{P_{05}} = \left[\frac{T_{01}}{T_{01} - (T_{01} - T_{05})/\eta_{tTT}}\right]^{\gamma/(\gamma-1)} \tag{4.10}$$

Similar expressions may be derived for the total-to-static isentropic efficiency and expansion ratio

$$\eta_{tTS} = \frac{h_{01} - h_{05}}{h_{01} - h_{5_{ss}}} = \frac{T_{01} - T_{05}}{T_{01} - T_{5_{ss}}} = \frac{1 - (T_{05}/T_{01})}{1 - (P_5/P_{01})^{(\gamma-1)/\gamma}} \tag{4.11}$$

and

$$\frac{P_{01}}{P_5} = \left[\frac{T_{01}}{T_{01} - (T_{01} - T_5)/\eta_{tTS}}\right]^{\gamma/(\gamma-1)} \tag{4.12}$$

4.2.4 Degree of Reaction

The degree of reaction (RN) of a turbine may be defined as the isentropic enthalpy change in the rotor divided by the isentropic enthalpy change across the whole stage. Thus

$$RN_s = \frac{h_{4_s} - h_{5_{ss}}}{h_{01} - h_{5_{ss}}} \tag{4.13}$$

It is, in fact, a measure of how much expansion occurs in the rotor relative to the total. Thus in a machine having 50 per cent reaction, expansion will be reasonably evenly divided between the stator (nozzles) and the rotor. If the reaction were 0 per cent, a pure 'impulse' turbine would be the result. Equation 4.13 implies a degree of reaction based on the energy available (in the isentropic case). It is more useful to base reaction on the actual energy transfer, that is

$$RN = \frac{\text{energy transfer due to change in static pressure in the rotor}}{\text{total energy transfer in the stage}}$$

$$= \frac{h_4 - h_5}{h_{01} - h_{05}} = \frac{(h_{04} - C_4^2/2) - (h_{05} - C_5^2/2)}{(h_{01} - h_{05})} \tag{4.14}$$

Thus,

$$RN = 1 - \frac{C_4^2 - C_5^2}{2(h_{01} - h_{05})}$$

From equations 4.6 and 4.7 and the velocity triangles in figure 4.3

$$RN = 1 - \frac{[(C_{\theta 4}^2 + W_4^2 - (U_4 - C_{\theta 4})^2] - [C_{\theta 5}^2 + W_5^2 - (U_5 - C_{\theta 5})^2]}{2(U_4 C_{\theta 4} - U_5 C_{\theta 5})}$$

$$= 1 - \frac{(W_4^2 - U_4^2 + 2U_4 C_{\theta 4}) - (W_5^2 - U_5^2 + 2U_5 C_{\theta 5})}{2(U_4 C_{\theta 4} - U_5 C_{\theta 5})}$$

therefore

$$RN = \frac{(W_5^2 - U_5^2) - (W_4^2 - U_4^2)}{2(U_4 C_{\theta 4} - U_5 C_{\theta 5})} \tag{4.15}$$

It is common to design for zero swirl at exit ($C_{\theta 5} = 0$) and often for the radial component of velocity at inlet to the rotor to equal the axial outlet velocity

$$C_{r4} = C_{a5}$$

Hence equation 4.14 becomes

$$RN = 1 - \frac{C_4^2 - C_5^2}{2U_4 C_{\theta 4}} = 1 - \frac{(C_{\theta 4}^2 + C_{r4}^2) - C_{a5}^2}{2U_4 C_{\theta 4}}$$

that is

$$RN = 1 - \frac{C_{\theta 4}}{2U_4} \tag{4.16}$$

If the rotor blades are radial, $\beta_{4b} = 0°$ and if $C_{\theta 4} = U_4$, hence the reaction is 50 per cent. It will be shown that it is difficult to design a radial turbine whose reaction is far from 50 per cent.

4.2.5 Blade speed Ratio (or Velocity Ratio)

The blade speed ratio (U_4/C_s) is the rotor tip velocity (U_4) divided by the velocity that would be achieved by the gas following isentropic expansion from the inlet conditions to the pressure at the exit from the turbine (total-to-static); that is

$$\frac{U_4}{C_s} = \frac{U_4}{\sqrt{[2(h_{01} - h_{5_{ss}})]}} = \frac{U_4}{\sqrt{\{2c_p T_{01} \ [1 - (P_5/P_{01})^{(\gamma-1)/\gamma}]\}}} \tag{4.17}$$

The use of the term 'blade speed ratio' has come from impulse steam turbine practice in which the enthalpy change in the rotor is zero. In that context the term refers to rotor blade speed/gas-jet speed ratio. Although the analogy does not hold when the degree of reaction is non-zero, the term remains commonly used, since it is a non-dimensional form of the rotor tip speed. Figure 4.4 shows a typical flow turbine isentropic efficiency plotted against the blade speed ratio. The turbine efficiency peaks at $U_4/C_s = 0.7$.

The relationship between the blade speed ratio and turbine efficiency is very important when designing and matching the turbine to the appropriate compressor. From the known turbine inlet temperature and expansion ratio, C_s can be calculated and the rotor tip diameter chosen (for a given rotational speed) to coincide with the U_4/C_s value for optimum turbine efficiency. The turbine efficiency/blade speed ratio diagram may also be used to specify instantaneous efficiency under pulsating inlet conditions for a quasi-steady calculation of turbine power (chapter 15).

4.2.6 Specific Speed

The concept of specific speed has already been discussed in chapter 3. This dimensionless parameter can be applied to the turbine in the same manner as it

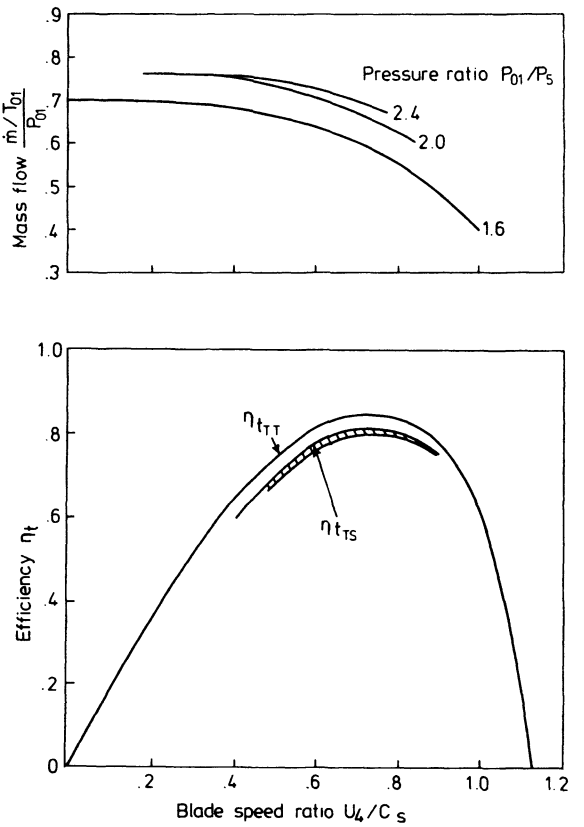

Figure 4.4 *An example of a radial flow turbine characteristic (based on Hiett and Johnston [1]*

was to the compressor. The definition of specific speed (*NS*) and specific diameter (*DS*) remain the same, namely

$$NS = \frac{N\dot{V}^{1/2}}{(HD)^{3/4}} \tag{4.18}$$

and

$$DS = \frac{D(HD)^{1/4}}{\dot{V}^{1/2}} \tag{4.19}$$

The concept has been developed for incompressible flow, but Balje [2] has shown that it also has some (approximate) validity to turbines with compressible flow. He illustrated how efficiency relates to specific speed and diameter (figure 4.5). In general, highest efficiency for a radial bladed rotor will occur when the specific diameter lies in the range 2.8 to 4.8 and the specific speed between 0.35 and 0.7.

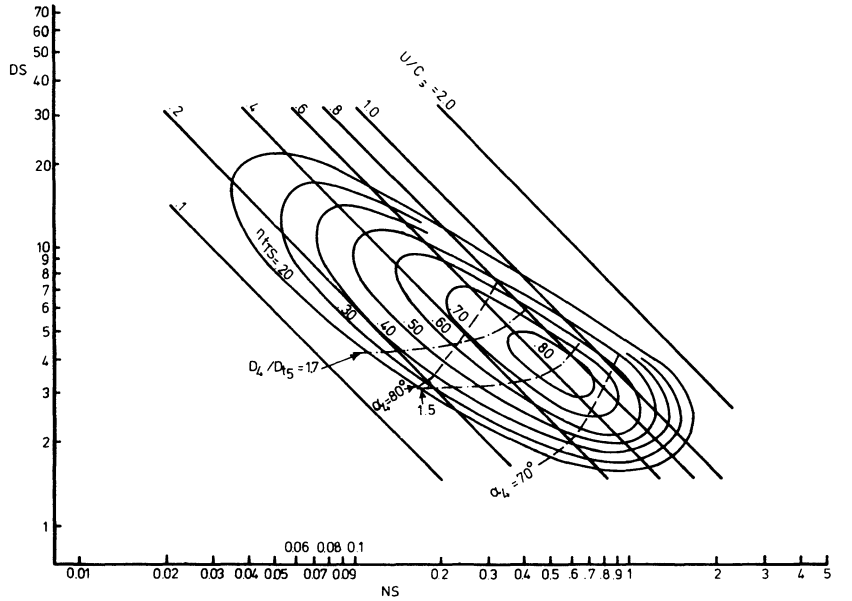

Figure 4.5 *Calculated non-dimensional performance diagram for single-stage radial turbines [2]*

4.3 One-dimensional Flow Analysis

One-dimensional analysis of the flow through the turbine provides the basis for the initial design. The pressure and relative velocity gradients across the channels, particularly of the rotor, where losses could occur due to flow separation at the channel walls and flow recirculation, are ignored. At a later stage the design can be modified with the help of more complicated three-dimensional analysis or according to guidelines based on the findings of experimental research work, to obtain optimum turbine performance.

In a similar manner to the one-dimensional flow analysis of the compressor, the steady flow energy equation, moment of momentum, continuity equation and thermodynamic equation of state are used to estimate a representative mean relative velocity and density at any cross-section through the channels in the turbine. The geometrical shape of each turbine component is then adjusted until reasonable blade loadings are achieved.

4.3.1 The Volute or Inlet Casing

The function of the volute will depend on whether the turbine has inlet nozzle vanes. If it has, then the volute must simply deliver a uniform gas flow to the nozzles. A single-entry volute casing is shown in figure 4.6. In addition, it is desirable that the flow angle does not depart far from the entry angle of the vanes,

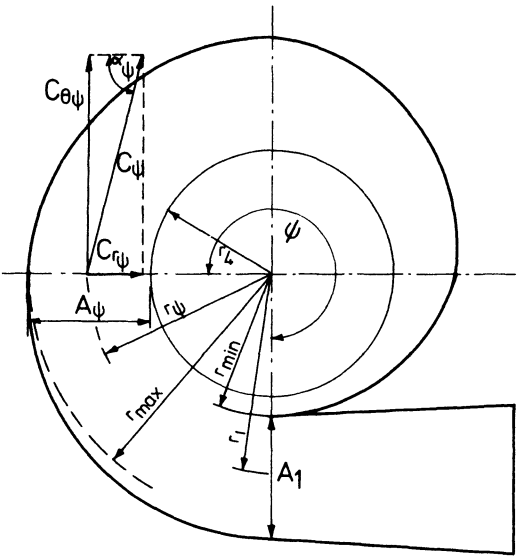

Figure 4.6 *Volute-type turbine scroll*

but since the velocity is low, losses will not be large if it does. Thus a simple cannister could be used. However, a spiral volute casing should be beneficial. This can be designed using incompressible flow theory with constant angular momentum (and hence uniform pressure). Thus, from figure 4.6

$$rC_\theta = \text{constant} = K \tag{4.20}$$

For incompressible flow, the mass flow rate at an azimuth angle ψ is

$$\dot{m}_\psi = \rho A_\psi C_{\theta\psi}$$

For uniform mass flow distribution

$$\dot{m}_\psi = \dot{m} \times \frac{\psi}{2\pi}$$

where $\dot{m}$ = total mass flow rate entering the volute. Hence

$$A_\psi = \frac{\dot{m}}{\rho C_{\theta\psi}} \times \frac{\psi}{2\pi}$$

Eliminating C_θ by using equation 4.20 gives

$$A_\psi = \frac{\dot{m}}{\rho} \times \frac{\psi}{2\pi} \times \frac{r_\psi}{K} \tag{4.21}$$

that is, the cross-sectional area of the volute reduces with the azimuth angle and mean radius. The mean radius will vary as the volute curves in round the circumference, but the reduction is not large when expressed as a fraction of radius. In consequence, the area is often reduced linearly with azimuth angle. The above

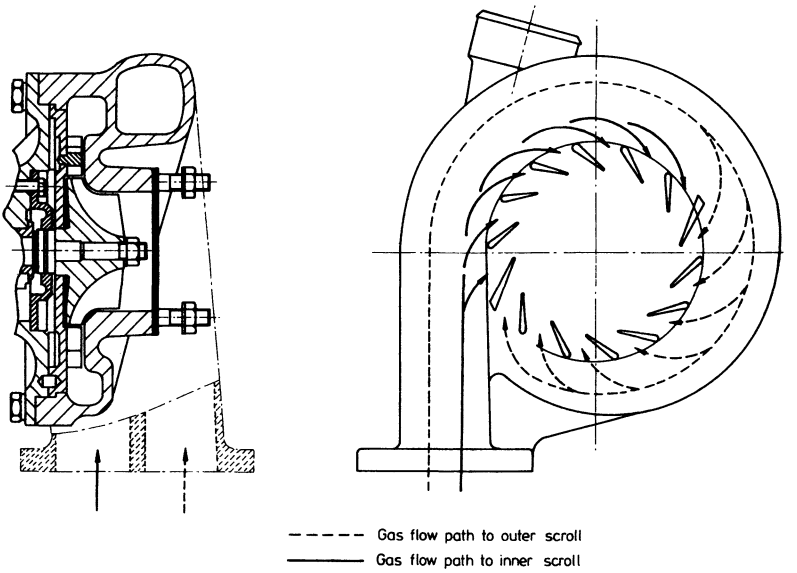

Figure 4.7 *Cross-section of CAV B01 turbine, with a double entry*

analysis has been developed for the case of a single-entry casing with the flow area reducing to zero. An identical analysis can be applied to each half of a double-entry volute.

Under the pulse turbocharging system a double or even triple-entry casing may be required to isolate the gas flow from each separate group of manifolds. This isolation holds throughout the inlet casing and the nozzle ring, and hence must be achieved by means of separate angular sectors (figure 4.7). It is a consequence that one entry passage will be longer than the other if a common flange is used at the exhaust manifold connection. Naturally the nozzles must be arranged to preserve the isolation between sectors as shown in figure 4.7.

It is common, whether the casing is single or double entry, to allow some reduction in flow area between the exhaust manifold flange and the point at which the scroll first admits to the turbine (cross-sectional area A_1, figure 4.6). This results in some flow acceleration and a compromise must be reached between the frictional losses that result from high velocities and the benefit of reduced turbocharger size and weight due to the smaller casing.

Many turbochargers are available in which the inlet nozzles have been eliminated. This is particularly common on automotive diesel engine turbochargers since they are required to operate over a very wide mass flow range. It follows that they operate away from the turbocharger's design point for most of the time and any fixed inlet nozzles would prevent the flow from adjusting to the changed conditions. As a result the rotor incidence angle departs from the optimum value. However, if the inlet nozzles are eliminated, the casing or volute must take over the function of flow guidance at entry to the rotor in addition to flow distribution

and acceleration. The geometry of the volute must determine the gas angle at volute exit or rotor tip (α_4). From figure 4.6

$$\cot \alpha_\psi = \frac{C_{r\psi}}{C_{\theta\psi}}$$

Denoting the effective volute inlet as station 1 (the point at which the scroll first admits to the turbine, figure 4.6), with r_1 being the radius of the centroid of section A_1,

$$r_1 C_{\theta 1} = r_4 C_{\theta 4}$$

(from equation 4.20). From conservation of mass

$$\dot{m} = \rho_1 A_1 C_{\theta 1} = \rho_4 2\pi r_4 b_4 C_{r4}$$

where b_4 = rotor inlet width. Thus

$$\cot \alpha_4 = \frac{\rho_1 A_1 C_{\theta 1}}{\rho_4 2\pi r_4 b_4 C_{\theta 4}} = \frac{\rho_1 A_1 r_4}{\rho_4 2\pi r_4 b_4 r_1}$$

$$= \frac{A_1}{r_1} \frac{\rho_1}{\rho_4} \frac{1}{2\pi b_4}$$

For incompressible flow

$$\cot \alpha_4 = \frac{A_1}{r_1} \frac{1}{2\pi b_4} \tag{4.22}$$

For a specified rotor tip width (b_4), the volute exit gas angle is defined by the ratio A_1/r_1. This value is often used to define casing geometry since it directly relates to the vane angle of an equivalent vaned inlet casing. Note that flow angle is independent of mass flow rate, hence the vaneless volute is only slightly better able to adjust to varying flow rates than a vaned housing. Even mass flow and flow angle distribution around the volute will be considerably more important than those in a casing with inlet nozzles. In consequence, the simple incompressible flow analysis leading to equation 4.22 is not wholly satisfactory, particularly if the assumption of constant mean radius is used. If the cross-sectional area is reduced linearly with azimuth angle ψ (or even the area divided by the mean radius), quite large variations in flow angle (α_4) result. Figure 4.8 illustrates this variation in flow angle for three different volutes, each designed with a constant A_1/r_1 value.

For the purpose of matching the turbocharger for a particular engine duty, a method of adjusting the flow angle at the rotor tip is required. If inlet nozzles are used it is simple to replace the nozzle ring by another in which the vanes are set at a different angle. If a nozzleless casing is used, the flow angle can be altered by increasing or reducing the cross-sectional area of the volute (that is, area A_1). The cross-sectional area of the scroll will be altered in proportion, all the way round the rotor. Thus a range of nozzleless inlet casings having different effective areas (or A_1/r_1) or a range of nozzle rings set at different blade angles are required for final matching of the flow characteristics to those of the engine (the procedure is fully described in chapter 10).

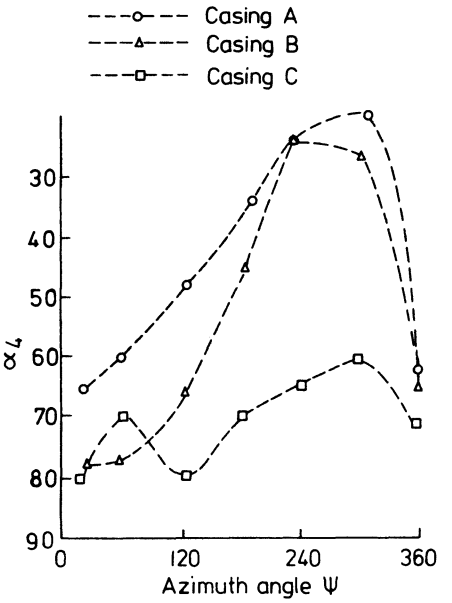

Figure 4.8 *Measured values of gas angle α_4 against azimuth angle ψ [3]*

4.3.2 The Inlet Nozzles

For reasons of simplicity and reliability, it is common to use uncambered (that is, having a straight axis) aerofoil section nozzles having quite robust trailing edges (figure 4.9). Even simpler straight parallel walled blades have been used, but at some penalty in efficiency. No general methods are available for calculating the optimum number of blades for a given duty, but clearly a large number will give better flow guidance at the penalty of increased frictional losses and flow blockage.

The function of the inlet casing and nozzles is to accelerate and direct the fluid flow at the required design angle to the rotor with the minimum loss. Since there is no work transfer, the stagnation enthalpy remains constant (neglecting heat transfer), but the stagnation pressure falls dependent on the magnitude of the friction loss in the inlet casing, incidence and friction loss in the nozzles. The

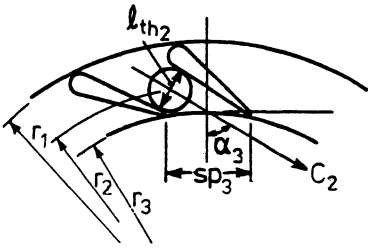

Figure 4.9 *Uncambered aerofoil nozzles*

total inlet casing and nozzle loss is usually expressed as a function of exit gas velocity and of a nozzle efficiency or loss coefficient.

Application of the steady flow energy equation with the assumption that exhaust gas may be considered as a perfect gas gives

$$T_2 = T_{01} - \frac{C_2^2}{2c_p} \tag{4.23}$$

$$\frac{P_2}{P_{01}} = \left(1 - \frac{C_2^2}{2c_p\,\eta_n T_{01}}\right)^{\frac{\gamma}{\gamma-1}} \tag{4.24}$$

where

$$\eta_n = \frac{h_{01} - h_2}{h_{01} - h_{2_s}}$$

If the length of the throat formed by two adjacent nozzle blades is l_{th_2} (see figure 4.9) and the width of the flow passage is b_2, then the mass flow rate is given by

$$\dot{m} = \rho_2 C_2 b_2 l_{th_2} z_2 \tag{4.25}$$

where z_2 = number of nozzles or vanes. The density will be given by

$$\rho_2 = \frac{P_2}{RT_2} \tag{4.26}$$

Hiett and Johnston, [1] from common steam turbine practice, have assumed that the flow angle at nozzle exit may be expressed as

$$\cos \alpha_3 = \frac{l_{th_2}}{sp_3} \tag{4.27}$$

where sp_3 is the circumferential spacing or pitch between blades at the trailing edge. Although equation 4.27 is an approximation, the error introduced is not great, particularly at high blade angles (measured from the radial direction). However, the efficiency of the rotor is sensitive to the inflowing gas angle.

4.3.3 The Vaneless Space

A vaneless space between the nozzle exit and rotor tip is usually introduced for mechanical and manufacturing reasons, but is kept small otherwise the advantage of using inlet nozzles may be lost. Analysis of flow in the vaneless space is similar to that in a vaneless diffuser. If wall friction is ignored (not an unreasonable assumption since, unlike the vaneless diffuser, the vaneless space is small), then angular momentum is conserved. Thus

$$r_3 C_{\theta 3} = r_4 C_{\theta 4}$$

(where 2 denotes nozzle exit throat and 4 denotes rotor inlet). From conservation of mass

$$\dot{m} = \rho_2 C_2 b_2 l_{th_2} z_2 = 2\pi r_4 b_4 \rho_4 C_{r_4} \tag{4.28}$$

Since

$$\tan \alpha_4 = \frac{C_{\theta 4}}{C_{r4}} \tag{4.29}$$

then

$$\tan \alpha_4 = \frac{r_3 \, C_{\theta 3} \, 2\pi r_4 b_4 \rho_4}{r_4 \, C_2 \, b_2 l_{th_2} z_2 \rho_2}$$

Since $C_{\theta 3}/C_2 = \sin \alpha_3$ then, assuming incompressible flow since the vaneless space is small

$$\tan \alpha_4 = \frac{r_3 2\pi b_4}{b_2 l_{th_2} z_2} \sin \alpha_3 \tag{4.30}$$

If the nozzle exit conditions are known, equation 4.30 gives the flow angle leaving the vaneless space.

4.3.4 The Rotor

In the rotor, energy transfer takes place from the fluid and hence there is a drop in enthalpy, pressure and absolute velocity.

The basic equation for energy transfer in the rotor has already been derived, namely

$$\dot{W} = \omega T = \dot{m}(U_4 C_{\theta 4} - U_5 C_{\theta 5}) = \dot{m} \, (h_{04} - h_{05}) \tag{4.31}$$

Hence

$$\frac{2\dot{W}}{\dot{m}} = 2 \, (U_4 C_{\theta 4} - U_5 C_{\theta 5})$$

$$= [U_4^2 + C_{\theta 4}^2 - (U_4 - C_{\theta 4})^2] - [U_5^2 + C_{\theta 5}^2 - (U_5 - C_{\theta 5})^2]$$

$$= [U_4^2 + C_{\theta 4}^2 - (W_4^2 - C_{r4}^2)] - [U_5^2 + C_{\theta 5}^2 - (W_5^2 - C_{a5}^2)]$$

from the velocity triangles (figure 4.3)

$$\frac{2\dot{W}}{\dot{m}} = (U_4^2 - W_4^2 + C_4^2) - (U_5^2 - W_5^2 + C_5^2)$$

hence

$$\frac{\dot{W}}{\dot{m}} = \tfrac{1}{2} \, [\, (U_4^2 - U_5^2) - (W_4^2 - W_5^2) + (C_4^2 - C_5^2) \tag{4.32}$$

The three bracketed terms in equation 4.32 illustrate key features of a radial flow turbine. The first term denotes a large positive contribution to turbine work due

to the change in radius ratio. Thus a radial inflow turbine ($U_4 > U_5$) is preferred to a radial outflow turbine, or indeed to an axial flow turbine. The second term shows that W_5 must exceed W_4 for positive work, that is, the flow must accelerate through the rotor, relative to the rotor (in a compressor it must decelerate). The third term shows that the absolute exit velocity must be minimised since this is a direct loss of potential turbine work. It is for this reason that exit swirl should be zero. Exit swirl is unnecessary and increases exit kinetic energy for a fixed mass flow rate.

In the special, but common case of a turbine with purely radial blades operating at a design point with a correct inlet flow angle (that is, $C_{\theta 4} = U_4$) and zero exit swirl (that is, $C_{\theta 5} = 0$), then

$$C_4^2 = W_4^2 + U_4^2 \text{ and } C_5^2 = W_5^2 - U_5^2$$

hence equation 4.32 reduces to

$$\frac{\dot{W}}{\dot{m}} = U_4^2 \tag{4.33}$$

(which is obvious from equation 4.31).

The layout of the rotor channel is not quite so critical as in the case of the compressor impeller, because the channel area is converging from rotor tip to the outlet and the mean relative velocity is accelerating along the channel. The distribution of average total temperature and density, and hence the relative velocity (for a given mass flow rate) along the rotor channel can be evaluated as follows. For example, at radius 'a' (see figure 4.10), from the energy transfer equation 4.32

$$\dot{W} = \dot{m}\tfrac{1}{2}[(U_4^2 - U_a^2) - (W_4^2 - W_a^2) + (C_4^2 - C_a^2)] \tag{4.34}$$

and from equation 4.5

$$\dot{W} = \dot{m}\left[(h_4 - h_a) + \frac{C_4^2 - C_a^2}{2}\right] \tag{4.35}$$

thus from equations 4.34 and 4.35

$$h_4 - h_a = \tfrac{1}{2}[(U_4^2 - U_a^2) - (W_4^2 - W_a^2)]$$

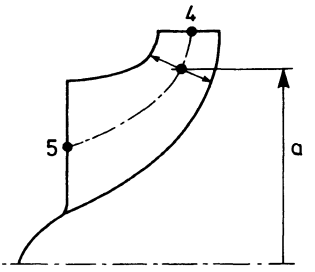

Figure 4.10 *Design of a rotor channel*

hence

$$c_p\,(T_4 - T_a) = c_p\,\Delta T_{4-a} = \tfrac{1}{2}\,[(U_4^2 - U_a^2) - (W_4^2 - W_a^2)] \tag{4.36}$$

for a non-reversible process

$$\Delta T_{(4-a)_S} = \Delta T_{4-a}/\eta_R$$

where η_R = rotor isentropic efficiency; and

$$\rho_a = \frac{P_a}{RT_a} = \frac{P_4\,[1 - (\Delta T_{(4-a)_S}/T_4)]^{\gamma/(\gamma-1)}}{R(T_4 - \Delta T_{4-a})} \tag{4.37}$$

From the continuity equation

$$W_a = \frac{\dot{m}}{A_a \rho_a}$$

hence

$$M_a = \frac{W_a}{\sqrt{[\gamma R(T_4 - \Delta T_{4-a})]}} \tag{4.38}$$

By this simplified one-dimensional treatment the rotor channel geometry can be checked to ensure gradual acceleration rates along the rotor passage.

The axial portion at the outlet from the rotor is called the 'exducer'. As already pointed out, the absolute exhaust kinetic energy is lost in the absence of an exhaust diffuser. Thus the exducer eye tip diameter should be large to reduce the exhaust velocity to a minimum. However, a compromise must be made to avoid excessively high Mach numbers at the exducer tip. There is also a limitation imposed on the diameter of the exducer tip. To ensure the desired angle of the fluid leaving the rotor, the exducer vanes have to be shaped with a gradual bend and a certain degree of blade overlap (figure 4.11).

Although no rigorous method is available for predicting the optimum number of rotor blades, Jamieson [4] has suggested a criterion for predicting the minimum number. Due to the relative eddy within the rotor passage (like that in the compressor impeller), the radial velocity will vary between the suction and pressure

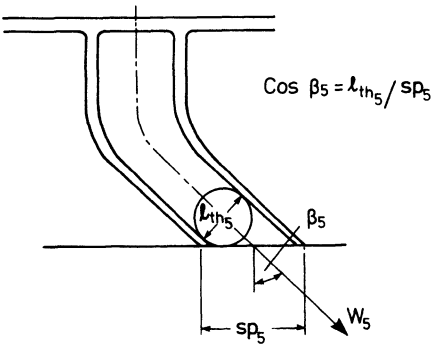

Figure 4.11 *The rotor exducer*

sides of the blades. Jamieson showed, for the case of incompressible flow in a purely radial machine, that the change of angular velocity is given by

$$\frac{\partial C_r}{\partial \theta} = -2\omega r$$

where ω = angular velocity of the rotor. Thus the maximum and minimum radial velocities (at either side of the passage) will be

$$C_{r\,max} = C_r + \tfrac{1}{2}\Delta C_r = C_r + \omega r \Delta\theta$$

and

$$C_{r\,min} = C_r - \tfrac{1}{2}\Delta C_r = C_r - \omega r \Delta\theta$$

where $\Delta\theta = 2\pi/Z$ = rotor blade spacing; C_r = mean radial component of velocity.

Jamieson argued that the minimum number of blades should be chosen such that at no point should the radial velocity become negative. The limiting case is likely to occur at the rotor tip. For $r = r_4$ and $C_{r4\,min} = 0$

$$\Delta\theta = \frac{C_r}{U_4}$$

At the design point flow conditions $U_4 = C_r \tan \alpha_4$, hence

$$\Delta\theta = \frac{1}{\tan \alpha_4}$$

Hence the minimum number of blades is

$$Z_{min} = \frac{2\pi}{\Delta\theta} = 2\pi \tan \alpha_4 \qquad (4.39)$$

Equation 4.39 is plotted in figure 4.12, which clearly shows that a large number of blades is required to avoid flow reversal when the flow angle is large. This

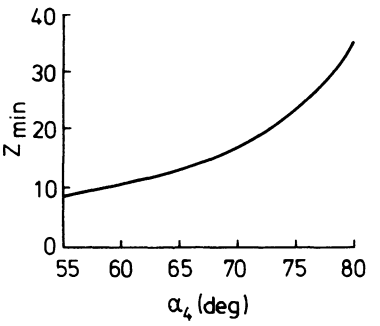

Figure 4.12 *Minimum blade number required to avoid flow reversal at rotor entry [4]*

number becomes impractical for small turbocharger turbines, due to the very narrow passage between blades at exit, causing casting and flow blockage problems. It should also be remembered that an increase in blade number is undesirable, from the point of view of inertia, on an automotive turbocharger. Fortunately, it appears that a reduction in blade number below that suggested by Jamieson's criteria does not result in a dramatic loss in efficiency. Hiett and Johnston [1] tested a 12-bladed rotor with a nozzle outlet angle of 77 °. Increasing the number of blades to 24 (by means of inserting splitter blades) resulted in only a small gain in efficiency (1 per cent). It is probable that other losses resulting from incidence effects at the rotor tip and viscosity in the flow passages are more complex than the concept of flow reversal due to the relative eddy. Similar marginal changes in efficiency, when halving the number of blades, were reported by Rohlik and Kovskey [5] and are shown in figure 4.13.

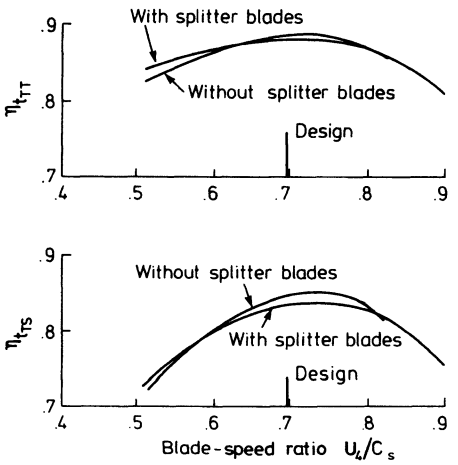

Figure 4.13 *Turbine efficiency with and without splitter blades [5]*

4.3.5 Exhaust diffuser

To enhance the performance of the radial flow turbine, the introduction of an exhaust diffuser provides a greater expansion ratio for the turbine, higher work extraction and in turn a higher stage efficiency. Normally small automotive turbochargers do not include an exhaust diffuser, but some of the large turbochargers incorporate exhaust diffusers in the outlet casing. In many applications an exhaust diffuser must be designed with a very short length after the turbine followed by some collecting device. Thus it is advantageous to use curved wall diffusers in place of the straight wall annular diffusers of short length.

A typical performance map of a straight wall annular diffuser is shown in figure 4.14 indicating the pressure recovery coefficient (*CP*) as a function of diffuser length (*l*) and area ratio (*AR*), with ideal inlet flow conditions. Actual turbine exit conditions are far from ideal and it is difficult to achieve the pressure recovery implied by figure 4.14 in this application.

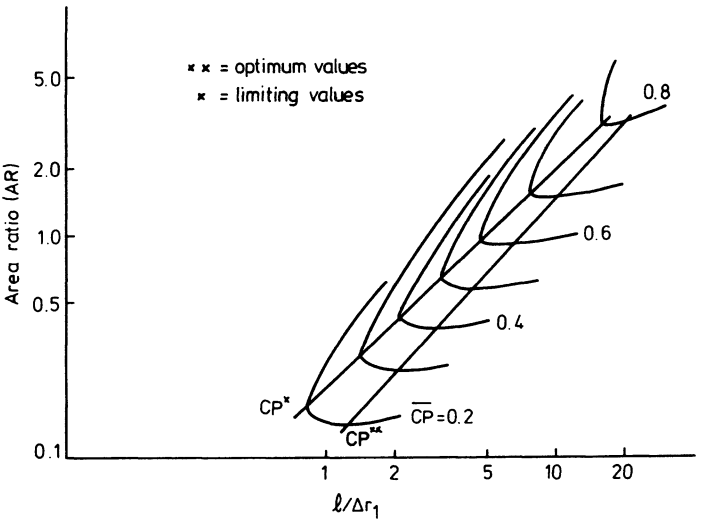

Figure 4.14 *Annular diffuser performance chart (blockage ~ 0.02) [6]*

4.3.6 Efficiency

The isentropic efficiency of a radial flow turbine is not easy to measure accurately and the result can vary greatly depending on test conditions. For example, results from hot tests will depend on the inlet gas temperature since this controls the heat transfer losses. The efficiency will be different from that commonly measured in 'cold' tests, usually using warm air simply to avoid freezing of the water vapour during expansion. Furthermore, if the turbine is operating under unsteady flow conditions of the pulse turbocharging system, its average operating efficiency will be lower than that obtained during steady flow tests. It is for these reasons that the turbocharger manufacturers are reluctant to make their efficiency curves readily available to customers. However, the trends of efficiency at off-design connditions (that is, as the gas angles depart from their design values) are well known.

If the total-to-total isentropic efficiency is plotted against the blade speed or velocity ratio (U/C_s), the resultant curve is relatively insensitive to pressure ratio (figure 4.15) particularly in turbines with nozzles. The total-to-static efficiency does depend on pressure ratio but only to a small extent (except at low nozzle angles, when the exit kinetic energy is significant, relative to turine work). The rather steep drop in efficiency as U/C_s increases above 0.8 is a characteristic of the radial flow turbine contrasting with that of an axial machine. At low flow rates, but high rotor speeds (high U/C_s), the flow becomes insufficient to overcome the centrifugal pressure field. The efficiency becomes zero at the runaway condition (approximately 1.1 to $1.2U/C_s$). Beyond this point the turbine will be acting as a compressor! Although it is unrealistic to consider this situation in the context of steady flow in a turbine, it is quite possible for the instantaneous flow

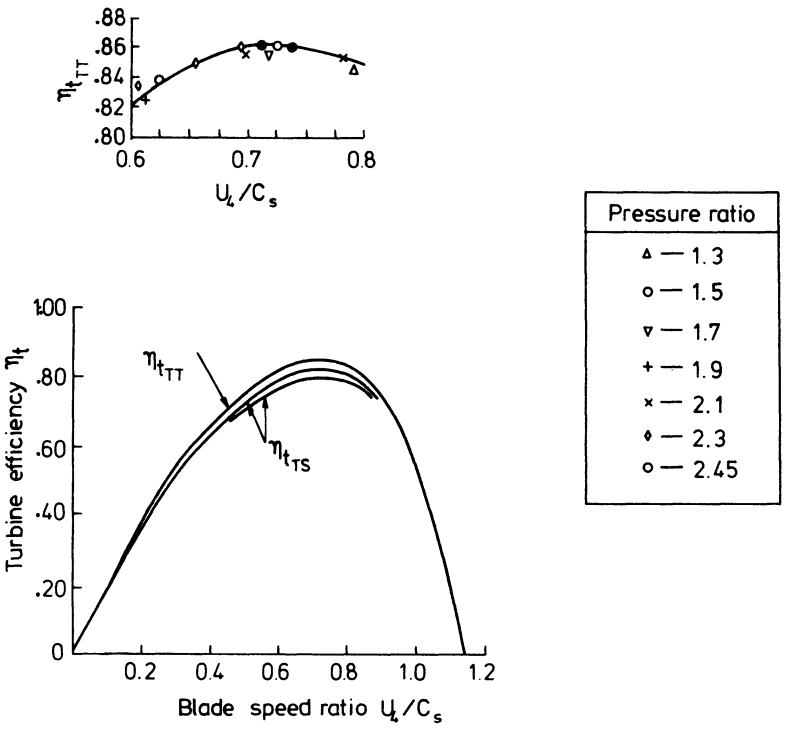

Figure 4.15 *Variation of turbine (with stator nozzles) efficiency with blade speed ratio [1]*

to move into this region during the unsteady flow conditions of pulse turbocharger operation.

From equation 4.33 the ideal specific work transfer at the design condition for purely radial blades will be given by

$$\frac{W}{\dot{m}} = U_4^2$$

For ideal flow with complete exhaust recovery, this will equal the isentropic stagnation enthalpy drop ($h_{01} - h_{5_{ss}}$). From equation 4.17 we obtain

$$\frac{U_4}{C_s} = \frac{U_4}{\sqrt{(2U_4^2)}} = \sqrt{\tfrac{1}{2}} = 0.7071$$

Thus optimum efficiency of an ideal radial flow turbine should occur at

$$\frac{U_4}{C_s} \approx 0.7$$

4.4 Energy Losses

In the simple one-dimensional analysis given above, no detailed account has been taken of energy losses, beyond the introduction of an all-enveloping efficiency term. However, when designing a radial flow turbine some knowledge of the source and magnitude of the various energy losses involved is vital if these losses are to be minimised. The actual fluid flow in a radial turbine is extremely complex since it is viscous and highly three-dimensional. However, considerable useful information has been accumulated by treating energy losses in terms of empirical loss coefficients that are modelled into the one-dimensional flow treatment as outlined above. Naturally, since the coefficients are empirical, they should not be applied to all classes of turbine with any expectation of great accuracy, but the data can usefully be applied in designing and developing similar types and sizes of machines and in predicting offdesign performance.

In a similar manner to that described for the centrifugal compressor, losses can be related to the Mach number at certain stations through the turbine.

There are several sources of energy loss in the radial flow turbine. These may be divided into those that occur in the stationary flow passages and those that occur in the rotor. Those in the rotor may be further sub-divided into incidence losses at the blade entry (sometimes called shock losses, although this may be misleading since shocks do not necessarily occur), fluid friction losses within the rotor passages, losses due to clearance between rotor and shroud and losses due to fluid friction between the rear face of the rotor and the adjacent wall of the casing. The losses are expressed as dimensionless loss coefficients although some users have suggested different bases for their presentation. A summary of the primary losses occurring in the radial flow turbine is illustrated in figure 4.16.

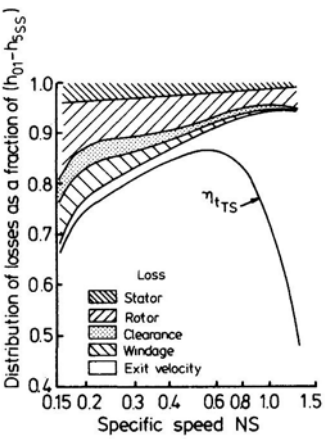

Figure 4.16 *Radial flow turbine distribution of losses [5]*

4.4.1 Nozzle Losses

The energy losses in the inlet casing and the nozzle ring are usually obtained from steady flow 'blowing rig' tests. With reference to the enthalpy/entropy diagram shown in figure 4.2 an enthalpy loss coefficient (*Ch*) may be expressed as

$$Ch = \frac{h_2 - h_{2_s}}{\frac{1}{2}C_2^2} \tag{4.40}$$

An alternative definition in terms of stagnation pressure used by Horlock, [7] is

$$CPL = \frac{P_{01} - P_{02}}{P_{02} - P_2} \tag{4.41}$$

which can be approximately related to *Ch* by

$$CPL \approx Ch \left(1 + \frac{\gamma M_2^2}{2}\right) \tag{4.42}$$

where M = Mach number.

The value of the loss coefficient will be a function of many parameters, such as Reynolds number, nozzle geometry, Mach number, etc. Benson [8] has illustrated the effect of Mach number on the nozzle loss coefficient for a small automotive turbocharger turbine fitted with 15 straight blades at a nominal 63 ° angle. *Ch* reduced with mass flow rate (figure 4.17). Benson states that the loss coefficient of the well-designed scrolls and nozzles combined is typically *Ch* = 0.1.

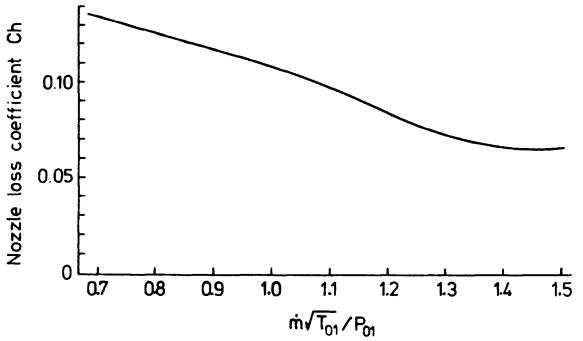

Figure 4.17 *Nozzle loss coefficient [8]*

4.4.1.1 Nozzle Gas Exit Angles

Before considering the losses associated with the rotor, it must be mentioned that the gas exit angle from the nozzles (or from the rotor blades) does not equal the blade angle. The deviation is a function of the throat width/blade pitch ratio (figure 4.9) and the local curvature of the nozzle blade (suction side) between

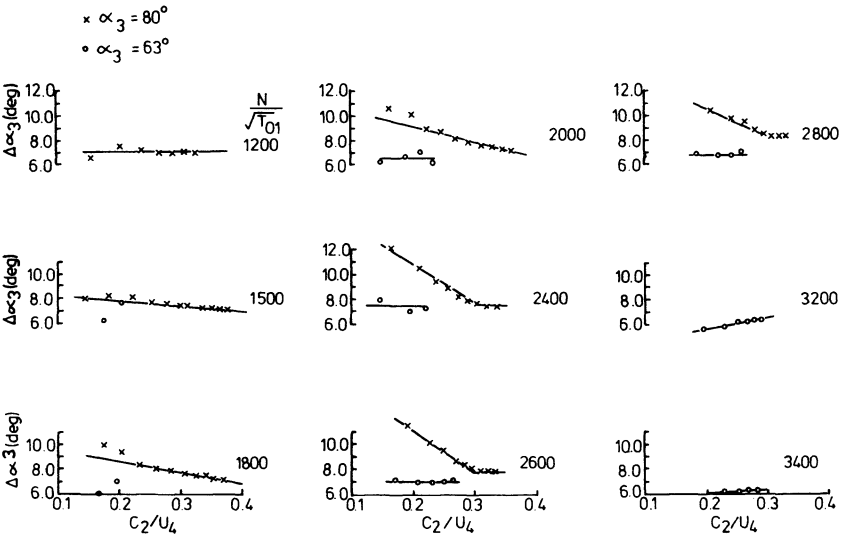

Figure 4.18 *Nozzle exit angle deviation ($\Delta\alpha_2$): CAV B01 turbine [8]*

throat and trailing edge. Hiett and Johnston [1] recommended using a flow angle calculated from $\alpha_3 = \cos^{-1}(l_{th2}/sp_3)$, but Benson [8] has shown (figure 4.18) that the deviation between nominal blade angle and the actual gas angle ($\Delta\alpha_3$) varies with exit velocity (C_2), rotor speed, and the blade angle itself. It is important that a correct gas angle is known since the incidence loss on the rotor is highly dependent on the actual gas inlet angle. Perhaps the most simple treatment is to evaluate the flow angle from the cosine rule as discussed above and, if at offdesign conditions, allow further deviation as a function of rotor speed if experimental data is available. [8]

4.4.2 Rotor Losses

It has already been stated that the energy losses in the rotor are derived from incidence effects, fluid friction in the passages, disc friction on the wheel and clearance effects, but these losses are interrelated. Although clearance losses may become quite significant on small mass-produced automotive turbochargers, it is usually the incidence and fluid friction effects in the rotor passage that dominate. Since it is particularly difficult to separate these two effects, it is common practice to predict an incidence loss and subtract it from the over-all rotor loss (measured experimentally), the resultant being attributed to passage friction. Although this procedure introduces the effect of errors in incidence loss prediction being masked, it is difficult to suggest a more rigorous approach that remains simple and within the concept of a simple one-dimensional flow model.

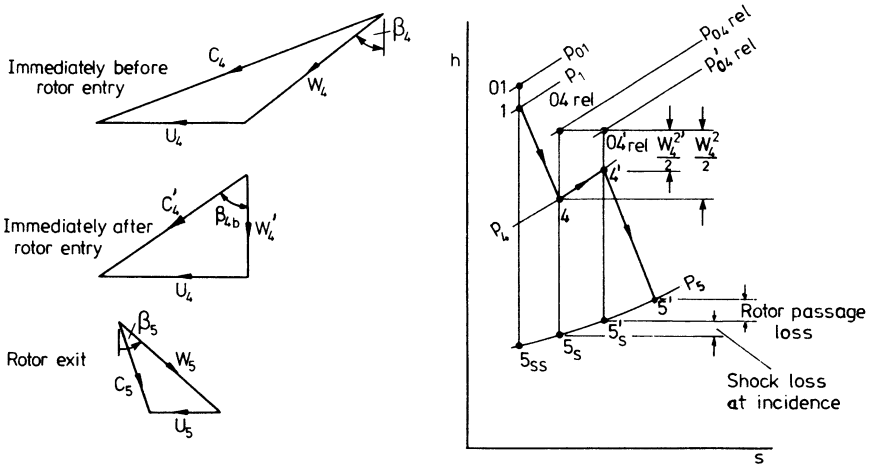

Figure 4.19 *Velocity triangles and h-s diagram for a 90° (radial) turbine at an offdesign condition*

4.4.2.1 Incidence Losses

Incidence loss models have been developed to allow for losses resulting from incorrect gas angles at offdesign conditions. Figure 4.19 shows a typical offdesign velocity triangle at the rotor entry. Immediately after entering the rotor, the gas is constrained to have a purely radial relative velocity (for a one-dimensional flow model of a radial bladed rotor), hence the actual gas angle is rapidly changed. In a real rotor the incidence angle between gas and rotor blade will cause flow separation and a subsequent mixing loss within the impeller. This loss is called an incidence loss in the one-dimensional flow model. It will be zero at the design point and will rapidly increase as conditions change.

Two separate approaches are commonly used to predict the incidence loss as the gas stream enters the rotor. In the first, often referred to as a 'constant pressure' model, it is assumed that the flow follows the blade angle β_4 and that the flow process occurs at constant pressure, with a corresponding entropy increase.

This model has been used by Whitfield and Wallace [9] and Benson *et al.* [10] The NACA model, reported by Futral and Wasserbauer [11] is based on the assumption that the complete tangential component of the relative kinetic energy is destroyed. Both Benson [8] and Whitfield and Wallace [9] have compared the two methods and concluded that there was little difference between them, those of Bridle and Boulter [12] nor Balje. [13] In figure 4.20 these predictions are compared on the basis of the loss of relative stagnation pressure (due to the assumed reduction in relative velocity [8]) for offdesign conditions on the turbine tested by Hiett and Johnston. [1]

Since the predictions do not result in greatly differing results, only the 'constant

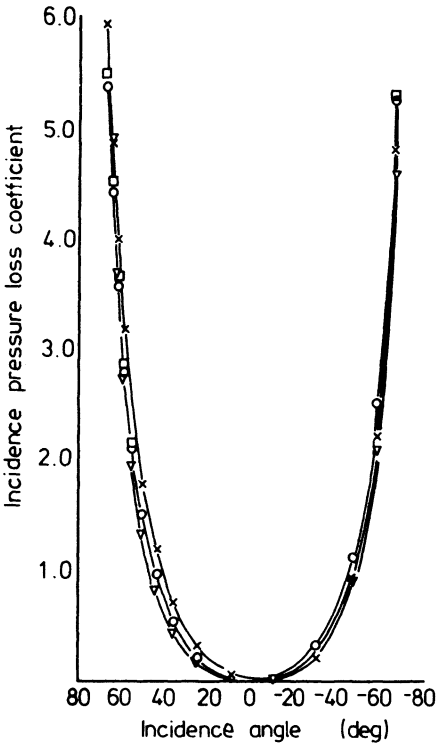

Figure 4.20 *Incident loss coefficients: comparison of loss coefficients at incidence – offdesign (Ricardo 70B turbine) [8]*

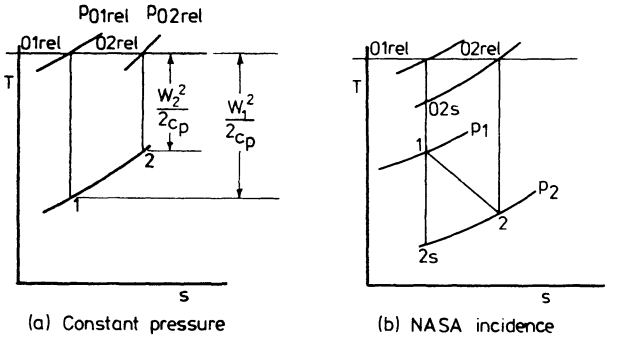

Figure 4.21 *T-S diagrams for loss models*

pressure' model will be considered in detail (figures 4.19 and 4.21a). Applying the steady flow energy equation to the relative flow at rotor entry gives

$$h_2 + \frac{W_2^2}{2} = h_1 + \frac{W_1^2}{2}$$

(where states 1 and 2 denote before and after the incidence loss) since heat and work transfer may be neglected in the nozzles. From the perfect gas equation this becomes

$$T_2 + \left(\frac{\gamma-1}{\gamma R}\right)\frac{W_2^2}{2} = T_1 + \left(\frac{\gamma-1}{\gamma R}\right)\frac{W_1^2}{2} \tag{4.43}$$

or

$$\frac{T_2}{T_1} = 1 + \frac{(\gamma-1)}{2\gamma R T_1}(W_1^2 - W_2^2)$$

From continuity

$$\rho_1 A_1 W_1 \cos\beta_1 = \rho_2 A_2 W_2 \cos\beta_2 \tag{4.44}$$

Since a constant pressure process is assumed

$$\frac{T_1}{T_2} = \frac{\rho_2}{\rho_1} \tag{4.45}$$

Eliminating W_2 from equation 4.44 and using equation 4.43 gives

$$\frac{T_2}{T_1} = 1 + \frac{(\gamma-1)}{2\gamma R T_1} W_1^2 \left[1 - \left(\frac{T_2}{T_1}\right)^2 \left(\frac{A_1 \cos\beta_1}{A_2 \cos\beta_2}\right)^2\right] \tag{4.46}$$

Since the sonic velocity (a) is given by

$$a^2 = \gamma R T$$

then, in terms of the relative Mach number (M)

$$M = \frac{W}{a}$$

and introducing the area ratio parameter (AR)

$$AR = \frac{A_1 \cos\beta_1}{A_2 \cos\beta_2}$$

equation 4.46 may be simplified to give

$$\frac{T_2}{T_1} = 1 + \frac{(\gamma-1)}{2} M_1^2 \left[1 - \left(\frac{T_2}{T_1}\right)^2 (AR)^2\right]$$

Solving for T_2/T_1 gives

$$\frac{T_2}{T_1} = \frac{-1 \pm \sqrt{\left[1 + 4\left(\frac{\gamma-1}{2}\right) M_1^2 (AR)^2 \left(1 + \frac{\gamma-1}{2} M_1^2\right)\right]}}{2(AR)^2 M_1^2 (\gamma-1)/2} \tag{4.47}$$

This can be transformed into the equivalent entropy increase by using the thermodynamic relationship

$$T\,\mathrm{d}s = \mathrm{d}h - v\,\mathrm{d}P$$

For a perfect gas undergoing a constant pressure process

$$s_2 - s_1 = \int_1^2 \frac{c_p}{T} dT = c_p \ln (T_2/T_1)$$

that is

$$s_2 - s_1 = \frac{\gamma R}{\gamma - 1} \ln \left(\frac{T_2}{T_1} \right) \tag{4.48}$$

The entropy rise (equations 4.47 and 4.48) is a function of the inlet Mach number (M) and the area ratio term (AR). In fact, AR is a function of the incidence angle. Consider figure 4.22 which illustrates an offdesign condition with a relative inlet gas angle β_4 and a (non-radial) blade angle β_{4b}. The constant pressure model implies that as the gas velocity changes direction as it enters the blades of the rotor, that is, through the incidence angle (i) where

$$i = \beta_4 - \beta_{4b}$$

In the simple case of a radially bladed impeller ($\beta_{4b} = 0$)

$$AR = \frac{A_4}{A_4'} \cos \beta_4 = \frac{A_4}{A_4'} \cos i$$

where

A_4 = area immediately before rotor entry

A_4' = area immediately after rotor entry.

Neglecting the thickness of the rotor blades, $A_4' = A_4$, hence

$$AR = \cos i \tag{4.49}$$

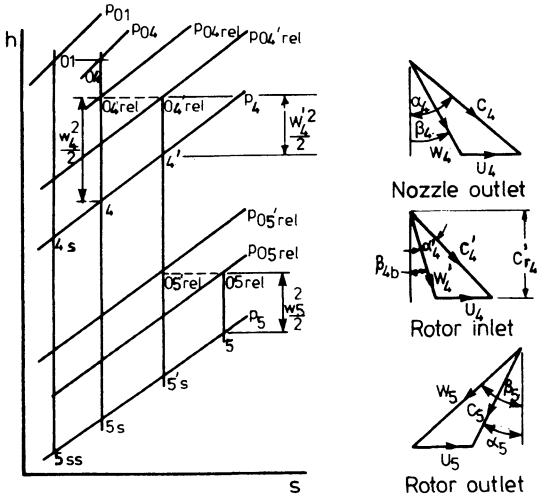

Figure 4.22 *T-S diagrams for rotor losses in radial turbine*

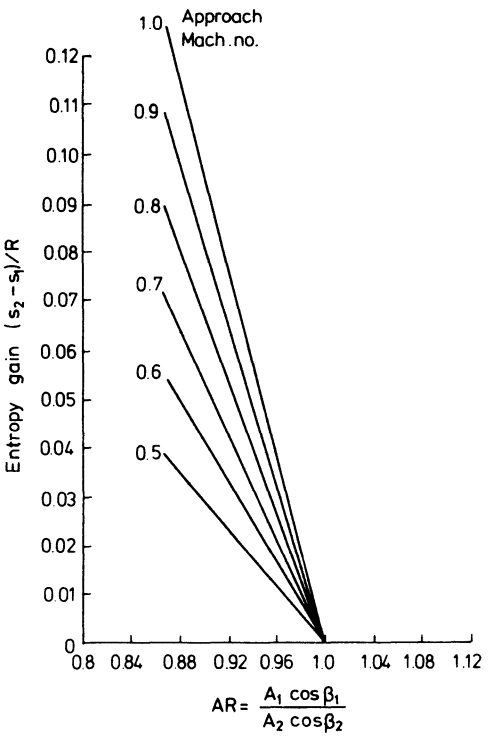

Figure 4.23 *Entropy gains given by the constant pressure model*

In the more general case of a non-radial blade

$$AR = \cos i - \sin i \tan \beta_{4b} \tag{4.50}$$

(again, neglecting blade blockage). Equation 4.48 is plotted in figure 4.23 which shows the effect of large incidence angles on energy loss (entropy gain) particularly at high inlet Mach number.

The constant pressure loss model assumes no blade blockage. If blockage were taken into account, it is possible that AR could exceed unity, resulting in the unrealistic situation of an entropy loss (that is, the model becomes invalid).

4.4.2.2 Fluid Friction Losses in the Rotor Passage

Several methods have been proposed for predicting the energy loss due to fluid friction within the rotor passage. Bridle and Boulter [12] considered the viscous drag separately in the radial and axial sections using the concept of an equivalent rotor with separate radial and axial components. The losses themselves were based on secondary flow losses in axial flow turbomachinery developed by Ainley and Mathieson [14] (see chapter 5). Futral and Wasserbauer [11] proposed that the

frictional loss is a function of the (relative) kinetic energy at entry and exit of the rotor, that is

$$L = K\left(\frac{W_4^2 + W_5^2}{2}\right) = \text{losses} \tag{4.51}$$

where K is an empirical constant and L can be related to a passage loss coefficient

$$Ch = \frac{h_5 - h_{5s}}{\frac{1}{2}W_5^2} = \frac{L}{\frac{1}{2}W_5^2} \tag{4.52}$$

Thus

$$Ch = K\left(\frac{W_4^2 + W_5^2}{W_5^2}\right) \tag{4.53}$$

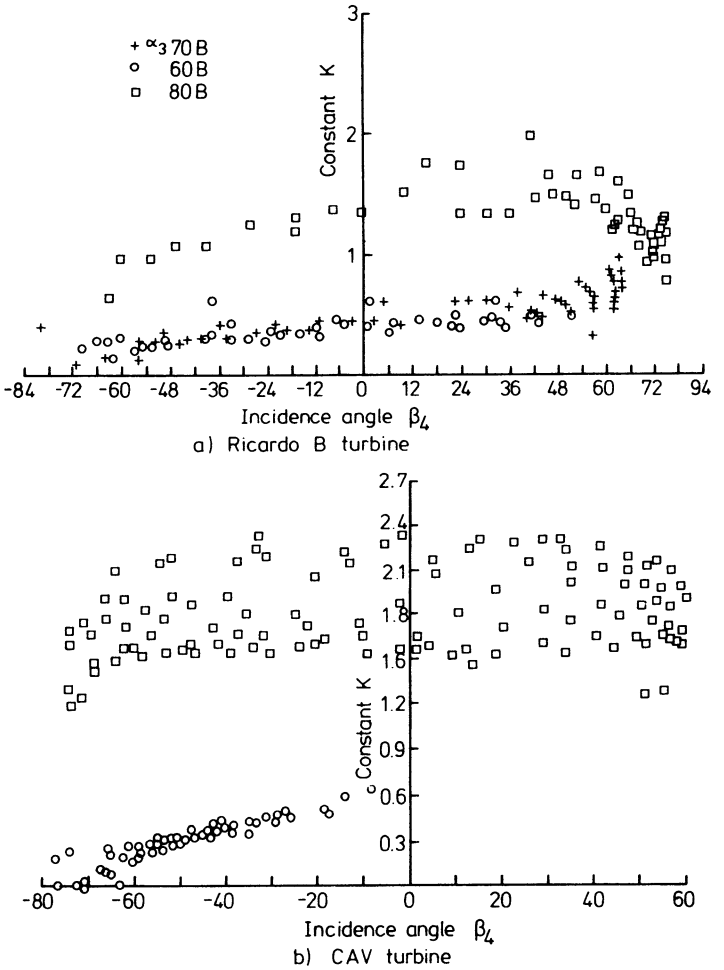

Figure 4.24 *Futral and Wasserbauer rotor loss coefficients [11]*

Benson [8] has evaluated K by subtracting the incidence loss from experimental values of the over-all rotor loss. The value of K is experimental and cannot be predicted but its value remained within 20 per cent of its mean as the incidence angle was varied over a large range (figure 4.24). Since at offdesign conditions the incidence loss dominates, it is not unreasonable to assume a constant mean value of K, although it will differ from one machine to another and will vary as the nozzle angle is changed. Futral and Wasserbauer analysed data from a 0.115 m diameter turbine and obtained a value of $K = 0.44$.

4.4.2.3 Disc Friction Losses

It is usual to express the disc friction loss between rotor back and housing in terms of a torque or power coefficient, although it is difficult in practice to separate it from the over-all rotor loss. For a rotating disc enclosed in a casing, Daily and Nece [15] have shown that the loss is a function of Reynolds number ($r_4 U_4/\nu = \omega r_4^2/\nu$) and the disc to casing clearance ratio (l_{cl}/r_4). The loss was expressed as a non-dimensional torque coefficient CTQ where

$$\text{torque} = CTQ \frac{\rho\omega^2}{2} (r_4^5 - r_5^5) \tag{4.54}$$

where r_5 and r_4 are the outer radius of the shaft retaining the rotor and the rotor tip radius respectively. The results are shown in figure 4.25, implying that the effect of Reynolds number dominates. For reasons of mechanical stress, a turbocharger rotor will not be shrouded (and the rear face may be scalloped out near the tip) so the true situation differs greatly from Daily and Nece's tests, although this data is widely used.

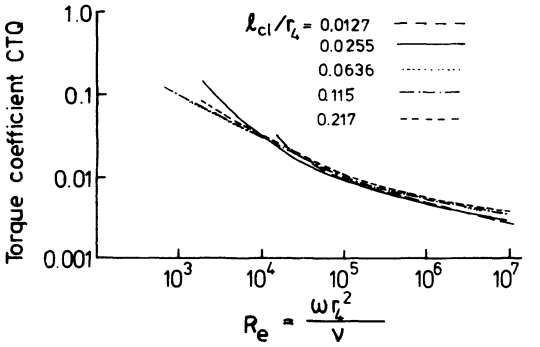

Figure 4.25 *Smooth disc torque coefficient [15]*

4.4.2.4 Clearance Losses

In a similar manner to the disc friction losses, clearance effects are usually lost in the over-all rotor loss coefficient. However, it is useful to try to estimate them so that a suitable compromise between manufacturing tolerance and the effect of

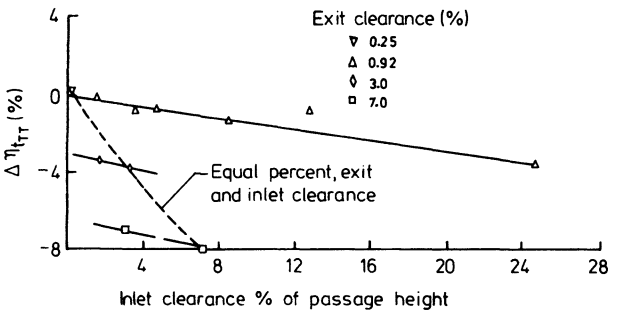

Figure 4.26 *Summary of inlet and exit clearance effects on total efficiency at design equivalent values of speed and pressure ratio [16]*

clearance on efficiency may be chosen rationally. This becomes particularly important for small automotive turbochargers where the combination of small physical size and the need for very low manufacturing costs combine to produce relatively large clearances. Excessive clearance will result in an efficiency drop and a loss in mass flow rate. Figure 4.26 illustrates the loss in efficiency as the blade-to-shroud clearance is increased. It is particularly interesting to note that the clearance at the rotor exit is far more influential than at the inlet (tip). This is probably due to the effect the exit blade-to-shroud clearance has on what fraction of the total mass flow is turned to the exit blade angle. At the inlet it is the nozzles (stator) that set up the flow angle, and the efficiency loss is due to flow leaking from the pressure to suction side of a blade, causing a small 'unloading' of the blade. This same phenomenon occurs at the exit, in addition to the gas angle effect already described. Clearance at the exit is largely a function of tolerances plus the journal bearing clearance. Unfortunately, rotor stability considerations tend to require quite large bearing clearances for the oil film. Tip clearance (or axial clearance) is largely a function of the differential expansion between rotor and housing, thrust bearing clearance and tolerance build-up.

4.4.2.5 Rotor Scalloping

Because of the high stress levels in turbocharger turbines, particularly at high temperature, material is sometimes removed from the rotor disc between the actual blades (figure 4.27). The reduced disc stress is partly counteracted by increased stress at the blade root but, since it is preferable for the blades to fail before the disc, scalloping is often useful. Additional gains result from the lower weight and inertia (for example, response and critical speeds of the rotor, etc.). Hiett and Johnston [1] showed that removing some disc material from between the blade tips did not seriously affect the turbine efficiency, because the flow path was not significantly changed. A small additional amount of scalloping resulted in a 2 per cent efficiency loss but a 25 per cent reduction in rotor weight and 45 per cent reduction in inertia.

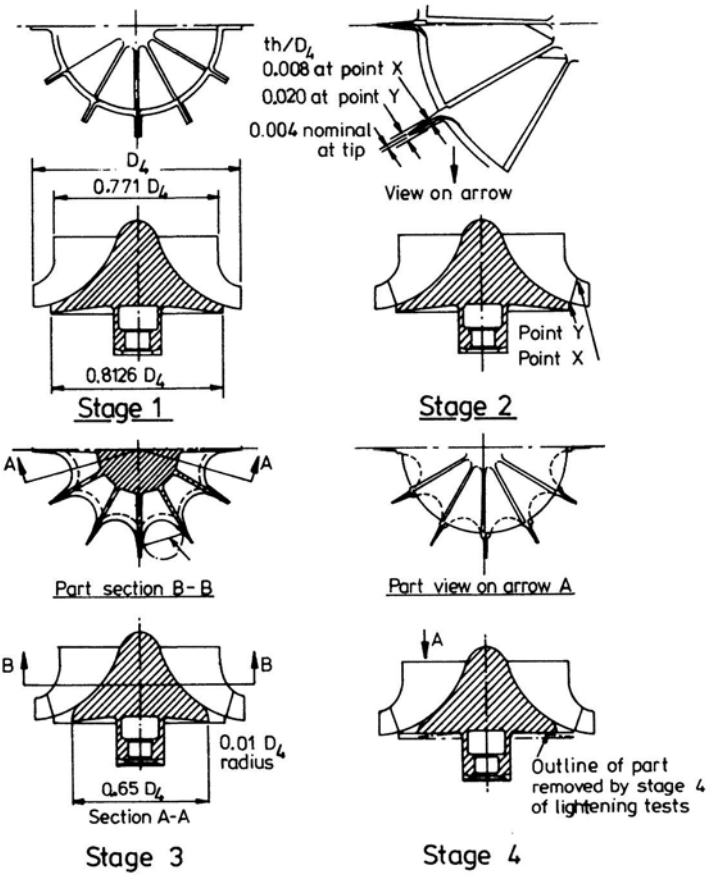

Figure 4.27 *Scalloped rotor [1]*

4.5 Three-dimensional Flow Models

The gas flow in the inlet casing and rotor of a radial flow turbine is viscous and three-dimensional. Under the pulse turbocharging system it is also highly unsteady. Thorough analysis of this situation is not yet a practical proposition and hence reliance is still placed on the concept of one-dimensional flow analyses combined with semi-empirical loss coefficients, as described above. However, attempts have been made to analyse three-dimensional inviscid flow and these can give a useful, if approximate, insight into what is happening in the machine.

Most widely used are the streamline curvature methods of Katsanis. [17, 18] The problem is reduced to hub-to-shroud and blade-to-blade two-dimensional analyses with inviscid flow. This, and similar methods, have been used by Barnard and Benson, [19] Benson *et al.*, [20] Cartwright, [21] Ariga *et al.* [22] and others. Figure 4.28 shows hub-to-shroud and blade-to-blade streamlines and relative velocity profiles predicted for a small automotive turbocharger turbine. The flow

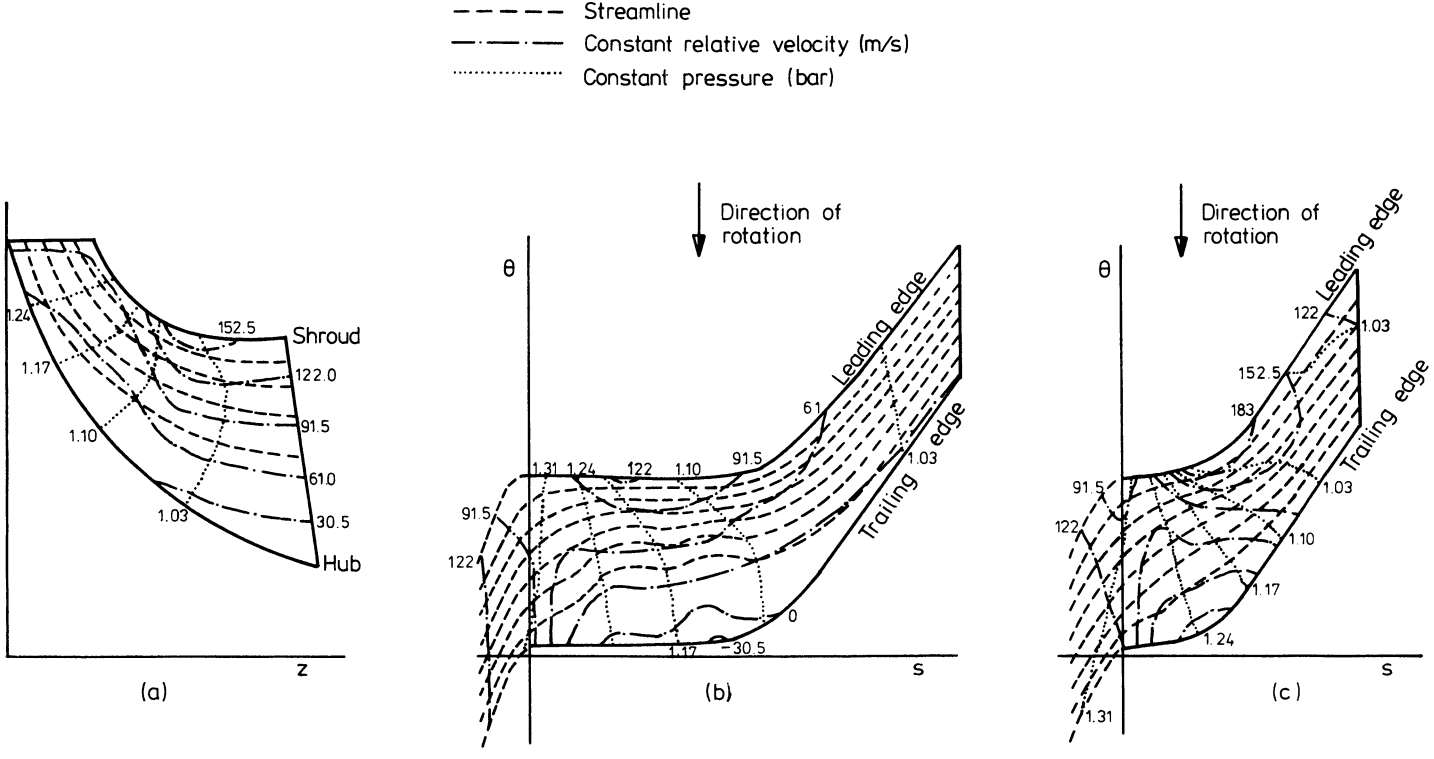

Figure 4.28 (a) *Flow pattern in meridional hub-to-shroud plane;* (b) *flow pattern in blade-to-blade plane on hub surface;* (c) *flow pattern in blade-to-blade plane at shroud surface [19]*

conditions are offdesign at a large incidence angle (59°). In the blade-to-blade plane, a negative velocity is predicted on the hub surface at the trailing edge of a blade. This implies that an eddy will be present at this position. It is also probable that flow separation will occur on the shroud, again at the trailing edge of a blade (figure 4.28c) where the relative velocity gradient becomes very steep. Although viscosity has been ignored and hence boundary layer growth and separation are absent from the model, these techniques can be useful in 'tidying up' a channel profile to reduce the possible effects of rapid decelerations, etc. Similar methods can be used to analyse flow in nozzles. Figure 4.29 shows predictions for the surface velocity distribution along the straight blades used by Hiett and Johnston [1] and alternative curved blades. The blade loading (velocity distribution) diagram obtained with the curved blades indicates an advantage over straight nozzle blades, by reducing the velocity difference from pressure to suction side, where they meet at the trailing edge.

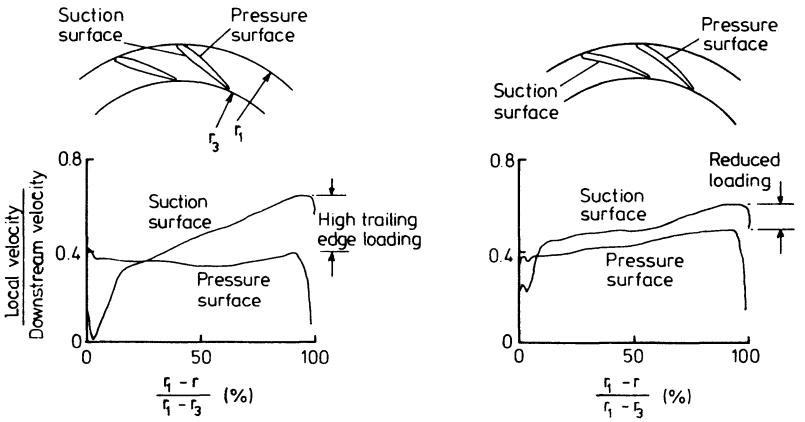

Figure 4.29 *Radial turbine nozzles [23]*

4.6 Unsteady Flow

Many diesel engines use the pulse turbocharging system. As a consequence, the turbocharger turbine is required to operate under non-steady flow conditions, with a double or sometimes triple-entry casing creating different instantaneous flow regimes in each sector. The variation in mass flow rate during an engine cycle is substantial, in some cases moving from zero flow to choke and back again. The degree of unsteadiness will depend on many factors, such as the number of engine cylinders connected to a turbine entry, degree of supercharge (that is, low or high pressure), type of turbine entry casing, etc. Even under a (nominally) constant pressure system, some flow unsteadiness will occur if the exhaust manifold volume is kept down to a reasonable size.

As the instantaneous mass flow rate arriving at the turbine varies from one extreme to another, the resultant gas angles in the machine will depart far from their design values, creating large incidence losses, boundary layer separation, etc.

It would be unreasonable to expect the turbine to operate at high efficiency under these conditions and it is indeed fortunate that radial turbines can accept unsteady flow without serious loss in performance. The actual performance produced by a particular machine will depend on the actual flow conditions to which it is subjected.

4.6.1 End-of-sector and Windage Losses

If the turbine is fitted with a nozzle ring and has a divided inlet, the division from two or three inlets is maintained to the low-pressure region at the nozzle exit. This implies that the division is in the form of separate angular sectors. At the join of each sector ('end of sector') some energy loss occurs even under steady flow conditions. This is usually due to a somewhat non-uniform flow distribution around each sector, combined with a less than perfect mass distribution between sectors creating different gas velocities and flow angles either side of the dividing nozzle blade. A mixing loss occurs. However, the loss is small. The end-of-sector losses only become significant when the instantaneous flow conditions on either side of the divider are substantially different. In fact, this must be the normal (pulse system) condition, otherwise there would be no point in dividing the turbine entry. Thus end-of-sector losses occur during unsteady flow and their value will depend on the flow conditions prevailing.

Windage losses also occur due to unsteady flow with the pulse operating system. They result from the instantaneous mass flow rate in one sector of the turbine dropping to zero. That part of the turbine wheel effectively 'windmills'. The magnitude of the loss (which is considerably greater than the end-of-sector loss) can be established from steady flow tests with admission through one sector only, that is, 'partial admission'. Figure 4.30 shows that the fall-off in efficiency is as large as 15 percentage points on a medium-sized radial turbocharger turbine. Benson and Scrimshaw [25] quote a drop in efficiency from 74 per cent to 63 per cent on an automotive-size turbocharger turbine. Undoubtedly some cross-flow occurs from the flowing sector to the non-flowing sector in the case of complete partial admission. On an engine the loss in efficiency will be considerably less,

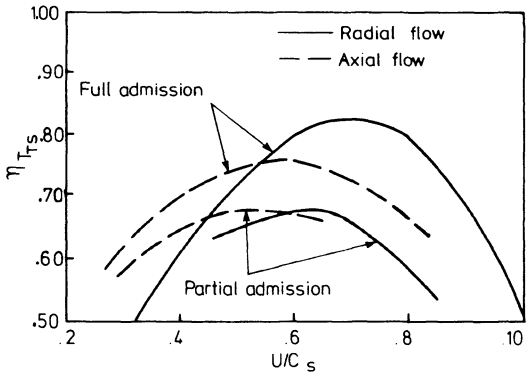

Figure 4.30 *Partial admission losses [24]*

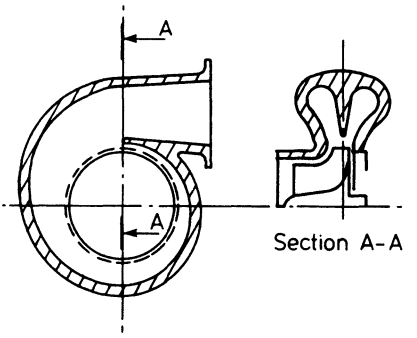

Figure 4.31 *Twin-entry volute casing*

since complete partial admission (that is, no-flow in one sector) only occurs for a small fraction of the time and may not occur at all.

If a nozzleless casing is used, the division between sectors will usually take the form of a wall in the radial plane (figure 4.31). Under steady flow conditions the mixing loss at the junction (equivalent to the end-of-sector loss) is likely to be greater than that of a casing with radially divided sectors but incidence loss reduces. However, under unsteady flow conditions with a phase difference between the flows, the gas flow situation will be very different. When unequal mass flows emit from each sector, the flow difference is likely to mix out before reaching the rotor blades. During the period when the flow through one inlet drops to zero, some reverse flow (from the other inlet) will occur, [26] but the remaining gas flow will enter the rotor around the complete periphery. Thus the complete partial admission situation, when some rotor passages have zero through-flow will not occur. As far as the rotor itself is concerned, a circumferentially divided inlet casing will reduce flow unsteadiness and eliminate complete windmilling. Against this are certain disadvantages. Although the connection between the inlets occurs after substantial area reduction where pressures have reduced, some interference in flow between one inlet branch and the other will occur. This may be undesirable for the exhaust and scavenging processes on the engine.

Over all, the benefits inherent in this type of divided casing usually outweigh the disadvantages and they are used on most small turbocharger turbines having vaneless casings.

4.6.2 Combined Effect of Unsteady Flow, Windage and End-of-sector Losses

The pressure fluctuation in the intake to the turbine may have a large order of magnitude and hence the energy available for conversion to useful work in the turbine is varying. Due to the inertia of the turbocharger rotor, this cyclic torque results in only small changes in turbocharger speed (typically of 2 to 5 per cent). For the purpose of considering gas angles in the turbine, it is reasonable to neglect this variation and assume a constant tip speed. As the instantaneous gas flow varies from its peak down to nearly zero value and back again, the blade speed ratio

(U/C_s) will vary from a small to a very large value. If it is assumed that the turbine behaves at any instant in an identical manner under steady or unsteady flow ('quasi-steady flow'), then the instantaneous turbine efficiency will vary with U/C_s, according to figure 4.30. In practice, the actual turbine performance is not fully in agreement with the quasi-steady assumption, but the trend is certainly correct. The average operating efficiency of the turbine will be dominated by the periods of time when the mass flow rate is large (the efficiency during periods of zero flow is relatively unimportant) and hence will be considerably higher than half the steady flow value. This is illustrated in figure 4.32 where the mass flow rate and efficiency from unsteady flow tests on a small double-entry turbine are plotted (against crank angle of an engine). Clearly the time-averaged value of turbine efficiency will be of the order of 50 per cent (cf. a peak value of 70 per cent). However, the mass flow average efficiency ($\int \dot{m}\eta_i \, dt / \int \dot{m}_i \, dt$) will be approximately 65 to 70 per cent. Thus the drop in efficiency due to unsteady flow operation is

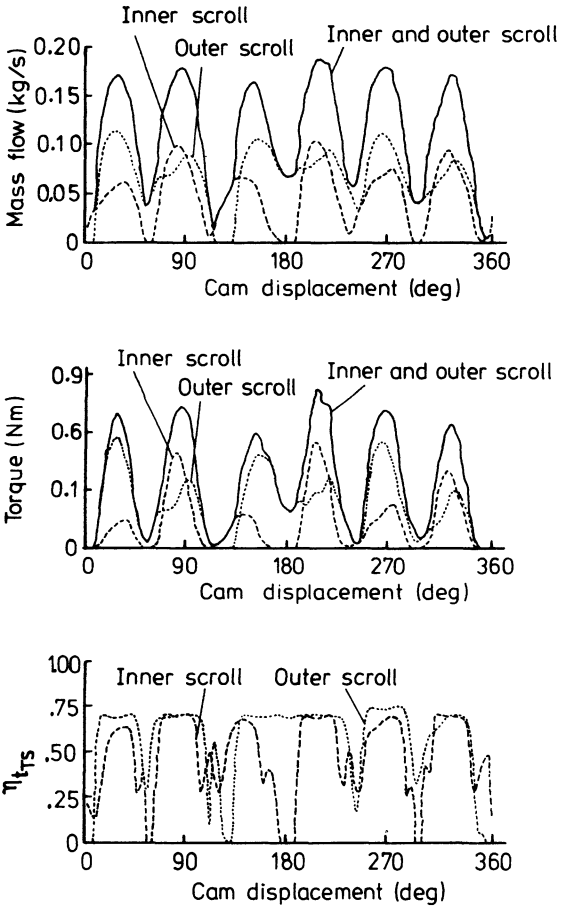

Figure 4.32 *Torque, mass flow and efficiency diagrams [25]*

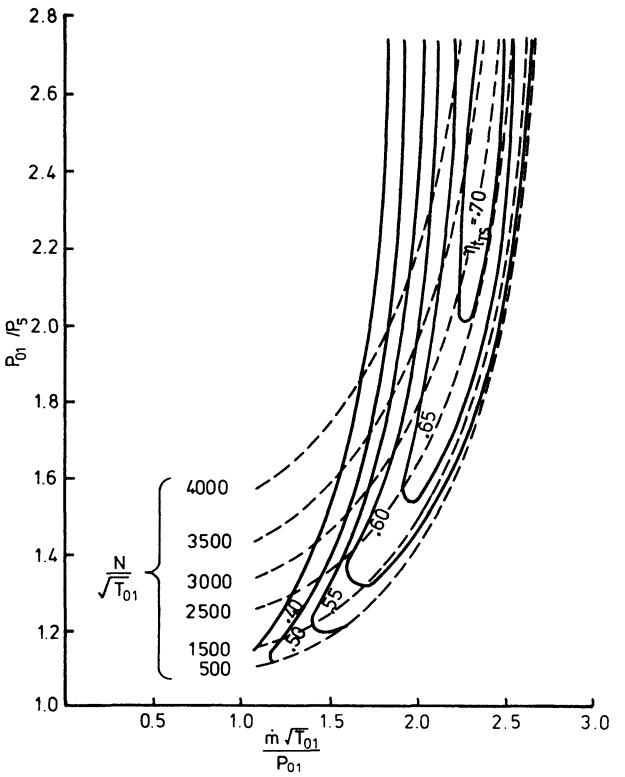

Figure 4.33 *Typical turbine characteristic (Holset Ltd)*

considerably lesss than might be expected considering the efficiency against U/C_s curve, in isolation, or complete partial admission data.

4.7 Turbine Characteristics and Flow Range

The performance of a radial flow turbine is best defined (chapter 2) by curves showing the relationship between expansion ratio, isentropic turbine efficiency and pseudo-non-dimensional mass flow rate and speed. A typical turbine characteristic, showing constant speed parameter $N/\sqrt{T_{01}}$ plotted against the non-dimensional mass flow rate ($\dot{m}\sqrt{T_{01}}/P_{01}$) and expansion ratio P_{01}/P_5 is given in figure 4.33.

Compared with the flow characteristic of an adiabatic nozzle (see figure 4.34) defined by the relationship

$$\frac{\dot{m}\sqrt{T_{01}}}{AP_{01}} = \sqrt{\left\{\frac{2\gamma}{(\gamma-1)R}\left[\left(\frac{P_5}{P_{01}}\right)^{2/\gamma} - \left(\frac{P_5}{P_{01}}\right)^{(\gamma+1)/\gamma}\right]\right\}} \qquad (4.55)$$

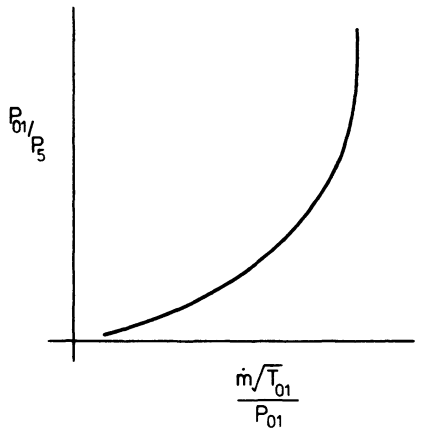

Figure 4.34 *Nozzle characteristic*

(where subscripts 01 and 5 relate to entry and exit) the principal difference is that the turbine characteristics are quite speed dependent.

In addition the turbine chokes at a much higher pressure ratio than the simple adiabatic nozzle. The latter phenomenon is not surprising since the turbine could be considered as two nozzles in series (that is, nozzle and rotor passages). The speed dependence principally arises from the effect of the centrifugal field created by the speed of the rotor. At low rotational speeds a certain inlet pressure is required for mass to flow through the turbine in the correct direction. At higher rotor speeds a greater inlet pressure will be required, since a higher centrifugal pressure field will oppose the gas motion.

The restricted presentation of the turbine expansion ratio against mass flow rate characteristics makes it difficult to study the efficiency contours as shown in figure 4.33. For this reason several other useful presentations are often used. Typical is the torque/speed presentation (figure 4.35) showing lines of constant expansion ratio and efficiency, and the efficiency against blade speed ratio diagrams previously mentioned (figure 4.30).

A turbocharger turbine is required to handle a very wide mass flow range in automotive application where the engine operates over a broad speed and load range.

The flow range ($\dot{m}\sqrt{T}/P$) of the radial flow turbine is limited by choking at high pressure ratios. No exact low flow limit exists, since in the ultimate situation the radial turbine can act as a compressor. The maximum flow through the turbine is limited by choking conditions in the nozzle throat (or throat of the nozzleless casing) or rotor exit. The critical pressure ratio between the inlet and the nozzle throat, when flow at the latter is sonic, is a function of the gas specific heat capacity ratio (γ), where

$$\frac{P_5}{P_{01}} = \left(\frac{2}{\gamma + 1}\right)^{\gamma/(\gamma-1)} \tag{4.56}$$

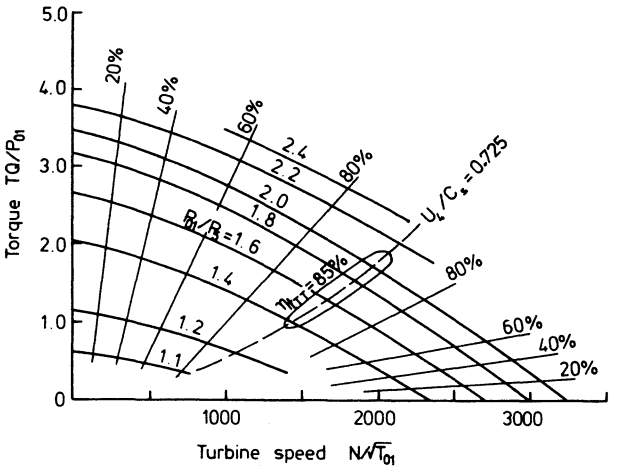

Figure 4.35 *Variation of troque with speed: Turbine with nozzles. [1]*

For diesel engine exhaust gas this will be approximately 0.55 (that is, an expansion ratio of 1.82:1), dependent on air/fuel ratio and exhaust temperature. For the normal 50 per cent reaction design, the expansion ratio across the rotor will be of a similar order, enabling the turbine to operate at an over-all expansion ratio approaching 3.5:1 before the flow becomes sonic. However, since turbine flow characteristics (see figure 4.33) become asymptotic to the choking conditions, and the rotor exducer may also choke, the turbine is almost choked at a considerably lower pressure ratio.

The effective area of the vaned nozzles depends on the vane angle and hence the choked mass flow will be altered by a change in nozzle angle. If a nozzleless inlet casing is used, the effective throat area will be dependent on the gas angle and exducer area. Gas angle control is achieved by varying the cross-sectional area of the scroll, since this increases or decreases the tangential component of velocity. Thus the choked mass flow rate will be a function of the effective area of the scroll and can be varied by changing scrolls.

As important as the choked flow rate is the need for high efficiency over a wide flow range. Although a turbine with inlet nozzles usually achieves a higher peak efficiency than one with a nozzleless casing (due to better and more uniform flow distribution and guidance around the rotor tip), the latter is better equipped to cope with offdesign conditions. Regardless of mass flow rate, the use of inlet nozzles will constrain the flow angle at entry to the rotor. As the flow rate moves away from design conditions, the inlet velocity will change in magnitude, not direction. Thus the relative velocity approaching the impeller tip will depart from the radial direction, creating an incidence loss. If a nozzleless casing is used, the flow angle can adapt to the flow rate. An incidence loss will still result, but the incidence angle (and hence the loss) will be less. Thus the nozzleless turbine has a wider efficient-flow range and is commonly used on turbochargers for engines working over wide speed and load ranges.

Not only does the choice of nozzle angle or scroll affect the choked mass flow

rate, but, since it changes the inlet velocity triangle, it affects the efficiency map. Changes in nozzle angle or casing will move the area of optimum efficiency across the working map of the turbine. If the changes in area or angle are large, the peak value of efficiency will probably also drop, since incidence losses will increase at what was previously the design point. However, changes of this type do provide an extremely useful method of tailoring the performance of a turbocharger to the requirements of a particular engine.

From the economic point of view it is desirable to produce a single turbocharger unit that can cover a wide range of engine sizes and hence of mean mass flow rates. To adapt a basic design of the turbine such that it can provide high efficiency over a very large mass flow range involves changing the effective choking area. There are three principal ways in which this can be done

(1) varying the angle of the nozzle blades (see figure 4.36a) or varying the turbine inlet casing cross-sectional area for nozzleless turbines;

(2) cropping the trailing edge of the nozzle blades to increase the effective throat area (figure 4.36b);

(3) axial cropping of the nozzle ring and rotor together with the provision of suitable sized turbine casings (figure 4.36c).

The method 3 has the most drastic effect on throat and rotor exducer area and hence mass flow rate, with the least loss in turbine efficiency. For these reasons a manufacturer may offer a basic design of a turbocharger with two or three rotors and corresponding turbine inlet casings to cover a large range of engine sizes. This can provide up to 50 per cent change in mean mass flow rate.

(a) Varying nozzle angle

(b) Radial cropping

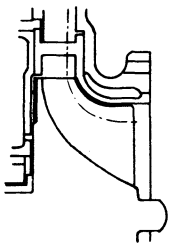

(c) Axial cropping

Figure 4.36 *Variation of turbine area*

To obtain optimum efficiency in between these rotors options 1 or 2 may be used. Option 2 is the simplest one, but it increases losses associated with the change in trailing edge thickness and nozzle gas outlet angle, and introduces a larger gap between nozzle and rotor tip.

Changes in nozzles or nozzleless casings, and rotors, are commonly called 'trim' or 'build' changes within a certain 'frame size' (turbine casing, centre casing and bearings) of the turbocharger. Together with similar build or trim changes on the compressor (discussed in chapter 3) this provides a very versatile and adaptable turbocharger unit not only to move the area of highest efficiency to the desired engine operating conditions but also to adapt the turbocharger unit to a reasonably wide range of engine sizes.

4.7.1 Variable geometry

Although the flow range of a particular turbine trim is large, operation away from the design point results in a loss of efficiency. As important is the fact that the

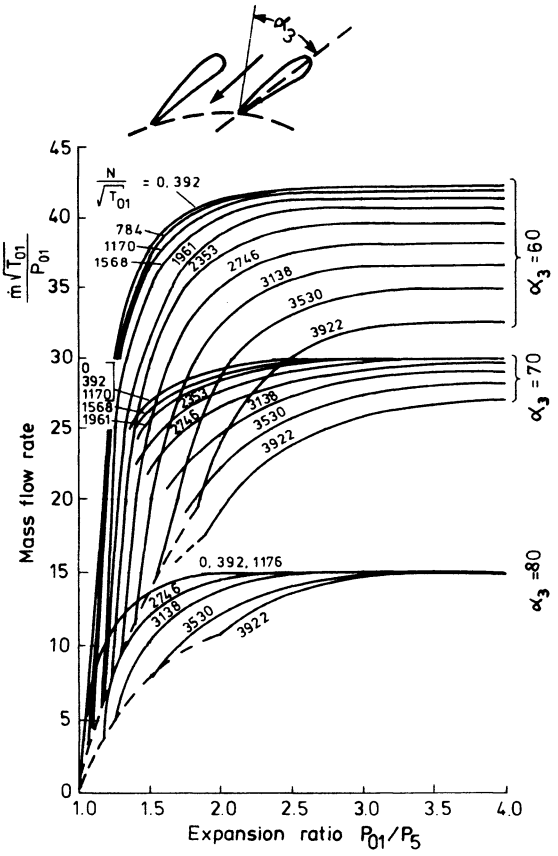

Figure 4.37 *Variable nozzle angle: mass flow characteristics [27]*

expansion ratio of the turbine will vary greatly with mass flow rate (figure 4.33).

Since compressor pressure ratio and turbine expansion ratio are directly related, boost will be low at low mass flow rates and high at high mass flow rates. This has serious consequences for an engine designed to operate over a large speed range. The engine may have insufficient boost at low speeds and be over-boosted at high speeds. Since a change in nozzle angle alters the throat area of the nozzles (figure 4.36a), and therefore controls the expansion ratio for a certain mass flow rate, it appears attractive to use adjustable nozzle vanes.

The performance of a turbine with variable nozzle vane angles can be illustrated by superimposing characteristics measured at various fixed settings (figure 4.37). Clearly major benefits are obtainable in terms of increased pressure ratio at low mass flows but, in practice, variable geometry has rarely been used except on gas turbine plant and some experimental turbochargers. The difficulties are essentially mechanical, such as obtaining reliable working for long periods of time while exposed to the action of high temperature and corrosive exhaust gas. Figure 4.38 shows the construction of one type of variable geometry system by Von de Nuell. [28] Another is shown by Berenyi and Raffa. [29] Perhaps an even greater deterrent has been the cost, which must include the control system. Relatively cheap control systems can be designed using the boost pressure as a pneumatic controller, but hydraulic systems are considerably better at overcoming any tendency for the nozzles to stick after long idle periods, since greater pressures may be used. The general adoption of variable geometry still awaits the design of a cheap and reliable system.

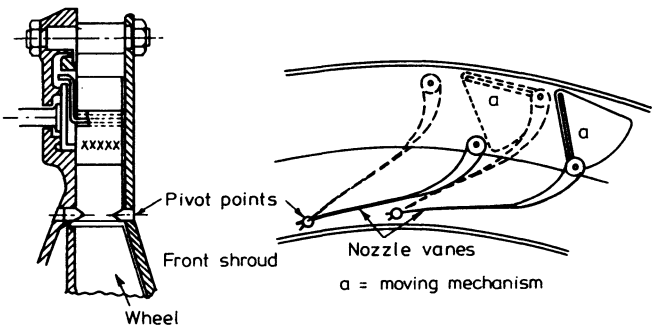

Figure 4.38 *Variable area nozzle with pivoted nozzle vanes for small, simple centripetal gas turbine [28]*

4.8 Turbine Rotor Stresses and Blade Vibrations

The rotor of the radial flow turbine is similar in shape to the centrifugal compressor and therefore the same methods of stress analysis are used (chapter 3). However, attention must be given to the high temperature and its distribution across the rotor.

Turbine blade vibration can be a particular problem of the pulse turbocharging system, since the highly unsteady inlet gas flow acts as a source of excitation. The

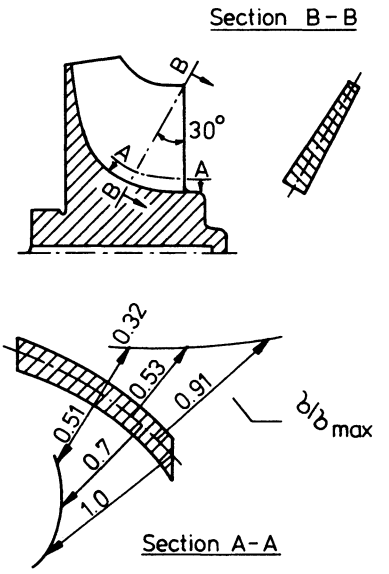

Figure 4.39 *Radial turbine: bending stress distribution around impeller blade [30]*

pulsating gas forces on the blades may be considerable and, since the variety of exhaust systems that are used is great, it can become difficult to control the vibrations, especially when engines operate over a wide speed range. Thus a vibration problem may develop on one engine (with a certain number of cylinders and operating speed) but not on others.

Most turbine blade vibration studies have been conducted on axial blades for gas turbine plant. The geometry of radial turbine blades is quite different. Firstly, the nozzle ring spacing is different from the rotor blade spacing, and secondly, the flow path is very long. It is the maximum stress points, due to the centrifugal loading, that are most vulnerable and this usually occurs at the blade root, near the trailing edge (figure 4.39). The stress levels under simulated pulse turbocharging conditions on an eight-cylinder engine were measured by Mann [30] and are reproduced in figure 4.40. The stress peaks indicate the 5th, 6th and 7th orders of resonance with the fundamental frequency of the rotor blades. Redesign of the blade thickness, etc., can eliminate a particularly high stress level associated with a particularly bad order of vibration, although there are limits to what can be achieved. If redesign is not possible, a damping wire may have to be inserted through all the blades, but this will undoubtedly reduce the turbine efficiency (for example, by 3 per cent).

4.9 Design of the Single-stage Radial Flow Turbine

The design procedure of a radial flow turbocharger turbine for constant pressure application is, in principle, similar to the design procedure outlined for the cen-

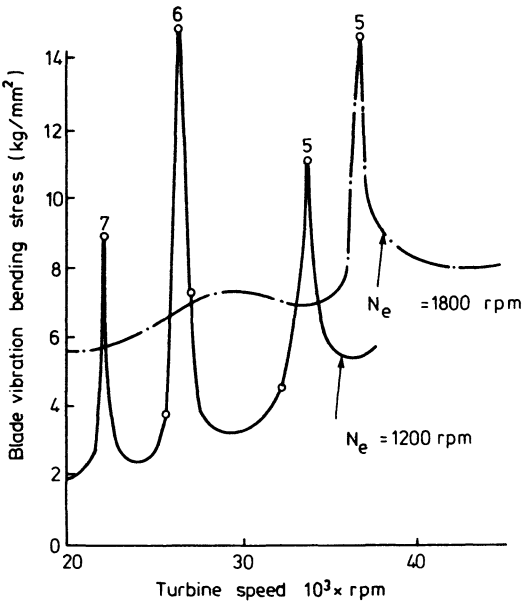

Figure 4.40 *Radial turbine: blade vibration level during partial admission, charging an eight-cylinder engine [30]*

trifugal compressor (chapter 3). The first step in the design is to establish the geometrical shape of the turbine components using one-dimensional analysis. For a nominal mass flow rate, inlet pressure and temperature, the inlet casing (volute) and nozzle throat area can be estimated from the continuity equation. However, the thermodynamic conditions to be created at the nozzle discharge have to be known. The standard approach is to first establish the thermodynamic state of the fluid at the rotor inlet. From the energy transfer and assumed degree of reaction (normally 50 per cent) and optimum blade speed ratio, the rotor inlet and outlet velocities can be calculated and the inlet conditions established. Then the nozzle ring and inlet casing geometry can be estimated assuring flow match at the inlet to the nozzle ring. A rotor hub wall profile of gentle curvature is assumed together with the number of rotor vanes. The shroud wall profile of the rotor is chosen to ensure gradual acceleration of the flow from inlet to outlet of the rotor. Normally purely radial rotor blades are adopted to avoid excessive stresses at the root of the vanes due to bending. Creep-stress limitation of the rotor material will influence the maximum vane height at the exducer. Once the blade shape is established, the next critical task for the rotor design is to examine the blade angle distribution and hub and shroud surface shapes using the quasi-three-dimensional analysis as guidance to minimise or eliminate flow separation regions.

There is no straightforward design method for radial turbines with pulsating flow and partial admission operation. One approach is to study the effect of typical exhaust pulse shapes on the changes in turbine efficiency as the blade speed ratio varies. From this analysis it is possible to select an optimum rotor tip diameter for a given rotational speed (dictated by the compressor) or conversely to select an optimum rotational speed for a given rotor tip diameter.

References

1. G. F. Hiett and I. H. Johnston, Experiments concerning the aerodynamic performance of inward flow radial turbines, *Proc. Inst. Mech. Engrs*, **178**, Pt 31 (II) (1963/4)
2. O. E. Balje, A study on design criteria and matching of turbomachines, *Trans. ASME J. Engng Power* (Jan 1962)
3. F. S. Bhinder, Investigations of flow in a nozzleless spiral casing of a radial-inward flow gas turbine, *Proc. Inst. Mech. Engrs*, **184**, Pt 3G(II) (1969/70)
4. A. W. H. Jamieson, The radial turbine, in *Gas Turbine Principles and Practice* (Newnes, 1955)
5. H. E. Rohlik and M. G. Kovskey, Recent radial turbine research at the NASA Lewis Research Centre, *ASME Paper 72-GT-42* (1972)
6. G. Sovran and E. D. Klomp, Experimentally determined optimum geometries and rectilinear diffusers with rectangular conical or annular cross section in *Fluid Mechanics of Internal Flow* (Elsevier, Amsterdam, 1967)
7. J. H. Horlock, *Axial Flow Turbines* (Butterworth, 1966)
8. R. S. Benson, A review of methods for assessing loss coefficients in radial gas turbines, *Int. J. Mech. Sci*, **12** (1970)
9. A. Whitfield and F. J. Wallace, Study of incidence loss models in radial and mixed flow turbomachinery, *Proc. Inst. Mech. Engrs, Conf. Publication 3* (1973)
10. R. S. Benson, W. G. Cartwright and S. K. Das, An investigation of the losses in the rotor of a radial flow gas turbine at zero incidence under conditions of steady flow, *Proc. Inst. Mech. Engrs*, **183**, Pt. 3H (1967/8)
11. S. M. Futral and C. A. Wasserbauer, Off-design performance prediction with experimental verification for a radial inflow turbine, *NACA TN D-2621* (1965)
12. E. A. Bridle and R. A. Boulter, A simple theory for the prediction of losses in the rotors of inward radial flow turbines, *Proc. Inst. Mech. Engrs*, **182**, Pt. 3H (1967/8)
13. O. E. Balje, A contribution to the problem of designing radial turbomachinery, *Trans. ASME*, **74** (1952)
14. D. G. Ainley and G. C. R. Mathieson, An examination of the flow and pressure losses in blade rows of axial flow turbines, ARC, R & M Z 891 (1955) (HMSO).
15. J. W. Daily and R. E. Nece, Chamber dimension effects on induced flow and frictional resistance of enclosed rotating discs, *Trans. ASME J. Basic Engng*, **82** (1960)
16. S. M. Futral and D. E. Holeski, Experimental results of varying the blade-shroud clearance in a 6.02 inch radial inflow turbine, *NASA TN D-5513* (1970)
17. T. Katsanis, Use of arbitary quasi-orthogonals for calculating flow distribution in the meridional plane of a turbomachine, *NASA TN-2546* (1964)
18. T. Katsanis, Use of arbitary quasi-orthogonals for calculating flow distribution on a blade to blade surface in a turbomachine, *NACA TN-2809* (1965)
19. M. C. S. Barnard and R. S. Benson, Radial gas turbines, *Proc. Inst. Mech. Engrs*, **183**, Pt. 3N (1968/9)
20. R. S. Benson, W. G. Cartwright and G. Woollatt, Calculations of the flow distribution within a radial turbine rotor, *Proc. Inst, Mech. Engrs*, **184**, Pt. 36 (1970)
21. W. G. Cartwright, A comparison of calculated flows in radial turbines with experiment, *SAE paper 72-GT-50* (1972)

22. I. Ariga, I. Watanabe and K. Fujie, Investigations concerning flow patterns within the impeller channels of radial inflow turbines with some reference to the influence of the splitter vanes, *Trans ASME* (1967)
23. D. J. L. Smith and D. H. Frost, Calculation of flow past turbomachine blades, *Proc. Inst. Mech. Engrs*, **184**, Pt 3G(II) (1969/70)
24. H. R. M. Craig and M. S. Janota, The potential of turbochargers as applied to highly rated 2-stroke and 4-stroke engines, *Proc. CIMAC* (1965) paper B.15
25. R. S. Benson and K. H. Scrimshaw, An experimental investigation of non-steady flow in a radial gas turbine, *Proc. Inst. Mech. Engrs*, **180**, Pt. 3J (1965/6)
26. F. Pischinger and A. Wunsche, The characteristic behaviour of radial turbines and its influence on the turbocharging process. *Proc. CIMAC* (1977)
27. F. J. Wallace, P. R. Cave and J. Miles, Performance of radial flow turbines under steady flow conditions with special reference to high pressure ratios and partial admission, *Proc. Inst. Mech. Engrs*, **184**, Pt 1, No. 56 (1969/70)
28. W. T. Von de Nuell, The radial turbine, in *Aerodynamics of Turbines and Compressors*, ed. W. R. Hawthorne (Oxford University Press, 1964)
29. S. G. Berenyi and C. J. Raffa, Variable area turbocharger for high output diesel engines, *SAE 790064*, Turbochargers and Turbocharged Engines, SP442 (February 1979)
30. A. Mann, The development of turbochargers for diesel engines with a high degree of charging, *Proc. CIMAC* (171) paper B.15.

5

The Axial Flow Turbine

5.1 Introduction

In the early days of turbochargers, axial flow turbines were used exclusively, assisted by experience gained from aircraft gas turbine technology after 1945. Indeed, it was largely turbine blade material developments, pioneered for gas turbines, that made diesel engine turbochargers practicable.

Currently all medium and large-size turbochargers retain axial flow turbines due to their high efficiency. Small engine turbochargers (such as those used on trucks) use radial flow turbines to reduce cost and because the efficiency of axial flow machines falls with their size, due to relatively large blade clearance effects.

The majority of diesel engines fitted with large turbochargers use the pulse turbocharging system, hence their turbines operate under highly unsteady conditions. It follows that much of current axial flow turbine research for aircraft gas turbines is of only limited value to the turbocharger designer. More recent large turbocharger installations tend to use constant pressure turbines, easing the turbine design task.

5.2 Elementary Theory

Usually a single-stage axial turbine is quite sufficient to expand the exhaust gas through the pressure ratios associated with single-stage compression (required by the majority of present-day turbocharged engines). If two-stage turbocharging is applied, it is normal to use two separate turbochargers with the turbines in series (see chapter 11). Thus the axial flow turbocharging turbine consists of a single row of nozzles (stator blades) and rotor blades.

Since the blade height of the axial flow turbine is usually small compared to the rotor diameter, it is sensible to consider the elementary theory of the gas flow through the turbine in terms of conditions at the 'mean blade height' diameter. This treatment is commonly referred to as the 'pitch line' analysis and will be implied, unless stated otherwise.

This one-dimensional analysis assumes average values of velocity, pressure and temperature for the cross-section, on the pitch line. Thus flow variations across a section of the channel are ignored.

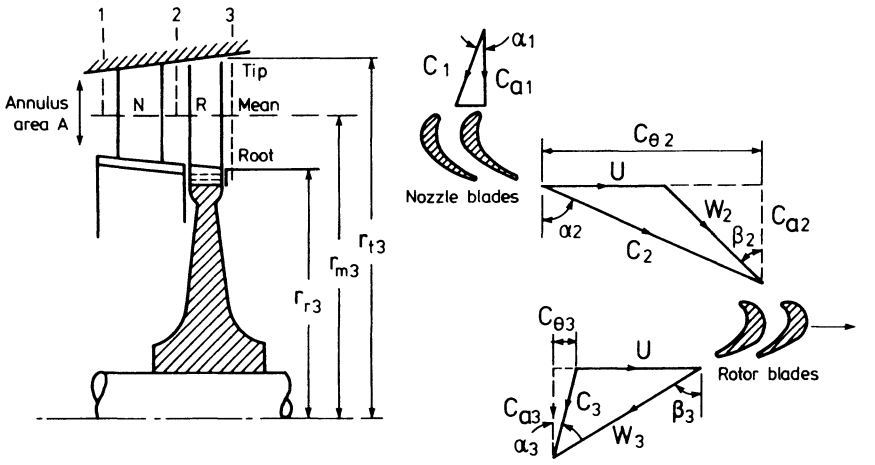

Figure 5.1 *Axial flow turbine stage [1]*

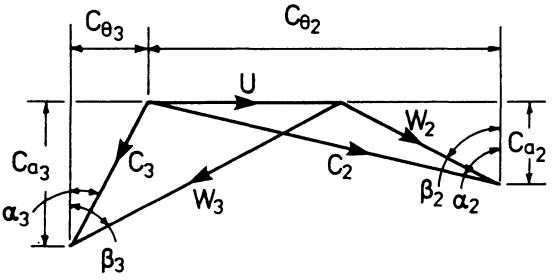

Figure 5.2 *Velocity diagram, rotor inlet and exit*

5.2.1 Velocity triangles and energy transfer

Figure 5.1 shows the nozzle (stator) and rotor blades of an axial flow turbine together with the velocity diagrams at the nozzle and rotor blade exits. The gas (at pressure and temperature P_1 and T_1 respectively) enters the nozzle with a velocity C_1 and at an angle α_1 (which may be zero). It is expanded in the nozzle vanes to a velocity C_2 at an angle α_2; α_1 and α_2 are the inlet and outlet blade angles of the nozzles. The rotor blade angle (β_2) must relate to the angle of the relative velocity vector (W_2) formed by the vector subtraction of the absolute velocity (C_2) and the rotor blade speed (U). The gas is further expanded in the rotor, leaving with velocity C_3 at an angle α_3 (this being commonly referred to as the 'swirl angle'). In a single-stage turbine, the inlet gas angle (α_1) will be zero (in a multi-stage turbine, α_1 will be the rotor exit swirl angle of the previous stage).

It is helpful to superimpose the two velocity diagrams at the blade exits (figure 5.2). The torque developed by the turbine will equal the rate of change of angular momentum, that is,

$$TQ = \dot{m}(C_{\theta 2} r_2 + C_{\theta 3} r_3) \tag{5.1}$$

Hence the energy transfer is

$$\dot{W} = \omega TQ = \omega \dot{m}(C_{\theta 2} r_2 + C_{\theta 3} r_3)$$

Considering flow conditions at mid-radius, r_2 will usually equal r_3, hence

$$\dot{W} = \dot{m} U(C_{\theta 2} + C_{\theta 3}) \tag{5.2}$$

or

$$\dot{W} = \dot{m} U(C_2 \sin \alpha_2 + C_3 \sin \alpha_3) \tag{5.3}$$

or

$$\dot{W} = \dot{m} U(C_{a2} \tan \beta_2 + C_{a3} \tan \beta_3) \tag{5.4}$$

5.2.2 Temperature Drop across the Turbine

The steady flow energy equation can be written as

$$\dot{Q} - \dot{W} = \dot{m} \left[h_b - h_a + \frac{C_b^2 - C_a^2}{2} \right]$$

When applied to a turbine, rewritten in terms of the stagnation enthalpy (h_0) with heat transfer neglected

$$\dot{W} = \dot{m}(h_{0a} - h_{0b})$$

Since no work is done in the nozzles, the stagnation enthalpy remains constant

$$h_{01} = h_{02} \tag{5.5}$$

For the rotor, using equation 5.2

$$\dot{W} = \dot{m}(h_{02} - h_{03}) = \dot{m} U(C_{\theta 2} + C_{\theta 3})$$

that is

$$h_{02} - h_{03} = U(C_{\theta 2} + C_{\theta 3}) \tag{5.6}$$

If the exhaust gas from the engine may be considered as a perfect gas, then the change in total temperature is given by

$$T_{02} - T_{03} = \frac{h_{02} - h_{03}}{c_p}$$

Hence

$$T_{02} - T_{03} = \frac{U(C_{\theta 2} + C_{\theta 3})}{c_p} = \Delta T_{0t} \tag{5.7}$$

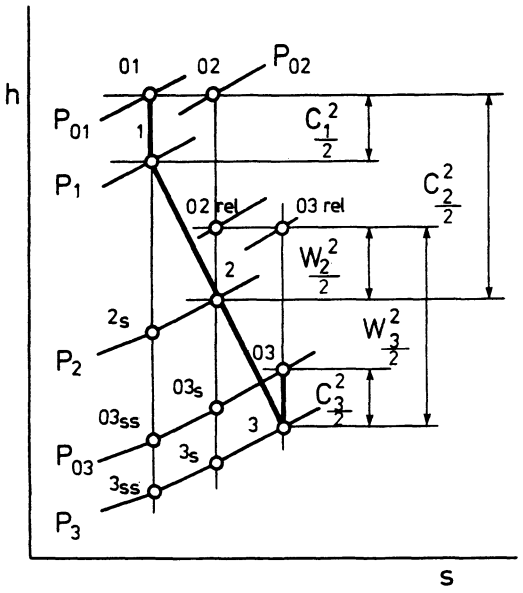

Figure 5.3 *h–s diagram for a turbine*

5.2.3 Isentropic Efficiency and Expansion Ratio

Figure 5.3 is an enthalpy/entropy diagram for flow through a turbine. The isentropic efficiency of the turbine on a total-to-total basis is given by equation 2.20. Using the notation of figure 5.3

$$\eta_{tTT} = \frac{h_{01} - h_{03}}{h_{01} - h_{03ss}} = \frac{T_{01} - T_{03}}{T_{01} - T_{03ss}} = \frac{1 - (T_{03}/T_{01})}{1 - (P_{03}/P_{01})^{(\gamma-1)/\gamma}} \tag{5.8}$$

giving

$$\frac{P_{01}}{P_{03}} = \left[\frac{T_{01}}{T_{01} - (T_{01} - T_{03})/\eta_{tTT}}\right]^{\gamma/(\gamma-1)} \tag{5.9}$$

Similar expressions may be derived for the total-to-static isentropic efficiency and expansion ratio

$$\eta_{tTS} = \frac{h_{01} - h_{03}}{h_{01} - h_{3ss}} = \frac{T_{01} - T_{03}}{T_{01} - T_{3ss}} = \frac{1 - (T_{03}/T_{01})}{1 - (P_3/P_{01})^{(\gamma-1)/\gamma}} \tag{5.10}$$

and

$$\frac{P_{01}}{P_3} = \left[\frac{T_{01}}{T_{01} - (T_{01} - T_3)/\eta_{tTS}}\right]^{\gamma/(\gamma-1)} \tag{5.11}$$

5.2.4 Degree of Reaction

Several different definitions of the degree of reaction are available. The concept is based on the fraction of the overall static pressure drop across the stage that occurs in the rotor. An extreme case might be a pure impulse turbine in which the complete pressure drop occurs in the nozzle (then the degree of reaction as defined above would be zero). This has been common practice in steam turbines, where the pressures, and hence leakages, can be very high, but is not used on gas turbines. Although the degree of reaction was conceived in terms of actual pressure drop, it is more convenient to define it in terms of total enthalpy drop, in an isentropic turbine, operating at the pressure ratio of the real machine.

Thus the degree of reaction (RN_s) may be defined as

$$RN_s = \frac{h_{2_s} - h_{3_{ss}}}{h_{01} - h_{3_{ss}}} \tag{5.12}$$

that is, the enthalpy change in an isentropic rotor divided by the enthalpy change across an isentropic stage.

Since the enthalpy drop across the stage is

$$h_{01} - h_{3_{ss}} = (h_{01} - h_{2_s}) + (h_{2_s} - h_{3_{ss}})$$

the expression for the degree of reaction becomes

$$RN_s = 1 - \frac{h_{01} - h_{2_s}}{h_{01} - h_{3_{ss}}} \tag{5.13}$$

The isentropic efficiency of the nozzles is defined by

$$\eta_n = \frac{\text{actual kinetic energy at nozzle exit}}{\text{theoretical kinetic energy obtained from isentropic expansion}}$$

that is

$$\eta_n = \frac{C_2^2}{C_{2_s}^2} = \frac{h_{01} - h_2}{h_{01} - h_{2_s}}$$

Equation 5.13 becomes

$$RN_s = 1 - \frac{C_2^2}{2c_p T_{01} \eta_n \left[1 - (P_3/P_{01})^{(\gamma-1)/\gamma}\right]} \tag{5.14}$$

A more convenient definition of degree of reaction that is frequently used with axial flow turbines is defined in terms of the static enthalpy drop, since this can be related to the velocity triangles. Thus, the degree of reaction becomes

$$RN = \frac{h_2 - h_3}{h_1 - h_3} \tag{5.15}$$

In many turbine designs there will be no change in kinetic energy over the

stage (following gas turbine practice, where a 'repeating stage' is ideal for multi-staging). Hence

$$\begin{aligned} h_1 - h_3 &= h_{01} - h_{03} \\ &= h_{02} - h_{03} \text{ (from equation 5.5)} \\ &= U(C_{a2} \tan \beta_2 + C_{a3} \tan \beta_3) \end{aligned}$$

from equations 5.4 and 5.6. In a repeating stage, $C_{a2} = C_{a3} = C_a$ (axial component of velocity), therefore

$$h_1 - h_3 = UC_a(\tan \beta_2 + \tan \beta_3) \tag{5.16}$$

Relative to the *rotor*, no work is done as the flow passes through the rotor, hence from the energy equation

$$\begin{aligned} h_2 - h_3 &= \tfrac{1}{2}(W_3^2 - W_2^2) \\ &= \tfrac{1}{2}(C_a^2 \sec^2 \beta_3 - C_a^2 \sec^2 \beta_2) = \tfrac{1}{2}C_a^2(\tan^2 \beta_3 - \tan^2 \beta_2) \end{aligned} \tag{5.17}$$

therefore

$$RN = \frac{h_2 - h_3}{h_1 - h_3} = \frac{C_a}{2U} (\tan \beta_3 - \tan \beta_2) \tag{5.18}$$

Since $\tan \beta_2 = (C_{\theta 2} - U)/C_a = \tan \alpha_2 - U/C_a$, then

$$RN = \tfrac{1}{2} + \frac{C_a}{2U} (\tan \beta_3 - \tan \alpha_2) \tag{5.19}$$

and the degree of reaction of an axial flow turbine may be freely chosen. In contrast, the radial flow turbine is limited by the centrifugal field and it becomes difficult to increase reaction beyond 50 per cent. There is little in favour of adopting zero reaction designs (these are used for high-pressure steam turbines for reasons already mentioned). There are two other important common designs: 50 per cent reaction and designs such that the exit velocity is wholly axial, although there is no reason why axial flow turbines should not be built with any value of reaction.

Consider the 50 per cent reaction design. This implies an equal enthalpy drop in rotor and stator, which seems a reasonable proposition. It follows from equation 5.19 that $\alpha_2 = \beta_3$ and that the velocity triangles are symmetrical (figure 5.4). From equation 5.4

$$\dot{W} = \dot{m}UC_a(\tan \beta_2 + \tan \beta_3)$$

But $\tan \beta_3 - \tan \beta_2 = U/C_a$ (from equation 5.18); eliminating β_2 gives

$$\dot{W} = \dot{m}UC_a\left(2 \tan \beta_3 - \frac{U}{C_a}\right) \tag{5.20}$$

For a design in which the exit velocity is purely axial (that is, $C_{\theta 3} = 0$ to reduce exit kinetic energy) then

$$\tan \beta_3 = \frac{U}{C_a}$$

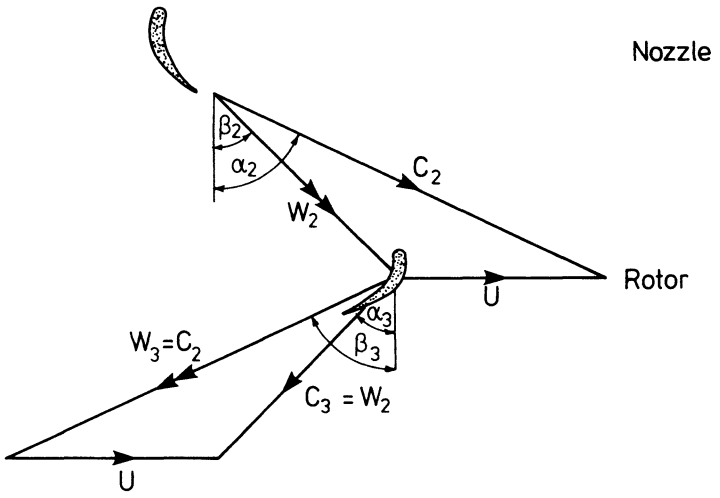

Figure 5.4 *Velocity diagram for a 50 per cent reaction stage*

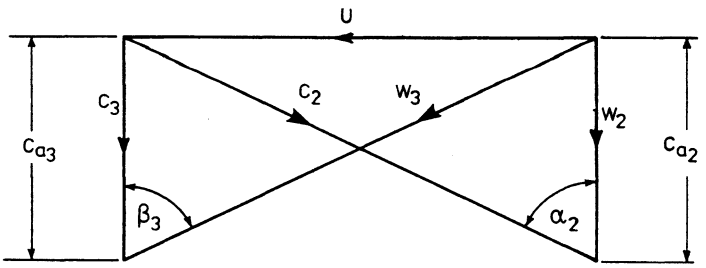

Figure 5.5 *Velocity diagram for a 50 per cent reaction stage, with zero exit swirl*

and the velocity triangles (with 50 per cent reaction) are as shown in figure 5.5. Then from equation 5.20, assuming constant axial velocity

$$\dot{W} = \dot{m}UC_a \tan \beta_3$$

and

$$\dot{W} = \dot{m}UC_a \tan \alpha_2 \qquad (5.21)$$

Zero exit swirl can be achieved with any degree of reaction. From equation 5.18 the reaction will be given by

$$RN = \frac{C_a}{2U}\left(\frac{U}{C_a} - \tan\beta_2\right)$$

$$= \tfrac{1}{2} - \frac{C_a}{2U}\tan\beta_2 \qquad (5.22)$$

5.2.5 *Blade Loading Coefficient*

The blade loading coefficient (ψ) is a useful dimensionless parameter which may be defined as

$$\psi = \frac{\dot{W}}{\dot{m}U^2}\left(\text{sometimes given as } \frac{2\dot{W}}{\dot{m}U^2}\right) \qquad (5.23)$$

Since the work done is equal to the stagnation enthalpy drop through the stage, then

$$\psi = \frac{h_{01} - h_{03}}{U^2} = \frac{c_p\,(T_{01} - T_{03})}{U^2} \qquad (5.24)$$

For this reason the blade loading coefficient is often referred to as the temperature drop coefficient. From equation 5.2

$$\psi = \frac{C_{\theta 2} + C_{\theta 3}}{U} \qquad (5.25)$$

From equations 5.20 and 5.23, for 50 per cent reaction

$$\psi(RN = 0.5) = \frac{C_a}{U}\left(2\tan\beta_3 - \frac{U}{C_a}\right)$$

$$= \frac{2C_a}{U}\tan\beta_3 - 1$$

or, in terms of blade angle (figure 5.4)

$$\psi(RN = 0.5) = \frac{2C_a}{U}\tan\alpha_2 - 1 \qquad (5.26)$$

If the exit velocity is purely axial, then from equations 5.21 and 5.23 and figure 5.1

$$\psi = \frac{C_a}{U}\tan\alpha_2 = \frac{C_a}{U} \times \frac{C_{\theta 2}}{C_a} = \frac{C_{\theta 2}}{U} \qquad (5.27)$$

or

$$\psi = \frac{C_a}{U}\left(\frac{C_{\theta 2}}{C_a} - \frac{U}{C_a} + \frac{U}{C_a}\right)$$

$$= \frac{C_a}{U}\left(\frac{C_{\theta 2} - U}{C_a} - \frac{U}{C_a} + \frac{2U}{C_a}\right)$$

$$= \frac{C_a}{U}\left(\tan\beta_2 - \tan\beta_3 + \frac{2U}{C_a}\right) \text{ (from figure 5.12 with zero exit swirl)}$$

$$= 2 + \frac{C_a}{U}(\tan\beta_2 - \tan\beta_3)$$

Hence from equation 5.18

$$\psi = 2(1 - RN) \tag{5.28}$$

5.2.6 Blade Speed Ratio (or Velocity Ratio)

A convenient way of presenting turbine isentropic efficiency as a function of the degree of reaction, is to use the blade speed or velocity ratio (U/C_s). This is the velocity (U) at the mean blade height, divided by the velocity that would be achieved by the gas following isentropic expansion to the pressure at the exit from the turbine (total to static) (see chapter 4)

$$\frac{U}{C_s} = \frac{U}{\sqrt{[2(h_{01} - h_{3ss})]}} = \frac{U}{\sqrt{\{2c_pT_{01}[1 - (P_3/P_{01})^{(\gamma-1)/\gamma}]\}}} \tag{5.29}$$

Figure 5.6 shows typical turbine characteristics plotted against the blade speed ratio. The peak efficiency moves to higher values of U/C_s with increasing reaction. For example, the efficiency of the low reaction (5 per cent) turbine peaks at $U/C_s = 0.4$, whereas the 50 per cent reaction design peaks at $U/C_s = 0.7$ like a radial flow turbine. In chapter 4 it was shown that the relationship between the blade speed ratio, degree of reaction and turbine efficiency is very important

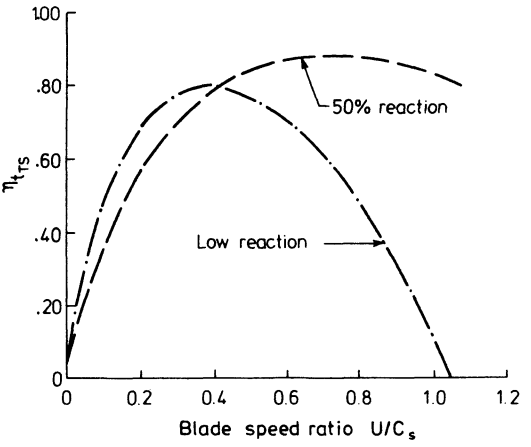

Figure 5.6 *Turbine efficiency against blade speed ratio and degree of reaction*

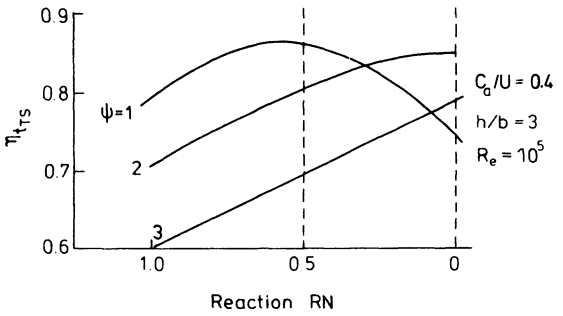

Figure 5.7 *Influence of reaction on total-to-static efficiency with fixed values of blade loading [2]*

when designing a turbine and matching it to the appropriate compressor. From a specified turbine inlet temperature and expansion ratio, C_s can be calculated. The diameter of the mean blade height may then be evaluated for chosen values of degree of reaction and rotational speed, to ensure optimum turbine efficiency.

5.2.7 Choice of Reaction and Blade Loading

The efficiency of an axial turbine is not governed by the blade loading and reaction, but they do affect the efficiency. The kinetic energy leaving the stage may be a major source of energy loss (since the total-to-static efficiency is of interest with respect to a single-stage turbocharger turbine), and this is related to the dimensionless parameters through the velocity triangles. Figure 5.7 shows the efficiency change with reaction for different values of blade loading, although it must be said that these are simply trends and their significance should not be over-stressed. Clearly it is difficult to achieve high efficiency with high blade loading, but it is difficult to avoid this situation when cost prohibits multi-staging. It is therefore necessary to use high blade speeds (high U, subject to stress limitations) and compromise between zero and 50 per cent reaction. The choice of reaction for an unsteady flow turbocharger turbine is discussed in section 5.8.

5.3 Vortex Blading

The axial flow turbocharger turbine is virtually always combined with a centrifugal compressor. This will usually result in the compressor diameter exceeding the mean diameter of a turbine designed to handle approximately the same mass flow. The result is that the turbine will have blades whose height is relatively small compared to the mean radius. In consequence the 'pitch line' analysis described above is reasonable. Turbine blades of constant cross-sectional geometry may be used, but since the rotor velocity will vary from hub to tip, the gas angles will vary with radius. It is desirable for efficiency, but not for stressing and manufacturing reasons, to use twisted blades which take account of this gas angle

variation. Such designs are commonly known as 'vortex blading'. The analytical method of calculating the radial variation is based on radial equilibrium conditions, and is outlined below. However, it is important to remember that vortex blading will cope with the radial variations at the design point flow and speed only. At offdesign, a different twist would be required, even to preserve the same incidence angle over the blade height. Since a turbocharger turbine will spend much of its working life at offdesign conditions and will commonly be used with highly unsteady inlet gas flow, the benefits of using vortex blading are less than would be gained on a gas turbine (or steam turbine) plant. Furthermore, even at the design point, the benefits may be marginal if the radius ratio (tip to hub) is small. For example, Johnston and Knight [3] have compared the efficiency of a single-stage turbine with small blade height fitted with vortex and constant angle blading. The difference did not exceed their margin for experimental error.

5.3.1 Radial Equilibrium

Some basic assumptions are usually made to simplify the analysis. The first is that the radial component of velocity is zero, the second that no flow variations around the circumference exist (that is, axisymmetric flow). For a more complete treatment the reader is referred to Horlock. [4] Having made the above assumptions, the basic radial equilibrium equation can be developed by considering the pressure and centrifugal forces on a fluid element. Using the notation of figure 5.8

$$(P + \mathrm{d}P)\,(r + \mathrm{d}r)\mathrm{d}\theta - Pr\,\mathrm{d}\theta - 2\left(P + \frac{\mathrm{d}P}{2}\right)\mathrm{d}r\,\frac{\mathrm{d}\theta}{2} = \rho\,\mathrm{d}r\,r\,\mathrm{d}\theta\,\frac{C_\theta^{\,2}}{r}$$

where the first two terms are derived from the pressure on top and bottom of the element, the third term from the mean pressure component on the side walls and the term on the right-hand side from the centrifugal field. Neglecting second-order terms, this equation may be simplified to give the basic radial equilibrium condition

$$\frac{1}{\rho}\frac{\mathrm{d}P}{\mathrm{d}r} = \frac{C_\theta^{\,2}}{r} \tag{5.30}$$

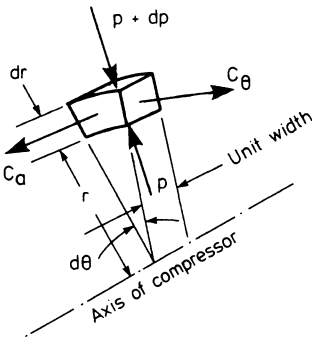

Figure 5.8 *Radial equilibrium: forces on a fluid element [1]*

From the definition of stagnation enthalpy

$$h_0 = h + \tfrac{1}{2}(C_a^2 + C_\theta^2)$$

(since $C_r = 0$) hence

$$\frac{dh_0}{dr} = \frac{dh}{dr} + C_a \frac{dC_a}{dr} + C_\theta \frac{dC_\theta}{dr} \tag{5.31}$$

But

$$T\,ds = dh - (1/\rho)dP, \text{ or}$$

$$T\frac{ds}{dr} = \frac{dh}{dr} - \frac{1}{\rho}\frac{dP}{dr} \tag{5.32}$$

Therefore equation 5.31 becomes

$$\frac{dh_0}{dr} - T\frac{ds}{dr} = \frac{1}{\rho}\frac{dP}{dr} + C_a \frac{dC_a}{dr} + C_\theta \frac{dC_\theta}{dr} \tag{5.33}$$

From equations 5.30 and 5.33

$$\frac{dh_0}{dr} - T\frac{ds}{dr} = C_a \frac{dC_a}{dr} + \frac{C_\theta}{r}\frac{d(rC_\theta)}{dr} \tag{5.34}$$

Assuming that the stagnation enthalpy and the entropy do not vary with radius, equation 5.34 reduces to

$$C_a \frac{dC_a}{dr} + \frac{C_\theta}{r}\frac{d(rC_\theta)}{dr} = 0 \tag{5.35}$$

which may be rewritten in the alternative form

$$\frac{d}{dr}(C_a^2) + \frac{1}{r^2}\frac{d}{dr}(rC_\theta)^2 = 0$$

5.3.2 Free Vortex Design

A special case of the above equation occurs when the axial velocity (C_a) is maintained constant across the radius. Then, equation 5.35 becomes

$$r\frac{dC_\theta}{dr} + C_\theta = 0$$

that is

$$\frac{dC_\theta}{C_\theta} = -\frac{dr}{r}$$

which may be integrated to give

$$\ln C_\theta = -\ln r + \text{constant}$$

that is $\ln(C_\theta \times r) = \text{constant} = \ln(r_m C_{\theta m})$ where m denotes mean values; thus

$$rC_\theta = \text{constant} = r_m C_{\theta m} \tag{5.36}$$

which is the equation for free vortex flow (already encountered in the vaneless diffuser of a radial compressor). The variation in angle with radius is easily calculated from the components of velocity.

From the velocity triangles (figure 5.1) and the knowledge that

$$rC_{\theta 2} = rC_{a2} \tan \alpha_2 = \text{constant}$$

and

$$C_{a2} = \text{constant and } C_{a3} = \text{constant}$$

the values of the gas angles (α_2 and α_3) at any radius (r) are related to the values at the mean radius (r_m) by the following

$$\left.\begin{aligned} \tan \alpha_2 &= \left(\frac{r_m}{r}\right)_2 \tan \alpha_{2m} \\ \text{and} \\ \tan \alpha_3 &= \left(\frac{r_m}{r}\right)_3 \tan \alpha_{3m} \end{aligned}\right\} \tag{5.37}$$

Also, since

$$\tan \beta_2 = \frac{C_{\theta 2} - U}{C_{a2}} = \tan \alpha_2 - \frac{U}{C_{a2}}$$

and

$$\tan \beta_3 = \frac{C_{\theta 3} + U}{C_{a3}} = \tan \alpha_3 + \frac{U}{C_{a3}}$$

Since $U = r\omega = (r/r_m)U_m$, this becomes

$$\left.\begin{aligned} \tan \beta_2 &= \left(\frac{r_m}{r}\right)_2 \tan \alpha_{2m} - \left(\frac{r}{r_m}\right)_2 \frac{U_m}{C_{a2}} \\ \text{and} \\ \tan \beta_3 &= \left(\frac{r_m}{r}\right)_3 \tan \alpha_{3m} + \left(\frac{r}{r_m}\right)_3 \frac{U_m}{C_{a3}} \end{aligned}\right\} \tag{5.38}$$

Examples of the variation of gas and blade angles with radius are shown in figure 5.9.

It is instructive to look at the variation in reaction with radius that results from the free vortex design. From equation 5.18 and the velocity triangles (figure 5.1), the reaction is given by

$$RN = \frac{C_a}{2U}\left(\frac{C_{\theta 3} + U}{C_a} - \frac{C_{\theta 2} - U}{C_a}\right)$$

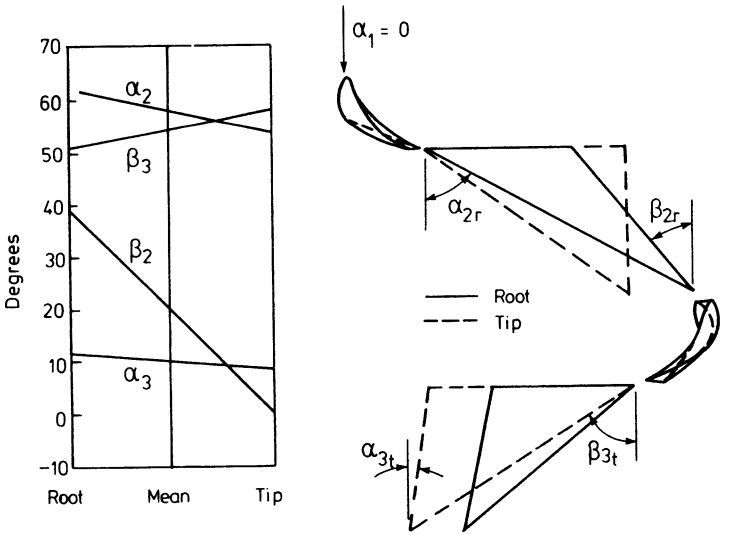

Figure 5.9 *Variation of gas angles with radius, free vortex design [1]*

$$= \frac{C_a}{2U}\left(\frac{C_{\theta 3} - C_{\theta 2}}{C_a}\right) + 1$$

that is

$$RN = \frac{C_{\theta 3} - C_{\theta 2}}{2U} + 1$$

$C_{\theta 2}$ and $C_{\theta 3}$ will vary with radius according to equation 5.36. Hence RN will vary with radius (r) as follows

$$RN = \frac{r_m}{r}\left(\frac{C_{\theta 3m} - C_{\theta 2m}}{2r\omega}\right) + 1 \tag{5.39}$$

It would not be sensible to allow compression (in a turbine) at any radius, hence the reaction at the root should be zero or greater. For zero reaction at the blade root

$$\frac{r_m}{r_r^2}\left(\frac{C_{\theta 3m} - C_{\theta 2m}}{2\omega}\right) = -1$$

Substituting into equation 5.39 gives the consequent reaction at any other radius, namely

$$RN_r = 1 - \left(\frac{r_r}{r}\right)^2 \tag{5.40}$$

Note that 50 per cent reaction will occur at radius

$$r \text{ (for } RN = 50\%) = r_r\sqrt{2}$$

Thus if zero reaction is selected at the blade root (hub) the reaction at the tip will exceed 50 per cent if the root/tip radius ratio exceeds $1/\sqrt{2}$ (0.707).

In deriving the above expressions the radial equilibrium equations have been applied at nozzle and rotor exit. In doing this it has been implicitly assumed that the flow is isentropic.

The specific work done at any radius may be obtained from equation 5.2, namely

$$\frac{\dot{W}}{\dot{m}} = U(C_{\theta 2} + C_{\theta 3})$$

Introducing the angular velocity (ω)

$$\frac{\dot{W}}{\dot{m}} = \omega(rC_{\theta 2} + rC_{\theta 3}) \tag{5.41}$$

It is clear from equations 5.36 and 5.41 that the specific work is constant over the radius and this is a convenient property. To obtain the total work, this value need only be evaluated at the pitch line and multiplied by the mass flow.

5.3.3 Constant Nozzle Angle Design

The free vortex design described above is only one possible design that satisfies radial equilibrium; other vortex designs may be used. It is particularly convenient to use a constant nozzle angle (for ease of manufacture) with twisted rotor blades only. Thus

$$\tan \alpha_2 = \frac{C_{\theta 2}}{C_{a2}} = \text{constant} \tag{5.42}$$

Hence

$$\frac{dC_{\theta 2}}{dr} = \frac{dC_{a2}}{dr} \tan \alpha_2$$

Thus the vortex flow equation (5.35) becomes

$$\frac{C_{\theta 2}}{\tan^2 \alpha_2} \times \frac{dC_{\theta 2}}{dr} + \frac{C_{\theta 2} r\, dC_{\theta 2}}{r\, dr} + \frac{C_{\theta 2}^2}{r} = 0$$

that is

$$(1 + \cot^2 \alpha_2) \frac{dC_{\theta 2}}{dr} + \frac{C_{\theta 2}}{r} = 0$$

Hence

$$\frac{dC_{\theta 2}}{C_{\theta 2}} = -\sin^2 \alpha_2 \frac{dr}{r}$$

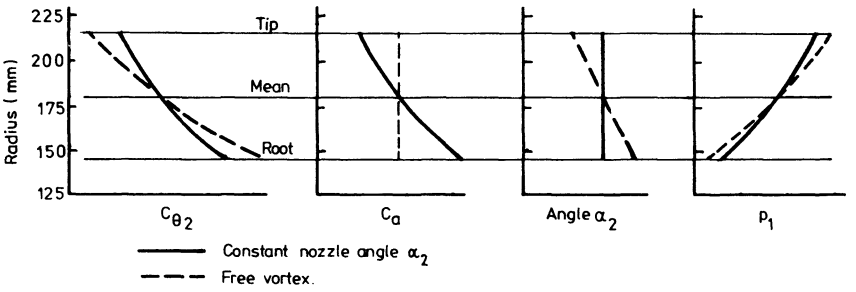

Figure 5.10 *Variation of velocity, nozzle angle and pressure with radius for free vortex and constant nozzle angle designs*

Integrating

$$\ln(C_{\theta 2}) = \ln(r)^{-\sin^2 \alpha_2} + \text{constant}$$

Hence

$$r^{\sin^2 \alpha_2} C_{\theta 2} = \text{constant}$$

A comparison of velocity, nozzle angle and pressure distribution with radius for free vortex and constant nozzle angle designs is shown in figure 5.10.

A third possible twisted blade design is based on a requirement of constant mass flow per unit area at any radius. This inherently results in a flow with no radial velocity component (which we have assumed all along, but in practice will not occur in a free vortex or constant nozzle angle design). Horlock [4] presents an analysis of this design.

5.4 Blade Profile, Spacing and Chord Length

Relationships between energy transfer and the gas angles have been developed including the effects of twisted (vortex) blading. But nothing has yet been said about the detail design of the blades themselves, their profile, pitch/chord ratio, aspect ratio, etc. The objective is to accept the approaching gas and turn it through the angle required with the absolute minimum loss. The velocity triangles specify the gas angles, but these may not always coincide with the blade angles (particularly at offdesign conditions) and hence the blade must cope with gas incidence.

5.4.1 Blade Profile

Various techniques have been used for designing and specifying blade profiles. Many successful designs have been based on blade shapes compounded from circular arcs and straight lines within the framework of specified inlet and outlet angles plus thickness, etc.

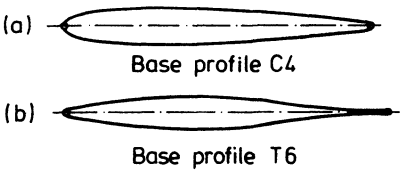

Figure 5.11 *Base turbine blade profiles [7]*

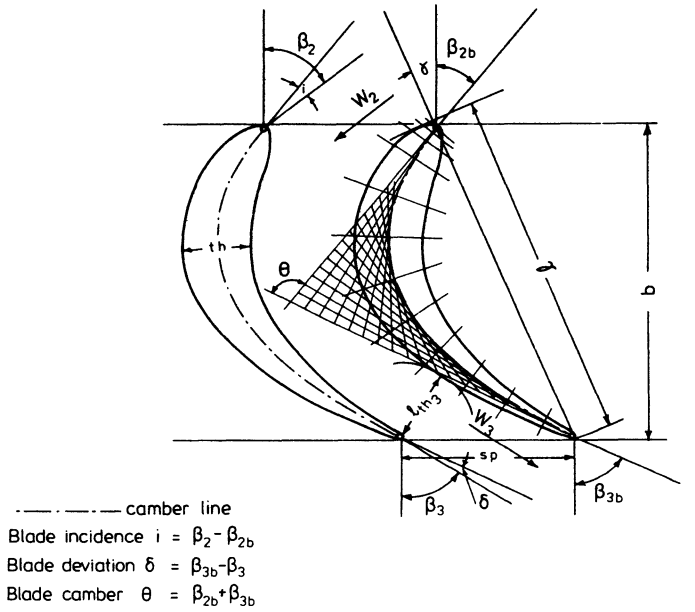

Figure 5.12 *Turbine blade curvature and camber*

An alternative technique is to relate the blade profile to a basic aerofoil shape (or base profile) having zero inlet and outlet blade angle (figure 5.11). This profile is then built up around a specified camber line (figure 5.12). The tangents of the camber line will, of course, equal the blade angles at entry and exit, while the camber line itself may be a circular or parabolic arc. The stagger angle (γ) is the angle of the chord line to the axis. Johnston and Smart [5] have reported on a typical design using this method. Dunavant and Ermin [6] developed two base profiles for reaction and zero reaction turbines, together with associated camber lines. The reaction design gave rapid turning in the early section of the blade where the Mach number is low, while the loading was distributed more evenly in the zero reaction design.

The gas exit angle will not equal the blade angle and hence it is important to

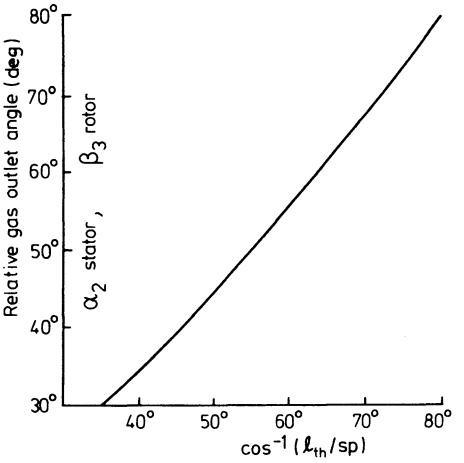

Figure 5.13 *Relationship between gas and blade outlet angles [7]*

know the deviation. It will be remembered from chapter 4 that the gas exit angle from a radial flow turbine is frequently calculated from the cosine rule, that is

$$\beta_3 \text{ (or } \alpha_2) = \cos^{-1}\left(\frac{l_{th}}{sp}\right)$$

where l_{th} is the throat width between blades and sp is the spacing. The procedure was derived from steam turbine practice, but it does tend to over-estimate the deviation in some rotor blades. Ainley and Mathieson [7] correlated the gas exit angle with the expression above (figure 5.13) for 'conventional' blades at Mach numbers below 0.5.

It may appear to the reader that the design of blades as described above is rather arbitrary. In fact the process has been one of trial and error, by practical tests on stationary 'cascades' of blades in a specially designed wind tunnel (see below). By this technique the most efficient blade profiles for various flow conditions have been established. This is not to say that other, superior, profiles do not exist. They do, and some of the more sophisticated techniques used to achieve these designs will be mentioned in section 5.6.

5.4.2 Cascade Testing

There are obvious practical difficulties associated with detailed tests on blade performance in a hot, running turbine. Furthermore it is no simple job to design and build a suitable set of rotor blades to test, for they must survive running conditions. It is clearly simpler to investigate flow through a stationary set of blades (a cascade) in a wind tunnel. Fortunately, being an axial flow machine, this does not involve the introduction of a significant error due to ignoring centrifugal and Coriolis forces (as would happen in radial flow blading) particularly if the blade height is small.

A cascade test will essentially be a test on a 'two-dimensional' blade (that is, the blades should be infinitely long and untwisted), although data may be related to any discrete section of a twisted turbine blade. Many of the basic turbine blade profiles in use have been developed solely from cascade testing. Basic blade performance data is derived from the measurement of pressures, velocities and flow angles (using pitot-static tubes and yaw-meters). In addition the pressure distribution along the blade surfaces may be measured. The quantity of tests required can become prohibitive since the effect of incidence angle, inlet Mach number, Reynolds number, etc., might be required. In practice, most tests are performed at the same inlet Mach number and Reynolds number ($Re > 2 \times 10^5$, see section 5.5). From the basic test data, the energy loss associated with that blade shape over a range of incidence angles may readily be established, and improved profiles developed. A large amount of data for many blade profiles is available.

5.4.3 Blade Spacing

The blade spacing is usually considered in terms of the pitch/blade chord ratio (figure 5.12, sp/l). If the blades are close together, they will guide the gas flow well, but the total surface area, and hence frictional losses, and boundary layer blockage will be high. Conversely few blades result in poor guidance and consequent high secondary losses (see section 5.5). Zweifel [8] has published a guideline, based on (full admission) cascade tests. Zweifel's optimum pitch/chord ratio is given by

$$\frac{sp}{l} = 0.8/[2 \cos^2 \alpha_2 \, (\tan \alpha_1 + \tan \alpha_2)] \tag{5.43}$$

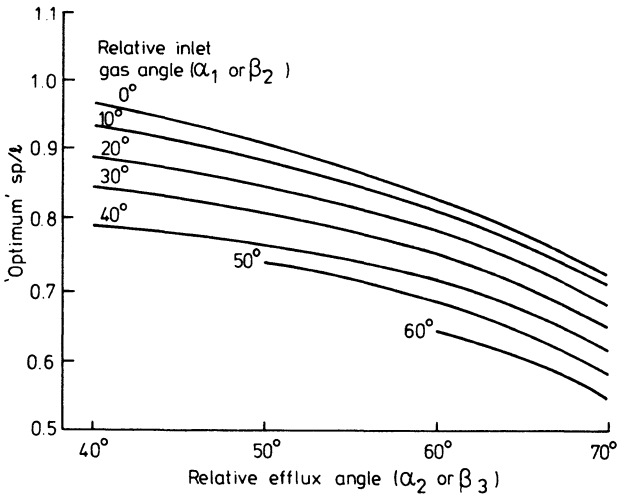

Figure 5.14 *'Optimum' pitch chord ratio, for minimum profile loss [1]*

A graph of 'optimum' pitch/chord ratio against exit angle (for specified values of inlet gas angle) may be extracted from Ainley's data.[7] Figure 5.14 illustrates that as the angular deflection is increased (that is, $\alpha_1 + \alpha_2$ or $\beta_2 + \beta_3$), so the pitch/chord ratio must be reduced for good flow guidance. Horlock [4] points out that Zweifel's prediction only agrees with Ainley's data for outlet angles in the range 60 to 70°. Fortunately, the pitch/chord ratio does not usually appear to be a critical parameter.

To avoid resonant frequency effects, the nozzle row and rotor should not have the same number of blades. However, since the optimum number will not be greatly different, it is common practice to use an even number of nozzle blades and an odd number of rotor blades.

5.4.4 Blade Height

The aspect ratio (height to blade chord length) is particularly important in turbocharger turbines, since it falls at the lower end of the axial turbine size spectrum, hence the blades are small. Furthermore, long blades increase the likelihood of blade vibration problems, particularly if the inlet gas flow is undergoing major pulsations (that is, the pulse turbocharging system). Short blades result in proportionally large tip clearances and excessive flow between pressure and suction sides of the blades. In aircraft gas turbines the optimum aspect ratio tends to be around 3 to 4. It will inevitably be much less in turbocharger turbines, but should not be less than 1.

5.5 Energy Losses and Blade Profiles

It is the detail design of the blades themselves that controls the flow pattern around them and hence any resulting energy losses. The blade design should deflect the gas through the desired angles and be able to cope with large incidence variation, which is inevitable in a turbocharger turbine, with minimum loss.

The energy losses may be expressed in a variety of ways. Various people have proposed loss coefficients based on the blade drag, entropy increase, nozzle kinetic energy, velocity, enthalpy and stagnation pressure losses but the last two are most commonly used. Thus the loss coefficient for the nozzle blades may be defined [1] as

$$Ch_n = \frac{h_2 - h_{2s}}{C_2^2/2} = \frac{T_2 - T_{2s}}{C_2^2/2c_p} \text{ or } CPL_n = \frac{P_{01} - P_{02}}{P_{02} - P_2} \tag{5.44}$$

In practice the values of these two coefficients do not differ much, but CPL_n is clearly easier to measure and Ch_n is simpler for a theoretical analysis.

A rotor loss coefficient must relate to entropy increases in the rotor regardless of what happens in the nozzle. Isentropic expansion through the rotor alone results in exit temperature T_{3s} hence

$$Ch_R = \frac{h_3 - h_{3s}}{W_3^2/2} = \frac{T_3 - T_{3s}}{W_3^2/2c_p} \text{ and } CPL_R = \frac{P_{02\,rel} - P_{03\,rel}}{P_{03\,rel} - P_3} \tag{5.45}$$

Note that the enthalpy loss coefficient is related to the kinetic energy relative to the rotor. This enables convenient measurements to be taken on static cascade wind tunnel blade tests. *Ch* and *CPL* are commonly referred to as the enthalpy and stagnation loss coefficients respectively.

It is important to be able to relate the loss coefficients to the over-all isentropic efficiency of the stage. For a single-stage turbocharger turbine, it is the total to static efficiency that is most relevant

$$\eta_{tTS} = \frac{h_{01} - h_{03}}{h_{01} - h_{3ss}}$$

But $h_{01} - h_{3ss} = (h_{01} - h_{03}) + (h_{03} - h_{3ss})$, therefore

$$\eta_{tTS} = \frac{1}{1 + (h_{03} - h_{3ss})/(h_{01} - h_{03})} \tag{5.46}$$

But

$$h_{03} - h_{3ss} = (h_3 - h_{3s}) + (h_{03} - h_3) + (h_{3s} - h_{3ss})$$
$$= Ch_R \tfrac{1}{2} W_3^2 + \tfrac{1}{2} C_3^2 + (h_{3s} - h_{3ss})$$

Since $h_{3s} - h_{3ss} \approx h_2 - h_{2s}$

$$h_{03} - h_{3SS} \approx Ch_R \tfrac{1}{2} W_3^2 + \tfrac{1}{2} C_3^2 + Ch_n \tfrac{1}{2} C_2^2$$

Substituting into equation 5.46 gives

$$\eta_{tTS} = \frac{1}{1 + \left(\dfrac{Ch_R W_3^2}{2} + \dfrac{Ch_n C_2^2}{2} + \dfrac{C_3^2}{2}\right) / (h_{01} - h_{03})} \tag{5.47}$$

The loss coefficients Ch_n and Ch_R take account of the energy loss from several sources. These are generally divided into four groups (although they may be further subdivided) as follows.

(a) Profile Losses

This is the energy loss due to boundary layer growth over the blade itself. It may include losses due to separation as the incidence angle increases. It is virtually impossible to isolate this loss in a real turbine hence predictions of profile loss are usually based on test results from cascade wind tunnels. The most commonly used prediction is that of Ainley and Mathieson [7] although others have been presented by Balje and Binsly, [9] Craig and Cox [10] and Traupel. [11] Denton [12] has surveyed and compared the various methods.

Since the profile loss is essentially a boundary layer loss (at zero incidence) it will be affected by Reynolds number, surface roughness, turbulence and the velocity distribution. Horlock [13] has presented a general review of boundary layer effects in turbomachinery. It is generally accepted that the blade boundary layers will be predominantly laminar for $Re < 10^5$, and that the loss varies with $Re^{-0.5}$. As Reynolds number increases, transition to a turbulent boundary layer

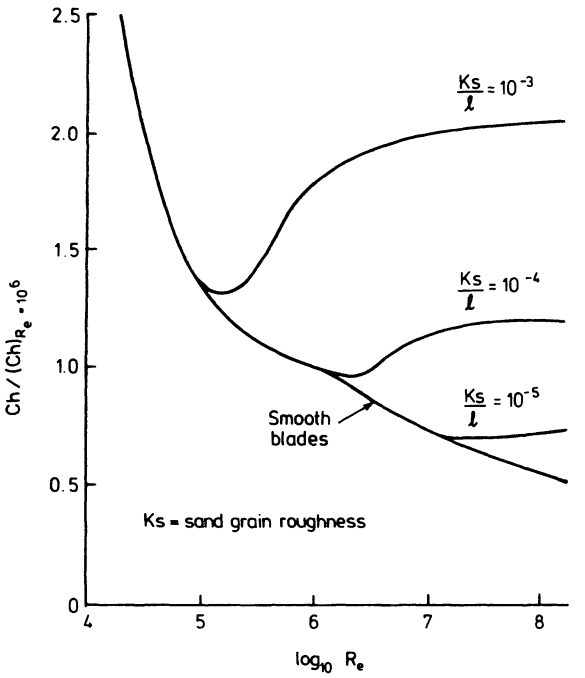

Figure 5.15 *The effect of Reynolds number and roughness on loss [12]*

is virtually complete when $Re > 10^6$ and then the loss varies with $Re^{-0.2}$ (for fully turbulent layers on smooth blades [12]). Roughness is particularly important at high Reynolds numbers as shown in figure 5.15. The effect of velocity distribution is related to the Mach number and the resultant loss seems highly dependent on the blade profile. [4]

Losses at the trailing edge of the blade are included in the profile loss. Both Ainley and Mathieson [7] and Markov [14] agree that the loss increases almost linearly with the ratio of the trailing edge thickness to the blade spacing. Fortunately turbine blades are usually less sensitive to large incidence angles than compressor blades. Soderberg [15] has presented the effect of incidence loss on the over-all (that is, not simply profile) loss as a function not only of incidence, but also of the blade thickness to chord length ratio (figure 5.16) although Horlock [4] suggests that the relationship is over-simplified. Both Ainley and Mathieson [7] and Craig and Cox [10] have presented incidence loss predictions in terms of a stalling incidence, defined as the incidence at which the loss is doubled (an arbitrary figure). The profile loss is modified in accordance with an incidence ratio expressed in terms of incidence over 'stalled' incidence angle.

(b) Annulus Loss

The profile loss accounts for losses associated with boundary layer drag on the blades themselves. Annulus loss terms account for drag on the inner and outer

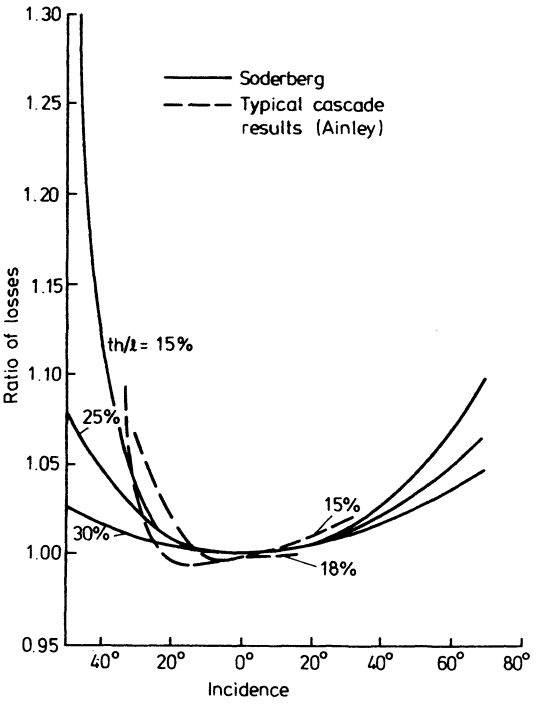

Figure 5.16 *Effect of incidence on losses [4]*

walls (figure 5.17). It is to be expected that the loss will be a function of the turbine geometry, in particular its significance will vary with the ratio of blade chord length to height ratio. In practice it is difficult to separate annulus and secondary losses during experimental tests [16] and hence the combined value is often presented. However Markov [14] and others have attempted direct boundary layer calculations.

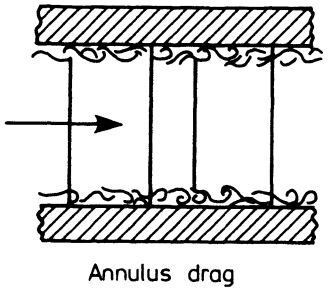

Figure 5.17 *Three-dimensional flow effect – annulus drag [1]*

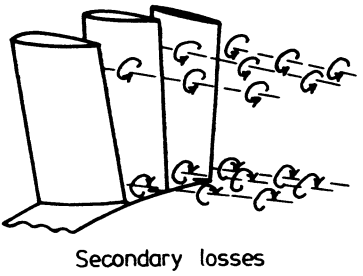

Figure 5.18 *Three-dimensional flow effect – secondary losses [1]*

(c) Secondary Losses

Substantial deflection of the boundary layers must occur through a blade row. This generates a vorticity component in the flow when the gas stream leaves the confines of the blades (figure 5.18). Theoretical analyses have been proposed which evaluate the loss resulting from mixing out of these flows but they appear to underestimate the over-all secondary losses. In consequence, semi-empirical expressions (such as those by Ainley and Mathieson [7] and Soderberg [15]) are more commonly used. Markov [14] has presented some data relating to turbines with very short blades. Dunham [17] has reviewed much published data.

(d) Tip Clearance Losses

Another main source of energy loss results from leakage over the blade tip. This becomes the dominant loss on very small axial turbines and is the main reason why their performance is poor relative to large jet-engine turbines. When both clearance and secondary losses are present it becomes almost impossible to separate their effects and hence reliable data is scarce. Soderberg [15] simply multiplied the calculated efficiency with zero clearance by the ratio of the flow area minus tip clearance to the total flow area. Ainley and Mathieson's expression [7] is more realistic and is based on correlating experimental data.

(e) Additional Losses

Although the losses (a) to (d) are usually the principal losses, others may occur in certain circumstances. For example, additional losses may occur at wall cavities between the nozzle and rotor at the hub, or may result from the use of lacing wires (see section 5.10). Craig and Cox [10] suggest that circular lacing wires will increase the mean blade loss by approximately 1 per cent of the local relative velocity head for every 1 per cent of the passage blocked by the wire.

5.5.1 Estimation of Design Point Efficiency

The overall efficiency of an axial flow turbine working at its design point may be estimated from predictions of the component losses. The preliminary design of the turbine will have been established from elementary theory applied at the pitch line followed by a check that reaction is greater than zero at the root. Root and tip velocity triangles are then established and the Mach numbers checked to avoid high losses. This assumes that a blade height and annulus area are established, having regard to Mach number, nozzle and rotor deflections, etc., plus centrifugal stress calculations. A worked example of the calculations up to this point (for a single-stage turbocharger turbine) is given by Horlock. [4] Assuming that conventional blading is used, the next step is to evaluate the probable losses and redesign if necessary.

It will have become clear that the most commonly used method of loss prediction is that of Ainley and Mathieson [7] modified in places to suit special circumstances.

5.5.2 The Ainley-Mathieson Correlation

The method, which is based on cascade test results, estimates the performance from flow conditions on the pitch line. First the profile drag at zero incidence is established from the data of figure 5.19, which predicts its variation with the pitch/chord ratio for various gas outlet angles. Figure 5.19 illustrates two cases, axial inlet ($\alpha_1 = 0$) and zero reaction ($\beta_2 = \beta_3$). (Note that the figures can be used for nozzle or rotor blades, since they relate to *relative* flow. Hence for a nozzle $\beta_2 = \alpha_1$ and $\beta_3 = \alpha_2$.) For blading between these two extreme cases an interpolation formula is used, namely

$$CPL_P = [\, CPL_{P(\beta_2=0)} + \left(\frac{\beta_2}{\beta_3}\right)^2 (CPL_{P(\beta_2=\beta_3)} - CPL_{P(\beta_2=0)}) \,] \left(\frac{th/l}{0.2}\right)^{\beta_2/\beta_3} \tag{5.48}$$

Equation 5.48 is a correction for the change in inlet angle for a specified outlet angle and hence a change in reaction. The term on the extreme right allows correlation at other thickness/chord (th/l) ratios than Ainley and Mathieson's 0.2 although will not be valid for values much different from 0.2.

The secondary and clearance losses will together be given by

$$CPL_S + CPL_{cl} = [Ch_S + 0.5\,(l_{cl}/h)] \left(\frac{C_{LF}}{sp/l}\right)^2 \left(\frac{\cos^2 \beta_3}{\cos^3 \beta_m}\right) \tag{5.49}$$

where $\beta_m = \tan^{-1}\,[(\tan \beta_2 + \tan \beta_3)/2]$ and C_{LF} is the blade lift coefficient; Ch_S is the secondary loss factor given by Ainley and Mathieson (figure 5.20) and l_{cl}/h is the clearance to blade height ratio. Note that Ch_S is a function of A_3/A_2 (where A is the annulus area) and takes some account of the degree of acceleration if the annulus area tapers. (Experience suggests that flow acceleration tends to help stabilise the boundary layers and hence reduce the loss.)

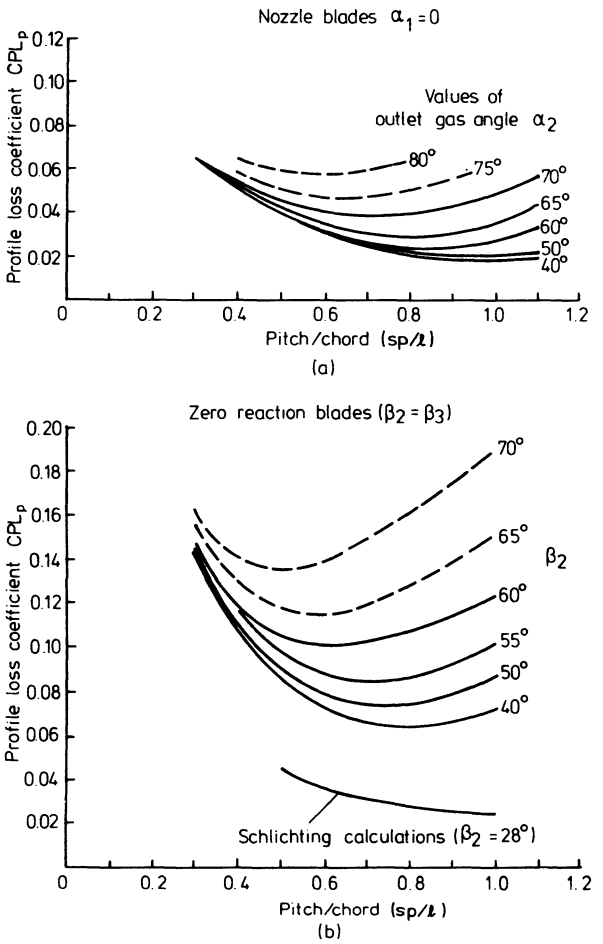

Figure 5.19 *Profile loss coefficients for conventional section blades at zero incidence [7]*

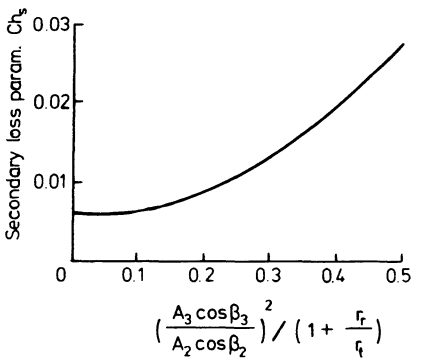

Figure 5.20 *Secondary loss parameter [7]*

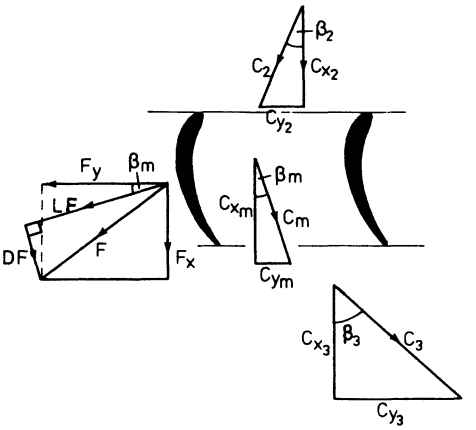

Figure 5.21 *Lift and drag forces on fluid within the blade row*

Consider the forces perpendicular to the mean velocity in the middle of the blade row (figure 5.21).

$$LF = F_y \cos \beta_m + F_x \sin \beta_m \tag{5.50}$$

The blade lift coefficient is defined as

$$C_{LF} = \frac{LF}{\frac{1}{2}\rho_m C_m{}^2 l} \tag{5.51}$$

where l = blade chord length. By application of the momentum equation, expressions can be developed for F_y and F_x [4] and equations 5.50 and 5.51 can be combined to give (with certain simplifying assumptions)

$$C_{LF} = 2\left(\frac{sp}{l}\right)(\tan \beta_2 + \tan \beta_3) \cos \beta_m \tag{5.52}$$

Ainley and Mathieson's data not only refers specifically to a thickness/chord ratio of 0.2 but also to a trailing edge thickness to pitch ratio (th_e/sp) of 0.02. Figure 5.22 predicts the variation of the over-all loss coefficient ($CPL_P + CPL_S + CPL_{cl}$) with trailing edge thickness. In effect this illustrates the penalty paid when having to use thick blades to help eliminate possible vibration problems.

It may be shown [1] that the enthalpy (Ch) and stagnation pressure (CPL) loss coefficients are related. For the nozzle

$$CPL_n = Ch_n \left(\frac{T_{02}}{T_{2s}}\right) \approx Ch_n \left(\frac{T_{02}}{T_2}\right)$$

For the rotor

$$CPL_R = Ch_R \left(\frac{T_{03rel}}{T_{3s}}\right)$$

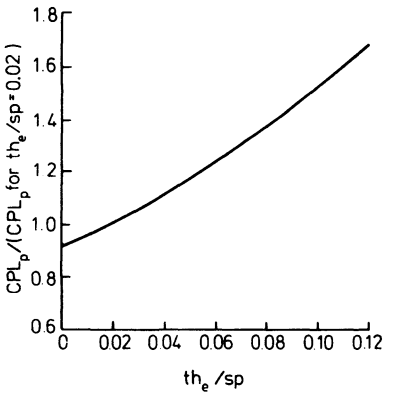

Figure 5.22 *Effect of trailing edge thickness on blade loss coefficient [7]*

The enthalpy loss coefficients may therefore be evaluated and the over-all (total-to-static) stage efficiency calculated from equation 5.47. A check is then made on the mean Reynolds number (averaged over the first nozzle row and last rotor row if multi-staged), since Ainley and Mathieson's data specifies $Re \approx 2 \times 10^5$. They proposed that the total-to-total efficiency can then be varied according to

$$(1 - \eta_{tTT}) \propto Re^{-0.2}$$

but the same relationship could reasonably be used with the total-to-static efficiency.

Although the Ainley-Mathieson method predicts reasonable efficiencies for aircraft turbines, it tends to be less accurate when applied to turbocharger turbines due to their low aspect ratio (blade span or height to chord length ratio) and large tip clearance (consequences of smaller size). Dunham and Came [18] have proposed that the secondary and tip clearance loss prediction of Ainley and Mathieson should, in these circumstances, be modified as follows.

(1) Function Ch_S (in equation 5.49 and figure 5.20) should be replaced by the expression

$$Ch_S = 0.0334 \left(\frac{l}{h}\right)\left(\frac{\cos\beta_3}{\cos\beta_2}\right) \tag{5.53}$$

(for nozzle put $\beta_2 = \alpha_1$ and $\beta_3 = \alpha_2$; h = blade height).

(2) Function $0.5(l_{cl}/h)$ in equation 5.49 should be replaced by the function

$$0.47 \left(\frac{l}{h}\right)\left(\frac{l_{cl}}{l}\right)^{0.78} \tag{5.54}$$

These modifications improve the predictions with low aspect ratios.

A typical breakdown of the principal losses, as predicted by Ainley and Mathieson is given in figure 5.23. An illustration of the trends in design point efficiency predicted by the Ainley-Mathieson method (given by Horlock [4]

and Shaw [19]) is reproduced in figure 5.24. Both total-to-static and total-to-total efficiencies are predicted for any degree of reaction against blade loading coefficient (ψ). The diagram refers to a single-stage machine with axial inlet flow, typical of a turbocharger turbine. The conclusion is that the best efficiency (total-to-static for a single-stage turbocharger turbine) will probably be achieved with a

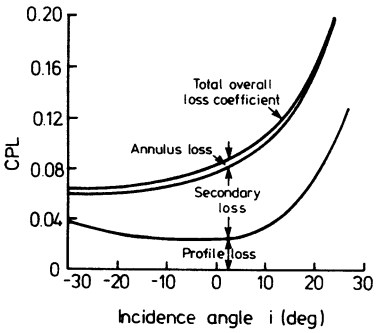

Figure 5.23 *Analysis of losses in flow through a row of turbine blades [7]*

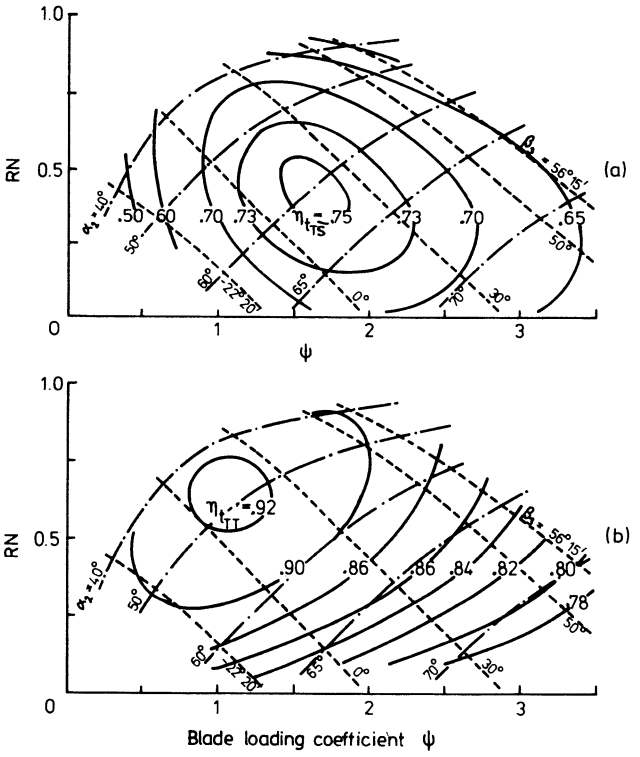

Figure 5.24 *Turbine stage efficiencies predicted by the Ainley-Mathieson method:* (a) *total-to-static efficiency;* (b) *total-to-total efficiency [19]*

blade loading coefficient around 1.5, and low or zero exit swirl resulting in about 30 to 40 per cent reaction.

5.5.3 Estimation of Offdesign Efficiency

The offdesign performance of a turbocharger turbine is particularly important for several reasons. Firstly, with pulse turbocharging the instantaneous mass flow rate will vary enormously, hence gas flows and angles will move away from the design point cyclically. Secondly, the engine to which the turbocharger is fitted

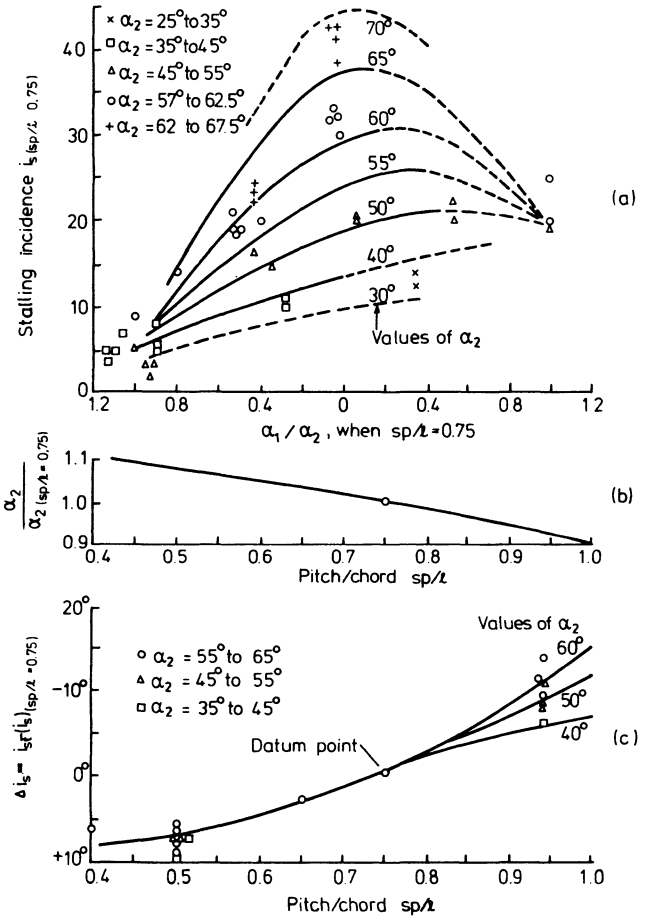

Figure 5.25 *Offdesign performance of cascades of turbine blades, for Re = 2 x 10^5, M < 0.5.* (a) *Stalling incidence of turbine blade sections when pitch/chord ratio = 0.75;* (b) *variation of exit gas angle with pitch/chord ratio;* (c) *variation of stalling incidence with pitch/chord ratio;*

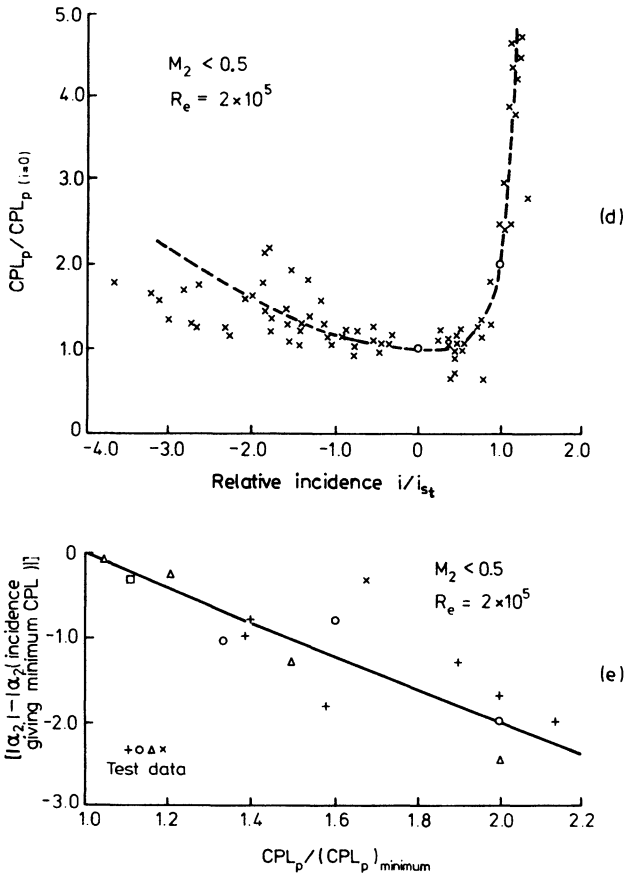

Figure 5.25 (d) *variation of relative profile loss with relative incidence;* (e) *variation of exit gas angle with relative profile [7]*

will certainly have to operate with a varying load and probably a varying speed. Finally, one basic design of turbine will be adapted to a range of engine sizes. The Ainley-Mathieson method takes account of offdesign conditions through the effect of increasing incidence angle. The procedure is first to evaluate the nominal 'stalling' incidence ($i_{st_{o.75}}$) for an equivalent cascade of 0.75 pitch/chord ratio from figure 5.25a [the value of gas exit angle (α_2) being 'corrected' from figure 5.25b if the pitch/chord ratio is other than 0.75]. The change in stalling incidence (Δi_{st}) due to the different pitch/chord ratio is found from figure 5.25c and hence the relevant stalled incidence evaluated from

$$i_{st} = i_{st_{o.75}} + \Delta i_{st}$$

The relative profile loss coefficient ($CPL_P/CPL_{Pi=0}$) is then found for the appropriate relative incidence (i/i_{st}) from figure 5.25d. The effect of incidence in

changing the gas outlet angle is given in figure 5.25e. For a more detailed description of the procedure the reader is referred to Ainley and Mathieson. [7]

The performance scheme of Craig and Cox [10] is also capable of predicting the effects of offdesign conditions.

5.6 Three-dimensional Flow Models

The analysis of flow through the axial turbine presented so far, has been confined to two-dimensions (with the exception of vortex blading) and semi-empirical techniques. Fortunately the flow in an axial turbine is predominantly accelerating and the boundary layers on the blades are usually thin. As a result, turbines with quite high efficiencies have been designed using the above techniques without detailed analysis of the blade shapes. However, as the demand for higher loadings and efficiency continues, local knowledge of the detailed flow pattern becomes more important. Several useful design techniques are now available, with different orders of complexity and realism. None truly models the actual flow situation in a working turbine and therefore, although useful, the analyses should be used with caution.

Broadly the methods can be divided into those that assume incompressible flow and those that do not. A second division may be made according to whether the model relates to a complete cascade of blades, or just to the channel between two adjacent blades. In the latter model, the flow conditions on the leading and trailing edges will not be accurate but the mathematical solution is simpler. A third division concerns the mode of operation of the model. Most predict the flow for specified blade shapes, but it can be argued that the reverse is more useful, namely to generate blade profiles from a specified velocity profile along the suction and pressure surfaces. Since such a variety of approaches to the problem are used and their complexity is beyond the scope of this book, discussion will be restricted to the objectives with only brief reference to the most commonly used methods.

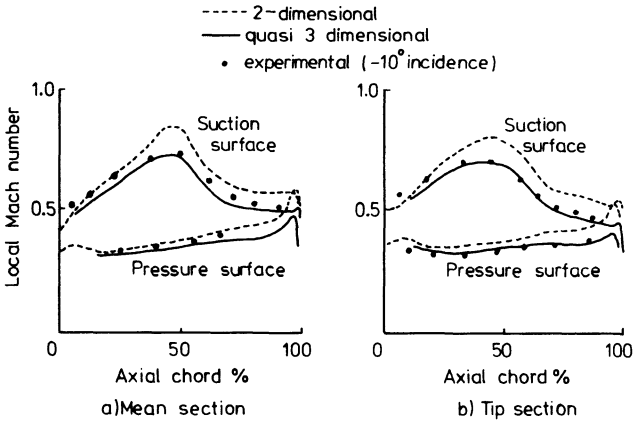

Figure 5.26 *Turbine stator blade: surface Mach number distribution [24]*

The initial approach (assuming incompressible flow) was to compute the 'potential flow' (that is, pressure and velocity distributions) outside the (thin) boundary layer in a passage formed by two adjacent bodies. Typical is Martensen's method [20] extended by Wilkinson. [21] A boundary layer calculation (either a full calculation or, more commonly, a semi-empirical diffusion ratio limit to avoid separation) is then conducted. Compressible flow models have more relevance to the actual flow in a turbine, widely used methods being those of Katsanis [22] and Stanitz. [23] Figure 5.26 illustrates predicted Mach number distributions (as the tip and mean radii) along a set of turbine nozzle blades. The important feature is the deceleration towards the trailing edge on the suction surface, since if it is too great, separation may occur. Japikse [25] recommends that the diffusion parameter (recovery of dynamic head at the minimum pressure point) should not exceed 0.4 to 0.5, although higher values are possible if the boundary layer is fully turbulent, to avoid separation.

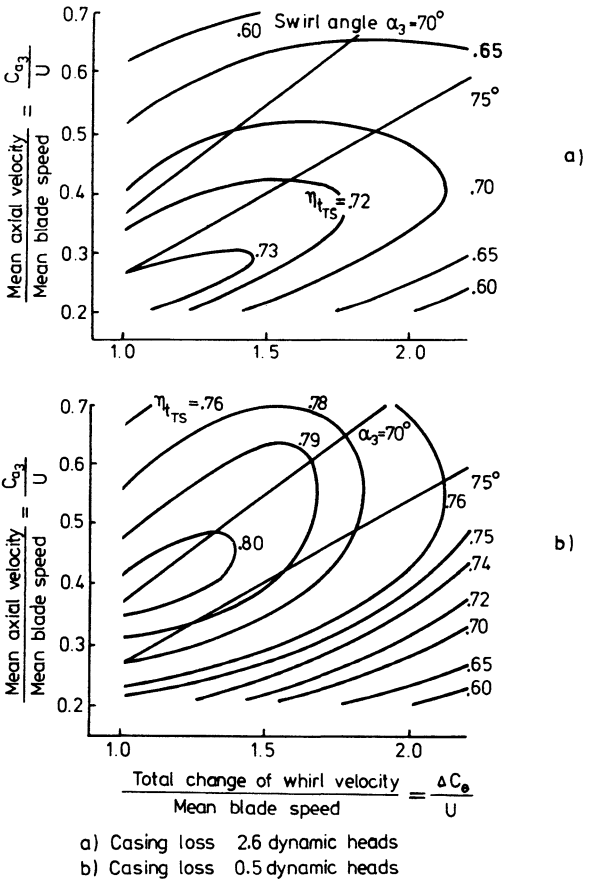

Figure 5.27 *Total-to-static turbine efficiencies for different exhaust casing losses [26]*

5.7 Inlet and Exhaust Casings

The discussion of energy losses and performance prediction (section 5.5) was concerned with the turbine stage alone. However, quite significant energy losses can occur in the inlet and exhaust casings of turbochargers. This can be particularly important if space is at a premium and passages with sharp radii are used, or if no attempt at exhaust diffusion is made. Furthermore there are losses associated with the multi-entry casing for pulse turbocharging systems. That casing design may have a major effect on the turbine total-to-static efficiency is shown in figure 5.27. The results show a different characteristic and a 7 percentage point gain in over-all efficiency resulting from a major improvement in casing design.

Particularly awkward problems arise on an intake casing with a multi-entry pulse system. For example, the gas flow from two separate intakes must be transposed into two 180° annular ducts, invariably in a very short distance (to keep turbocharger size down). A typical example of the problem is shown in figure 5.28. Quite apart from the loss in the casing, the major problem is that of obtaining even velocity distribution and flow angle. Simpson and Scarlett [26] mapped the pressure drop and flow angle over the annular nozzle inlet area of such a casing, during steady flow tests. Figure 5.29 shows the results in terms of a pressure loss coefficient CPL_k where

$$CPL_k = \frac{\text{total pressure drop}}{\text{inlet kinetic head}} \tag{5.55}$$

and the incidence at the nozzle blades. Clearly flow conditions near the ends of

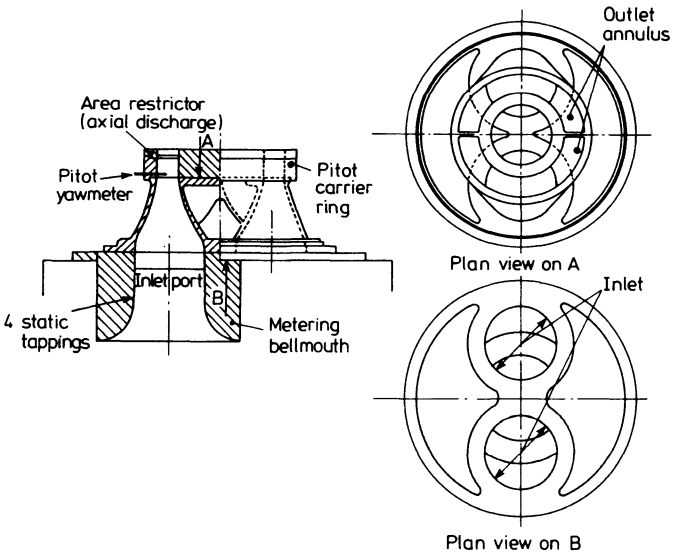

Figure 5.28 *General arrangement for inlet casing tests [26]*

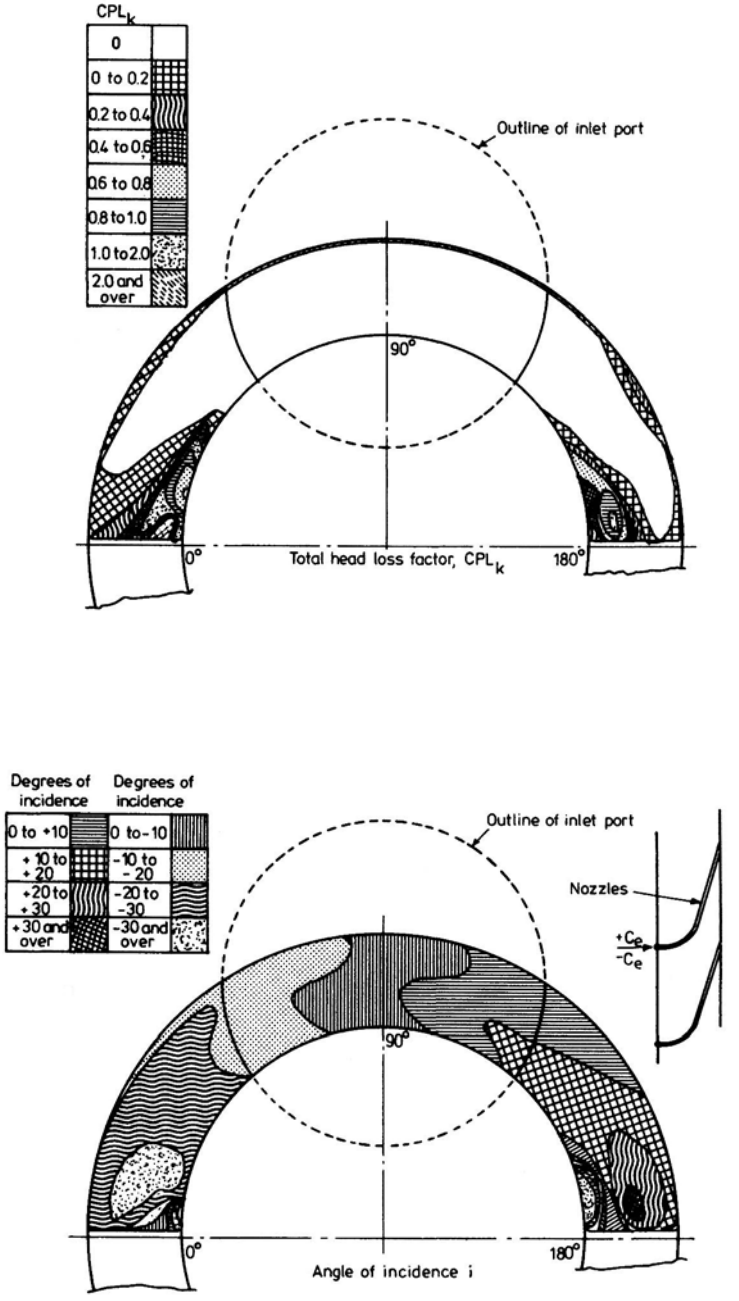

Figure 5.29 *Inlet casing test results, angular variation of pressure loss coefficient and incidence [26]*

the arcs are unsatisfactory, particularly near the blade roots, although the overall pressure loss in the casing is low. Casings for constant pressure operation (and some pulse systems) will use a single-entry casing. Multi-entry pulse systems may have up to four entries, although 'end of sector' losses will increase with each additional entry.

Since all kinetic energy leaving a turbocharger turbine is lost, it is advantageous to diffuse the exit flow as much as possible. For a fixed exhaust back pressure, greater diffusion will result in a lower rotor exit pressure and hence greater turbine work. Usually it is difficult to diffuse purely in the axial direction without the turbocharger becoming excessively long, hence diffusion is required during transition from axial to radial flow. A radial exit naturally simplifies access to end mounted bearings.

Simpson and Scarlett [26] tested a model turbine with a variety of axial to radial diffusion profiles. The general arrangement of their model is shown in figure 5.30 (the swirl vanes simulating the turbine), and some test results in figure 5.31 where CPL_q is defined similarly to CPL_k (equation 5.55) but relating

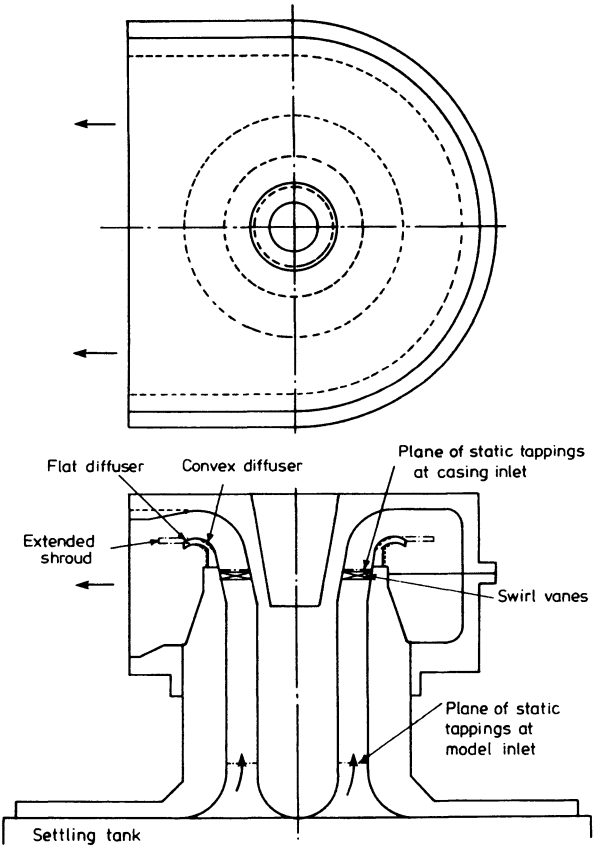

Figure 5.30 *General arrangement of exhaust diffuser tests [26]*

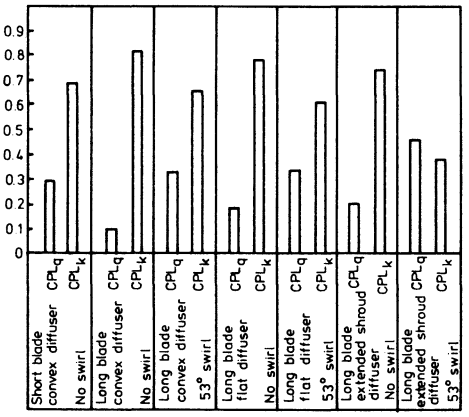

$$CPL_q = \frac{\text{static pressure change}}{\text{isentropic inlet dynamic head}}$$

$$CPL_k = \frac{\text{total pressure drop}}{\text{isentropic inlet dynamic head}} = \left[1-\left(\frac{A_1}{A_2}\right)^2\right] - CPL_q$$

Figure 5.31 *Full admission test result [26]*

to static pressure gain. Clearly the flat extended diffuser shroud produced maximum static pressure gain. Further tests with a reduced casing volume (using a shorter axial length) showed little loss in performance suggesting that the original design in figure 5.30 was larger than necessary. A small deterioration in diffuser performance resulted when half the inlet casing was blocked off (that is, complete partial admission) except when the 180° blocked sector was placed in line with the casing outlet flange.

5.8 Partial Admission and Unsteady Flow

A turbocharger turbine designed for pulse operation will operate with highly unsteady flow and will usually require two or more separate intake sectors. The separation of these intakes is preserved through the nozzle to the rotor entry so that interference between various exhaust manifolds is minimised (see chapter 7). Thus the change in performance due to unsteady flow and partial admission go together. However it is often more convenient to try to separate the effects.

5.8.1 Partial Admission

The gas flow entering each sector of a multi-entry turbine will be unsteady, may have quite different pressure wave forms and will certainly be out of phase (otherwise there is no point in using more than one entry). Thus at any instant in time, the instantaneous mass flow rates and pressures in the sectors will differ,

and some blade passages may contain no flow at all. The resulting losses may conveniently be divided into 'end-of-sector' and 'windage' losses. The latter dominate.

The windage loss will be the power required to drive the turbine when no gas is flowing through it at all. This situation can, momentarily, arise with a single-entry turbine, but will more commonly affect only part of the turbine wheel when the gas flow in one sector falls to zero. The phenomenon can be modelled in steady flow tests by blanking off a complete turbine inlet sector. Test results are shown by Suter and Traupel, [27] Craig *et al.*, [28] Dibelius, [29] and others. A typical comparison of turbine efficiency under full and partial admission can be made from figures 5.32 and 5.33, both from the same twin-entry turbine but

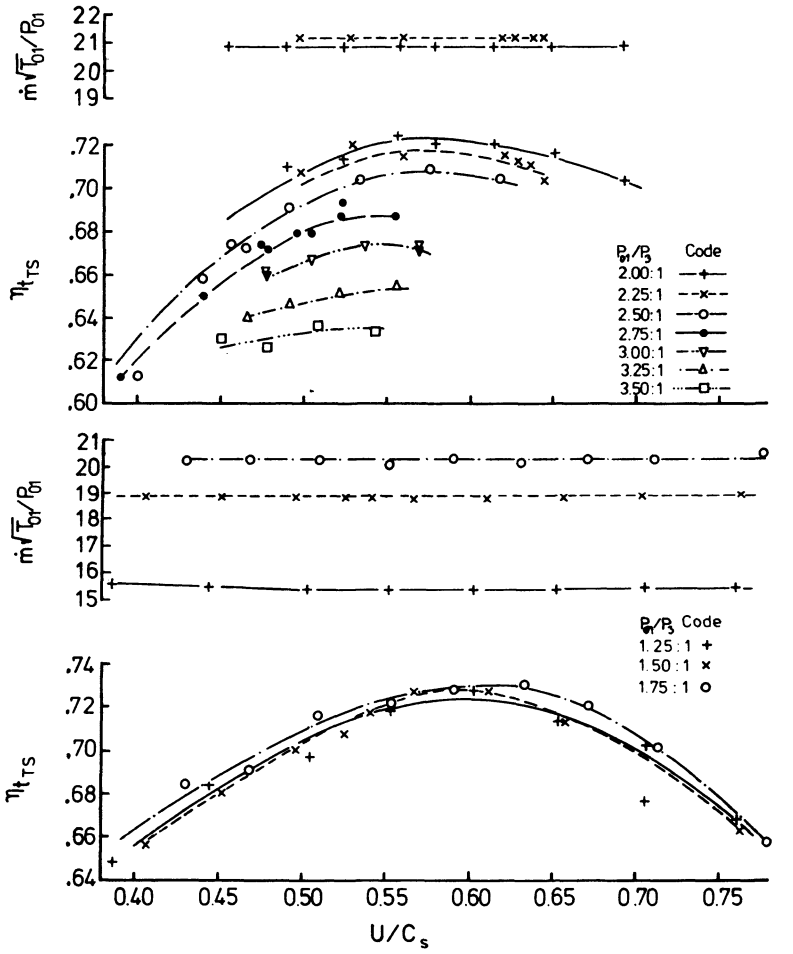

Figure 5.32 *Steady flow turbine performance, varying U/C_s and pressure ratio, full admission [28]*

figure 5.33 incorporates the loss due to one sector being completely blanked off. The efficiency loss is approximately 11 per cent and peak efficiency occurs at a lower blade/speed ratio, particularly at low pressure ratios. Suter and Traupel [27] suggest that the loss may be correlated by the following expression

$$\dot{W}_w = K_1 \left(\pi D_m h \frac{\rho U_m^3}{2} \right) (1 - \epsilon) \tag{5.56}$$

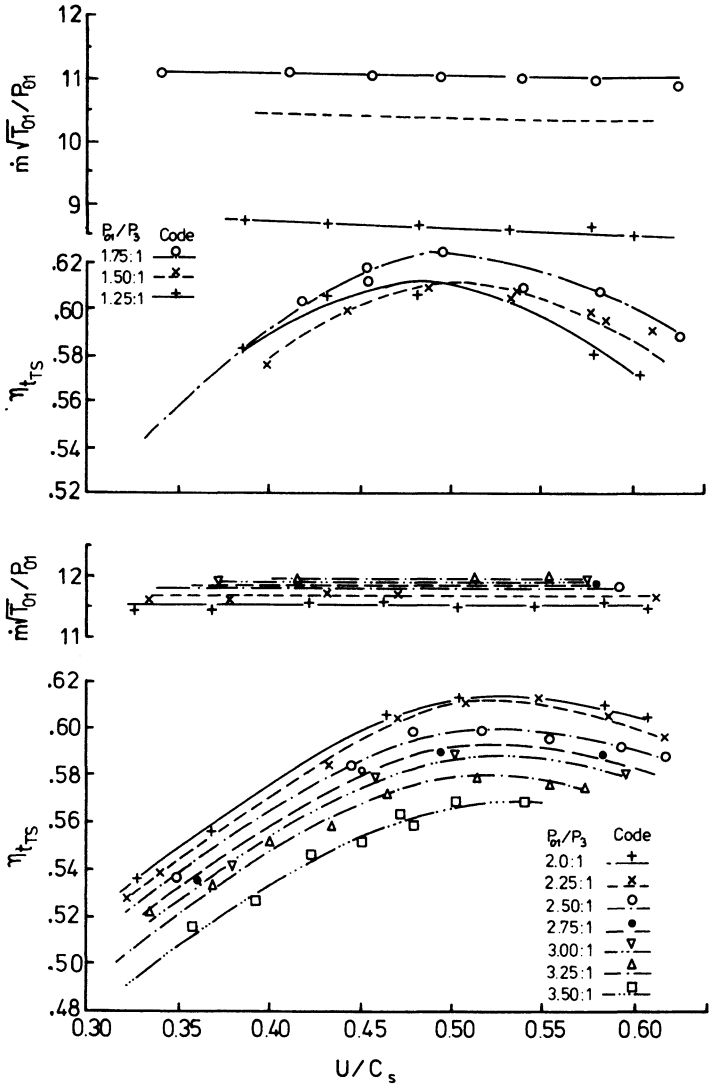

Figure 5.33 *Steady flow turbine performance, with complete partial admission (one entry blocked) [28]*

where $\dot{W}_w$ = power loss (windage)

K_1 = empirical constant

D_m = mean diameter

h = blade height

ϵ = arc of admission (as a fraction of 360°)

U_m = mean blade speed

Their own results suggest a value of 0.1 for K_1.

Figure 5.33 includes the losses due to windage and end-of-sector effects. At the join of two sectors the flow conditions entering the passage between two rotor blades will be highly disturbed (due to unequal flows in the two sectors) resulting in inefficient operation. The end-of-sector losses will be lower in magnitude than the windage loss, since a smaller sector of the turbine wheel is involved, but will not be insignificant. Suter and Traupel [27] suggest that the end-of-sector loss may be approximated by

$$\dot{W}_{es} = K_2 \left(\frac{b}{D_m}\right)\left(\frac{C_s}{U_m}\right)\frac{\dot{m}U_m^2}{\epsilon} \tag{5.57}$$

where $\dot{W}_{es}$ = end-of-sector power loss

K_2 = empirical constant

b = blade axial width (that is, axial component of blade chord)

C_s = isentropic velocity equivalent ($\sqrt{2\Delta h_s}$)

$\dot{m}$ = mass flow rate.

Figure 5.34 shows the reduction in total-to-static efficiency due to partial admission obtained by Dibelius [29] during steady flow tests. The efficiency is shown for full admission, half admission, admission in two quarter sectors and finally one quarter sector, in all cases plotted against a head coefficient $2\Delta h_s/U_m^2$. The partial admission losses are shown to be most severe with quarter admission (as would be expected) particularly when the blade speed is high relative to the expansion ratio (that is, low $2\Delta h_s/U_m^2$).

5.8.2 Unsteady Flow

Since the flow at entry to the nozzles will be axial in a single-stage turbocharger turbine, the energy losses in the stationary passages will not be substantially affected by unsteady flow (changing incidence losses will not occur). However, some boundary layer separation may result during periods of high instantaneous flow rates; therefore it would be unrealistic to expect no change in nozzle energy losses.

During unsteady flow conditions the gas velocity leaving the nozzle will be varying considerably in magnitude but little in direction. The instantaneous

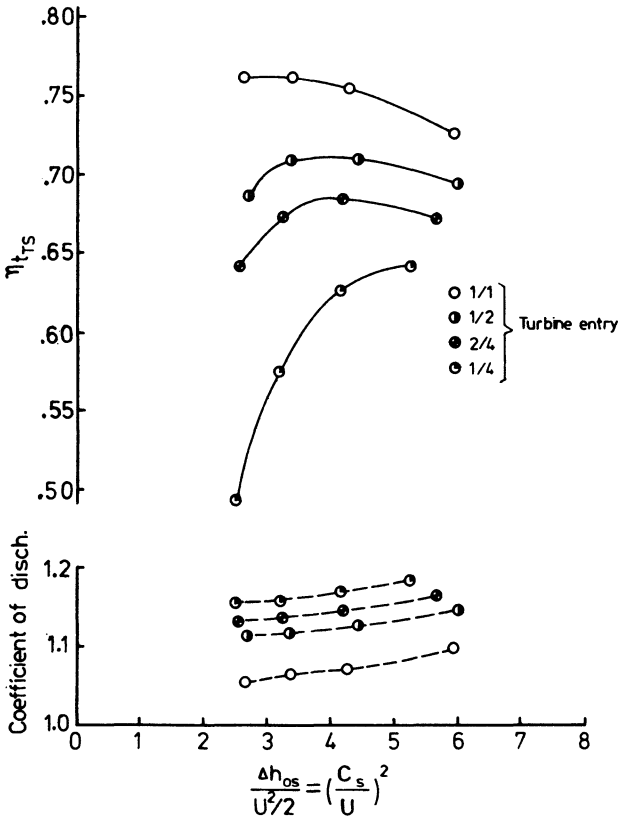

Figure 5.34 *Efficiency with full, half, two quarter and quarter admission [29]*

velocity may drop to zero resulting in windage losses as described above. However, in the less extreme case of a pulsating flow whose mean is close to the design point of the turbine, the velocity triangle at the rotor entry will alter according to the instantaneous gas velocity. The rotor speed will remain approximately constant due to its inertia. Hence the incidence angle between the resultant gas relative velocity and the rotor blade angle will oscillate from a large positive to a large negative value. The incidence will in turn cause losses to increase (figure 5.25). The value of this increase in energy loss may be estimated using the offdesign procedure described in section 5.5. However, evidence suggests that a turbine operating under unsteady flow conditions does not behave exactly as the sum of its performance under assumed 'quasi-steady' conditions; [30, 31] the difference increases as pressure ratio and pulse frequency increase. This error is more fully described in chapter 15, but does not affect the basic discussion presented here since it is relatively small.

If it is assumed that the quasi-steady flow analysis is realistic, then clearly the performance of the turbine under unsteady flow conditions will depend on the

cyclic change of the incidence angle, etc. Thus it will depend on the pulse amplitude, shape and frequency. These factors themselves depend both on turbine area, engine exhaust manifold configuration (see chapters 6 and 7), the timing at which the exhaust valve opens, whether the engine is a two or four-stroke type, etc. The consequence is two-fold. Firstly, no two results from separate unsteady flow tests may be compared without qualification, and secondly, the mean turbine efficiency obtained from a machine will depend not just on the turbine, but also on the engine that generates the unsteady flow. The latter point is one reason why turbocharger manufacturers are often reluctant to offer their efficiency characteristics to potential customers.

Craig and Janota [31] have predicted the performance of an axial flow turbine under unsteady, partial admission conditions for several common exhaust manifold configurations used with the pulse turbocharging system. The calculations were based on a realistic pulse shape for a two-stroke engine, and used a predictive technique similar to that of Ainley and Mathieson [7] plus Suter and Traupel's partial admission model. [27] Figure 5.35a shows the predicted 'base line' performance under steady flow constant pressure conditions for four geometrical configurations (used to adjust the flow range of a basic machine to a particular engine – see section 5.9). The precise values of peak efficiency shown are relatively unimportant since the objective is to compare performance under 'constant pressure' and 'pulse' operation. A relatively small deterioration in performance results when the same single-entry casing connects to three cylinders in a pulse turbocharging system (figure 5.35b). If a twin-entry casing is used, each entry connected to two-cylinders, a larger deterioration in turbine efficiency results (figure 5.35c), whereas if only one cylinder is connected to each entry, efficiency falls even further, particularly as U/C_s departs from the optimum. As the number of cylinders connected to a turbine entry is reduced, so the windage losses will increase due to the longer interval of low mass flow between engine exhaust pulses. The subject is discussed in detail in chapter 7.

Under steady flow conditions a gas turbine is usually most efficient when the reaction is relatively high (for example, up to 50 per cent). However, under highly unsteady flow the choice of reaction may not be so clear. Consider a series of pressure pulses arriving at the turbine. An impulse turbine will cope well with the peak of the pressure pulse (low value of U/C_s). Since windage losses increase with speed squared (equation 5.56), the low speed of the impulse design will also keep these losses low. However, a penalty will be paid due to incidence loss during the mean flow period of the pulse. A higher reaction (and blade speed) will suit the mass flow at the mean of the pulse but will be offdesign at the peak. It is important for the designer to choose the optimum reaction, since this is one of the few freedoms open to him; remember that he must accept radial inlet flow and preferably zero exit swirl (to maintain a high total-to-static efficiency) in a single stage. It is normal to design for zero reaction at the blade root (since a negative reaction is not desirable) in order to cope best with the high mass flow during the peak of the pulse. Thus the pitch line reaction will be lower than that of a turbine designed for constant pressure operation. Daneshyer *et al.* [30] tested turbines with reactions at the root of -10, 0 and 20 per cent under steady and pulsating flow. They concluded that the conventional zero reaction at the root design was not the optimum; the turbine benefited from increased reaction both

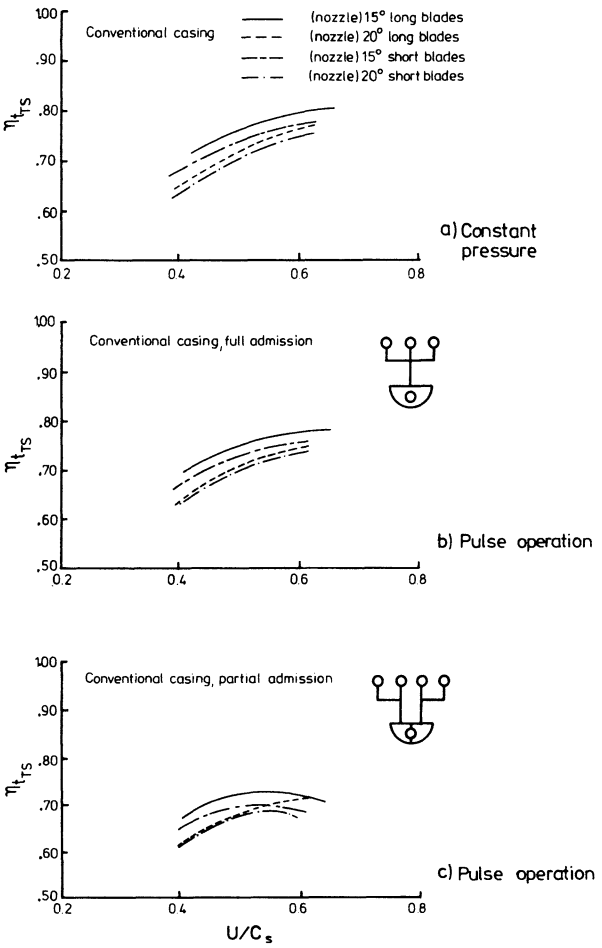

Figure 5.35 *Turbine efficiency prediction, for constant pressure and pulse operation with two or three cylinders per turbine entry [31]*

under steady and unsteady flow. In practice the benefit will be dependent on pulse shape and, as stated by Daneshyer *et al.* [30] may not be apparent if long windage periods (for example, with one or two cylinders to a turbine inlet) occur.

5.9 Turbine Characteristics and Flow Range

An axial flow turbine will be fitted only on the larger sizes of turbocharger. These turbochargers will be used for marine and industrial engines rather than automotive types. In consequence they do not have to operate over quite such a large

flow range as the radial turbine fitted to an engine whose speed and load vary greatly. Unfortunately this apparent benefit only helps the turbine marginally since it may still be required to operate under the highly fluctuating inlet conditions associated with pulse turbocharging. A further problem arises since one basic turbocharger design must be capable of adaptation to a large range of diesel engines for purely economic reasons.

The calculation of offdesign performance of a single-stage axial turbine has already been discussed. As the mass flow rate departs from the optimum, the primary source of increased energy loss is that due to incidence. Fortunately, the gas flow through the axial flow turbine is predominantly accelerating. This tends to stabilise the boundary layers and delay separation. As a result the increase in loss with incidence is not severe and the axial flow turbine has a reasonable efficiency over quite a large flow range. The axial machine is more fortunate than the radial flow turbine since there is no opposing centrifugal field.

The effective limits to the useful performance of the axial flow turbine are low efficiency at low mass flow rates and choking at high mass flow rates. A typical set of turbine characteristics is shown in figure 5.36 based on the presentation commonly used by turbine designers (that is, total-to-total efficiency and dimensionless mass flow plotted against pressure ratio for various values of non-dimensional speed parameter). Figure 5.37 shows similar characteristics in which the total-to-static efficiency is plotted against blade speed ratio.

Choking will usually occur at the throat of the nozzles at an over-all pressure ratio of between 2 and 3, dependent on the degree of reaction. At lower flow, the mass flow rate for a specified expansion ratio will exhibit some speed dependence, but considerably less than that of a radial machine (due to the existence of a speed-dependent centrifugal field in the latter). Thus the axial flow turbine mass flow characteristic (frequently called the 'swallowing capacity curve') may be considered as approximately a unique line similar to that obtained from a fixed area orifice or nozzle. The effective area of an equivalent single nozzle can

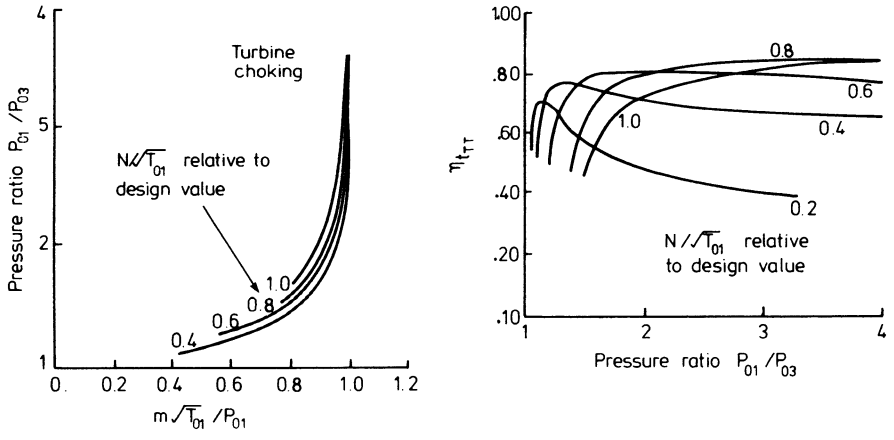

Figure 5.36 *Turbine characteristics [1]*

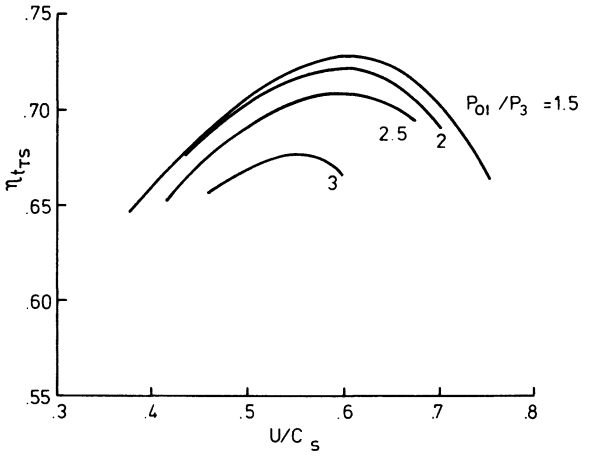

Figure 5.37 *Turbine efficiency against blade speed ratio [28]*

be estimated by considering the throat area of the turbine nozzles and the duct area at rotor blade exit as two nozzles in series.

It has already been mentioned that the axial flow turbine maintains a reasonable efficiency as flow is reduced but eventually a point does come at which the efficiency becomes unacceptable. It is therefore important to choose a blade profile providing good performance under high incidence. Since, during unsteady flow operation, it is most important to maintain high efficiency when the mass flow rate is high, the design point can be biased in this direction relative to the mean mass flow rate.

The problem of flow range resolves primarily into adapting a single turbocharger design to a range of engine sizes and hence mass flow rates. To adapt a basic design of turbocharger turbine such that it can provide high efficiency over a very large mass flow range involves changing the effective choking area. Thus the throat area of the nozzles must be altered. There are four principal ways in which this can be done

(1) varying the angle of the nozzle blades (figure 5.38a);
(2) changing the nozzles for a set having a different exit angle (figure 5.38b);
(3) cropping the trailing edge of the nozzle blades to increase the effective throat area (figure 5.38c);
(4) changing the height of the nozzle and rotor blades together with provision of suitably sized inlet and exhaust casings (figure 5.38d).

It will be clear from figure 5.38 that method (4) will have the most drastic effect on throat area and hence choked mass flow rate. For this reason a manufacturer may offer a basic design of turbocharger with two or three blade heights to cover a large range of engine sizes. This would typically result in a choked mass flow change of around 50 per cent. To obtain optimum efficiency in between these points, one of options (1), (2) or (3) may be used. It is difficult to justify producing multiple ranges of turbine nozzle blades with different exit angles

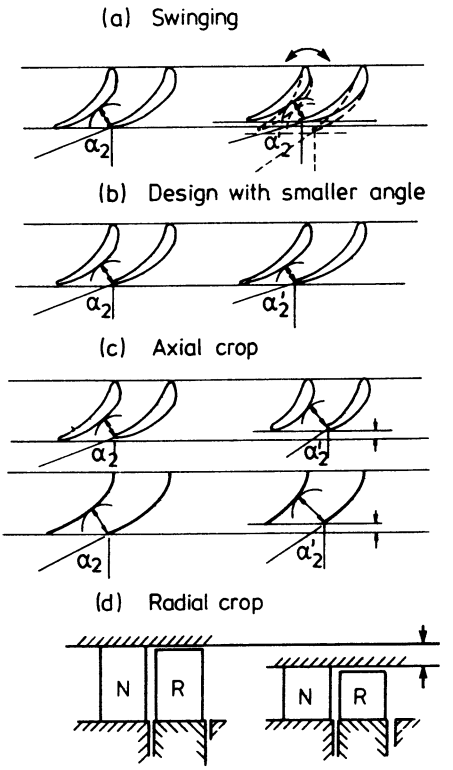

Figure 5.38 *Methods of altering the effective nozzle area*

hence option (2) may be discarded. Varying the blade angle can be achieved if the blade mounting is designed accordingly, but it does result in some clearance being required at hub and tip plus some nozzle incidence loss. Although the technique is used it is simpler to design a rigidly fixed blade and to crop its trailing edge. This, the more commonly used method, can increase losses associated with the trailing edge thickness and introduce a large nozzle/rotor interspace. Hence some small penalty is paid in efficiency.

5.10 Blade Stress, Fixing and Vibration

The design of the turbine blade profile is governed not just by aerodynamics, but by the stress levels involved. Clearly the maximum operational speed will be governed by the stresses in both the rotor blades and the disc. Turbine blade vibrations can readily be excited by the highly unsteady flow resulting from pulse system operation and this may govern the minimum blade thickness used in practice, since thicker blades will be stiffer and have higher natural frequencies. Thus the turbine design may be severely constrained by stress in the rotor blades, root fixing and vibration problems.

5.10.1 Rotor Blade Stresses

The stresses that act on the rotor blades are due to centrifugal tensile stress, centrifugal bending stress, gas pressure bending stress and thermal stress. Dundas [32] has shown that the centrifugal stress at the blade root (the highest stress point) may be calculated from

$$\sigma_{c\,max} = \frac{\rho\omega^2 r_m^2 (1 - \Lambda)^2}{2} \left\{ 1 + (AR - 1) \left(\frac{2 - 3\Lambda + \Lambda^3}{3(1 - \Lambda)(1 - \Lambda^2)} \right) \right\} \quad (5.58)$$

where $\Lambda = r_{hub}/r_{tip}$

AR = blade taper = A_{tip}/A_{hub}.

The stress depends on the material density, taper and the product of annulus area times speed. It is the speed that is the dominant variable and hence will be limited by $\sigma_{c\,max}$. Centrifugal bending stress will also be present if the blade is non-radial.

Work is obtained from the turbine due to the change of angular momentum of the gases passing through the blades. This change in momentum produces the force required to turn the rotor and therefore must exert a bending moment on the blades. Gas bending moments will be developed about the axial and tangential directions but the former will dominate. Cohen *et al.* [1] quote a useful approximation for the stress due to gas bending, namely

$$\sigma_{gb\,max} \approx \frac{\dot{m}(\bar{C}_{\theta 2} + \bar{C}_{\theta 3})}{Z} \frac{h}{2} \frac{1}{Il^3} \quad (5.59)$$

where the bar denotes mean values

Z = number of blades
h = blade height
l = chord
I = smallest value of the root section modulus of a blade of unit chord.

For a fuller treatment the reader is referred to Horlock [4] and Dundas. [32]

The centrifugal stress will usually dominate, but the gas bending stress may be more important since it will not be steady. It is useful to superimpose an additional component to the bending stress to allow for the flow unsteadiness, that is

$$\sigma_{max} = \sigma_{c\,max} + \sigma_{gb\,max}(1 + k) \quad (5.60)$$

where k will depend on the amplitude of the fluctuating forces, etc. [33]

Choice of a satisfactory stress level will be made from creep strength and fatigue data for suitable materials (see Chapter 2).

5.10.2 Rotor Disc Stresses

Rotor disc stresses will be due to the centrifugal load of the blades, the centrifugal load of the disc and the effect of a thermal gradient across it. The load of the

blades will be fixed, hence it is the hoop stress due to the rotation of the disc itself that must be evaluated. For a solid disc of constant thickness, the mean and maximum hoop stresses will be given by [4]

$$\sigma_{h\ mean} = \frac{\rho U_{max}^2}{3} \tag{5.61}$$

$$\sigma_{h\ max}\ (\text{at centre}) = \frac{\rho U_{max}^2}{8}\ (3 + \nu) \tag{5.62}$$

where U_{max} occurs at the outer rim and ν = Poisson's ratio. For a full treatment of an arbitrary shaped disc see Dundas. [32] The thermal stress imposed by the temperature difference between rim and centre leads to a high compressive hoop stress at the rim.

5.10.3 Blade Fixing

Many techniques have been tried for fixing the blades to the rotor disc. Small experimental turbines have used a single machined forging for blades and disc, a single casting and blades welded to the rim. However, by far the most common method is to use separate blades restrained by a 'fir-tree' root (figure 5.39). The blades themselves are usually a slightly loose fit in the rim but will be restrained from axial movement. When running the blades will be held by the separations of

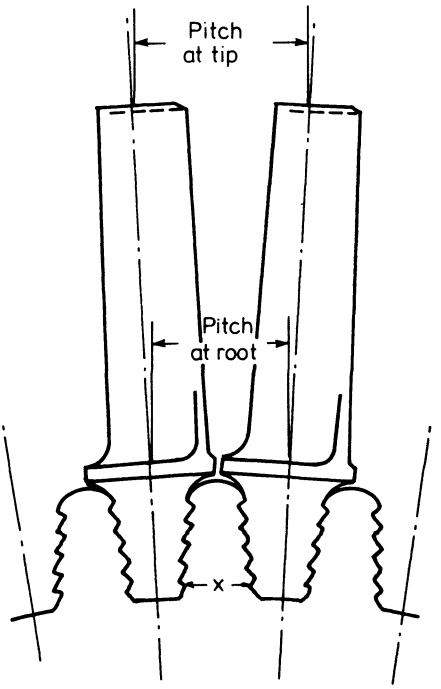

Figure 5.39 *'Fir-tree' root, turbine blade fixture [1]*

the fir-tree due to centrifugal force, a small amount of movement being beneficial in damping blade vibration. The complex 'fir-tree' must be accurately machined otherwise the serration will not be uniformly loaded (the load will be redistributed by local yielding if the non-uniformity is small). A large amount of photo-elastic and finite difference stress research has been devoted to the fir-tree but further discussion is beyond the scope of this book. However, one important point should be made: the blade must fail before the disc. This will help in designing a casing to restrain the consequences of failure since the fractured components will be smaller and lighter.

5.10.4 Blade Vibration

The subject of turbine blade vibration is immensely complex, but the fundamental principle is simple: avoid resonance. In a gas turbine plant vibrations are induced in the rotor blades as they pass through the wakes of the stator blades in addition to the basic problem of rotor speed passing through a multiple of the blade natural frequency. For a turbocharger turbine the problem is compounded by the unsteady flow inherent in the pulse turbocharging system. Gisiger [34] and Brock and Scarlett [35] have reported typical investigations into turbine blade failures on turbochargers.

Although realistic attempts have been made (see Dundas [32] for a resumé) to predict the natural frequencies of turbine blades, they are usually determined experimentally. The techniques used in avoiding vibration problems are limited. The primary method is to use a stiff enough blade but this naturally results in thick blades and poor aerodynamic performance if carried to excess. A secondary method is to use a damping wire fed through a hole in the blades. This again will result in an aerodynamic penalty but it is effective in reducing large amplitude vibrations at the upper end of the turbocharger speed range. At lower speed, when the engine speed and load are low, the turbine inlet temperature is low and the wire may not be in good contact with all the blades. At higher turbocharger speeds the stress level in the wire will exceed the elastic limit and good contact will be ensured. A final method, used on gas turbine plant, is to use blade tip shrouds, but economic manufacturing techniques and stress levels usually prohibit their use on turbochargers.

Particular problems that occur under pulse operation usually develop when large amplitude pulsations combine with unfavourable groupings of cylinders to a turbine entry. Basically the objective should be to avoid large discontinuities in the flow arriving at the turbine. Some combinations of engine firing order and manifold connections are more favourable than others. Operation with a pulse converter (double or multi-entry) is described in detail in chapter 8, but it may be mentioned that by reducing turbine inlet fluctuations, blade vibration problems are greatly eased. A full discussion of the effects of various engine and turbine combinations on blade vibration is given by Kirsten. [36]

5.11 Design of a Single-stage Axial Flow Turbine

The design of a turbocharger turbine depends on the turbocharging system. For

constant pressure operation a high degree of reaction (for example 50 per cent, at the mean blade height) and a well-designed exhaust diffuser give best performance. Pulse turbocharging with three cylinders connected to a turbine entry is also satisfactory with this type of turbine blading.

There is no straightforward design method for pulse turbocharging with partial admission, particularly when individual or pairs of cylinders are connected to a turbine inlet. One approach is to study the effect of typical exhaust pulse shapes on changes in turbine efficiency as the blade speed ratio varies (that is, assuming quasi-steady flow). This procedure may be repeated for turbines having different degrees of reaction, aspect ratio, pitch chord ratio and blade profiles. Some of this information will be available from experimental tests, but much will have to be predicted using the methods outlined. In general, it will be found that a low reaction turbine with a high aspect ratio results in the most efficient energy conversion of pulsating flows, with partial admission.

The design of a single-stage turbine is primarily based on the 'pitch line analysis'. For a nominal mass flow rate and energy transfer, the velocity triangles at the mean blade height are estimated from the momentum equation. The energy and continuity equations, together with the appropriate loss coefficients enable the thermodynamic state of the fluid to be established at the inlet and outlet of rotor and stator. The degree of reaction must be chosen to establish the optimum blade speed ratio at the design point. Consideration must be given to established limitations of gas deflection angles to avoid excessive losses across either row of blades. In addition, the creep stress limitations of the rotor blade material will influence the maximum safe annulus flow area, through its relationship with blade height and rotor speed.

To satisfy radial equilibrium with vortex-type blading, the velocity triangles at the root and tip of the blades must be constructed. At the root section, a check should be made to avoid recompression due to negative reaction.

Cascade data may be used to select a standard blade profile, the optimum number of blades, pitch chord ratio and the correct incidence angles at the design section, root and tip of the stator and rotor blades. The incidence angle must be chosen to minimise drag at design and offdesign conditions: it will depend greatly on the gas deflection angle. A constraint may be placed on the blade exit angle, since this may affect the throat area of the passage between the blades, and hence control mass flow rate. A correction may have to be made to achieve the design mass flow rate, at the penalty of a deviation between desired gas exit angle and the blade exit angle.

The actual cross-sectional profile of the blade is obtained by 'wrapping' the standard aerofoil section around a camber line. The passage between the blades must be checked for convergence to ensure that the throat occurs at the trailing edge on the concave side of the blades. The design sections established at the root, mean and tip are then stacked (on their centres of mass) to enable the blade surfaces to be constructed. In gas turbine design, it is common practice to offset the stacking points, thereby creating a bending force to partially counterbalance gas bending stresses. This technique is undesirable if the gas flow is highly unsteady as it is with pulse turbocharging, since negative transient stresses may be introduced reducing the rotor blade life through fatigue failure.

Cascade data may be used to estimate losses in the rotor and stator blading

and over-all stage performance at the design point followed by detailed quasi-three-dimensional flow analysis, and iteration on blade profile to improve aerodynamic performance. Offdesign performance may be predicted using the data of Ainley and Mathieson. [7]

References

1. H. Cohen, G. F. C. Rogers and H. I. H. Saravanamuttoo, *Gas Turbine Theory* (Longman, 1972)
2. S. L. Dixon, *Fluid Mechanics, thermodynamics of turbomachinery* (Pergamon, 1975)
3. I. H. Johnston and L. R. Knight, Tests on a single-stage turbine comparing the performance of twisted with untwisted rotor blades, *ARC R&M2927* (1953)
4. J. H. Horlock, *Axial Flow Turbines* (Butterworths, 1966)
5. I. H. Johnston and D. E. Smart, An experiment in turbine blade profile design, *ARC CP941* (1967)
6. J. C. Dunavant and J. R. Ermin, Investigation of a related series of turbine blade profiles in cascades, *NACA TN3802* (1956)
7. D. G. Ainley and G. C. R. Mathieson, A method for performance estimation for axial flow turbines, *ARC R&M2974* (1957)
8. O. Zweifel, The spacing of turbomachine blading, especially with large annular deflection, *Brown Boveri Rev.* (December 1945)
9. O. E. Balje and R. L. Binsley, Axial turbine performance evaluation, *ASME J. Engng Power* (October 1968)
10. H. R. M. Craig and H. J. A. Cox, Performance estimation of axial flow turbines, *Proc. Inst. Mech. Engrs,* **185** (1970/71)
11. W. Traupel, *Thermische Turbomaschinen* (Springer-Verlag, 1966)
12. J. D. Denton, A survey and comparison of methods for predicting the profile loss of turbine blades, *Proc. Inst. Mech. Engrs. Conf. Publication 3,* (1973)
13. J. H. Horlock, Boundary layer problems in axial turbomachines, in *Flow Research on Blading* (Elsevier, 1970)
14. N. H. Markov, Calculation of the aerodynamic characteristics of turbine blading, trans. Associated Technical Services (1958)
15. C. R. Soderberg, Unpublished notes, MIT gas turbine laboratory (1949) – see Horlock [4] for details
16. P. M. Came, Secondary loss measurement in a cascade of turbine blades, *Proc. Inst. Mech. Engrs. Conf. Publication 3* (1973)
17. J. Dunham, A review of cascade data on secondary losses in turbines, *J. Mech. Engng. Sci.,* **12** (1970)
18. J. Dunham and P. M. Came, Improvements to the Ainley-Mathieson method of turbine performance prediction, *Trans. ASME, 70-GT-2, J. Engng. Power,* **92** (1970)
19. R. Shaw, Efficiency predictions for axial flow turbines, *Int. J. Mech. Sci.,* **8** (1966)
20. E. Martensen, Calculation of pressure distribution over profiles in cascade in two-dimensional potential flow by means of a fredholm integral equation. *Archs ration. Mech. Analysis,* **3** (1959)
21. D. H. Wilkinson, A numerical solution of the analysis and design problems for flow past one or more aerofoils or cascades, *ARC R&M3545* (1967)

22. T. Katsanis, A computer program for calculating velocities and streamlines on a blade to blade stream surface of a turbomachine, *NASA TN D4525* (1968)
23. J. D. Stanitz, Design of two-dimensional channels with prescribed distributions along the channel walls, *NACA TN 2593-2595* (1952)
24. D. J. L. Smith and D. H. Frost, Calculation of the flow past turbomachine blades, *Proc. Inst. Mech. Engrs.*, **184**, Pt 3G(iii) (1969-70)
25. D. Japikse, Turbocharger turbine design and development, Lecture B2, Turbocharging the Internal Combustion Engine, Fluid Dynamics Institute, Darmouth College, New Hampshire, USA, and Imperial College, London (1979)
26. C. W. Simpson and D. E. Y. Scarlett, Pressure losses in the inlet and outlet casings of axial flow turbines for turbochargers, *Proc. Inst. Mech. Engrs.*, **182**, Pt.3d, (1967/8)
27. P. Suter and W. Traupel, Untersuchungen über den ventilationsverbrauch von turbinenrädern. Report No. 4, Institute for Thermal Machines, Zurich, English Translation BSRA No. 917 (1959)
28. H. R. M. Craig *et al.*, An investigation of steady and unsteady flow through a Napier turboblower turbine under conditions of full and partial admission, *Proc. Inst. Mech. Engrs.* **183**, Pt.1 (1968/9)
29. G. Dibelius, Turbocharger turbines under conditions of partial admission, *Brown Boveri Rev.*, **52**, No. 3 (1965)
30 H. Daneshyer *et al.*, A comparison of the performance of three model axial flow turbines tested under both steady and pulse flow conditions, *Proc. Inst. Mech. Engrs.* **184**, Pt.1 (1969/70)
31. H. R. M. Craig and M. S. Janota, The potential of turbochargers as applied to highly rated 2-stroke and 4-stroke engines, *Proc. CIMAC,* paper B.14 (1965)
32. R. E. Dundas, Design of the gas turbine, *Sawyer's Gas Turbine Engineering Handbook,* 2nd ed. (Gas Turbine Publications, 1972)
33. H. D. Emmert, Current design practices for gas turbine power elements, *Trans. ASME,* **72**, No.2 (1950)
34. H. Gisiger, Turbine blade failures in the turbocharger of a locomotive engine, *Sulzer Tech. Rev.,* **45**, Research No. (1963)
35. E. K. Brock and D. E. Y. Scarlett, Prediction of diesel engine performance, *DEUA publication 319* (1968)
36. W. Kirsten, Influence of exhaust manifold arrangements on blade vibrations in turbocharger turbines, *Brown Boveri Rev.*, **58**, No. 415 (1971)

6

Constant Pressure Turbocharging

6.1 Introduction

The basic objective of turbocharging is simply stated: to supercharge the engine using the energy of the exhaust gases to drive a compressor via a turbine. A considerable fraction of the energy released by combustion of the fuel/air mixture in any engine is lost through the exhaust system (30 to 40 per cent). In the design of a turbocharging system it is of the utmost importance to utilise the exhaust gas energy leaving the engine and arriving at the turbocharger turbine to full advantage. Two principal systems have been briefly introduced in chapter 1. In this chapter the constant pressure (or 'single-pipe') system will be considered in detail, together with a discussion of its application to two-stroke and four-stroke engines designed for various duties.

6.2 The Energy Available in the Exhaust System

Figure 6.1 shows the ideal limited pressure engine cycle in terms of a pressure/volume diagram (not specific volume) for the naturally aspirated engine. Superimposed is a line representing isentropic expansion from point 5, at which the exhaust valve opens, down to the ambient pressure (P_a) which could be obtained by further expansion if the piston were allowed to move to point 6. The maximum theoretical energy that could be extracted from the exhaust system (the so called 'blow-down' energy) is represented by the shaded area 1-5-6.

Considering now the supercharged engine, the ideal four-stroke pressure/volume diagram would appear as shown in figure 6.2, where P_1 is the supercharging pressure and P_7 the engine back pressure (in the exhaust manifold). Process 12-1 is the induction stroke, during which fresh charge at the compressor delivery pressure enters the cylinder. Process 5-1-13-11 represents the exhaust process. When the exhaust valve first opens (point 5) some of the gas in the cylinder escapes to the exhaust manifold expanding along line 5-7 if the expansion is isentropic. Emptying of the cylinder causes the pressure of the remaining gas in the cylinder to fall down the line 5-13. The piston then moves during the expulsion stroke, 13-11, displacing the cylinder contents through the

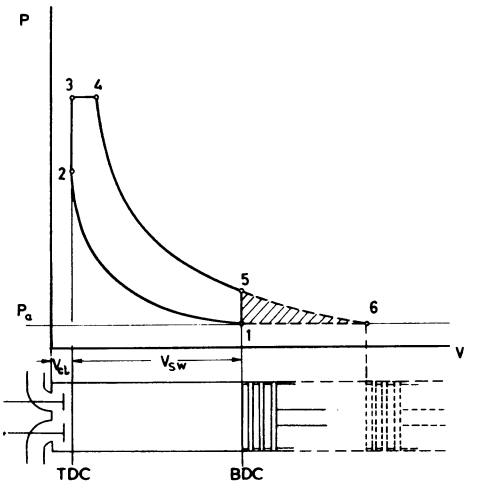

Figure 6.1 *Ideal limited pressure cycle, naturally aspirated*

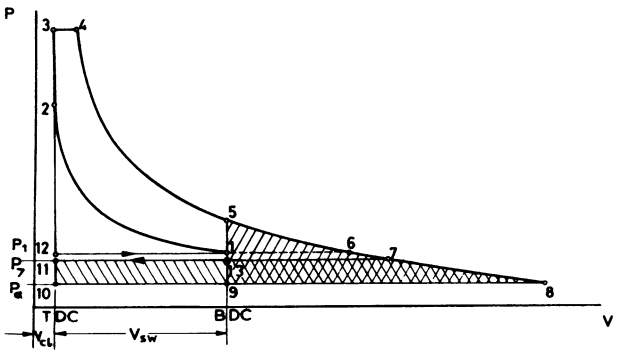

Figure 6.2 *Supercharged ideal limited pressure cycle, four-stroke engine*

exhaust valve into the exhaust pipe against the back pressure P_7. At the end of the exhaust stroke the cylinder retains a volume (V_{cl}) of residual combustion products, which for simplicity can be assumed to remain there. The maximum possible energy that could be extracted during the expulsion stroke will be represented by the area 7-8-10-11, where 7-8 represents isentropic expansion down to the ambient pressure.

There are two distinct areas in figure 6.2 representing energy available from the exhaust gas, the blow-down energy (area 5-8-9) and the work done by the piston (area 13-9-10-11). The maximum possible energy available to drive a turbocharger turbine will clearly be the sum of these two areas. Although the energy associated with one area is easier to harness than the other, it is difficult to devise a system that will harness all the energy. To achieve that, the turbine inlet pressure must rise instantaneously to P_5 when the exhaust valve opens,

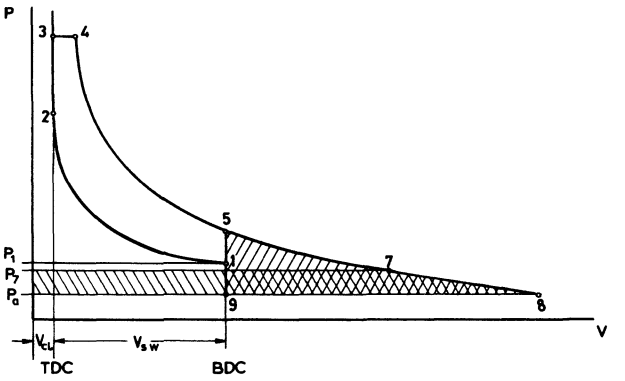

Figure 6.3 *Supercharged ideal limited pressure cycle, two-stroke engine*

followed by isentropic expansion of the exhaust gas through P_7 to the ambient pressure ($P_8 = P_a$). During the displacement part of the exhaust process (expulsion stroke) the turbine inlet pressure must be held at P_7. Such a series of processes is impracticable.

Consider the simpler process in which a large chamber is fitted between the engine and the turbine inlet, in order to damp down the pulsating exhaust gas flow. By forming a restriction to flow, the turbine may maintain its inlet pressure at P_7 for the whole cycle. The available work at the turbine will then be given by area 7-8-10-11. This is the ideal constant pressure system. Next consider an alternative system, in which a turbine wheel is placed directly downstream of the engine close to the exhaust valve. If there were no losses in the port, the gas would expand directly out through the turbine along line 5-6-7-8, assuming isentropic expansion. If the turbine area were sufficiently large, both cylinder and turbine inlet pressures would drop to P_9 before the piston had moved significantly up the bore. Hence the available energy at the turbine would be given by area 5-8-9. This can be considered the ideal pulse system. The systems commonly used and referred to as 'constant pressure' and 'pulse' are based on the above principles but in practice they differ from these ideals.

Although the diagrams illustrating the energy available at the turbine are based on the four-stroke engine cycle, similar diagrams can be constructed for a two-stroke engine. Apart from the change in valve or port timing, the work done by the piston is replaced by the energy transferred from the compressor to the scavenge air (see figure 6.3). For clarity, scavenge in the overlap period in the case of the four-stroke engine has been ignored, although the four-stroke engine might pass a significant quantity of scavenge air when turbocharged.

6.3 Constant Pressure Turbocharging

With constant pressure turbocharging, the exhaust ports from all cylinders will be connected to a single exhaust manifold, whose volume will be sufficiently large to damp down the unsteady flow entering from each cylinder in turn. Only

one turbocharger need be used, with a single entry, but in some cases more than one are fitted so that a reasonable boost pressure is maintained in the event of one turbocharger failing. When the exhaust valve of a cylinder opens, the gas expands down to the (constant) pressure in the exhaust manifold without doing useful work. However, not all of the 'pulse' energy is lost. From the law of conservation of energy, the only energy actually lost between cylinder and turbine will be due to heat transfer. With a well-insulated manifold, this loss will be very small and can be neglected. Consider what happens to the gas leaving the cylinder, expanding down into the exhaust manifold, then flowing through the turbine. The process is shown on the enthalpy/entropy diagram (figure 6.4). (If the gas is considered 'perfect' then the enthalpy/entropy diagram can be regarded as a

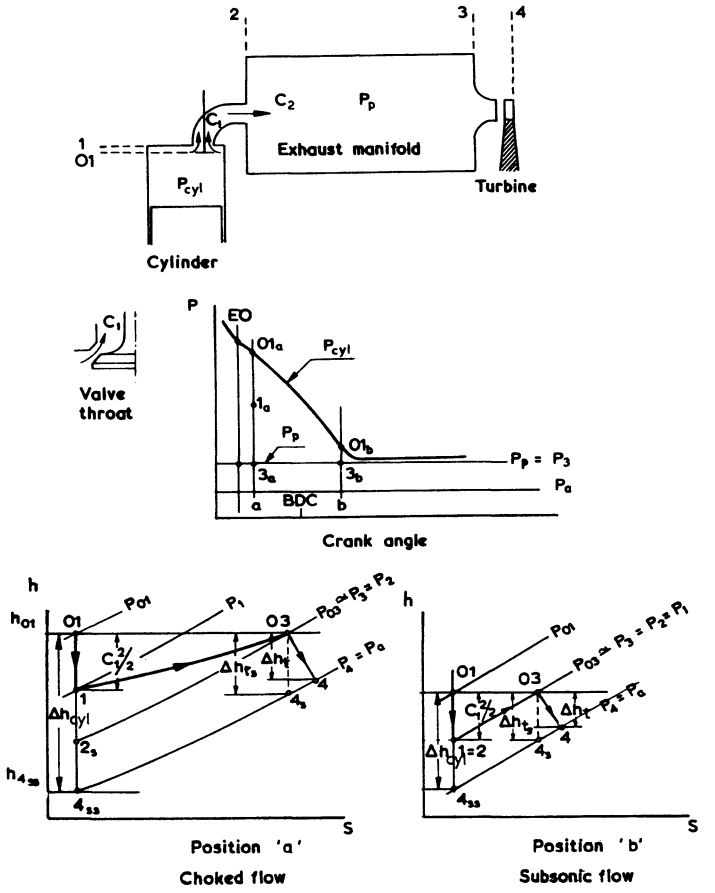

Figure 6.4 *Constant pressure turbocharging: large exhaust manifold volume.* Δh_t *= enthalpy change across turbine;* Δh_{t_s} *= isentropic enthalpy change across turbine expansion ratio;* Δh_{cyl} *= enthalpy available when exhaust valve opens;* $h_{4\,ss}$ *= enthalpy after isentropic expansion from 01 to turbine exit pressure (atmospheric)*

temperature/entropy diagram.) At the moment of exhaust valve opening, the cylinder pressure P_{cyl} will be much higher than the exhaust manifold pressure P_p. Considering first the crank position 'a' on the pressure/crank angle diagram. Point 01_a denotes stagnation conditions in the cylinder and h_{01_a} is the stagnation enthalpy of the gas in the cylinder. P_p ($=P_3$) is the pressure in the exhaust manifold and P_4 is the pressure at turbine exit, normally equal to the atmospheric pressure P_a.

During the early stages of valve opening (when the effective throat area of the valve is very small) the pressure ratio across the valve or port will be above the choked value. Hence the gas flow will accelerate to sonic velocity C_1 in the throat (process 01-1 on the enthalpy/entropy diagram) followed by a shock wave at the valve throat and sudden expansion to the exhaust manifold pressure P_p (process 1-03). Due to turbulent mixing and throttling, no pressure recovery occurs. The stagnation enthalpy remains unchanged and hence the flow from valve to the turbine is shown by line 1-03 and is accompanied by an entropy increase.

As the valve continues to open, the cylinder pressure will fall and flow through the valve becomes subsonic as indicated by point 'b' on the pressure/crank angle diagram. In this case the flow will accelerate to value $C_1 = C_2$ (process 01-1) in the exhaust valve throat expanding to pressure P_3 in the exhaust manifold. Finally, work is done in the turbine along line 03-4. The energy available for doing useful work in the turbine is given by $h_{03} - h_{4_s} = \Delta h_{t_s}$ and is converted to $h_{03} - h_4 = \Delta h_t$ in the turbine, whereas the energy available from the cylinder is $h_{01} - h_{4_{ss}} = \Delta h_{cyl}$. Clearly it is the lack of recovery of the kinetic energy leaving the valve throat and the throttling losses which lead to poor exhaust gas energy utilisation with the constant pressure system.

Since the stagnation temperature of the gas in the exhaust manifold (T_{03}) remains equal to the cylinder release value (T_{01}), the actual volume of the gas at turbine inlet, exceeds the value that would result from isentropic expansion to point 7 (figures 6.2 and 6.3). Thus not all the pulse energy is lost, some of it is recovered in the form of a higher inlet temperature at the turbine.

Typically, a constant pressure exhaust manifold will consist of a large diameter pipe running along the exhaust side of an engine, with each exhaust port connected to it via a short pipe. A single turbocharger mounted at one end, or possibly over the centre, would commonly be used. If two are used, one would probably be mounted at each end. On a vee engine, the large bore manifold will usually lie between the banks with the inlet valves arranged to be on the outside.

The volume of the exhaust manifold should be sufficient to damp pressure pulsations down to a low level. Thus the volume required will depend on cylinder release pressure (point 5, figures 6.2, 6.3) and frequency of the exhaust gas pulsations coming from each cylinder in turn. Pulse amplitude will be a function of engine loading (BMEP or boost pressure), the timing at which the exhaust valve opens, turbine area and exhaust manifold volume. Frequency will be dependent on the number of cylinders. The effect of engine speed will be less significant since the duration of the exhaust process from each cylinder will be relatively constant in terms of crank angle, rather than time, and a suitable turbine area will be chosen at the operating speed and load. Thus it is inappropriate to give a general rule that the manifold volume should be x times the total swept volume of the engine. Clearly x will be larger on an engine with few

cylinders than on an engine with many cylinders, and its value will be some compromise between an acceptable total volume for installation and the volume required to damp out the pulses. For guidance however, it can be stated that the volume would normally be in the range of 1.4 to 6 times the total swept volume of the engine.

If the exhaust manifold volume is not sufficiently large, the 'blow-down' or first part of the exhaust pulse from a cylinder will raise the general pressure in the manifold. If the engine has more than three cylinders, it is inevitable that at the moment when the blow-down pulse from one cylinder arrives in the manifold, another cylinder is nearing the end of its exhaust process. The pressure in the latter cylinder will be low, hence any increase in exhaust manifold pressure will impede its exhaust process. This will be particularly important where the cylinder has both inlet and exhaust valves partially open (valve overlap) and is relying on a through-flow of air for scavenging of the burnt combustion products. A rise in exhaust manifold pressure at this time is virtually inevitable in an engine with more than three cylinders, unless the volume is large. This will be particularly important on a two-stroke engine, since if the exhaust pressure exceeds inlet pressure during scavenging, the engine cannot run at all.

Any heat lost from the exhaust manifold will result in reduced energy available at the turbocharger turbine, therefore it is sensible to insulate the manifold. When the large surface area of the manifold is considered, it is not surprising that such insulation can significantly increase the boost delivered by the turbocharger compressor.

It may already be clear that the constant pressure system has some advantages and disadvantages over the pulse system. These will be considered in detail after the pulse system is fully described but some points are relevant here. Firstly, virtually by definition, conditions at the turbine entry are steady with time. Thus all the losses in the turbine that result from unsteady flow are absent. Furthermore, a single-entry turbine may be used, eliminating 'end-of-sector losses'. Thirdly, since a single turbocharger can be used on all multi-cylinder engines (many of which might otherwise require two or more), it will be a large unit. Due to the difficulties of maintaining close tolerances and small clearances in small machines, larger machines have lower leakage losses and hence have higher efficiency. All of the above result in a high average turbine efficiency under constant pressure operation, even though the inlet pressure may not strictly be absolutely constant. [1] Furthermore, if the turbine is specifically designed for constant pressure operation it may have a high degree of reaction (for example, 50 per cent) which, coupled with an exhaust diffuser, brings additional gains in efficiency.

From a purely practical point of view, the exhaust manifold is simple to construct although it may be rather bulky, particularly relative to small engines with few cylinders. However, for large engines with many cylinders (for example, V16), the convenience of being able to join all cylinders to a common exhaust manifold with a single turbocharger on top, alongside or at either end of the engine, is useful. A major disadvantage of the constant pressure system arises when the engine load is suddenly increased or a rapid engine speed increase is required. The pressure in the large volume is slow to rise, hence the energy available at the turbine increases only gradually. Turbocharger, and therefore

engine response will be poor. This subject is discussed in detail in chapter 12, but it is clear that the poor response of the constant pressure turbocharging system restricts it from consideration for applications when frequent load (or speed) changes are required.

The turbocharging system will affect the engine through three parameters only: the boost pressure and temperature in the inlet manifold and the pressure in the exhaust manifold. Hence it is these three factors that must be examined when considering a turbocharging system. The effect of the first two is obvious. The objective of turbocharging is to increase the pressure in the inlet manifold in order to trap a greater mass of fresh air in the cylinder when the inlet valve closes. This is partially offset by any increase in temperature, but enables more fuel to be burnt and power output to rise. The importance of the exhaust manifold pressure depends on whether the turbocharged engine is a four-stroke or a two-stroke. The subject will be discussed in detail later, but it is useful to consider, when comparing turbocharging systems, that several arrangements might enable a certain boost pressure to be developed. The merits of the different systems can then be compared by considering the exhaust manifold pressure developed and its effect on engine performance.

By considering the energy balance for the turbocharger when running with a constant exhaust pressure, it is simple to derive a relationship between the exhaust manifold pressure (P_p) and the boost pressure (P_m). The power required to drive the compressor may be expressed as

$$\dot{W}_c = \dot{m}_a \, c_{pa} \, T_a \, [(P_m/P_a)^{(\gamma_{a-1})/\gamma_a} - 1] / \eta_c$$

The power developed by the turbine is

$$\dot{W}_t = \dot{m}_e \, c_{pe} \, T_p \, [1 - (P_a/P_p)^{(\gamma_{e-1})/\gamma_e}] \, \eta_t$$

Since $\dot{m}_e = \dot{m}_a + \dot{m}_f$ or $\dot{m}_e/\dot{m}_a = 1 + 1/AFR$ and the energy balance for the turbocharger is

$$\dot{W}_c = \dot{W}_t \times \eta_{mech}$$

then

$$c_{pa} \, T_a [(P_m/P_a)^{(\gamma_{a-1})/\gamma_a} - 1] / \eta_c = \eta_{mech} \, \eta_t \, (1 + 1/AFR) \, C_{pe} \, T_p \times [1 - (P_a/P_p)^{(\gamma_{e-1})/\gamma_e}]$$

or

$$[(P_m/P_a)^{(\gamma_{a-1})/\gamma_a} - 1] = [1 - (P_a/P_p)^{(\gamma_{e-1})/\gamma_e}] \, \eta \times (1 + 1/AFR) \, (c_{pe}/c_{pa}) \, (T_p/T_a) \qquad (6.1)$$

where $\eta = \eta_{mech} \, \eta_t \, \eta_c$

Thus the relationship between the inlet manifold pressure (P_m) and exhaust manifold pressure (P_p) is a function of the over-all turbocharger efficiency (η), the turbine inlet temperature (T_p) and, to a lesser extent, the air/fuel ratio (AFR).

The air/fuel ratio at full load will be governed by the onset of black smoke in the exhaust. The turbine inlet temperature will also be dependant on air/fuel ratio, the amount of cool scavenge air passing through the cylinders and heat loss from the exhaust manifold. It will also be controlled by the timing of exhaust valve opening, although naturally this will be optimised for engine, rather than turbine considerations (clearly by advancing the valve opening point, the energy available at the turbine will increase; however, the effective expansion stroke of the engine is reduced hence power output and efficiency can suffer). Thus it is largely the over-all turbocharger efficiency that governs the relationship between exhaust and inlet manifold pressures, particularly on four-stroke engines with little scavenge air.

Equation 6.1 was plotted, for a compressor pressure ratio of 2, in figure 1.9, showing the dominant effects of turbocharger efficiency and turbine inlet temperature on the pressure ratio between inlet and exhaust manifolds. It is important to realise that if the turbine inlet temperature is held constant (for metallurgical reasons), then higher turbocharger efficiencies are required to maintain a favourable scavenge pressure ratio (inlet manifold to exhaust pipe) at higher boost pressures.

Although the turbocharger efficiency (and air/fuel ratio, through the turbine inlet temperature) governs the relationship between exhaust and inlet pressures, it is the turbine area that controls the exhaust pressure itself, since it acts as a restricting orifice (the situation is less simple on a two-stroke engine). By fitting smaller and smaller turbines to a four-stroke engine it is theoretically possible to develop very high exhaust pressures and correspondingly high levels of energy available at the turbine. This should allow very high boost pressures to be obtained (subject to the relationship described above). Although the argument is sound when considering reasonable pressure ratios, the practical effects of turbine speed and inlet temperature limitations combined with decreasing turbocharger efficiency at high pressure ratios and poor engine scavenging, prevent very high pressure ratios being developed in practice. Thus it is the turbine area that principally decides the exhaust manifold pressure, and the air/fuel ratio and turbocharger efficiency that fix the relationship between inlet and exhaust pressure at the cylinders.

The choice of boost pressure for a specific engine, although developed by the turbocharger, will be limited by constraints imposed by engine design. For example, the engine will be designed to sustain a certain maximum cylinder pressure, to survive a certain level of thermal loading, etc. Thus the engine designer will have some clear idea of the boost pressure required, and the turbine area will be matched to provide it. Thus, when comparing different turbocharging systems it is convenient to compare their performance at a specified boost pressure.

With constant pressure turbocharging, the amount of scavenge air that passes through the cylinder (expelling exhaust residuals out of the clearance space) is directly governed by the pressure drop between inlet and exhaust manifold and the valve overlap period if the engine is a four-stroke. A two-stroke engine is not self-aspirating and hence this pressure drop is the only factor that expels the exhaust gas and charges the cylinder with fresh air. This difference has major implications concerning the turbocharging system. Therefore the application of

the constant pressure system to two and four-stroke engines will be discussed separately.

6.4 Four-stroke Engines with Constant Pressure Turbocharging

Four-stroke engines are self-aspirating. They have a discrete intake and exhaust stroke. Virtually regardless of the pressure in the exhaust manifold, piston motion during the exhaust stroke will displace most of the gas, thus a four-stroke engine will run with a high 'back-pressure'. However, the situation is undesirable for three reasons. Firstly, work is done by the piston in expelling exhaust gas, resulting in less useful engine power output and lower efficiency. Secondly, if the exhaust pressure exceeds the inlet pressure, a considerable quantity of residual gas will be left in the cylinder, reducing the volume and purity of fresh air drawn in during the next intake stroke. Thirdly, some blow-back of combustion products (residual gas) into the intake manifold may occur during valve overlap, resulting in an undesirable build-up of carbon particles. Clearly it is desirable to avoid developing an exhaust manifold pressure greater than that in the inlet manifold (compressor delivery).

Since naturally aspirated engines run with virtually equal inlet and exhaust pressures, no significant scavenging of the residual gas takes place. When turbocharging, advantage can be taken of the potential difference in manifold pressures to generate a scavenge air throughput to clear the cylinder of residual combustion products. Thus a pressure drop between intake and exhaust is desirable during the period of valve overlap. The magnitude of the pressure drop required to achieve good scavenging without an excessive and wasteful through-flow of air, will be dependent on the amount of valve overlap used on the engine. Valve timing will itself depend on the primary application of the engine, since an engine with large valve overlap will not run well over a wide speed range.

Consider the idealised intake and exhaust process shown in figure 6.5. During the intake process (0–1) the pressure on the piston crown (the boost pressure P_1) exceeds the crankcase pressure on the underside (ambient pressure P_a). Hence

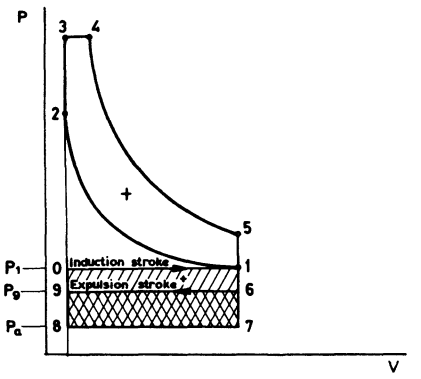

Figure 6.5 *Ideal intake and exhaust process: four-stroke engine*

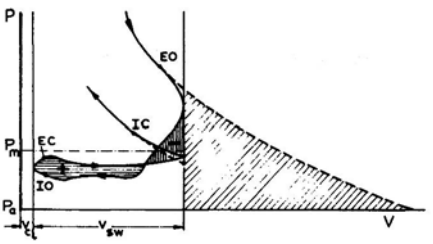

Figure 6.6 *Real gas exchange process: four-stroke engine [3]*

useful work will be done by the compressed fresh air on the piston (denoted by the area 0-1-7-8). During the exhaust stroke (the displacement 6-9), gas pressure on the piston crown (P_9) again exceeds crankcase pressure (P_a) but the piston motion opposes the resultant force, hence the piston is doing work on the exhaust gas. The net gain or loss (gain in this case) of useful work during this 'gas exchange' process will be given by the area 1-6-9-0. This work benefit is only gained at the expense of compressor work, although that is desirable since it in turn is derived from exhaust gas energy which is normally wasted. This is one reason why a turbocharged engine may be more efficient than a naturally aspirated engine. In practice the 'gas exchange' process will be far from the ideal shown in figure 6.5, due to many factors. The resulting diagram will appear like that of figure 6.6. where IO, IC, EO and EC denote the points at which the inlet and exhaust valves start opening and finish closing. The net gas exchange or 'pumping' work will be the total of positive work minus negative work between the moment of exhaust opening and inlet closing.

It can be argued that the merit of a turbocharging system can be measured, on a comparative basis, by the net work done during the gas exchange period for a specified boost pressure (see for example, Meier [2]). Although not an exact method of comparison (since, for example, optimum valve timing might be different with different turbocharger arrangements) it is a useful parameter. Ryti and Meier [3] have evaluated the contribution of the gas exchange work (in terms of the parameter $\Delta P_{ge}/P_m$ where ΔP_{ge} = gas exchange work/swept volume) for a typical industrial four-stroke engine turbocharged by the constant pressure system. Figure 6.7 shows this parameter and its variation with boost pressure ratio P_m/P_a for a range of over-all turbocharger efficiencies (based on thermodynamic calculation). Also shown are the air delivery ratio (ADR), volumetric efficiency (η_{vol}) and mean turbine inlet temperature (T_t). The volumetric efficiency is based on inlet manifold conditions and may be defined as

$$\eta_{vol} = m_c/V_{sw}\rho_m \tag{6.2}$$

where m_c is the mass of fresh air trapped in the cylinder per cycle. Clearly η_{vol} can be slightly greater than unity if fresh charge scavenges residual combustion products from the clearance volume. The air delivery ratio is defined as

$$ADR = m_{tot}/V_{sw}\rho_m \tag{6.3}$$

where m_{tot} includes scavenge air passing through the cylinders. It is an approximate measure of how much scavenge air passes through the cylinder ($ADR > 1$).

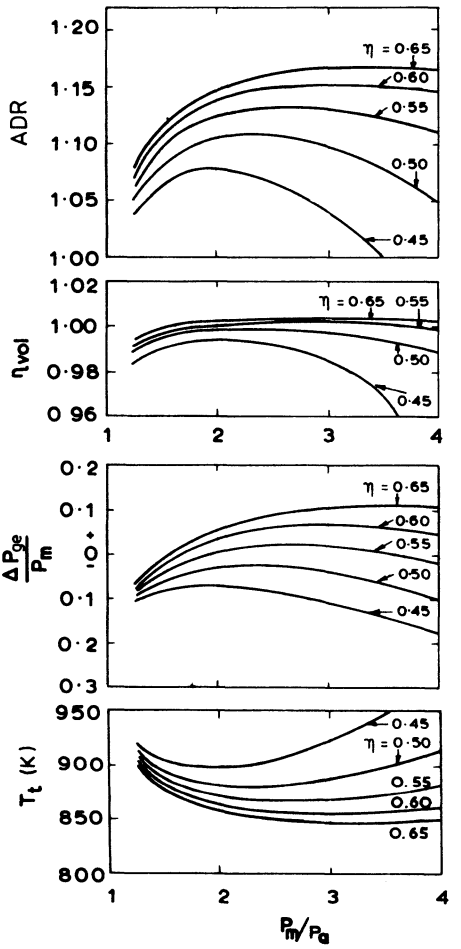

Figure 6.7 *Parameters affecting the gas exchange process on a four-stroke engine, with constant pressure turbocharging [3]*

The data shown refers to full-load conditions only and has been extended to include high pressure ratio (4:1). Valve overlap is 100°. Consider first the graphs of air delivery ratio and volumetric efficiency. If the air delivery ratio falls below 1.1 then the volumetric efficiency (that is, effectiveness in trapping fresh air in the cylinders) decreases. Little benefit is obtained by increasing *ADR* beyond 1.15 because some of the fresh charge is probably blown through into the exhaust manifold. Hence an air delivery ratio between these limits is ideal, with the valve timing used on this engine. Consider next the effect of turbocharger efficiency on all four curves. It is clear that the effect of over-all turbocharger efficiency becomes substantially more important as the boost pressure is raised. For low pressure ratios, a high turbocharger efficiency certainly reduces the pumping work (possibly changing from a loss to a gain) and is therefore beneficial, but

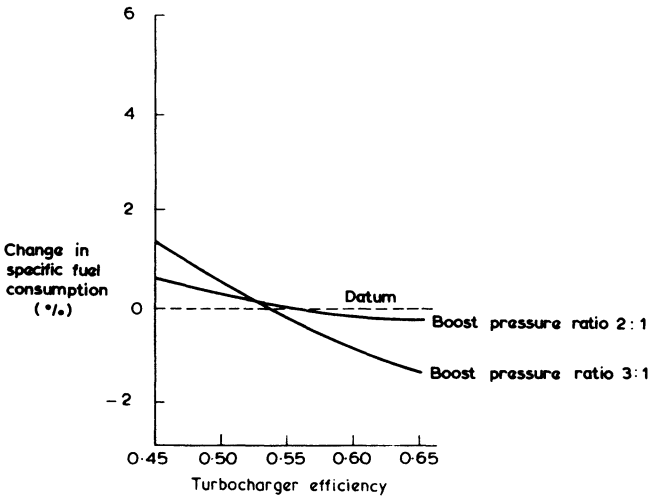

Figure 6.8 *Effect of turbocharger efficiency on specific fuel consumption [3]*

not critical. If the pressure ratio required is high, turbocharger efficiency becomes critically important.

The gas exchange work parameter directly affects specific fuel consumption and changes in one are reflected in changes in the other. Thus the effect of turbocharger efficiency on specific fuel consumption can be extracted from figure 6.7. The result (for two pressure ratios) is shown in figure 6.8 as a gain or loss in specific fuel consumption relative to an arbitrary datum.

The present discussion of constant pressure turbocharging has related only to full engine load and speed. However, engines for most applications are required to operate at part load for much of the time. The engine is controlled through its fuel injection system, hence under part load conditions the *volume* of fresh air drawn into the cylinder will not change significantly, but the quantity of fuel injected will. The governor, if used, will adjust the quantity of fuel injected to maintain the speed required. Thus the principle change will be to the air/fuel ratio and hence, as far as the turbocharger is concerned, the exhaust temperature. The lower exhaust temperature is equivalent to reduced energy arriving at the turbine hence turbine and therefore compressor work drops. The boost pressure is therefore lower resulting in a reduced *mass* of fresh charge being drawn in to the cylinder. Hence the boost pressure, mass flow rate and turbine inlet temperature all fall. The fall in boost pressure will not create any problems unless the exhaust pressure has not dropped by a comparable amount.

Consider again the energy balance for the turbocharger (equation 6.1). At low loads, the turbine inlet temperature ($T_t = T_p$) will drop and, since the mass flow rate and pressure ratios will also have fallen: the turbocharger is probably operating away from the design point condition on the turbine and compressor characteristics. Figure 6.9 shows the pressure drop between inlet and exhaust manifold ($\Delta P_{cyl} = P_m - P_p$), for several values of turbine inlet temperature. This must be combined with the effect of a low turbocharger efficiency (figure

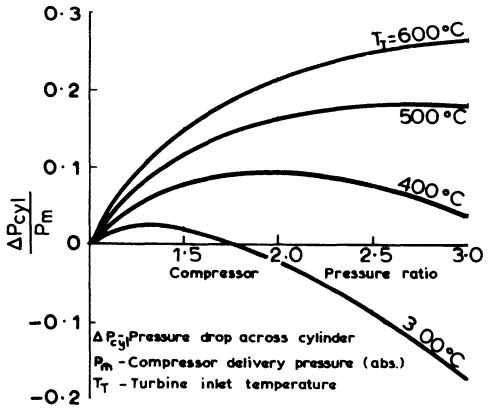

Figure 6.9 *Relationship between compressor pressure ratio and* $\Delta P_{cyl}/P_m$ *for a turbocharger over-all efficiency of 60 per cent, with variable turbine inlet temperature*

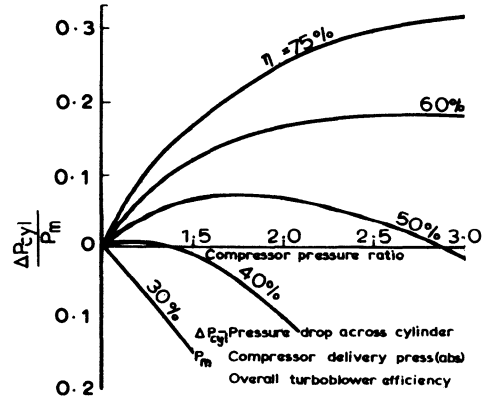

Figure 6.10 *Relationship between compressor pressure ratio and* $\Delta P_{cyl}/P_m$ *for a turbine inlet temperature of 500 °C, with variable turbocharger efficiency*

6.10). Clearly, at part load engine operation the pressure drop between inlet and exhaust will deteriorate and will eventually become negative. Scavenging will be impaired, the gas exchange work will become a loss and hence power output and efficiency will fall. Thus the constant pressure system is not ideal for part load operation.

Similar conditions apply at high-load but low-speed operation of the engine (automotive applications). The turbine area is too large at these conditions, leading to a small compressor pressure rise and low compressor efficiency. However, the situation is not as serious as that at part load, since the air/fuel ratio and hence turbine inlet temperature remains high.

6.5 Two-stroke Engines with Constant Pressure Turbocharging

The two-stroke engine is neither self-aspirating nor self-exhausting. It relies on a positive pressure drop between the inlet and exhaust manifolds in order to run at all. The scavenging process, in which fresh charge is forced in and residual gas forced out, is the key to a successful two-stroke engine. It follows that the two-stroke engine is far more dependent on a reasonable pressure drop being developed across the cylinder than is the case with the four-stroke engine. The four-stroke engine can work with an adverse pressure gradient, the two-stroke will not.

Several different scavenging systems have been developed for two-stroke engines. Those in common use are the cross, loop and uniflow scavenging systems. The last may use inlet ports with exhaust valves in the cylinder head or inlet and exhaust ports with opposed pistons. The systems are illustrated in figure 6.11 with typical corresponding scavenge efficiencies, but it is outside the scope of this text to discuss them in detail. The scavenge efficiency may be defined as the mass of fresh air retained in the cylinder divided by the mass of air required to fill the cylinder volume at manifold density. Scavenge ratio is the total mass of air supplied (including scavenge air) divided by the mass of air required to fill the cylinder volume at inlet manifold density. Generally the uniflow system will be better at using the fresh inlet charge to sweep out all the residual combustion products, but no system is perfect, since there is inevitably some mixing of a fresh charge and burnt products.

To obtain reasonable scavenging however, it is essential to pass some air right through the system and to waste. The amount of 'excess air' required will depend

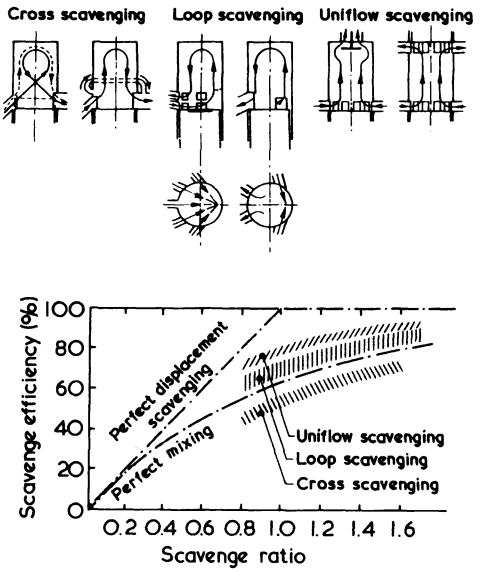

Figure 6.11 *Two-stroke scavenging systems [4]*

on the scavenging efficiency of the system being used and many other factors. It is therefore impossible to quote general rules, but the amount will vary from 10 to about 40 per cent (uniflow to cross-scavenging). The consequence to the turbocharger is two-fold. Firstly, the gas in the exhaust manifold will be diluted with cool scavenge air, lowering the turbine inlet temperature. Secondly, a penalty must be paid for compressing the excess air since, although it will be expanded through the turbine in due course, only part of the energy expanded will be regained, due to compressor and turbine inefficiencies. Thus the turbocharger will have a more difficult job than on a four-stroke engine, since it *must* provide a positive pressure drop across the cylinder, and is required to work under the adverse conditions mentioned above. It was for these reasons that many turbocharged two-stroke diesel engines first appeared with some form of mechanically driven compressor assistance, and many now operating on the constant pressure system still retain the principle.

The general equation for the energy balance of a turbocharger under constant pressure operation (equation 6.1) and the curves that result (figures 6.9 and 6.10) are just as valid for the two-stroke engine and the four-stroke, but the exhaust temperature will be lower with the former. Typical values of mean turbine inlet temperature on highly rated two-stroke and four-stroke engines at full load might be 400 and 500 °C respectively. Figure 6.12 shows the relationship of pressure drop (inlet to exhaust) to pressure ratio for a turbine inlet temperature of 400 °C. Comparison of figures 6.12 and 6.10, which may be assumed to represent two-stroke and four-stroke operation respectively, shows that at full load, the four-stroke engine will perform adequately if the turbocharger efficiency is 50 per cent or more, while the two-stroke engine will require a turbocharger efficiency approaching 60 per cent. A large well-designed turbocharger can develop 60 to 65 per cent over-all efficiency, but some allowance must be made for a reduction in efficiency in service (due to fouling, the build-up of dirt and

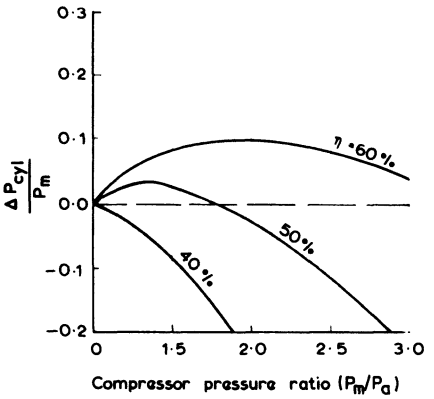

Figure 6.12 *Relationship between compressor pressure ratio and* $\Delta P_{cyl}/P_m$ *for a turbine inlet temperature of 400 °C, for variable turbocharger efficiency*

carbon). Usually an allowance of 5 per cent will be reasonable, with good maintenance. In practice this means that a well-designed engine having a good scavenging system, with little pressure loss, will run satisfactorily at full load provided that it has a well-matched efficient turbocharger. Large slow-speed engines are in this category at present but no small higher-speed two-stroke engine can run with a constant pressure turbocharging system without some other aid to scavenging. This is due to the lower efficiency of very small turbochargers and the high pressure losses in the scavenge ports and valves of a high-speed engine.

At part load, the turbine inlet temperature will fall due to the lower air/fuel ratio. Turbocharger efficiency will probably also fall, since the turbocharger would usually be matched for optimum working conditions near full load (although this depends on engine duty). It is obvious from figures 6.10 and 6.12 that if the turbocharger inlet temperature drops below 300 °C and the turbine efficiency below 55 per cent, then the engine will stop. Thus all two-stroke engines using the constant pressure turbocharging system require some additional aid for scavenging, for starting and at part load operation. This is a major disadvantage of the constant pressure system. As turbocharger manufacturers have improved the efficiencies of their machines and engine manufacturers have improved the design of their components, enabling the engine to withstand high pressures and temperatures, so the constant pressure system becomes more attractive. If a high turbocharger efficiency is available, the pressure drop obtained across the cylinder becomes increasingly favourable as the compressor pressure ratio increases (figure 6.10, $\eta = 75$ per cent). Thus the constant pressure system is used on several highly rated modern two-stroke engines that are not required to work over a wide load (or speed) range.

An important exception to the above occurs in the case of a gas, rather than diesel, engine. The gas engine operates at a richer air/fuel ratio and a lower compression ratio (to avoid 'knock' as in a spark-ignition petrol engine). In consequence a greater proportion of energy is rejected to the exhaust system and the turbine inlet temperature is significantly higher. Many constant pressure turbocharged natural gas engines are running (particularly in the United States) with turbochargers alone, once the load has increased to above about half full-load. Land [5] has described the development of such an engine.

Having established that a constant pressure turbocharged two-stroke diesel engine will require some aid for scavenging, there are several potential arrangements. Aid could be provided by a rotary compressor, a simple fan or a reciprocating pump, connected either in series or parallel with the turbocharger compressor. For clarity, the scavenging aid will be referred to as a scavenging pump and the turbocharger compressor as simply the compressor. Consider first the series system. The scavenge pump can be placed either before or after the compressor. If the scavenge pump is placed before the compressor, then air flow through the pump will be governed by its speed and possibly its pressure ratio (depending on the type of pump). This concept can, however, result in an excessively large scavenge pump being required. Furthermore, the air flow through the engine will virtually be fixed by the speed of the scavenge pump alone, and will not increase with load. Clearly this is a pointless arrangement if pump and engine are constrained to run at the same speed. A more sensible variation of this system is to use an electrically driven fan for the first stage of

compression, since its speed may be controlled independently of the engine, and it may be turned off when the turbocharger provides sufficient boost on its own.

Some engines use a mechanically driven reciprocating scavenge pump (from the crankshaft) as a second stage of compression following the turbocharger compressor. [4] A similar arrangement is to use the underside of the piston as a reciprocating scavenge pump – a relatively simple arrangement on a cross-head engine. With this system the air flow through the engine is governed by engine speed (that is, the speed of the pump) and engine load, since at high loads the turbocharger will raise the density of the air entering the scavenge pump. With all types of reciprocating scavenge pump, the unsteady nature of the flow can create surge problems in the centrifugal turbocharger compressor. An adequate margin between the average mass flow rate at the operating condition and surge must be maintained. A reasonably large receiver between compressor and pump will help.

Some small two-stroke engines use Roots or screw (Lysholm) compressors as a scavenge pump, driven direct from the crankshaft. The Roots blower usually has a rather low efficiency (typically 55 to 65 per cent), peak efficiency occurring at a very low pressure ratio (figure 6.13) due to air leaking (and recirculating) between the rotors and wall. A particular disadvantage of the Roots compressor is its noise. Screw-type compressors are quieter and more efficient. Furthermore

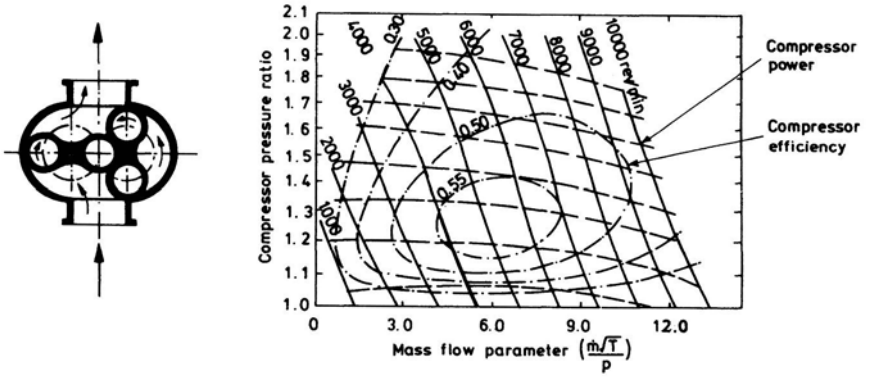

Figure 6.13 *Typical Roots compressor performance*

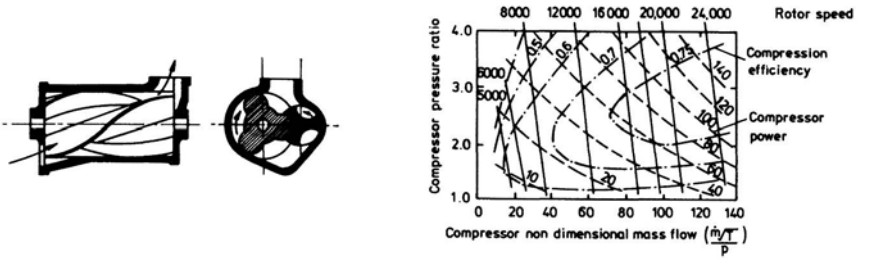

Figure 6.14 *Typical screw (Lysholm) compressor performance*

they can maintain a high efficiency over a much wider pressure ratio range, up to 3:1 if required (figure 6.14). Unfortunately they are considerably more expensive to manufacture and are therefore used where their better performance can be fully justified economically. Typically however, most two-stroke engines with Roots or screw scavenge compressors are either pulse turbocharged or are not turbocharged at all.

From time to time experiments have been conducted with other aids to scavenging, such as a mechanical drive to the turbocharger and an oil-driven Pelton wheel on the compressor shaft. Compressed air injection into the turbocharger compressor has been successfully used on two-stroke gas engines.

References

1. T. Azuma, Y. Tokunaga and T. Yura, Characteristics of exhaust gas pulsation of constant pressure turbocharged diesel engines, *ASME J. Engng Power*, **102** (October 1980) (also CIMAC, Vienna, 1979)
2. E. Meier, Two-stage turbocharging, *Brown Boveri Rev.*, **52**, No.3 (1956)
3. M. Ryti and E. Meier, On selecting the method of turbocharging four-stroke diesel engines, *Brown Boveri Rev.*, **56**, No. 1 (1969)
4. G. Gyssler, Problems associated with turbocharging large two-stroke diesel engines, *Proc. CIMAC* (1965) paper B.16
5. M. L. Land, Performance and operation of spark-ignited gas engines, *Proc. Inst. Mech. Engrs*, **181**, Pt.1 (1966/7)

7

Pulse Turbocharging

7.1 Introduction

It was the development of the pulse turbocharging system in the early 1930s (although patented by its inventor, Alfred Buchi, in 1925) that was the major breakthrough in the history of turbocharging. Although the constant pressure system is widely used on certain types of engine, the vast majority of turbocharged engines in Europe use the pulse system. However, the pulse system that has been successfully developed is not the true impulse arrangement described in section 6.2. In the practical pulse system an attempt is made to utilise the energy represented by both the 'pulse' and 'constant pressure' areas of figure 6.2. The objective is to make the maximum use of the high pressure and temperature which exist in the cylinder at the moment of exhaust valve or port opening, even at the expense of creating highly unsteady flow through the turbine. In most cases the benefit from increasing the available energy will more than offset the loss in turbine efficiency due to unsteady flow.

7.2 The Pulse Turbocharging System

The available exhaust energy obtained with the constant pressure system has been discussed in detail in section 6.3. Consider now a much smaller exhaust manifold as shown in figure 7.1. Due to the small volume of the exhaust manifold, a pressure build-up will occur during the exhaust blow-down period. This results from the flow rate of gases entering the manifold through the valve exceeding that of gas escaping through the turbine.

At the moment the exhaust valve starts to open, the pressure in the cylinder will be 6 to 10 times atmospheric pressure, whereas the pressure in the exhaust manifold will be close to atmospheric. At crank position 'a', a short period after valve opening, the pressure drop across the valve is above the choking (critical) pressure ratio, hence the flow in the valve-throat will be sonic, process 01-1 (figure 7.1, position 'a'). Further expansion of the gas to the exhaust manifold pressure, P_3, occurs by sudden expansion at the valve throat, since no pressure recovery occurs due to turbulent mixing. The stagnation enthalpy remains constant hence the flow from the valve throat is shown by line 1-03 accompanied by an entropy increase. Finally the gas expands through the turbine to atmos-

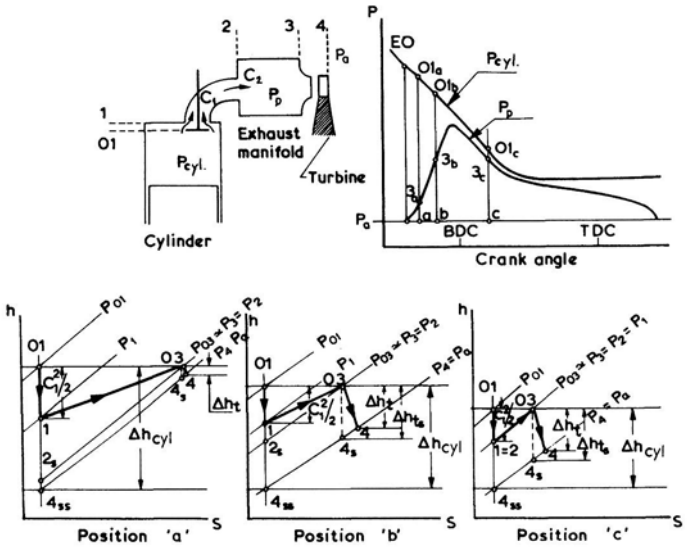

Figure 7.1 *Pulse pressure turbocharging: small exhaust manifold volume*

pheric pressure (process 03-4), doing useful work, equivalent to Δh_t. The outflowing gas from the cylinder loses a very large part of its available energy ($\Delta h_{cyl} - \Delta h_t$) in throttling and turbulence after passing the minimum section of the exhaust valve. The throttling losses are very large if the ratio of valve throat area to manifold cross-section area is very small and the pressure drop across the valve is very large, during the initial stages of valve opening.

Following further opening of the exhaust valve the cylinder pressure (P_{01}) falls, but the pressure in the exhaust manifold (P_3) increases. At crank position 'b' the manifold pressure increases to point 3b, reducing the throttling losses across the valve (process 1-03, figure 7.1, position 'b'). The pressure drop across the turbine (P_{03}/P_4) is now much larger than at position 'a', transferring the available energy ($h_{03} - h_{4_s}$) to the turbine, which represents a much larger proportion of the available energy in the cylinder (Δh_{cyl}).

At crank position 'c' the flow through the exhaust valve is sub-sonic. The throttling loss is reduced and is equivalent to the kinetic energy $C_2^2/2 = C_1^2/2$ at entry to the exhaust manifold. During the exhaust stroke, in the case of the four-stroke engine, or scavenge period in the case of the two-stroke engine, the flow process follows approximately the constant pressure pattern as described in section 6.3. At exhaust valve or port closure, the pressure in the exhaust manifold approaches the atmospheric value.

With pulse operation, a much larger portion of the exhaust energy can be made available to the turbine by considerably reducing throttling losses across the exhaust valve and port. The speed at which the valve opens to its full area (steepness of the valve area opening period), and the size of the exhaust manifold, become important factors so far as energy utilisation is concerned. If the exhaust valve can be made to open faster, the throttling losses become smaller during the initial exhaust period. Furthermore, the smaller the exhaust manifold, the

faster the rise in manifold pressure becomes, contributing to a further reduction in throttling losses in the early stages of the blow-down period. A small exhaust manifold also causes a much more rapid fall of the manifold pressure (P_3) towards the end of the exhaust process improving scavenging and reducing pumping work in a four-stroke engine.

So far, a single-cylinder engine connected to a small exhaust manifold has been discussed. However, the problem becomes more complicated when considering a multi-cylinder engine. Since the turbocharger may be located at one end of the engine, narrow pipes are used to connect the cylinders to the turbine to keep the exhaust manifold size as small as possible. By using narrow pipes the area increase following the valve throat is greatly reduced, keeping throttling losses to a minimum.

Consider again a single-cylinder engine, connected to a turbine by a long narrow pipe as shown in figure 7.2. Since a large quantity of exhaust energy becomes available in the form of a pressure wave, which travels along the pipe to the turbine at sonic velocity, the conditions at the exhaust valve and turbine are not the same at a given time instant. Thus the flow processes at exhaust pipe entry (across the valve) and at the turbine end, have to be presented separately as shown in figure 7.2. For simplicity, pressure wave reflections in the pipe are ignored.

During the first part of the exhaust process, in the choked region of flow through the valve, the gas is accelerated to sonic velocity, C_1, at the valve throat. Since the contents of the pipe are initially at rest at atmospheric pressure, sudden expansion takes place across the valve throat, process 01-1-02. However, some of the kinetic energy $C_1^2/2$ is retained as $C_2^2/2$ dependent on the valve throat area/pipe cross-section area. As the valve opens further (see crank position 'a') the pressure at the exhaust pipe entry rises rapidly. This is firstly because a certain

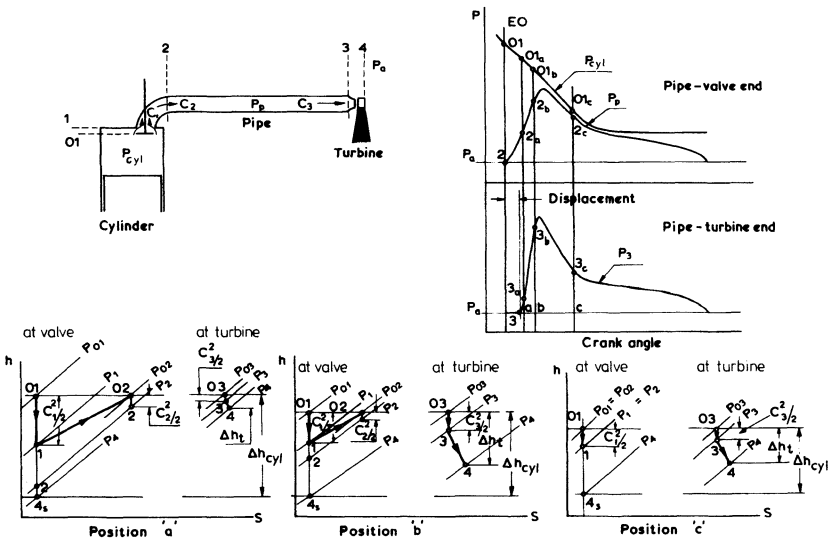

Figure 7.2 *Pulse pressure turbocharging: narrow exhaust pipe*

time is required for the acceleration of the outgoing gases, and secondly because the gases enter the exhaust pipe from the cylinder at a higher rate (velocity C_2) than they are leaving the exhaust pipe at the turbine end (velocity C_3). The rapid pressure rise at the pipe entry is transmitted along the pipe in the form of a pressure wave (travelling at sonic velocity) and will arrive at the turbine displaced in time. The displacement is a function of the length of the pipe. At crank position 'b' the pressure drop across the valve is noticeably reduced due to the rapid drop in cylinder pressure (P_{01}) and the rise in pipe pressure (P_2), and also because the valve throat area/pipe area ratio has increased. Both effects considerably reduce throttling losses (process 01-1-02-2, figure 7.2, position 'b'). The velocity (C_3) at the turbine end of the pipe is greater than velocity (C_2) after the valve, due to the arrival of the high pressure wave at the turbine end.

In the sub-critical flow region of the blow-down period, the pressure in the exhaust falls at the same time as that in the cylinder, position 'c'. The velocity (C_1) at the valve throat is equal to the velocity (C_2) in the pipe, since the valve is fully open. At the turbine the exhaust gas expands from P_{03} to atmospheric pressure, P_a, doing useful work in the turbine (Δh_t) along line 03-3-4.

It has been established that the pulse turbocharging system results in greater energy availability at the turbine. As the pressure wave travels through the pipe, it carries a large proportion of pressure energy and a small portion of kinetic energy, which is affected by friction. The gain obtained through the use of a narrow exhaust pipe is achieved partly by reducing throttling losses at the early stages of the blow-down period and partly by preserving kinetic energy ($C_2^2/2$). Thus small-diameter exhaust pipes are *essential* (and, up to a point, the smaller the better) since this will preserve high gas velocity from the valve to turbine. However, if the pipes are made too narrow, viscous friction at the pipe wall will become excessive. Pipe friction will increase the pressure drop from valve to turbine, raising the pressure at the valve throat and hence reducing scavenge air flow and increasing piston pumping work. In addition, since convective heat transfer is velocity dependent, the high velocity of the gas in the pipe will increase heat transfer losses from the manifold (ignored in the simplified analysis presented earlier). The optimum exhaust manifold pipe diameter will be a compromise, but the cross-sectional area should not be significantly greater than the geometric valve area at full lift, for a four-stroke engine. A slightly larger area is sometimes used on two-stroke engines, when scavenging is critical and the pressure on the exhaust side of the valves or port must be kept low. Naturally the exhaust pipe must be kept free of sharp bends and should be short to avoid excessive friction losses.

A typical example illustrating the gain in available exhaust gas energy when using narrow pipes is shown in figure 7.3. This test data was obtained on a single-cylinder loop-scavenged high-speed two-stroke engine with three types of exhaust manifold: a compact type (pipe diameter = pipe length) and two narrow pipes (pipe area/cross-section port area ratio of 1.78 and 1.03). All the tests refer to the same engine speed, BMEP, boost pressure, air flow rate and turbine (represented by a simple nozzle in these tests). It is interesting to note that the difference in available energy between the three types of exhaust manifold is not as significant as might be expected, and is predominantly affected by the volume of the exhaust manifold, rather than length of the exhaust pipe. This means that

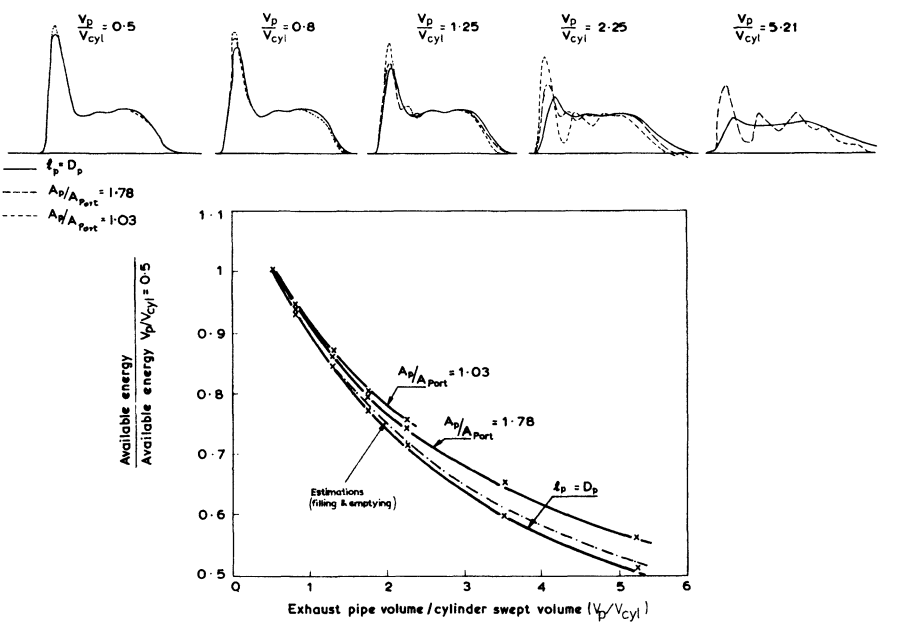

Figure 7.3 *Effect of exhaust manifold shape on available energy [1]*

the gain in available exhaust gas energy associated with a narrower pipe is mainly due to the reduction in exhaust manifold volume. A secondary effect is due to lower throttling losses in the blow-down period due to the reduced pipe cross-section area/valve area ratio.

The trends shown in figure 7.3 are typical of a two-stroke loop-scavenged engine in which the blow-down pulse represents only 35 per cent of the total available energy for the whole exhaust pulse. The blow-down pulse represents a larger proportion of the whole exhaust pulse energy in four-stroke engines, hence the advantage of using a narrow cross-sectional area will be slightly larger.

In order to increase the proportion of the energy leaving the cylinder that is made available to the turbine, it is desirable to open the exhaust valve as fast as possible so that P_3 increases rapidly (figure 7.4). However, valve assembly inertia forces will impose a limit to what can be achieved. By ensuring a good aerodynamic form for the exhaust valve or increasing the number of exhaust valves, the effective valve cross-sectional area/time diagram can be improved without a corresponding increase in the acceleration forces.

The principal method of increasing (or reducing) the available energy at the turbine is common to both pulse and constant pressure systems. The available energy is governed by, among other factors, the pressure at the valve throat (P_1) or the exhaust manifold pressure (P_3). This in turn is controlled by the flow area of the turbine. By reducing the turbine area, pressure P_3 will be increased and vice versa. This enables the energy utilisation of the turbine to be adjusted within wide limits, as shown in figure 7.5 when matching a turbine to a particular engine.

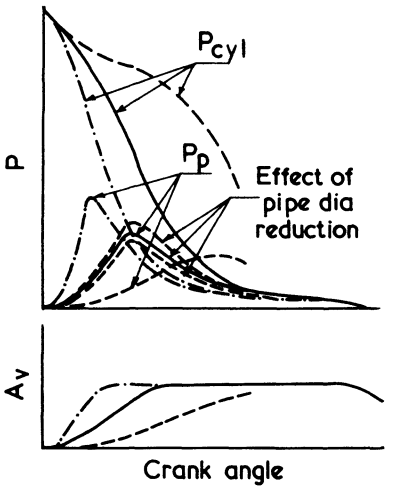

Figure 7.4 *Effect of valve area time diagram and pipe diameter [2]*

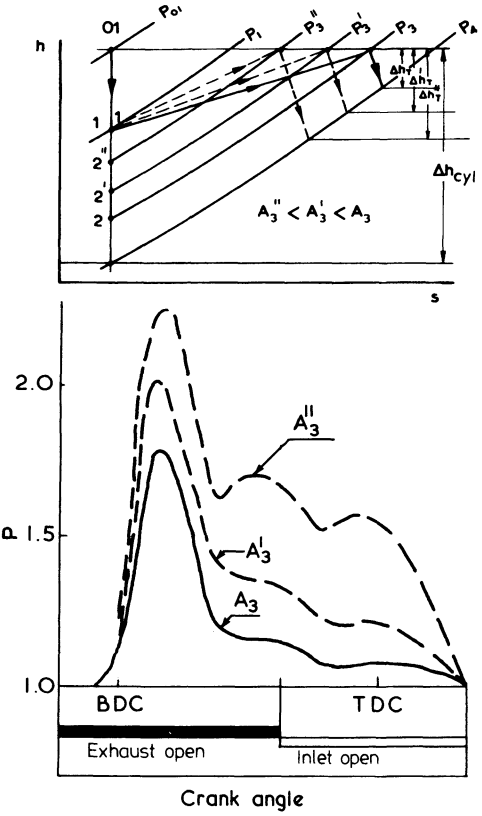

Figure 7.5 *Effect of progressively reducing turbine area (A_3)*

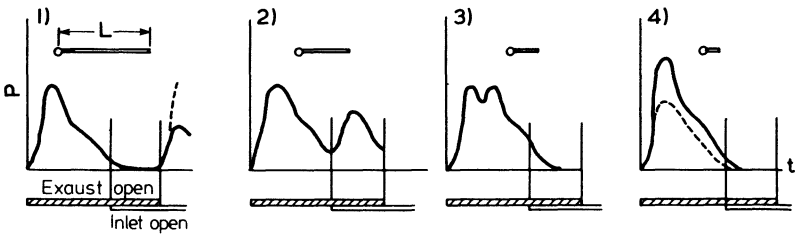

Figure 7.6 *Influence of pipe length on energy utilisation and gas exchange [2]*

The actual flow through a pulse exhaust system is, of course, highly unsteady and is affected by pulse reflections from the turbine and closed exhaust valves. Consider, for simplicity, a single-cylinder engine connected through a narrow exhaust pipe to a turbine (figure 7.2). During the first part of the exhaust process the pressure rises in the pipe at the valve and is transmitted along the pipe in the form of a pressure wave.

The pressure wave arriving at the turbine (P_3) will be partially reflected by the small throat area of the turbine. The reflected pressure wave will return along the pipe and may impede flow at the exhaust valve, dependent on the time at which it arrives there. The reflection time is a function of the exhaust pipe length (and, to a smaller extent, temperature, since the velocity of sound is a function of temperature). The effect of the reflected wave on the pressure at the exhaust valve (P_2) is shown in figure 7.6, with four exhaust pipe lengths. Superimposed on the time axis are the exhaust and inlet valve opening periods. If the exhaust pipe is long (case 1), the reflected wave may arrive after the exhaust valve has closed, having no effect. If the pipe were shorter (case 2), the reflected wave arrives in the middle of the scavenge period, preventing a two-stroke engine from running and seriously impairing the performance of a four-stroke engine. A much shorter pipe (case 3) results in a partial addition of pressure waves, creating a second pressure peak in the middle of the exhaust process. This secondary pressure peak raises the available energy in the manifold. However, since it occurs during the second part of the exhaust process (after blow-down) when the piston is displacing the exhaust gas, this gain will be at the expense of increased piston pumping work and some scavenging interference. If the exhaust pipe is very short (case 4), the pressure waves will be virtually superimposed, increasing the available energy during the important blow-down period yet maintaining good scavenging.

In figure 7.6 the pressure waves are shown on a time basis, but the figures can be considered on a crank-angle basis. It will then be evident that as engine speed changes (horizontal scale magnified or reduced), the effective time of arrival of a reflected pulse, in crank-angle terms, will vary. Hence the exhaust pipe length is critical and must be optimised to suit the speed range of the engine. The interference of reflected pressure waves with the scavenging process is the most critical aspect of a pulse turbocharging system, particularly on engines with very long exhaust pipes and substantial valve overlap. It is on these engines

that the pressure wave travel time, when expressed in terms of crank angle, will be longest since

$$\text{reflection time, } t = \frac{2l}{a} \quad \text{(from valve to turbine and back)}$$

where a = sonic velocity
l = pipe length.

If the engine speed is N (rev/min), then the reflection time or lag in terms of crank angle ($\Delta\theta$) is given by

$$\Delta\theta = N \times 360 \times 2l/(a \times 60) = 12lN/a \tag{7.1}$$

Sonic velocity (a) may be expressed as

$$a = \sqrt{(\gamma RT)} \tag{7.2}$$

where T is the mean exhaust gas temperature. Hence

$$\Delta\theta = 12lN/\sqrt{(\gamma RT)} \tag{7.3}$$

Evidently if the engine speed is high and the pipe length long, $\Delta\theta$ will be large. An automotive diesel running at 2000 rev/min with a 450 °C exhaust temperature

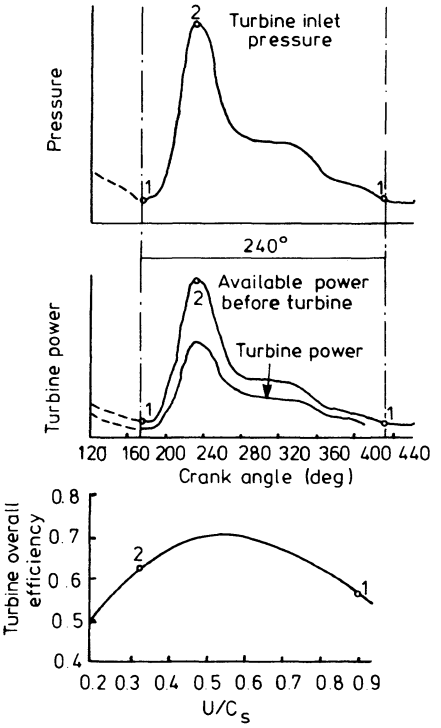

Figure 7.7 *Turbine inlet pressure, power and efficiency curves*

and a pipe length of 0.8 m would experience a lag of 35°. However at low speed the lag would be less (18° at 1000 rev/min). Only if a very long exhaust manifold were used would direct reflection be as bad as case 2 in figure 7.6, on such an engine.

Next consider conditions at the turbine entry. The bulk of the energy arriving is contained in a pressure pulse (figure 7.7, top). The total energy arriving at the turbine will be given by

$$E_{\text{tot}} = \int_0^{720} \dot{m} h_{0_t} \, \mathrm{d}\theta \tag{7.4}$$

(for a four-stroke engine where θ = crank angle) and the total power output of the turbine will be given by

$$\dot{W}_{\text{tot}} = \int_0^{720} \dot{m} h_{0_t} \eta_t \, \mathrm{d}\theta \tag{7.5}$$

In figure 7.7 (bottom) a typical turbine efficiency curve is shown. If quasi-steady flow is assumed, then the instantaneous turbine efficiency will be that corresponding to the appropriate instantaneous value of blade speed ratio (U/C_s). The values of efficiency coinciding with the peak and a low point of the pressure diagram are illustrated. For much of the remainder of the engine cycle the turbine will be windmilling and decelerating. When the next exhaust pulse arrives, part of its energy will be used to accelerate the turbocharger again, hence energy is wasted. Thus energy is wasted due to a low average turbine efficiency resulting from the very unsteady flow and windmilling during no-flow conditions.

On a multi-cylinder engine, narrow pipes from several cylinders can be connected through a single branched manifold to one turbine. Consider the three-cylinder four-stroke, automotive engine shown in figure 7.8. Due to the phase angle between the cranks of the three cylinders, the opening periods of the exhaust valves follow successively every 240° with very little overlap between them. Thus a sequence of pressure pulses arrives at the turbine (figure 7.9). This virtually eliminates the long periods of pure windage, although the average turbine efficiency will remain lower than that obtained with a correctly matched

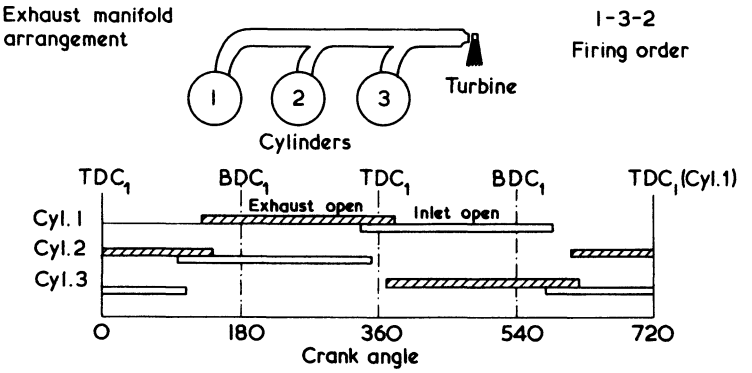

Figure 7.8 *Pulse system: three-cylinder four-stroke engine with automotive-type valve timing*

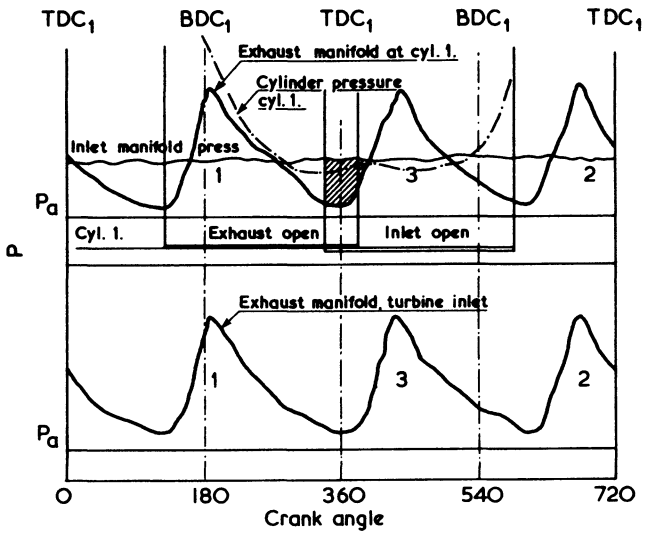

Figure 7.9 *Exhaust pressure diagrams: three-cylinder four-stroke engine with automotive-type valve timing*

constant pressure system, operating near the peak of the turbine efficiency curve. The remaining important point to consider is the exhaust pressure close to the valves, during the valve overlap (scavenging) period. As with the constant pressure system, a good pressure drop between inlet and exhaust manifold during the period when both valves are open is important in the case of a four-stroke engine with significant valve overlap and vital for a two-stroke engine. In figure 7.9 the pressure histories in the manifolds near an inlet and exhaust valve are shown, the pressure drop during the period of valve overlap being cross-hatched. Clearly, at the running condition shown, the pressure drop is favourable.

The diagrams in figures 7.8 and 7.9 have been deliberately drawn for a three-cylinder four-stroke engine with short, narrow exhaust pipes and automotive-type valve timing. Such an engine rarely exists, but is a convenient unit on which to present some important aims of pulse turbocharging. One objective is to increase average turbine efficiency by reducing windage periods, while avoiding interference with scavenging of one cylinder due to the effect of the blow-down pulse from another. The pressure pulse exhausting from a cylinder travels along the manifold until it reaches a junction. At the junction it divides into two pulses (each of smaller magnitude due to the effective area increase), one travelling down each pipe. One pulse will travel towards the turbine, the other will arrive at the exhaust valve of another cylinder. It is the later pulse, from cylinder number 3 (figure 7.9), that has arrived near cylinder 1 just at the end of the scavenge period of cylinder 1, that could be a problem. If it had arrived earlier, it would have interfered with scavenging. This type of interference, due to the *direct* action of a pressure wave from another cylinder, is quite separate from the action of a pressure pulse *reflected* from the turbine, whether the latter started from cylinder 1, 2 or 3. The pipe lengths in figure 7.8 have deliberately been kept short so that the reflected pulses are almost superimposed on the initial

pulse (case 4 in figure 7.6). This will not always be the case, so the effect of both types of possible pulse interference must be considered. It should be mentioned that if the direct pulse meets a closed exhaust valve at cylinder 1 (as it has in the figure) it will be reflected and will eventually arrive at the turbine some time after the first component of the pulse from cylinder 3.

The over-all pressure wave system that occurs in a manifold such as that in figure 7.8 will be very complex, with pulses propagating from each cylinder, pulse division at each junction, total or partial reflection at an exhaust valve (dependent on whether it is closed or not) and reflection from the turbine. Since the turbine is a restriction, not a complete blockage, the reflection from it is only partial. Fortunately, pulse division at junctions weakens the pulses (due to the area increase) and hence the system of pressure waves is weakened at each point, and successively with each reflection. Thus it is usually the direct pulses and those from the first reflections that are important. The complexity of the pressure wave system does, however, make theoretical calculations a difficult process.

Most engines have four or more cylinders, but it is convenient to consider a six-cylinder engine next. Figure 7.10 shows valve timing of a typical automotive six-cylinder diesel engine and its firing order. It is obvious that if all six cylinders were connected to a single-entry turbine through narrow pipes, the pressure waves from each cylinder would significantly interfere with the exhaust processes of each other during valve overlap and the exhaust stroke, thus increasing pumping losses. The effect would be poor engine performance. The two-stroke engine could not operate under these conditions. The difficulty can be avoided by simply connecting the cylinders in two groups of three, either to two different turbines, or to separate sections of a single turbine. If the correct cylinders are grouped together, then the pressure pulse system in each group will be the same as that shown in figure 7.8. From figure 7.10 it is clear that cylinders 1, 2 and 3 may form one group and cylinders 4, 5 and 6 the other, but the arrangement

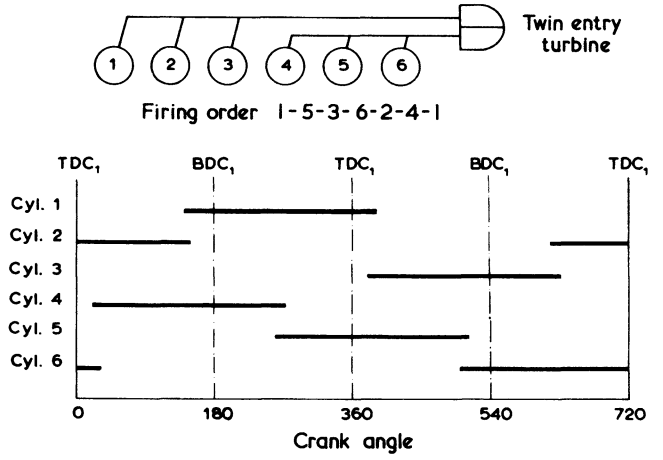

Figure 7.10 *Exhaust valve timing for an automotive six-cylinder four-stroke engine*

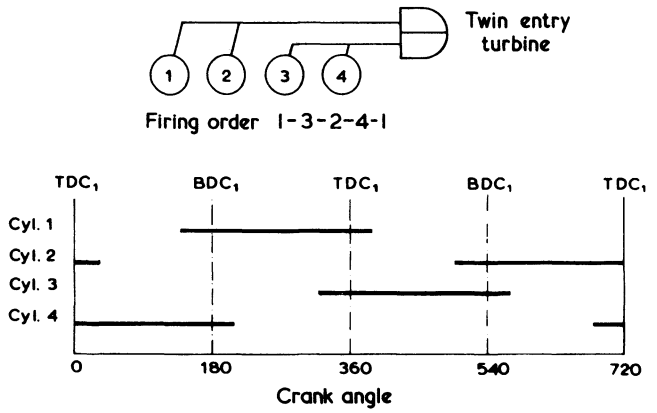

Figure 7.11 *Exhaust valve timing for an automotive four-cylinder four-stroke engine*

would differ if the firing order of the cylinders were changed. It may be concluded that the six-cylinder engine is similar to the three-cylinder, from the turbocharging point of view, but turbine performance may be slightly worse due to end-of-sector losses in a divided turbine system.

It is usually disadvantageous to connect more than three cylinders to a single turbine entry. Thus, for the four-cylinder engine shown in figure 7.11, pairs of cylinders (1-2 and 3-4) would be connected to a twin-entry turbine. On engines with other numbers of cylinders, the general rule will be to connect cylinders whose firing sequences are separated by 240° crank angle (in the case of four-stroke) and 120° (two-stroke) to a turbine inlet, and select those cylinders whose exhaust processes are evenly spaced out. However, this is not always possible. For example, on a vee engine, the vee angle will introduce an additional phase lag (or lead) to the firing intervals between cylinders. In such cases, the more basic rule of avoiding direct pressure wave interference must be observed. Some exhaust manifold arrangements for common firing orders on several engine forms are given in figure 7.12. In several cases (seven, eight and twelve-cylinder engines) an additional option will be a choice between two twin-entry turbochargers or one four-entry unit. The former option is more commonly used, since end-of-sector losses in the turbine are reduced and two smaller turbochargers are often cheaper and easier to install.

Before discussing the application of the pulse system to four-stroke and two-stroke engines in detail, some general points relating to the pulse system are appropriate. The principal advantage of the pulse over the constant pressure system is that the energy available for conversion to useful work in the turbine is greater. However, this benefit is reduced or eliminated if the energy conversion process is inefficient. The operation of radial and axial flow turbines under partial admission, unsteady flow conditions has been discussed in other chapters. The single pulse developed in figure 7.7 clearly will result in low average turbine efficiency due to a long windage period, and quite significant mass flow when the equivalent steady state turbine efficiency is low. Thus the benefits of pulse energy will be lost by turbine inefficiency. Of course, it is difficult to use the

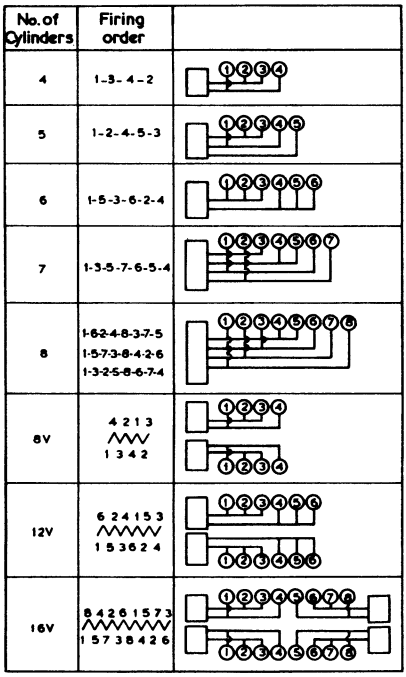

Figure 7.12 *Exhaust pipe arrangements for four-stroke engines*

alternative 'constant pressure' system with a single-cylinder engine – the example has merely been given to illustrate the penalty when one cylinder of a multi-cylinder engine is connected to a single turbine entry (unfortunately this may be necessary on some engines, for example, the five-cylinder engine in figure 7.12). With three cylinders to a turbine entry (figure 7.9), the average turbine efficiency will be higher since windage periods are almost eliminated. The efficiency can be better still if the valve timing has a larger overlap by using long exhaust periods (290°) as is the practice in medium-speed diesel engines. However, turbine efficiency, averaged over the unsteady flow cycle, will be lower than that obtained in a well-matched steady flow system. If two cylinders are connected to a turbine entry, the average turbine efficiency will be lower than would be the case with three cylinders, since (short) windage periods would exist. Thus the pulse turbocharging system is most suitable for those engines whose exhaust manifolds may connect groups of three cylinders to a turbine entry. However, even if this is not possible, the loss in turbine efficiency due to partial admission and unsteady flow is usually more than offset by the additional energy available at the turbine, hence the pulse system is by far the more widely used.

The pulse system has several other attractive features over the constant pressure system. If the system is properly designed, it will usually be possible to arrange for the pressure just downstream of the exhaust valve to fall substantially below the cylinder and inlet manifold pressure during the valve overlap period (figure 7.9). Hence reasonable scavenging can be ontained even at low engine load when the exhaust gas temperature, turbine efficiency and hence

boost pressure are low. For the same reason if the over-all turbocharger efficiency falls slightly (due to fouling in service), scavenging is not seriously impaired. From the practical point of view, the pulse system is attractive on engines with small number of cylinders, since the exhaust system is simple and compact.

For many applications a further advantage of the pulse system is the far superior acceleration response of the system when fast load changes occur (chapter 12). The small volume of the exhaust manifold results in rapid transfer of energy by pressure waves to the turbine.

One of the important disadvantages of the pulse system has already been touched on, namely poor performance when one or two cylinders only are connected to a turbine inlet, particularly if the pressure ratio is high. In these arrangements, the pressure downstream of the exhaust valves may be virtually ambient before the valve opens. Hence, using the logic of figure 7.2, little of the first part of the pressure pulse will be used effectively at the turbine. The higher the supercharging pressure ratio, the higher the cylinder pressure will be at the moment when the exhaust valve opens, hence the more significant this loss will be. At the same time turbine efficiency will be poor due to partial admission and the highly unsteady flow. Another important disadvantage of the pulse system has also been implied, namely a problem of poor gas exchange if pressure waves arrive at an exhaust valve at the wrong time. Some engines, having long pipes, may even be speed limited to avoid this happening. Undesirable pulse interference may occur on only one cylinder, in which case that cylinder may run at a very low air/fuel ratio due to bad scavenging unless fuel delivery is reduced accordingly. In this latter case, over-all power output is naturally reduced.

Usually, a turbocharger correctly matched to an engine operating with the pulse system will use a larger turbine than would be fitted for constant pressure operation. With the pulse system, the mass flow through the turbine is intermittent, taking place over shorter time intervals, hence the turbine must be sized to accept a high instantaneous flow rate, especially for two-cylinder/pipe and one-cylinder/pipe systems. Figure 7.13 compares the turbine area per cylinder needed for three or two-cylinder groups when operating with the pulse and constant pressure system, as a function of the compressor pressure ratio. Thus the ideal size ratio between turbine and compressor is different in pulse and constant pressure operation and often a larger frame size turbocharger will have to be used with the

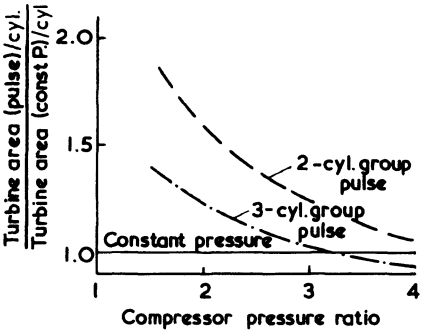

Figure 7.13 *Turbine area with pulse and constant pressure turbocharging [4]*

pulse system. This can lead to less efficient operation of the compressor in the low mass flow range.

Although the pulse system provides convenient and compact exhaust manifolds on engines with few cylinders (for example four and six-cylinder), when engines have large numbers of cylinders (for example a V16) the arrangement of air and exhaust pipes can become very complex, often using several turbochargers. The complex high-temperature exhaust pipe system creates major thermal expansion problems on large engines which must use long pipes. Expansion joints become essential on these engines and they can become a major source of engine unreliability, particularly on highly rated engines whose exhaust pressures, as well as temperatures, are high. Usually stainless steel bellows-type joints are used, but these suffer from vibration and fatigue and must be replaced at regular intervals. Several types of sliding joints have also been used, usually with piston ring seals but these are often less successful. On most engines, one or the other of these types can be developed quite successfully, particularly if the manifolds themselves are sufficiently rigid (or mechanically restrained) to avoid imposing an additional vibration level to the joint. In cases where a reliable expansion joint cannot be developed, more drastic measures must be taken. Two options are open, either to water cool the complete manifold or to change to the constant pressure system. In the former case the energy transmitted to the turbine will be significantly reduced (perhaps by 5 per cent) and the cooling system of the engine will need to be enlarged. The approach is therefore unattractive. The option of a constant pressure system will introduce the advantages and disadvantages already discussed. An expansion joint will then be required only between manifold and turbine (since the latter is rigidly fixed to the cylinder block), rather than at several places in the manifold. [3]

On a large industrial or marine engine the pulse exhaust manifolds will be lagged to prevent energy loss between cylinders and turbine, to reduce the fire hazard of hot pipes and to reduce engine room temperature. On small (automotive size) engines the manifolds are left unlagged for convenience. The small size and low weight of an automotive turbocharger enables it to be mounted rigidly on the exhaust manifold and to move with the pipes as they expand. Only on the larger sizes of automotive engine will expansion joints be desirable, where an end-mounted turbocharger is used.

Many of the points discussed above are reported in detail by Ryti and Meier, [4] Gyssler, [5] Jenny, [2] Herger and Jenny, [6] Craig and Janota, [7] Decollogny and Meier, [8] and Wallace. [9] An additional point is that the exhaust manifold for pulse turbocharging must be designed, once the diameter is chosen, for minimum energy loss. Thus all sharp bends, rough castings, poorly designed junctions and area restrictions must be avoided, otherwise a reduction in available energy at the turbine, results.

7.3 Four-stroke Engines with Pulse Turbocharging

The important factors that must be considered when using the pulse turbocharging system on a four-stroke engine have been mentioned in section 7.2. Most significant of these are the effects of pressure waves on the exhaust and scavenging

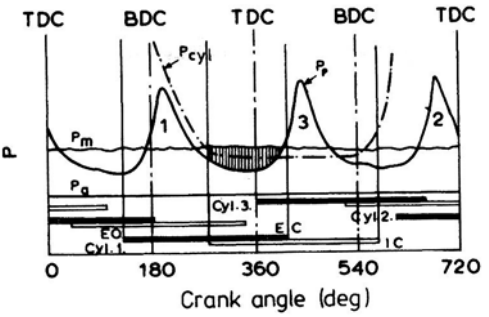

Figure 7.14 *Exhaust pressure diagram: three-cylinder group*

process and the boost developed by the turbocharger under pulsating turbine inlet flow.

Figure 7.14 shows exhaust, cylinder and inlet manifold pressures measured on a four-stroke engine in which the cylinders are connected in groups of three. The valve timing is typical of medium-speed engines. This diagram represents the almost ideal case of pulse operation for several reasons. Firstly, the exhaust pressure wave has built up rapidly, increasing energy available at the turbine. The pressure drop between cylinder and valve is low for much of the exhaust process, minimising the effect of kinetic energy being generated and then wasted. The pressure in the exhaust manifold (measured near the exhaust valve), falls to below the intake manifold pressure before the inlet valve begins to open, and continues to fall. The favourable pressure drop between inlet and exhaust is maintained for the full period of valve overlap, creating good scavenge air flow, with the maximum pressure drop coinciding with the period when the combined (inlet and exhaust) valve area is a maximum. At the turbine inlet, the flow will be unsteady but windage has been eliminated since the pressure is above ambient at all times. It follows that turbine efficiency is good, being almost as good as that of the constant pressure system.

The only danger evident from figure 7.14 is the fact that pressure pulse 3 (directly from cylinder 3) arrives just as the exhaust closes. No harm is done in this case, but there would have been if it had arrived earlier. Thus if the period of exhaust valve opening were made significantly longer, undesirable pulse interference would occur. Scavenging exhaust products of a four-stroke engine is not difficult, but the effect of exhaust pressures during the blow-down period, valve timing and valve overlap also have a significant effect in terms of the pumping work done by the piston during the gas exchange process. The ideal conditions are to have the peak of the blow-down pulse occurring just before the piston reaches the bottom dead centre crankshaft position followed by a very rapid pressure drop to below the boost pressure level during the exhaust stroke.

If two cylinders are connected to a turbine entry, the direct pressure pulse from one cylinder will usually arrive substantially after the exhaust valve of the other has closed (figure 7.15). Problems are more likely to arise from the reflected pulse (from the turbine), affecting an individual cylinder of a large engine running at high speed. For example, cylinder number 8 of the eight-cylinder

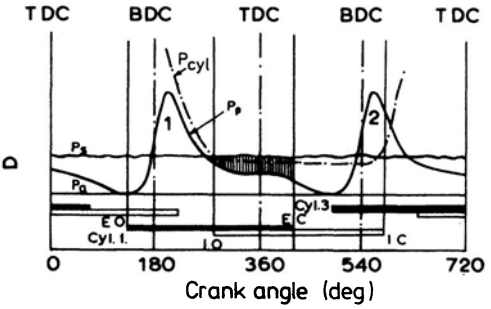

Figure 7.15 *Exhaust pressure diagram: two-cylinder group*

engine shown in figure 7.16 might receive a reflected pulse after a considerable time lag due to the long pipe length (equation 7.3). An example is shown in figure 7.16, where the blow-down pulse from cylinder 8 reflected from the closed end of cylinder 1 and, strengthened by the reflection from the turbine, has arrived at the valve during the critical period of valve overlap, raising the cylinder pressure to equal the inlet manifold pressure for almost the whole 'scavenge' period. This can only be avoided by keeping the exhaust pipes as short as possible (for example, by using a centrally mounted turbocharger on the engine of figure 7.16, but this may not be acceptable for installation reasons). If it is impossible to shorten the pipes, poor performance from that particular cylinder must be accepted or a change made to a pulse converter (chapter 8) or constant pressure system. Obviously the same pulse reflection problem can also occur on engines with three and one cylinder connected to a turbine entry.

The effectiveness of the pulse turbocharging system is governed by the gas-exchange process and the over-all efficiency of the turbocharger under unsteady flow conditions. It is difficult to draw general conclusions from individual engine test results due to the difficulty of isolating the effects of various design features (speed, valve timing, pipe lengths and many other parameters). For this reason it is useful to use turbocharged engine performance prediction methods (described in chapter 15) when looking at the general effectiveness of pulse turbocharging. Figure 7.17 shows the predicted values of some important parameters on pulse turbocharged industrial engines whose exhaust manifolds

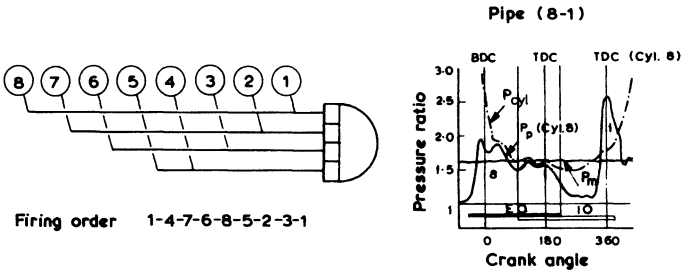

Figure 7.16 *Pulse interference on eight-cylinder in-line engines*

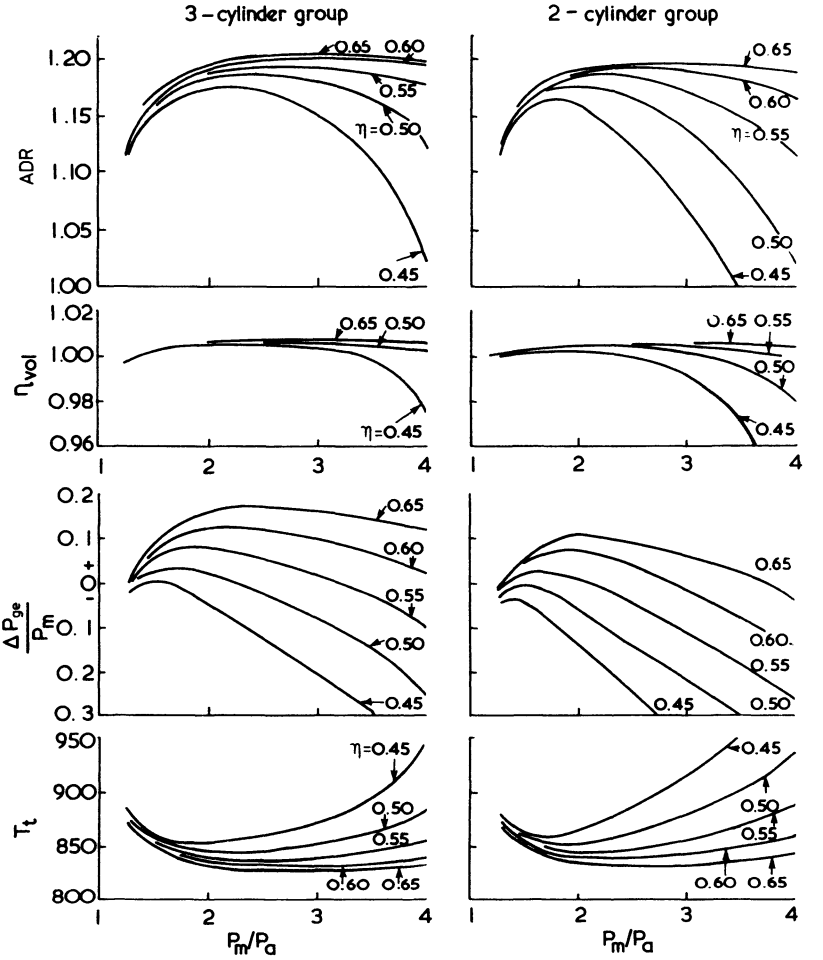

Figure 7.17 *Comparison of air delivery ratio, volumetric efficiency, gas exchange work and exhaust temperature as a function of compressor pressure ratio and over-all turbocharger efficiency: operation with the pulse system four-stroke engine [4]*

group two and three cylinders together (the parameters were defined in section 6.4). Consider first the three-cylinder group (on the left). The air delivery ratio (*ADR*) and volumetric efficiency (η_{vol}) curves show that excellent scavenging is obtained with an over-all turbocharger efficiency of 45 per cent or more, up to boost pressure ratios of 3:1. Only at higher pressure ratios is a turbocharger efficiency above 45 per cent required. Thus for all normal purposes, the benefit of high turbocharger efficiency is only gained in terms of a more favourable pumping loop (positive work output from the pistons during the gas-exchange process). In terms of specific fuel consumption the move from a turbocharger efficiency of 45 to 65 per cent at a boost pressure ratio of 3:1, results in a

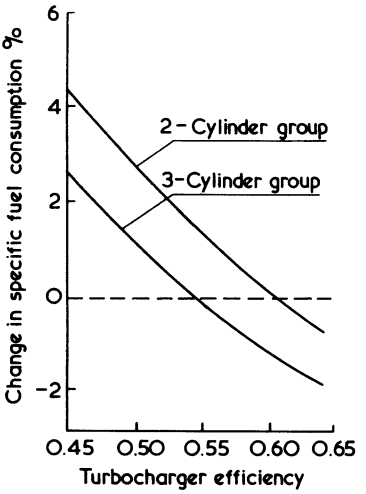

Figure 7.18 *Effect of turbocharger efficiency on specific fuel consumption pulse system – 3:1 compressor pressure ratio [4]*

benefit of approximately 4 per cent (figure 7.18). In addition, the turbine inlet temperature is reduced by 50 °C.

Turning to the predictions for an engine with two cylinders connected to a turbine entry (right-hand side of figure 7.17) the poor turbine operating conditions are reflected in a general requirement for a higher turbocharger efficiency. An over-all value of 50 per cent or greater is required for good scavenging at pressure ratios above 2:1. Below 2:1, a turbocharger efficiency of 45 per cent is satisfactory, with little to be gained from higher values. At high pressure ratios the turbocharger efficiency must be high to avoid excessive pumping work and maintain an acceptable turbine inlet temperature. Considering again the change of turbocharger efficiency from 45 to 65 per cent at a 3:1 pressure ratio, the effect on specific fuel consumption (due to the positive work during gas exchange) is a gain of approximately 5 per cent (figure 7.18).

In general, it can be concluded that pulse turbocharging of the four-stroke engine with the three-cylinder group arrangement provides the best utilisation of exhaust gas energy for engines operating up to 3:1 compressor pressure ratio (corresponding to a BMEP of 20 bar) with single-stage turbocharging. At higher ratings the single-stage low-reaction turbine cannot efficiently handle the large pressure drop of the blow-down pulse (see chapters 4 and 5) and the constant pressure system becomes more attractive, particularly for engines with a large number of cylinders.

The increased throttling losses, pumping losses, undesirable pulse reflections, windage and end-of-sector losses in the turbine associated with the two-cylinder and one-cylinder groups of 4, 8, 16 and 5, 7, 10, 14 or 20-cylinder engines can be a serious disadvantage of the conventional pulse turbocharging system at pressure ratios above 2:1 (BMEP of 13.5 bar).

7.4 Two-stroke Engines with Pulse Turbocharging

It has been made clear in section 6.5 that it is the effectiveness of scavenging that is the key to successful and efficient operation of the two-stroke engine. It has also been shown that, with the constant pressure system, the turbocharger is not self-supporting over the complete operating range of the engine. During the scavenge period the piston of the two-stroke engine moves only slightly and hence no work is done by the piston that could be utilised to supply energy lacking in the exhaust system.

Turbocharging with the pulse system provides substantial pressure energy at the turbine during the blow-down period and very effective scavenging at part load operation. This is achieved by keeping the exhaust manifold volume small and avoiding long pipes which could cause pulse reflections that interfere with scavenging. Thus two-stroke engines operating with the pulse system have turbochargers fitted very close to the cylinders, one turbocharger serving only two or three cylinders.

Comments made in section 7.3 regarding the efficiency at which the turbine converts the available exhaust pulse energy when one, two or three cylinders are connected to a turbine entry, relate to both two and four-stroke engines. The only major difference in this respect is that the shape of the exhaust pressure diagram is different, due to the long scavenge period (figure 7.19). The diagram tends to consist of quite distinct 'blow-down' and 'scavenge' periods. The energy of the blow-down pulse represents about 35 to 60 per cent of the over-all pulse energy, dependent on the scavenge system used, and the point of exhaust valve opening. Figure 7.19 illustrates a typical pressure diagram with one cylinder

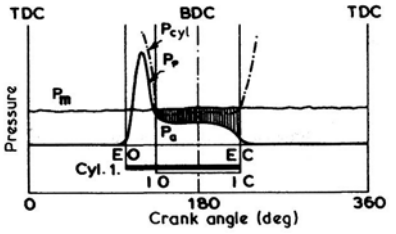

Figure 7.19 *Exhaust pressure diagram: one-cylinder group*

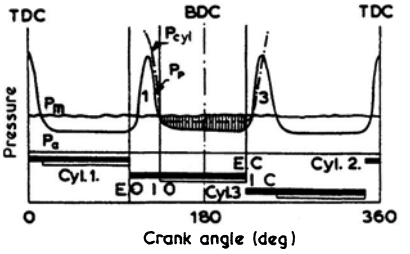

Figure 7.20 *Exhaust pressure diagram: three-cylinder group*

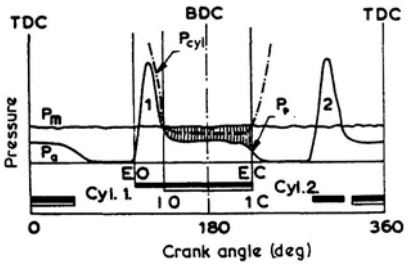

Figure 7.21 *Exhaust pressure diagram: two-cylinder group*

connected to a turbine entry. Figures 7.20 and 7.21 show diagrams with three and two cylinders connected to a turbine entry respectively.

If a two-stroke engine has a good scavenging system and the exhaust system is designed to enable the pressure drop between inlet and exhaust manifolds to be large during the scavenge period, then the pulse system enables the engine to run in a self-sustained condition without any auxiliary scavenging aid. The combination of good scavenging, high energy available at the turbine and efficient turbocharger operation enables the two-stroke engine to run, self-sustained, over the whole operating range.

It has been found in practice that best results are obtained with the three-cylinder group exhausting at 120° crank angle firing intervals (figure 7.20). Although the turbocharger will operate less efficiently when the exhausts are grouped in pairs (figure 7.21), the engine should still be able to operate self-sustained over its full speed range.

Since the designer of a uniflow scavenge engine with exhaust valves is free to choose his valve timing, if unfavourable groups of cylinders or other reasons result in low turbocharger work output, the point at which the exhaust valve opens may be advanced, increasing the 'release' pressure and temperature. This will raise the energy available at the turbine, enabling the engine to run self-sustained. However, there are two disadvantages. Firstly, the effective stroke of the piston is reduced, reducing the useful power output from the piston, and secondly, the high release temperature will impose higher thermal effects on exhaust valves, manifold and turbine. In some cases, carefully designed small exhaust manifolds with a two-cylinder group can preserve more blow-down energy at the turbine than in the case of the three-cylinder group, without the need for appreciably advancing the exhaust valve opening point.

Exhaust port timing can be altered on opposed piston engines by adjusting the position of the ports, up or down the cylinder, or by altering the phase angle (crank lead) between the opposing pistons. However, the increased volume of the exhaust manifold, imposed by the exhaust port belt, results in less efficient utilisation of the pulse energy. Thus the opposed piston two-stroke engine requires auxiliary air assistance at very low part load duties.

On some (rare) occasions it is possible to use the reflected pressure pulse to aid the gas-exchange process on a two-stroke engine. If the combination of engine speed, exhaust pipe length and valve timing is such that the lag of the reflected pulse is a little less than the full opening period of the exhaust valve, then the

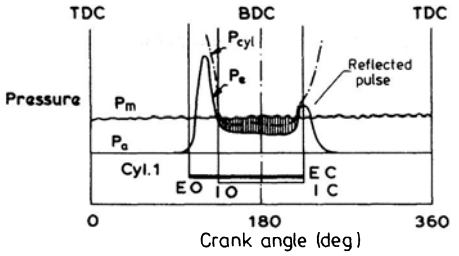

Figure 7.22 *Effect of a reflected pressure pulse arriving at the end of the scavenge period of a two-stroke engine*

exhaust pressure diagram near the valve might look like that shown in figure 7.22. By raising the exhaust pressure just as the valve is closing, it is possible to force the cylinder pressure to rise and equal the inlet manifold pressure when inlet and exhaust valves close. This will increase the mass of fresh charge trapped in the cylinder. Due to the momentum of the inflowing gas, it is sometimes possible for the cylinder pressure to exceed both inlet and exhaust pressures in a carefully designed system. However, if the reflected pressure wave arrives somewhat early, when the exhaust valve area is large and scavenging is not yet complete, then the mass trapped in the cylinder will have a high residual gas content. Furthermore combustion products may be blown right through into the inlet manifold where carbon deposits may build up. This situation should not be accepted, but may occur at low engine speeds, when the pulse lag (from equation 7.3) becomes shorter. Clearly, when attempting to use this reflected pulse, the effect of pressure wave dynamics must be checked over the complete speed range of the engine.

The major disadvantage of the scheme outlined above can be avoided if use is made of the direct pressure pulse from an adjacent cylinder, rather than a reflected pulse originating from the cylinder in question to aid the gas exchange process. For example, with a three-cylinder group (figure 7.20), the phase interval between cylinders (120°) is close to the opening period of the exhaust valve. If the exhaust period exceeds 120° and the direct pressure wave travel time is very short, then pressure pulse 3 might arrive at the end of the exhaust period of cylinder 1, raising the mass of fresh air trapped in the cylinder as described above. The lag between exhaust valve opening (cylinder 1) and pulse 3 arriving has two components: the phase angle between cylinders and the pressure wave travel time. The first will dominate and is constant in terms of crank angle, hence the effect of engine speed is small. The disadvantages of the system are that wave travel time must be short hence pipes must be short (thus an adjacent cylinder must be favourably timed), and the exhaust period may have to be rather long. If the latter is the case, then the expansion stroke is artificially reduced which may offset any potential gain in engine performance.

If two cylinders are connected to a turbine entry (figure 7.21) it will not be possible to use pressure wave interference to help increase the trapped mass (although, theoretically, it may be possible to use the reflected pulse). However, if the valve timing is rather conservative (that is, of short duration) then it may

be possible to connect four cylinders, each firing at 90° intervals, to a turbine entry. The pulse from one cylinder travelling direct to a second may, if the pipes are not too short, arrive just at the end of the exhaust process of the second cylinder. However, since the exact timing of the interfering pulse is critical, there are few engines on which this scheme is beneficial.

The disadvantage of loop and cross-scavenged engines is not only poor scavenging but the fact that the use of inlet and exhaust ports results in restrictive timing. As the piston uncovers and then covers the inlet and exhaust port, symmetrical valve timing is unavoidable. The exhaust lead over the inlet is a function of the height of the ports in the cylinder and will result in exactly the same lag at valve closure. Thus, towards the end of the scavenge period the pressure in the exhaust manifold drops rapidly and leakage of the charge into the exhaust occurs while the exhaust ports remain open. Due to this lag, the exhaust lead must be limited or rotary exhaust valves have to be fitted. This complicates the installation and the exhaust manifold volume is increased, which may prevent the turbocharger from providing sufficient air for the engine to run without a scavenging aid.

Increased engine ratings and improved turbocharger efficiency (approaching 65 per cent for large units), has reduced the disadvantage of the constant pressure system over the pulse system on large two-stroke engines. Thus for simplicity and reliability MAN converted to the constant pressure system in 1974. To reduce costs further, and simplify the installation, MAN replaced the under piston pumps by electrically driven scavenge pumps fitted in front of the turbocharger compressors. Similarly, in recent years, Sulzer and B & W engines have changed to the constant pressure system.

References

1. M. S. Janota, A. J. Hallam, E. K. Brock and S. G. Dexter, Prediction of diesel engine performance and metal temperature using digital computers, *Proc. Inst. Mech. Engrs.*, **182**, Pt.3L (1967/8)
2. E. Jenny, Utilization of exhaust gas energy in the supercharging of the four-stroke diesel engine, *Brown Boveri Rev.*, **37**, No.11 (1950)
3. P. S. Vaughan, The development of high specific output, four-stroke, supercharged diesel engine, *Proc. CIMAC* (1965) paper A.14
4. M. Ryti and E. Meier, On selecting the method of turbocharging four-stroke diesel engines, *Brown Boveri Rev.*, **56**, No.1 (1969)
5. G. Gyssler, Problems associated with turbocharging large two-stroke diesel engines, *Proc. CIMAC* (1965) paper B.16
6. H. Herger and E. Jenny, Turbocharging of diesel engines – present state and future developments, *Proc. CIMAC* (1957)
7. H. R. M. Craig and M. S. Janota, The potential of turbochargers as applied to highly rated two and four-stroke engines, *Proc. CIMAC* (1965) paper B.14
8. G. Decollogny and E. Meier, Considérations sur les écoulements non-stationnaires dans les collecteurs d'un moteur diesel suralimenté et leurs aspects pratiques, *J. Soc. Ing. Auto.*, **35**, No.8/9 (1962)
9. F. J. Wallace, Vergleich der Gleich-druck und Stoss-aufladeverfahren bei der Abgasturboaufladung von Dieselmotoren mit hohem Aufladedruck, *MTZ*, **25**, No.5 (1964)

8

Pulse Converters and Summary of Turbocharging Systems

8.1 Introduction

The pulse turbocharging system has been found to be superior to the constant pressure system on the majority of today's diesel engines. Generally, it is used on all but highly rated engines designed for constant speed and load or marine applications. In chapter 7 it was made clear that the pulse turbocharging system is usually most effective when groups of three cylinders are connected to a turbine or turbine entry. When one or two cylinders are connected to a turbine entry, the average turbine efficiency and expansion ratio tend to fall due to the wide spacing of exhaust pulses. The 'pulse converter' has been developed to overcome some of these disadvantages on certain engines (although some versions are suitable for use on any engine) as a compromise between the pulse and constant pressure turbocharging system.

The term 'pulse converter' was first used by Birmann. [1] His objective was to design a device that preserved the unsteady flow of gases from the cylinder during the exhaust and valve overlap periods, yet maintained steady flow at the turbine. In this way he hoped to achieve good scavenging and high turbine efficiency. Figure 8.1 shows one of the devices proposed. All the cylinders are connected to a single-entry turbine, resulting in a continuous, and almost steady flow, and high turbine efficiency. To achieve good scavenging, Birmann proposed a 'jet-pump' system, using a high velocity jet of gas issuing from a central nozzle to reduce the pressure in short pipes at the exhaust valves. The high velocity jet

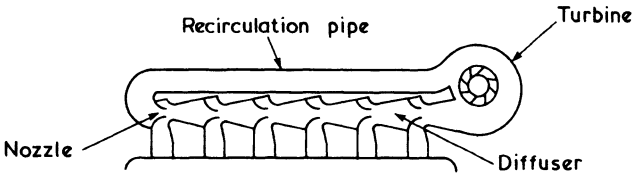

Figure 8.1 *Schematic of early Birmann pulse converter*

should create a suction effect in the surrounding area, due to the conservation of momentum. The by-pass tube was used to provide the jet for the first cylinder (so that some gas circulated at all times) and to maintain an almost constant pressure at the jet nozzles (reducing the filling and emptying losses of a normal pulse exhaust system).

The system shown in figure 8.1 has several disadvantages.

(1) There is insufficient length between exhaust ports to permit efficient pressure recovery in the diffusers.

(2) Each nozzle must be larger than the last, resulting in high manufacturing cost.

(3) Frictional and diffusion losses will be high, since much of the exhaust gas will pass through several ejectors and diffusers.

(4) The whole installation is bulky and complex.

(5) The large total volume of the installation can result in poor performance when starting and accelerating, as in the constant pressure turbocharging system.

Birmann gradually developed refinements of his pressure pulse-energy converting system (pulse converter), but it never achieved wide acceptance possibly due to the problem of trying to optimise the size of the ejector nozzles and amount of recirculation. Furthermore, the extremely turbulent nature of the gas flow entering the diffusers must have resulted in poor diffusion which, when combined with high jet velocities, would imply high losses. Consequently the energy available during expansion through the turbine is reduced, although the steady flow conditions would aid efficient conversion of this energy into useful work.

No doubt stimulated by Birmann's work (and in particular his simpler pulse converter [2, 3, 4, 5, 6]), Brown Boveri and Sulzer initiated a test programme with pulse converters on a four-stroke diesel engine in 1957. This work was reported by Decollogny and Meier [7] and later, more comprehensively, by Petak. [8] Rather than apply a complex 'ejector-junction-diffuser' arrangement at each cylinder, pairs of cylinders were joined in the conventional arrangement of a pulse system. The pulse converter was used only to join groups of cylinders (figure 8.2) that would normally be kept separate. Thus, for example, four cylinders of an

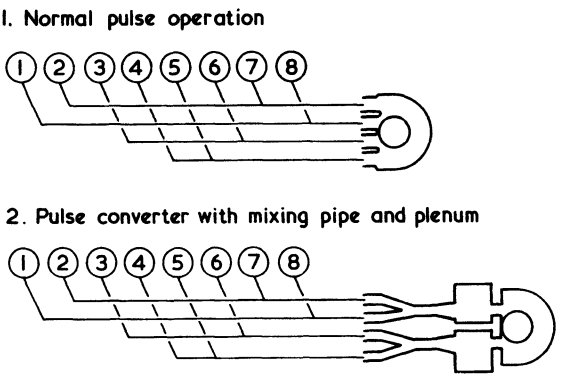

Figure 8.2 *Petak's pulse converter*

eight-cylinder engine might be connected to a single turbine entry rather than two. The four cylinders are chosen such that their exhaust processes successively follow each other, resulting in continuous admission of exhaust gas to the turbine. This reduces the unsteadiness that results when only two cylinders are connected to a turbine entry, but does not eliminate it. The plenum chamber (figure 8.2) is substantially smaller than that associated with constant pressure turbocharging, but is an additional aid in reducing unsteady flow.

By achieving steadier flow at the turbine entry, the average operating efficiency of the turbine improves. However, it is important that the pulse converter does not hinder the exhaust process at the valves. In particular, the scavenging process is very reliant on achieving a low pressure downstream of the exhaust valve during the relevant portion of the exhaust process. Birmann's device was principally aimed at improving scavenging by lowering this pressure.

If an engine has very little valve overlap (short exhaust periods), it may be possible to connect four suitable cylinders to a single turbine entry with only a small amount of interference between the exhaust processes. However with the normal valve timing of a turbocharged industrial or marine engine, the four exhaust periods (typically $> 240°$) will be too long to avoid substantial overlapping of the exhaust processes from the four cylinders during a $720°$ cycle.

Figure 8.3 illustrates the problem with pulse turbocharging. The cylinder pressure is dropping during the exhaust process and falls below the pressure of the charging manifold at the beginning of the scavenge period. However, the

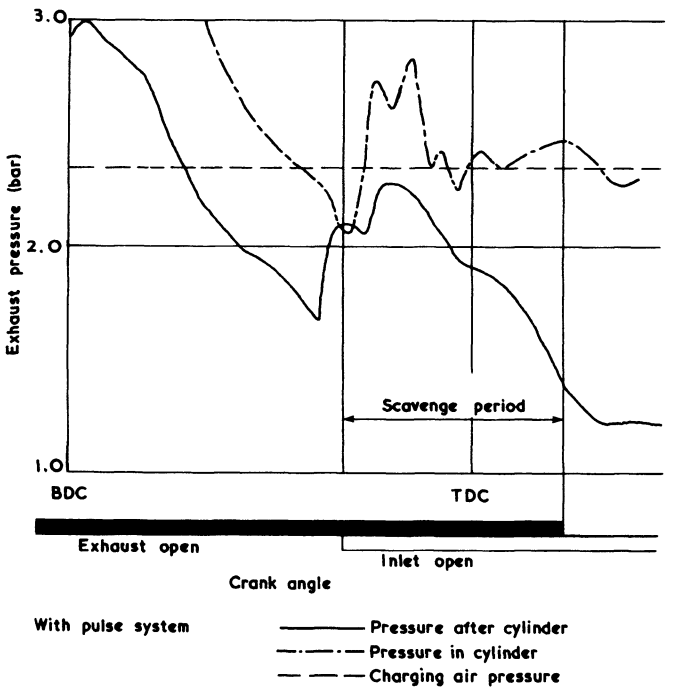

Figure 8.3 *Exhaust pressure wave interference during scavenging*

arrival of an exhaust pressure pulse from another cylinder raises the pressure downstream of the exhaust valve, just at the critical scavenge period. The result is that flow through the exhaust valve is reduced and cylinder pressure rises to exceed that of the charging air manifold. Virtually no scavenging is possible.

To avoid a deterioration of the scavenging process, the 'pulse converter' must prevent, or at the very minimum reduce, the effect of a pressure wave from one cylinder interfering with the exhaust process of another. It is the area reduction in the inlet nozzles, converting pressure to velocity at the junction, that reduces pressure wave propagation from one branch to another. However, to be very effective, large area reduction is required introducing significant throttling losses at the junction. Thus a pulse converter should be assessed on the basis of lack of flow unsteadiness at the turbine, minimum loss of available energy at the turbine and minimum exhaust pulse interference between cylinders.

8.2 Simple Pulse Converters

The majority of pulse converters in use today are based on the concept of minimum energy loss even if this means not only a loss of all suction effect, but some pressure wave interference during scavenging. [9,10,11,12] To avoid high mixing losses at the junction, the area reduction in the inlet nozzles is usually small, (junction area > 50 per cent of pipe area) while the mixing length and plenum chamber used by Petak, and often the diffuser, are omitted completely. These simple pulse converters have the added advantage of adding little over-all length to the exhaust system. A typical example (from a four-cylinder engine) is shown in figure 8.4. The pulse converter is specified by the nozzle and throat area ratios. Clearly no suction effect will be generated by such a pulse converter, but the flow losses through it will be very much less than those in more complex designs.

Figure 8.5 illustrates the propagation of a pressure wave through a pulse converter junction (using a water table analogy). The pressure wave enters from the

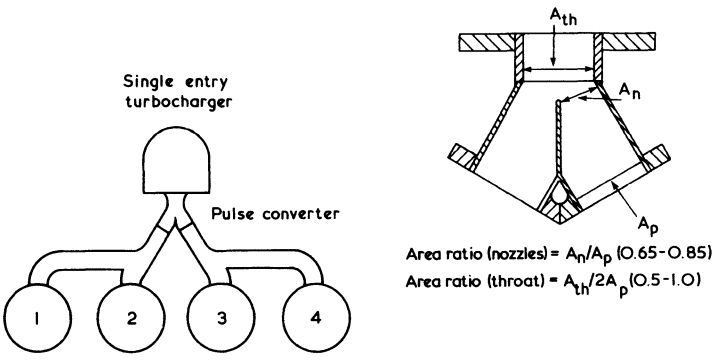

Figure 8.4 *Exhaust manifold arrangement (four-cylinder engine) and pulse converter details*

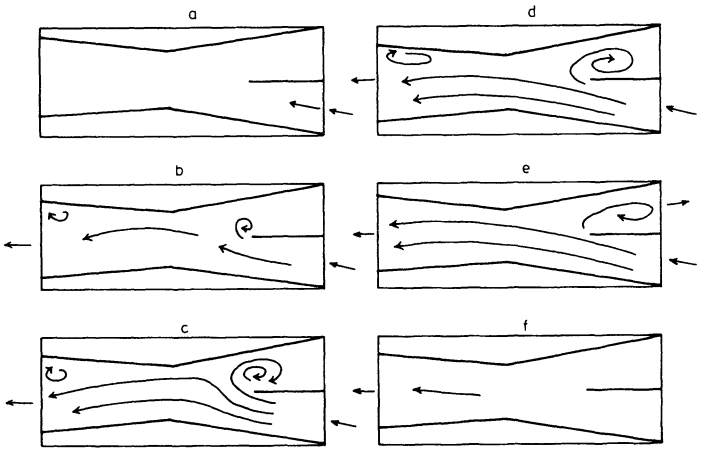

Figure 8.5 *Flow visualisation in a model pulse converter, with a pulse entering from the lower right-hand inlet and flowing to the turbine on the left*

lower right-hand branch. As flow enters the junction a vortex is set up at the entry from the upper branch. This partially blocks the branch. In addition, the highly turbulent nature of the flow ensures that any movement up that branch is unlikely to be significantly diffused in the expanding section. Thus the junction does not eliminate the propagation of a pressure wave from one inlet branch to another, but it does reduce it. The reduction in amplitude of this potentially troublesome pressure wave will be governed by the detailed design of the junction and by the area of the inlet nozzles. The latter will, of course, control the momentum of the jet issuing from an inlet nozzle.

Whether the propagation of a pressure pulse from one branch to another will interfere with the exhaust and scavenging process of a particular cylinder, and if so by how much, will depend on the exhaust valve timing, engine speed, firing interval between cylinders, lengths of exhaust pipes, turbine area and cylinder release pressure. Thus different engines will accept different levels of pulse propagation through the pulse converter. Adjustments of the area reduction at the inlet nozzles and, to some extent, the common throat area after the junction, allow some control of pressure pulse propagation to be achieved. However, the common 'throat' area is frequently the turbine inlet flange area.

Tests on a model pulse converter [13] have shown that the area reduction at the inlet nozzles has to be severe to reduce pulse propagation substantially. The penalty accompanying large area reductions in the inlet nozzles is higher internal 'losses' and hence reduced energy available for useful expansion through the turbine. In practice this means that the minimum possible area reduction is used, consistent with reasonable scavenging. It follows that the design of the pulse converter is a compromise between minimum losses and reduction of pulse interaction between the inlet branches. The compromise adopted may vary from one engine design to another, depending on the amount of pulse interference, etc.

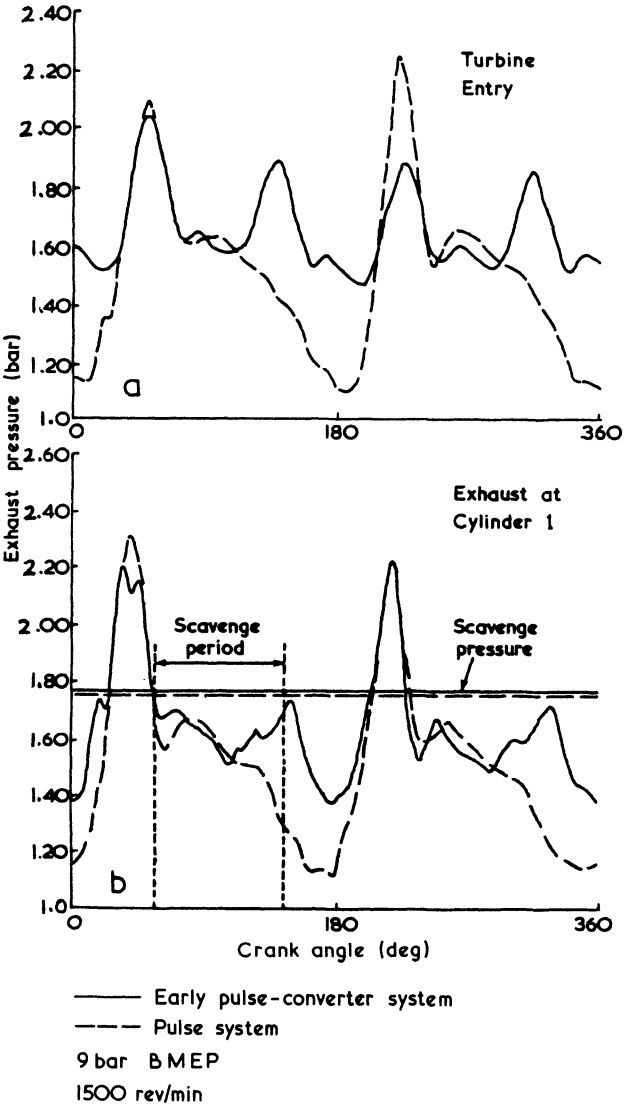

Figure 8.6 *Comparison of exhaust pressure diagrams with pulse and pulse converter systems (four-cylinder two-stroke engine)*

8.3 The Application of Pulse Converters to Two-stroke Engines

The two-stroke engine is not self-aspirating hence the application of turbocharging systems and their influence on the scavenging process is particularly critical. However, many two-stroke engines have run successfully with pulse and constant

pressure systems and, more recently, pulse converters. The majority of medium and slow-speed uniflow scavenged two-stroke engines are able to run with no additional aid to scavenging. However, this is not the case with two-stroke engines that are required to operate over a very wide speed and load range. For this type of duty (for example, automotive) a separate mechanically driven scavenge blower is required. Thus the engine duty and its scavenging arrangement will impose certain requirements on the turbocharging system.

Figure 8.6 compares the exhaust pressure diagrams measured near an exhaust valve and at the turbine entry on an engine with pulse and simple pulse converter turbocharging systems. The engine is a four-cylinder automotive unit with a Roots blower fitted in series with the turbocharger compressor. The pulse converter arrangement is that shown in figure 8.4, with a nozzle/inlet pipe area ratio of 0.75.

Considering the turbine entry diagram, by connecting four cylinders to a turbine entry, partial admission losses have been eliminated and the entry conditions, although not steady, exhibit far less severe fluctuations. The result should be an improvement in the average operating efficiency of the turbine. The pressure diagrams recorded in the exhaust pipe near cylinder 1 show a similar pattern during the early part of the scavenge period but not towards the end. The effect of an exhaust pressure pulse from cylinder 3 arriving, with reduced amplitude, at cylinder 1, raises the exhaust pipe pressure towards the end of the scavenging period. If this pulse had a large amplitude and arrived earlier in the scavenge period, engine performance would be adversely affected. By arriving with reduced amplitube, late in the scavenge period, this pressure pulse in fact aids performance. By raising the exhaust port pressure up to almost equal the boost (or scavenge) pressure at the moment of valve closure, the density of the fresh air trapped in the cylinder increases. Scavenging is not unduly impaired since the pressure drop between the intake and exhaust ports of the cylinder is very favourable during the period when the instantaneous valve area is greatest.

The combined effect of superior turbine admission conditions and increased charge density at the moment of valve closure results in a substantial improvement in engine performance (figure 8.7). The increased boost generated by more efficient turbine operation allows a smaller capacity Roots blower to be fitted (blower B, figure 8.7). The specific fuel consumption improves due to the reduction in power required to drive the blower.

If the two-stroke engine is not required to work over such a large speed and load range as an automotive unit, it is usually possible to dispense with the scavenge blower and rely on the turbocharging system to provide sufficient boost pressure. In this case any improvement in turbine performance due to the pulse converter will be reflected directly in increased specific air consumption. There is no scavenge blower to absorb extra power as a result of increase air flow hence the engine is in a better position to benefit. Figure 8.8 shows results from tests on a medium-speed (450 rev/min), four-cylinder two-stroke diesel engine fitted with a pulse converter. Clearly good scavenging has been achieved and the pulse converter has reduced specific fuel consumption, turbine inlet termperature and, therefore, thermal loading.

The reduction of area in the inlet nozzles of the pulse converter governs the transmission of a pressure wave from one inlet branch to another, and the losses

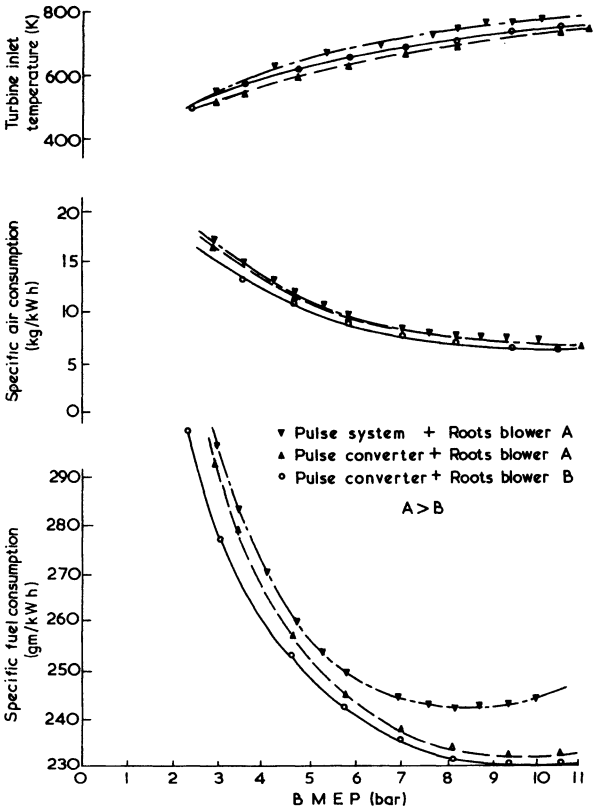

Figure 8.7 *Comparison of performance at 1500 rev/min of pulse and pulse converter systems (four-cylinder two-stroke engine)*

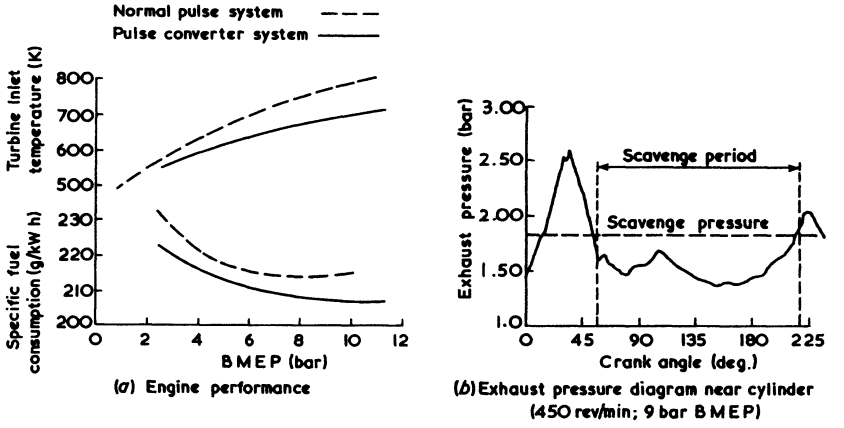

Figure 8.8 *Simple pulse converter performance on a four-cylinder medium-speed two-stroke engine [9]*

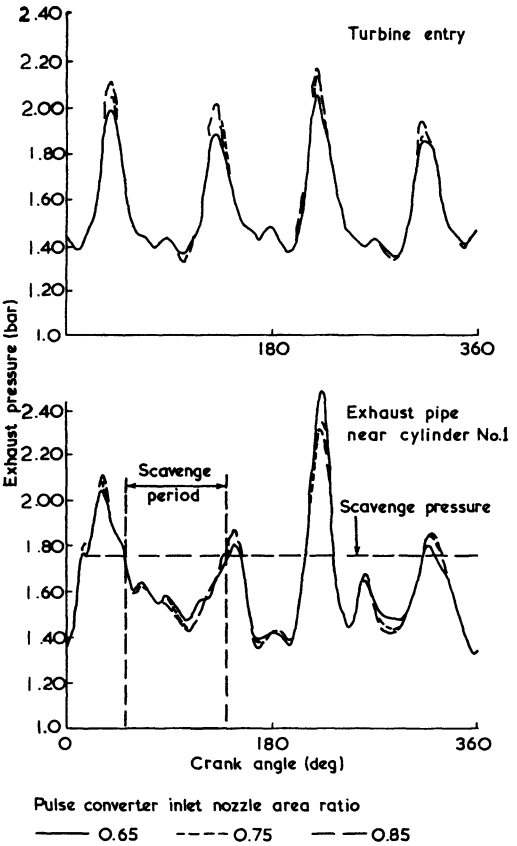

Figure 8.9 *Comparison of exhaust pressure diagrams with pulse converters of different area ratios (1500 rev/min, 9 bar BMEP)*

through to the turbine inlet. The common throat that follows the junction generally has a less significant effect since, with simple pulse converters, its area is generally governed by the intake area of the turbine casings available.

Large area reductions in the inlet nozzles can reduce the propagation of a pressure pulse from one inlet branch to another [14, 15] but only at the expense of increased throttling losses. Figure 8.9 shows exhaust pressure diagrams obtained with pulse converters having three different inlet nozzle area ratios, but they are identical in other respects. The smaller nozzles marginally reduce the amplitude of the interfering pulse arriving at the end of the scavenge period, but the effect is small.

Clearly the pulse converter has to be matched for a particular engine and duty. Figure 8.10 shows the specific fuel consumption of the same engine with the three different pulse converters fitted at varying loads and speeds. Although differences are small, the smallest pulse converter is superior at low speeds but inferior at high speeds. The latter effect probably results from high throttling losses when the mass flow rate is high, which outweighs, the benefit of reduced

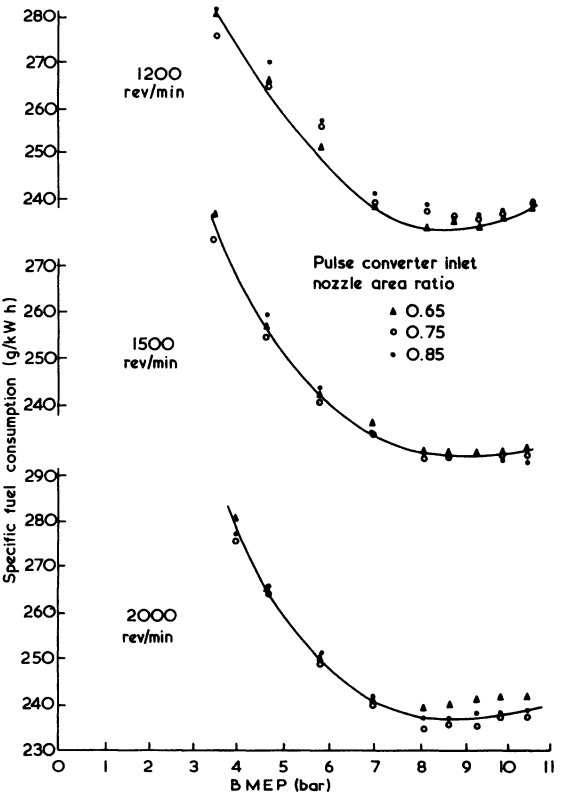

Figure 8.10 *Pulse converter matching curves*

pulse interference. The pulse converter having an inlet nozzle area ratio of 0.75 is probably the optimum.

A set of exhaust pressure diagrams (taken near the valve) at constant load but varying engine speed (figure 8.11) shows that the pulse converter reduces pulse propagation at all speeds. There is no critical speed at which it becomes most effective. However, the over-all performance of an exhaust pipe system that includes a pulse converter is speed sensitive. Clearly the arrival time of an exhaust pulse relative to the scavenge period of another cylinder is very important. The pressure pulses travel at sonic velocity (a) and since

$$a = \sqrt{(\gamma RT)} \tag{8.1}$$

it follows that the wave travel time will principally be a function of load (via the effect of air/fuel ratio on T, γ and R) rather than engine speed. In terms of crankshaft rotation, this time lag will convert to a varying crank angle interval. Thus the time of arrival of the interfering exhaust pulse will vary relative to the scavenge period of another cylinder. In figure 8.11 this difference is very small, since the engine is small and the total pressure wave travel time is in the order of 10 to 30° crankshaft rotation. However, with large engines, the total pressure wave travel

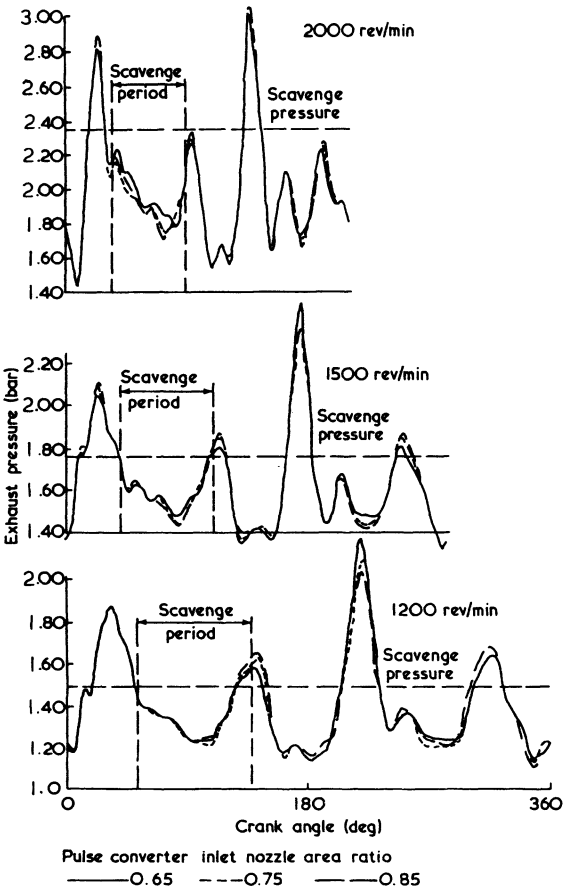

Figure 8.11 *Exhaust pressure diagrams (near cylinder) at varying speed and constant load (9 bar BMEP)*

time will be much longer and hence the influence of engine speed on the timing of pressure pulse interference is more significant.

Exhaust pressure diagrams recorded at constant engine speed but increasing load are shown in figure 8.12. Clearly pressure wave propagation is reduced in proportion to the amplitude of the initial pulse hence there is no general load sensitivity. However, an engine fitted with pulse converters can be more difficult to start than a normal pulse turbocharged engine.

When matching a turbocharger, the turbine area is adjusted to generate a certain mean expansion ratio. This in turn results in sufficient turbine work for the compressor to develop the desired boost pressure. In pulse turbocharging, a series of exhaust gas pulses pass through the turbine. If these pulses are spaced out in time and do not overlap with each other, then the turbine area, in principle, need not be increased to accommodate however many pulses of gas follow each other through the turbine. Of course, in practice turbine area will be changed slightly in order to develop the same boost pressure with different average turbine

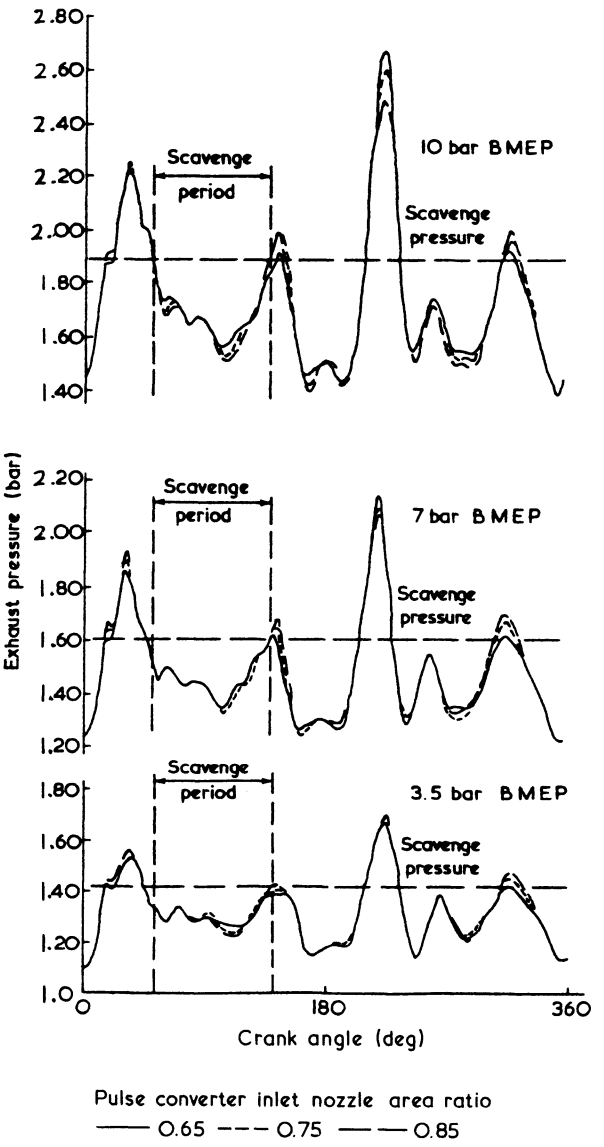

Figure 8.12 *Exhaust pressure diagrams (near cylinder) at constant speed (1500 rev/min) and varying load*

efficiencies. Thus in general it may be said that the so-called rule of 'turbine area per pulse' prevails. That is, irrespective of the number of cylinders connected to a turbine entry (one, two, three or four) the turbine area remains approximately the same when the turbocharger is matched to the engine at a given rating. A

small area adjustment, to alter turbine available energy, offsets the effects of any increase or decrease in windage and end-of-sector losses and will be adequate for different arrangements. In contrast, with constant pressure turbocharging, turbine area selection will depend more on the steady mass flow rate and expansion ratio, and therefore increases with the number of cylinders.

Considering a simple four-cylinder engine with pulse or pulse converter turbocharging systems, in one case a twin-entry turbine will be used while a single-entry unit will suit the pulse converter. Each sector of the twin-entry unit will receive two pulses per cycle, whereas the single-entry unit will receive four equally spaced pulses. Since the number of pulses in the sequence will not substantially alter the desired turbine area, the single-entry unit will require the same area as one sector of the twin-entry unit. In other words the total turbine area is halved.

In practice, some overlap of the four pulses occurs (figure 8.6) hence turbine area is reduced by somewhat less than half (40 per cent in figure 8.6). This may result in the turbocharger having a smaller basic frame size than that required with pulse turbocharging, although the flow requirements at the compressor are not reduced. However, on some engines a reduced number of turbochargers may result (that is, a change from two twin-entry units on an eight-cylinder engine with pulse turbocharging to one twin-entry unit with the pulse converter).

Turbine area is primarily chosen to achieve a desired boost pressure level but it controls the general pressure level in the exhaust manifold at the same time. Since this pressure level will increase as turbine area is reduced, it follows that the amplitude of pulses entering the pulse converter will also increase. Fortunately the pulse converter tends to reduce the transmission of these pressure waves in proportion to their original amplitude, but clearly the lower the turbine entry pressure the less pressure pulse interference between the cylinders will occur. It follows that the pulse converter will operate most satisfactorily if the over-all efficiency of the turbocharger is high, so that a relatively high boost pressure can be developed with maximum turbine area.

8.4 The Application of Pulse Converters to Four-stroke Engines

Four-stroke engines are self-aspirating and hence the design of the inlet and exhaust system, while very important, is less critical. Thus four-stroke engines are generally somewhat less sensitive to details of the turbocharging system when starting for example, and at low loads. Although less critical, factors that enhance the performance of the turbocharged two-stroke engine such as a good pressure drop between the intake and exhaust ports during scavenging, will also benefit the four-stroke engine. The four-stroke engine can function without scavenging, but good scavenging will always improve its performance. Similarly, an efficient exhaust system and turbocharger will enable a larger turbine area to be used (for the same boost pressure), reducing exhaust manifold pressure and hence pumping work during the exhaust process.

The period available for scavenging the four-stroke engine is during the overlap between the start of the intake process and the end of the exhaust process. Since the inlet valve remains open substantially longer than this, raising the exhaust pressure at the end of the scavenge period cannot trap more air in the cylinder.

Thus, unlike the two-stroke, no advantage can be taken from a nominally 'interfering' pressure pulse to trap more air in the cylinder. The arrival of a pressure pulse (via the pulse converter) during the period of valve overlap will impair scavenging no matter when it arrives, on a four-stroke engine. Clearly this situation should be avoided, but it will rarely be possible to avoid some pulse interference. It follows that the pulse converter must again be designed to reduce interference as far as possible without significantly reducing the energy available for useful expansion at the turbine. The amount of pulse reduction required in the pulse converter will depend on when in the scavenge period the interfering pulse arrives. It will have least effect when the exhaust valve is almost closed.

Figure 8.13 shows exhaust pressure diagrams measured near cylinder 1 of an in-line eight-cylinder medium-speed four-stroke engine, fitted with pulse converters having different area ratios. The effect of the exhaust pulse from cylinder 2 is to influence the pressure at cylinder 1, via the pulse converter, during the scavenge period of the latter. With no inlet area reduction at the pulse converter (that is, a simple pipe junction), the exhaust pressure rises above the charging pressure for a significant part of the scavenge period (cylinder 1). The pulse converter with an inlet nozzle area ratio of 0.7 reduced this interference resulting in a 4 per cent increase in air flow rate and a small reduction in fuel consumption.

The smaller pulse converter (0.5 area ratio) has significantly increased throttling losses, resulting in a deterioration of engine performance, probably due to the higher exhaust pulse pressure at the valve.

The influence of engine speed acts through the timing of pressure pulses from one cylinder relative to another just as on two-stroke engines. Thus the exhaust pipe lengths as well as engine speed and load are controlling parameters. Exhaust

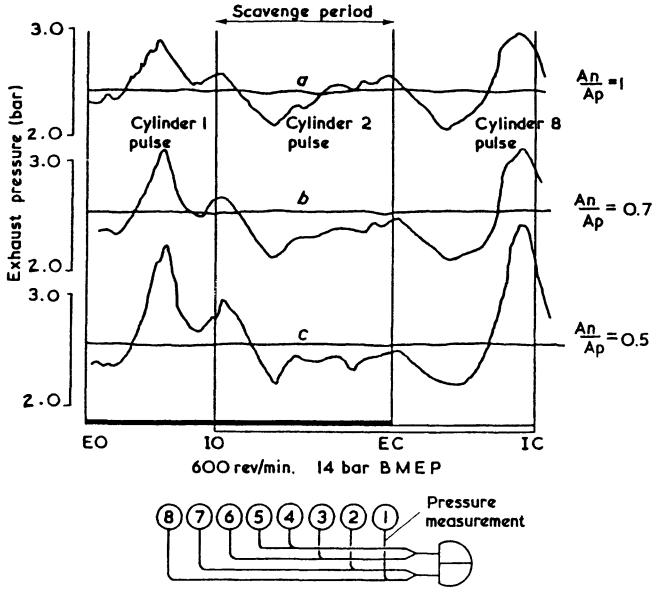

Figure 8.13 *Exhaust pressure measured at cylinder 1 with (a) 1, (b) 0.7 and (c) 0.5 area ratio pulse converters [16]*

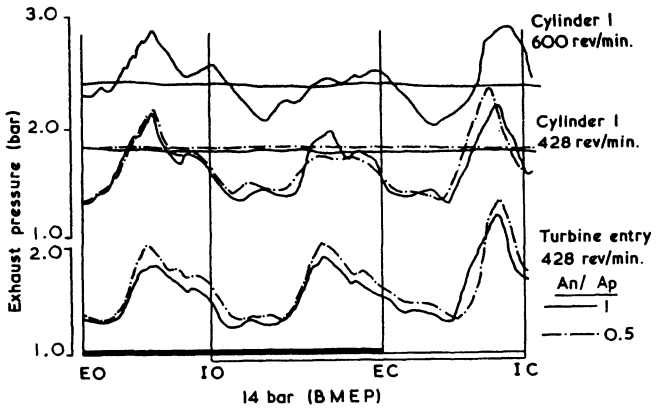

Figure 8.14 *Comparison of exhaust pressures at 600 and 428 rev/min [16]*

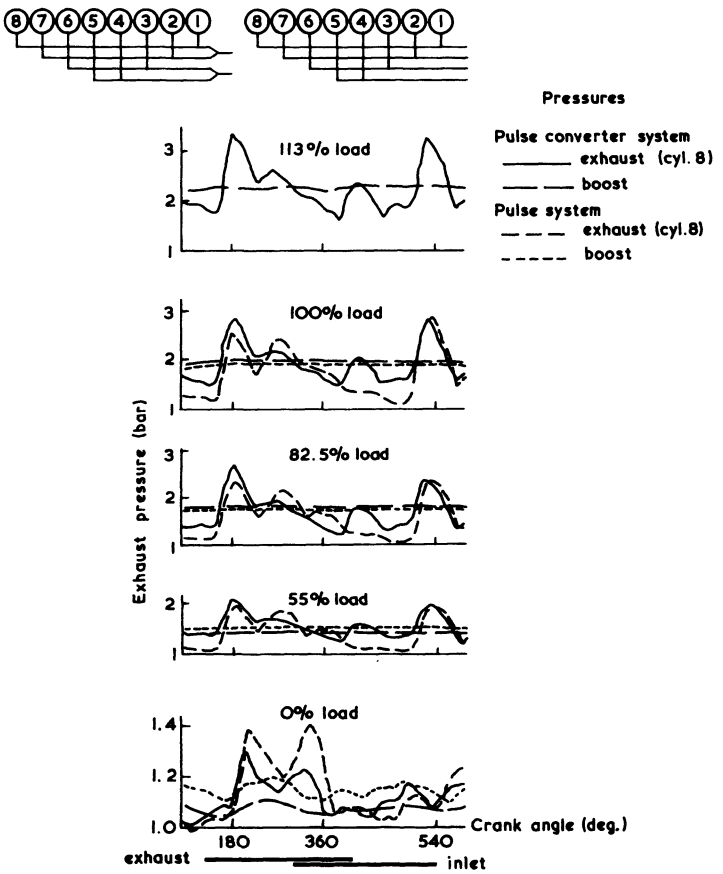

Figure 8.15 *Pulse and pulse converter performance comparison at varying load (medium-speed four-stroke engine) [11]*

pressure diagrams taken at two engine speeds are shown in figure 8.14. The pressure wave travel time from cylinder 2, through the pulse converter and round to cylinder 1 is roughly constant in terms of time. Thus at the lower engine speed the wave travel time reduces when expressed in terms of degrees of crankshaft rotation. The interfering pulse arrives earlier and affects scavenging adversely. Thus a pulse converter with greater area reduction at the inlet nozzles would be required if performance at the lower speed were important.

Figure 8.15 shows exhaust pressure diagrams with pulse and pulse converter turbocharging systems on an eight-cylinder engine at constant speed but different loads. During the valve overlap period, the pressure drop between intake and exhaust manifolds is more favourable with the pulse converter system on this particular engine. The pulse converter does tend to retain this advantage down to low loads, but the charging pressure falls more rapidly than with conventional pulse turbocharging. Thus the benefit of a higher charging pressure at full load with the pulse converter is reversed at low load.

Since the timing of interfering exhaust pulses is governed by pressure wave velocity and distance travelled, the lengths of the various parts of the exhaust manifold can have an important influence on pulse converter design. In some cases it may prohibit the use of a pulse converter, since adjustment of the inlet area ratio can only have a limited effect on pulse reduction before throttling losses become excessive.

For the cylinder and turbocharger arrangement shown in figure 8.13, the shortest path length for an interfering pulse is between cylinders 2 and 1, while the longest is between cylinders 7 and 8. Figure 8.16 compares the exhaust pressure diagrams at cylinders 1 and 8. Due to the short wave travel time, cylinder 1 suffers from interference early in its scavenge period, while cylinder 8 suffers interference much later, when the exhaust valve is nearly closed.

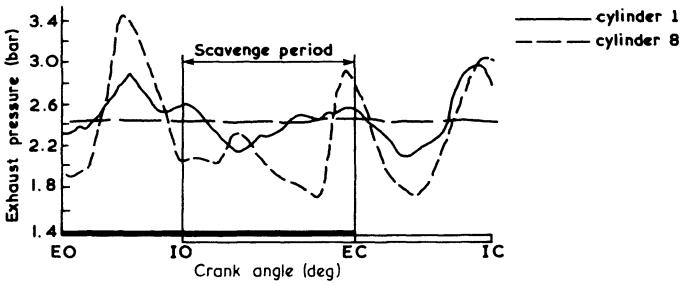

Figure 8.16 *The effect of exhaust pipe length on pressure pulse interference with a pulse converter*

8.5 Engine Arrangments, Firing Order and Valve Timing

The data used to illustrate the effect of a pulse converter has been obtained from four and eight-cylinder in-line engines. Yet engines have been produced with almost any number of cylinders between 1 and 20, many in vee form although three cylinders is the usual minimum for turbocharging. Engines with four, eight or sixteen cylinders tend to be the 'natural' ones for pulse converters, but this

results from the pulse converter being developed to overcome the disadvantages of the pulse system with these engines. The reasons have been explained, but to summarise, it is due to the fact that since the cylinders cannot be grouped in threes per turbine entry (under the normal pulse system), partial admission losses occur and the turbine loses efficiency due to highly unsteady flow.

When cylinders can be grouped in threes (six, nine and twelve-cylinder engines), turbine inlet flow is continuous, although not steady. The pulse system usually works well with these engines and it is unlikely that the use of a simple pulse converter will improve performance. The pulse converter becomes advantageous when cylinders would normally be grouped in pairs with pulse turbocharging (four, eight and sixteen-cylinder engines). However, care must be exercised when the pulse converter links cylinders from both branches of a vee engine due to the effect of the vee angle on the firing interval between cylinders. This can result in pulse interference during critical phases on the exhaust process.

Other engines can use pure pulse turbocharging or combinations of pulse and simple pulse converter systems. For example, the vee 10 cylinder engine shown in figure 8.17 (firing order 1, 6, 2, 7, 4, 9, 5, 10, 3, 8) can use a combination of pulse turbocharging for cylinders 2, 3, 6 and 9 and pulse converters for 1, 4, 5, 7, 8 and 10 (arrangement D). The exhaust periods are shown for a vee angle of 45°, and the firing order given. With normal pulse turbocharging (arrangement A) it would be possible to connect cylinders into five pairs without interference of their exhaust processes. Pairings might be as follows: 1-5, 2-3, 4-10, 6-9, 7-8. This scheme has disadvantages. Two turbochargers with different inlet housings would be required (a twin entry and a three entry) creating problems with matching and spares.

An alternative grouping for pulse turbocharging would be to join cylinders (arrangement B): 1-4, 2-3, 5, 6-9, 7-8, 10. This would enable two three entry turbochargers to be used, but their efficiency would suffer from windmilling through one sector while the exhaust valves of cylinders 5 or 10 were closed. A third scheme (arrangement C) might be to link cylinders: 2-3-5, 1-4, 6-8-9, 7-10.

Two twin-entry turbochargers could be used, with good admission characteristics, but it is evident from figure 8.17 that pressure pulse interference from cylinder 3 on cylinder 5 and from cylinder 6 on cylinder 8 is probable. Thus scavenging of cylinders 5 and 8 will be poor unless pulse converters are fitted. A similar alternative (arrangement D) would be to connect cylinders: 1-4-10, 2-3, 5-7-8, 6-9. This has an advantage over the previous grouping since the interfering pulses will be delayed by longer path lengths (for example, from 1 to 10 and from 7 to 5). However, if the valve timing, engine speed and exhaust pipe lengths are such that pressure wave interference will harm engine performance, then pulse converters may be introduced to protect cylinder 7 from the exhaust process of cylinder 5, and 10 from 1.

Similar combinations of pulse and pulse converter systems can be used on engines with other numbers of cylinders, but no general rules are appropriate to all engines. The best arrangement for any particular engine will depend on its firing order, phase angle between banks (vee engines) valve timing, speed range, pipe lengths and turbine area, since these are the parameters that control the exhaust dynamics.

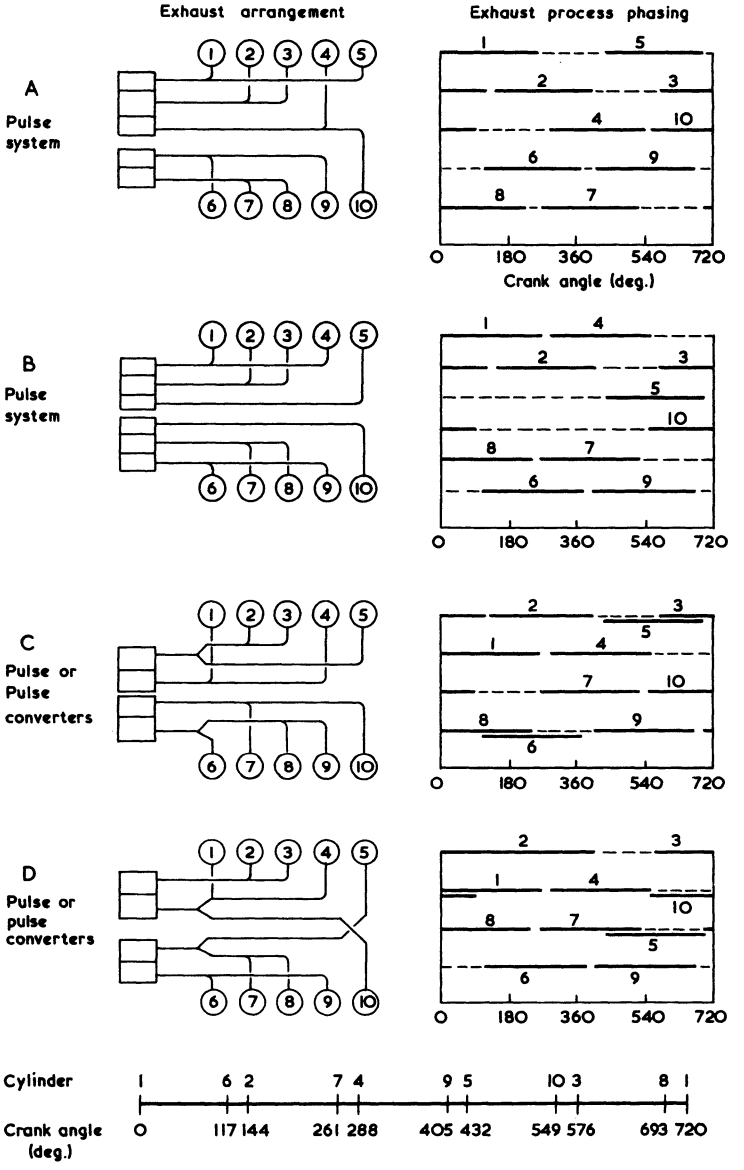

Figure 8.17 *Pulse and simple pulse converter turbocharging systems on a V10 engine*

8.6 Multi-entry Pulse Converters

The design of pulse converters need not be restricted to two inlet branches and a single exit to the turbine. Petak [8] tested designs with three entries. However, a

logical step beyond the simple type of twin-entry pulse converter is to try to connect all the cylinders of an engine to a single turbine entry. The objective is to try to minimise pulse interference by a combination of three factors

(1) area reduction at the inlet nozzles;

(2) by connecting a large number of cylinders together, the effect of one exhaust pulse on the others is reduced;

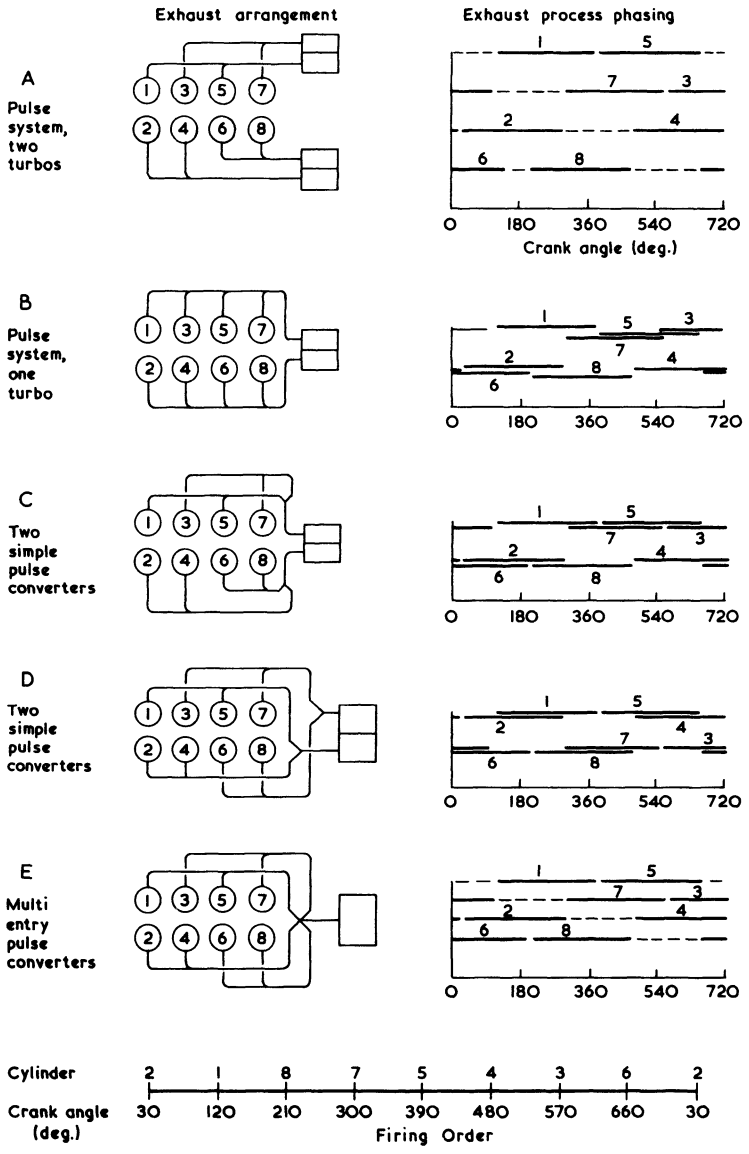

Figure 8.18 *Pulse and pulse converter turbocharging systems for an automotive V8 engine*

(3) by connecting a large number of cylinders to a single turbine inlet, the turbine area is very large compared with the cross-sectional area of each exhaust pipe.

Consider the V8 automotive engine shown schematically in figure 8.18. This has a 90° vee angle, exhaust pipes on the outside of the vee and a firing order 2, 1, 8, 7, 5, 4, 3, 6. The ideal pulse turbocharging system (A), uses two small twin-entry turbochargers, one for each bank. Although the exhaust pulses reaching each turbine inlet are not equally spaced, there will be no overlap between them with conventional automotive valve timing. A widely used alternative system has one twin-entry turbine with an entry for each bank (B). However, even with little

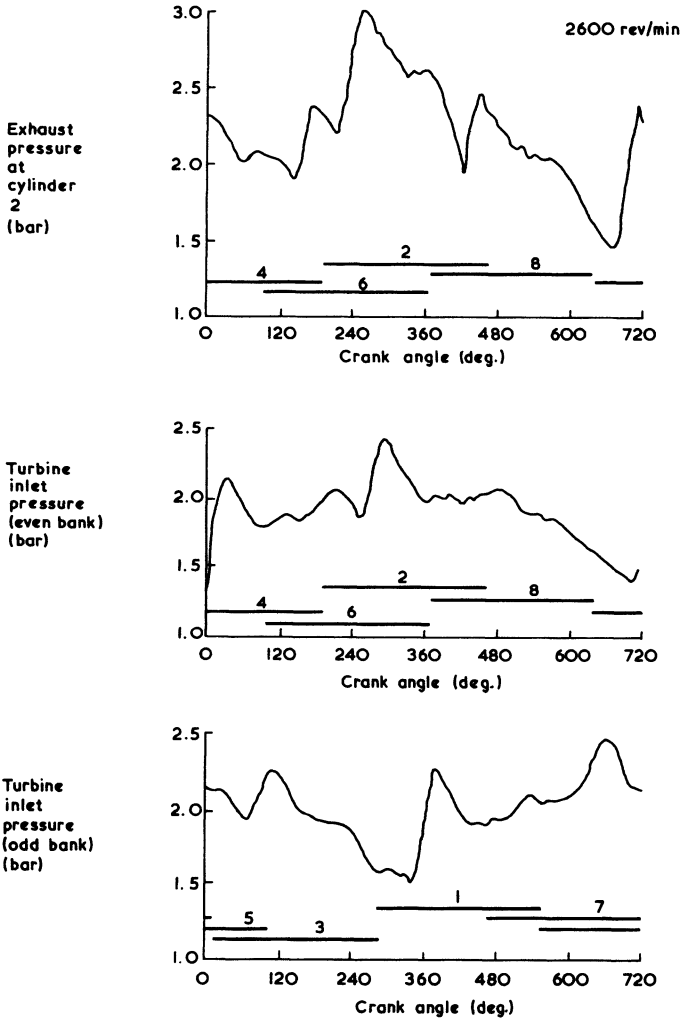

Figure 8.19 *Exhaust pressure diagrams, full load and speed, with pulse turbocharging (V8 automotive engine)*

valve overlap, the four exhaust processes in each branch of the exhaust system interfere badly. Figure 8.19 shows the turbine inlet pressure diagrams (both entries) and the exhaust pressure diagram adjacent to cylinder 2, for system B. Although windage periods are absent, due to continuous flow (from four-cylinders) through the turbine, the flow is highly unsteady and peaks at the period when exhaust processes from cylinders 4, 6 and 2 come together. On the odd-numbered bank, peak flow occurs when the pulses from cylinders 1, 7 and 5 build up.

A multi-entry pulse converter turbocharging system can be fitted to this type of engine in order to improve turbine inlet conditions and reduce exhaust process interference between cylinders, without the expense of two turbochargers.

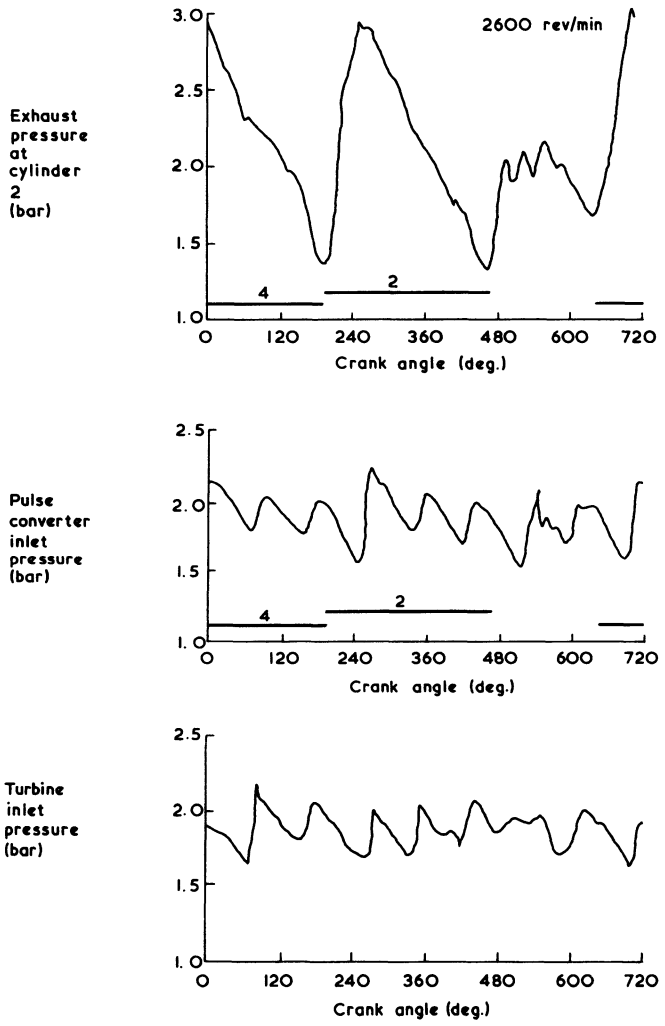

Figure 8.20 *Exhaust pressure diagrams, full load and speed, with a multi-entry pulse converter (V8 automotive engine)*

Exhausts are paired for optimum pulse spacing (figure 8.18E) as with the twin-turbocharger pulse system. Thus four pipes connect to one single-entry turbocharger through a four-inlet pulse converter. Two alternative exhaust systems using simple twin-entry pulse converters and a twin-entry turbine are shown in figures 8.18C and D. The latter is the better arrangement, since it avoids the double overlap of exhaust process 7 with those from cylinders 1 and 5 (that is, pulses are more evenly spaced in arrangement D than C).

With the multi-entry pulse converter system (figure 8.18E) the exhaust pulses arriving at the turbine are spaced equally, every 90°. Equal spacing is a very desirable requirement of the multi-entry system, since it relies on the fact that the influence of any individual exhaust process from a cylinder is small relative to the combined effect of them all. If the exhaust processes from two or three cylinders were close together, pressure would build up in the system and the last cylinder in the group to exhaust would be opposed by an unduly high pressure.

Exhaust pressure diagrams (system E, figure 8.20) show that the multi-entry pulse converter has not eliminated unsteady flow at the turbine, but comparison with figure 8.19 reveals a significant improvement, with the highest peak and lowest trough removed. If these are likely to be the least efficient points of turbine operation (low and high U/C_s respectively) then average turbine efficiency will improve. In addition, one or two percentage points in efficiency will be gained by using a single-entry housing. Whether these efficiency gains are found in practice depends on how well the turbine characteristics match the requirements of the engine. Generally, benefits at high speed and load will be achieved with a deterioration at low speed and load. [17]

Data from an automotive engine (figures 8.19 and 8.20) is influenced by the relatively low turbocharger efficiency on this type of unit, wide speed range, low valve overlap and modest loads. In contrast, medium-speed engines generally operate at higher ratings, have larger and therefore more efficient turbochargers, and use substantial valve overlap for effective scavenging. The large exhaust pressure pulses generated by highly rated engines, and the difficulty of achieving efficient utilisation of this energy in the turbine, means that benefits resulting from

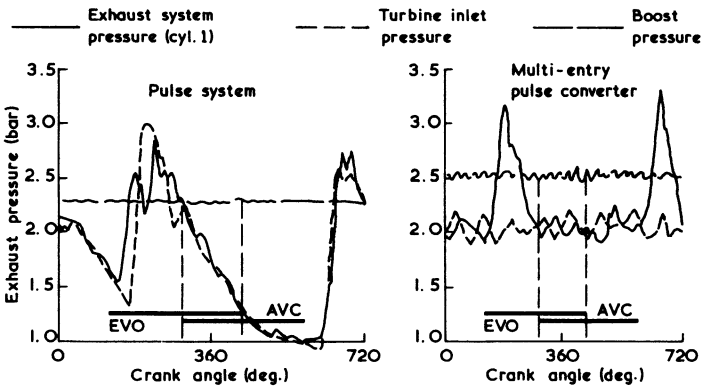

Figure 8.21 *Comparison of exhaust pressure diagrams with pulse and multi-entry pulse converter turbocharging systems (V8 medium-speed engine) [18]*

steadier turbine admission increase at higher BMEPs. However, more care has to be taken to ensure favourable exhaust pressures at the valves during the overlap period.

Figure 8.21 compares pressure diagrams, during gas exchange, on a more highly rated V8 engine with large valve overlap, with pulse and multi-entry pulse converters. A more favourable pressure drop between inlet and exhaust is obtained early in the scavenge period, with the latter system. More important, large turbine inlet pressure fluctuations and periods of no admission are eliminated.

The examples given above are V8 engines, but multi-entry pulse converters can be used on engines with more than eight cylinders, particularly those unfavourable for normal pulse turbocharging (fourteen, sixteen cylinders, etc.). Figure 8.22 shows the gas exchange diagram from a highly rated medium-speed V14 engine, using a multi-entry pulse converter and a single-entry turbine on each bank of seven cylinders. The intake to exhaust pressure drop is favourable for scavenging. The pulse converter, a simple casting, is shown in figure 8.23, but a more favourable arrangement is to assemble the four inlet pipes as quadrants on a circle.

Multi-entry pulse converters have successfully been used on eight, fourteen,

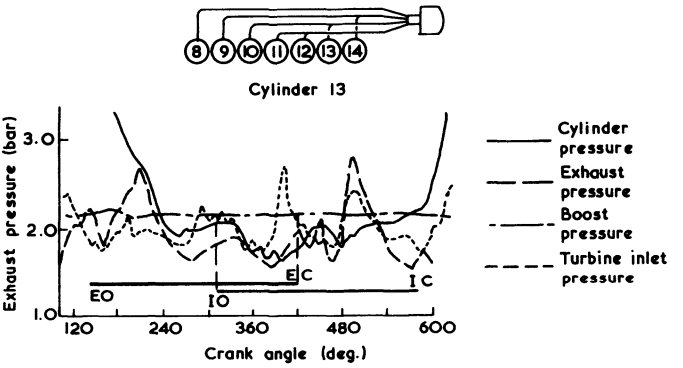

Figure 8.22 *Exhaust pressure diagrams from a V14 engine with multi-entry pulse converters [19]*

Figure 8.23 *Multi-entry pulse converter [19]*

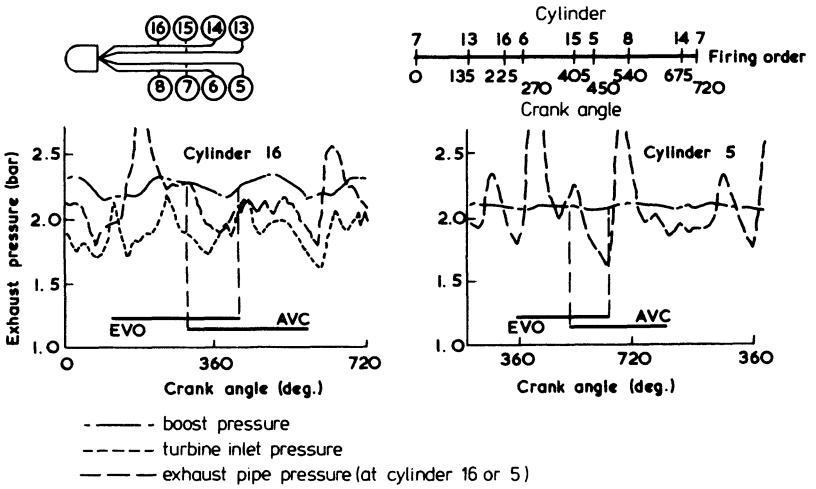

Figure 8.24 *Exhaust pressure diagrams from a V16 engine with unequal firing intervals and a multi-entry pulse converter [18]*

sixteen and even nine cylinder engines. [20] However, there are situations where the multi-entry system is not advantageous, principally when the firing interval between cylinders is not even. Consider the application to the rear eight cylinders of the V16 engine shown in figure 8.24. Due to the 45° vee angle, the exhaust processes are separated by 45, 90 and 135° (that is, 90 - 45, 90 and 90 + 45) intervals. Turbine entry conditions are not particularly steady. For example, the combination of exhaust pulses from cylinders 5 and 15 (45° apart) impair scavenging of cylinder 16.

The multi-entry pulse converter system tends to suit engines with large numbers of cylinders and evenly spaced firing intervals, operating at high loads. It ranks between the simple pulse converter and constant pressure systems as far as turbine admission conditions and general performance are concerned.

Currently, the original pulse converter concept of Birmann (figure 8.1) is receiving renewed interest as engine ratings continue to increase. Curtil and Magnet [21] have shown that a refined and simplified version of the Birmann device (called a modular pulse converter by Curtil and Magnet), can give excellent performance at high ratings. A schematic of the system, and details of the junction, are given in figure 8.25. The initial nozzle, fitted at each exhaust port, accelerates the flow, reducing pressure. The cross-sectional area of the main pipe is kept relatively small to maintain a high velocity, but low pressure. Thus the exhaust manifold pressure is low relative to the boost pressure, ensuring good scavenging and reducing piston pumping work. A diffuser connects the narrow main pipe to turbine inlet. Figure 8.26 compares the performance of a nine-cylinder high-speed industrial and marine engine with a conventional multi-entry system and the modular pulse converter. The comparison favours the latter, by a small margin, but the principle advantage comes from the simplicity of the exhaust manifold system (figure 8.25).

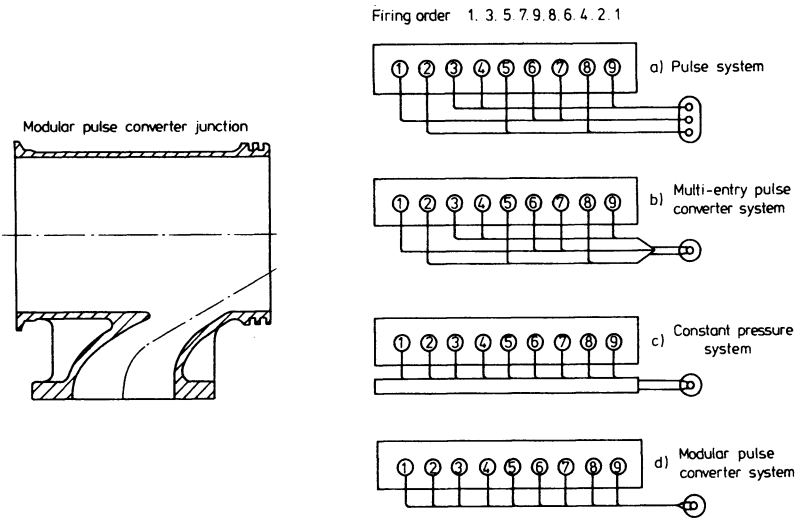

Figure 8.25 *SEMT-Pielstick modular pulse converter and pipe arrangements with various turbocharging systems on a nine-cylinder engine [21]*

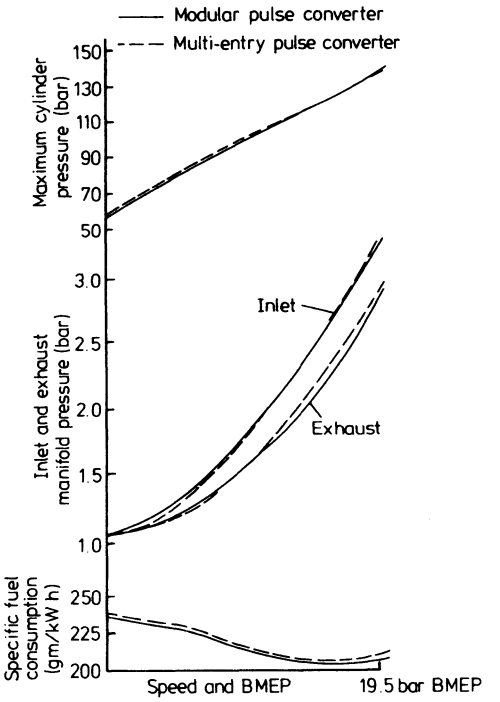

Figure 8.26 *Performance comparison between multi-pulse and modular pulse converter systems (propeller law) [21]*

8.7 Summary of Turbocharging Systems

Many of the factors influencing the choice between pulse, pulse converter and constant pressure turbocharging systems have been discussed in the previous three chapters. It remains to highlight the dominant factors and relate these to particular engine applications. In fact the choice depends primarily on the application for which the engine is designed and secondly on the over-all efficiency of the turbocharging system at the normal rating of the engine. Finally, cost and reliability are increasingly important considerations.

8.7.1 Four-stroke Engines

Most turbocharged four-stroke engines today use the pulse system, since the benefit of increased available energy at the turbine outweighs any losses in turbine efficiency relative to the constant pressure system.

From the discussion in section 6.3 and 6.4 it is evident that with constant pressure turbocharging the performance of an engine at part load is poor, suffering from reversal of flow in the scavenge period and negative pumping work. However, with increase in engine output (at constant speed) at a certain pressure level, dependent on the turbocharger efficiency and exhaust temperature, the pressure drop across the cylinders becomes positive, aiding scavenging and providing positive pumping work. With increase in exhaust manifold pressure the throttling losses at the exhaust valves are reduced, resulting in further improvement in exhaust gas energy utilisation. Thus as the engine rating increases, and hence the compressor pressure ratio rises, constant pressure turbocharging becomes more effective.

At low turbocharger pressure levels, pulse turbocharging with its efficient utilisation of the blow-down pulse and effective scavenging is superior to the constant pressure system. As the power of the engine increases, the amplitude of the blow-down pulses rises, causing stronger pulse reflections from the turbine and exhaust manifold branches. Reflected pressure waves of high amplitude (due to choking at the turbine nozzles) can cause interference with effective scavenging and a considerable increase in negative pumping work, reflected in rising specific fuel consumption. At compressor pressure ratios approaching 3:1 and above, the single-stage turbine of the turbocharger imposes limitations on the efficient use of the pulse system. The low reaction axial flow turbine (suitable for partial admission operation) capable of efficient energy conversion up to 2.5:1 expansion ratio (chapter 5), can no longer efficiently absorb blow-down pulses of approaching 5:1 expansion ratio. Thus there is a noticeable drop in turbine efficiency with further increase in engine rating. It is therefore not surprising that as pressure charging levels rise, the constant pressure system begins to look more attractive, unless two-stage turbocharging is used (chapter 11). However, the ideal three-cylinder group of the pulse system provides superior performance over the constant pressure system within wide limits. It is the inferior performance of the two-cylinder and single-cylinder groups (four, five, seven, eight, ten, fourteen, sixteen and twenty-cylinder engines) suffering from less efficient use of exhaust gas energy and inefficient operation of the turbine under partial admission conditions, which show the serious disadvantages of the pulse system in the case of highly

charged engines. However, the use of pulse converters can bring the performance of those engines in line with those of six, nine, twelve and eighteen-cylinder engines.

Figures 6.7 and 7.17 can be used to compare predicted engine performance for constant pressure operation and pulse operation with three-cylinder and two-cylinder groups. With the three-cylinder group the pulse system is clearly superior to the constant pressure system up to high pressure ratios (3:1) showing better scavenging, a pumping work gain and lower turbine inlet temperature. When pairs of cylinders are grouped (two-cylinder group), the changeover point between pulse and constant pressure superiority occurs at a much lower presure ratio, the exact point being dependent on actual turbocharger average efficiency and may lie as low as 2:1 pressure ratio. A serious drawback of the constant pressure system, of course, is the poor response of the engine to sudden load increase and speed change (see chapter 12).

In general it can be concluded that with moderately charged engines (below 14 bar BMEP) the pulse system is superior to constant pressure turbocharging. It gives a good acceleration characteristic, excellent scavenging at part load and little adverse effect on engine performance if turbocharger efficiency falls due to compressor fouling in service. At higher charging levels, engines consisting of three-cylinder groups (six, nine, twelve and eighteen-cylinder engines) and operating with the pulse system show superiority over constant pressure turbocharged variants. This means that the constant pressure system is most suitable on engines that are quite highly turbocharged and whose number of cylinders cannot be grouped in threes under the pulse system. The constant pressure system is further excluded from use in engines that must operate for long periods at part load or for vehicle applications where quick response to engine load and speed changes and good low-speed torque is required. Thus the primary application of engines for which the constant pressure system is best suited is highly rated engines that are required to run at or near their rated power output for most of their working life. However, with the progressive increase in engine ratings, where low-load operation will be relatively infrequent, the constant pressure system becomes more attractive when the performance over the whole load range is considered. Use of auxiliary aids to improve acceleration, or low load operation, broadens the use of constant pressure turbocharging. The constant pressure system may also be used on lower rated engines, where possible loss in performance is sacrificed for a cheaper, simpler and more reliable system, particularly on engines with a large number of cylinders (ten, fourteen, sixteen, twenty).

Pulse converters are used on reasonably highly rated engines that would normally be pulse turbocharged, but have unfavourable numbers of cylinders. Whether simple twin-entry or multi-entry systems are used is dependent on the spacing of exhaust processes in time. Thus a V8 engine, which has particularly difficult exhaust phasings, benefits from a pulse converter system at relatively low BMEP (figure 8.27).

8.7.2 Two-stroke Engines

The uniflow scavenged type of two-stroke engine, in which some control of the

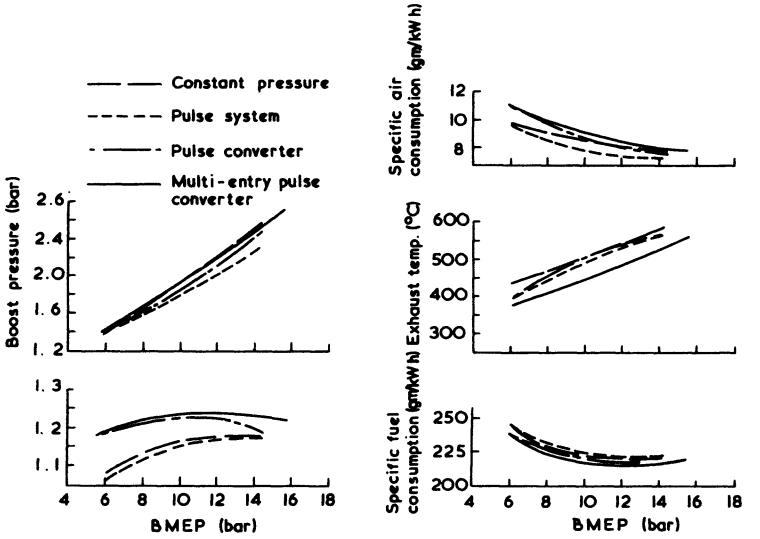

Figure 8.27 *Engine performance comparison with constant pressure, pulse and pulse converter systems: V8 engine, four-stroke [18]*

amount of energy supplied to the turbine is achieved by early opening of the exhaust valve, successfully operates with the pulse system and turbocharger alone. However, with an increase in engine rating, the loss in piston work (due to early opening of the exhaust valve) outweighs the additional work that the turbocharger is able to provide. Like the four-stroke engine, there is a cross-over point where use of constant pressure turbocharging becomes more advantageous than the pulse system. With an over-all turbocharger efficiency of 62 per cent and dependent on the engine layout and cylinder groups, the changeover point may occur as low as 12 bar BMEP. However, the use of pulse converters largely eliminates the difference in performance between engines with unfavourable numbers of cylinders (that is, 4, 5, 7, 8, 10, 14, 16) and the preferred three-cylinder groups (with 6, 9, 12, 18 cylinders).

The automotive vehicle two-stroke engine, including the uniflow scavenge type, requires assistance during scavenging (usually from an engine-driven Roots blower in series), since it has to cover a wide engine speed and load range and the efficiency of the small turbocharger is rather low (50 per cent). With scavenge assistance the constant pressure system does not seriously impede the acceleration characteristic of the engine, hence the choice of constant pressure or pulse system is mainly based on economic grounds and the simplicity and reliability of the plant. A smaller scavenge pump, better specific fuel consumption at low speed and part load operation and a better low-speed torque characteristic are the main advantages of using the pulse system. Constant pressure turbocharging provides a much simpler and more reliable exhaust manifold, especially on an engine with a large number of cylinders, and a longer life expectation of the turbocharger turbine.

The rail traction two-stroke engine also requires auxiliary air assistance at part

load and low-speed operation. Gearing of the turbocharger permanently to the engine shaft or coupling through a free-running clutch avoids the use of a separate scavenge pump. The choice of a constant pressure or pulse system is based on the same assumptions as discussed for the automotive type.

The large marine uniflow scavenged two-stroke engine with pulse turbocharging requires no scavenge pumps and represent a very efficient and simple installation. Some manufacturers however, prefer to retain under piston pumps in series with the turbocharger to ensure excellent manoeuvrability at very low speed and load (in harbour). In this application the constant pressure system is preferred, allowing greater flexibility in turbocharger installation.

In the case of the large cross and loop-scavenge marine engines operating with the assistance of under piston pumps or electrically driven fans, constant pressure turbocharging is preferred to the pulse system, to achieve a simpler exhaust installation and more efficient operation at high rated outputs.

Pulse converters can be used successfully on two-stroke engines with cylinder numbers unfavourable to pulse turbocharging. In many cases, advantage can be taken of nominally 'interfering' pressure pulses to increase the mass of fresh charge trapped in the cylinder as the exhaust closes.

References

1. R. Birmann, Exhaust energy converting means for internal combustion engines, US Patent No. 2406656 (1946)
2. R. Birmann, A look at turbocharging, *Diesel Power and Transportation* (January 1954)
3. R. Birmann, Better superchargers bring wider usage, *SAE J1* (August 1954)
4. R. Birmann, Aerothermodynamic considerations involved in turbocharging four and two cycle diesel engines, *ASME Paper 55-OGP-10* (1956)
5. P. J. Louzecky, Design and development of a two-cycle turbocharged diesel engine, *Trans. ASME*, **79** (1957)
6. De Laval Steam Turbine Co., Improvements in or relating to turbochargers for internal combustion engines, British Patent No. 797248 (1958)
7. G. Decollogny and E. Meier, Considérations sur les écoulements non-stationnaires dans les collecteurs d'un moteur diesel suralimente et leurs aspects pratiques, *J. Soc. Ing. Auto.*, **35**, No. 8/9 (1962)
8. H. Petak, Erfahrungen mit einfachen Pulse convertern an viertakt Dieselmotoren, *MTZ*, **25**, No. 5 (1964); English translation: *Sulzer Tech. Rev.*, Research Number (1966)
9. M. S. Janota, D. H. Taylor and N. Watson, Application of pulse converters to two-stroke diesel engines, *Gas and Oil Power*, No. 746 (1968)
10. M. S. Janota and N. Watson, Pulse converters – a method of improving the performance of the turbocharged diesel engine, *Proc. Inst. Mech. Engrs*, **187**, No. 51 (1973)
11. E. Meier, The application of pulse converters to four-stroke diesel engines with exhaust gas turbocharging, *Brown Boveri Rev.*, **55**, No. 8 (1968)
12. G. Zehnder, Pulse converters on two-stroke diesel engines, *Brown Boveri Rev.*, **55**, No. 8 (1968)
13. N. Watson and M. S. Janota, Non-steady flow in an exhaust system with a pulse converter junction, Paper 27, Conference on Unsteady Flow, University of Salford, 1971.

14. N. Watson, Pulse converters for turbocharged diesel engines, Ph.D. Thesis, University of London, 1970
15. T. Nakada and M. Yumoto, The exhaust pipe system of supercharged diesel engine, *IHI Engng Rev.*, **6**, No. 2 (1973)
16. S. K. Sinha and D. W. H. Tennant, Discussion of reference 10 above
17. N. Watson and B. S. Holness, Engine and turbocharger interaction with multi-entry pulse converters, Paper C65/78, Turbocharging and Turbochargers Conference, Inst. Mech. Engrs (London, 1978)
18. E. Meier, Development of exhaust-gas turbochargers and pressure charging systems for diesel engine with high mean effective pressures, *Proc. CIMAC* (1973) paper 2
19. Y. Takemoto, Supercharging systems on four-stroke medium speed diesel engine, I.S.M.E. (Tokyo, 1973)
20. G. Zehnder and E. Meier, Exhaust gas turbochargers and systems for high-pressure charging, *Proc CIMAC* (1977) paper 8
21. R. Curtil and J. L. Magnet, Exhaust pipe systems for high-pressure charging, Paper C50/78, Turbocharging and Turbochargers Conference Inst. Mech. Engrs (London, 1978).

9

Charge Cooling, the Inlet and Exhaust Systems

9.1 Charge Cooling

The principal reason for turbocharging is to increase the power output of an engine without increasing its size. This is achieved by raising the inlet manifold pressure, hence increasing the mass of fresh air drawn into the cylinders during the intake stroke and allowing more fuel to be burnt. However, it is impossible to compress air without raising its temperature unless the compressor is cooled. Since the objective is to raise the density of the air, this temperature rise partly offsets the benefit of increasing the pressure, since

$$\rho = P/RT \tag{9.1}$$

The objective must therefore be to obtain a pressure rise with a minimum temperature rise. This implies isentropic compression (figure 9.1) in which case the temperature rise will be given by the equation

$$\Delta T_s = (T_2 - T_1)_s = T_1 \left[(P_2/P_1)^{(\gamma-1)/\gamma} - 1\right] \tag{9.2}$$

Unfortunately due to inefficiencies in practical compressors, the actual tem-

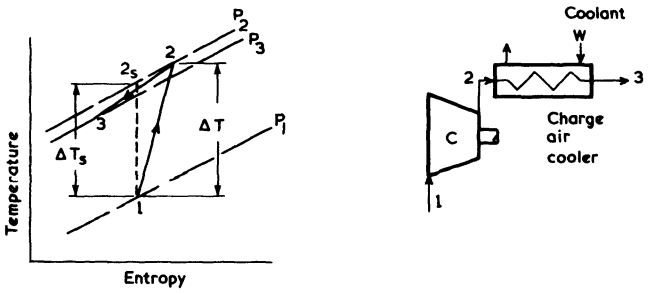

Figure 9.1 *Charge air cooling, with a pressure loss*

perature rise will be greater than that given by equation 9.2. In terms of the isentropic efficiency of the compressor (η_c) it will be given by

$$\Delta T = T_2 - T_1 = (T_2 - T_1)_s/\eta_c = T_1 \left[(P_2/P_1)^{(\gamma-1)/\gamma} - 1\right]/\eta_c \tag{9.3}$$

The more efficient the compressor, the closer the temperature rise approaches the isentropic temperature rise (figure 9.1).

Denoting states 1 and 2 as the inlet and outlet to the compressor, and using equations 9.1 and 9.3

$$\rho_2 = P_2/RT_1 \left\{1 + \left[(P_2/P_1)^{(\gamma-1)/\gamma} - 1\right]/\eta_c\right\} \tag{9.4}$$

or

$$\rho_2/\rho_1 = (P_2/P_1)/\left\{1 + \left[(P_2/P_1)^{(\gamma-1)/\gamma} - 1\right]/\eta_c\right\} \tag{9.5}$$

Equation 9.5 is plotted in figure 9.2 for a range of pressure ratios and compressor efficiencies. Several points emerge. Firstly, the benefit obtained by raising inlet manifold pressure is reduced substantially due to the temperature rise in the compressor, which itself is dependent on compressor efficiency. Secondly, the advantage of high compressor efficiency in helping to hold the boost temperature down is relatively small, but worthwhile. Thirdly, in absolute terms, the benefit that can be obtained by cooling the compressed air back to near ambient conditions is substantial, and increases with pressure ratio. Clearly it is attractive to try to cool the air between compressor delivery and the intake to the cylinders.

A further advantage of charge cooling is that the lower inlet temperature at the cylinders will result in lower temperatures throughout the working process of the engine (for a specified BMEP) and hence reduced thermal loading. Figure 9.3 illustrates the compressor outlet temperature variation with pressure ratio and compressor efficiency for a typical inlet condition. In terms of delivery temperature, the benefit of correctly matching the turbocharger such that the

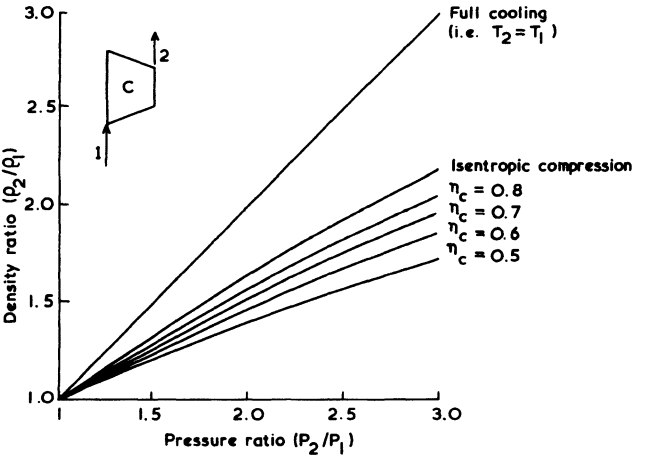

Figure 9.2 *Effect of compressor efficiency on air density in the inlet manifold*

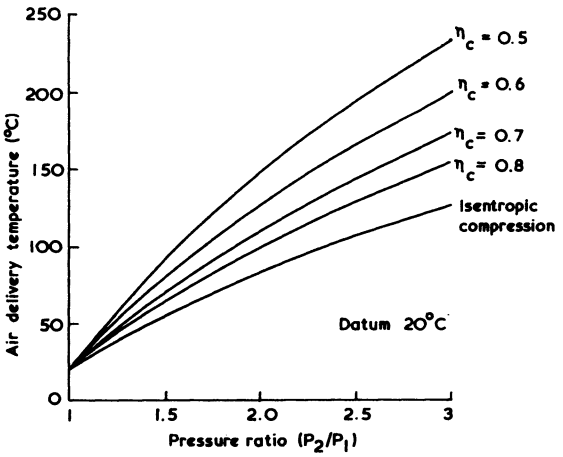

Figure 9.3 *Effect of compressor efficiency on charge air temperature*

operating line of the engine falls in an area of high efficiency on the compressor map is clear.

By using a charge air cooler after the compressor and before the intake to the cylinders (aftercooling), the density of the air entering the cylinders will be increased, enabling more fuel to be burnt. The reduction in temperature achieved by the cooler will be a function of the temperature of the cooling medium available and the effectiveness of the cooler, the latter being expressed as

$$\epsilon = \frac{\text{actual heat transfer}}{\text{maximum possible heat transfer}}$$

For a perfect gas this is equivalent to

$$\epsilon = (T_2 - T_3)/(T_2 - T_w) \tag{9.6}$$

The effectiveness (ϵ) is sometimes called the thermal ratio. From equation 9.6 it is evident that the effectiveness and the temperature drop between the 'hot' air inlet and the 'cold' cooling medium govern the extent of cooling achievable. Clearly the cooling medium should be as cold as possible, hence a supply of cooling water at ambient temperature will be more useful than the cooling water system of the engine.

From equation 9.6 the inlet temperature to the cylinders is given by

$$T_3 = T_2(1 - \epsilon) + \epsilon T_w \tag{9.7}$$

From equation 9.3 this becomes

$$T_3 = T_1\{1 + |(P_2/P_1)^{(\gamma-1)/\gamma} - 1|/\eta_c\}(1 - \epsilon) + \epsilon T_w \tag{9.8}$$

Equation 9.8 has been plotted with a range of values for cooler effectiveness in figure 9.4, for fixed values of compressor efficiency and cooling water temperature. Both the benefit from high effectiveness and the over-all benefit of aftercooling can be seen from figure 9.4 and by comparison with the $\eta_c = 0.7$ line in

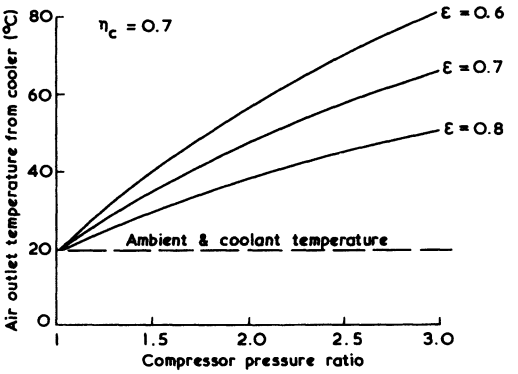

Figure 9.4 *Intercooler effectiveness and inlet manifold temperature*

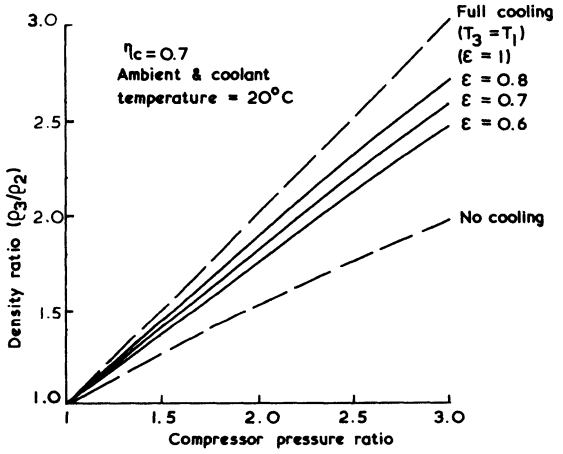

Figure 9.5 *Effect of charge cooling on inlet air density*

figure 9.3. In figure 9.5 the effect on density ratio is shown. Compared to the uncooled case, in which the temperature rise in the compressor offsets about half of the benefit due to increased pressure, the cooler enables all but about 20 per cent of the pressure rise to be used.

Poor compressor efficiency will increase the air temperature entering the cooler (figure 9.3) and therefore raises the temperature difference (T_2 - T_W) in equation 9.6. It follows that the aftercooler partially offsets the effect of a low compressor efficiency in terms of temperature, but not pressure, for a certain work input.

The advantages of charge cooling are clear, but although the technique is commonly used (particularly on highly rated engines), it is not universally adopted. Aftercooling does have some disadvantages. From the fluid dynamics point of view, one problem is that air flow through the cooler results in a pressure loss, since narrow flow passages are required for effective cooling. This will

result in some offset against the density increase from cooling (figure 9.1). The pressure drop through an intercooler will be a function of its size and detail design. A very large intercooler will be awkward to install on an engine, may cost more than a compact one, but will probably have a higher effectiveness, and low pressure loss. The loss in pressure is usually expressed as a function of the dynamic head of the inflowing air

$$\Delta P_{cool} = K_1 \rho C^2/2$$

where K_1 is approximately constant. Since $\dot{m} = \rho AC$ and $\rho = P/RT$

$$\Delta P_{cool}/P_2 = K_2 [\dot{m}\sqrt{(T_2)}/P_2]^2 \tag{9.9}$$

where K_2 is a constant.

Typical effectiveness and pressure loss characteristics for a charge air cooler are shown in figure 1.15.

The second disadvantage is a more practical problem. A source of cold air, or preferably water (due to its higher heat transfer coefficient), must be available. This may be easy to arrange, (for example in marine applications) but is not always possible. If the boost pressure is low and the available coolant relatively warm (such as the cooling water system of the engine) charge cooling will produce only marginal benefit and at full power only. A third disadvantage will be cost, but the benefits of charge cooling will outweigh the additional cost on all but low-rated engines. Finally, excessive charge cooling can cause condensation in the inlet manifold.

Air-to-air (figure 9.6a) charge cooling may be adopted in locations where a cooling water supply is not available, and high ambient temperatures make installation of a local closed system unattractive. In these cases, radiator cooling of the engine oil and water cooling system is usually arranged, directly behind a remote air-to-air charge cooler. Very large coolers may be used since the spatial limitations imposed when mounting a cooler directly on the engine are removed. Thus a very high effectiveness (up to 0.95) may be achieved, with consequent benefits in engine performance.

An interesting alternative air-to-air charge cooling system for vehicle engines uses bleed air from the turbocharging system to drive the cooling air supply fan (figure 9.6b). Around 5 to 10 per cent of the air flow through the compressor is used to drive an impulse-type turbine, built around the circumference of a fan. The fan delivers atmospheric cooling air for the charge cooler. [1] The advantage of the system is that cooling air flow tends to increase as it is required by the engine, but matching is a complex process.

Air-to-water cooling systems can use the normal water cooling system of the engine (figure 9.6c) or a separate closed water cooling system with its own water-to-air radiator (figure 9.6d). The advantage of the former system is simplicity of installation, but cooling is limited by the high water temperature (typically around 90 °C). Indeed charge air heating is likely to occur at low speed and low load. The indirect system shown in figure 9.6d has a greater cooling potential, since the water temperature can be set lower than that of the normal engine cooling system, is more compact on the air side than system 'a', but involves the expense of two heat exchangers.

A comparison of engine performance with the two most compact systems

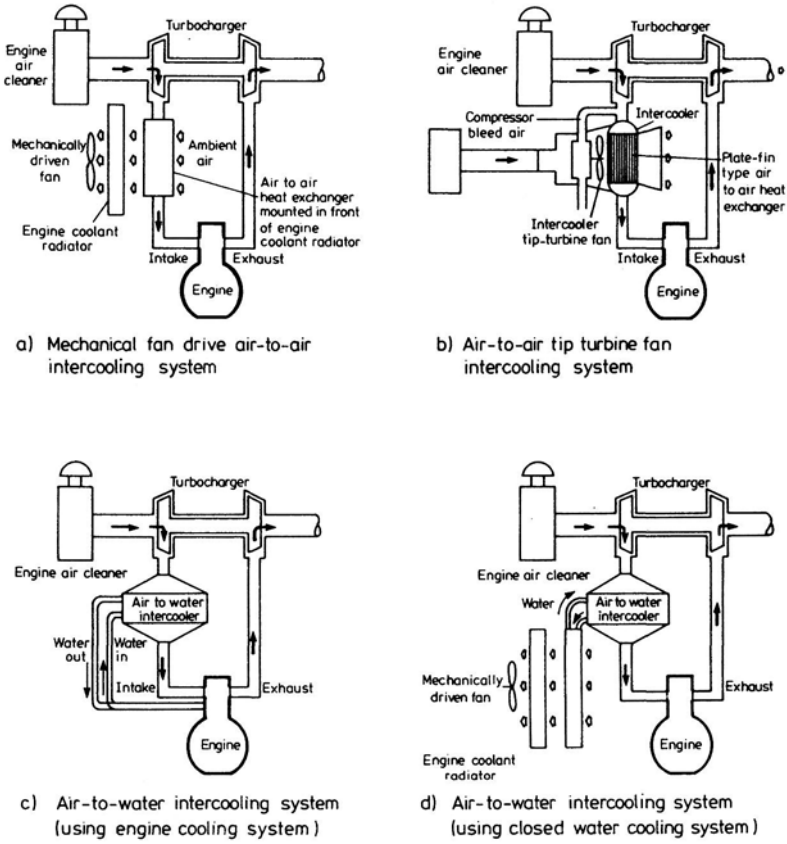

Figure 9.6 *Types of charge air cooling systems (adapted from McLean and Ihnen [2])*

(system b, air-to-air tip fan and system c, air-to-water, engine coolant) is given in figure 9.7. The air-to-air system shows a clear benefit in achieving a lower cylinder intake air temperature due to the lower temperature of the coolant, and the consequent benefit in engine performance.

9.2 The Design of Charge Coolers

If the charge cooler is mounted on the engine, it must be designed as an integral part of the engine to keep the air pipe lengths compact, and some compromise between size (hence cost) and cooling capacity must be achieved. The design will therefore be tailored to a particular engine.

Since the cooler will be mounted on a vibrating engine and must withstand the delivery pressure of the compressor it must be robust. Service life and maintenance periods must not be less than those of the basic engine, particularly with respect to performance deterioration due to fouling on the cooling water or air side. Compactness is important on the majority of installations, particularly

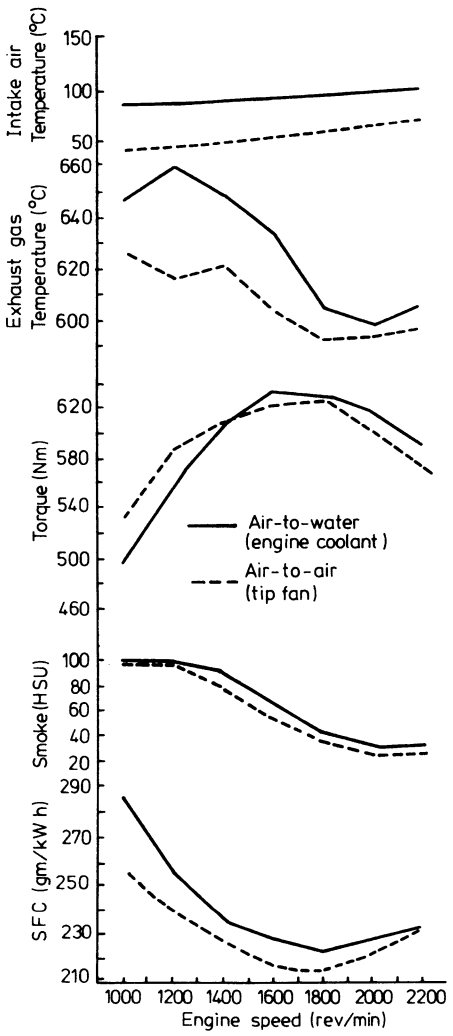

Figure 9.7 *Comparison of engine performance with ambient air and engine water as the coolant [2]*

on high speed engines where the mass flow rate of air is large relative to the size of the basic engine. Clearly the design will be a compromise between cooling capacity and its benefit in engine power and efficiency together with pressure loss, size and cost.

In designing a heat exchanger the two most important parameters to consider are the heat transfer rate between the air and coolant and the pressure drop due to fluid friction. The latter will be most important on the gas side, since it affects charge density, but cannot be ignored on the coolant side since power will be required for coolant circulation. The coolant will be water or air. The high heat transfer coefficient of water means that the pressure drop on the water side is unlikely to be large in a sensibly designed unit. However, if ambient air is to be

the coolant, it is easy to expend considerable energy due to mechanical pumping power overcoming friction in the core of the heat exchanger. Since mechanical energy obtained from heat is achieved by a process of low over-all efficiency, this must be avoided.

The heat transfer rate per unit surface area will increase with the fluid velocity, but at a rate that is somewhat less than the first power of velocity. In contrast, the power required to overcome friction will increase by something approaching the cube of velocity. It follows that to reduce the pressure loss through the cooler, the number of flow passages (and therefore flow area) can be increased reducing the pressure loss by a much greater margin than the accompanying loss in heat transfer rate per unit area due to lower velocities. The pressure drop relationship forces the designer to aim for low velocities. Since the thermal conductivities of gases are low (relative to liquids) the combination of the above two factors results in a low heat transfer rate per surface area on the air side (or sides). Typically an air-to-air heat exchanger will require about ten times the surface area of a comparable water-to-water cooler (that is, for the same heat transfer rate and pumping power [3]). Two results follow. Firstly, an air-to-air cooler will be substantially larger than a water-to-water cooler with the equivalent cooling effect and coolant inlet temperature. Secondly, an air-to-water cooler will benefit from a much larger heat transfer area on the air side than the water side. This latter requirement can be met by using fins on the gas side – figure 9.8 which illustrates the range of common heat exchanger surface configurations. The arrangements with one secondary surface (fins on gas side only), typical of air-to-water coolers are shown in the centre, while those with two secondary surfaces, suitable for air-to-air cooling, are shown on the right. The coolers without primary surfaces are more suitable for liquid-to-liquid cooling and would be too bulky for charge cooling. Note that in the tubeless monopack system (air-to-air), the gases need not always cross at right-angles (each in its own layer

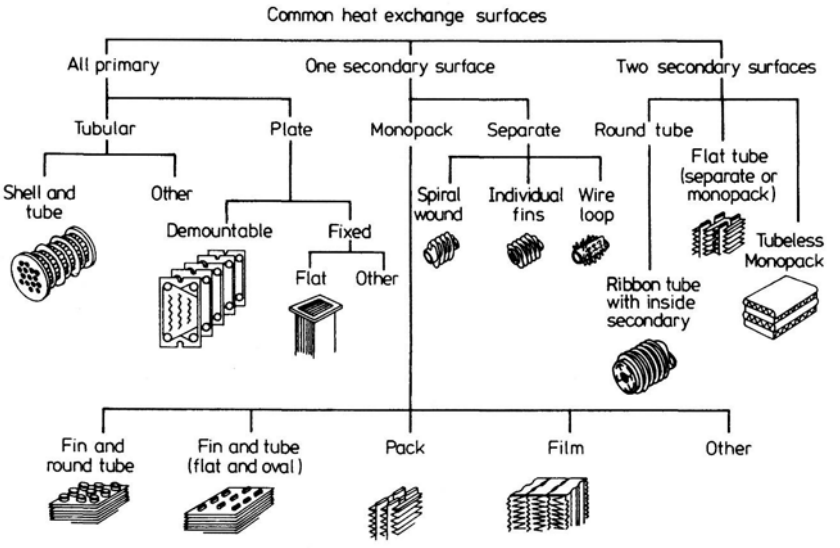

Figure 9.8 *Common heat-exchanger surfaces [4]*

of the sandwich) as shown. It should be mentioned that the build-up of a thick boundary layer will adversely affect the conductance. It follows that it is sensible to interrupt the surfaces to break up the boundary layers even at some penalty in increasing pressure loss. Curved or wavy passages can be used, but a most effective way is to arrange the gas flow to be normal to the tubes so that a new boundary layer builds up on each tube.

Most charge coolers use water as the cooling medium and therefore require a secondary surface (fins) only on the air side. The source of water will affect the design. Three sources may be considered: raw water from the sea or a river, water from a separate closed cooler system and water from the cooling system of the engine. When 'raw' water is used the major problems that occur are due to fouling and corrosion. Thus the material selected for the water tubes and jackets must have good corrosion resistance. [4, 5] It is important that the water is adequately strained to prevent ingress of mud and gritty material, and that ease of cleaning is considered at the design stage. If gradual fouling goes undetected it is quite possible for the engine to become significantly overloaded thermally. Naturally the larger the tubes the likelihood of blockage is less, but a penalty is paid since the cooler will be less compact. Generally however, larger tubes are required when using raw water than would be the case if a closed water circuit were used. Little fouling will occur if a closed circuit cooling water system is used and reasonable preventive measures are taken.

Fouling is also a problem on the air side since a build-up of dirt increases the pressure loss through the cooler and reduces the heat transfer. A small amount of dirt on the fins has little effect, but in time, it does tend to build up, often aided by the ingestion of oil mist. Eventually the build-up can result in complete bridging (blockage) across the cooling fins. It is unfortunate that washing of the turbocharger compressor by water injection can result in dirt being deposited in the cooler. On large industrial engines the cooler should be designed for regular cleaning without removal from the engine. These coolers are therefore frequently designed such that the heat transfer matrix may be removed while the casing remains in position. Steam, or compressed air, cleaning is then relatively easy. In other designs it is simple to remove the side walls for access. Of course, due to the air filtration requirement of the engine, the amount of dirt build-up will vary greatly from one engine type to another.

If an air-to-air charge cooler is used then two secondary surfaces may be required and dirt may build up on either. On the air coolant side, unfiltered air may result in rapid blockage if the air inlet is near a dusty environment. Usually though, maintenance is relatively easy and fouling is evident without any dismantling being necessary.

There are several conflicting requirements when installing a charge cooler on an engine. If an air-to-air cooler is to be used it will usually be mounted slightly remote from the engine (in front of the cooling water radiator on a truck) where space is available. A penalty is paid in that the volume between compressor and cylinders is large, affecting transient response. If an air-to-water cooler is used, this will usually be mounted on the engine so that the unit becomes a compact package. Pressure then exists to keep the charge cooler as small as possible, but some compromise is required between size, effectiveness, pressure loss and fouling resistance. Usually on very large engines separate coolers may be mounted below each turbocharger at the side of the engine. On medium-speed engines the coolers will be mounted adjacent to each turbocharger, usually at the end of

the engine. On smaller engines a single turbocharger and cooler will be used, the latter being mounted almost anywhere convenient on the engine. Small automotive-size engines, which are produced in large numbers, can usually justify specially designed coolers, the housing often being a casting including the inlet manifold. Several typical installations are shown by Forbes and Hampson. [6] The inlet duct design is important since the cooling effect is considerably reduced when the air flow is unevenly distributed. For even distribution, the inlet system must be planned with care and the flow resistance in local bends must be lower than that through the cooler. Installation problems become particularly severe on highly rated high-speed engines, since the required cooling area increases with mass flow rate.

9.3 Charge Air Cooling and Engine Performance

The effect of charge cooling is to increase the density of the air entering the cylinders for a certain boost pressure. The relationship between charge cooler effectiveness, coolant temperature, pressure ratio, compressor efficiency and charge density has been derived in section 9.1. It remains to look at the effect on over-all engine performance. It is the effect of charge cooling on power output and efficiency within the constraints of specified maximum cylinder pressure, thermal loading and exhaust temperature limits, that is of interest.

For a constant power output, charge cooling will reduce charge temperature and hence thermal loading. Alternatively, since the charge density increases with aftercooling, more fuel can be burnt raising the power output in proportion to the density (all other factors being assumed equal). The additional cost of the intercooling equipment is offset by this higher power output. Thus, from figure 9.5, the use of an aftercooler of 0.7 effectiveness permits an increase of power output from 1.55 to 1.82 times the naturally aspirated power output at a 2:1 pressure ratio. At a 2.5:1 pressure ratio the increase is from 1.76 to 2.20 times the naturally aspirated power output. However, in practice thermal loading or other factors limit the increase.

Consider first engine performance with and without a charge air cooler, with no change in maximum fuelling. Results computed for an engine operating over a wide speed range are shown in figure 9.9. Intercooling obviously reduces inlet manifold temperature substantially and this effect is followed right through the cycle, lowering heat transferred to the cylinders. Air flow increases, weakening the air/fuel ratio which in turn reduces the turbine inlet temperature. The latter results in a drop in specific energy at the turbine, hence boost pressure will also reduce, but not enough to offset the density gain due to the lower charge temperature. The combined effects of weaker air/fuel ratio, reduced heat transfer to combustion chamber walls (due to lower gas temperature) and changes in ignition delay and combustion rate, lead to a reduction of specific fuel consumption of nearly 6 per cent. The gain in BMEP will be the same. However, both improvements will occur largely at low engine speeds, since the charge air cooler is most effective at low air flows (figure 1.15).

Figure 9.10 shows the over-all match superimposed on the compressor characteristic, illustrating that charge air cooling moves the operating regime

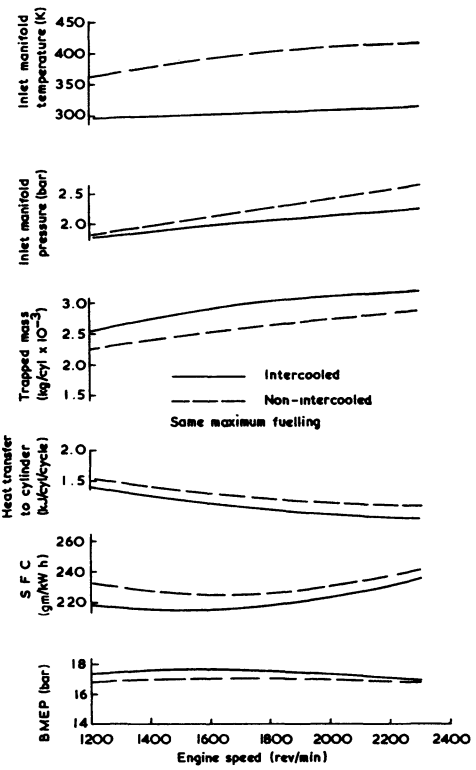

Figure 9.9 *The effect of intercooling on engine performance (with no change in fuelling)*

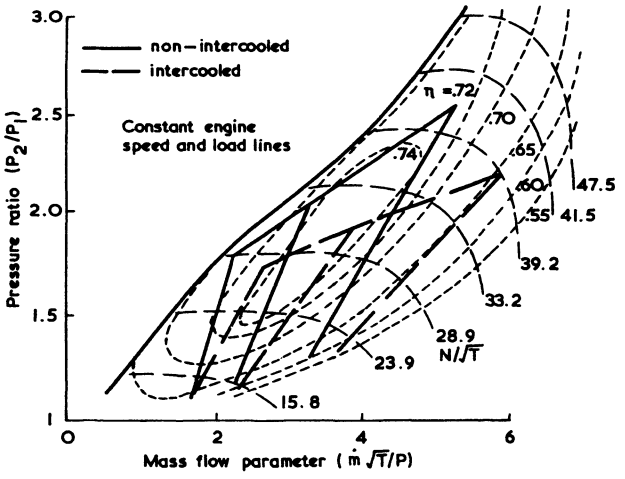

Figure 9.10 *Comparison of intercooled and non-intercooled engine operating maps on compressor characteristic*

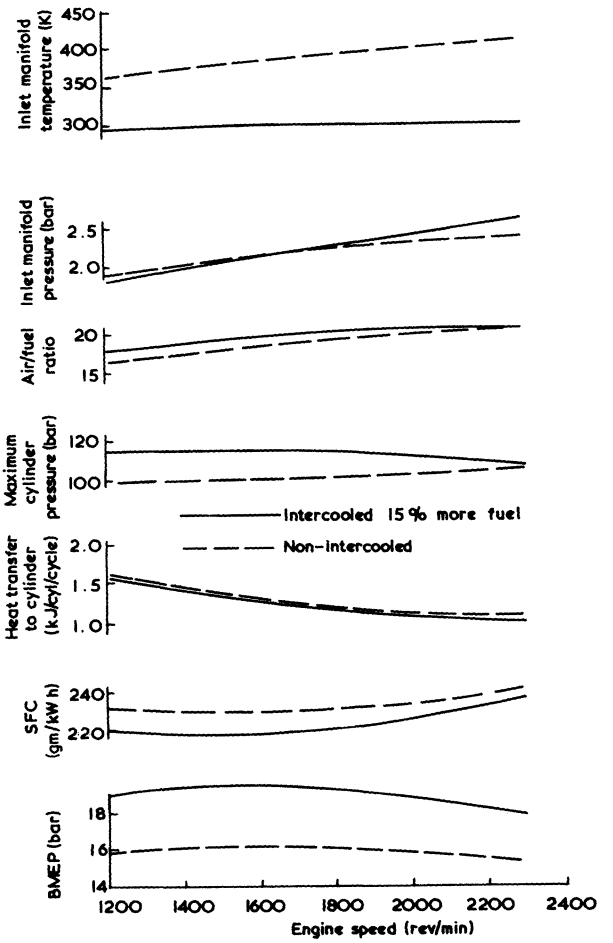

Figure 9.11 *The effect of intercooling on engine performance (increased fuelling)*

away from the surge line. Constant speed engine operating lines tend to run more nearly parallel to the surge line, which may ease the problem of matching in many applications. However, the over-all air flow characteristic for a variable-speed engine does widen, hence matching could be more difficult in this particular application.

Consider next the more realistic situation in which advantage is taken of charge cooling to increase fuelling, although not to the extent that the minimum air/fuel ratio returns to its previous value (figure 9.11). Again with no change in turbocharger match, BMEP increases from 16 to 19.5 bar (22 per cent) and specific fuel consumption is reduced by 6 per cent (largely due to indicated power increasing, but not engine friction). These results are obtained with fuelling adjusted to achieve no increase in thermal loading of the combustion chamber. However, the maximum cylinder pressure has risen from 105 to 118

bar (12.5 per cent). In this particular test, increased air flow through the compressor has moved the characteristic point at full power to an area of lower compressor efficiency. Thus air/fuel ratio at full power is much the same with and without the charge cooler.

Analysis of these results shows that charge cooling enables substantial power increases to be achieved without increasing thermal loading. Specific fuel consumption may also benefit due to the increase in power developed in the cylinder without a corresponding increase in engine frictional losses, and the weaker air fuel ratio. The obvious problem is that the maximum cylinder pressure rises with power output, though fortunately not linearly.

If two-stage turbocharging is adopted then both interstage and aftercooling may be used. Since the temperature rise per stage will be a function of stage inlet temperature, intercooling reduces the high-pressure compressor work. Thus interstage cooling has the two-fold benefit of reducing inlet manifold temperature and compressor work. The disadvantages are the large size of heat exchanger required to achieve significant interstage cooling, since the air inlet temperature from the first stage will not be particularly high. Thus a large cooler is required. Use of a small intercooler of consequent low effectiveness and high air side pressure loss will be counter-productive.

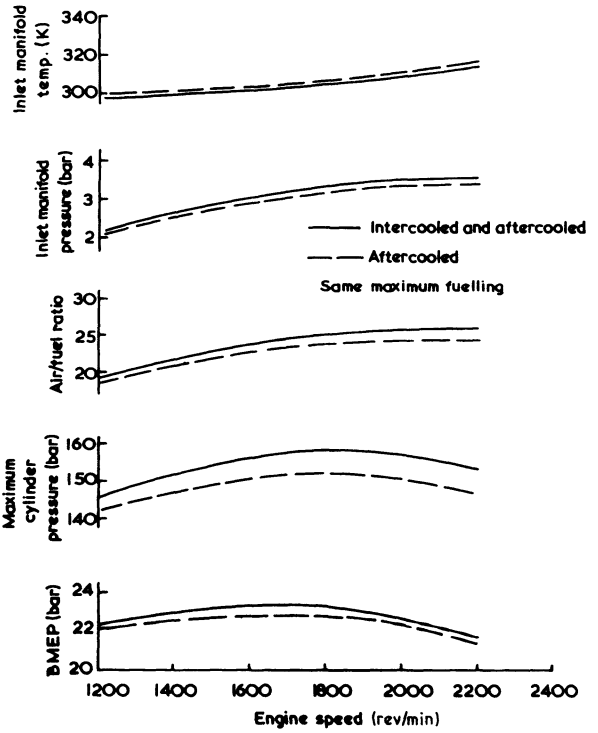

Figure 9.12 *The effect of interstage cooling on two-stage turbocharged engine performance*

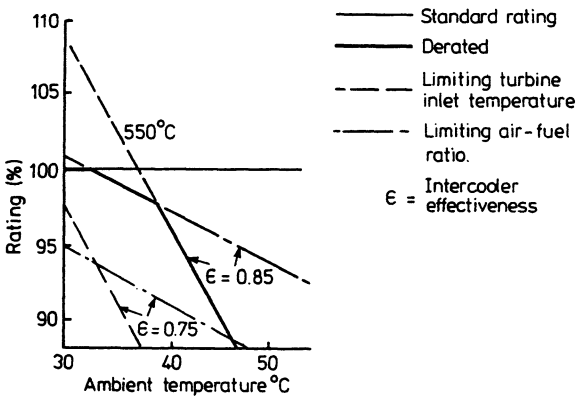

Figure 9.13 *Intercooler effectiveness and engine rating [7]*

Figure 9.12 compares predictions of full load engine performance with a two-stage aftercooled engine with and without an interstage cooler, with no change in maximum fuelling. A reasonably large cooler is used, having an effectiveness of 0.8 at full power. Interstage cooling raises BMEP by 1.5 per cent and reduces specific fuel consumption by the same amount. The large rise in peak cylinder pressure is partly due to changes in combustion rate. By taking full advantage of the situation and increasing fuelling to achieve the same air/fuel ratio, the gain in power output would be 12 per cent.

The necessity for achieving high cooler effectiveness has been illustrated in terms of its controlling influence on inlet manifold air density (figure 9.5). Figure 9.13 shows how the rating of a charge cooled medium-speed four-stroke engine is governed by the effectiveness of the cooler. If the rated power is limited by minimum air/fuel ratio up to a turbine inlet temperature of 550 °C and by the temperature thereafter, an increase in effectiveness from 0.75 to 0.85 allows power to be raised by between 6 and 10 per cent, dependent on the ambient temperature.

The benefits of intercooling are quite clear. Whether it is used in practice will depend on the availability of a coolant at a low temperature and economic considerations. In terms of the latter it is usually found that intercooling is fully justified on all reasonably high-rated engines. Often, for economic reasons, manufacturers will wish to offer a range of power outputs all based on one basic engine design. It may be convenient to offer three ranges based on a naturally aspirated, turbocharged and turbocharged plus aftercooled versions. Since mechanical and thermal loadings will be greater in the higher-power versions, the naturally aspirated version may be rather over-designed, but the economics of producing more engines of a single basic design may offset the extra cost.

9.4 The Inlet System

The charge cooler must be an integral part of the inlet system of the engine and, because of its importance, it has been discussed in detail. However, the remainder

of the system, comprising the air filter, inlet ducting and manifold, is also important. The first two will influence the over-all performance due to the pressure drop resulting from the air flow through them. The design of the inlet manifold may influence the distribution of air between the cylinders and, together with the intake ducting, may affect the likelihood of compressor surge occurring.

An inlet duct before the air cleaner is often used in marine and stationary applications, to bring outside air into the engine room. Sometimes silencers are placed in the inlet duct. Naturally the duct should be as straight and free-flowing as possible resulting in a pressure loss of less than 0.005 bar although a greater loss may have to be accepted if space is a major factor. The air cleaner will be particularly important on small engines, its filtering requirement being determined by engine wear and contamination rather than by turbocharger or intercooler fouling. On larger engines, fine filtration is not necessary although some build-up of dirt in compressor and cooler occurs. Usually industrial turbochargers are supplied complete with an air filtration system, although this will be as much a silencer as a filter (see chapter 14). It is the pressure drop through the filter on a small engine, and in particular its increase with use, that dominates the intake pressure loss. It is difficult to build filters to trap sufficiently small particles to prevent engine wear without introducing large pressure drops, and still achieve high noise reduction, all in a small size. The subject is discussed by Sherburn, [8] Wadman [9] and others, but the immediate concern is to establish the effect of pressure loss on engine performance.

The effect of a specific intake restriction will vary from engine to engine since it depends on whether the consequent mass flow reduction results in a decrease or increase in the compressor efficiency. This, in turn, depends on where the operation lines of the engine lie on the compressor map. Intake restriction will reduce mass flow rate; this will often result in an increased efficiency but the surge margin (the distance from the surge line on the compressor map) will be reduced. Figure 9.14 shows that a turbocharged engine can be rather insensitive to inlet system pressure loss. In practice what happens is that the pressure loss

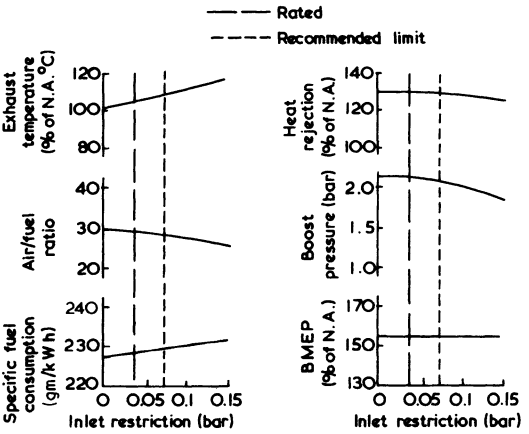

Figure 9.14 *Influence of inlet restriction on engine performance [10]*

increases between services as the filter gradually blocks. The air flow rate is reduced, but since the fuel system remains untouched, the air/fuel ratio is reduced. Exhaust temperature increases the specific turbine work, hence compressor pressure ratio rises slightly, partially offsetting the pressure loss. Thus the absolute inlet manifold pressure falls by less than the expected amount. A high exhaust temperature and a smokey exhaust will eventually result if the pressure loss becomes substantial. For an automotive engine an intake pressure loss of less than 0.04 bar is desirable, allowing for double this as the filter becomes dirty in service.

The intake manifold, between compressor and engine must be sufficiently large to damp down the pressure fluctuations caused by the intermittent intake processes of the cylinders. If it is too small then manifold pressure will reduce towards the end of each induction process, and since the turbocharger maintains an almost constant speed, the compressor may surge. The volume of inlet manifold required, relative to the swept volume of the engine, will reduce with increasing numbers of cylinders, and will be more critical with a two-stroke engine than a four-stroke. Usually, a compromise is reached between the effects of pressure fluctuation and installation and engine maintenance difficulties resulting from bulky manifolds. In addition, a large inlet manifold significantly slows the response of a turbocharged engine when acceleration is required or load changes occur. A particularly serious situation can result from a rather tortuous path to one cylinder. This situation tends to occur on a vee engine when auxiliary equipment is installed between the vee near the front of the engine, resulting in a restricted passage to the two front cylinders. Since the nominal fuel distribution between cylinders is equal, the air flow restriction effectively reduces the air/fuel ratio in those cylinders. The result may be a smoke or even thermal loading problem.

Actual inlet manifolds tend to take the form of ducts or pipes rather than large volumes. As a result pressure wave effects induced by the intake process can be amplified. It is these pressure waves that can cause surge when the 'mean' mass flow rate lies above the 'steady state' surge value. In terms of mass flow rate measured at the air intake, usually with a damping chamber in the system, the effective surge line appears to have moved to the right on the compressor map. The problem is usually the result of the frequency of the intake pulses exciting several natural frequencies of the 'air column' in the intake pipes, or receiver (figure 9.15) and seems to occur most frequently on medium-speed

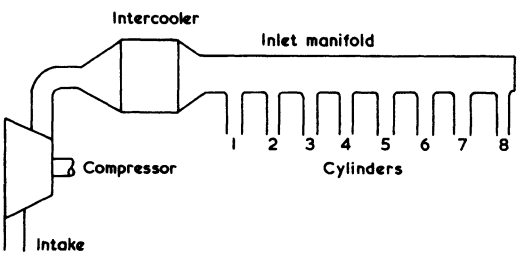

Figure 9.15 *Typical intake system on an in-line eight-cylinder engine*

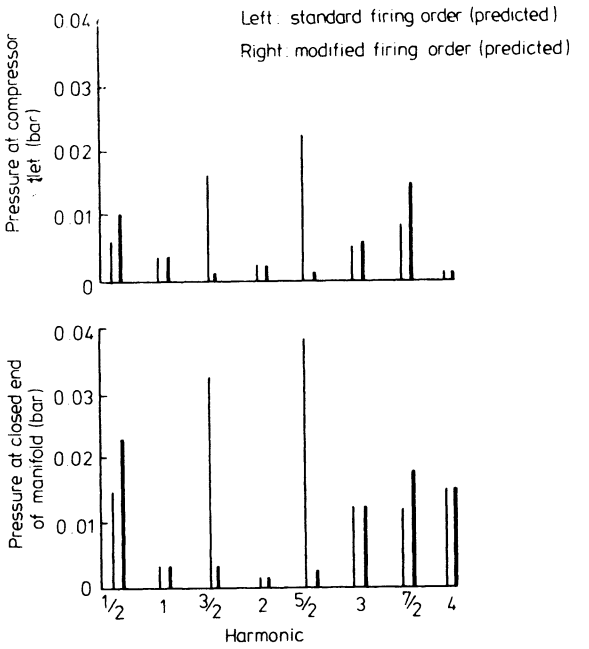

Figure 9.16 *Partial amplitude of pressure wave harmonics in the inlet manifold of an in-line eight-cylinder engine [13]*

four-stroke engines. It is possible to calculate the pressure wave action using the method of characteristics [11] or the concept of impedance. [12]

Generally the intake pipes are designed to be as short as possible, and little scope is available for altering the receiver length to tune out an undesirable natural frequency. A change to a larger cross-sectional area of the receiver will always help reduce the amplitude of the pressure waves. If the problem persists or no room is available to increase the volume of the receiver, then damping orifices can be inserted. These will, of course, create an undesirable pressure loss if they are small enough to be effective and are therefore a last resort. It is often better to connect the air inlet pipe to a position near the centre of the receiver, and this can sometimes reduce the transmission of pulsations to the compressor. The arrangement is commonly used on vee engines. The pressure pulse interference can be particularly bad when certain firing orders are used, which must be remembered at the early design stages. For example, Meier [13] shows the partial amplitudes of the harmonic pressure pulsations in the intake of an eight-cylinder engine with alternative firing orders (figure 9.16), firing order 1 being 1-7-4-6-8-2-5-3 and firing order 2 being 1-2-4-6-8-7-5-3. In the latter case, the large partial amplitudes of the 3/2 and 5/2 harmonics have been eliminated, an improvement that would undoubtedly widen the effective operating range of the compressor and result in more even inflow into the cylinders.

An important conclusion may be drawn at this stage, namely that the surge line shown on the turbocharger compressor performance maps is, of necessity,

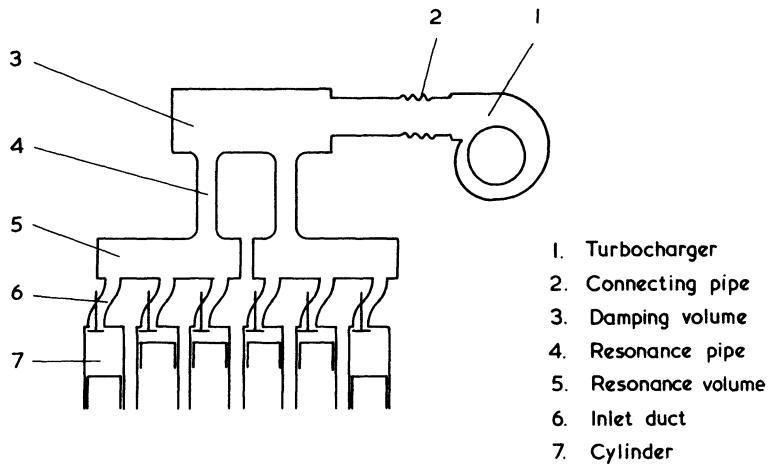

Figure 9.17 *Dynamic charging of the intake system on a turbocharged engine [14]*

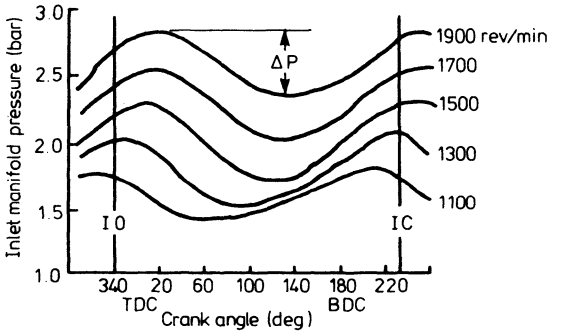

Figure 9.18 *Intake manifold pressure variation during the intake process with dynamic charging [15]*

only a guide. The position of the effective surge line, when the compressor is fitted to an engine, will depend on the individual installation.

It is difficult to use the pressure wave action in the intake manifold, to aid filling of the cylinders, without causing compressor surge. However, figure 9.17 illustrates a system in which tuned volumes and resonance pipes (Helmholtz resonator) are used to increase the effective volumetric efficiency at low engine speeds. The intake system is split, according to the firing order, so that the two delivery ports of the damping volume experience pressure fluctuations that are exactly out of phase. Thus the damping volume need not be large.

Figure 9.18 shows instantaneous pressures in the resonance chambers during the period when the inlet valve is open, at different engine speeds. High pressures are generated shortly after the valve opens and before it closes, but the effects are delayed as speed increases. The high pressure developed as the valve closes

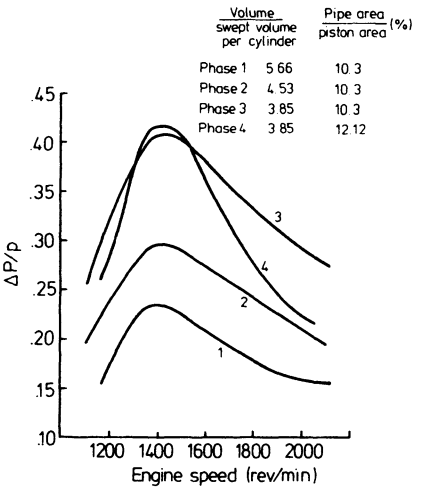

Figure 9.19 *Effect of resonant volume and resonant pipe diameter of the amplitude of inlet manifold pressure variation [15]*

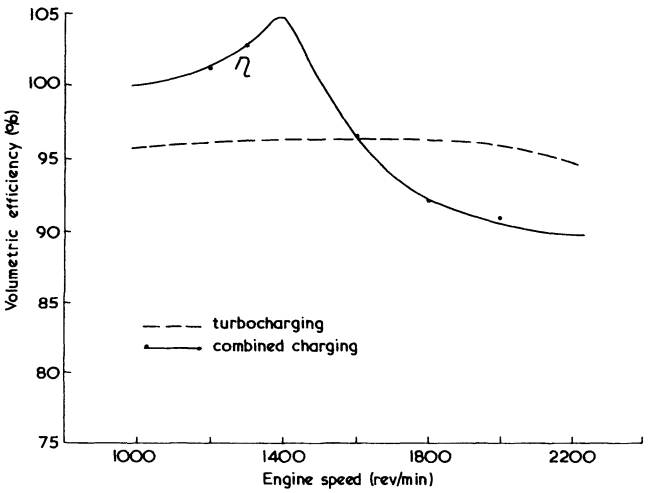

Figure 9.20 *Effect of dynamic charging on volumetric efficiency over a speed range [14]*

increases the mass of air trapped in the cylinder (or volumetric efficiency), at low and medium speeds. The frequency and amplitude of the pressure pulsations are governed by the length and cross-sectional area of the resonance pipe (4, figure 9.17) and the capacity of the resonant volume (5, figure 9.17). Figure 9.19 shows the pressure pulse amplitude, divided by the mean pressure ($\Delta P/P$) with four different combinations of volume and pipe area, with the resonant pipe length being adjusted to obtain the same resonant frequency. Figure 9.20

is an example of the effect of a resonant system, designed to improve low-speed torque of an engine, on volumetric efficiency. An incidental advantage of the system, caused by the increase in mass flow at low speeds, and a reduction at high speeds, is a small reduction in the required flow range of the turbocharger compressor.

Regarding maintenance, it should be remembered that the consequences of using a very dirty air filter may not simply be confined to a loss in performance, high thermal loading and a smokey exhaust. Since the pressure right through the compressor will be lower than normal, the balance in thrust loadings between compressor and turbine will be disturbed. The results can be a high loading on the thrust bearing with the possibility of failure if the air filter is not changed. Furthermore, the low compressor pressure will aggravate any tendency for oil leakage to occur through the piston ring or labyrinth seals into the compressor, resulting in high oil consumption, a possible increase in exhaust smoke and an increased rate of fouling from dirt accumulation.

Many engines (having more than six cylinders) are fitted with more than one turbocharger, since it will often be easier and cheaper to install two or three small turbochargers than one large version. A choice may be made whether to use a common or separate air receiver. Both arrangements are successfully used. A major advantage of a common receiver is that the engine can run with boost from one turbocharger if the other fails. The damaged turbocharger may be isolated or removed and the engine, running with fewer turbochargers and its fuelling reduced to suit, will produce somewhere between its normal and naturally aspirated power. This facility might, for example, be particularly valuable for a ship far from its home port or spares. The disadvantage may result from the fact that two turbochargers, particularly small cast impeller units, might well have slightly different characteristics. If the constant speed compressor characteristics are rather flat, it is possible for the two to require quite different mass flow rates for the same pressure ratio. One compressor is then likely to induce surge in the other. Using separate intake systems with a small linking pipe, small enough to damp the mass flow through it, is one solution. Alternatively, quite separate manifolds may be used. Of course, if separate manifolds are used and the turbochargers have slightly different characteristics, then some cylinders will be more highly loaded than others.

9.5 The Exhaust System

The most important aspect of the exhaust system is the manifolding between cylinders and turbine. Due to the importance of this aspect, the subject has been comprehensively covered elsewhere. However, the exhaust pipe system from the exhaust of the turbine to atmosphere must not be neglected and is discussed here.

The exhaust system from the turbine onwards (henceforth called simply the exhaust or exhaust system) affects the engine-turbocharger combination in two ways. The first, results from the kinetic energy content of the gases leaving the turbine. In particular, the kinetic energy leaving the radial flow turbine can be substantial and it is desirable to convert as much of it as possible to pressure.

Since the ambient pressure at the end of the exhaust pipe is not controllable, the greater the conversion of kinetic energy to pressure that occurs in the exhaust, the lower will be the absolute pressure at the turbine exit. It follows that turbine work will be greater, since its expansion ratio has increased. Exhaust diffusers have been discussed in chapters 4 and 5. In axial flow turbochargers the outlet casing will inevitably already include a diffuser.

The second effect that the exhaust system has on the turbine is related, namely the influence of direct pressure loss in the pipe on turbine exit pressure and hence its work output. The direct pressure losses will result from pipe friction, losses in bends, the silencer and some types of exhaust brakes. The exhaust system should be as straight as possible, any bends that are necessary being of large radius. Its cross-sectional area is dependent on the total length, number of bends, etc., but should be much greater than the exit area of the turbine.

Provided that no sharp bends are used and that the exhaust pipe diameter is sufficient, it will be the silencer that creates the largest pressure loss in the exhaust system. Fortunately the turbine, in extracting energy from the exhaust gases, reduces the noise emission from the exhaust pipe (relative to a naturally aspirated engine of the same power output) hence silencing is less of a problem. The deterioration in engine performance as turbine exit pressure rises will vary from one engine to another, dependent on whether turbocharger efficiency improves or reduces as the mass flow and pressure ratio change. However, some performance reduction is inevitable. Figure 9.21 illustrates the deterioration in engine performance as the turbine back-pressure is raised on a medium-speed industrial engine. Note the rising turbine inlet temperature. Figure 9.22 shows similar trends on a turbocharged automotive (truck) diesel engine. A commonly recommended maximum back-pressure is 0.05 bar at the turbine exit. The exhaust pipe length must not be such as to cause resonance.

Exhaust brakes are sometimes used on automotive four-stroke diesel engines. When the driver presses the brake pedal a valve is closed (partially closed, it being a proportional device) in the exhaust pipe restricting the flow of exhaust gases. At the same time the fuel supply is shut down, hence the engine is being driven

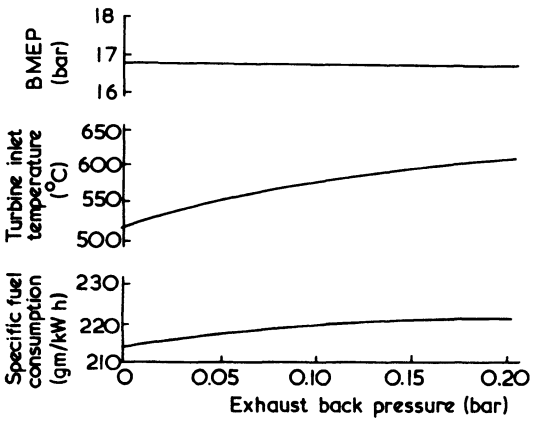

Figure 9.21 *Influence of exhaust back-pressure (gauge) on a medium-speed engine*

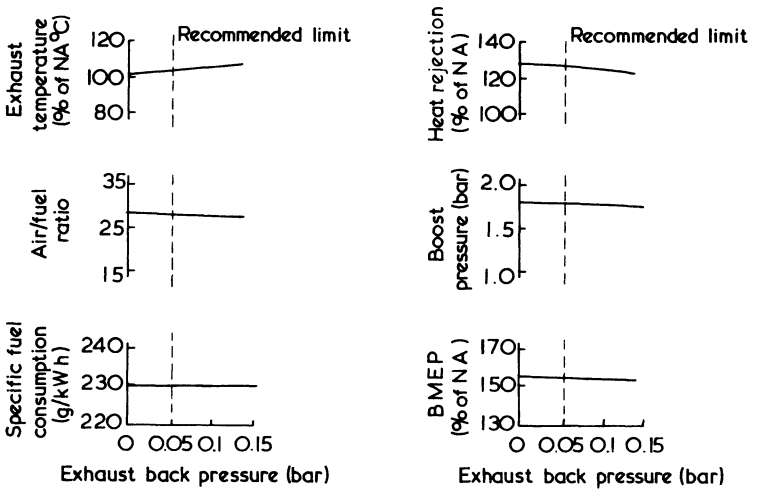

Figure 9.22 *Influence of exhaust back-pressure (gauge) on engine performance [10]*

like a compressor, but from the inertia of the moving vehicle. The engine acts as a brake by absorbing power and this power increases as back-pressure is placed in the exhaust. Some of the devices can cause a significant flow restriction even in the off position, and this must be taken into account in choosing pipe diameter and valve size.

The exhaust brake may be positioned before or after the turbocharger. The downstream position is most common, since this overcomes the difficulties associated with a twin-entry turbine housing and gas temperature is lower improving reliability, and more freedom remains for choosing a convenient mounting position. The disadvantages of this system are high gas pressure at the turbine with potential leakage into the turbocharger housing and high loading on the thrust bearings of the turbocharger. However, most modern turbochargers are designed to accept this condition for the short periods of time when an exhaust brake is in use.

References

1. G. Holzhausen, F. J. Pekar and A. F. Jeney, Integral air-to-air intercooling: A way to improve fuel economy, gaseous emissions, and increase output, *Proc. CIMAC* (1975)
2. D. H. McLean and M. H. Ihnen, The design and development of an air-to-air intercooled engine for agricultural tractor application, *ASME paper 78-DGP-28* (1978)
3. W. Kays and A. L. London, *Compact Heat Exchangers*, 2nd ed. (McGraw-Hill, 1964)
4. G. A. Montgomerie and M. K. Forbes, Cooling equipment for internal combustion engines, *Proc. Inst. Mech. Engrs.*, **181**, Pt.1 (1966/7)
5. A. Mani, Aspects in the design of intercoolers, *Brown Boveri Rev.*, **58**, No.415 (1971)

6. M. K. Forbes and R. J. Hampson, Some present day aspects of charge air cooling, *DEUA Publication 347* (March 1972)
7. W. Lowe, The effect of ambient and environmental atmospheric conditions, *Proc. Inst. Mech. Engrs.*, **184**, Pt.3P (1969/70)
8. P. E. Sherburn, Air cleaner design – present and future, *SAE 69007* (1969)
9. B. W. Wadman, Air cleaners for high output engines, *Diesel and Gas Turbine Progress* (June 1969)
10. H. G. Holler, The influence of induction and exhaust system design on power producing characteristics of diesel engines, *SAE Trans.* No.700535, **79**, (1970)
11. R. S. Benson and J. Foxcroft, Non-steady flow in internal combustion engine intake and exhaust systems, *Proc. Inst. Mech. Engrs.*, **184**, Pt.3b(1) (1969/70)
12. M. Ryti, Pulsations in air intake systems of turbocharged diesel engines, *Brown Boveri Rev.*, **52**, No.3 (1965)
13. E. Meier, Developments of exhaust-gas turbochargers and pressure charging systems for diesel engines with high mean effective pressures, *Proc. CIMAC* (1973) paper 2
14. G. Cser, Some results of combined charging application, Turbocharging and Turbochargers Conference, *Inst. Mech. Engrs.*, (London, 1978) paper C64/78
15. M. C. Brands, Helmholtz tuned induction system for turbocharged diesel engine, *SAE 790 069*, SP79/442 (1979)

10

Turbocharger Matching

10.1 Introduction

Naturally aspirated diesel engines are capable of operating over wide speed ranges. The maximum useful speed will usually be limited by poor volumetric efficiency, the inertia of the reciprocating parts or, in the case of some small high-speed engines, high frictional losses and poor combustion. An engine that is designed for variable speed operation will usually exhibit some deterioration in performance both at extreme low and high speeds. This is due to high gas frictional losses in the inlet valves and the use of valve timing optimised in the mid-speed range and a gradual mismatch between fuel injector characteristics and swirl. However, the useful speed range can be wide, since reciprocating machinery is well suited to cater for a wide range of mass flow rate.

The performance of turbomachines is very dependent on the gas angles at entry to the impeller, diffuser and turbine rotor. The blade angles are set to match these gas angles, but a correct match will only be obtained when the mass flow rate is correct for a specified rotor speed. Away from this 'design point' the gas angle will not match the blade angle and an incidence loss occurs due to separation and subsequent mixing of high and low-velocity fluid. These losses will increase with increasing incidence angle, hence turbomachines are not well suited for operation over a wide flow range. Their use as superchargers is due to their high design point efficiency and their ability to 'accept' high mass flow rates through small machines.

It is clear that a turbomachine is not ideally suited to operate in conjunction with a reciprocating machine, hence the combination of diesel engine and turbocharger must be planned with care. 'Matching' of the correct turbocharger to a diesel engine is of great importance and is vital for successful operation of a turbocharged diesel engine. The over-all objective of turbocharger matching is to fit a turbocharger with the most suitable characteristics to an engine in order to obtain the best over-all performance from that engine. The turbocharger will not be operating at its high efficiency flow area over the complete working range of the engine, if the latter is large (as in the case of an automotive engine). It follows that it is possible to 'match' the turbocharger correctly only at a particular point in the operating range of the engine. For example, if an engine is required to run for most of its life at constant speed and full load, the turbocharger will be chosen such that its high-efficiency operating area coincides with

the pressure ratio and mass flow requirements of the engine at that condition. If the engine is required to operate over a broad speed and load range, then a compromise must be made when matching the turbocharger. This compromise will principally be governed by the duty for which the engine is required.

The basic size of the turbocharger will be determined by the quantity of air required by the engine. This will be a function of swept volume, speed, rating (or boost pressure), density of air in the inlet manifold, volumetric efficiency and scavenge flow. If these parameters are known an initial estimate of the air mass flow rate may be made: for a four-stroke engine

$$\dot{m} \approx \frac{N}{2} \times V_{sw} \times \rho_m \times \eta_{vol} \tag{10.1}$$

With little valve overlap, the volumetric efficiency will be less than unity and may be estimated from values obtained under naturally aspirated operating conditions or from previous experience. With large valve overlap, the clearance volume will be scavenged and some excess air will pass into the exhaust.

$$\eta_{vol} = f(\eta_{vol*}; \frac{CR}{CR - 1}; ADR)$$

where η_{vol*} = volumetric efficiency, naturally aspirated. For a two-stroke engine (with scavenge pump assistance)

$$\dot{m} = N \times V_{sw} \times \rho_m \times \eta_{vol} \tag{10.2}$$

where V_{sw} is now the swept volume of the scavenge pump.

The density of the air in the inlet manifold will be given by

$$\rho_m = \frac{P_m}{RT_m} \approx \frac{P_2}{RT_2} \tag{10.3}$$

The boost pressure (P_m) will have been estimated for the engine to produce its target power output, subject to expected thermal and mechanical stresses. By assuming a value for the isentropic efficiency of the compressor (total-to-static) the boost temperature (T_m) may then be estimated

$$T_m = T_a + \frac{T_a}{\eta_c}\left[\left(\frac{P_m}{P_a}\right)^{(\gamma-1)/\gamma} - 1\right] \approx T_1 + \frac{T_1}{\eta_c}\left[\left(\frac{P_2}{P_1}\right)^{(\gamma-1)/\gamma} - 1\right] \tag{10.4}$$

The isentropic efficiency of the compressor may be taken from compressor maps. If the compressor efficiency is quoted on the total-to-total basis, a correction of a few percentage points down on the total value is required.

For an engine using aftercooling the boost temperature (T_m) has to be reduced according to the equation

$$T_m = T_2(1 - \epsilon) + \epsilon T_w \tag{10.5}$$

From equations 10.1 to 10.5 and known values of ambient temperature and pressure, and required compressor pressure ratio, the mass flow rate at maximum power can be estimated.

By looking at the basic guide lines presented in the turbocharger manufacturers'

literature (such as that shown in figure 10.1), or the complete compressor characteristic curves (figure 10.2), a basic 'frame size' of turbocharger may be selected. The final choice of compressor will be made bearing in mind the complete operating lines of the engine over its whole speed and load range, superimposed on the compressor characteristic. The compressor 'trim' or diffuser will be chosen to allow a sufficient margin from surge while ensuring that the operating lines pass through the high-efficiency area. This will be discussed in detail in section 10.2.

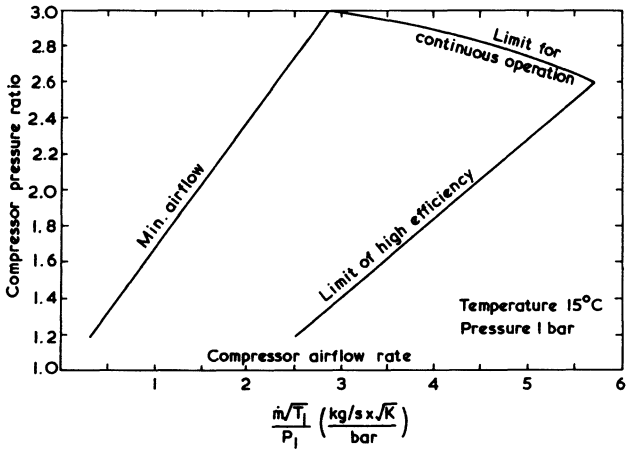

Figure 10.1 *Compressor airflow range*

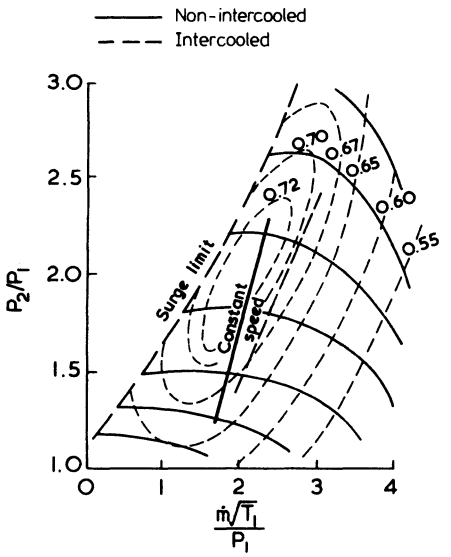

Figure 10.2 *Superimposition of engine running lines on compressor characteristics, constant engine speed, with and without charge air cooling*

Once the basic frame size and compressor have been established, the turbine must be matched by altering its nozzle ring, or volute if it is a radial flow machine. The effective turbine area will change, raising or lowering the energy available at the turbine and hence adjusting the boost pressure from the compressor. Although it is possible to calculate the over-all performance of a turbocharged engine and hence establish the most suitable turbocharger match, final matching will always take place on the test bed or, in some cases, when the engine is installed. In consequence, it is important when matching on a test bed to ensure that the correct air filter, intake and exhaust systems are used.

Turbocharger matching, particularly on a new engine, can be a lengthy process since many dependent parameters are involved. Although the basis is to match the turbocharger to the engine, it may well be necessary to improve the performance of the combination by engine design changes at the same time. Some such changes – adjustment of the fuel injection system, for example – are obviously essential. Others that may be desirable include alteration to the valve area and timing. It will not be possible to discuss all these factors in detail and the broad principles of matching fuel injection systems, swirl, optimisation of valve timing, etc., are not substantially different from those pertaining to naturally aspirated engines. Most large industrial highly rated turbocharged engines are designed as such from the outset today, and it is less common for a naturally aspirated design to be uprated by turbocharging in this class of engines. The designers will know from experience approximately what valve timing, injection pressures, etc., will be suitable, although factors such as these will be modified in the light of subsequent testing. Manufacturers of smaller engines however, sometimes turbocharge engines that were originally designed for naturally aspirated use. Fortunately, if modest power gains are sought (up to 50 per cent), major redesign is seldom necessary since the maximum cylinder pressure may be held down by an engine compression ratio reduction, and thermal stresses are not usually a major problem. However, if greater power gains are required the engine will probably require major redesign.

10.2 Air Flow Characteristics of Engine and Turbocharger

10.2.1 Four-stroke Engine

The air flow rate through a turbocharged (non-aftercooled) diesel engine will be a function of the engine speed, compressor delivery air density and the pressure differential between intake and exhaust manifolds during the period of valve overlap. If the engine is run at constant speed, but steadily increasing load, then the mass flow rate will increase approximately with the increasing charge density. The air flow through the engine may be superimposed on a turbocharger compressor characteristic, as shown in figure 10.2, the slope being governed by the density ratio. When matching a turbocharger to an engine with this operational requirement, the objective will be to choose a compressor such that the constant engine speed line falls through the middle of the high-efficiency area of the compressor map. If an aftercooler is fitted, then, as load increases, the cooling effect will increase charge density more rapidly for a corresponding boost

pressure, hence the slope of the constant engine speed air flow line on the compressor characteristic will be less steep (figure 10.2). Again, to match the turbocharger for this duty, the objective will be for the operating line of the engine to pass through the high-efficiency region of the compressor characteristic.

Consider next an engine running at constant load (BMEP) but increasing speed. As the engine speed increases so will the volumetric flow rate of air. The effective flow area of the turbocharger turbine remains almost constant hence turbine inlet pressure will rise. As discussed in chapter 7, the result is an increase in energy available for expansion through the turbine and hence increased boost pressure at the compressor. Thus the constant load line of the engine will not lie horizontally on the compressor characteristic, but will rise with engine speed (figure 10.3), the slope depending on whether the engine is aftercooled or not. If the engine is required to operate over a range of speeds and load (for example, an automotive unit), then a set of constant speed and constant load lines may be drawn on the compressor characteristic to represent the operating range (figure 10.4). The complete engine characteristic must lie between the compressor surge line and the limit imposed by low efficiency or possibly turbocharger over-speed at high mass flow rates.

The margin between surge and the nearest point of engine operation must be sufficient to allow for three factors. Firstly, pulsations in the intake systems may well induce surge when the mean flow lies close to the nominal surge line. Secondly, if the air filter becomes excessively blocked in service, the air flow rate through the engine will reduce, but the turbine work will be maintained by a hotter exhaust as the air/fuel ratio gets richer. Thus boost pressure may not fall and some movement of the engine operating line towards surge may occur. A larger movement towards surge will result if the engine is operated at altitude. The effect of altitude operation on turbocharged engine performance is discussed

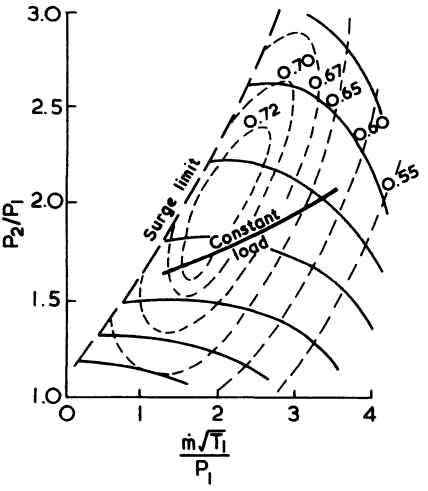

Figure 10.3 *Superimposition of engine running lines on compressor characteristics: constant engine load*

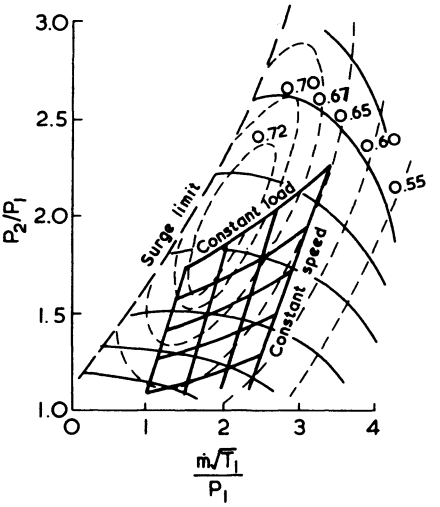

Figure 10.4 *Superimposition of engine running lines on compressor characteristics: constant engine load and speed lines*

in section 10.9. The combined effect of the three factors affecting surge margin will vary from one engine for one application, to another. In general, however, a margin of at least 10 per cent (of mass flow rate) between surge and the nearest engine operating line should be allowed. On engines with a small number of cylinders a 20 per cent margin will sometimes be required.

Generally, the turbocharger turbine can operate efficiently over a wider mass flow range than its compressor. It follows that it is more important to examine the engine air flow plotted on the compressor map than on the turbine map. This is indeed fortunate since if the turbine is operating under the pulse system with highly unsteady flow, it is not realistic to plot a 'mean' value on the turbine map. The result can be quite misleading, which is one of the reasons why turbocharger manufacturers are reluctant to offer turbine characteristic maps to many of their clients. To assess accuratley the operating area on a turbine map would require a plot of instantaneous gas flow and pressure ratio over a full range of engine operating conditions. The information is very difficult indeed to measure accurately. Probably the best that can be done [1] is to predict the instantaneous values using the methods outlined in chapter 15.

Figure 10.5 shows the turbine characteristic in terms of mass flow parameter against speed parameter, along lines of constant pressure ratio, with efficiency loops superimposed. This presentation enables the pulsating flow through the turbine to be illustrated, and its effect on turbine matching. The vertical lines denotes full load engine operation at four speeds. At any engine speed, the top point denotes the maximum amplitude point on the pressure wave passing through the turbine, and the bottom point corresponds to a pulse minimum. The line joining these points is vertical, since turbocharger speed varies only slightly at constant engine speed. At low engine speed (1000 rev/min), the pressure pulses are likely to be separated by short periods of zero flow, hence the pulse

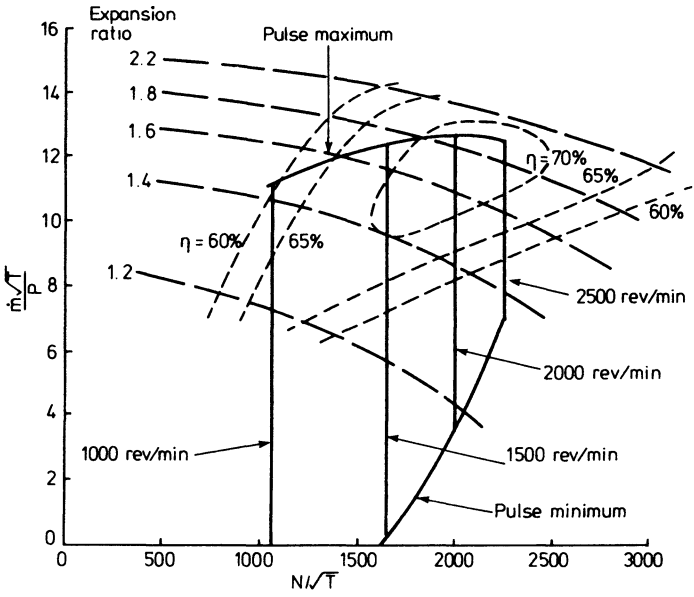

Figure 10.5 *Turbine performance map with pulse flow operating lines superimposed*

minimum corresponds to a mass flow parameter value of zero. In figure 10.5, optimum turbine efficiency coincides with a high pressure ratio point on the 2000 rev/min line. Since the point of maximum mass flow is also the point of highest pressure ratio, optimum turbine efficiency coincides with a high instantaneous mass flow rate, at 2000 rev/min.

Maximum instantaneous turbine power will be developed when the combination of mass flow rate, pressure ratio and efficiency are optimum, since

$$\dot{W}_{t_i} = \dot{m} c_p T_p \left[1 - (P_a/P_p)^{(\gamma_e - 1)/\gamma_e}\right] \eta_t$$

Maximum total turbine power must be calculated by integrating instantaneous power, over an engine cycle, since

$$\dot{W}_t = \frac{1}{720} \int_0^{720} \dot{W}_{t_i} \, d\theta$$

This will occur when peak efficiency falls at a point associated with just less than maximum pressure ratio or mass flow rate. Thus the turbine match shown in figure 10.5 is optimum for the engine speed range of 1700 to 2500 rev/min, at full load. If peak turbine efficiency is required at low speed, then a turbine having a high efficiency area at lower rotational speeds, will be optimum.

The compressor may be matched initially by choosing the best combination of impeller and diffuser such that the engine operating characteristics lie within the guide lines given above. Final matching will depend on the type of power

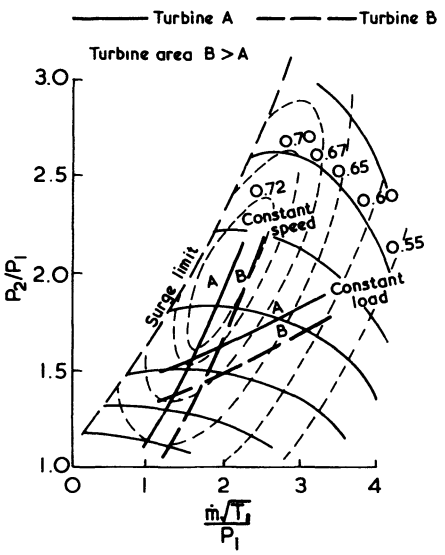

Figure 10.6 *Superimposition of engine running lines on compressor characteristics: effect of turbine area*

or torque curve required from the engine for a certain application, and will be discussed later. However, it has been pre-supposed that the turbine is able to provide sufficient power to drive the compressor and produce the air flow conditions discussed. Since the useful flow range at the turbine is wider than that at the compressor, the turbine supplied by the turbocharger manufacturer will inevitably be able to cope with the necessary mass flow. Whether it produces sufficient power depends on its efficiency and the turbine area (since this dominates the energy available for useful expansion). The turbine nozzle ring or volute controls its effective area. Thus the effective area at the turbine will be adjusted (by changing the components mentioned above) to achieve the desired boost level from the compressor. If turbine area is reduced, then the compressor boost pressure and the mass flow rate will go up, the former by a larger amount than the latter since charge temperature will also rise. The effect, in terms of the engine operating lines superimposed on the compressor characteristic is shown in figure 10.6.

10.2.2 Two-stroke Engines

The air flow characteristics of a two-stroke engine will depend on whether the engine is fitted with a turbocharger alone or has an auxiliary scavenge pump or blower. Consider first the situation when a turbocharger is used on its own. During the period when the inlet ports are open, the exhaust ports or valves will also be open and the air flow rate will depend on the pressure drop between intake and exhaust manifolds. The physical arrangement is analogous to flow

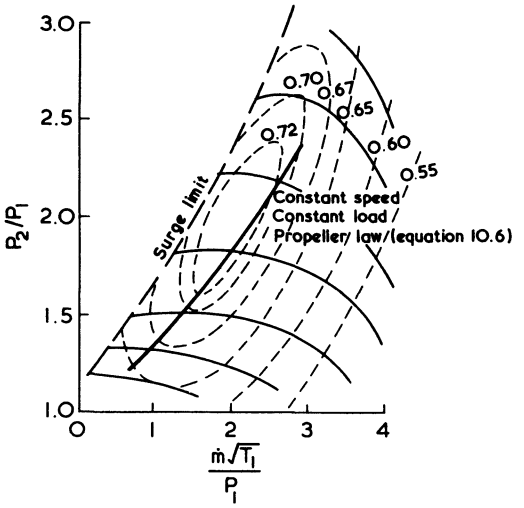

Figure 10.7 *Superimposition of engine running lines on compressor characteristics: propeller law, two-stroke engine*

through two orifices placed in series. The mass flow against pressure ratio characteristic for steady flow through two orifices in series is a unique curve and it follows that the two-stroke engine will exhibit a similar characteristic. Thus the engine operating line, when superimposed on the compressor characteristic will be a unique curve, almost regardless of engine load or speed (figure 10.7). Fortunately the compressor characteristics are well suited to this type of demand, as shown in figure 10.7, and it is relatively easy to match the turbocharger. If an aftercooler is fitted (which it is on most engines of this type) the mass flow/pressure ratio curve will have a different slope (smaller gradient) which suits the compressor characteristic even more.

If scavenge pumps or positive displacement compressors are placed in series with the turbocharger compressor on a two-stroke engine, then the air flow characteristic will be dominated by the scavenging device. For example, a reciprocating scavenge pump will exhibit much the same flow characteristics as a four-stroke engine, hence when constant load and speed operation lines are plotted on the compressor characteristic, the result is little different from that shown in figure 10.4. Somewhat similar characteristics are obtained if a rotary compressor (for example, a Roots blower) is used, although small differences will result from different compressor characteristics. In general, however, the matching problem will not be significantly different from that of a four-stroke engine and the comments previously made apply. The additional difficulty that does arise is that the scavenge blower must also be matched to the engine at the same time, since a compromise must be reached between scavenge blower and turbocharger work.

Generally the turbocharger will be expected to do as much of the compression work as possible. Depending on the quality of the scavenging system, turbocharger efficiency, use of pulse or constant pressure turbocharging, etc.,

the turbocharger may well be able to provide sufficient boost pressure at full power but not at low load. The subject has been discussed in detail in chapters 6 and 7. It follows that the work division between turbocharger and auxiliary compressor may well be governed by the requirement for adequate scavenging (and hence engine performance) for part load operation. The final balance will vary from engine to engine since many different factors are involved. An example, involving an application where a wide speed and load requirement exists, is discussed in section 10.8.

10.3 Matching for Constant Speed Operation

The most common application requiring a constant speed diesel power source is electricity generation, either for steady base load or stand-by units in the event of failure of an external supply. It is a relatively simple requirement from the point of view of turbocharger matching, as mentioned in section 10.2. The difficulties are associated more with the tight speed-governing requirements (since the frequency of alternating current generation will be governed by engine speed) rather than turbocharger matching, during sudden load changes. This latter situation is discussed in chapter 12.

The basic compressor characteristics resulting from this varying load at constant speed application is shown in figure 10.2. Small adjustments in turbine area will affect both the boost and exhaust pressures, hence pumping work and the resultant fuel consumption of the engine. Within the limits of acceptable mechanical and thermal loading of the engine, turbine matching will be used to achieve optimum performance and fuel consumption. Figure 10.8 shows the effect of turbine area changes on the specific fuel consumption with varying load at constant speed. Matching will be a compromise between performance at low and high load. If the diesel generator is required for base load operation, then the turbocharger will be matched at the rated load (full line in figure 10.8). Otherwise a larger nozzle ring or volute will be fitted to improve part load efficiency. The small nozzle increases piston pumping work and hence increases fuel consumption, except at high load, when the engine benefits from the extra air which results from more turbine and compressor work.

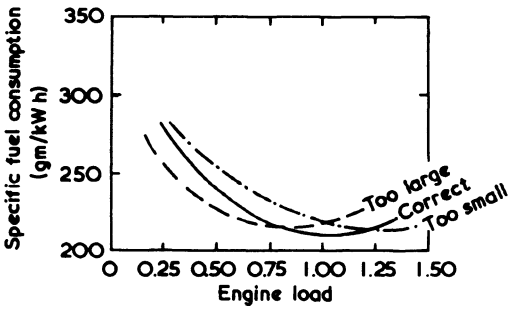

Figure 10.8 *Optimum turbine matching for fixed load, constant speed*

Fine tuning of the turbine match produces the smaller changes in engine performance shown in figure 10.9. This is a more highly rated engine (17 bar BMEP) with large valve overlap. The flow characteristics of the three turbine trims used are given in figure 10.10. In this case, the smaller turbine, although benefitting from increased available energy, has a lower efficiency than the larger trims (being cropped from a larger design). In addition the high exhaust pressure level developed by the small effective flow area of the turbine, has an adverse effect on the scavenge air flow during valve overlap. These effects combine to impair engine performance with the smaller turbine trim.

In figure 10.11 the engine air flow rates are superimposed on the compressor map, with each of the three turbine trims. Clearly the choice of compressor

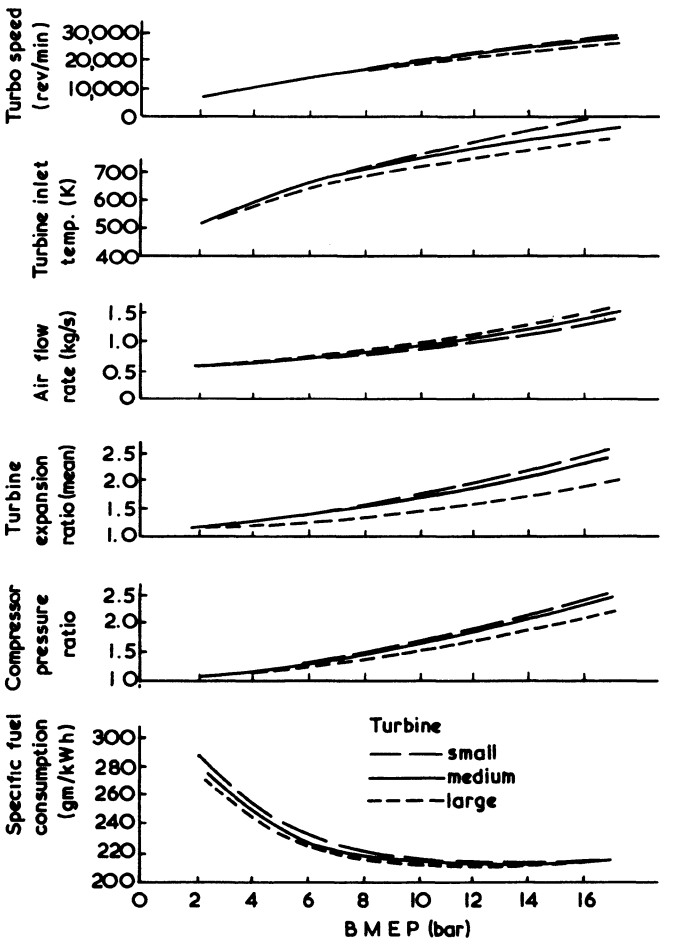

Figure 10.9 *The effect of small turbine area change on engine performance at constant speed*

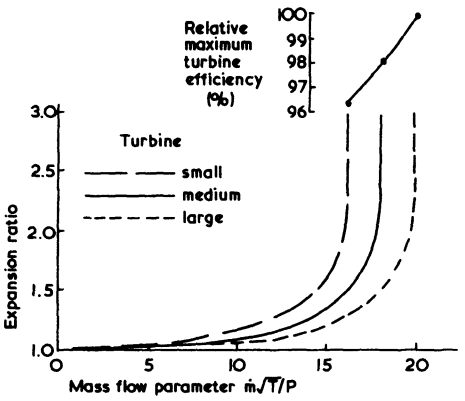

Figure 10.10 *Turbine trims used in figure 10.9*

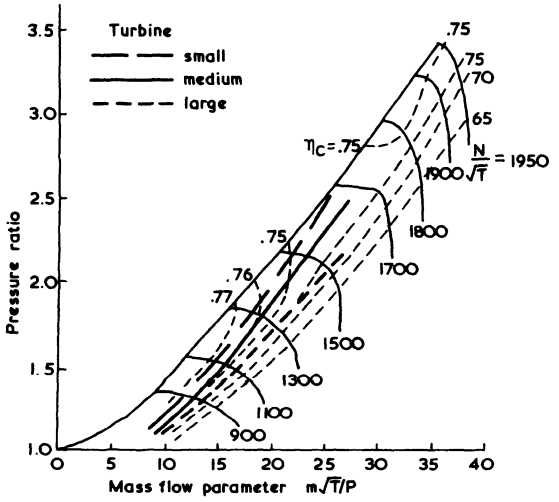

Figure 10.11 *The effect of turbine matching on compressor requirement for constant engine speed operation*

is correct with the medium turbine, but a smaller compressor trim would be needed to avoid surge with the smallest turbine, and a slightly larger variant to achieve optimum compressor efficiency with the largest turbine.

10.4 Matching the Marine Engine

The required power/speed characteristics of the marine engine are governed by the performance of the propeller, and will therefore depend on whether a fixed or variable pitch propeller is used.

The characteristics of the fixed pitch propeller are such that the power requirement increases with the cube of the speed (the well-known 'propeller law')

$$\dot{W} \propto N^3 \tag{10.6}$$

Thus BMEP increases with speed squared (figure 10.12). It happens that the output characteristics of the turbocharged engine are ideal for this application, hence matching is a case of optimisation rather than compromise. Compressor pressure ratio rises with engine speed as well as with load. The reason may be found in the flow characteristics of the turbine. As engine speed increases, so does the air flow through it (equation 10.1, for a four-stroke engine). The flow characteristic

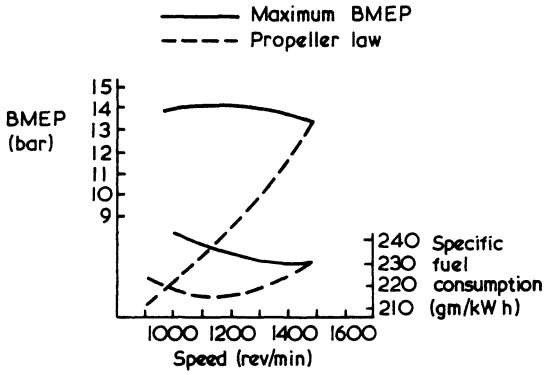

Figure 10.12 *Engine performance comparison at maximum BMEP and propeller law*

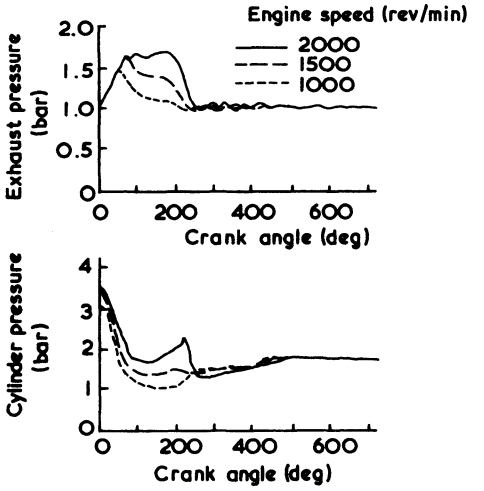

Figure 10.13 *The effect of engine speed on the exhaust process of a single-cylinder engine [2]*

of the turbine (figure 10.10) is such that the expansion ratio is forced to increase with air flow and therefore engine speed (figure 10.13). The torque developed by the turbine is largely a function of expansion ratio and turbine inlet temperature, if changes in efficiency are small, since

$$TQ = \dot{W}/2\pi N = [1 - (P_a/P_p)^{(\gamma_e - 1)/\gamma_e}]\ T_t c_{p_e} \eta_t\ \dot{m}/2\pi N \qquad (10.7)$$

Thus turbine, and hence compressor, torque rises with engine speed. The boost pressure developed by the compressor is largely a function of torque input from the turbine, hence speed and load. However, optimum specific fuel consumption will occur at lower speeds, where mechanical friction losses are lower.

10.4.1 The Four-stroke Engine with Fixed Pitch Propeller

Figure 10.14 illustrates a typical operating line on the compressor characteristic for fixed pitch propeller operation of a four-stroke engine. Two important facts are clear. Firstly, if the turbocharger is correctly matched, the compressor is working in an area of reasonably high efficiency at all engine speeds and loads, but if highly rated, the surge margin will be governed by mid-speed performance, due to the 'waist' shown in the surge line.

When matching at full speed the turbine will be matched to produce maximum engine power output, subject to thermal and mechanical limits. Generally the result will also be minimum specific fuel consumption. If different turbine areas are tried, various boost pressures will be developed and the propeller law working line will move across the compressor map. The compressor diffuser (or the complete assembly) will be changed to ensure that the operating line falls through the optimum efficiency area with a sufficient surge margin to allow for intake pul-

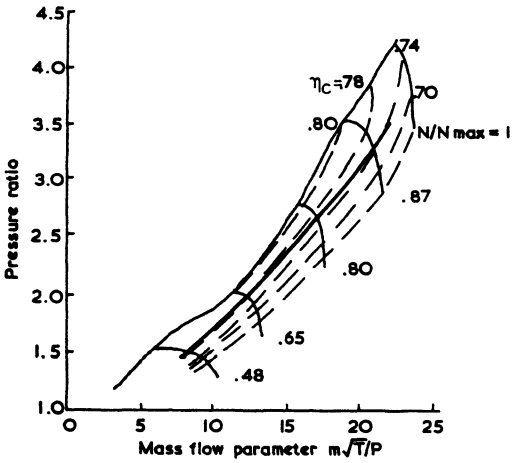

Figure 10.14 *Compressor match for a four-stroke engine with fixed pitch propeller [3]*

sations, and compressor fouling in service. When matching, the power output, specific fuel consumption and exhaust temperature will be monitored, but generally there will be no major conflict between variables.

It is common practice among the builders of medium and slow-speed diesels to offer a large range of power outputs by offering engines with increasing numbers of cylinders, each cylinder being virtually a self-contained unit fixed to a common crankcase. For convenience the engine may be rated at X kW (or BHP) per cylinder producing, for example, $12X$ kW in V12 form. A problem then sometimes arises in achieving the same power output per cylinder on those engines which have favourable numbers of cylinders for pulse operation (for example, 12) and those that do not (for example, 8, see chapter 7). In the latter case poor turbine efficiency due to the highly unsteady entry flow must be compensated for by reducing turbine area to increase the energy available at the turbine. The result will be a higher exhaust temperature and possibly a small deterioration in specific fuel consumption due to increased pumping work.

Frequently, several medium-speed engines will be used in a single vessel, with perhaps two engines geared down and geared together driving each propeller. The requirement can arise, if one engine fails, of driving the propeller with one engine only. If the engine-turbocharger combination has been matched for optimum performance when producing half of the maximum power required by the propeller, then the match will be unsuitable for operation as one engine. Naturally this engine cannot drive the propeller at full speed (it will not have the power), but it is theoretically capable of turning it at nearly three-quarters of its maximum speed due to the power requirement being proportional to the cube of the speed (propeller law). Consider what happens if the engine runs at

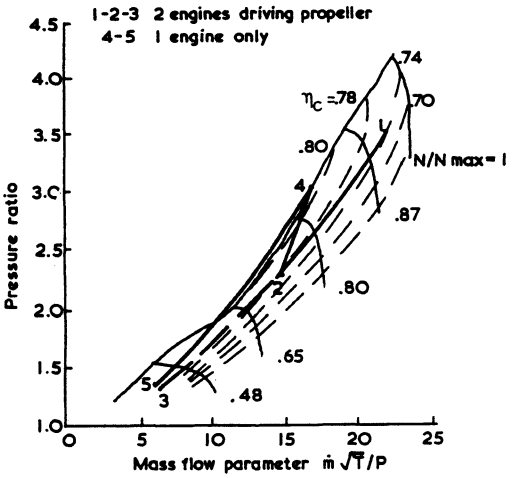

Figure 10.15 *Engine mass flow characteristic superimposed on compressor map when one of two engines is running, with a fixed pitch propeller [3]*

70 per cent of full speed, remembering that the power required is double what would be required from each engine if both were running at that speed. If both engines were running, the operating point would be that denoted by point 2 in figure 10.15, but point 4 with one engine. Unless the compressor is matched with a very large surge margin, surge is inevitable. Thus the optimum match with both engines working correctly is compromised.

10.4.2 The Four-stroke Engine with Variable Pitch Propeller

A much broader power/speed requirement is obtained from a variable pitch propeller. At each pitch setting, the propeller law will apply and hence the characteristic will be an envelope of propeller law curves. Figure 10.16 illustrates how the power curve of the engine will cut across an 'extreme pitch' curve if the propeller is matched to require full engine power at its rated speed at optimum

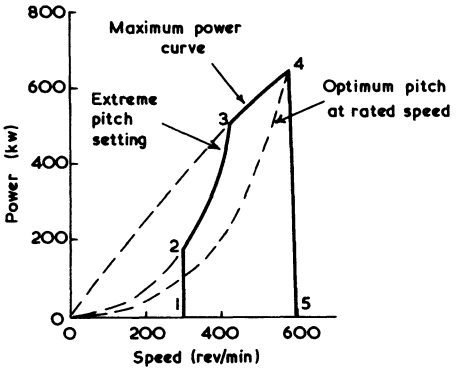

Figure 10.16 *Propeller law power curves with a variable pitch propeller [3]*

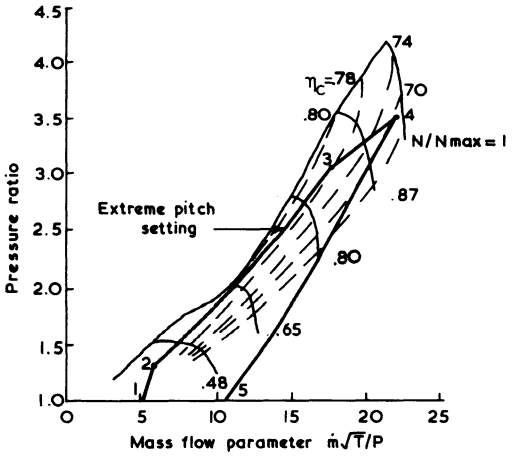

Figure 10.17 *Compressor matching with a variable pitch propeller [3]*

pitch. Lines 1-2 and 5-4 denote minimum and maximum engine speeds. When plotting the resultant operating regime on the compressor characteristic (figure 10.17) it can be seen that it is the 'extreme pitch' curve that determines the surge margin, not the maximum speed point (4). The engine can still be matched for optimum performance at full speed, but the compressor will have to be chosen to allow line 2-3 to be well clear of surge. This may result in a small penalty in performance at point 4.

10.4.3 The Two-stroke Engine with Fixed Pitch Propeller

The different types of scavenging system used by two-stroke engines have been described in earlier chapters. In general, only pulse turbocharged uniflow scavenged engines can operate without a scavenge pump or fan in addition to the turbocharger over the complete operating range required. This class includes the very large opposed piston and 'valve in head' marine two-stroke engines. The power required by the propeller will naturally be governed by the propeller law and it follows that, if the engine is matched at its rated speed, the equilibrium running line will fall on the compressor map in a similar manner to the four-stroke engine. However, the air flow characteristics will be governed by the scavenge period, and may be simulated by two orifices in series (that is, to represent the intake and exhaust of the engine). This characteristic suits the compressor well, and matching is usually a reasonably straightforward exercise similar to that described for four-stroke engines.

If scavenge pumps are used, the division of work between them and the turbocharger will influence the matching process. Generally though, the capacity of the scavenge pumps will have been estimated and the turbocharger is matched for optimum performance in conjunction with those pumps. A change in pump capacity might follow, depending on the success of the matching exercise, in which case the whole procedure must be repeated. To ensure that the engine will not stall at low speeds, the scavenge pumps must supply sufficient air to raise the inlet manifold pressure above that in the exhaust. If the turbocharger compressor precedes the scavenge pump, then the air flow characteristics obtained on the compressor map at low speeds, will be highly dependant on the capacity of the scavenge pumps. Thus a range of air flow requirement curves could be plotted on the compressor map. At low speeds the air flow will depend principally on the pump speed, but at higher speeds, the influence of the turbocharger compressor will significantly affect air flow by increasing the charge density at entry to the scavenge pumps.

10.5 Matching for Diesel-Electric Traction

Diesel generators are frequently used for rail traction since the characteristics of the basic diesel engine are not ideally suited for direct drive. In particular, the locomotive engine requires high torque at zero speed, to accelerate a heavy train from rest. Sufficient voltage can be generated (by a diesel generator) to produce the excitation necessary at the electric drive motors. The power needed to accelerate the electric motor from zero speed is less than the capability of the diesel

engine at higher speeds. If the turbocharger is matched to the engine at its rated speed and load, the equilibrium running lines will usually be quite well positioned on the compressor map at other speeds and loads. A possible area of trouble is surge at low speed and high load, and this may mean that the compressor build finally chosen leaves a rather large surge margin at full power.

Since, like the automotive engine, the diesel-electric locomotive unit is mobile, it is possible that it may be required to operate at altitude. The turbocharger must be matched to allow sufficient surge margin, and, if it is known that the engine will run at a particularly high altitude, the fuel injection system and turbocharger match will need to be adjusted to suit. The engine will effectively need derating to prevent over-loading at altitude (see section 10.9).

10.6 Matching for Other Industrial Duties

The power/speed requirements for other industrial duties will generally fall between those of an automotive engine and the other applications described above. A typical industrial application might be the drive to a reciprocating compressor. The compressor can be operated over a reasonably wide speed range, from zero to full load as the control valves open or close. The resultant operating area on the engine and compressor maps is similar to the requirements for an automotive engine (section 10.7). The surge margin will be governed by full load operation at low speeds and this will force the full speed and load point well away from surge and possibly into a low efficiency area of compressor operation.

10.7 Matching the Four-stroke Automotive Engine

Turbocharger matching for many industrial and marine duties is relatively straightforward due to the limited speed and load ranges required. Matching the turbocharger to an automotive engine is considerably more difficult due to the wide speed and load variations encountered. Although the power required to propel a vehicle increases rapidly with speed, it is inappropriate to design an engine with this type of output. Consider the power and torque curves of two different engines as shown in figure 10.18.

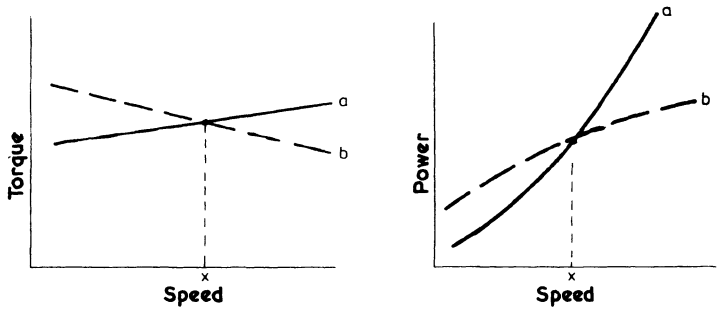

Figure 10.18 *Power and torque curves*

If two identical vehicles (with engines 'a' and 'b') are running along a flat road at speed x, both could be using the same maximum torque output from their engines. When the vehicles arrive at a small hill, the engine load will increase but, since both engines are already producing their maximum torque at that speed, the speed must fall. As engine speed falls, the engine in truck 'b' will produce more torque to meet the increased load applied, enabling the engine to propel the vehicle up the hill at a somewhat lower speed. In contrast, the engine in truck 'a' will produce less torque as its speed drops, compounding the deceleration of the vehicle. Vehicle speed will fall rapidly forcing the driver to change to a lower gear. Although the situation has been over-simplified, it illustrates the requirement for a torque curve that rises as speed falls, otherwise driving the vehicle will be tiring due to the need for frequent gear changes. Such a torque curve is said to have good 'torque back-up'. Pulse turbocharging is essential in obtaining a good torque back-up at low engine speed.

With good torque back-up, the vehicle will benefit from high torque at low speeds to provide a margin for acceleration and to allow the vehicle to lug up very steep hills with a limited number of ratios in the gearbox. Figure 10.19 shows the ability of a truck to climb hills if constant power is available over the whole speed range. Superimposed is the vehicle's hill-climbing ability in each gear ratio (five-speed gearbox) with a more typical engine fitted. The shaded portions represent running conditions falling below the maximum power output of the engine but are not achievable in practice because the engine cannot develop sufficient torque at that speed. These areas are also shown, but more clearly, in the power availability envelopes of figure 10.20. By increasing engine torque at less than full speed, the left-hand part of the power envelope in each gear will rise, possibly at the expense of maximum power. However, the result will probably be a more useful power availability for a fixed number of gear ratios. Otherwise the only method of reducing the shaded areas is to use a gearbox having more ratios.

Clearly the turbocharged automotive diesel engine should not be matched at full power and a compromise must be reached between power and a suitably

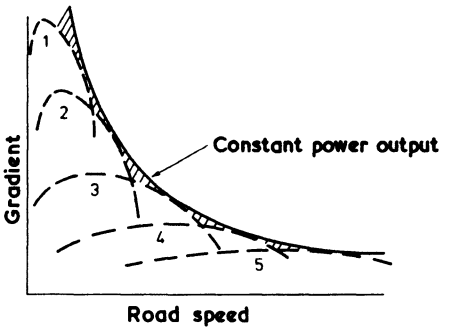

Figure 10.19 *Gradient against speed ability of a truck with a five-speed gearbox [4]*

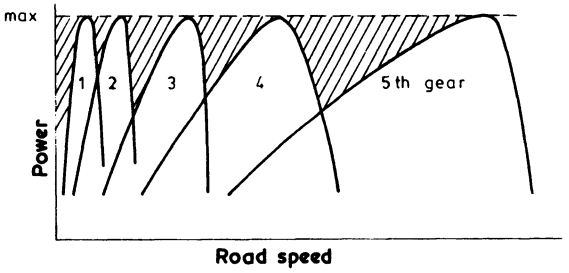

Figure 10.20 *Power/speed envelope for a five-speed gearbox truck*

shaped torque curve. Figure 10.21 shows a typical torque curve for a naturally aspirated automotive diesel engine (curve 'a'). Torque back-up may be defined as

$$\frac{\text{maximum torque - torque at maximum speed}}{\text{torque at maximum speed}}$$

Maximum torque of engine 'a' occurs at 54 per cent of its maximum speed, and the torque back-up is 16 per cent. Since the engine will not normally be required to work below about 40 per cent of the maximum speed, torque rises with reducing speed over half the useful speed range. This characteristic is, fortunately, a reasonable compromise between power and low-speed torque, enabling trucks to use five or six-speed gearboxes.

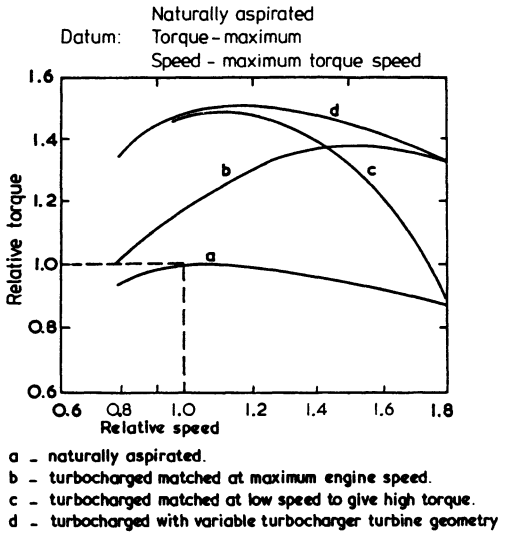

Figure 10.21 *Torque/speed relationships: naturally aspirated and with quite different turbocharger matches*

Although it has been made clear that it is not sensible to match the turbocharger at the maximum speed of the engine for this application, the torque curve that might result is shown in figure 10.21 (curve b). The result is a totally inappropriate torque curve. An alternative is to match the turbocharger to produce maximum torque at the same speed as might be expected on a naturally aspirated engine (curve c), if possible. Excellent torque back-up is obtained but the maximum power output (torque x speed) is considerably reduced.

Before discussing the merits of compromise solutions between the extremes shown in figure 10.21, it is worthwhile considering what engine or turbocharger limitations might prevent such curves being obtained in practice. Engine performance will typically be limited (for reliability) by a maximum value of cylinder pressure and possibly exhaust temperature (since the latter is an approximate guide to thermal loading, for example at the exhaust valve). In addition, a limit will be imposed by the acceptable (or legislated) exhaust smoke level, which will be determined largely by the quantity of air delivered by the turbocharger. The turbocharger will be limited by a maximum safe rotational speed and turbine inlet temperature (governed by the creep and scaling properties of the turbine wheel and housing). Depending on engine rating, some or all of these factors will limit engine performance. These limits can be superimposed on the torque (or BMEP, since torque $\approx$ BMEP) curve as shown in figure 10.22, where the maximum possible torque curve is shown. However, the position of most of these limiting lines will move if the turbocharger match is changed.

It is clear from figure 10.22 that the factor that is most restrictive when trying to achieve a desirable torque characteristic is the low-speed smoke limit. This comes as no surprise since, in section 10.4, it was explained that it is normal for boost pressure to rise with engine speed, as a direct result of the air flow characteristics of the turbocharger turbine. For example, the flow characteristics of

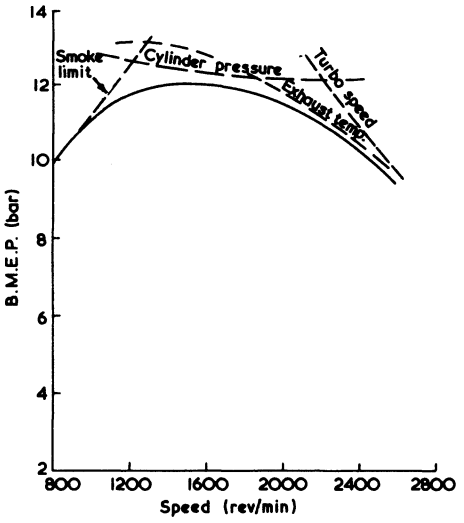

Figure 10.22 *Turbocharger and engine limitations [5]*

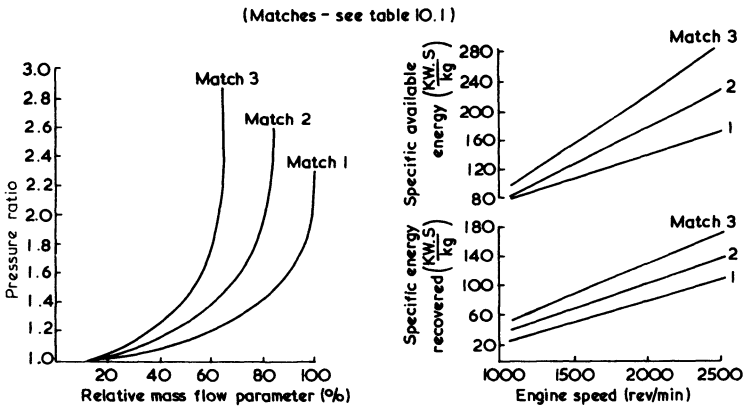

Figure 10.23 *Turbine flow characteristics and resultant energy utilisation of the turbine [6]*

three radial turbine trims (volutes) are shown in figure 10.23. The smallest area volute will generate the highest turbine inlet pressure and therefore the highest specific available energy at the turbine. Allowing for the variation of turbine efficiency over the pulsating and mean flow range, specific energy recovered by the turbine also increases substantially with engine speed. This characteristic is a consequence of the almost constant effective flow area of a fixed geometry turbine. Thus the natural characteristic of the turbocharged truck engine will be

TABLE 10.1 *Turbocharger and Fuelling Changes*

Match	Comment	Peak Compressor Efficiency (%)	Peak Turbine Efficiency (%)	Relative Turbine Area	Maximum Fuelling (relative)
1	Baseline	70	68	100	100
2	Smaller turbine	75	73	82.8	100
3	Smallest turbine	75	67	66.0	100
4	Match 2 plus increased fuelling	75	73	82.8	114
5	Match 4 plus waste gate	75	73	82.8	114
6	Match 4 with tailored fuelling	75	73	82.8	114
7	Match 2 increased fuel and limited speed range	75	73	82.8	118

compressor work (and therefore boost pressure) rising with engine speed. The smoke limit is caused by insufficient boost pressure, and hence air flow, at low engine speeds.

If the fuel delivered to the cylinders is allowed to increase with speed, to match the increase in air flow, then torque curve b (figure 10.21) will result. In order to achieve a more acceptable torque curve, the fuel delivery (per cycle) is held relatively constant over the speed range and efforts are made to raise boost pressure at low speed. Two techniques are available to achieve this. Either the turbocharger efficiency must be raised at this operating point, or the thermodynamic availability of energy delivered to the turbine (that is, specific available energy, figure 10.23) must be increased. Both techniques are usually adopted, and will be discussed under the headings of turbine and compressor matching.

10.7.1 Turbine Matching

Figure 10.23 shows that by reducing turbine area, for example from match 1 to match 3, specific available energy at the turbine increases at all speeds. If the fuel delivery schedule is unchanged, then boost pressure increases as shown in figure 10.24, weakening the air/fuel ratio and reducing low-speed smoke. Match 2 is based on a small turbine area reduction, hence the increase in available energy at low speed is small (figure 10.23). However, turbine operation is more efficient with this build, hence the benefit in actual turbine work is more substantial.

The benefit of reduced smoke at low speeds does not come without accompanying disadvantages. Figure 10.23 shows that with the smallest turbine (match 3), the expansion ratio across the turbine will be very high at the maximum engine speed, when air flow is greatest.* Thus the piston must pump the exhaust

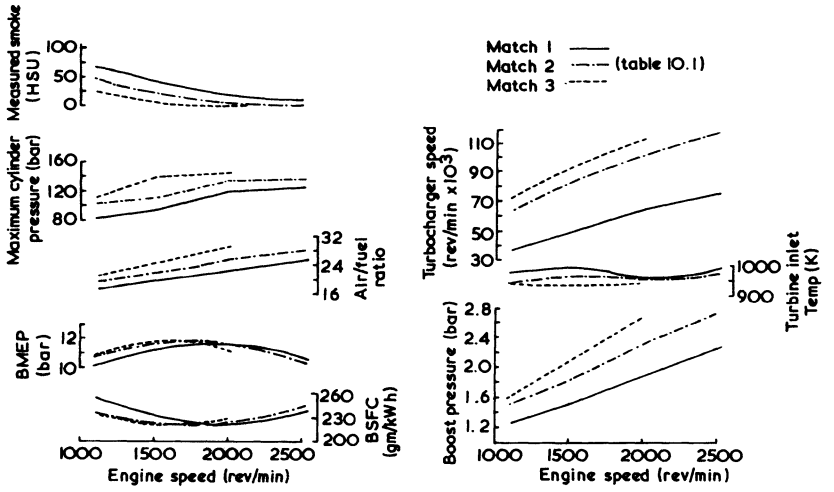

Figure 10.24 *The effect of turbine match on engine performance with no change in fuelling [6]*

gases out against a high pressure, resulting in poor net power output and fuel consumption. This is seen as low BMEP and high BSFC at high engine speed (2000 rev/min) with match 3, figure 10.24. In addition, the engine exceeds the allowable limits of maximum cylinder pressure and turbocharger speed. Thus match 2 is a reasonable compromise, except that maximum power (BMEP at maximum speed) is marginally less than that achieved with match 1.

Ideally a variable geometry turbine is required. This would have the effective turbine area of match 1 at full engine speed, but the effective area of match 2 at mid-speed and match 3 at low speed. This would offer the low exhaust smoke, low fuel consumption and high BMEP of match 3 at 1000 rev/min, with the low cylinder pressure and low fuel consumption of match 1 at 2500 rev/min. This is an ideal that has attracted turbocharger and engine manufacturers for many years, since it reduces the speed dependence of turbine specific available energy shown in figure 10.23. The problem is one of engineering a cheap, reliable and effective system, and has not been solved to date. Prototypes exist, but no system is currently available in mass production. Experimental results with a prototype variable geometry system are presented in chapter 11.

By taking advantage of the extra air flow generated by match 2, fuelling may be increased over the complete speed range in order to raise torque and restore the maximum power output of match 1. Figure 10.25, match 4, is the extreme case, in which fuelling is increased (with turbine 2) until the original maximum air/fuel ratio is achieved. Naturally, low-speed smoke has reverted to its former value, but a substantial increase in power output has been obtained, without loss of torque back-up or a substantially higher turbine inlet temperature. A small deficit in fuel consumption at high speeds is countered by a substantial improvement at low speeds. The disadvantages are high mechanical loading (maximum

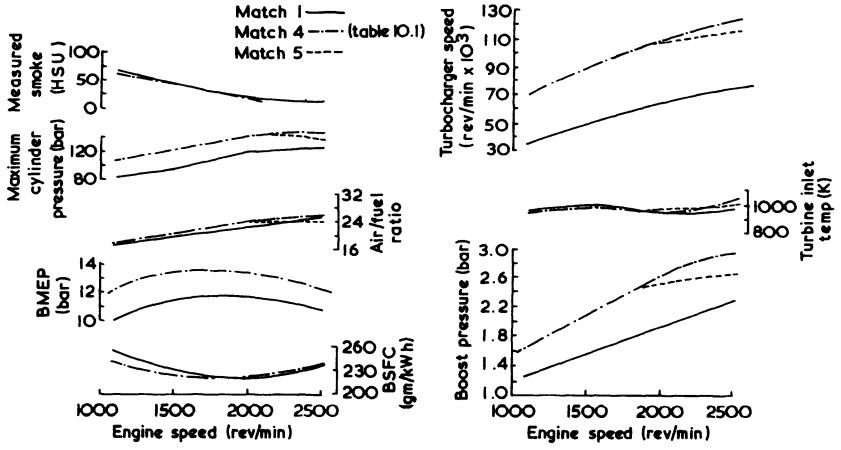

Figure 10.25 *The effect of turbine match on engine performance at constant minimum trapped air/fuel ratio [6]*

* Turbocharger specifications are given in table 10.1.

cylinder pressure and turbocharger speed). In practice, a complete envelope of performance options between matches 1 and 4 is available by suitable choice of turbine trim and fuel setting.

Further 'fine-tuning' of the turbine may be achieved by selecting from different components having approximately the same effective area at the mid engine speed condition, but whose flow and efficiency variations differ over the working range of the engine (see chapter 4 and Watson [1]).

10.7.2 Exhaust Waste Gates and Automotive Engines

The problem of over-speeding the turbocharger and coping with high cylinder pressures becomes prominent when engines which operate over a very wide speed range are turbocharged and matched for good torque back-up. The small turbocharged passenger car diesel engine falls into this category. A method of avoiding this problem is to by-pass some of the exhaust gas around the turbine (figure 10.26) at high speed and load. Thus, when a small turbine is fitted to achieve good low-speed boost, the massive increase in specific available energy at the turbine at high speed is alleviated by increasing the effective flow area out of the exhaust manifold. This has two effects. Firstly, only part of the exhaust gas flow goes through the turbine. Secondly, the increase in flow area reduces the exhaust pressure that would otherwise build up. Both measures reduce turbine work and hence boost pressure. In addition, the second factor reduces pumping work during the exhaust stroke and would, for example, moderate the loss in BMEP and deterioration in fuel consumption shown in figure 10.24, match 3, at high speeds.

The by-pass valve will usually be built into the turbine casing, and will consist of a spring-loaded valve acting in response to the inlet manifold pressure acting on a controlling diaphragm. Different combinations of spring load, diaphragm area and valve area can be used to achieve a wide variety of boost pressure variations with engine speed. Disadvantages are increased cost, potential unreliability and the restriction to a single-entry turbine housing. Thus some of the

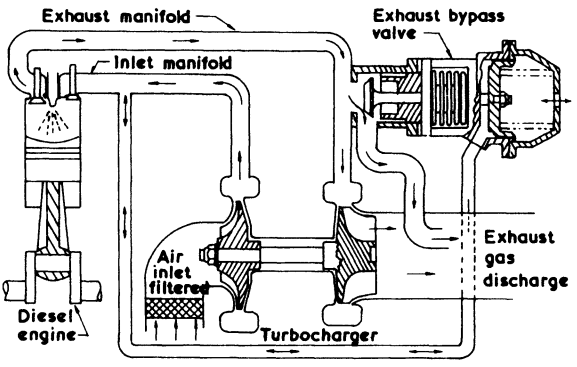

Figure 10.26 *Turbocharger exhaust by-pass valve [7]*

benefit of good pulse energy utilisation at low speed (chapter 7) is lost, particularly on six and eight-cylinder engines.

Figure 10.25, match 5, shows how an exhaust waste gate may be used to reduce the high boost pressure developed by a small turbine (match 4) and hence control turbocharger speed and, to a lesser extent, maximum cylinder pressure.

10.7.3 Fuel System Matching

Development of fuel injection pumps and associated equipment has introduced additional freedom to vary fuel delivery over the speed range of an engine. The turbocharger matching process must be closely linked with fuel system matching even after optimum injection rates, pressures, nozzle sizes and swirl have been achieved.

Tailoring of the fuel delivery characteristic is a method of achieving good torque back-up within the framework of engine and turbocharger limitations (figure 10.22). For example, match 6, figure 10.27, is identical to match 4, except that maximum fuelling is restricted at high speeds in order to limit the maximum turbocharger speed. Fuelling is gradually restricted from 2000 rev/min upwards, but a reduction from 1500 rev/min upwards would reduce not only turbocharger speed but maximum cylinder pressure. Thus impressive torque back-up would be achieved, but at the expense of a low maximum power output.

At the other end of the speed range, excessive smoke can be reduced by restricting fuelling until sufficient boost is available to generate a reasonable air/fuel ratio. Thus a spring-loaded diaphragm senses boost pressure and allows the maximum fuel stop to open as engine speed increases. Since fuelling is restricted only when the boost pressure is zero or low, torque is only reduced at

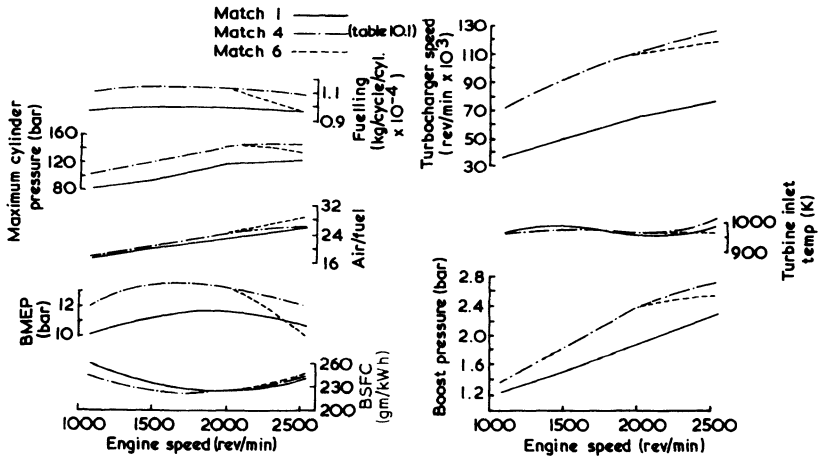

Figure 10.27 *The effect of turbine match and fuel control on engine performance [6]*

very low speeds, that is, below that at which maximum torque is achieved. The device is commonly called an 'aneroid' (fuel controller).

10.7.4 Engine Speed Range

The difficulty of achieving a satisfactory match over a wide speed range has been explained. In certain circumstances it may be advantageous to reduce the rated speed of an engine while increasing BMEP to achieve the same maximum power output.

By reducing the turbine area and increasing fuelling (figure 10.25, match 4), high BMEP is obtained. If maximum rated speed is reduced from 2500 rev/min to 2000 rev/min (an extreme case), excessive turbocharger speed is avoided. Naturally the final drive gear ratio of the truck must be raised to compensate, hence the engine is working at a higher load than would normally be the case at the same vehicle speed and load. Since specific fuel consumption reduces with load, fuel savings are possible.

Figure 10.28 illustrates the fuel consumption of a truck with a conventional turbocharger (match 1), and a reduced speed (match 7), with the same maximum power output. The four diagrams denote operation at maximum speed (top), 80, 60 and 40 per cent of maximum speed (bottom). In all cases the speed of the match 7 engine is 84 per cent of the match 1 engine, with the final drive of the vehicle adjusted accordingly. The BMEP with match 7 is higher than with match 1, in order for both systems to develop the same power at their respective maxi-

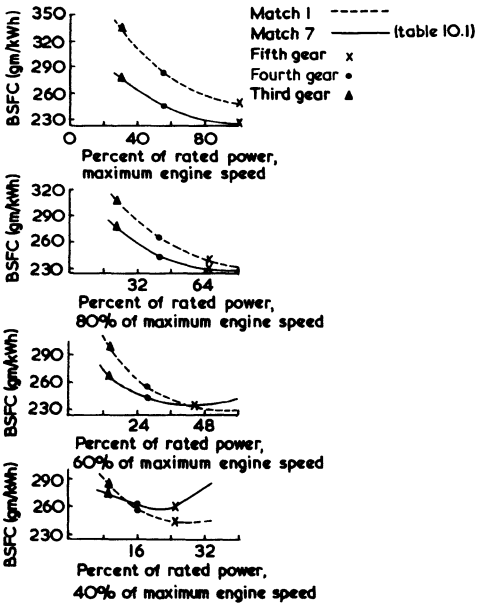

Figure 10.28 *The effect of reducing rated speed and increasing BMEP on steady speed fuel consumption [6]*

mum speeds. The right-hand points on the top diagram (denoted x) represent operation with the vehicle running at full speed along a flat road in fifth gear. Each engine is at full load and maximum speed. The specific fuel consumption is lower with match 7, since this engine is operating at lower speed and higher load, where engine efficiency is superior. The other points on the top diagram (denoted by • and Δ) represent full engine speed in fourth and third gear, again with the vehicle driving steadily along a flat road. In these cases, vehicle speed is lower, hence the engine is operating at less than rated power (or BMEP) but its maximum speed. Match 7 remains more efficient than match 1 because BMEP is higher and speed lower.

At lower engine speeds the same basic trends are shown but the difference between match 1 and match 7 reduces as engine speed reduces and changes sign at very low speeds. Thus limiting speed range is seen to result in a significant improvement in fuel consumption over most of the operating range of the vehicle, except in high gear at low speeds. This advantage primarily results from the fact that running at lower engine speeds substantially reduces mechanical friction in the engine while higher load operation only causes a marginal increase.

10.7.5 Compressor Matching

Since the truck engine operates over a wide speed and load range, the air flow requirements cover large areas of the compressor map. A typical superimposition

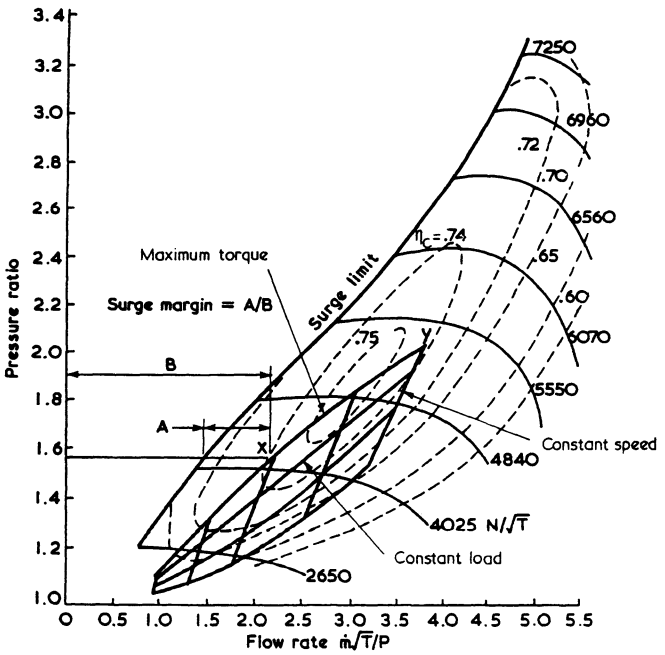

Figure 10.29 *Engine operation area superimposed on compressor map, showing surge margin*

of engine air flow on the compressor map is given in figure 10.29, showing lines of constant engine speed (1000, 1500, 1900, 2400 and 2800 rev/min) and load (3.85, 6.17 and 8.48 bar), and the maximum torque curve.

Selection of the correct compressor is largely a matter of ensuring a sufficient surge margin (A/B, figure 10.29) and that the operating points at maximum torque and power (points X and Y, figure 10.29) occur at reasonable compressor speed and efficiencies. Thus the compressor shown in figure 10.29 is a satisfactory choice, since the operational area is clear from the surge line and lies in an area of high efficiency. However, a slightly larger compressor might result in more of the operating regime experiencing higher compressor efficiency, with a less generous surge margin. A small improvement in low speed boost could also be obtained if maximum compressor efficiency occurred at a lower pressure ratio (for example, 1.6 compared with 1.8 in figure 10.29).

Reducing turbine area will raise the boost pressure, reducing the surge margin (compare figures 10.29 and 10.30) and therefore a smaller compressor trim may be required in some cases. However, the surge margin shown in figure 10.30 is adequate, the compressor being well matched.

Figure 10.31 shows a poor compressor match, using too small a compressor trim on an intercooled engine. At maximum speed and load (point Y) the compressor efficiency is low. Boost pressure actually falls as the engine speed increases from 2400 and 2800 rev/min as a result. It may occasionally be convenient to

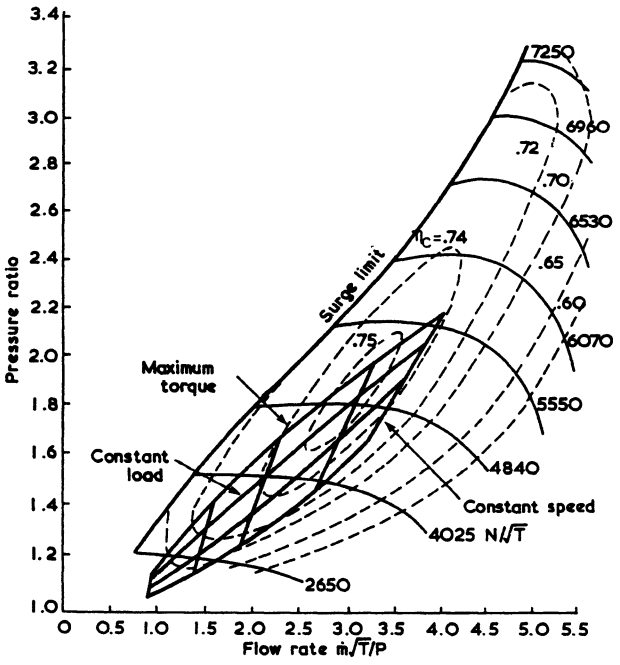

Figure 10.30 *Engine operation area superimposed on compressor map, showing surge margin with reduced turbine area*

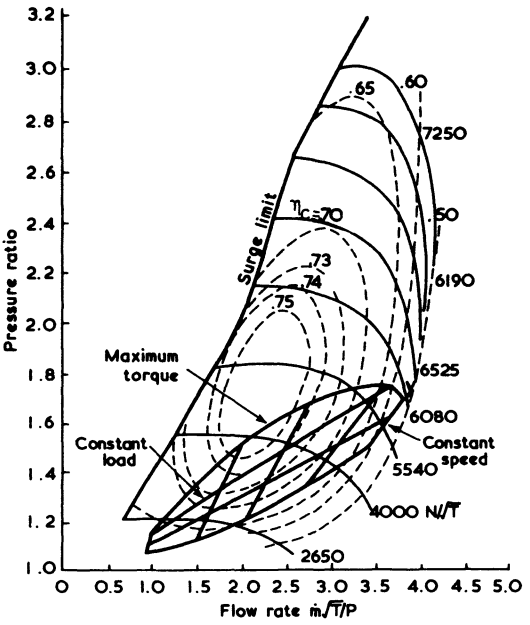

Figure 10.31 *An incorrectly matched compressor on a charged cooled engine*

deliberately match into an inefficient region at maximum engine speed and load, in order to hold the boost pressure and therefore maximum cylinder pressure down. However, an excessive reduction in efficiency occurs in the extreme case shown, and piston pumping work during gas exchange will suffer.

10.8 Matching the Two-stroke Automotive Engine

Few manufacturers now produce automotive two-stroke engines, General Motors (Detroit Diesel) being the only large company involved. Turbocharging the two-stroke automotive diesel engine involves some additional concepts to those already discussed above. Since the engine must work over a wide speed and load range, and must be capable of starting from a battery, some form of assistance will be required to produce the pressure drop from intake to exhaust manifolds so essential for scavenging at cranking speeds. Normally a Roots blower is used, placed in series after the turbocharger compressor. As explained in section 10.2, the Roots blower will ensure that the air flow characteristics are similar to those of a four-stroke engine. However, the balance of work between Roots blower and turbocharger will affect the power output, torque curve and specific fuel consumption.

Similarly to a four-stroke engine, the boost pressure will rise with speed and load. It follows that the Roots blower will be expected to provide most of the boost pressure at low speeds and loads, yet a reducing proportion of the total

as speed and load rises. The capacity of the Roots blower will be governed by the need for acceptable performance at low speeds. The roots blower absorbs power from the crankshaft of the engine, hence it reduces the power available at the flywheel. The larger the capacity of the Roots blower, the greater the loss in engine power output. Specific fuel consumption deteriorates. If the Roots blower is too small, scavenging at low speeds will be poor. If it is too large, then power will be wasted in developing an excessive boost pressure at high speeds and loads, where the turbocharger alone could provide sufficient boost.

Both the Roots blower and turbocharger must be matched to the engine together. Figures 10.32 to 10.34 show the performance obtained from an automotive two-stroke engine at three speeds, during turbocharger and Roots blower matching tests. At low speeds (figure 10.32), the larger Roots blower (85) substantially reduces specific fuel consumption and turbine inlet temperature. To achieve anything approaching the same performance with the smaller Roots blower (75), the turbocharger must be encouraged to do more work, by reducing turbine area (that is, increasing nozzle stator angle). At medium speeds, the differences in specific fuel consumption are smaller (figure 10.33). However, the

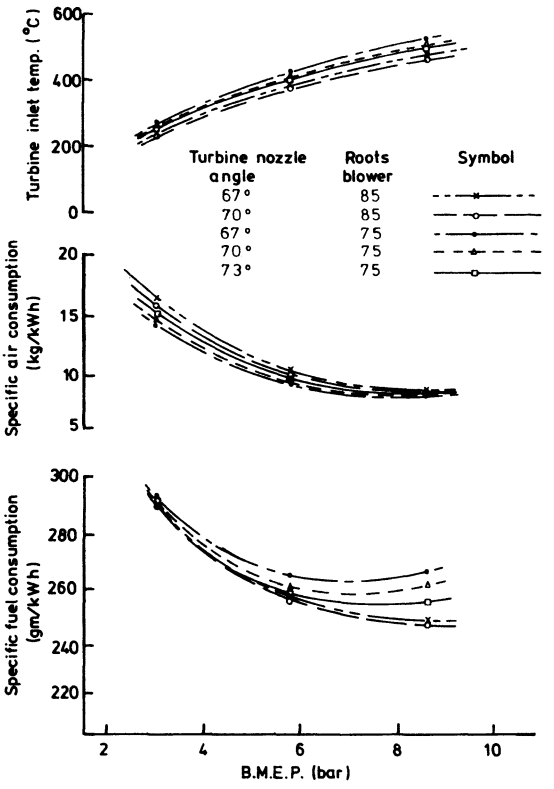

Figure 10.32 *Two-stroke turbocharger and Roots blower matching curves at 1000 rev/min*

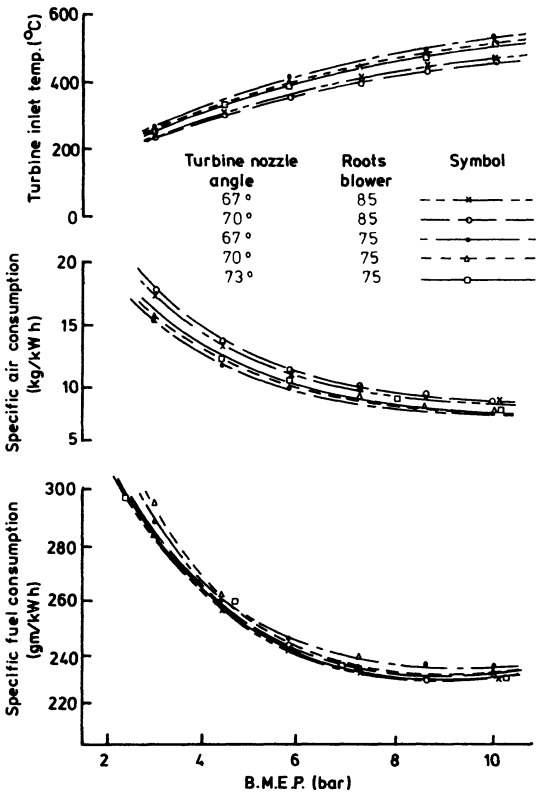

Figure 10.33 *Two-stroke turbocharger and Roots blower matching curves at 1500 rev/min*

air flow (or specific air consumption) is significantly greater with the larger Roots blower. Scavenging improves, but the gain is offset by the additional power absorbed by the Roots blower. At high speed (figure 10.34), the engine benefits little from the additional air flow from the larger blower, since the turbocharger is providing enough boost for good scavenging when the smaller blower is fitted. Thus a saving in blower power is reflected in superior fuel consumption. Any scavenging benefit obtained by fitting the larger blower is marginal and is not offset by its extra power requirement. Thus these figures illustrate the conflict between performance at high and low speed. A sensible compromise is to fit the larger Roots blower and the smallest turbine housing shown.

10.9 Changes in Ambient Conditions

Changes in inlet air density may be caused by ambient temperature and pressure changes at sea level, or operation of the engine at altitude. The change of air

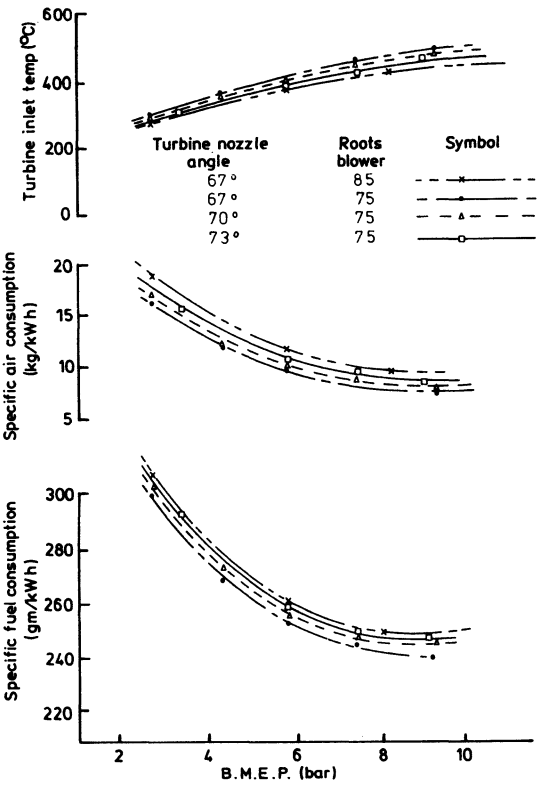

Figure 10.34 *Two-stroke turbocharger and Roots blower matching curves at 2000 rev/min*

flow may readily be predicted if the engine is naturally aspirated, but this is more difficult if the engine is turbocharged.

In mobile applications, such as a truck, the engine may be required to operate at sea level in a cold winter climate and perhaps at altitude during a hot summer. Thus the final compressor and turbine matches selected will be something of a compromise, particularly if the pressure ratio is high. The match selected will suit the normal operating environment of the engine, but with sufficient margins on surge, turbine inlet temperature and turbocharger speed to cover other conditions.

If the engine is designed for stationary applications, its operating altitude will be known, hence the manufacturer will have the option of rematching the turbocharger to suit the environment. The alternative will be to derate the engine for operation at altitude.

Although operation under changing ambient conditions introduces additional complications for the manufacturer of a turbocharged engine (such as reduction of the surge margin), the turbocharging system does offer partial compensation

for reducing air inlet density at altitude. If variations in turbocharger efficiency are ignored for simplicity, the energy equation for constant pressure turbocharging (equation 6.1) may be written as

$$[(P_2/P_1)^{(\gamma_{a-1})/\gamma_a} - 1] = K(T_3/T_1)\,[1 - (P_1/P_3)^{(\gamma_{e-1})/\gamma_e}] \qquad (10.8)$$

where K is a constant. As air density and therefore air mass flow rate reduce, so the turbine inlet temperature (T_3) will rise due to the richer air/fuel ratio. This means that the ratio of compressor to turbine pressure ratios will be altered in favour of the compressor. Its pressure ratio will increase, partially offsetting the reduction in air inlet density. It is also apparent from equation 10.8 that as ambient pressure (P_1) falls, so the expansion ratio of the turbine increases, raising compressor pressure ratio, provided that the turbine inlet pressure (P_3) does not fall at the same rate as ambient pressure.

An increase in ambient temperature (T_1) however, has an undesirable effect on the turbine to compressor energy balance, hence the turbocharger will tend to amplify the effect of such a change on air flow rate.

10.9.1 Operation under Changing Ambient Conditions, without Rematching

Large variations in ambient conditions can lead to problems due to compressor surge, excessive cylinder pressure, turbine inlet temperature, turbocharger speed or smoke emission. The actual performance of an engine under varying ambient conditions will depend on several factors which, for convenience of explanation, were assumed to be constant in the simplified analysis given above. For example, if air mass flow rate and compressor pressure ratio change, movement across the operating map of the compressor will be accompanied by an efficiency change. It follows that engines of similar performance at sea level will not necessarily perform comparatively at altitude. Techniques have been developed for accurately predicting the effect of varying ambient conditions (see chapter 15), but these require detailed turbine and compressor maps. A simpler, but less rigorous approach, is to correlate the performance of existing engines obtained when operating at altitude, or in very hot and very cold climates.

The parameter that limits engine performance will depend on the design of individual engines. At high ambient temperatures (figure 10.35), the limits are

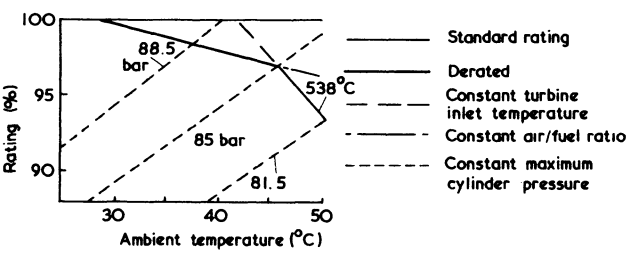

Figure 10.35 *Engine limitations at high ambient temperatures [8]*

likely to be smoke, due to reducing air flow, then turbine inlet or exhaust valve temperature or thermal loading of the engine. At low ambient temperature, maximum cylinder pressure or compressor surge (due to high pressure ratio, see equation 6.1) may be a limiting factor. It will be the limitations of a particular engine and turbocharger combination that will govern to what extent fuelling must be reduced, derating the engine for acceptable reliability or smoke emission. Low temperature, through its influence on compressor pressure ratio, can lead to compressor surge if the temperature change is very great.

Operation at altitude is usually, but not always, accompanied by a reduction in temperature. Through the combined effects of the rich fuel/air ratio on turbine inlet temperature and low turbine exit pressure, the turbocharging system offers partial compensation of the inlet air density reduction at altitude. Thus an engine may have to be derated, but not by as much as a naturally aspirated engine.

The effect of altitude on a turbocharged truck engine at full power, with and without intercooling, is shown in figure 10.36. Although the absolute inlet manifold pressure reduces with altitude, the reduction is smaller than that of ambient pressure (figure 10.37). Turbocharger speed increases due to the increase in turbine inlet temperature and expansion ratio. It can be seen that thermal limits and the maximum permissible turbocharger speed will be the limiting factors, particularly the latter. Movement towards the surge on the compressor map is shown in figure 10.38 for the non-intercooled engine, operating at part speed and load.

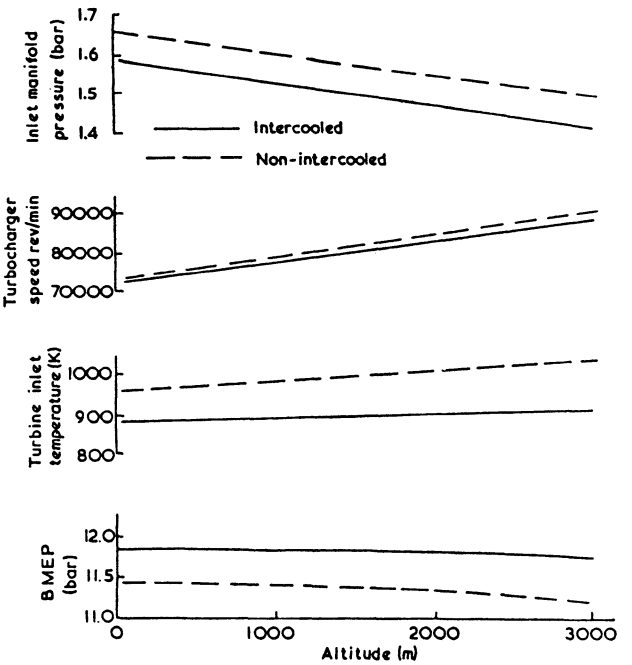

Figure 10.36 *The effect of altitude on truck engine performance*

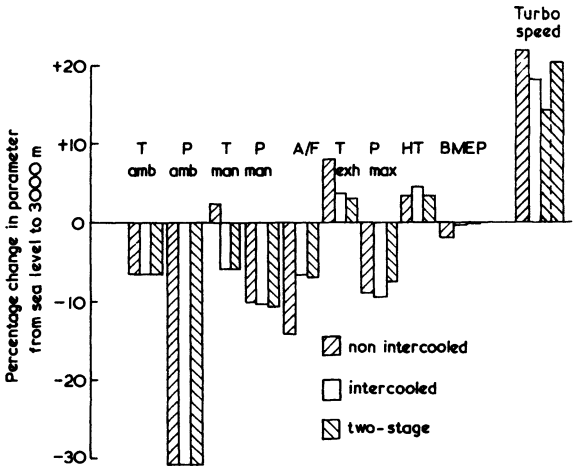

Figure 10.37 *Relative change in performance parameters at altitude*

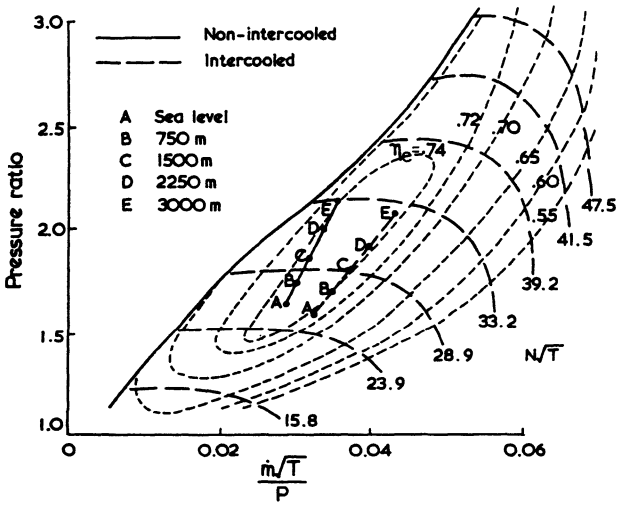

Figure 10.38 *Reduction in surge margin at altitude (part speed and load)*

If a stationary engine is not rematched for operation at altitude, then initially smoke emission, followed by turbocharger speed or inlet temperature will be the factors governing the reduction in fuelling and therefore rated power output, required. CIMAC (Conseil International des Machines à Combustion) recommend an empirical formula for derating at altitude, based on a limitation of constant turbine inlet temperature. The formula is

$$\dot{W}_{alt} = \dot{W}_{ref}\left[K - 0.7(1-K)\left(\frac{1}{\eta_{mech}} - 1\right)\right] \qquad (10.9)$$

TABLE 10.2 *Exponents in CIMAC formula for derating at altitude*

Four-stroke Turbocharged Diesel Engines			
	m	n	q
Without charge cooling	0.7	2.0	–
With charge cooling	0.7	1.2	1.0

where

$$K = \frac{\dot{W}_{alt(ind)}}{\dot{W}_{ref(ind)}} = \left(\frac{P_{a(alt)} - hf\phi_{alt}P_{svp}}{P_{a(ref)} - hf\phi_{ref}P_{svp(ref)}} \right)^m \times \left(\frac{T_{ref}}{T_{alt}} \right)^n \left(\frac{T_{cool(ref)}}{T_{cool(alt)}} \right)^q$$

Values of the indices m, n and q are given in table 10.2.

10.9.2 Rematching to Suit Local Ambient Conditions

If the turbocharger is selected to suit the local ambient condition, additional density compensation can be provided in some cases. By reducing the turbine trim, more work can be extracted from the turbine enabling boost pressure to be raised, offsetting the loss in ambient density. This will, for example, delay the smoke limit or turbine inlet temperature limit to higher altitudes or ambient temperatures (compare figures 10.35 and 10.39). Thus derating may be avoided altogether or reduced. However, the influence of a more restrictive turbine on exhaust manifold pressure levels must be considered. Some engine performance deficit may occur.

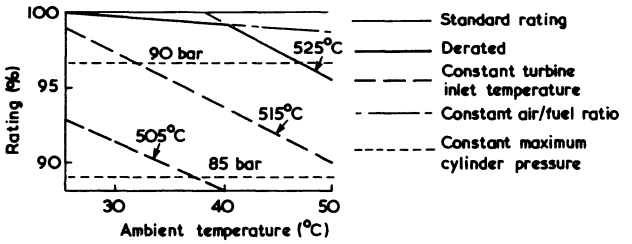

Figure 10.39 *Engine limitations at high ambient temperatures with appropriately matched turbocharger [8]*

References

1. N. Watson, Turbocharging in the 1980's, current trends and future prospects, *SAE 790123*, Turbochargers and Turbocharged Engines, SP442 (1979)

2. J. D. Ledger, Computer aided design of the exhaust of a turbocharged diesel engine, Interactive Systems, On-line Eurocomp (1975)
3. E. Meier, Development of exhaust gas turbochargers and pressure charging systems for diesel engines with high mean effective pressures, *Proc. CIMAC* (1973)
4. E. Kellett and J. F. Betteridge, Achieving constant horsepower by turbocharging, *Engine Des. Appl.* (November 1965)
5. I. W. Goodlet, Turbocharging of small engines, *Proc. Inst. Mech. Engrs.*, **188**, No.3/74 (1974)
6. N. Watson, M. Marzouk and Z. Baazaari, Turbocharging system options for vehicle engines, Paper C61/78, Turbocharging and Turbochargers Conference, *Inst. Mech. Engrs* (London, 1978)
7. W. E. Woolenweber, The turbocharger – a vital part of the engine intake and exhaust systems, *SAE 700534* (1970) (also in SP359, Pt. 18)
8. W. E. Lowe, The effect of ambient and environmental atmospheric conditions, *Proc. Inst. Mech. Engrs.*, **184**, Pt.3P (1969/70)

11

High-output Turbocharging

11.1 Introduction

The demand for higher and higher power outputs from a specified size of diesel engine continues. Higher outputs may be achieved by increasing speed and/or BMEP. In the last 25 years there has been a steady increase in rated mean effective pressure (figure 1.5) but only a relatively small speed increase. There are many reasons why it is difficult to increase the speed of an engine substantially. Limitations arise due to the inertia of reciprocating parts, deterioration of volumetric efficiency, air/fuel mixing problems, etc. Some limitations are absolute, in that engine damage will result if a certain speed is exceeded; others result in a progressively deteriorating engine fuel consumption (efficiency). Furthermore different limitations affect different types (and sizes) of engine. However, the potential for increasing engine speed is rather limited, although gradual progress will be made (figure 11.1).

Major increases in BMEP have followed the introduction of turbocharging and charge air cooling, to all types of engines. Although this has not been achieved without mechanical problems, the over-all reliability of quite highly rated engines is significantly better than was the case many years ago. There remains considerable scope for further increasing mean effective pressures, supported by encour-

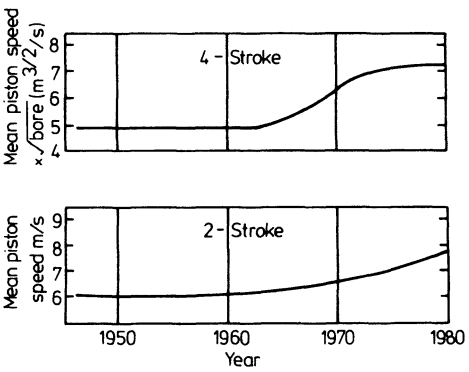

Figure 11.1 *Average increase in piston speed since 1945 [1]*

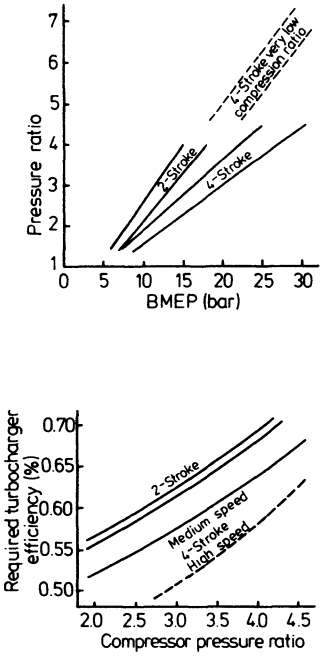

Figure 11.2 *Required pressure ratio and turbocharger efficiencies at high BMEP [2]*

aging performance of certain experimental engines that have run up to 30 bar BMEP. However, both engine and turbocharger design limit the mean effective pressures that may be used commercially at any specified time in the development story of turbocharged diesel engines. The basic engine limitations are the value of maximum cylinder pressure (that is, stress limits), thermal loading and possibly the fuel injection system (due to the difficulty of injecting rapidly at very high pressure). The single-stage turbocharger is limited, principally, by its over-all efficiency and flow range at high pressure ratios, turbine inlet temperature and speed.

Figure 11.2 shows the compressor pressure ratio necessary to achieve BMEPs from 7 to 17 bar on two-stroke engines and 10 to 28 bar on four-stroke engines. The bands shown cover a variety of different engine designs, using different turbocharging systems, but all are industrial and marine rather than vehicle engines. The turbocharger efficiency (over-all), required to reach these pressure ratios and ratings is also shown, the wide band for four-stroke engines resulting from the variety of turbocharging systems used.

Many techniques are available to help improve the performance of the turbocharging system at very high boost pressures, and the offdesign performance at moderately high pressures. The methods can be divided into those that improve the efficiency or characteristics of the turbocharging system (at high pressure ratios), such as two-stage turbocharging, variable geometry turbocharging, and those that use an external energy supply to aid the turbocharger. Among the

latter are compound engines and combustion of fuel/air in parallel with the combustion chamber of the engine purely to increase turbine work (for example, the 'Hyperbar' system). One important method of achieving high output from turbocharged diesels is to aftercool the air leaving the compressor. Charge cooling has been fully described (chapter 9), and must be considered essential for high-output turbocharging. However, before discussing the methods of achieving high output, the engine and turbocharger limitations must be defined in more detail.

11.2 Engine Limitations

As boost pressure is raised it is obvious that the maximum cylinder pressure achieved during combustion will also rise, generating high stress in many mechanical components. Figure 11.3 shows how peak cylinder pressure increases with boost pressure as the latter is raised to attain high BMEP. This diagram relates to a medium-speed four-stroke engine with a compression ratio 10.5:1. Fortunately we have not yet reached the metallurgical limits of the standard cast and fabricated components, provided that they are adequately designed and cooled. Thus reliability at high engine loads is largely a function of detailed design, manufacturing technique and cost. It is not within the scope of this chapter to discuss details of engine design, since information is given in many technical papers (for example, CIMAC conference proceedings). However, it is useful to obtain an idea of what levels of pressures and component temperatures are involved. Figure 11.4 shows the performance of a medium-speed four-stroke diesel engine using two-stage turbocharging with interstage and aftercooling. The turbocharger was matched for optimum performance at 24 bar BMEP. At 28 bar BMEP the maximum cylinder pressure reached 180 bar with a boost pressure ratio of 4:1. The mean turbine inlet and exhaust valve temperatures were not excessive (570 and 400 °C respectively). Although other component temperatures at this BMEP are not available, figure 11.5 shows the temperature profiles at various critical components (piston, exhaust valve, cylinder head and liner) at 24.15 bar BMEP. These figures were obtained on a standard production engine designed

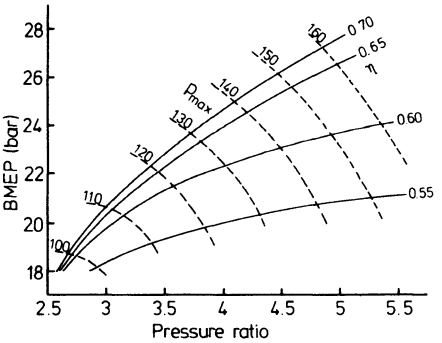

Figure 11.3 *The influence of compressor pressure ratio and BMEP on peak cylinder pressure [3]*

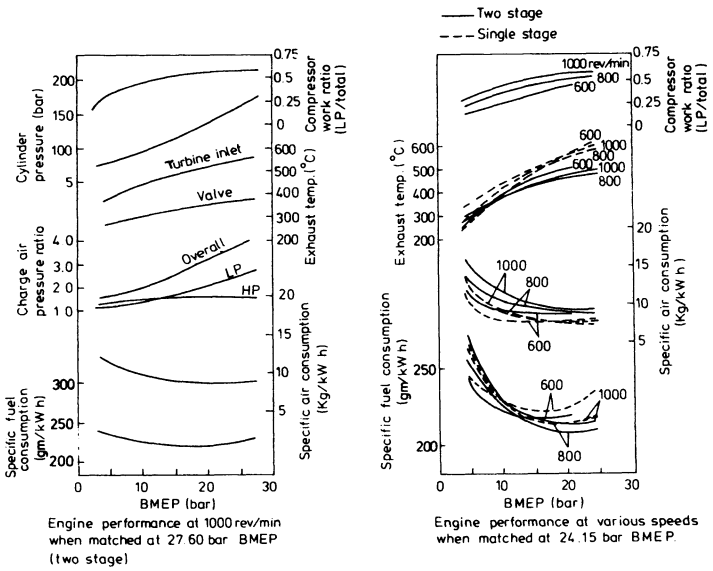

Figure 11.4 *Performance of medium-speed four-stroke diesel engine at very high output [4]*

for operation at considerably lower loads and point to the fact that an engine could be designed to run at significantly higher mean effective pressures than normal today.

It is possible to limit the direct mechanical loads due to cylinder pressure by reducing the compression ratio. This technique results in a loss of thermodynamic cycle efficiency but this will be offset at full load by an apparent gain in mechanical efficiency, since mechanical losses will not increase in proportion to BMEP. Typical compression ratios of medium-speed four-stroke engines have reduced from 16 to 17 on naturally aspirated engines in 1950 to 11 to 12 in 1980, reflecting the need to limit maximum cylinder pressure when turbocharging for higher BMEP. The minimum compression ratio that may be used will be governed by the ability of the engine to start from cold and to idle smoothly with a clean exhaust. For the medium-speed diesel engine the minimum compression ratio is about 11 if starting aids are not to be used. 13 to 14 is the normal minimum for swirl chamber, diesel injection engines.

Ideally, a variable compression ratio engine is required, running with high compression ratio when starting or operating at low load, and reducing compression ratio at high load. Thus high compression temperature is achieved at low loads for good combustion, and maximum cylinder pressure is restricted at

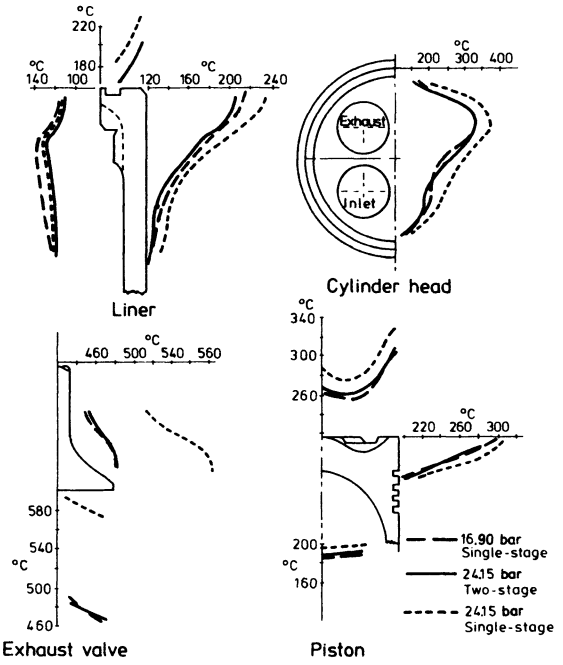

Figure 11.5 *Metal temperature of combustion chamber components [4]*

high load. Numerous systems with varying degrees of complexity have been tested, most relying on varying oil pressure in a cavity separating the piston crown from its body. [5] However, the cost, complexity and potential unreliability of the systems have kept them out of commercial production.

An alternative approach is the 'variable geometry' combustion chamber system of SEMT-Pielstick, based on an indirect injection or pre-combustion chamber system (figure 11.6). As the piston approaches TDC, the piston plug virtually closes the connecting passage. The geometry of the chambers is then such that the compression ratio generated in the pre-chamber exceeds that in the main chamber. The small size and compact shape of the pre-chamber make it much easier to contain a higher pressure than the main chamber.

The Miller turbocharging system [6] can be used to reduce pressure and/or temperature, by altering valve timing. If the inlet valve is closed *before* TDC, then cylinder pressure and temperature will fall from around the inlet manifold values at inlet valve closure (IVC) to lower values at BDC. Relative to an engine having inlet valves that close at BDC or later, the cylinder pressure and temperature at the beginning of compression are lower, and hence peak cylinder pressure and temperature reduce. An obvious disadvantage is that the mass of air trapped in the cylinder reduces, but the Miller system compensates for this by using a higher compressor pressure ratio, and therefore inlet manifold air density. If the objective is to reduce the maximum cylinder pressure of a diesel engine, then the compressor pressure ratio must only be raised sufficiently to

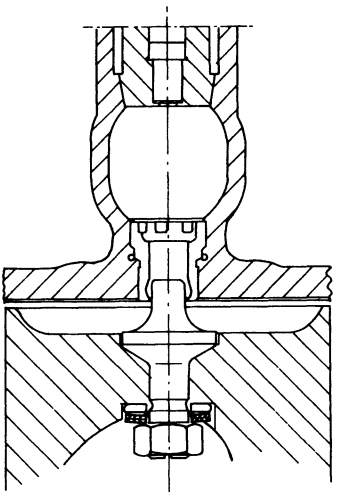

Figure 11.6 *Arrangement of the variable geometry combustion chamber on the SEMT-Pielstick PA 4-185 engine*

offset the loss in trapped mass in the cylinder. Usually the charge air cooling system will be designed to maintain the same inlet manifold air temperature, hence the increase in air density will be proportional to the increase in absolute inlet manifold pressure. A simplified example follows, based on part of an ideal cycle in which the inlet valve would normally close at BDC.

Assume an absolute boost pressure of 2 bar, a cylinder volume at BDC of V and a volumetric compression ratio of 10:1. Assuming isentropic compression with an index of 1.4, the compression pressure at TDC (assumed to be before combustion) is given by

$$P_{TDC} = 2\left(\frac{10}{1}\right)^{1.4} = 50.24 \text{ bar}$$

Now assume that the Miller system is used, with the inlet valve closing when $V_{cyl} = 0.9V$. The boost pressure must be raised to 2(10/9) = 2.22 bar to retain the same trapped mass in the cylinder, assuming no change in inlet manifold temperature. The effective compression ratio is reduced to 9:1, hence

$$P_{TDC} = 2.22\left(\frac{9}{1}\right)^{1.4} = 48.12 \text{ bar}$$

Thus compression pressure is reduced by 4.22 per cent.

In order to retain the ability to start from cold and operate effectively at low load, a variable valve timing system should be used, advancing IVC as above, towards full load. An additional disadvantage is the need for a high turbocharger pressure ratio.

Figure 11.7 shows the performance of a medium-speed four-stroke marine diesel engine using the Miller system, combined with two-stage turbocharging to achieve the high boost pressure required. Variable inlet valve timing is used, with

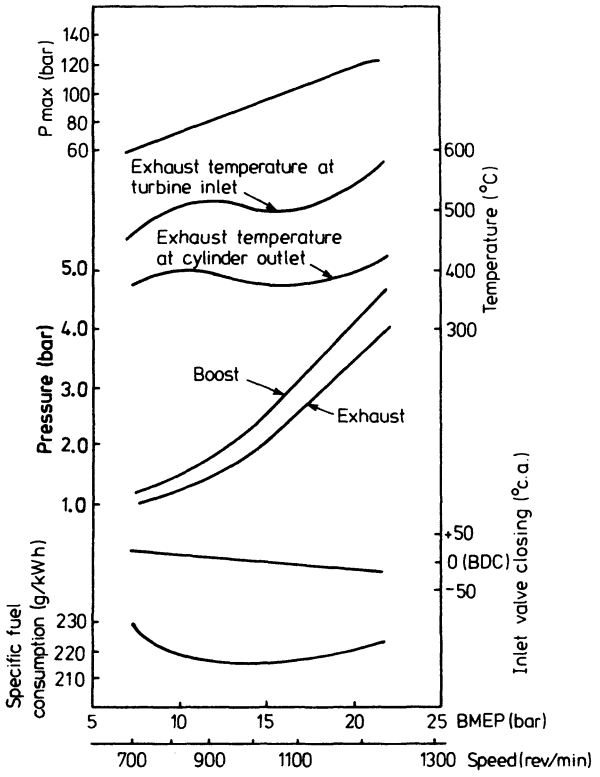

Figure 11.7 *Propeller law performance with the Miller system and two-stage turbocharging [7]*

intake closure around 20° BBDC at 22 bar BMEP. Maximum cylinder pressure is 128 bar, with a compressor pressure ratio of 4.6:1. The combination of the Miller system with two-stage turbocharging is discussed in detail in section 11.5.

The Miller system is particularly attractive for natural gas engines, since compression temperature may be reduced allowing much higher compressor pressure ratios, or engine compression ratios, to be used without causing combustion knock. Figure 11.8 shows computed cylinder pressure and temperature during the end of the intake stroke and beginning of the compression stroke, with variable intake valve closing. As intake valve closure is advanced from 60° ABDC through 40°, 20°, BDC and 55° BBDC, so boost pressure has been raised to maintain the same cylinder pressure during compression (that is, more than that required to retain the same trapped mass). The temperature during the compression stroke progressively reduces. With spark ignition, variable valve timing is not necessary and the compressor pressure ratios required are normally low enough for single-stage turbocharging to be adequate.

The most common method used to reduce maximum cylinder pressure on very highly rated diesel engines is to use a fixed, low compression ratio. This reduces engine cycle efficiency, but can allow power output to increase substan-

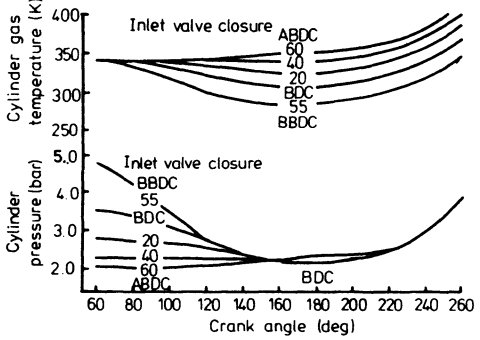

Figure 11.8 *The effect of varying inlet valve closure on cylinder pressure and temperature, with boost pressure changing to produce the same compression pressure [8]*

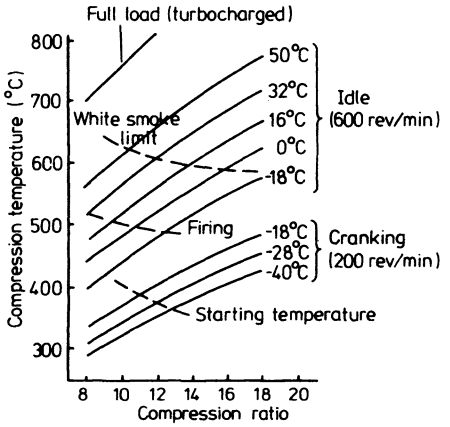

Figure 11.9 *Relationship between compression ratio, compression temperature and ambient temperature for diesel combustion [9]*

tially. The reduction in the fraction of indicated power lost to friction may be enough to offset the loss in cycle efficiency, resulting in little change in specific fuel consumption. The major problem that results is low compression temperature and pressure in the absence of boost pressure when starting the engine or running at low load. Either electrical heating or pilot fuel burning systems can be used to heat air in the inlet manifold for cold starting. To improve ignition and combustion at low load, some engine manufacturers shut the coolant flow to charge air coolers or by-pass air around them.

Figure 11.9 shows the relationship between compression ratio and compression temperature at various ambient air temperatures. The diesel starting and firing temperatures denote ignition of No. 1 diesel fuel and sustained firing temperature. Also shown is the compression temperature required to avoid white smoke emission due to poor combustion. This shows, for example, that this engine will

not start with a compression ratio below 11:1, if the ambient temperature falls below -18 °C. Having started, white smoke will be emitted when idling with a charge air temperature below 43 °C.

Increased thermal loading is usually a much more difficult problem since it is not amenable to simple remedial measures such as reducing the compression ratio. Although this will help by reducing temperature throughout the cycle, the benefit is marginal in non-quiescent chambers since combustion and heat transfer are dominated by the effect of air movement. Thermal loading can be reduced by using the high boost pressure to achieve a specified power output with a high trapped air/fuel ratio, but this technique will raise maximum cylinder pressure and therefore may not be acceptable.

Probably the most common type of thermal failure results from a fatigue crack formed under load cycling conditions. This may result in early failure in service following satisfactory endurance testing at continuous high load. The cyclic variation in temperature varies approximately inversely as the square root of engine speed and will therefore be smaller in high speed engines. However, even on a low-speed engine, quite high stress may be acceptable, if the total number of cycles in service is small (for example, an ocean-going vessel spending most of its time at constant engine speed and load). Not all thermal problems are of this type. Others include exhaust valve burning, injector nozzle over-heating, lubrication breakdown and piston ring scuffing, carbonisation of the lubricant, etc.

Figure 11.10 shows a typical temperature distribution from the gas to the water coolant at the valve bridge of a cylinder head. To reduce thermal stress the metal thickness must be reduced as much as possible, but this may be incompatible with resistance to gas pressure, particularly on large engines. One solution is to use 'strong-back' or 'twin deck' construction in which the thermal loads are carried by a thin section which has a number of supports transmitting the pressure load to a well-cooled heavier 'strong-back'. This gets the cooling passages close enough to the gas face in complex cast components such as the cylinder head. Even more effective is to use a machined flame plate of thin steel giving the cooling water direct access to the exhaust valve seat insert (figure 11.11). Drilled passages are also frequently used to cool cylinder liners on large engines and can

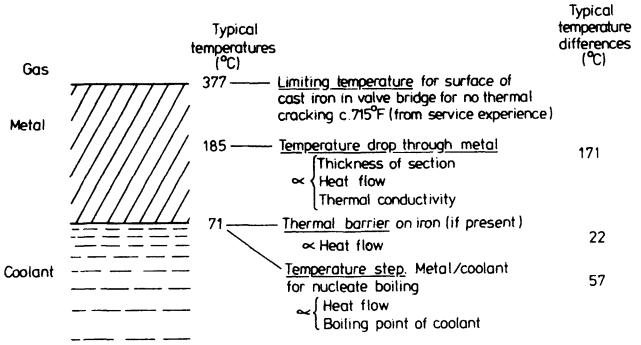

Figure 11.10 *Factors affecting metal temperatures [10]*

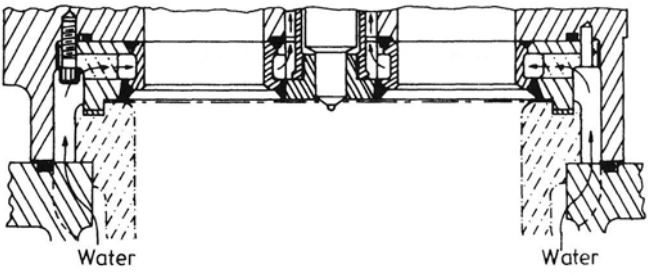

Figure 11.11 *Ruston 'flame plate' cylinder head [11]*

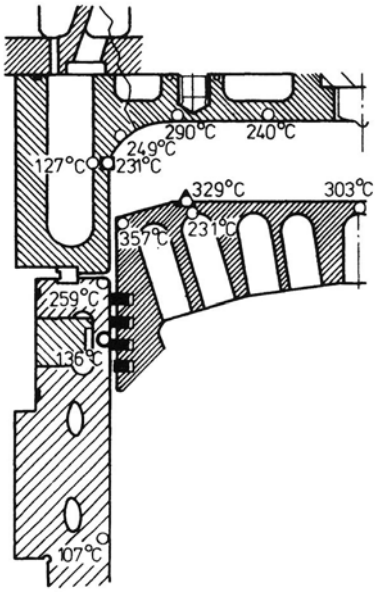

Figure 11.12 *Drilled liner cooling passages on a MAN two-stroke engine*

be very effective where the over-all thickness of the liner is large in order to resist mechanical stresses (figure 11.12).

The piston is obviously a critical component since it is difficult to arrange for delivery of a cooling medium. Unfortunately water cooling can only be used in cross-head-type engines where adequate sealing from the crankcase is possible. Oil cooling is used in more conventional engines even though the heat transfer coefficient is many times less than water. Either 'solid' (that is, through a passage full of oil) or oil jet and 'cocktail shaker' type cooling are used.

Over-heating of the fuel injector can be a particular problem on small engines since the nozzle face area tends to be rather large yet the fuel through-flow (which acts as a coolant) remains small. At the other extreme an engine burning heavy residual oil can also experience problems since the fuel must be pre-heated

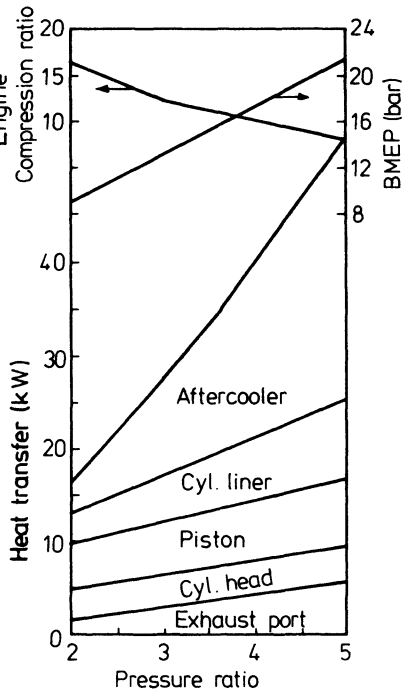

Figure 11.13 *Breakdown of heat losses with increased boost pressure [12]*

to enable it to be pumped through the injector; virtually no fuel cooling is possible. Water-cooling passages can be drilled in the injector body itself or a water jacket may be placed around the injector in these cases.

Figure 11.13 shows calculated heat transfer to charge air cooler, cylinder liner, piston, cylinder head and exhaust port as turbocharger pressure ratio increases from 2 to 5, while compression ratio is reduced to limit maximum cylinder pressure to 120 bar. Most apparent is the very large heat rejection to the charge air cooler required to keep the boost air temperature constant. More important to thermal stress is the heat rejected to cylinder components. Fortunately heat transferred to cylinder head and piston only increases slightly, but that to the liner shows a substantial increase. This results from high cylinder gas temperature for a longer part of the expansion stroke with a reduced compression ratio engine. The data relates to an air-cooled vehicle type engine, with an air/fuel equivalence ratio kept constant at 2.2. On medium-speed engines, increasing air supply (particularly scavenge air flow since this does not affect peak cylinder pressure) is a powerful method of controlling exhaust valve thermal loading.

Introduction of more fuel and the formation of a good combustion mixture with an increase in engine rating presents certain problems. Increase in injection pressure and use of larger injector orifices gives satisfactory results at full load operation. However, at part load, the larger orifices cause difficulties in the formation of a good mixture due to over penetration of the spray, resulting in exhaust

smoke. Combustion itself does not present any particular difficulties for engines operating at high mean effective pressures.

In general it can be concluded, following experimental work carried out on a single-cylinder medium-speed four-stroke diesel engine operating up to 35 bar BMEP and 1500 rev/min, [13] that it is possible to contain the thermal and mechanical loads with relatively unsophisticated cylinder components up to 39 BMEP, provided that an adequate air flow through the engine can be maintained. The same comments can be applied to truck engines at BMEPs of up to 18 bar. [9]

11.3 Single-stage Turbocharger Limitations

The limitations of single-stage turbocharging are turbine inlet temperature, rotational speed and stress, compression efficiency and flow range (particularly at high pressure ratios) and turbine efficiency at high expansion ratios.

The turbine inlet temperature of most current turbochargers is limited to around 650 to 750 °C and this appears quite adequate for high-output engines. Many industrial engines are limited to exhaust valve temperatures below 600 °C to prevent exhaust valve fouling when operating on heavy fuels. The developments in aircraft gas turbine technology have resulted in turbine inlet temperatures exceeding those likely to be encountered on even the most highly rated turbocharged diesel, hence there is unlikely to be any immediate absolute limit. However, possible increases in temperature are limited by the cost of high-temperature materials combined with difficulties in machining, plus extra complexity should cooled blades be required. Certain other measures may be taken to control turbine inlet temperature when a cheap mass-produced unit with a low acceptable temperature limit is used. For example, the air/fuel ratio may be increased (at the expense of cylinder pressure) or valve overlap may be increased to provide more dilution by cool scavenge air.

The maximum rotational speed is governed by stress limits in the turbine rotor or compressor impeller, but neither can be isolated from temperature. The creep properties of the turbine material at elevated temperature are particularly important. The compressor cannot be ignored since the temperature rise through it at high pressure ratios limits the use of cast aluminium alloys.

Currently most conventional medium-speed four-stroke engines operate at a BMEP of around 15 bar, requiring a compressor pressure ratio of 2.5:1 (figure 11.2). This implies an impeller tip speed of 365 m/s. Increasing the rating to 20 or 25 bar requires a pressure ratio of 3.3 and 4.1:1 respectively, with impeller tip speeds of 415 and 445 m/s. Since mechanical stress increases with the square of rotational speed, stress is raised by 28.8 per cent for a rating of 20 bar, and 44.6 per cent for 25 bar. The exit air temperature at a pressure ratio of 4.1:1, an efficiency of 75 per cent and an inlet temperature of 20 °C is 214 °C. The impeller material must be selected with a view to its high-temperature fatigue properties as a result. Titanium is particularly suitable, and for this reason is used in the new range of Brown Boveri turbochargers (series 4), for requirements exceeding a 3.5:1 pressure ratio. However, it is very expensive and difficult to machine, hence it can only be justified in high-pressure high-BMEP applications.

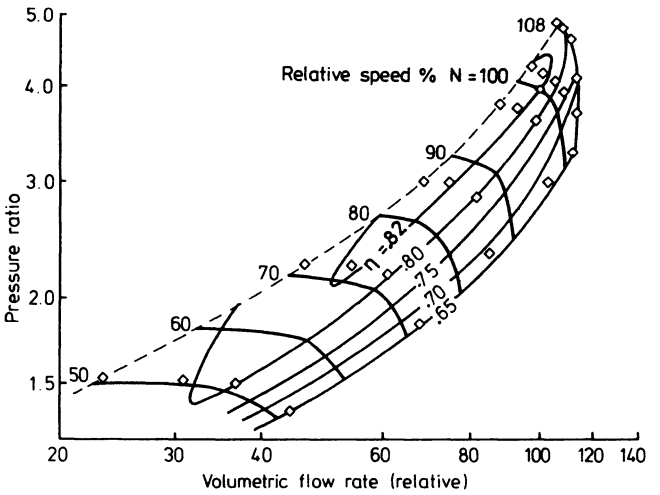

Figure 11.14 *Brown Boveri VTR 454 compressor performance map*

The problem of deteriorating efficiency and flow range at high pressure ratios has been discussed in chapters 3, 4 and 5. The maximum practical pressure ratio that can be used will depend on the application, since this governs the importance of flow range. Generally however, compressor efficiency will begin to fall off when the Mach number at the impeller eye tip substantially exceeds unity. The pressure ratio at which this occurs will depend on the geometry of the particular compressor (impeller) but normally occurs at pressure ratios about 3.5 with the standard-type turbocharger compressor. Thus at a pressure ratio of about 3.5 or 4:1 a point can be observed above which compressor efficiency falls and the useful operating range of the compressor characteristic narrows, creating difficulties in matching to ensure a safe margin from surge at reasonable compressor efficiency. This problem can be overcome by using a more sophisticated design of the compressor (chapter 3). For example, figure 11.14 shows the compressor map of the Brown Boveri VTR 454, designed for operation at 3.5 to 4:1 pressure ratio with high efficiency.

The low-reaction single-stage axial flow turbine, is most suitable for pulse turbocharging with partial admission operation but suffers from falling efficiency above an expansion ratio of 2:1 (chapter 5). The introduction of a high degree of reaction single-stage axial flow turbine with an exhaust diffuser, or the use of a radial flow type turbine permits efficient operation at higher expansion ratios (up to 4:1). However, the rather poor partial admission performance of these turbines means that they are most suited for constant pressure turbocharging systems.

In general the over-all turbocharger efficiency approaches 62 per cent for full admission operation at pressure ratios between 2.5 and 3:1 with most existing medium and large-size turbochargers. New designs of turbochargers will maintain this efficiency at pressure ratios above 3.5:1.

11.4 Single-stage Turbocharging of Marine and Industrial Engines

Experimental four-stroke medium-speed diesel engines have been running at BMEPs of up to 27 bar with single-stage turbocharging at a pressure ratio of 3.72:1, [14] and an engine compression ratio of 11:1. For reasons given elsewhere conventional compressor and turbine efficiencies are low at this high pressure ratio, resulting in insufficient air flow to keep exhaust gas temperature down. As a result, operation with heavy fuel oils will cause deposition problems on turbine blades and exhaust valves. If valve seat temperatures are limited to around 450 °C and turbine inlet temperatures to around 550 °C to ensure satisfactory operation with heavy fuel, a BMEP limit of 20 bar is imposed. Raising boost pressure by increasing turbocharger efficiency can raise this limit to 22 to 24 bar BMEP, using new turbocharger designs (figure 11.14).

If the compressor pressure ratio is in the range 3.5 to 4:1, and pulse turbocharging is used, then the amplitude of the pressure pulses at the turbine will be very large and turbine efficiency poor. Comparison of figures 6.7 and 7.17 shows that the constant pressure turbocharging system is superior at this rating. Thus constant pressure turbochargers will be used unless the engine is required to respond rapidly at low load. [15] At slightly lower ratings pulse or pulse converter systems are favoured.

Highly rated two-stroke engines are now rated at 13 bar BMEP and more. Future developments are likely to increase these ratings to 15 or 16 bar, requiring compressor pressure ratios of 3.7:1 (figure 11.2). Although most current turbochargers are capable of operating at this pressure ratio, their efficiencies are not high enough (figure 11.2) to offset the low exhaust temperature of the two-stroke engine. Some of these engines have therefore used two-stage turbocharging. With single-stage turbocharging, the constant pressure system is preferred, because the very high amplitude pressure waves generated with pulse turbocharging, reduce turbocharger efficiency. To start the engine, and operate at low loads, an aid to

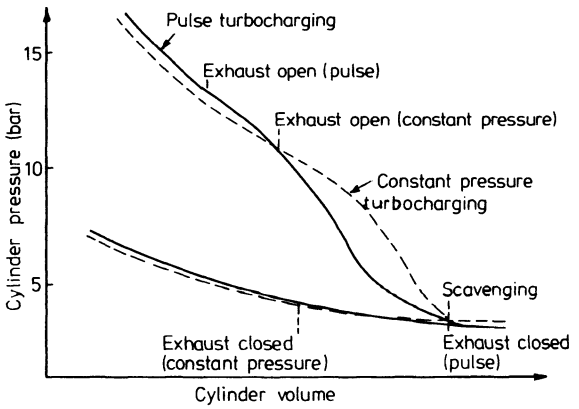

Figure 11.15 *Cylinder pressure during gas exchange with valve timing optimised for pulse and constant pressure operation (two-stroke engine) [16]*

scavenging is required since the turbocharger alone cannot provide sufficient boost pressure. Usually, a simple electrically driven fan is used.

A further benefit of the constant pressure system is shown in figure 11.15. Since the exhaust pressure is low when the exhaust valve starts to open, the rate at which the cylinder gases flow out through the exhaust valve is more rapid with the constant pressure system than the pulse system. As a result, the exhaust valve may be opened later, giving a longer effective expansion stroke. The cylinder pressure is higher approaching BDC, doing useful piston work, and then falls more rapidly close to BDC. Oestergaard [16] reports a 7 per cent benefit in specific fuel consumption, mostly due to this effect.

11.5 Two-stage Turbocharging of Marine and Industrial Engines

In the early years of turbocharger development multi-stage compressors and turbines were built. At that time, knowledge was not adequate to design turbomachines of the pressure ratios required in single-stage form with high efficiency. As knowledge was accumulated, both the efficiency and pressure ratios rose, enabling much simpler single-stage turbochargers to be built, capable of developing pressure ratios of 3:1 or more. Although it is quite feasible to build single-stage centrifugal compressors with much higher pressure ratios, it becomes increasingly difficult to maintain high efficiency over an acceptable flow range. Two-stage turbocharging is an alternative (figure 11.16). Two turbochargers are placed in series so that the low-pressure (LP) unit is driven by the energy of the exhaust gases leaving the high-pressure (HP) unit. Thus if each compressor can develop a pressure ratio of say 3:1, the two-stage system can result in an (theoretical) over-all ratio of 9:1 with no loss of compressor efficiency, although obviously such a high pressure ratio is not yet practical on diesel engines.

The major advantage of two-stage turbocharging comes from the fact that two machines of normal pressure ratio and efficiency can be used. High over-

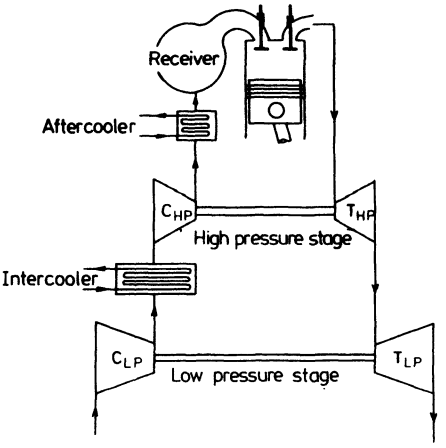

Figure 11.16 *Two-stage turbocharging with single-stage turbochargers*

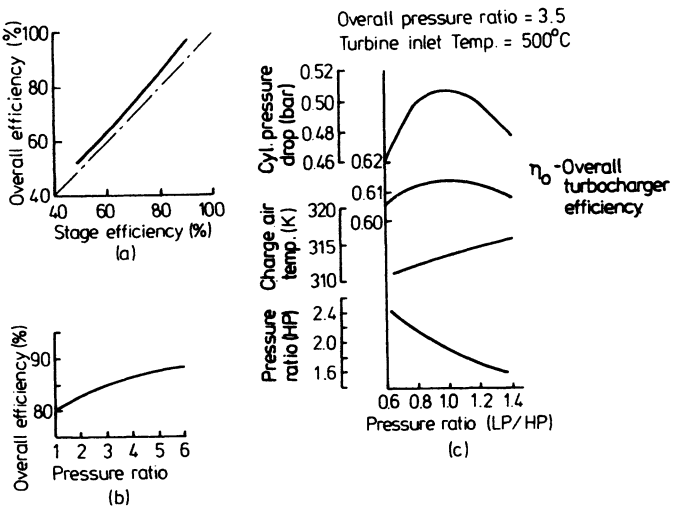

Figure 11.17 *Over-all and stage efficiencies, two-stage compression with intercooling [17]*

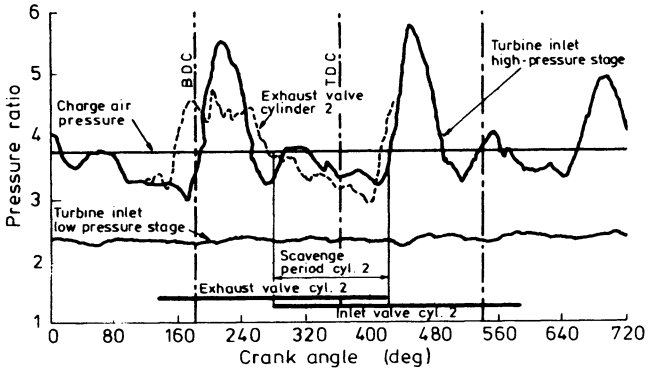

Figure 11.18 *Pressure-time diagram at turbine inlets with two-stage turbocharging [4]*

all pressure and expansion ratios may be developed using conventional turbochargers. The primary disadvantages are the increased cost of the additional turbocharger plus intercooler (if fitted) and manifolding, and the over-all bulk of the system.

Interstage cooling is an additional complication, but the reduction in temperature at the inlet of the HP compressor has the additional advantage of reducing the HP compressor work for a given pressure ratio, since this is a function of compressor inlet temperature. This increases the effective over-all efficiency of the turbocharging system. Figure 11.17 compares the over-all efficiency of a two-stage compressor system relative to a single-stage system, showing the benefit of

inter-stage cooling and the higher efficiency of each of the two stages due to their lower pressure ratio.

The turbines also benefit from the lower expansion ratio per stage. Figure 11.18 shows pressure crank-angle diagrams taken in the exhaust manifold before the HP and LP turbines, and near an exhaust valve, on a medium-speed six-cylinder engine operating at 24 bar BMEP. The HP turbine operates with the pulse system, since this gives best results with the turbine expansion ratio varying from 2.3 at its peak down to 1.37 at the lowest mass flow rate condition. A twin-entry radial flow turbine is used for the HP stage, and a single-entry unit for the LP stage. Since the exhaust gas from all cylinders passes together through the low-pressure stage, and the interstage ducting has a significant volume, this stage operates at constant pressure. The expansion ratio of the LP stage is 2.4:1. At these expansion ratios, the turbines can operate much more efficiently than would be the case with a single-stage system. With pulse turbocharging the expansion ratio of a single-stage system would vary from 5.5 to 3.2:1. If a constant pressure system were used, the expansion ratio of a single stage would be around 3.7:1. Turbine efficiency would be low with either system.

Figure 11.19 compares engine performance with single and two-stage turbocharging, with the turbochargers correctly matched for each system at each load. This figure is not a continuous curve produced with a fixed turbocharger build, but enables the optimum system to be determined over the BMEP range of 7 to 27 bar. At the low end of this range there is no difference in performance, and even at the maximum rating achieved with the single-stage system (20 bar), specific fuel consumption differences are small. However, the two-stage sys-

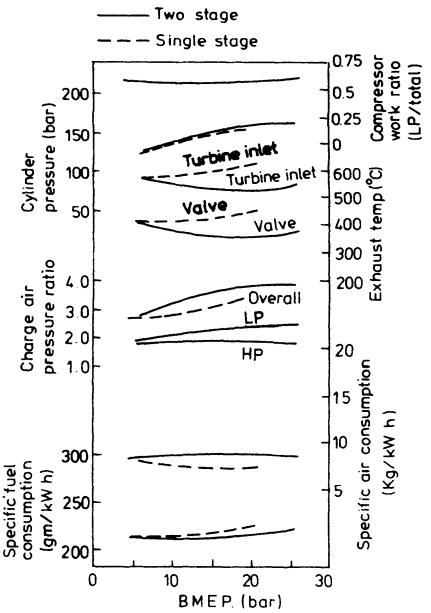

Figure 11.19 *Engine performance plot of optimum turbocharges matches [4]*

tem, through greater turbocharger system efficiency, provides a higher boost pressure, greater specific air consumption and therefore lower exhaust valve and turbine inlet temperatures. Thermal loading is reduced, opening the way to higher ratings with the two-stage system.

Another advantage of two-stage turbocharging is the moderate rotational speed at which both stages operate, compared with the very high speed of a high-pressure ratio single-stage unit. This is beneficial in terms of impeller and turbine blade stresses, bearing life and turbocharger noise level.

When matching turbochargers with a two-stage system, it is the effective area of the two turbines in series that has the most effect on engine performance. It will be obvious that the volumetric flow rate through the LP compressor and turbine will be substantially greater than those of the HP compressor and turbine, and therefore that the LP turbocharger must be larger than the HP unit. Figure 11.20 shows that optimum compression is achieved with an equal work share between stages, and therefore the pressure ratio of each stage must be approximately equal (dependent on whether interstage cooling is used). This requires the LP turbine nozzle area to be almost double that of the HP stage, but Takemoto

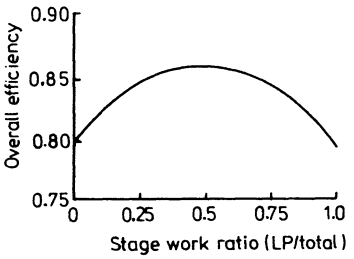

Figure 11.20 *Optimum work share for two-stage compression with intercooling [17]*

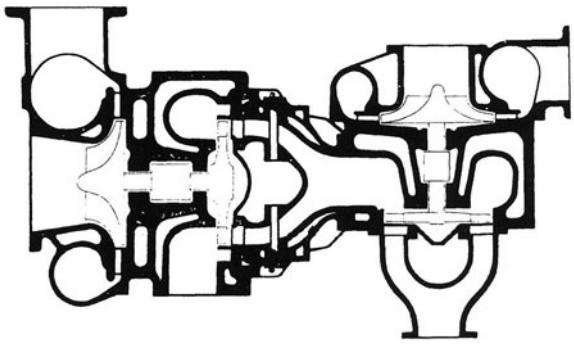

Figure 11.21 *Cross-section of a Hispano Suiza two-stage turbocharging unit: left, the low-pressure stage; right, the high-pressure stage*

and Hashimoto have shown [18] that engine performance is insensitive to a variation in LP/HP nozzle area ratio from 1.7 to 1.47.

Although two-stage turbocharging has several attractive features, it is only in the late 1970s that the first commercial engines using the system were announced, and very few have been produced. The greatest disadvantages are the obvious ones of additional cost, complexity and bulk. Some attempts have been made to reduce the bulk by combining two stages into one twin-shaft turbocharger. Figure 11.21 illustrates a design assembled largely from existing single-stage components.

A less obvious disadvantage of the two-stage systems is that performance is often poor at low load and speed. To a large extent this is caused by the fact that, relative to a single-stage system, the pressure ratio per stage is low. As speed or load reduce with a single-stage very high-pressure turbocharger, the presssure ratio drops and both compressor and turbine efficiency are likely to increase. Figure 11.22 shows an engine operating line, at constant speed and varying load, superimposed on the HP and LP compressor maps of a two-stage system. Because the over-all pressure ratio is shared between two stages, the full-load operating points coincide with high efficiency on both HP and LP compressors. However, as load is reduced, pressure ratio falls and compressor efficiency drops, particularly on the HP unit. The same will be true with the turbines. Thus the over-all turbocharger system efficiency falls with reducing load with a two-stage system whereas the opposite will be true with a high-pressure ratio single-stage system. Woschni *et al.* [20] have shown that this can cause an increase in thermal load, as engine load is reduced from full load along a propeller law curve.

The Miller turbocharging system (section 11.2) is one method of reducing this effect. Advancing the opening and closing point of the inlet valve as load is decreased, from the very retarded condition normal with the Miller system at full load, has two effects. First, volumetric efficiency improves, hence more air is trapped in the cylinders. This is shown in figure 11.23, where boost pressure and cylinder pressure at IVC are shown along a propeller law load-speed relationship, with constant valve timing and Miller-type variable valve timing. The data assumes single-stage constant pressure turbocharging, not a two-stage system, but

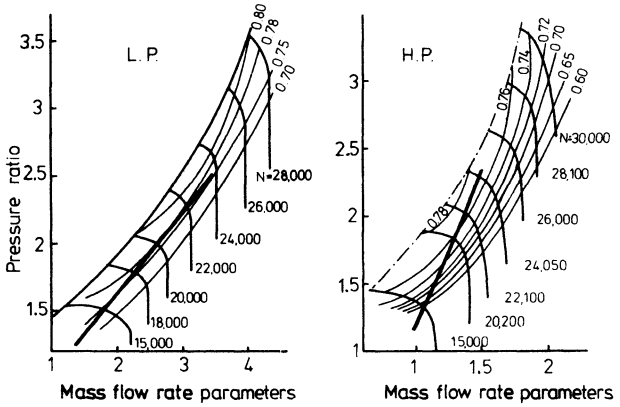

Figure 11.22 *Constant speed operating lines with two-stage turbocharging [19]*

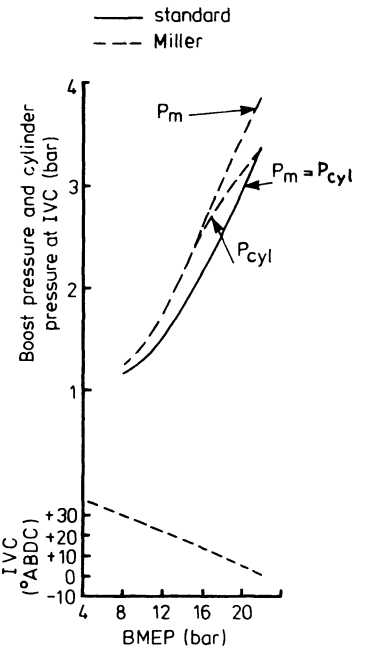

Figure 11.23 *Boost pressure and cylinder pressure at IVC with standard and Miller (variable) valve timing [21]*

the important effect is that caused by the variable valve timing. With optimum conventional valve timing, cylinder pressure at IVC will virtually equal the boost pressure. In figure 11.23 this is shown along the complete curve with fixed valve timing of 30° ABDC. The boost pressure is higher with the Miller system, and the valve timing is deliberately non-optimised at full load, hence cylinder pressure at IVC is 0.5 bar below boost pressure, at 22 bar BMEP. As load and speed reduce, so valve timing is retarded closer to the optimum, raising cylinder pressure at IVC closer to the higher boost pressure of the Miller system. The mass of air trapped in the cylinder increases relative to that with conventional timing. Full advantage has been taken of this effect by Chellini, [7] in the result shown with two-stage turbocharging and the Miller system in figure 11.7.

11.6 Two-stage Turbocharging of Vehicle-type Engines

Figure 11.24 shows that the specific cost, volume and weight of vehicle-type diesel engines reduce as rated BMEP increases. Most current turbocharged vehicle diesel engines are rated at 10 to 12 bar BMEP, but this is likely to increase gradually. Higher BMEP is required for certain duties, such as military applications, and very high pressure ratios are required to retain BMEPs of 12 bar up to very high altitudes common in many countries. Two-stage turbocharging has therefore been proposed for these engines, to enable high boost to be developed

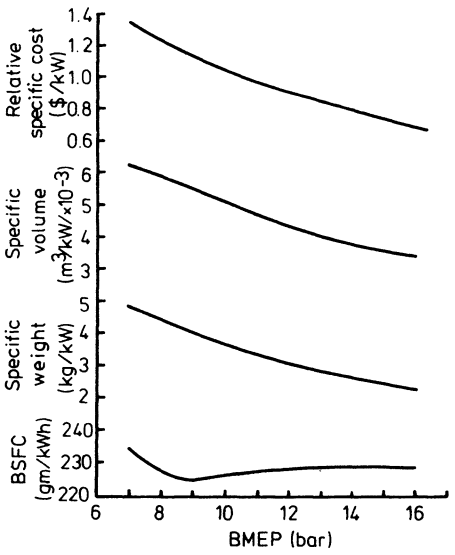

Figure 11.24 *The case for the high BMEP truck engine [9]*

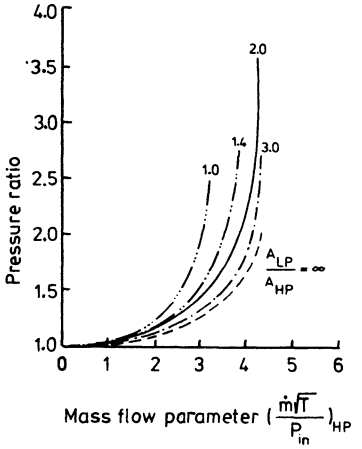

Figure 11.25 *Over-all flow characteristics of two turbochargers in series, fixed high-pressure, varying low-pressure unit*

over a wide engine speed range. The important requirement is high torque at low speeds, hence turbocharger boost pressure should not fall rapidly as engine speed is reduced. The relative match of the two turbochargers can be used to optimise low-speed boost, [22] for the same performance at rated speed and load.

Figure 11.25 shows the over-all pressure ratio against mass flow parameter for two turbines in series, in simplified form and neglecting rotor speed effects. A range of flow characteristic curves is shown with one HP turbine, but varying LP

turbine effective area. The extreme right-hand curve denotes a single-stage turbocharger, choking at a pressure ratio around 2:1. The addition of an LP turbine reduces the mass flow rate at the pressure ratio of 2:1. The ratio of effective areas of the two turbines (LP/HP) is shown for each line. Comparing the lines representing the single-stage turbocharger, and the two-stage system with an area ratio of 2(that is, $A_{LP} = 2A_{HP}$), it can be seen that the maximum mass flow parameter is governed by choking of the HP unit. This occurs when its pressure ratio is about 2:1, and the over-all two-stage pressure ratio is 3.5:1. Smaller LP turbines cause the system to choke when the LP turbine chokes, at a lower HP mass flow parameter.

Now consider an engine operating at rated speed and load, with a turbine pressure ratio of 3.5:1. The same mass flow parameter could be achieved with three of the curves shown (single-stage, area ratio 2 or 3). Thus with any of these systems, the same performance might be achieved at this condition, assuming identical efficiencies of turbines and compressors, for simplicity. As engine speed is reduced from this condition, mass flow rate will fall. The operating point on the turbine flow characteristic will move down and to the left. Figure 11.25 shows that at mass flows less than the choked value, the pressure ratio of the turbine is higher with the two-stage system. Thus if turbine efficiencies are similar, turbine torque at medium and low engine speeds, and therefore compressor boost, will be highest with area ratio 2, and will typically be 50 per cent higher than the single-stage system. Thus an optimum two-stage system can substantially improve low-speed boost, relative to a single-stage system.

In section 11.5 it was shown that minimum compressor work with a two-stage system occurs with an equal work share. Figure 11.26 shows the work share (HP/LP) and how it varies over the mass flow range, with the turbocharger matches of figure 11.25. With the optimum (for low-speed boost) turbine area

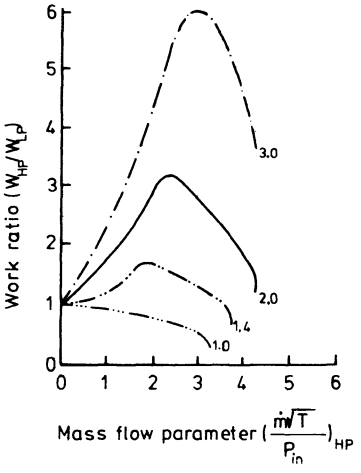

Figure 11.26 *Work ratio variation with area ratio of two turbochargers in series (fixed high-pressure, varying low-pressure unit)*

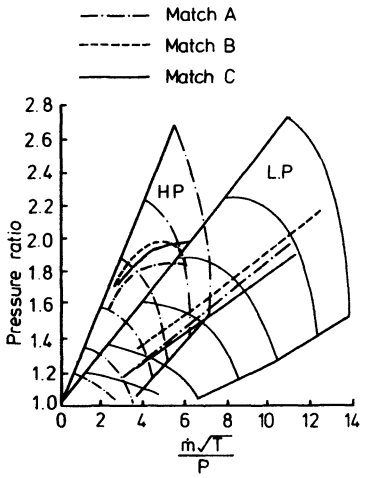

Figure 11.27 *Effect of varying two-stage turbocharger match on compressor requirements*

TABLE 11.1 *Two-stage turbocharger matches for figures 11.27 and 11.28*

MATCH	Peak Compressor Efficiency (%) HP	LP	Peak Turbine Efficiency (%) HP	LP	Relative Turbine Area (%) HP	LP	Injection Timing
A	70	70	68	68	100	178	std.
B	70	70	68	68	78	144	std.
C	70	70	68	68	100	200	5° retard

ratio of 2, the work share is almost equal at the choked condition, but HP turbine work dominates as mass flow rate is reduced to about 50 per cent of choked flow. This represents almost the full speed range of an engine. Two conclusions may be drawn. Firstly, it is impossible to maintain an equal work share unless an undesirably small LP turbine is fitted. Secondly, relative to the HP turbine and comressor, LP turbine torque and therefore compressor boost, falls rapidly as engine speed is reduced. This has implications in terms of the compressor map widths required for the two stages. Figure 11.27 shows the maximum torque operating lines of a two-stage turbocharged vehicle engine, superimposed on both HP and LP compressor maps. The three turbine matches shown are specified in table 11.1, but all three show that HP boost remains high over the complete engine speed range, whereas LP boost falls as speed is reduced. The turnover in HP boost is largely caused by changes in turbine efficiency ignored in the simplified discussion given above. LP compressor selection is simplified by the narrow operating range, but a wide area of efficient operation is required for the HP compressor.

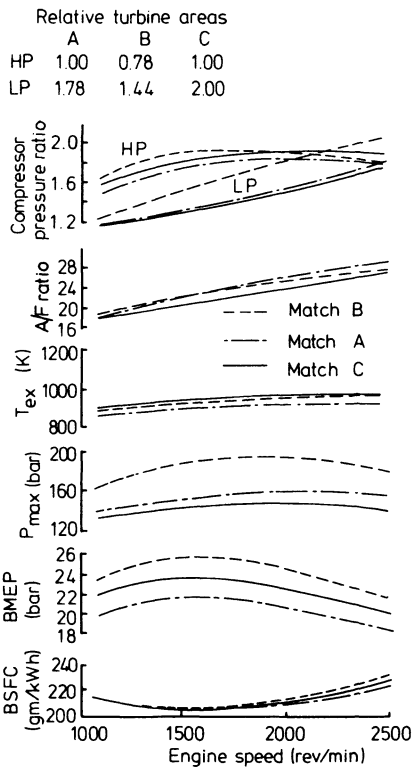

Figure 11.28 *The effect of varying two-stage turbocharger match on engine performance*

Figure 11.28 shows engine performance with the three turbocharger matches listed in table 11.1. All three matches have a LP/HP area ratio close to 2, but both turbines are small with match B, creating excessive LP boost and maximum cylinder pressure. Match C uses a slightly larger LP turbine than match A, reducing LP boost by a small amount. However, this reduces the back pressure on the HP turbine, allowing its work to increase, hence HP compressor ratio increases. Note that very high BMEP and good low-speed torque can be achieved with match C. This is achieved with a reasonable cylinder pressure, by using a low engine compression ratio (12:1), and retarded injection, without a fuel consumption penalty at full load.

11.7 Variable Geometry Turbocharging

The potential of variable geometry turbine nozzles has been exploited in small gas turbines for many years. By varying blade angle with speed or mass flow rate, both the effective turbine area (dominated by the passage width between stator

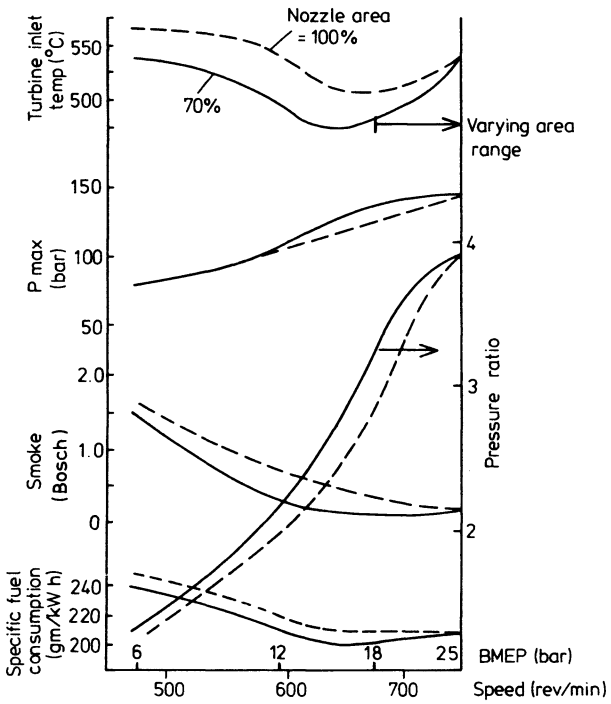

Figure 11.29 *Engine performance with two-stage turbocharging and variable HP turbine area [23]*

blades) and incidence losses at the rotor may be controlled. In particular, the effect of turbine area control improves utilisation of the exhaust gas energy by the turbine at low engine speeds (chapters 6 and 7), without over-speeding the turbocharger or over-boosting the engine at high engine speed, by increasing effective turbine area under these conditions. The potential benefits are particularly worth while for engines whose load and speed change substantially (for example, vehicle applications). However, the additional cost and complexity are more likely to be accepted on the more expensive highly rated engines. Thus, for example, MAN have proposed using a variable geometry HP turbine in a two-stage system to improve the part load and speed performance along a propeller law, overcoming the problems discussed in section 11.5. [23] An axial flow turbine is used, with rotating stator blades. Figure 11.29 shows that closing the nozzle blades as speed and load reduce, increases boost pressure with a beneficial effect on exhaust smoke, turbine inlet temperature and specific fuel consumption.

The disadvantage of variable geometry is the extreme difficulty of engineering a cheap and reliable system, particularly with a small radial flow turbine as used where the benefits of variable geometry are potentially greatest (vehicle engines). For example, figure 11.30 shows the performance of a truck engine fitted with alternative vaneless radial turbine housings, having a small and a large effective area. The smallest housing gives best performance at low speed,

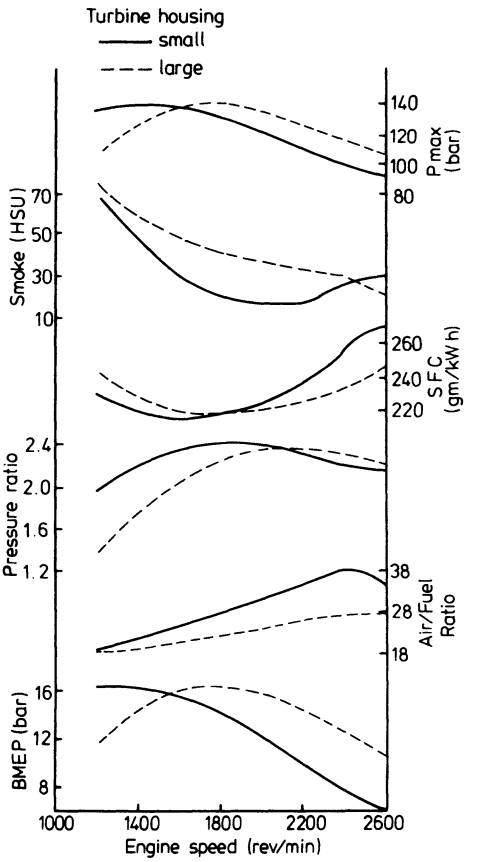

Figure 11.30 *Engine performance with different turbine housings [24]*

since the engine benefits from the additional boost and air flow. At high speed, excessive exhaust manifold pressure results in poor performance relative to that achieved with the large housing. Potentially, a variable geometry system could produce the characteristic of the small turbine housing at low speed and the larger housing at high speed.

Berenyi and Raffa [25] have tested an experimental variable geometry radial flow turbocharger on a high-output military vehicle engine. Variable angle turbine nozzle blades and compressor diffuser blades were used, the latter to achieve a very wide surge-free operating range imposed by high boost being developed at low engine speed with the turbine nozzle area at a minimum. Figure 11.31 shows the performance achieved, compared to the standard turbocharging system with fixed geometry. The turbocharger used by Berenyi and Raffa was a complex and expensive prototype. It remains to be seen whether simpler and cheaper variable geometry systems become available in the future.

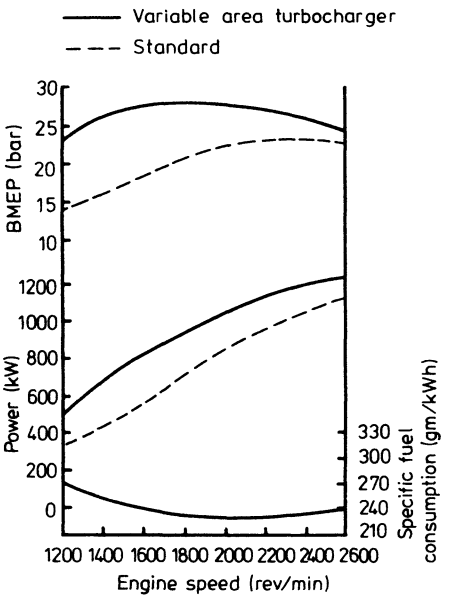

Figure 11.31 *Engine performance with fixed and variable geometry turbocharger [25]*

11.8 'Hyperbar' Turbocharging

The 'Hyperbar' turbocharging system has been developed to overcome some of the practical difficulties inherent in using conventional turbocharging systems on very high-output engines, particularly those required to operate over a large speed range. These difficulties may be summarised as follows

(1) low turbocharger efficiency at very high pressure ratios
(2) high peak cylinder pressure
(3) low boost at low engine speeds
(4) poor starting and light load running with low engine compression ratio
(5) insufficient compressor map width at high pressure ratio
(6) slow turbocharger acceleration.

The Hyperbar system uses a combustion chamber placed between the exhaust ports of the engine and the turbocharger turbine. Additional fuel is burnt in this combustion chamber to increase turbine and therefore compressor work, overcoming disadvantages (1) and (3) above. The system is shown diagrammatically in figure 11.32. In order to provide sufficient air for the auxiliary combustion chamber, some air from the turbocharger compressor by-passes the engine directly to the combustion chamber. This by-pass is also used to restrict compressor mass flow variation as engine speed and engine airflow change, overcoming item (5) above.

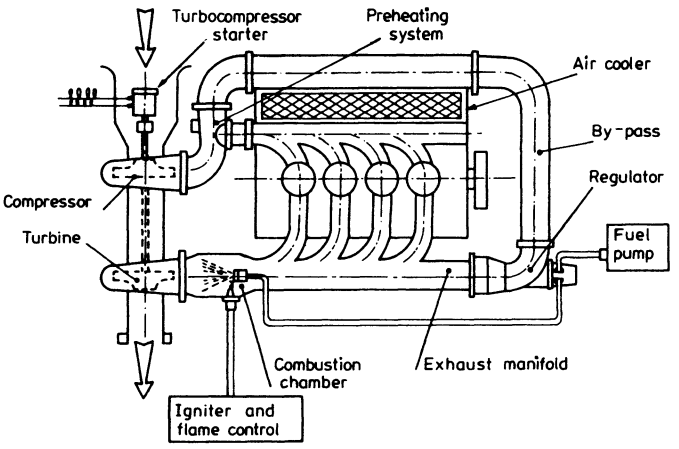

Figure 11.32 *Schematic of Hyperbar turbocharging system [26]*

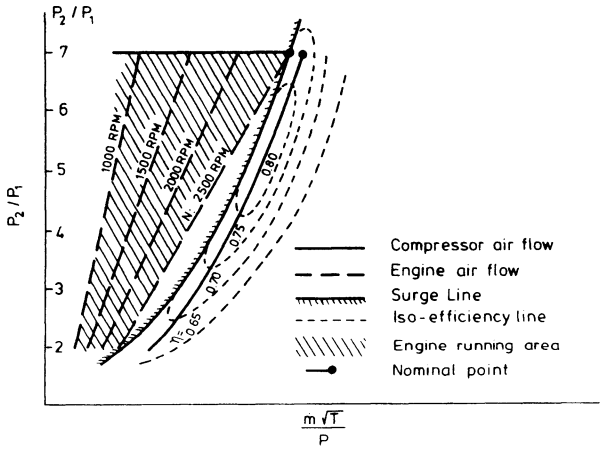

Figure 11.33 *Engine and compressor air flow requirements, at varying engine speed and load, with the Hyperbar turbocharging system [26]*

Figure 11.33 shows engine and compressor air flows, superimposed on a very high-pressure ratio, single-stage compressor map. This means that the compressor is easily matched to the engine and that the compressor may be designed for high efficiency and pressure ratio without sacrifice to achieve a wide flow range.

The Hyperbar turbocharging system is designed to operate with very high compressor pressure ratio and very low engine compression ratio, overcoming item (2) above. For example, Melchior and Talamon [26] report tests in which the Hyperbar system is used to raise compressor pressure ratio from 2.8:1 to 7.26:1 (using a two-stage system), while engine compression ratio is reduced

from 13:1 to 7:1. BMEP increased from 17 to 30 bar with no increase in maximum cylinder pressure (140 bar).

An additional disadvantage of conventional systems listed above (4) is poor starting and light load running with low engine compression ratio. The Hyperbar uses an electric starter motor to rotate the turbocharger rotor, with the engine air by-pass open. The air flow is sufficient to enable the auxiliary combustion chamber to be started. The turbocharger starter motor is then decoupled, allowing the turbocharger to operate like a free-running gas turbine. The engine may then be cranked over by normal means, and air is drawn into the combustion chambers. Normally this air would be at atmospheric pressure and temperature and the compression ratio of the engine would not be high enough for self-ignition. However since the 'gas turbine' part of the Hyperbar system is self-sustaining, a reasonable boost temperature and pressure can be developed before the engine fires. By by-passing the charge air cooler, warm air from compressor exit is delivered to the cylinders aiding in-cylinder ignition. The charge air cooler may also be by-passed during light load operation to maintain high charge air temperature and good combustion. At higher loads, a gradual transition to full aftercooling is required to limit thermal loading of the engine.

The auxiliary combustion chamber can also be used to improve turbocharger and engine response to rapid load and speed demand changes. This can be achieved by increasing auxiliary combustion chamber fuelling rapidly to accelerate the turbocharger when required., and by maintaining fuelling at light load and low speed to prevent the turbocharger speed from ever falling to a low value. This overcomes the final disadvantage (6) given above.

However, the Hyperbar system does have disadvantages. An obvious one is complexity, due to the auxiliary combustion chamber and by-pass valve, plus the fuel and air control systems required for them. A second disadvantage is the fuel consumption penalty of the auxiliary combustion chamber.

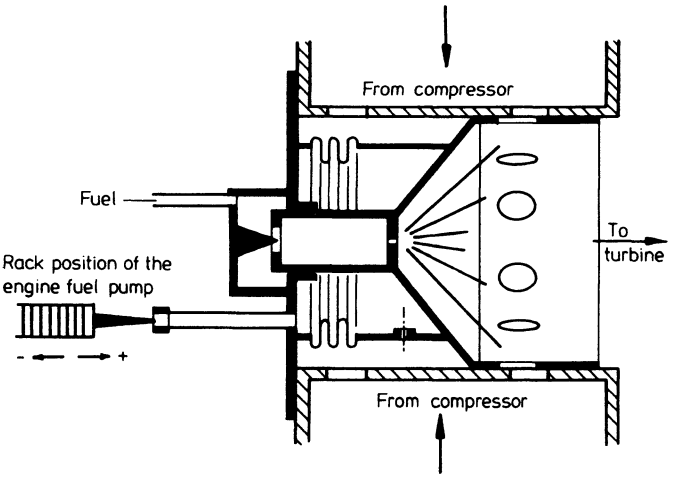

Figure 11.34 *Hyperbar auxiliary combustion chamber schematic [27]*

The by-pass valve and its control system are actually quite simple. It consists of a large poppet valve between compressor delivery and the exhaust manifold system, the valve having a very large diameter stem. Exhaust manifold pressure acts on the complete face of the valve (area A_{ex}). The compressor delivery pressure acts on the rear of the valve face (area $A_{ex} - A_{valve\ stem}$). Thus a pressure differential ($\Delta P = P_m - P_p$) is automatically maintained as a function of boost pressure (P_m) and the ratio of valve stem to head area. This pressure differential is optimised for scavenging and piston pumping work during the gas exchange process.

The combustion chamber and its fuel control systems are more complex. Figure 11.34 shows the combustion chamber in simplified form. It is based on small gas turbine combustion practice, with a central continuous flow fuel injector and atomiser. The fuel flow rate is governed by fuel pressure prior to the injector, which itself is controlled by movement of the combustor under the influence of turbine inlet pressure. The air supply to the combustor comes from the by-pass valve. Combustion products mix with the exhaust gas from the engine, prior to entering the turbine.

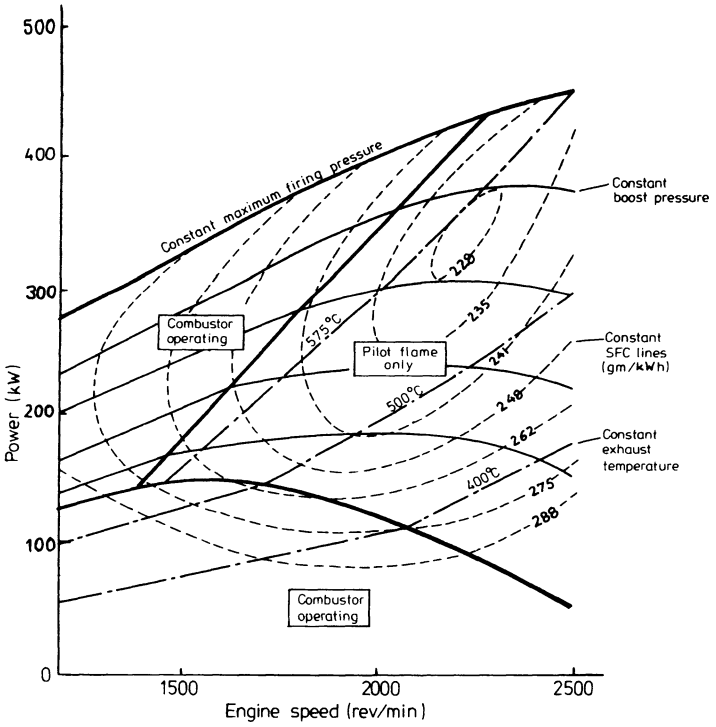

Figure 11.35 *Performance map showing operating area where combustor is required to achieve high torque and good combustion at low load [26]*

The deficit in over-all fuel consumption, due to the fuel requirement of the auxiliary combustion chamber, will vary substantially with engine load and speed. At rated speed and load, the auxiliary fuel supply can usually be reduced to a pilot level sufficient to retain combustion, hence over-all specific fuel consumption is only 2 to 8 per cent more than a conventionally turbocharged engine at a lower rating. [26] Auxiliary fuelling will be required at low speed, to increase boost pressure and therefore engine torque and to drive the additional by-pass air flow through the compressor. It is also required at low load to keep compressor boost pressure and therefore temperature high, for good combustion with the low engine compression ratio. Figure 11.35 shows these three regimes of operation of the auxiliary burner, superimposed on the engine performance map, together with lines of constant boost pressure. Table 11.2 shows computed by-pass air flow, and auxiliary combustion chamber fuel flow, expressed as a fraction of the engine air and fuel flows over a large speed and load range. At 21 bar, 2500 rev/min, the air and fuel flows are sufficient for pilot combustion. As speed is reduced to 1500 or 1000 rev/min the auxiliary fuel supply rises to 40 per cent of the engine fuel flow in order to maintain constant BMEP and constant air/fuel ratio (to maintain acceptable thermal loading). The by-pass air flow rises to 60 per cent. Reducing load to 5 bar BMEP further increases the fuel requirement of the auxiliary combustion chamber, until at low speed and load it exceeds that of the cylinders.

Wallace and Winkler [28] have compared predicted engine performance with the Hyperbar system (table 11.2) and a conventional two-stage turbocharger system. They conclude that the Hyperbar system is best able to provide any desired torque-speed curve, including very high torque at low speed. However, the fuel consumption penalty will vary from 8 per cent in the high-speed and load operating range to 30 per cent at low speed and load. These calculations may not

TABLE 11.2 *Prediction of by-pass air flow and auxiliary combustion chamber fuel flow [28]*

Engine Speed (rev/min)	By-pass Air Flow Ratio (%) / By-pass Fuel Flow Ratio (%)			
2500	7.4 / 2	33.1 / 2	33.5 / 2	30.9 / 10
2000	39.9 / 10	40.3 / 2	40.3 / 2	38.3 / 35
1500	49.4 / 40	49.8 / 2	49.3 / 20	47.2 / 85
1000	60.3 / 40	60.2 / 25	60.0 / 50	60.0 / 150
Mean effective pressure (bar)	21	15	10	5

be representative of a well-optimised Hyperbar system, certainly the specific fuel consumption claimed by Hyperbar (figure 11.35) at low speed and load are better than the above.

No engine is in full production with a Hyperbar system, but some experimental engines entered daily use on French railways in 1979/80. Currently the system is seriously considered for applications requiring very high specific power output and rapid response, for example, military vehicles and some railway applications. The complexity, cost and fuel consumption penalty may be reduced with progressive development in time, leading to more widespread use, but these judgements cannot be made at present.

11.9 Compound Engines

Compound engines are characterised by some mechanical linkage and power transmission between the exhaust-gas driven turbine and the crankshaft of the engine. The objective is not necessarily to achieve very high output, but to increase over-all engine efficiency by harnessing exhaust gas energy into useful power output from the engine. However, since the power transmission between turbine and crankshaft increases the complexity and cost of the engine system, compounding has usually been associated with high-output engines on which the extra cost can be justified. Rapidly increasing fuel costs from 1973 have led to re-examination of the potential of compound engines, even at conventional ratings.

Quite a larger number of compound engines of varying degrees of complexity have been proposed. Only a small number have reached the prototype stage and very few have been built prior to 1980. The best known are the Wright aircraft engine built in the early 1950s, prior to commercial turbine engines, and the Napier Deltic engine.

Two simple turbo-compound engine arrangements are shown in figures 11.36a and b. Arrangement (b) uses a fixed-ratio reduction gearbox between the turbocharger and crankshaft, while the arrangement (a) allows the compressor and turbine to be separated and run at different speeds. These simple schemes have two disadvantages associated with the gearbox between turbocharger and engine. Firstly, it will be obvious that a very high gear ratio is required and that the rotational speed of the turbocharger input shaft gear is high. For example, a typical turbocharged truck engine may operate at 2500 rev/min, with a turbocharger speed of 80 000 rev/min at rated speed and load. The design of a gearbox with a reduction ratio of 32 and an input speed of 80 000 rev/min, perhaps transmitting around 15 kW, is a formidable task. The second disadvantage is that the characteristics of the engine and turbocharger combination will be changed substantially if a fixed gear ratio exists between them. For example, consider the turbocharger speed against engine speed characteristic of the freely turbocharged engine, match 1, in figure 10.24. If the same boost pressure is to be retained at full speed, the compressor speed must be 73 000 rev/min for an engine speed of 2500 rev/min, requiring a gear ratio of 29.2:1. At 1000 rev/min this would produce a turbocharger speed of 29 200 rev/min which is 19 per cent less than that of the freely turbocharged engine. Thus low-speed boost pressure will be inadequate.

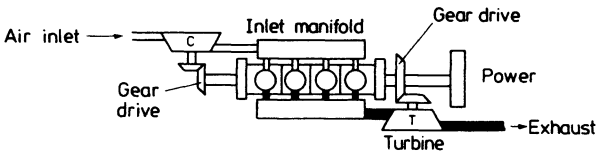

(a)

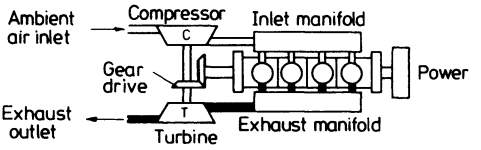

(b)

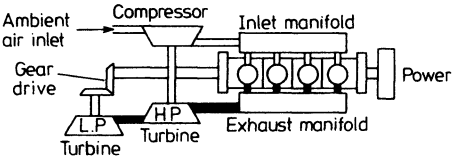

(c)

Figure 11.36 *Turbo-compound engine arrangements*

If a small turbine housing is selected (match 2 in figure 10.24) and the 29.2:1 gear ratio is retained, then the boost pressure developed by match 1 will be obtained at maximum engine speed, and surplus turbine power will be transmitted to the crankshaft of the engine. Engine efficiency will improve by a few per cent, but at the expense of poor low-speed performance. However, as load is reduced, turbocharger speed and therefore boost pressure are constrained to remain unchanged. Turbine power reduces as the exhaust gas temperature falls, until a point is reached beyond which turbine power is insufficient to drive the compressor. Power will then be transmitted from the crankshaft of the engine to the turbocharger. The turbocharger is then providing higher boost than required, at the expense of engine efficiency. Thus the simple compound scheme with a fixed gear ratio is unsatisfactory.

An obvious solution to this problem is to use a variable speed gearbox, but this makes the gearbox design problem substantially more difficult. This scheme was used on the Napier Nomad two-stroke diesel aircraft engine, built, but never put into production, in the early 1950s (figure 11.37). More complex schemes with a variable gear ratio and variable geometry turbocharging have been proposed by Wallace. [30] Excellent torque characteristics have been demonstrated but at

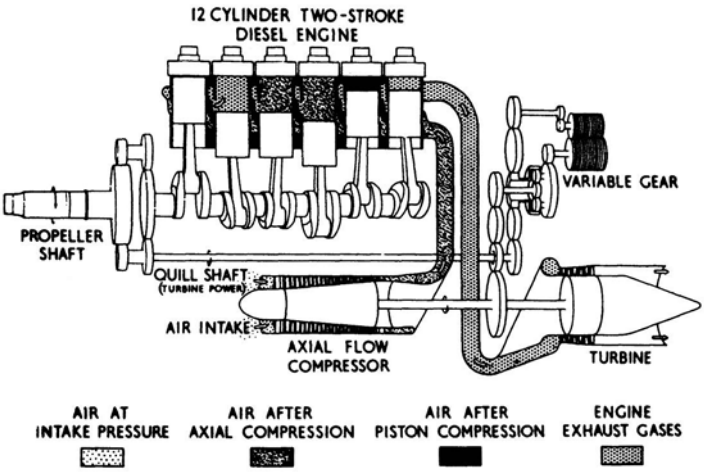

Figure 11.37 *Schematic of Napier Nomad compound aircraft diesel engine [29]*

the expense of considerable complexity and with only small gains in efficiency.

One simpler method of improving the low speed problem is to replace the turbo compressor of figure 11.36a by a Roots or Lysholm compressor, having the characteristics shown in figures 6.13 and 6.14. With these compressors, the mass flow rate is proporational to engine speed, and pressure ratio is almost independent of speed. Thus a relatively constant boost pressure can be maintained over the whole engine speed range. However, the compressors are large, expensive and noisy, and the system suffers from the same part load disadvantage mentioned above.

An alternative scheme is to use a second LP turbine in series with a conventional turbocharger turbine, the LP turbine being compounded with a fixed gear ratio (figure 11.36c). This scheme has the complexity of an additional turbine, but allows the turbocharger to work in the conventional turbocharger manner, and prevents power transfer from the engine to a compressor. Like a conventional two-stage turbocharged engine, the LP turbine is large and runs at a lower rotational speed as a result. Thus the gear ratio and the input shaft speeds are lower, easing the gearbox design problems.

The addition of an LP turbine has two effects. Power is generated by the turbine and transmitted to the crankshaft of the engine and the exit pressure of the turbocharger turbine is raised. The latter effect reduces turbocharger power, hence a smaller turbine must be used to preserve the required boost pressure. Turbine inlet pressure rises, increasing piston pumping work during the gas-exchange (intake and exhaust) process, which offsets part of the benefit from compounding on over-all engine efficiency.

The available energy at the LP turbine will increase with engine speed and load, due to the influence of air/fuel ratio on exhaust gas temperature and the flow characteristic of the turbine. Thus the power transferred to the crankshaft will be significant at high speed and load, but actual values are determined by the turbocharger match selected, and system efficiencies. The back pressure felt

by the turbocharger turbine will also be highest at high speed and load, hence turbocharger boost will vary slightly less with speed than normal.

Little data is available in published literature analysing compound systems in detail, but the benefit achievable is highly dependent on turbocharger and gearbox efficiency, and matching constraints. Kamo and Bryzik [31] have predicted an improvement in brake specific fuel consumption from 202 to 183 g/kWh (9 per cent) at rated speed and load. Way and Wallace [32] have predicted the thermal efficiencies shown in figure 11.38. The difference between the turbocharged and compound engines (in standard form, that is, otherwise a conventional engine design) is 3 percentage points (or 8 per cent difference) over most of the speed range at full load. Like Kamo's data, this relates to compound scheme (c) in figure 11.36.

Other proposed compounding schemes include use of a heat exchanger at the turbine exhaust, heating a fluid operating a closed Rankine power generation cycle. [33] These schemes offer greater potential fuel economy saving but are more complex and expensive, and fall outside the scope of this book.

Recently considerable research and development work has been directed at combining compound systems with engines designed for greatly reduced heat

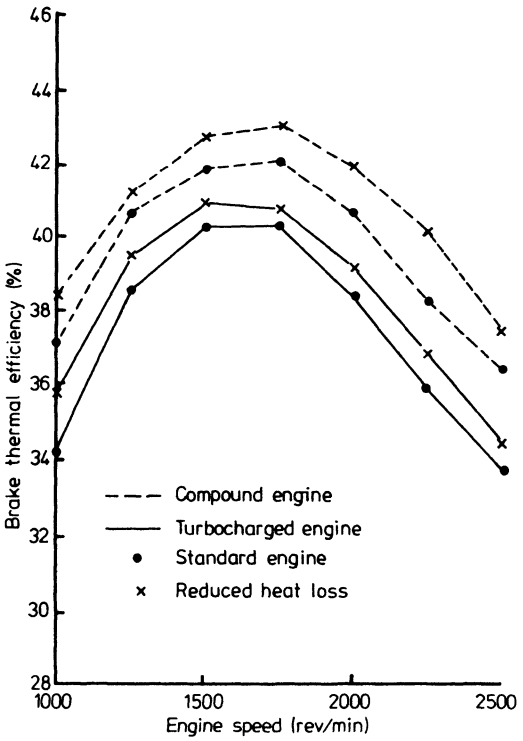

Figure 11.38 *Comparative thermal efficiency of standard and reduced heat loss engines in turbocharged and compound form [32]*

transfer from the cylinder and the exhaust system. These so-called 'adiabatic turbo-compound engines' are discussed in the following section.

11.10 Insulated Engines

Increasing fuel costs have forced engine designers to consider reducing the heat loss through combustion chamber walls in order to improve engine efficiency. An insulated engine is one in which no heat from the cylinder gas escapes through the combustion chamber walls to the surroundings. Such an engine design has the obvious advantage of not needing a cooling system and the disadvantage of posing a very difficult design problem to the manufacturer. Here we are more concerned with the effects on the turbocharging system and engine efficiency, but the implications of the insulated concept must be considered first.

Two idealised systems could be proposed, both of which reduce the heat loss to the surroundings to zero, except through the exhaust system. In the first system, the normal cooling system of the engine is removed and all the water jackets and surroundings filled with an insulating material. Obviously the combustion chamber wall surfaces will be much hotter than before but the heat transfer from gas to wall will not be zero. The new cylinder wall temperature will stabilise so that heat transfer from gas to wall during the high gas temperature part of the engine cycle (combustion and expansion) will be balanced by heat transfer from wall to gas during the low gas temperature part (intake and compression). The net heat transfer will be zero, not the instantaneous heat transfer; we shall call this an 'uncooled' engine. In the second system, both the instantaneous and net heat transfer are reduced to zero; this will be called an 'adiabatic' engine. Figure 11.39 shows calculated instantaneous heat flux for a conventional engine and uncooled and adiabatic versions, illustrating the effects shown above.

In figure 11.39, the reduction in heat transfer during the expansion stroke is about 30 to 40 per cent for the uncooled engine. The benefit in indicated thermal efficiency is small (4 per cent). [34] During the intake stroke the negative heat transfer (to the gas) is significant, reducing volumetric efficiency substantially. Indeed Zapf has calculated that if the air/fuel ratio of the standard engine is retained, then the IMEP will fall from 10 to 7.3 bar as a result. This

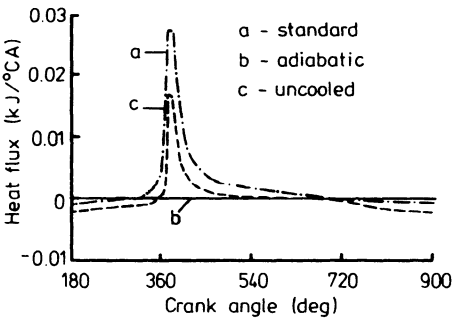

Figure 11.39 *Heat transfer from combustion chamber with insulated engine [34]*

major disadvantage of the uncooled engine does not effect the adiabatic engine. Its IMEP rises to 11.9 bar and its indicated thermal efficiency by 13 per cent.

The adiabatic concept is therefore much more attractive, but how can it be achieved? The assumption of zero instantaneous heat transfer implies a zero gas-to-wall heat transfer coefficient or that gas and wall temperatures are always equal. Neither of these ideas is possible, but something close to the second might be achieved if the thermal capacity of the cylinder wall is very small (low density and specific heat capacity). Wallace *et al.* [35] have shown that this ideal can only be achieved by using an infinitely thin, fully conducting metal shield, backed by perfect insulation. However, even if the metal shield were a 0.01 mm thick copper element, the resultant fluctuation in surface temperature would be reduced to about ±40 °C, with a gas temperature fluctuation of ±1000 °C. Thus the ideal cannot be realised in a practical system.

As a result, effort is mainly directed at overcoming the disadvantages of the more practical, uncooled engine approach, which are low volumetric efficiency and small thermal efficiency gains. Turbocharging can be used to offset the effect of low volumetric efficiency, by raising boost pressure, but maximum cylinder pressure limitations may restrict the benefit achieved. Turbo-compounding, as discussed in section 11.9, can further improve the thermal efficiency of the engine. Analysis of the uncooled engine concept, or a more practical system with

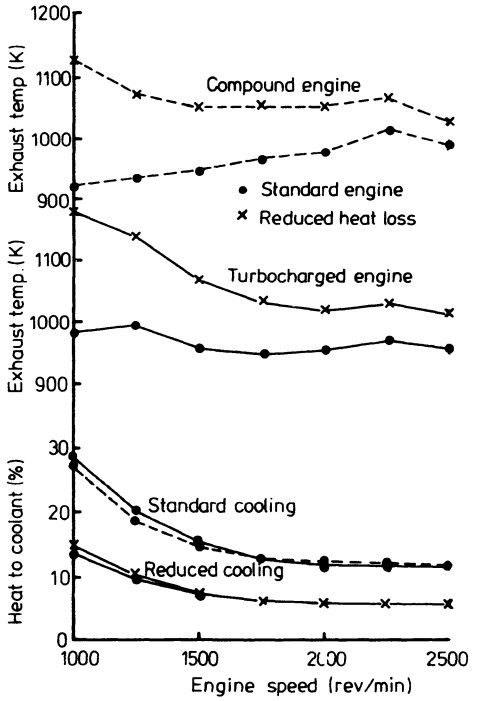

Figure 11.40 *Exhaust temperatures and percentage heat loss for turbocharged and compound engines, with reduced heat loss [32]*

reduced heat loss, shows that most of the energy saved by reducing heat transfer is delivered to the exhaust from the cylinders, in the form of a higher exhaust temperature (figure 11.40). Thus the energy available at the turbine increases. This is fortunate if a higher boost pressure is required to offset the effect of low volumetric efficiency, but the additional turbine energy should be more than enough for this task. Thus additional energy is potentially available for compounding.

The combined benefits of compounding and reduced heat transfer, are shown in figure 11.38. The combined effects improve thermal efficiency by about 11 per cent (or 4 percentage points) over the complete speed range. These calculations are based on compound scheme (c) of figure 11.36, and a reduction in total heat transfer of about 50 per cent. Kamo and Bryzik [31] predict a combined benefit of 23 per cent. Although this figure takes account of power saved by removing the cooling fan and water pump, and is based on a 75 per cent reduction of heat transfer, it is more optimistic than the projections of Way and Wallace. [32]

Unfortunately, difficulties in designing engines with heat transfer reduced to these levels, mean that experimental data has not yet been published to verify either prediction. The future of insulated turbo-compound engines is largely dependent on high-temperature materials technology, since combustion chamber surface temperatures will be substantially higher than those of conventional engines. Ceramics are being considered for the gas side face of combustion chambers, [36] due to their strength at very high temperatures. However, development work is currently in its infancy. [37]

References

1. M. S. Janota and D.H.C. Taylor, Development trends in turbocharging the medium speed diesel engine, *Combust. Engine Prog* (1970)
2. K. Kunberger, New BBC turbochargers, *Diesel and Gas Turbine Progress Worldwide* (November/December 1978)
3. G. Zehnder and E. Meier, Exhaust gas turbochargers and systems for high-pressure charging, *Proc. CIMAC* (1977) paper A.8
4. D.H.C. Taylor, M. Whattam and M.S. Janota, Comparison of single and two-stage turbocharging on a medium-speed four-stroke diesel engine at high BMEP, *Proc. CIMAC* (1971) paper A.19
5. J.R. Grundy, L.R. Kiley and E.A. Brevick, AVCR-1360-2 High specific output-variable compression ratio engine, *SAE 760051* (1976)
6. R. Miller and H.U. Lieberkerr, The Miller supercharging system for diesel and gas engines, *Proc. CIMAC* (1957)
7. R. Chellini, GMT uprates diesel by 40%, *Diesel and Gas Turbine Progress Worldwide* (January/February 1980)
8. H. Reulein, Einfluss der Turbokühlung und des Miller-Verfahrens auf die Liestung von aufgeladenen Gasmotoren, *MTZ*, **31** (1970)
9. R. Kamo, Higher BMEP prospects for vehicular diesels, Paper C62/78. Turbocharging and Turbochargers Conference, Inst. Mech. Engrs (London 1978).
10. C.C.J. French, Taking the heat of the highly boosted diesel, *SAE 690463* (1969)

11. Ruston and Hornsby Ltd, UK Patent No. 977678
12. P. Tholen and I. Killman, Investigations on highly boosted turbocharged air-cooled diesel engines, *ASME Paper 77-DGP-11* (1977)
13. C.C.J. French and D.H.C. Taylor, An investigation into diesel engine operation at very high ratings, *Proc. CIMAC* (1975)
14. H. Zapf and G. Athenstaedt, Test results and operating data of highly supercharged medium-speed four-stroke diesel engines up to an MEP of 27 bars, *Proc. CIMAC* (1975)
15. E. von Schnurbein, Constant pressure turbocharging for medium-speed four-stroke engines, Paper C57/78, Turbocharging and Turbochargers Conference, Inst. Mech. Engrs (London, 1978)
16. A. Oestergaard, Development of two-stroke uniflow-scavenged engines, *Diesel and Gas Turbine Progress Worldwide* (June 1979)
17. O. Syassen, Zukunftsaussichten der zweistufigen Aufladung für Zweitakt und Viertakt-Grossdieselmotoren, *MTZ*, **39** (1976)
18. Y. Takemoto and K. Hashimoto, Development of two-stage turbocharging system on a four-stroke medium-speed diesel engine, *Proc. CIMAC* (1977)
19. R. Herrmann and B. Treuil, Nouvelles perspectives de développement des moteurs diesel à 4 températures, *Proc. CIMAC* (1975)
20. G. Woschni, E. Beineke and H. Flenker, Calculation of the performance of one and two stage turbocharged medium speed diesel engines. Paper C53/78, Turbocharging and Turbochargers Conference, Inst. Mech. Engrs (London, 1978)
21. E. Meier, The Miller system - a possible solution to present problems with highly charged four-stroke engines, *Brown Boveri Rev.* **64** (1977)
22. N. Watson, M. Marzouk and Z. Baazaari, An evaluation of two-stage turbocharging for efficient, high-output, diesel engines, *ASME Paper 78-DGP-2* (1978)
23. K. Kunberger, New diesel highlights from MAN, *Diesel and Gas Turbine Progress Worldwide* (January/February 1980)
24. M.S. Ghadiri-Zareh and F.J. Wallace, Variable geometry versus two-stage turbocharging of high output diesel engines, Paper C63/78, Turbocharging and Turbochargers Conference, Inst. Mech. Engrs (London, 1978)
25. S.G. Berenyi and C.J. Raffa, Variable area turbocharger for high output diesel engines, *SAE 790064, Turbochargers and Turbocharged Engines, SP442* (1979)
26. J. Melchior and T. Andre-Talamon, Hyperbar System of high super-charging, *SAE 740723* (1974)
27. T. Andre-Talamon, New aspects of turbocharger utilization with Hyperbar parallel supercharging, Paper C66/78, Turbocharging and Turbochargers Conference, Inst. Mech. Engrs (London, 1978)
28. F.J. Wallace and G. Winkler, Very high output diesel engines - a critical comparison of two-stage turbocharged, Hyperbar and differential compound engines, *SAE 770756* (1977)
29. H. Sammons and E. Chatterton, Napier Nomad aircraft diesel engine, *SAE Trans.*, **63**, No 107 (1955)
30. F.J. Wallace, The differential compound engine, *SAE 670110* (1967)
31. R. Kamo and W. Bryzik, Adiabatic turbocompound engine performance prediction, *SAE 780068* (1978)
32. R.J.B. Way and F.J. Wallace, Results of matching calculations for turbocharger and compound engines with reduced heat loss, *SAE 790824, Diesel Engine Thermal Loading, SP 449* (September 1979)

33. C.J. Leising, G.P. Purokit, S.P. De Gray and J.G. Finegold, Waste heat recovery in truck engines, *SAE 780686* (1978)
34. H. Zapf, Grenzen und Möglichkeiten eines unärmedichten Brennraumes bei Dieselmotoren, *VDI-Ber.*, No. 238 (1975)
35. F.J. Wallace, R.J.B. Way and H. Vollmert, Effect of partial suppression of heat loss to coolant on the high output diesel engine cycle, *SAE 790823, Diesel Engine Thermal Loading, SP 449* (September 1979)
36. J.H. Stang, Designing adiabatic engine components, *SAE 780069* (1978)
37. M.C. Brands, J.R. Werner, J.L. Hoehne and S. Kramer, Vehicle testing of Cummins turbocompound diesel engine, *SAE 810073* (1981)

12

Transient Response of Turbocharged Engines

12.1 Introduction

The major increase in diesel engine ratings that has occurred over the last 30 years (figure 1.5) has largely come about due to turbocharging and subsequent charge cooling. Supercharging pressures have risen steadily, and it has become evident that some difficulties associated with turbocharging have become more significant at these higher ratings. The principal limitations – mechanical stresses of engine and turbocharger, thermal loading, turbocharger flow range and efficiency – have been discussed in chapter 11. An additional problem that has become more serious at the high pressure ratios now in use, is poor performance under transient conditions.

The problem of poor performance under changing load or speed conditions must be attributed to the nature of the energy transfer path between engine and turbocharger. It takes time to fill inlet and exhaust manifolds and raise their pressure. Under accelerating conditions, only part of the energy used by the turbine is delivered to the compressor, the remainder is required to overcome the inertia of the turbocharger and accelerate its rotating components. Energy required for the latter can be provided only at the expense of the former. Thus the supercharging pressure developed at any moment when the engine is accelerating or being subjected to an increasing load, is likely to be below that developed when operating steadily at the same instantaneous engine speed and fuel rack position. This implies that the air supplied will be less than that normally supplied for combustion of the quantity of fuel being injected. Combustion will deteriorate, causing smoke emission and possibly limiting the instantaneous torque developed by the engine. Thus poor acceleration or response to a load increase may result. In an extreme case the engine might stall, but usually the problem is a smokey exhaust and an unacceptably slow response time.

Figure 12.1 shows the performance parameters of a high-speed diesel engine during a fast load application, without change of governor setting. Full load is applied in about 1 s yet it takes about 4 s for the turbocharger to reach its final steady state speed. As the load is applied, the engine speed drops. The governor responds quite rapidly, reaching maximum fuelling in about 1.5 s from the moment of load application. However, since the boost pressure rises slowly the

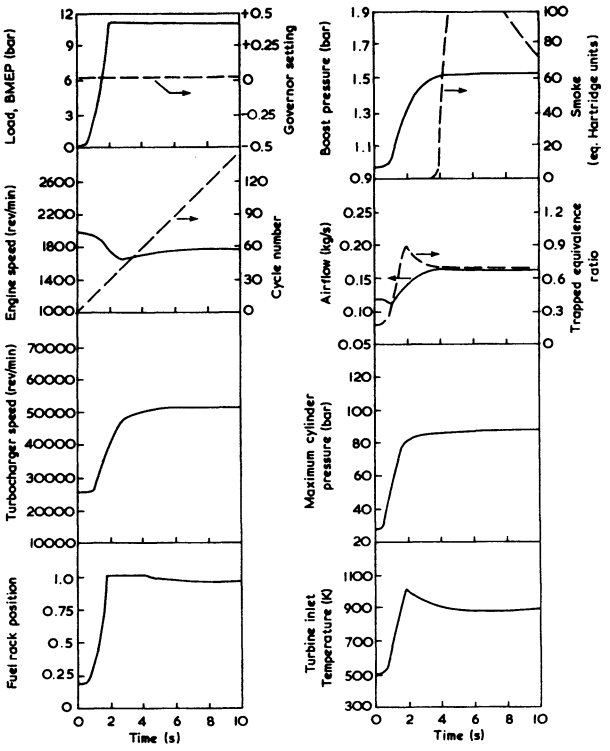

Figure 12.1 *Engine response to a fast load application*

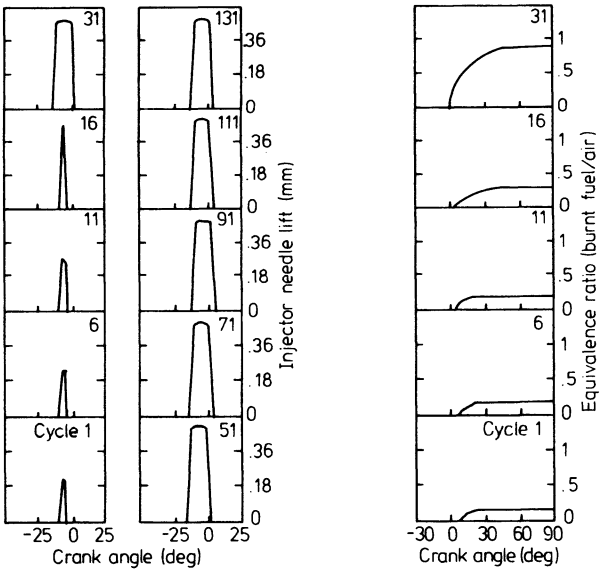

Figure 12.2 *Detailed engine performance parameters during the load change shown in figure 12.1*

fuel/air ratio becomes excessively rich. Figure 12.2 shows the injector needle lift diagrams for one cylinder at various points during the transient sequence of figure 12.1. At cycle 1, the load applied externally to the engine is zero, hence sufficient fuel is being injected only to overcome friction of engine and load. By cycle 16 (fourth diagram up), the governor has responded sufficiently for the injector to reach full lift and between cycles 16 and 31 full fuelling is reached (1 to 2 s). Also shown in figure 12.2 are predicted curves of instantaneous charge equivalence ratio in the cylinder (based on fuel burnt and air trapped in the cylinder at IVC). Following the start of combustion the equivalence ratio rises to reach a steady value at the end of combustion. Since the equivalence ratio is equal to unity for a stoichiometric mixture, it is apparent that the fuel/air ratio has become very rich indeed. The equivalence ratio is 0.9 during cycle 31; not surprisingly, the exhaust smoke level will be excessively black.

Figure 12.3 shows individual cylinder and exhaust manifold pressure diagrams recorded during the load application. The cylinder pressure diagram responds according to the fuel supplied. The exhaust manifold (turbine entry) diagrams show the exhaust pulses from three cylinders of a six-cylinder engine connected to one turbine inlet of a twin-entry turbine. Note that little rise in exhaust pressure occurs until between cycles 16 and 31. This is the point at which the load application becomes rapid and it is clear that the exhaust manifold pressure, and hence turbine energy, increases almost as soon as the fuel rack has responded. This leads to the important conclusion that energy has been transmitted to the turbine rapidly, in this case, but the inertia of the turbocharger is too great for the compressor to supply sufficient air to prevent an objectionable exhaust smoke level occurring.

On more highly rated engines, the difference between no-load and full-load fuelling would be greater, hence much richer fuel/air ratios could develop, leading to very poor combustion and engine stall.

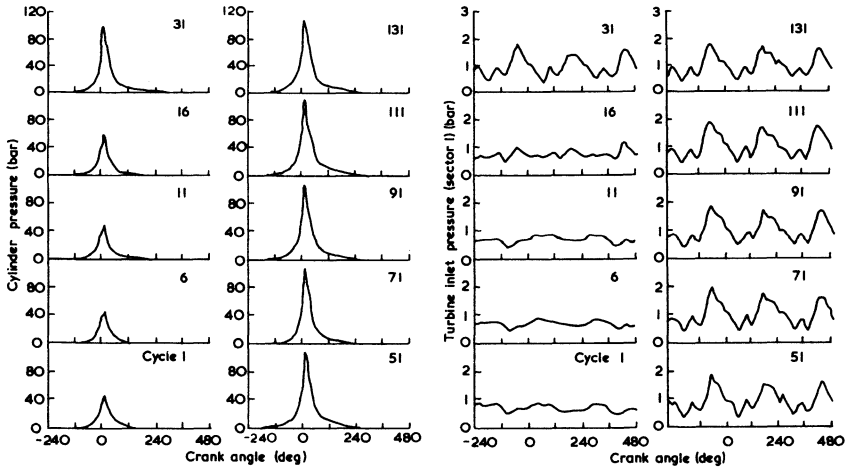

Figure 12.3 *Cylinder and exhaust pressure diagrams measured during the load change shown in figure 12.1*

Methods of predicting the transient response of turbocharged diesel engines are presented in chapter 15.

12.2 The Importance of Rapid Response

Having discussed the influence of turbocharger delays on engine performance, it is useful to look at some engine applications in which the response is important.

Load changes on electrical power generators can be large and sudden. Figure 12.4 illustrates engine response to a step load decrease on a diesel generator and a step load increase. Speed droop and voltage dip are important criteria in this instance, but note that the engine speed stabilises long before the turbocharger delivers its new, steady boost pressure. During the latter period the governor is in

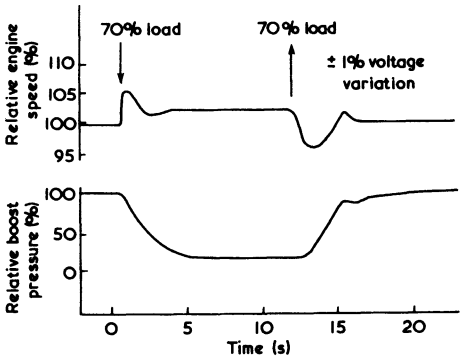

Figure 12.4 *Diesel generator response to sudden load changes [1]*

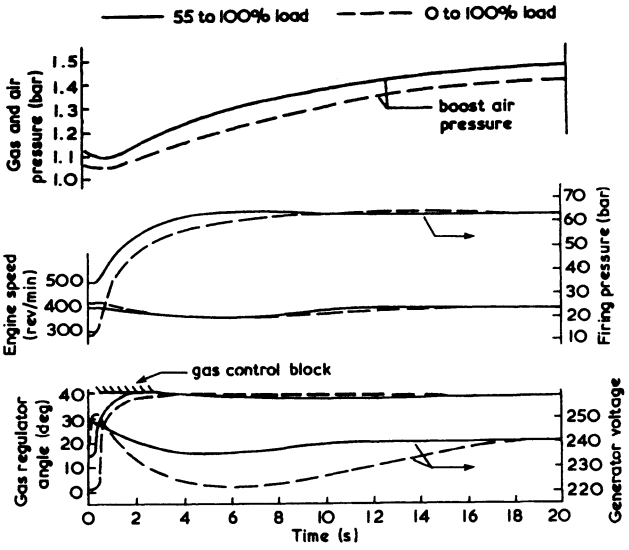

Figure 12.5 *Natural gas engine generator response to load changes [2]*

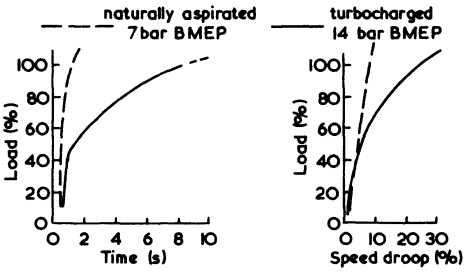

Figure 12.6 *Recovery period and dynamic speed droop comparison [2]*

control, maintaining the correct engine speed through a slightly rich fuel/air ratio until the turbocharger has accelerated to a new steady speed.

Figure 12.5 shows, in more detail, the response to sudden electrical load increases on a turbocharged natural gas engine. The dashed line denotes a 0 to 100 per cent load application, the solid lines a 55 to 100 per cent load application. Steady conditions are reached in 18 and 8 s respectively, with the speed and voltage droop not exceeding 10 per cent.

Theoretically, a step input of 100 per cent load will stall an engine if the fuel input is not allowed to exceed the full load steady state value at any time. Thus a fuelling overload of about 10 per cent is usually accepted, above steady state values, or the engine must be rated above the expected maximum load, or sudden load applications are restricted.

Figure 12.6 compares the recovery period and speed droop of two diesel generators – one naturally aspirated, the other turbocharged – to sudden load applications. If a temporary speed droop of 10 per cent is considered acceptable, then the naturally aspirated engine can accept a full load application satisfactorily. The turbocharged engine, however, will exceed this speed droop if a load greater than 70 per cent of full load is suddenly applied.

If the rating of the turbocharged engine is low, then the quantity of excess air (that is, above that required for a stoichiometric homogeneous mixture) at no load, may be quite sufficient to support combustion at maximum fuelling. However, if the engine is designed to operate with a high compressor pressure ratio, then full fuelling at virtually no-load boost pressure can result in an instantaneous fuel/air ratio richer than stoichiometric. Combustion will suffer sufficiently for power output to fall and the engine may stall. Thus response of a diesel generator depends on engine rating.

A further example of the need for rapid response is the manoeuvring characteristics of a ship-handling tug. A vessel of this type is required to change from full ahead to astern, quite rapidly. Typically the propeller should have reversed within 10 s, leading to the reversal of the vessel in 30 to 40 s. Vessels of this type, and others, frequently use highly pressure charged medium-speed diesel engines with a reverse reduction gearbox and a fixed pitch propeller. Figure 12.7 illustrates the sequence of events during a typical full ahead to full astern manoeuvre. At point 1 the vessel is moving ahead at 6.5 knots, when the control level is moved from full ahead to full astern. At this moment, fuel is cut off and neutral is

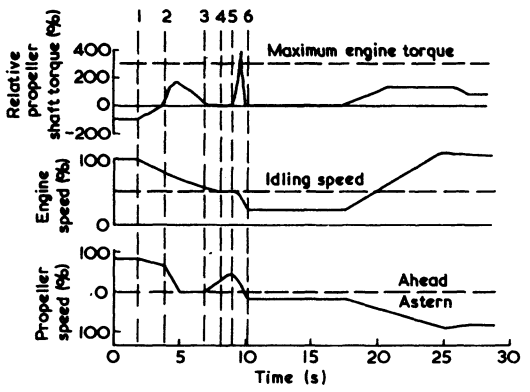

Figure 12.7 *Full ahead to full astern manoeuvre of a diesel-engined tug [1]*

selected in the gearbox. The engine speed starts to fall, but the propeller is decelerated more rapidly by the application of a shaft brake at point 2. The propeller has stopped within 5 s. The astern clutch is selected at point 4 when the engine is close to idling. The clutch takes time to engage (from points 5 to 6), but the propeller shaft brake must be released prior to clutch take-up (point 3). Since the vessel is moving forward at this moment, the propeller is induced to turn freely in the 'forward' direction. Thus when the clutch takes up, the propeller is rapidly brought to a halt and reversed. Clearly the instantaneous torque developed in the shaft during this action is very high and can result in a severe speed drop at the engine. This is the danger point, and a complete stall could occur.

12.3 Industrial Engines

12.3.1 Inertia

The inertia of the turbocharger rotor and of the engine-load combination, both influence the response to changes in load or demand speed. A high combined engine and load inertia will help maintain speed following a sudden load application, and is therefore useful for power generation. However, this will impair engine acceleration when a change in speed is required.

The effect of the combined inertia of engine and load will be illustrated for the case of a sudden load application to a medium-speed engine, typical of generating-set applications. The solid line in figure 12.8 illustrates engine response to a rapid load application, equivalent to 16.5 bar BMEP. As the load is applied, engine speed drops. The governor responds rapidly, with maximum fuel pump rack position being reached in about 0.5 s. Turbocharger acceleration is very slow (solid line), with a speed increase from 10 000 to 20 000 rev/min taking almost 4 s. During this period maximum fuelling is supplied, but the air supply is that of a naturally aspirated engine for the first 2 s. The result is an equivalence ratio reaching a value of 1.5, substantially richer than stoichiometric, and almost double

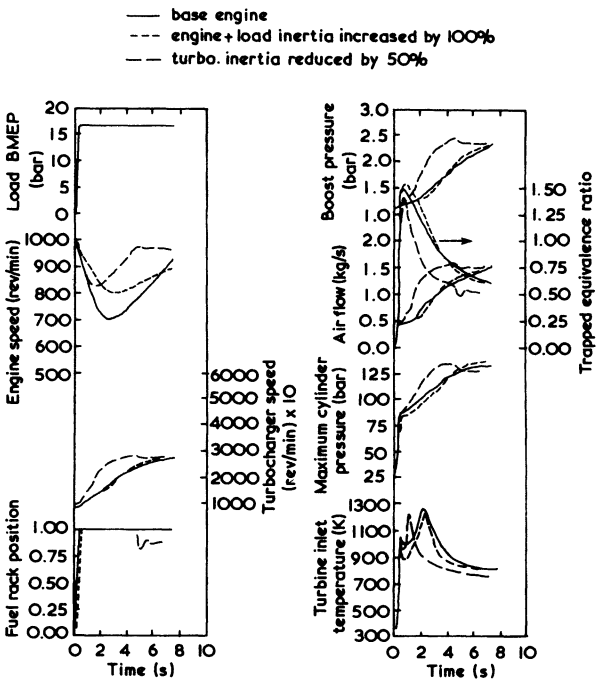

Figure 12.8 *Effect of engine and turbocharger inertia on engine response to a rapid load application*

the maximum steady speed value expected. Combustion deteriorates and engine speed continues to fall. About 2 s after this load application, the turbocharger has accelerated just sufficiently for the boost pressure and hence air flow to begin to increase significantly. Combustion begins to improve and deceleration of the engine is halted and reversed. As boost is built up, the equivalence ratio improves more and more and the engine accelerates back towards the required speed. During this load application, the speed drop is 30 per cent (from 1000 to a minimum of 700 rev/min), which is unacceptable for a normal generating set.

If the inertia of the engine and load combination is increased, then the greater stored kinetic energy will help reduce the deceleration of the engine as load is applied. The effect of a 100 per cent increase in combined engine and load inertia (figure 12.8) reduces speed drop from 30 to 20 per cent (from 1000 to a minimum of 800 rev/min), without improving turbocharger acceleration or any change in the maximum equivalence ratio. However, although speed drop has reduced, the increased inertia of the system means that it is more difficult for the engine to accelerate back up to the initial speed. The total recovery time from load application to the final steady speed, increases. Thus increased systems inertia reduces speed drop but may increase response (or recovery) time.

Reducing the inertia of the turbocharger can reduce speed drop and recovery time. Figure 12.8 shows that a 50 per cent reduction in turbocharger inertia reduces the speed drop of this medium speed engine, to 17 per cent (1000 to 830 rev/min),

and almost halves total response time. This is achieved with the original value of combined engine and load inertia. The benefit of reduced turbocharger inertia is shown in much more rapid turbocharger acceleration. The turbocharger response is still not sufficient to prevent the maximum equivalence ratio from substantially exceeding stoichiometric, but a weaker fuel/air ratio is developed much earlier. Thus combustion improves sooner, enabling the engine deceleration to be halted and reversed after about 1 s, compared with 2 s with the previous turbocharger inertia. Reducing turbocharger inertia is the most effective method of improving response.

There may be several possible methods of reducing the inertia of the turbocharger system, apart from the manufacturer's efforts at the design stage.

The turbocharger match most suitable for a particular engine and duty could in some cases occur at the low flow end of a particular turbocharger frame size or range. A change to the largest build from a smaller sized range may often be accepted with little penalty on steady speed performance, but with an inertia reduction. Alternatively, if the flow requirements lie in the mid-range of one basic frame size supplied by a particular manufacturer, the same requirement may be met by a unit at the top of a smaller frame size from another manufacturer, For engines having six cylinders or more, a reduction in inertia might be achieved by replacing a single large turbocharger with two small units.

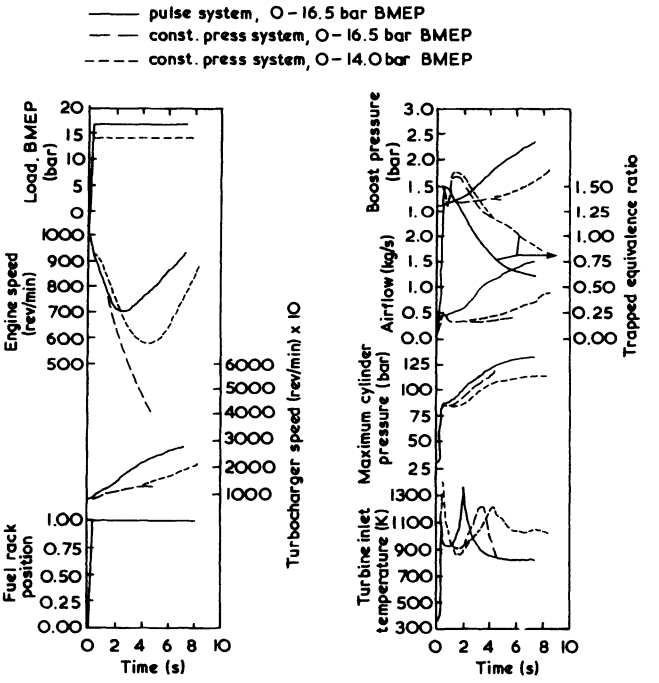

Figure 12.9 *Effect of the turbocharging system on engine response to a rapid load application*

12.3.2 Turbocharging System

A serious drawback of the constant pressure turbocharging system is its poor response to a sudden increase in load or speed. This is mainly due to the relatively large exhaust manifold which obviously takes longer to 'fill', increasing energy transmission time and reducing the availability of the exhaust energy arriving at the turbine.

The effect of changing from pulse to constant pressure turbocharging on the load acceptance of a medium-speed engine is shown in figure 12.9. The six cylinders of the engine are allowed to discharge into one common manifold whose volume is five times the total volume of the original manifolds, while a single-entry turbine housing replaces the previous twin-entry one. Very slow turbocharger response causes a long period with very rich fuel/air ratio. Combustion never recovers and the engine stalls; the maximum load applied has to be reduced from 16.5 to 14.0 bar BMEP to prevent engine stall.

The volume of the inlet, as well as the exhaust manifold, has some effect on the response of the engine. The larger the inlet manifold, the longer the time needed for the turbocharger to build up manifold pressure. If air-to-air coolers are mounted slightly remote from the engine, the over-all quantity of air stored in the pipes and cooler can become quite significant. However, scope for reduction in inlet manifold volume will usually be small when charge cooling is not used, or when compact air-water coolers are mounted on the engine.

12.3.3 Turbocharger Match

Stringent requirements concerning transient performance and speed governing introduce new constraints to the relatively simple matching process of constant speed engines. During a sudden load application, the transient air flow characteristic (superimposed on the compressor map) may shift towards the surge line, hence a relatively large surge margin is desirable.

Highly rated medium-speed engines generally use large overlap to promote good scavenging at rated speed and load. In addition to removing combustion products from the cylinders, the increased air flow into the exhaust system cools exhaust valves and the turbocharger turbine. In order to achieve good scavenging, it is important to maintain a favourable pressure drop between inlet and exhaust port, during the valve overlap period. The turbocharging system will have been matched to achieve this, under steady speed conditions. However, this requirement may not be met under transient conditions.

Figure 12.10 shows the effect of varying the size of the turbine nozzle ring on steady speed performance at the rated speed and load of a pulse turbocharged engine. Two adjacent nozzle ring sizes (immediately above and below the datum build) are considered. This engine has large valve overlap, for the reasons given above. Reducing turbine nozzle area increases turbine available energy, hence the boost pressure is highest with this nozzle. The trapped mass of air in the cylinder is greatest as a result. However, the small turbine nozzle increases exhaust system pressure substantially, hence the pressure difference between inlet and exhaust manifolds reduces and scavenge air flow suffers. The reduction in scavenge air flow

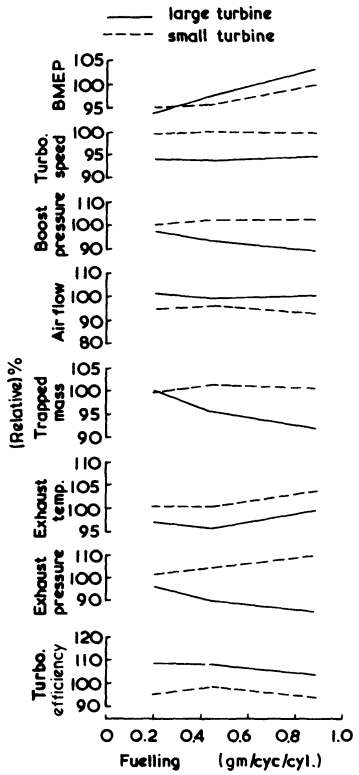

Figure 12.10 *Effect of turbine area on steady speed performance of a medium-speed engine (relative to base match, %)*

is sufficient for the total (scavenge plus trapped) air flow to be lowest with this nozzle, even though the trapped component is the greatest. With the large turbine area, boost is insufficient to deliver enough fresh air to the cylinder at full load and the trapped mass is only 92 per cent of that with the datum nozzle ring. Thus the datum turbine build is the optimum.

Load acceptance with these three alternative nozzle rings is shown in figure 12.11. Under transient conditions, turbocharger lag results in the exhaust manifold pressure rising before the boost pressure builds up. Thus the inlet to exhaust manifold pressure ratio is adverse and an engine with large valve overlap such as this experiences reverse flow from exhaust to inlet system, through the cylinders. The smaller the turbine area, the worse this situation becomes, hence the engine response is best with the largest of these three turbine trims. However, if the engine has much less valve overlap, it would not experience reverse flow, and the smallest turbine trim would provide highest boost and best response.

12.3.4 Fuel Control System

The poor response of a highly rated turbocharged engine is caused by the inertia

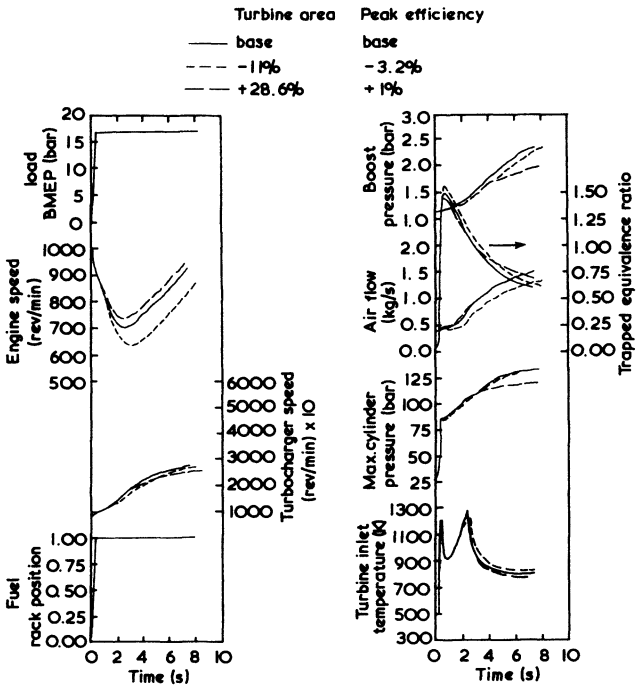

Figure 12.11 *The influence of effective turbine area on the response of a medium-speed turbocharged diesel engine (steady speed performance shown in figure 12.10)*

of the turbocharger, but is often made worse by the very fuel-rich equivalence ratios encountered as a result. This was illustrated in section 12.3.1, with reference to figure 12.8 in particular. In some cases, the use of a fuel control system, to limit fuel delivery until the turbocharger has built up sufficient boost pressure, can improve response. Figure 12.12 illustrates this.

The fuel system on the base line engine allows a 10 per cent over-fuelling under transient conditions, relative to the fuel delivery at rated steady full-load conditions. During the sudden load acceptance shown in figure 12.12 the instantaneous trapped fuel/air equivalence ratio in the cylinders reaches a value of 1.5. Combustion can be improved by eliminating this over-fuelling margin, resulting in a smaller speed drop. However, the engine is slow to reaccelerate relative to the base line engine. This results from the fact that once the boost pressure has built up, the engine could benefit from the extra 10 per cent of fuel supplied in the base line case.

A fuel control system, sensitive to boost pressure, can be used to combine the smaller speed drop with reduced initial fuelling, with better recovery with excess fuelling. Thus fuelling can be tailored to boost pressure for optimum response, as shown in figure 12.12. Relative to the base line case, this reduces peak equivalence ratio from 1.5 to 1.35, speed drop from 300 to 250 rev/min, and response time from 8 to 7 s.

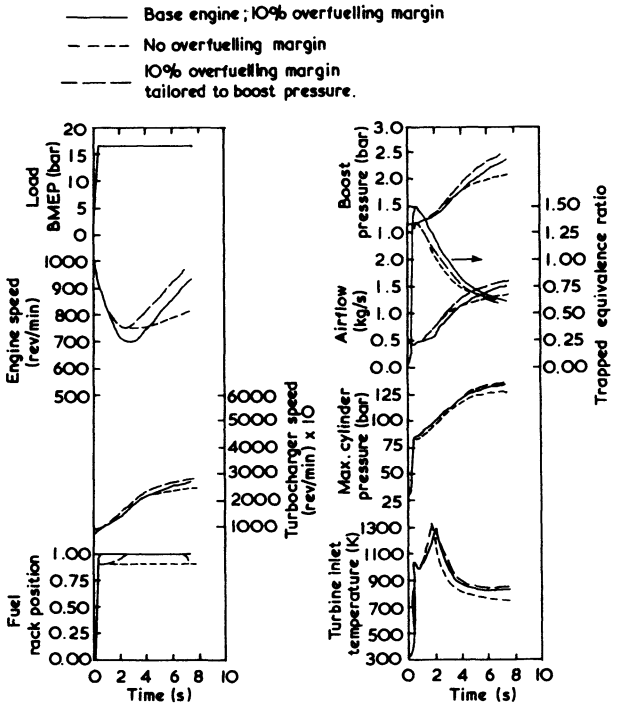

Figure 12.12 *Effect of tailoring maximum fuelling on engine response to a rapid load application*

The use of a fuel control system, often called an 'aneroid' or rack limiter, becomes more important as engine rating increases. This results from the fact that the difference between full-load fuelling at a high rating, and the maximum fuel delivery for good combustion with zero boost pressure, increases.

12.3.5 Valve Timing

The large valve overlap on the engine described in section 12.3.3 is a case where the optimum, determined at steady engine speed, adversely influences response.

When subjected to sudden loading, the governor will respond faster than the turbocharger, producing an over-rich fuel/air mixture. Resulting pressure in the cylinder and exhaust manifolds will be higher than those normally associated with the current boost pressure. Clearly scavenging will be poor and in some cases substantial reverse flow of combustion products into the inlet manifold will occur.

Load acceptance can be improved with less valve overlap, as shown in figure 12.13. The standard valve overlap period for this medium-speed engine, 149°, can be reduced to 109° by delaying the opening point of the inlet valve by 40° and reducing its dwell period. The effect is a substantial improvement in response,

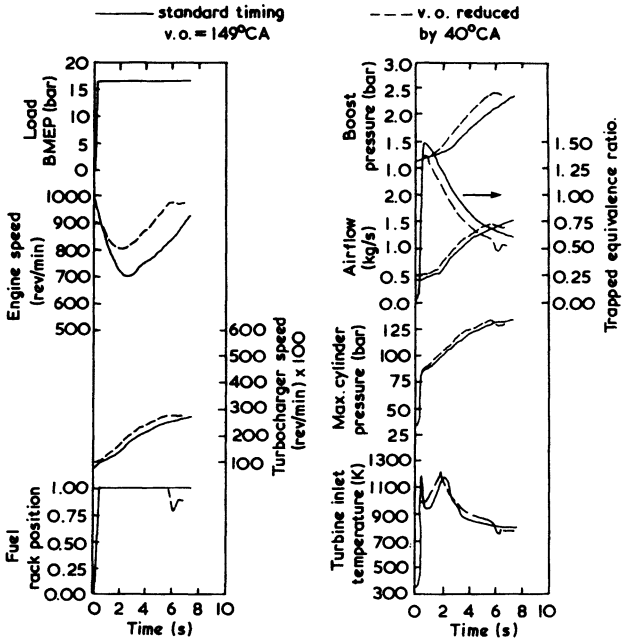

Figure 12.13 *Effect of valve overlap on load acceptance of a medium-speed turbocharged diesel engine*

maximum drop in engine speed and recovery time being reduced by 35 and 27 per cent respectively. As a result of reducing reverse flow into the air chest, the trapped mass of fresh air increases bringing down the trapped equivalence ratio, from a peak of 1.5 to 1.3. Energy release in the cylinder increases due to more complete combustion and response improves.

12.4 Vehicle Engines

12.4.1 Engine Acceleration

Vehicle engines are subject to frequent accelerations, hence their response to changes in desired speed is important. Since the ratings (BMEP) of these engines are lower than typical medium-speed industrial engines, boost pressure is not as high. As a consequence, response is less of a problem. However, more stringent exhaust smoke limitations are imposed.

Figure 12.14 shows the response of a truck engine to a sudden change in 'throttle' position, with no load applied to the engine. The 'throttle' is in fact the input to the speed governor of the engine. The governor senses that engine speed must be increased, and the fuel pump rack is rapidly moved to the maximum fuelling position. The turbocharger accelerates, but very little boost is developed. Insufficient air is supplied causing a large puff of black smoke from the exhaust.

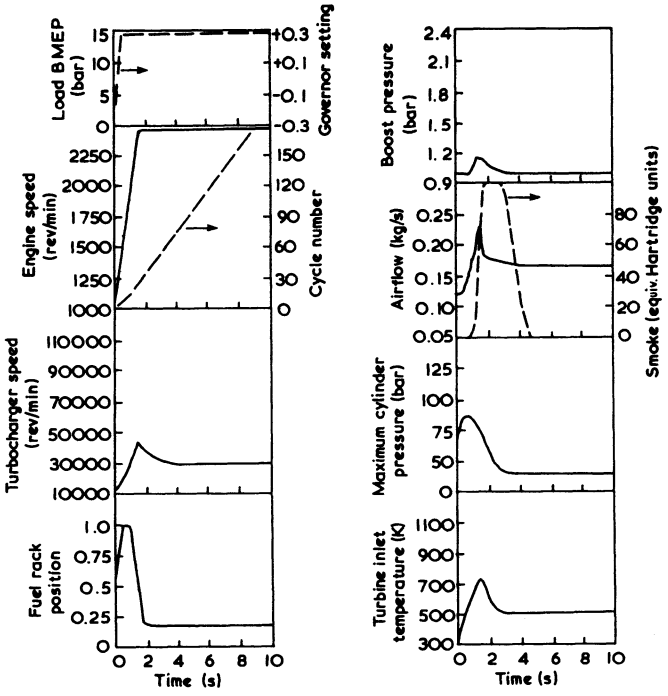

Figure 12.14 *Free (no-load) acceleration of a truck engine*

Under these conditions the engine is behaving virtually as a naturally aspirated engine that is momentarily overfuelled by a margin sufficient to cause smoke, but not sufficiently for combustion (heat release) to deteriorate significantly. Engine acceleration is rapid; only the exhaust smoke level is a problem.

The differences between this and the medium-speed engine discussed previously are that the truck engine has little valve overlap hence no scavenging air flow, and that the rating is not high enough for maximum fuelling to cause the trapped equivalence ratio to exceed the stoichiometric value at zero boost pressure. The engine will respond to changes in turbocharger match, turbocharger inertia and fuel control system, but its response will be less sensitive to changes than the medium-speed engine.

Acceleration under load is a requirement met when vehicles overtake. Figure 12.15 shows the acceleration of the same truck engine, but under a steady load equivalent to 7.5 bar BMEP (a test at steady load is not truly representative of a vehicle accelerating, but is convenient for analysis). The standard engine has no fuel control system. The governor rapidly moves the fuel pump rack to supply maximum fuelling. The turbocharger accelerates rather slowly hence combustion becomes fuel-rich and a substantial cloud of exhaust smoke results. Since the engine is accelerating against a load, its acceleration is slower than that shown in figure 12.14. As a result the fuel pump rack is held at maximum fuelling for longer, and the exhaust smoke is worse.

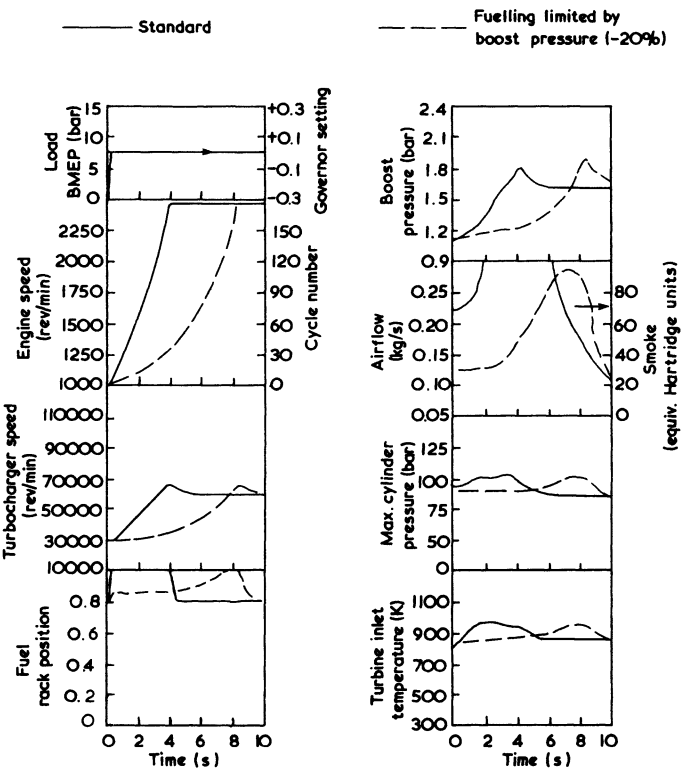

Figure 12.15 *The effect of boost control of fuelling on acceleration under load*

A fuel control system can be used to control exhaust smoke while accelerating. These devices can take many forms, but the simplest consists of a diaphragm which in response to boost pressure, adjusts the maximum fuel stop. Figure 12.15 shows the result of fitting a fuel controller that restricts fuelling by 20 per cent at zero boost pressure. Initially the governor responds very rapidly, moving the fuel pump rack to its (limited) full fuelling position. Since this is less than that with the standard system, both the engine and turbocharger accelerate more slowly. However the fuel/air ratio is prevented from becoming as bad, and exhaust smoke is reduced substantially. Thus the fuel controller is seen to be an effective method of exhaust smoke control under transient conditions, but a conflict between rapid response and low exhaust smoke is apparent.

Changes in turbocharger match influence response and exhaust smoke when accelerating, since they alter acceptable steady speed fuel delivery. The effect of changing turbocharger match and fuel delivery on a truck engine at steady speed was discussed in chapter 10, with the matches specified in table 10.1. Acceleration under a steady load is compared for two of these matches, in figure 12.16. With match 3 (see table 10.1), a small turbine is fitted, generating high boost pressure; combined with standard fuelling, the fuel/air ratio is low. When accelerating, engine response is rather slow but exhaust smoke is moderate. The fuel pump

rack limit is set at a higher value with match 4 (14 per cent more than match 3), but the turbine area is larger to prevent excessive cylinder pressure and turbocharger speed. Engine response with match 4 is more rapid, due to increased fuelling, but as a result exhaust smoke is worse.

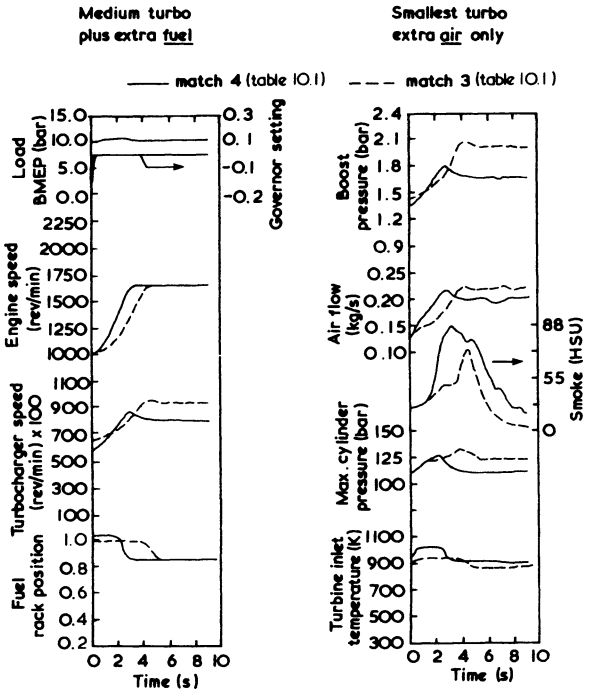

Figure 12.16 *Effect of turbocharger match and fuelling on engine acceleration (for matches, see table 10.1)*

12.4.2 Load Applications

Vehicle engines are also subject to load applications but these are generally less rapid than those experienced by generating sets. For example, high loads can be applied to truck engines when engaging the clutch after a gear change. Earth-moving vehicles experience load applications as part of their normal duty; the same is true of agricultural tractors as ploughs are engaged.

Figure 12.17 shows the response of the same truck engine to a load application, with different turbocharger systems, but without a fuel control device. A zero to almost full load application, with the base line turbocharging system, causes engine speed to fall from 2000 to 1750 rev/min. The speed governor has quite different characteristics to that of the medium-speed engine due to the engine duty. In the case of the medium-speed engine, the governor is required to return engine speed to its previous level (within 2 per cent) to maintain the fre-

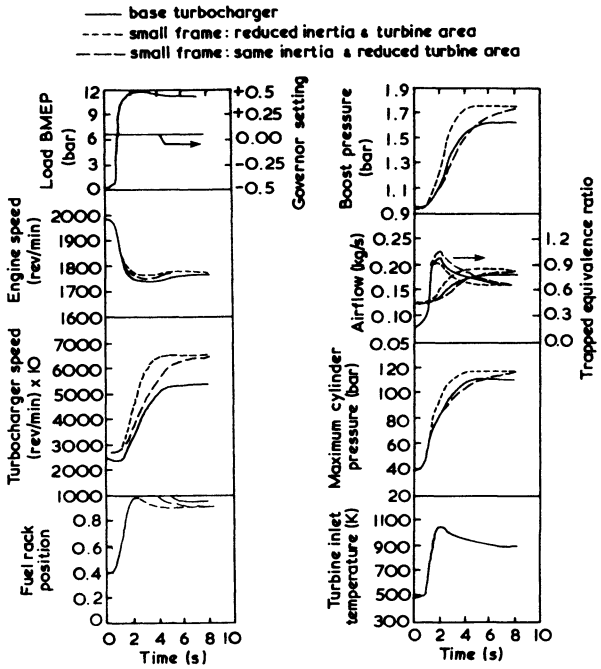

Figure 12.17 *Effect of turbocharger match on load acceptance of an automotive diesel engine*

quency of its electrical generating set load. The final speed droop (final minus initial speed) must be very low. This is not important on a vehicle engine, since the driver is continuously altering his pedal position to suit conditions. Thus less precise governing is required: indeed very precise governing makes the vehicle difficult to drive in changing traffic conditions.

A change to a smaller design of turbocharger (smaller 'frame' size), results in reduced turbocharger diameter (17 per cent), reduced inertia (52 per cent) and reduced turbine area (22 per cent). The turbocharger accelerates much more rapidly (figure 12.17), reducing the maximum trapped equivalence ratio from 1.00 to 0.9. As a result, exhaust smoke (not shown in figure 12.17) reduces. Also shown in figure 12.17 is response calculated (see chapter 15 for the method of calculation) with the small turbocharger but with the inertia of the base line turbocharger. Turbocharger acceleration is similar to the base line system, but since the turbocharger compressor is smaller, it has to rotate faster to produce the same boost pressure. As a result the instantaneous air supply lags behind that of the base line engine. This shows that turbocharger inertia is important, even in vehicle applications with modest engine ratings. t engine ratings.

Figure 12.18 shows vehicle engine response to a 16 bar BMEP load application, with three different turbocharging systems and engine ratings (single-stage turbocharged, single-stage with aftercooling and two-stage turbocharged with inter and aftercooling). This figure shows that, for the *same* load application, the turbo-

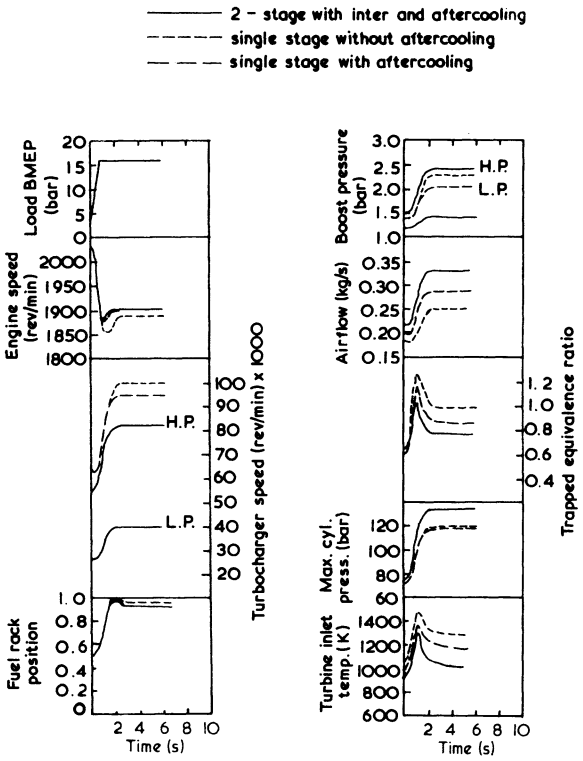

Figure 12.18 *Load acceptance of an automotive pulse turbocharged diesel engine using single and two-stage turbocharging*

charging system designed to supply the highest boost pressure at steady speed, also supplies the greatest air flow under transient conditions. With no charge air cooler and single-stage turbocharging, the maximum trapped equivalence ratio exceeds 1.2, but with two-stage turbocharging and very effective charge cooling, this is reduced to 1.0. Thus the more highly rated engine will respond better to the same load application, although it will not respond as well as a larger naturally aspirated engine developing the same maximum power.

12.5 Energy Addition

None of the factors discussed above utilises additional energy to help accelerate the turbocharger. One method of doing this is to use a store of compressed air, since it is an air deficiency that results in the poor response of turbocharged engines. Many industrial and marine engines have compressed air stores available for starting the engine, and diesel engined trucks are frequently fitted with air-brake systems. Thus part of an air supply and storage system may readily be available, although an air-brake reservoir of a truck must be used exclusively for braking, for safety reasons.

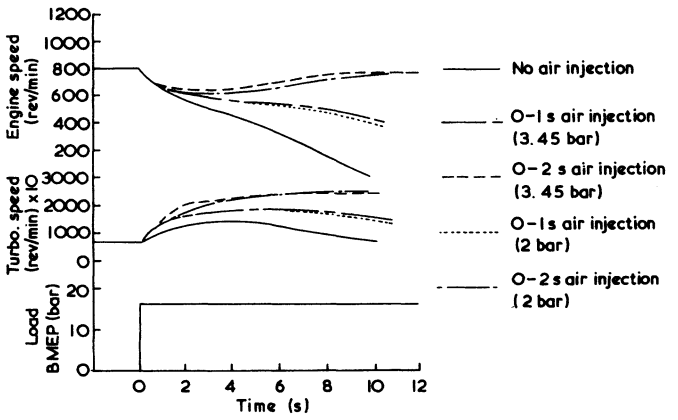

Figure 12.19 *The effect of compressor air injection on load acceptance [3]*

During transient operation, air may be injected into the inlet manifold, exhaust manifold, turbine rotor or compressor impeller. The latter technique has been widely reported. [3, 4, 5] Three air injection nozzles were chosen, as far as possible to impart maximum momentum to the rotor. The system was designed [3] such that the injected air would be 50 per cent of the total, under a supply pressure of 3.5 bar, at the nominal design speed of the turbocharger, but would only be used for short bursts.

The effect of air injection into the compressor impeller on engine response is predicted in figure 12.19. If a sudden load step equivalent to a BMEP 16.8 bar is applied to this industrial engine, when running at 800 rev/min, the solid lines show that it would stall. A burst of air injection for a minimum of between 1 and 2 s is required to prevent stalling. To maintain the required injection pressure for a burst of this duration would require an air store equivalent to 10 to 15 times the swept volume of the engine, at a pressure of 7 bar. A disadvantage, in addition to the air storage problem, is that a succession of rapid load changes may leave the reservoir empty. The system also requires a well-developed control mechanism. Air injection can also reduce the period of excessive smoke after gear changes, when a truck accelerates. [5] Figure 12.20 illustrates the potential increase in engine acceleration achievable (under full load) with inlet manifold air injection. This figure shows 'full throttle' acceleration from the same initial speed and load; after 4 s the engine with air injection has accelerated more rapidly (to 2035 instead of 1580 rev/min), and is producing substantially more power.

Schulmeister [7] has shown that air injection into the cylinders of an engine, through the air start valves often fitted to industrial and marine engines, is also very effective at improving response. However, air injection is not the only method by which additional energy may be supplied. Another has already been discussed (chapter 11), namely the Hyperbar system. This system can be used to overcome transient response problems in two ways. Firstly, by maintaining combustion in the exhaust at all times, turbocharger speed can be kept high, even at no load on the engine. Thus when full load is applied, the speed increase demanded of the

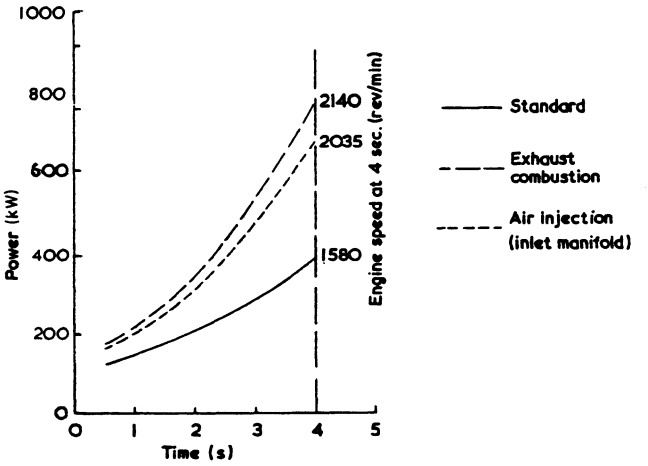

Figure 12.20 *Engine acceleration with exhaust combustion and air injection [6]*

turbocharger can be small or, in an extreme case, zero. Normally it would not be economical to keep the turbocharger at full speed at all times, so some turbocharger acceleration is required. Additional energy may then automatically be supplied to the turbine from fuel injected into the exhaust system combustion chamber. Figure 12.20 also shows engine acceleration with an exhaust combustion chamber, similar to the Hyperbar system.

Timoney [8] has shown that a Pelton wheel turbine may be fitted to the shaft of a turbocharger, operated by high-pressure (for example, 100 bar) lubricating oil. This technique may be used to improve turbocharger acceleration under transient conditions. A suitable control system is required. Figure 12.21 compares

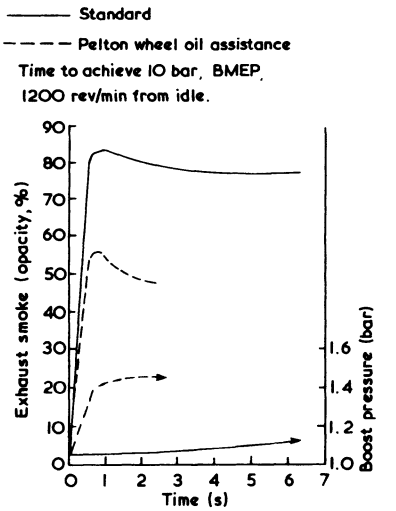

Figure 12.21 *The effect of Pelton wheel oil assistance to the turbocharger on engine response [8]*

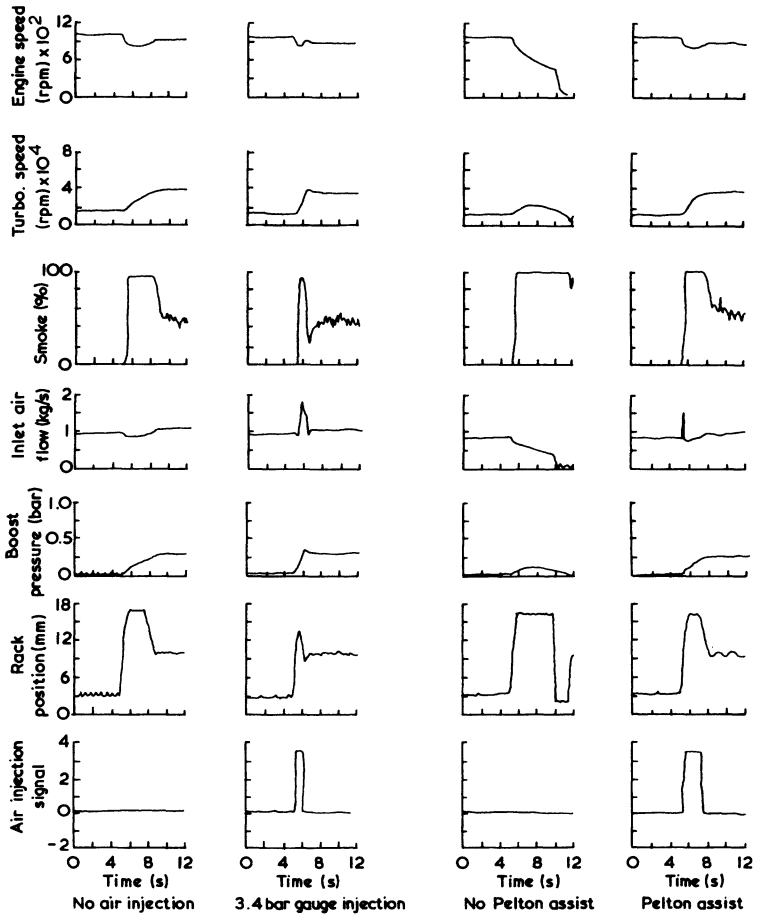

Figure 12.22 *Comparison of air injection and Pelton wheel oil assistance on response to a step load application [5]*

exhaust smoke and boost pressure during a 'full-throttle' acceleration. However, this is not a simple exercise, since is involves switching very high-pressure oil systems on and off quite rapidly. Winterbone *et al.* [5] have compared engine response to a load application with air injection and the Pelton wheel hydraulic assist systems. Figure 12.22 shows air injection to be the superior system. An additional disadvantage of the Pelton wheel is the windage loss at steady state and low efficiency when not in use.

It should be mentioned that some compound engines and Comprex [9, 10] supercharged engines will also respond more favourably than a turbocharged engine, due to direct mechanical energy transfer to the compressor in the former, and energy transfer via pressure waves travelling at sonic velocity in the latter. Figure 12.23 compares truck engine acceleration with turbocharged and Comprex supercharged versions of the same engine. The acceleration diagrams show BMEP

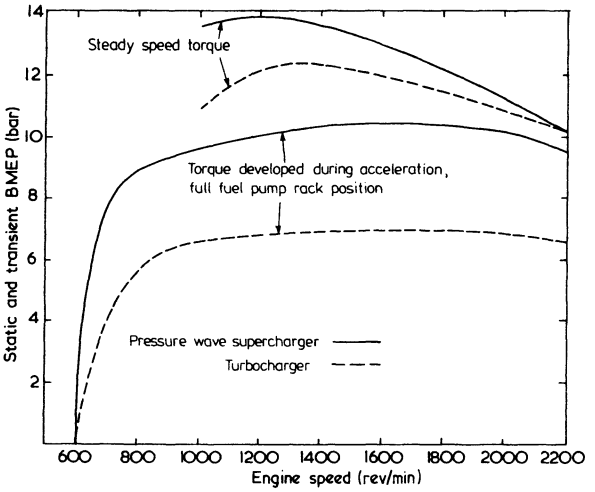

Figure 12.23 *Comparison of instantaneous BMEP when accelerating with steady speed-torque curve, with turbocharger and Comprex pressure wave supercharger [9]*

developed as a function of engine speed under 'full-load' or 'full-throttle' conditions, with the engine accelerating a large inertia mass, representative of a vehicle. The steady speed BMEP curves are shown for comparison, revealing that under transient conditions neither engine can generate true full-load BMEP, but that the Comprex supercharged engine is substantially better than the turbocharged engine.

References

1. D. A. Gillespie, R. N. Smith and P. J. Taylor, Automatic Control and associated problems with high pressure charged engines, *Proc. CIMAC* (1968) paper B.15
2. W. Klaurig and K. Will, Automatic operation of highly rated, spark ignition, turbocharged gas engines with special regard to their torque characteristics, *Proc. CIMAC* (1968) paper B.9
3. J. D. Ledger, R. S. Benson and H. Furukawa, Improvement in transient performance of a turbocharged diesel engine by air injection into the compressor, *SAE 770122* (1977)
4. R. S. Benson, A. G. Mortimer, A. Stotter and D. E. Winterbone, Transient response of turbocharged diesel engines Part 2, application to a heavy truck, a study of the dynamic performance of the engine, *SAE 770122* (1977)
5. D. E. Winterbone, R. S. Benson and P. Kenyon, Transient response of turbocharged diesel engines, Part 1, a comparison of two methods of improving response, *SAE 770123* (1977)
6. J. R. Grundy, L. R. Kiley and E. A. Brerick, AVCR 1360 – 2, high specific output variable compression ratio diesel engine, *SAE 760051* (1976)
7. R. Schulmeister, Untersuchungen zur Vebesserung der Lastannahme aufgeladener Dieselmotoren, *MTZ*, **41**, No. 5 (1980)

8. S. G. Timoney, High pressure turbocharging of 2-stroke engines, *SAE 690747* (1969)
9. J. Summerauer, F. Spinnler, A. Mayer and A. Hafner, A comparative study of the acceleration performance of a truck diesel engine with exhaust gas turbocharger and with pressure wave supercharger Comprex. Paper C70/78, Turbocharging and Turbochargers Conference, Inst. Mech. Engrs (London, 1978)
10. J. C. Hauser, Versuche und Rechnungen zum transienten Verhalten aufgeladener Fahrzeugmotoren, Paper 80.4.2.6, 18th FISITA Congress, Hamburg (1980).

13

Turbocharging the Petrol Engine

13.1 Introduction

Turbochargers have commonly been used on diesel engines for many years. In contrast, few turbocharged petrol engines have been built until recently and it is unlikely that a large fraction of the world's petrol engines will be so equipped. It is the difference in the combustion system between diesel and petrol engines that prevents the full potential of turbocharging from being obtained on the latter.

13.2 Petrol Engine Combustion and Knock

The method of fuel preparation in a petrol engine is fundamentally different from that of a diesel engine. Air alone is drawn into the cylinders of a diesel engine, it is then compressed and fuel is injected only at the moment when combustion is required. The air and fuel are mixed and self-ignition occurs, since the compressed air temperature is high. Fuel and air are pre-mixed before the air enters the cylinders of a petrol engine. Whether a carburettor or manifold petrol injection system is used, the cylinder compresses a homogeneous air and fuel mixture, the proportion of fuel being carefully controlled. The exceptions are some 'stratified charge' engines, which are closer to diesel engines in concept and will be mentioned later. The homogeneous mixture is ignited by the spark plug. Unlike a diesel engine, the rate at which combustion proceeds is not governed by the air/fuel mixing process but by heat and mass transfer from an area that is burning to an area that is not, and the temperature increase due to continued compression. Thus a flame advances across the combustion chamber, from the spark plug, until all the fuel is burnt.

Self-ignition is avoided by keeping the compression ratio low enough to hold the temperature of the mixture below the self-ignition point of the fuel, and by using a fuel having a high self-ignition temperature. Consider what would happen if the compression ratio were very high and self-ignition occurred before the plug sparked. Since the air and fuel exist in a uniform mixture it can be assumed that all of the fuel will self-ignite at almost the same moment. Combustion would certainly be rapid enough to be termed an explosion, and it is unlikely that the

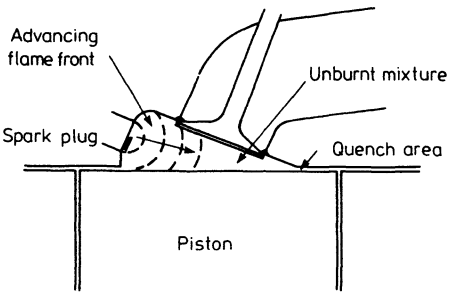

Figure 13.1 *Flame propagation in a spark-ignition engine*

engine would survive the experience without damage. Combustion must be fast, since little time is available, but not instantaneous.

Figure 13.1 illustrates the flame front propagating from the spark plug through the combustion chamber. The rate at which it progresses is governed by local turbulence, heat transfer between the burning and unburnt region, compression heating of the unburnt gas due to the piston motion and expansion of the burning mixture, air/fuel ratio and heat transfer to the surrounding walls (which will slow down the combustion process). Since the unburnt gas that is remote from the advancing flame front (often called the 'end gas') is heated by compression and, to some extent, by radiation, etc., this gas can reach its self-ignition temperature before the flame front arrives. A large volume of this gas might reach this condition, in which case explosive burning of the end gas would occur. This extremely rapid combustion generates a high rate of pressure rise in the cylinder, the impulsive force causing the bearings to 'knock', hence the general adoption of this name for the phenomenon (otherwise called 'detonation').

Rapid knocking combustion generates intense pressure wave action in the combustion chamber and very high local heat transfer rates to the piston and cylinder head walls. Since knock is most likely to occur at the furthest point from the spark plug, it is in these areas that local piston damage usually occurs. Several methods are used to reduce the likelihood of knock occurring in an engine. Firstly, the compression ratio must be kept low enough to hold the compression temperature rise to an acceptable limit. Secondly, fuels having a high self-ignition temperature are specified. The self-ignition temperature is dependent on many factors, the principal ones being fuel properties, air/fuel ratio and pressure. Generally the 'knock resistance' of a fuel is measured in terms of the octane scale, the higher octane fuels having a higher self-ignition temperature. High-octane fuels are produced by appropriate processing and selection following distillation of the basic crude oil and by the inclusion of certain aditives, such as tetraethyl lead. A third method of reducing the likelihood of knock occurring is to try to hold down the maximum distance of the spark plug from the extremity of the combustion chamber. Finally, the end gas may be kept relatively cool by arranging a high wall surface area to gas volume ratio at the combustion chamber extremities. Heat transfer to the walls tends to 'quench' the gas, hence the name 'quench area' (figure 13.1).

Recent pressure to reduce the emission of lead and hydrocarbons from the engine (a considerable fraction of hydrocarbon emission comes from the quench areas) means that it is becoming more difficult to ensure knock-free running, unless the compression ratio of the engine is low. The important point is that any measures that might increase the temperature of the mixture towards the end of the compression stroke are undesirable. Unfortunately, turbocharging does just this. By raising inlet manifold pressure and temperature, the pressure and temperature of the mixture in the cylinder will be raised throughout the compression stroke. Since the manufacturer will originally have allowed a certain margin clear of knock, it may be possible to supercharge the engine very mildly without inducing knock, but the safe margin will be reduced. Otherwise, measures such as low compression ratio, retarded ignition timing or charge air cooling, must be used to offset the effect of the temperature rise in the compressor.

13.3 Compression Ratio and Boost Pressure

Many turbocharged petrol engines have a low compression ratio in order to avoid combustion knock. Figure 13.2 shows the relationship between the geometric compression ratio of the engine and the over-all effective compression ratio at increasing boost pressure. Thus, for example, a compression ratio of 9:1 for a naturally aspirated engine must be reduced to 6.7:1 if a boost of 0.5 bar is to be used, with no change in other knock-controlling parameters. This compression ratio reduction does not reduce the mass of mixture trapped in the cylinder when the inlet valve closes (at least, not significantly), but it does offset the temperature rise in the turbocharger compressor. Thus by reducing compression ratio, a safe knock-free margin can be obtained. In addition, by reducing peak combustion chamber pressure, the increased mechanical loading on the engine will be controlled.

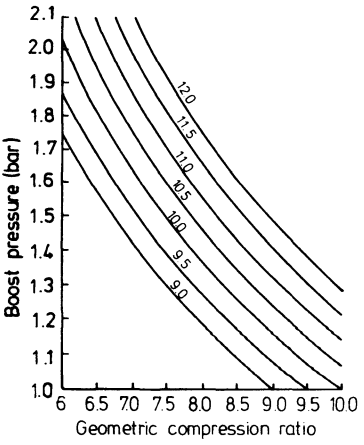

Figure 13.2 *Relationship between boost pressure, geometric compression ratio, and effective compression ratio (effective ratio shown by curved lines) [1]*

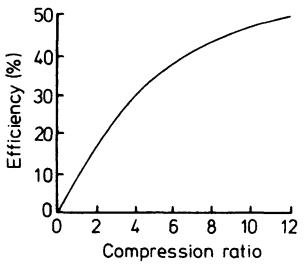

Figure 13.3 *Ideal Otto cycle efficiency with a stoichiometric mixture*

The basic efficiency (and hence power output for a specified fuel input) of the thermodynamic cycle on which the engine operates is largely governed by the compression ratio (or rather the expansion ratio). Thus by reducing the compression ratio to avoid knock, the efficiency of the basic thermodynamic process is reduced. As a result it is probable, but not certain, that the over-all efficiency of the engine will suffer. The fall-off in efficiency with low compression ratios is by no means linear. Figure 13.3 shows the efficiency of the simple fuel/air Otto cycle plotted against compression ratio. Although by no means wholly realistic, it illustrates that a 25 per cent reduction in compression ratio (from 10:1), reduces the efficiency by only 10 per cent. In addition to the losses occurring in the basic thermodynamic processes, friction in all the bearings and other mechanical debits will reduce the power output transmitted to the flywheel. Since the reduced compression ratio partly offsets the increase in cylinder pressure due to turbocharging, the mechanical loads (and hence frictional losses) may not change significantly with turbocharging. Thus the absolute power loss due to friction will remain steady. Consider the simplified example of an engine with a 10:1 compression ratio producing a power output of 100 kW with 46 per cent 'cycle' efficiency and a 70 per cent 'mechanical' efficiency. The potential power is 312 kW of which 143 kW arrive at the pistons and 43 kW is then lost due to mechanical inefficiences (312 x 0.46 = 143, 143 x 0.7 = 100). If the engine is turbocharged such that 1.5 times as much mixture is trapped in the cylinder, and the compression ratio is reduced to 7.5 (cycle efficiency 42 per cent, figure 13.3). The potential power is 468 hp and the power delivered by the pistons is 196 kW (312 x 1.5 = 468, 468 x 0.42 = 196). If the mechanical losses remain unaltered at 43 kW, the power output at the flywheel is 153 kW (196 - 43 = 153), and the over-all efficiency is 32.7 per cent (153/468) compared to 32.1 per cent (100/312) of the normal engine. Thus power output has increased substantially with a small gain in efficiency. Of course, this is not a very realistic example, since actual engine efficiences are lower, but it does show that turbocharging can improve the efficiency; however, it may not in some cases.

For a particular target power output an appropriate boost pressure will be chosen, having estimated any power loss due to a low compression ratio. The compression ratio actually used can only be determined experimentally, allowing a suitable knock-free margin. Alternatively, the compression ratio may be lowered and the boost pressure tailored to produce the knock-free margin required. Usually the latter technique will be used in first prototype development,

and the former for pre-production development. Unfortunately, no general rules on the choice of compression ratio can be given since it greatly depends on the individual engine size, detailed design, carburation, turbocharger boost control system and the nature of available fuels. Usually, a compression ratio some 2 ratios lower than normal would be used for a moderate boost pressure (0.5 bar), if no other technique were used to prevent knock.

Most important is the fact that whatever modifications are made to the engine, the charge temperature should be kept as low as possible so that the compression ratio can be maintained as high as possible commensurate with freedom from knock. This consideration is affected by several factors, the most important being the boost control system, carburation and whether an aftercooler is used.

Figure 13.4 shows the trade-off between boost pressure, charge air temperature, air/fuel ratio and fuel octane number at the knock limit, with a fixed compression ratio and optimum (that is, knock-limited) ignition timing. As expected, octane number has a strong influence on the permissible boost pressure, and so does charge air cooling. In addition richer fuel/air ratios permit a higher boost pressure.

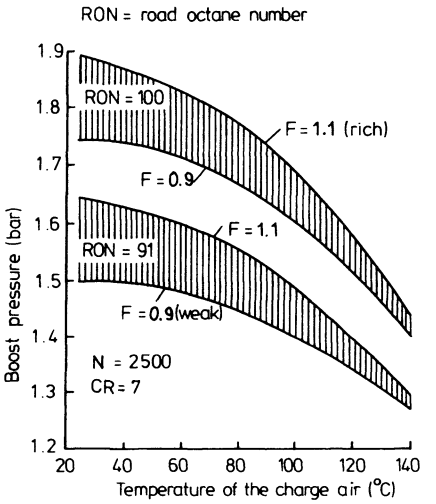

Figure 13.4 *Influence of charge temperature on charge pressure (knock-limited) with different air/fuel ratios and fuel qualities [2]*

13.4 Ignition Timing and Knock

A technique for reducing the tendency of the engine to knock that is an alternative or complementary to reduced compression ratio, is retarded ignition timing. Retarding combustion reduces the temperature of the end gas by delaying its heating relative to the TDC piston position. Thus the cylinder volume is increasing at the critical time, reducing the compression and temperature rise that would otherwise occur. Retarding ignition reduces engine efficiency by shortening the

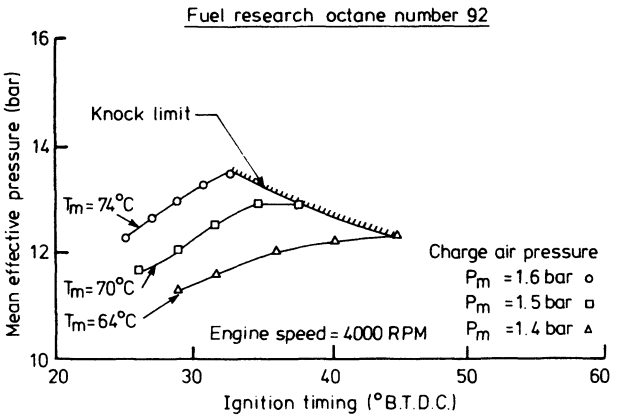

Figure 13.5 *Knock-limit dependence on spark timing, charge air temperature, and charge air pressure [3]*

effective expansion stroke. However, relative to reducing compression ratio, it is a more flexible technique, since it is relatively easy to retard ignition only when the boost pressure is high enough to induce knock.

Figure 13.5 shows the knock-limited ignition timing of a turbocharged engine at three compressor pressure ratios, with a fixed compression ratio of 6.9:1. At boost pressure ratios of 1.4, 1.5 and 1.6:1 the manifold air temperatures are 64, 70 and 74 °C respectively. The combined effects of increased pressure and temperature mean that the ignition timing must be retarded from 45 ° BTDC at a boost pressure of 1.4 bar, through 38 ° BTDC at 1.5 bar to 33 ° BTDC at a boost of 1.6 bar. Retarded timing may therefore be used to achieve a higher knock-limited boost pressure. In figure 13.5, the increase in boost from 1.4 to 1.6 bar has raised BMEP from 12.3 bar to 13.5 bar.

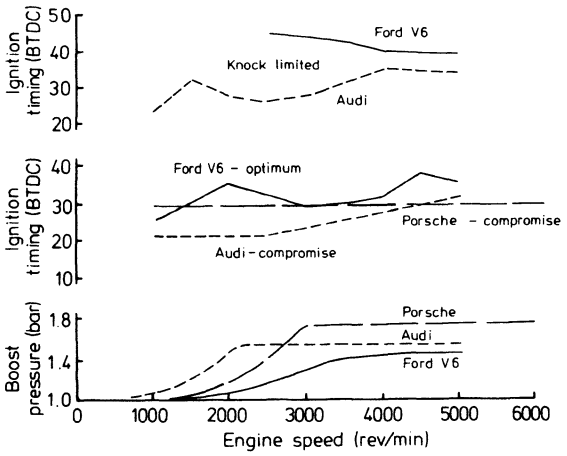

Figure 13.6 *Ignition requirements for turbocharged engines (Porsche; [4] Ford V6; [5] Audi [6])*

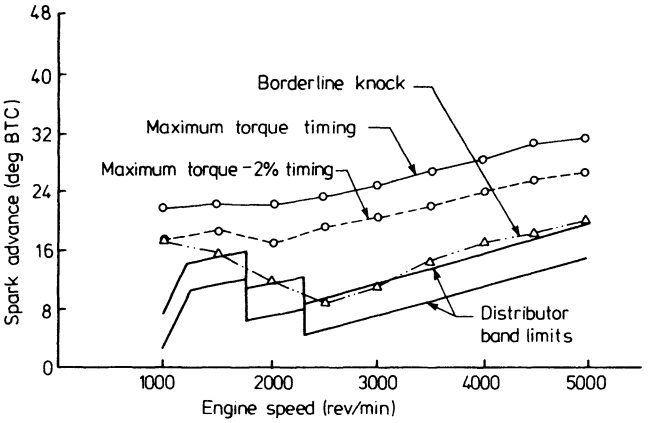

Figure 13.7 *Engine spark advance data at wide open throttle [7]*

To avoid an unnecessary fuel consumption penalty with retarded timing, the technique should only be used when the turbocharger does develop a high boost pressure. Thus at low speeds and part load, conventional timing is retained. The simplest method of achieving this requirement is a boost pressure retard system built into the normal vacuum advance diaphragm of the ignition distributor. Figure 13.6 shows knock-limited optimum and compromise ignition timings used on three very different experimental turbocharged engines. Comparing the Audi and Ford, boost pressure is developed at a lower speed on the former, requiring boost retard above 1500 rev/min for the Audi, but 2000 rev/min for the Ford.

Figures 13.7 and 13.8 show the ignition timing requirements of the Ford Mustang engine. [7] At wide open throttle (figure 13.7) the timing for maximum brake torque (MBT) minus 2 per cent coincides with borderline knock at 1000 rev/min. As speed increases, boost builds up and ignition timing must be retarded relative to the MBT requirement, to avoid knock. The Ford ignition system senses boost pressure and retards timing in two discrete steps as shown by the distributor band limit curves of figure 13.7. At reduced throttle openings

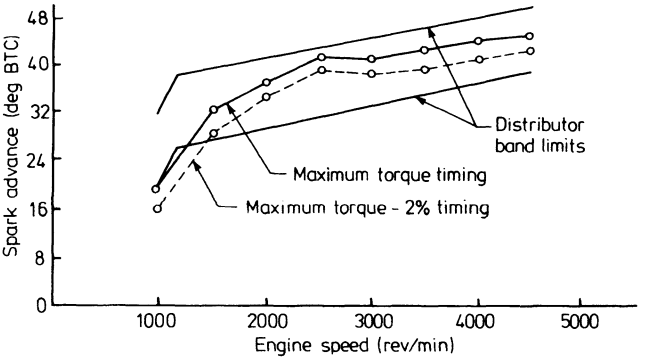

Figure 13.8 *Engine spark advance data at 30 cm Hg depression [7]*

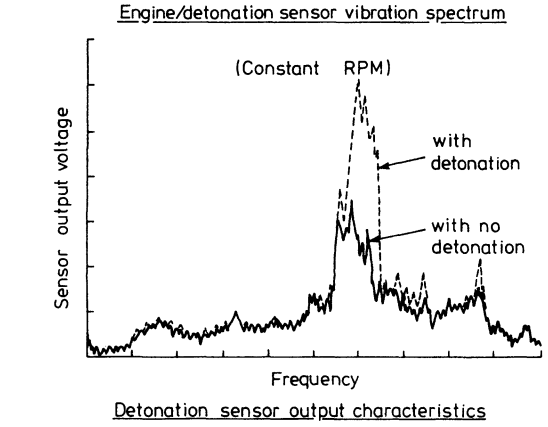

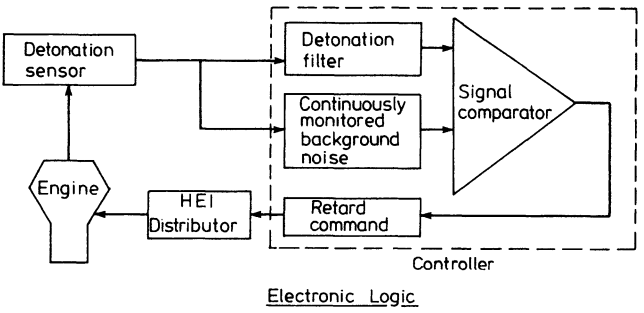

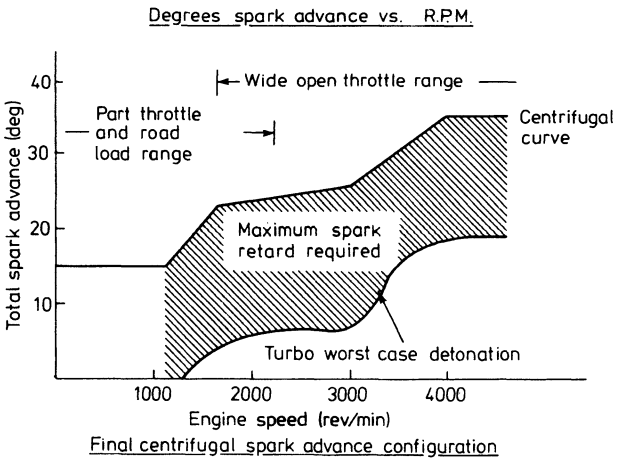

Figure 13.9 *Buick knock sensor and electronic spark control [8]*

(figure 13.8) MBT timing advance may be used free of borderline knock, since the turbocharger is providing no boost.

A more complex timing system is used on the turbocharged Buick V6 engine. [8] Since the objective of timing retard is to prevent knock, Buick have linked ignition timing to a knock-detection sensor. The sensor detects above normal vibration levels on the inlet manifold, a symptom of the rough combustion and very rapid cylinder pressure oscillations, when the end gas pre-ignites (figure 13.9). By suitable setting of the sensitivity of the system, the condition at which mild knock is beginning can be detected. An electronic controller retards ignition timing as a function of the severity of knock. Figure 13.9 also shows the centrifugal timing advance used on the Buick and the amount of retard necessary to avoid detonation under the most adverse operating conditions at each speed. In contrast to the results shown in figure 13.5, the Buick engine in turbocharged form retains the compression ratio (8:1) of the naturally aspirated engine. However, a rich fuel/air ratio is also used to help control knock at full throttle (see figure 13.4).

One undesirable feature of retarded timing is an increase in heat rejection to the exhaust system, since the complete combustion and expansion process is delayed. Thus the turbine inlet temperature rises (figure 13.10). Although the increase is small, the very high temperature of petrol engine exhaust gas (up to 1000 °C) is a problem for the turbine manufacturer and can cause oxidation of lubricating oil. Furthermore the potential power increase obtainable by turbocharging with retarded timing alone is limited. Higher boost pressures can be used if compression ratio is also reduced. A change to a cooler spark plug will usually be required to hold the tip temperature to normal limits.

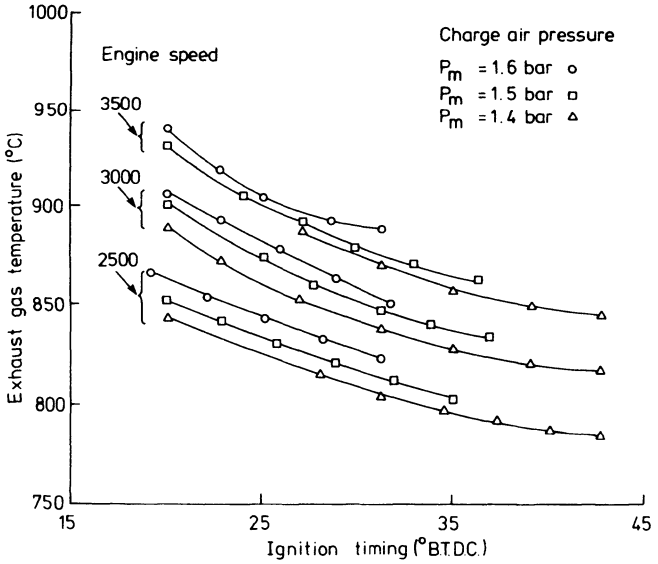

Figure 13.10 *Exhaust gas temperature dependence on spark timing and charge air pressure [3]*

13.5 Charge Air Cooling

The temperature rise in the compressor and its effect on knock can be offset by charge air cooling. Comparison of figures 13.5 and 13.11 shows that charge air cooling to an air temperature of 45 °C enables the knock-limited ignition timing to be advance by 10 °. However, the low boost pressure of the turbocharged petrol engine means that the temperature difference available between ambient air and the compressed air is small. A large air cooler is therefore required to achieve a major reduction in temperature and low-pressure loss. The benefit in terms of power output can be seen by comparing figures 13.5 and 13.11 but it is doubtful whether the extra cost, complexity and volume are warranted in passenger car applications, other than very expensive sports cars. An additional disadvantage is a deterioration in engine response due to the increase in total inlet manifold volume, and pressure loss in the cooler itself.

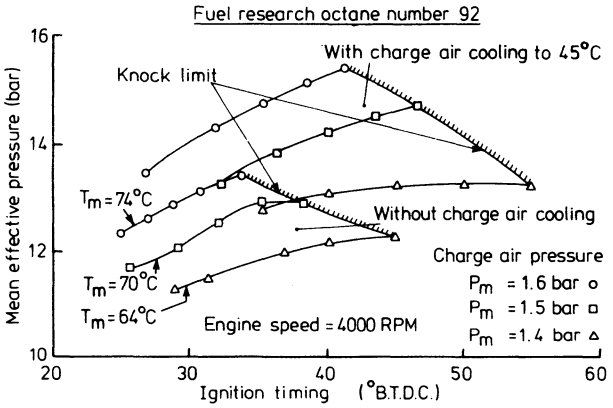

Figure 13.11 *Knock-limited dependence on spark timing and charge air pressure with charge cooling [3]*

13.6 Carburation and Fuel Injection

In principal, four options are open to manufactures of turbocharged petrol engines when considering the fuel system. Firstly, either a carburettor or fuel-injection system may be used. Secondly, the air and fuel may be mixed either before or after compression. The large majority of petrol engines are fitted with carburettors, since these are considerably simpler and cheaper than fuel injection systems. It follows that most manufacturers will want to retain carburettors on a turbocharged engine. Fuel-injection systems are generally fitted to more expensive high-performance engines, but their adoption on a turbocharged engine can overcome some particular difficulties associated with carburetted turbocharged petrol engines.

Whether a carburettor or fuel-injector is used, the objective is to measure the air flow rate through the engine and meter the correct amount of fuel, then evaporate it, and thoroughly mix it so that a homogeneous mixture of the correct

proportions is drawn into the cylinder at all times. The simplest flow measuring system is the venturi, in which air is drawn through a flow restriction, accelerates and drops in pressure. If incompressible flow is assumed, then

$$P_1 - P_2 = \tfrac{1}{2}\rho\,(C_2^2 - C_1^2) \tag{13.1}$$

where $P_1 - P_2$ = pressure drop from inlet to throat
C_1, C_2 = gas velocities at inlet and throat
ρ = air density.
Since the mass flow rate is given by

$$\dot{m} = \rho AC = \rho A_1 C_1 = \rho A_2 C_2 \tag{13.2}$$

then

$$P_1 - P_2 = \Delta P = \tfrac{1}{2}\frac{\dot{m}^2}{\rho}\left(\frac{1}{A_2^2} - \frac{1}{A_1^2}\right) \tag{13.3}$$

Thus the pressure drop is a measure of the mass flow rate, and is used to control the fuel flow rate. Unfortunately, even if the pressure drop through the venturi is small enough for the assumption of incompressible flow to be reasonable, the relationship between pressure drop and air mass flow rate does depend on the inlet density. Thus carburettors based on the simple venturi system tend to depart from their correct air/fuel metering performance when the inlet air density changes. This is already a significant problem due to under-bonnet temperature changes on naturally aspirated engines, but can become more serious on turbocharged engines. In particular, if the carburettor is placed after the compressor, large inlet density changes occur. The greater the density change, the more difficult it will be for the carburettor to work correctly. If a normal type of carburettor is used it must be accepted that it will not provide ideal fuel metering over the full range of engine performance. While the effect might be slight on a mildly turbocharged petrol engine, this type of installation will become less satisfactory on engines with higher boost pressures.

Inlet manifold fuel injection systems do not usually use venturi flow measurement, although the alternative methods adopted vary widely. However, they do have the advantage that flow measurement need not take place at the same position as fuel injection. Thus air flow can be measured before the compressor, even if the fuel is injected after the compressor. It follows that it is simpler to adapt the systems to cope with a wider range of inlet manifold pressures, from vacuum at idling to boost at full speed and power. Higher fuel pressures may be required, however.

Due to the lack of proper density compensation, the use of a carburettor placed after the compressor becomes less attractive the higher the boost pressure. However, the system has many other attractions. The principal advantage occurs when a manufacturer wishes to offer a turbocharged (higher power) option, based on an engine that is normally manufactured in naturally aspirated form, but at a relatively low additional cost. Naturally if the standard inlet manifold and carburettor can be retained, a significant cost saving is achieved. Since the engine is based, with the minimum number of modifications, on a naturally aspirated engine, it is unlikely that a high boost pressure will be used and the carburettor can be jetted

to cope, although it may not provide the ideal air/fuel ratio over the whole speed-load range. The fuel float chamber must be maintained at the compressor boost pressure so that the pressure head across the fuel jet is maintained. Generally, some sort of damping or plenum chamber will be required to eliminate swirl in the air leaving the compressor and to obtain a 'static' (see chapter 2) pressure at the carburettor inlet. It is this static pressure that must be fed to the float chamber. One method of achieving this is to enclose the complete carburettor in a large plenum chamber, although the control cables, etc. (throttle, choke, fuel line) must be sealed as they pass through the chamber walls. Regardless of the exact position of the plenum chamber, it must be designed to eliminate, not encourage swirling air flow, otherwise the distribution of fuel/air mixture may vary from one cylinder to another. More refined methods are usually used.

Since the carburettor is pressurised it follows that a high-pressure fuel pump will be required to deliver sufficient fuel to the carburettor. However, when the engine idles, the boost pressure will be zero and the fuel needle valve in the float chamber may not be able to oppose the high fuel pressure. Thus the fuel pressure must be regulated such that it maintains a value around 20 to 30 kN/m^2 above the boost pressure, whatever the boost pressure may be. A simple three-way (recirculating) regulating valve may be used, in which the high inlet pressure is modulated by returning excess fuel to the tank.

In addition to the problem of poor air/fuel metering, the 'pressurized' carburettor does have other disadvantages. Two have already been mentioned, namely a requirement for a complex fuel system and the need for seals where cables pass through the plenum chamber to the carburettor, or on the throttle spindles if the carburettor is separated from the plenum chamber. Turbocharged petrol engines often suffer from high engine compartment temperatures due to large, very hot exhaust surfaces. If a pressurised carburettor is used, an additional amount of heat comes from the compression temperature rise, particularly if the carburettor is placed in the plenum. The float chamber can become excessively warm resulting in fuel boiling, particularly when idling after high-speed runs. Every effort must be made to keep the under-bonnet temperature down by good ventilation and heat shielding. Uneven fuel and air distribution problems usually can be overcome by suitable design of the plenum, possibly by the insertion of baffles inside it, and although often a problem in the early development stages, it should not be difficult to overcome. Finally, referring back to the problem of knock, the use of a carburettor placed after the compressor will result in a higher mixture temperature during the intake process and hence a slightly lower knock-limited boost pressure than would result if the carburettor were placed before the compressor. This is due to the effect of fuel evaporation (latent heat). Consider the two alternative systems shown in figure 13.12. Neglecting the pressure drop through the carburettor, the following relationships may be established

$$T_{2a} = T_1 \left(1 + \frac{(P_2/P_1)^{(\gamma-1)/\gamma} - 1}{\eta_c}\right) \tag{13.4}$$

which may be expressed as

$$T_{2a} = T_1 (1 + K)$$

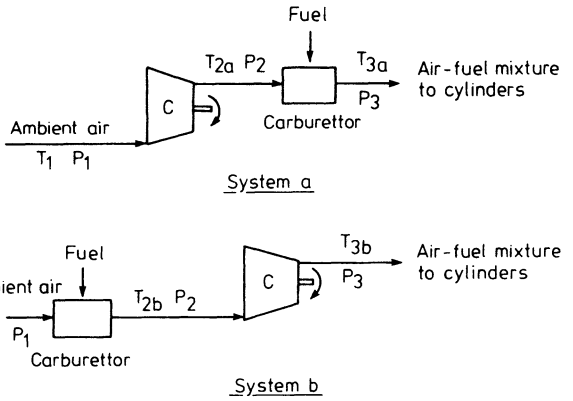

Figure 13.12 *Temperature rise with pressurised and non-pressurised carburettors*

If the enthalpy of evaporation of the fuel results in a temperature drop of ΔT_{carb} in the carburettor, then

$$T_{3a} = T_1 (1 + K) - \Delta T_{carb} \tag{13.5}$$

If the same mass flow rates of air and fuel occur in system b, and the compressor pressure ratio remains unchanged, that is

$$\left(\frac{P_3}{P_2}\right)_b = \left(\frac{P_2}{P_1}\right)_a$$

then

$$T_{3b} = T_{2b} \left(1 + \frac{(P_3/P_2)^{(\gamma-1)/\gamma} - 1}{\eta_c}\right) \tag{13.6}$$

or $T_{3b} = T_{2b} (1 + K)$ hence $T_{3b} = (T_1 - \Delta T_{carb}) (1 + K)$, or

$$T_{3b} = T_1 (1 + K) - \Delta T_{carb} (1 + K) \tag{13.7}$$

Comparing equations 13.5 and 13.7 it is clear that

$$T_{3b} < T_{3a}$$

hence a higher boost pressure or compression ratio (knock limited) may be used with system b.

By placing the carburettor before the compressor, it will work under ambient pressure so that a normal type of fuel system may be used and the carburettor, when properly jetted, will operate normally over the whole speed and load range. Full advantage can be taken of the enthalpy of evaporation (latent heat), although this can result in poor cold starting of the engine and poor mixture distribution. A water-heated jacket may be required, negating the evaporation benefit, or fuel arriving at the compressor will be in the liquid phase, and will tend to collect in the lowest part of the volute, resulting in a momentary weak mixture at the cylinders. Some turbochargers can be supplied with a water jacket formed in the

compressor cover. [9] However, water heating should be avoided if possible. In addition, fuel droplets may cause erosion damage at the leading edge of the compressor blade by impingement. More important is the fact that placing the carburettor before the compressor substantially increases the fuel-wetted surface of the inlet manifold. This can significantly weaken the fuel/air ratio of the mixture entering the cylinders during warm-up from a cold start, when a water jacket is ineffective. Emmenthal *et al.* [10] recommend an electrically heated grid after the carburettor to improve driveability and reduce emissions following a cold start. The compressor volute itself may require additional sealing where it joins the turbocharger body, to avoid fuel leakage. Many carburettors incorporate correction jetting to counteract low-speed enrichment under heavily pulsating air flow, but the compressor and inlet duct may damp these down to some extent, hence modified jet balance may be required. In addition, a rather small choke diameter is sometimes used to provide maximum power enrichment by creating a larger than normal pressure drop through the carburettor.

Lubricating oil leakage from the turbocharger into the inlet manifold will inevitably result if reliance is placed solely on the normal type of piston ring seal found on diesel engine turbochargers. This results from the large vacuum formed in the compressor when the throttle of the carburettor is closed (the problem will not exist if the carburettor is placed between compressor and engine). The vacuum draws oil mist from the turbocharger body past the piston ring seals and into the compressor tip. Although attempts are sometimes made to vent the area behind the piston ring 'seal', this alters the effective idling mixture strength in the manifold since a significant amount of air can be drawn in. The most effective alternative is to use a mechanical face seal, designed for very high-speed operation. A small stationary carbon ring is lightly loaded against a rotating, very finely ground, thrust face, forming an oil-tight seal. Most manufacturers of small turbochargers offer this facility, but it does increase turbocharger cost.

A problem that can result from the throttle being placed after the compressor,

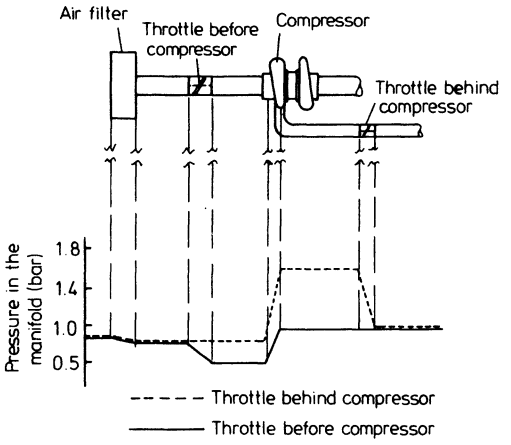

Figure 13.13 *Pressure in the intake system of a turbocharged petrol engine with the intake throttle before or behind the compressor [2]*

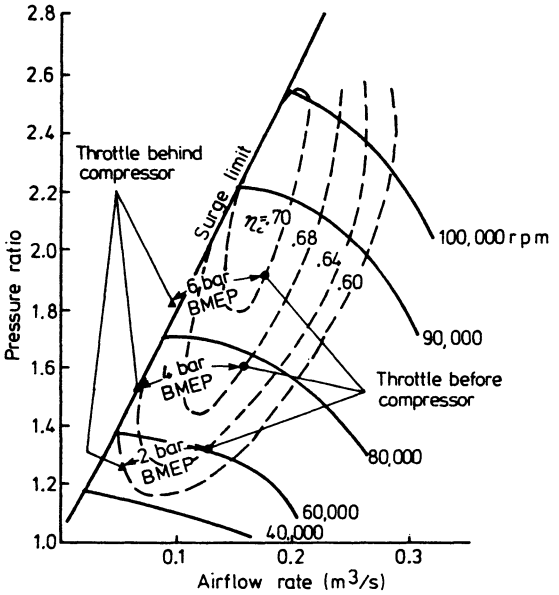

Figure 13.14 *Air flow at different loads, throttling before or behind the compressor [2]*

is surge when the throttle is closed. If the throttle is placed before the compressor, the air entering the compressor is of low density (low pressure, figure 13.13). For the same engine performance at part load, the air mass flow through the engine must be similar, whether the throttle is before or after the compressor. Thus placing the throttle before the compressor increases the volumetric air flow rate through the compressor. Figure 13.14 shows engine air flow characteristics at part load, superimposed on the compressor map, with both throttle positions, illustrating the higher volumetric flow with the throttle preceding the compressor. In the alternative position, volumetric flow will be low, leading to compressor surge as the throttle is closed. This is due to the turbocharger inertia momentarily maintaining high rotational speed and very high pressure ratio, but flow reducing instantaneously when the intake throttle closes. This can be avoided by leaving a large surge margin or by placing an auxiliary throttle before the compressor.

If fuel and air are metered and mixed before the compressor, then it is important to keep the manifold between compressor and the inlet ports short and its surface area and volume small. In particular any expansion into a large chamber will result in fuel vapour condensing and dropping out of the air stream. This and large fuel-wetted surfaces, can result in poor mixture distribution, since the liquid fuel will predominantly run into the nearest and lowest inlet ports, particularly during acceleration. However, a narrow short pipe will tend to maintain the swirling flow leaving the compressor, and this in itself can result in unfavourable mixture distribution. It requires careful design to break up this swirl without causing droplet condensation.

Generally it may be stated that positioning the carburettor before the compressor is the potentially better system since the air/fuel ratio can be controlled

more closely. However, unless the system is well engineered in all respects, it will not prove superior to the pressurised carburettor, particularly if the maximum boost pressure is low.

13.7 Inlet and Exhaust Manifolds

The design of the inlet system may be substantially different from that used on a naturally aspirated engine, particularly if the carburettor is placed before the compressor. The primary objectives will be to minimise the volume between carburettor and cylinder head (to improve response), encourage good fuel droplet break-up and mixing, avoid fuel condensation, encourage even mixture distribution between cylinders, eliminate swirling air movement and keep the temperature of the mixture down. These objectives are sometimes achieved by accepting a pressure loss that would not be tolerated on a naturally aspirated engine. The reason is due to the almost embarrassingly large amount of energy available in the exhaust system at full speed, enabling boost pressures far above the knock-limited value to be generated. Some flow loss, at full throttle and speed, reduces boost pressure, the loss being low when the boost pressure, and hence mass flow rate, are also small. A perforated plate can be used at the entry to the inlet manifold to reduce swirl and aid mixture distribution, but this method is not to be encouraged since restrictors reduce pressure, but not temperature.

Although the potential boost available from the turbocharger is excessive at full engine speed and throttle, the opposite is so at low speeds (a full discussion of the problem is given later). Thus the exhaust manifold must be designed to ensure the maximum utilisation of exhaust gas energy at relatively low engine speeds. Thus the pulse turbocharging system should be adopted, with short, narrow exhaust pipes and, if possible, no more than three cylinders connected to each turbine entry. Long pipes have been used to allow some cooling of the exhaust gas before it reaches the turbine, but pressure wave action can cause problems, the energy available for expansion through the turbine is reduced at low speeds, engine compartment temperatures increase and turbocharger response suffers. Generally provided that the pipe bore does not fall below the maximum valve area at full lift, the narrower and shorter the pipes, the better low-speed performance will be. Usually a large-bore exhaust pipe will be used from the turbine exhaust onwards, together with a low-loss silencer. A small-bore system will create a flow restriction and back-pressure at the turbine exit. Although this need not be a problem, because the turbocharger can be matched accordingly, it can be dangerous if the exhaust system subsequently develops a major leak. The back-pressure will reduce and turbocharger work will increase, possibly resulting in excessive boost pressure, combustion knock and engine damage. Unless a deliberate restriction is inserted at the turbine exhaust for matching purposes, it is preferable to use a low-loss exhaust system, but this may be impossible with a catalytic converter.

Both single or twin-entry turbochargers can be used on four-cylinder engines although the latter, with a divided exhaust manifold, will produce better low-speed torque. Six-cylinder engines are easily matched by a divided manifold and twin-entry turbine housing, while V8 engines can be fitted with a single twin-entry

turbocharger (four cylinders to each entry), or two smaller twin-entry turbochargers with the manifolds separated into pairs. In practice, it is difficult to combine a twin-entry turbine with a waste-gate boost control system (see section 13.8). In addition, thermal stresses are very severe in a divided housing, hence most turbocharged petrol engines use single-entry turbines.

Total inlet and exhaust manifold volume will be governed by the configuration of the engine. Thus a six-cylinder in-line engine can have a very compact system, unlike a V8 with exhaust pipes on the outside of each bank of cylinders. However, low volume systems can be designed for vee engines with suitable positioning of the turbocharger and exhaust pipes.

A particularly critical aspect of inlet and exhaust manifolds on turbocharged petrol engines is the choice of gaskets. The inlet system must withstand higher pressure than normal, while the exhaust system must accept not only higher pressures, but higher temperature and loading due to the weight of the turbocharger. It is not usually desirable to allow the full weight of the turbocharger to be carried by the exhaust manifold but any supporting brackets must be designed so that they do not oppose thermal expansion of the system. At full power, the exhaust temperature can reach 900 °C, hence thermal stresses in the manifold will fracture a poorly designed component. Expansion joints may be required. Efforts should be made to duct cooling air around the exhaust manifold and turbine and to allow this air to leave the engine bay readily so that engine compartment temperature is low.

13.8 Turbocharger Boost Pressure Control System

To understand the need for boost pressure control systems on turbocharged petrol engines, it is useful to draw some parallels with diesel engine turbocharging, since this has been discussed at length. Firstly, the petrol engine works over a wider speed range, typically up to 5000 rev/min. Secondly, the air/fuel mixture must be kept relatively close to the stoichiometric value rather than varying over a very wide (and much weaker) range. Thirdly, the boost pressure must be limited to avoid knock. The problems involved in matching the turbocharger over the normal speed range of an automotive diesel engine have already been discussed, but they become more severe over the wider speed range of the petrol engine. Since the air/fuel ratio is much richer than that used, even at full load, on diesel engines, the exhaust temperature is higher. Thus, for the same mass flow rate, the energy available in the exhaust gas at turbine entry is greater, yet the permissible boost pressure is lower. There is an excess of energy in the exhaust system (at full power) and the boost pressure must be limited. In addition the effect of the very large air flow range from low to high speeds, amplifies the problem of insufficient boost at low speed that was discussed in relation to the diesel engine (section 10.7.1). Efforts must be made to limit boost at high speed, but raise it at low speed.

13.8.1 Matching the Turbocharger for the Desired Maximum Boost Pressure

The simplest method of achieving a specified boost pressure at maximum speed

and load is to match the turbocharger accordingly. The boost pressure can be limited by fitting a large turbine, but this technique has major disadvantages and is not recommended. The turbine area will be governed by the mass flow through it at full power. Since the petrol engine operates over a very wide speed range, the mass flow will be very much less at low speeds. Under these conditions the turbine area will be relatively large and hence the energy available for expansion will be correspondingly small (figure 10.23) resulting in little or no boost pressure being developed. Aggravating the situation will be low turbocharger efficiency due to operation far from the design point conditions of the compressor. The over-all result will be a boost pressure and engine torque curve rising rapidly at high speed, with low boost at low speed. Such a curve, with no torque back-up, is totally unacceptable for the automotive application since continual gear changing will be required.

It may be possible to develop some torque back-up at speeds below the maximum, if the turbocharger is chosen such that it can be matched into the (low-efficiency) choking region at full engine speed. As speed is reduced the working point will move through an area of higher turbocharger efficiency and this may compensate for a reduction in energy available at the turbine, particularly if the exhaust manifold has been designed for a maximum pulse utilisation at lower speeds. However, it is very unlikely that torque back-up can be maintained right down to normal running speeds, without over-speeding the turbine at maximum engine speed, and inefficient compression raises charge temperature, which should be avoided.

13.8.2 Pressure-relief Valve in the Intake System

If a smaller turbocharger is fitted, the combination of higher efficiency at low flow rates and increased turbine energy (due to the reduced turbine area) will result in higher boost pressures over the whole speed range. A 'blow-off' or relief valve can be fitted to the intake manifold to prevent the boost pressure rising above its knock-limited value (figure 13.15). It is sometimes claimed that use of a blow-off valve lowers engine thermal efficiency, since compressed air, for which turbine work has been done, is dumped to the atmosphere without doing useful

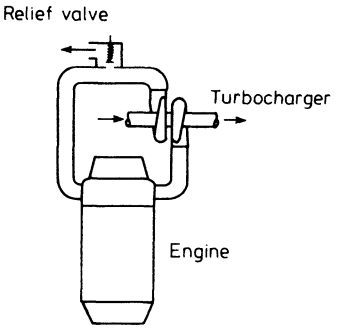

Figure 13.15 *Compressor pressure-relief valve control system*

work. However, since the turbine work is extracted from exhaust energy that would otherwise go to waste, the argument is not wholly valid. A small degradation in efficiency may result from the increased pumping work due to the higher exhaust pressure resulting from a small turbine area, as will be shown later.

If the carburettor is placed before the compressor a simple blow-off system cannot be used since an air/fuel mixture is involved. A modification is to recirculate the blown-off mixture back into the compressor eye (after the carburettor, so that the air/fuel mixture is not disturbed). The disadvantage of this system is that hot mixture (due to compression) is being recirculated, resulting in a higher mixture temperature at the cylinders and hence the knock-limited boost pressure will be lower. Thus the blow-off valve system is best suited to the pressurised carburettor or fuel-injection systems. Although the blow-off air is warm, it is possible to direct it over the exhaust manifold and turbine to cool these components, when they are hottest (at full power). The minimum turbocharger size is limited by its maximum speed at full power, as will become clear when the systems are compared.

13.8.3 Exhaust Waste Gate Systems

The exhaust waste gate has already been mentioned with reference to the turbocharged diesel engines (section 10.7.2). It consists of a valve allowing exhaust gas to by-pass the turbine. Clearly, since the exhaust gas energy of the turbocharged petrol engine is excessive at full speed and load, this is an excellent method of controlling boost pressure. Figure 13.16 illustrates the principle, in which the boost pressure acts on a diaphragm, opening the waste gate when the boost pressure reaches a pre-determined limit. The system has several advantages over the direct-relief valve system described above. The major benefit results from the fact that since not all the exhaust gas passes through the turbine, and no more than the air requirement of the engine passes through the compressor, then a smaller turbocharger (particularly the turbine) can be used. The small turbocharger is best able to provide sufficient boost at low speed (when the waste gate is closed), and reduces turbocharger lag due to its low inertia, especially if the waste gate is closed during acceleration. With careful design of the waste gate valve, the boost curve can be tailored to produce an optimum torque curve within the constraints of

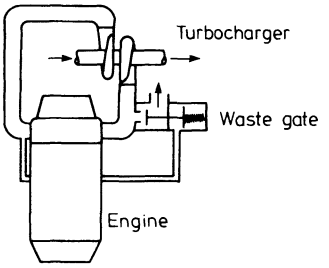

Figure 13.16 *Boost pressure-sensitive waste gate control system*

knock limits. Saab have proposed using a combustion knock sensor to open the waste gate, rather than boost pressure.

The major problem associated with waste gate systems is their cost and potential unreliability, due to the very high temperature and corrosive environment in which they must operate. It is a dificult design problem to satisfy both of these constraints, but suitable turbochargers with built-in waste gate systems are available.

13.8.4 Variable Geometry Turbines

By altering the angle of the turbine inlet nozzles (when fitted) both the effective area of the turbine (and hence energy availability) and the efficiency characteristic alter. By opening the nozzles at full engine speed and closing them at low speed, exhaust gas energy utilisation can be adjusted to suit low and medium-speed performance while preventing the turbocharger from over-speeding. The difficulty is one of engineering a cheap and reliable variable geometry turbine together with the associated control system. It is questionable whether a commercially acceptable system will ever be in widespread use, although the potential benefits are high.

13.8.5 Exhaust Restrictors

All the above systems rely on moving parts and therefore are potentially unreliable (particularly those in the exhaust system). A turbine exhaust restrictor is a fixed nozzle, placed after the turbine in its exhaust system. As the mass flow rate through the engine increases at high speed, so the pressure drop across the restrictor increases, raising the back-pressure on the turbine and reducing its effective expansion ratio. Thus turbocharger work is modulated by a rising back-pressure. Since the pressure drop increases approximately with the mass flow rate squared, the modulation becomes progressively more effective at higher engine speeds and loads. Flow losses at low speeds will be lower. The result is an acceptable boost pressure (and hence engine torque) curve. It is simple and reliable and permits a small turbine to be used, but it has serious disadvantages. The high exhaust manifold pressure and temperature generated aggravate gasket leakage problems, and increase the pumping work of the engine during the exhaust process. Furthermore the whole exhaust system becomes rather hotter than it would if an unrestricted exhaust were used. An additional disadvantage of a fixed restrictor system is that it is affected by atmospheric pressure variations.

13.8.6 Inlet Restrictors

The basic characteristics of a restrictor can be used in the inlet system as well as the exhaust. They can be placed either before or after the compressor. They allow the compressor to generate a high pressure ratio but prevent the engine from feeling the normal consequences. Like the exhaust restrictor, they become pro-

gressively more effective as mass flow rate increases (that is, with speed and load) and can produce quite acceptable torque curves. Their main disadvantage results from the fact that throttling (which is their function) is basically a constant enthalpy process. For a perfect gas (the air or air/fuel mixture may be assumed to behave approximately as a perfect gas), this implies a constant temperature process. Since the compressor is generating a high pressure ratio it is also generating a large temperature rise, which the restrictor is not modulating. Hence the knock-limited boost pressure is low.

13.8.7 Comparison of Systems

Comparison of engine performance when fitted with different boost control systems is difficult and can be misleading. This is due to the very large number of dependent variables acting during engine tests (turbocharger efficiency at the working point, variation in air/fuel ratio, actual characteristics of the control system used, etc.). It is impossible to keep all of these parameters constant. In order that a more informative picture is presented, a comparison based on predicted performance at a fixed air/fuel ratio and turbocharger efficiency will be given.

The predictions are based on the performance of an engine with an exhaust restrictor. [5] The performance of this engine has been predicted (within 5 per cent) by Baazaari, [11] using the methods outlined later (chapter 15). Predictions have also been made using other control systems, but assuming that the alternative systems could be tailored to produce the same boost pressure curve (in practice, they would not) as the exhaust restrictor. Figure 13.17 illustrates the basic performance that would result from use of a variable area turbine, an exhaust waste gate, a turbine outlet restrictor, a compressor relief valve, and compressor outlet and inlet restrictors for the hypothetical situation in which all systems produce

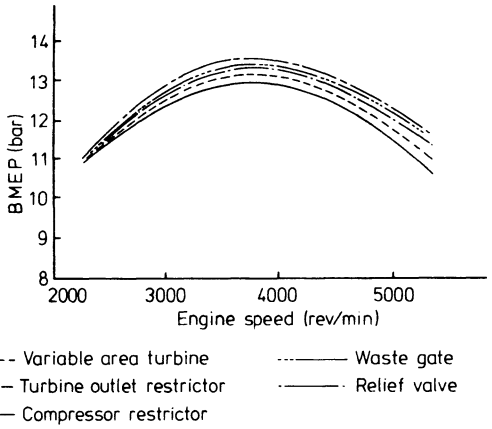

Figure 13.17 *The effect of different control systems on BMEP, when matched for the same boost pressure at all speeds [11]*

the same boost characteristics. Virtually no difference in specific fuel consumption (that is, engine efficiency) results but a span of 5 per cent in torque or BMEP occurs due to the difference in air flow rates, the variable geometry and waste gate systems being superior, the compressor restrictors worst.

The comparisons shown in figure 13.17 assume conditions that may not be achievable in practice, and ignore the fact that higher mixture temperature in the cylinders will exist in some systems relative to others. For example, the engine may well knock if compressor restrictors are used. An alternative basis of comparison assumes that the mean gas temperature in the cylinders, at the moment of ignition, remains the same as that predicted with the exhaust restrictor (at maximum speed and load). Thus all systems should be knock-free and may operate to produce their natural air flow characteristics at lower speeds. On this more realistic basis, the compression ratio of the engine will be adjusted so that the maximum mixture temperature at ignition is the same for all systems. The resultant engine performance curves are shown in figure 13.18. Note that the use of a variable area turbine allows the highest compression ratio (7.6:1) to be used, giving highest torque. A 5:1 compression ratio must be used with the compressor restrictors, resulting in a drop (relative to the variable geometry system) of 14 per cent in BMEP and a 7 per cent increase in specific fuel consumption. The other systems lie between, their order of merit being exhaust waste gate, compressor relief valve, turbine outlet restriction (these three being the most commonly used in practice) then compressor restrictors. Figure 13.19 shows the full-load engine operating line plotted with the same axes as a compressor characteristic, showing the high pressure ratio resulting from the use of compressor restrictors and the potential danger of turbocharger over-speed if a small turbocharger is used in conjunction with a compressor relief valve. A very wide flow range compressor would certainly be required with the latter system.

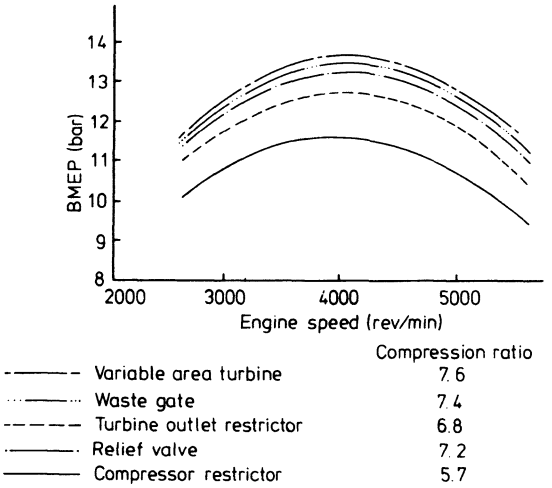

Figure 13.18 *The effect of different control systems on BMEP when matched to give the same cylinder temperature prior to ignition [11]*

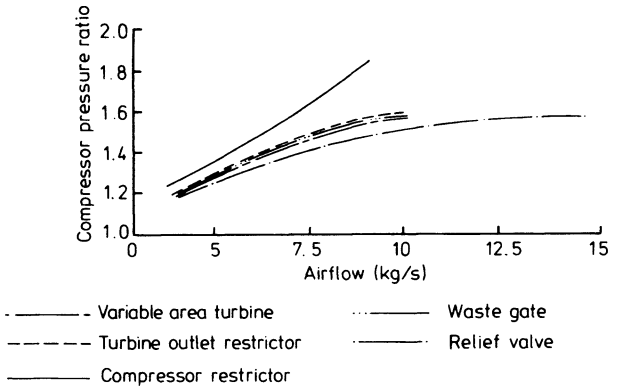

Figure 13.19 *The effect of different boost control systems on the compressor requirements [11]*

These results show that an exhaust waste gate or a variable geometry turbine are by far the most effective boost control systems.

Low-speed boost, and therefore torque, may be improved by reducing turbine area and increasing the mass flow through the waste gate at high speeds. Figure 13.20 illustrates the principle, and the benefit in low-speed torque. Also shown is the disadvantage, namely high fuel consumption, particularly at high maximum

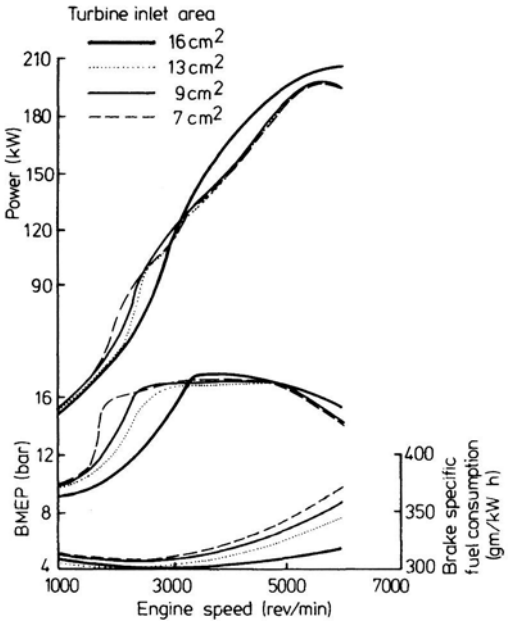

Figure 13.20 *Influence of the turbine housing inlet area on torque characteristics and power output [2]*

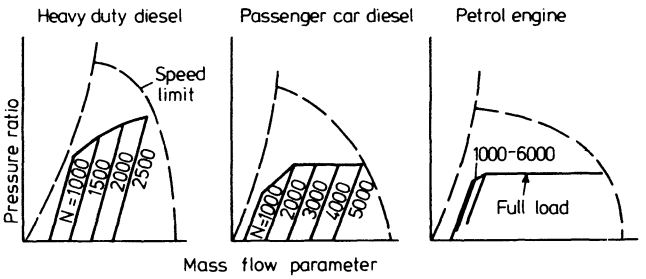

Figure 13.21 *Compressor maps of a turbocharged heavy-duty diesel engine, a diesel passenger-car engine, and a petrol engine [2]*

engine speed, due to the very high exhaust pressure developed and unfavourable piston pumping work.

At this point it should be mentioned that under normal roadgoing operating conditions, full throttle operation is not maintained long enough for the turbine inlet temperature or even turbocharger speed, to reach steady state values. Thus the turbine area used in practice can be smaller than that selected by steady dynamometer testing.

Superimposition of engine air flow lines on the compressor map is used to select the appropriate compressor as is normal for a diesel engine. However, due to four effects, the result is different, in terms of compressor requirement. These effects are

(1) low boost pressure requirement,
(2) use of an exhaust waste gate,
(3) greater operating speed range,
(4) operation at a narrow band of air/fuel ratio.

The consequences, in terms of compression requirement, are shown in figure 13.21. On the left is the typical high-pressure ratio, small-speed range, heavy-duty diesel. The passenger-car diesel (centre) has a wider speed range and therefore air flow requirement. A waste gate is used to limit cylinder pressure at high speed, hence the pressure ratio is modest. The petrol engine has a very wide speed range and a limited pressure ratio, hence a very wide mass flow range compressor is required. Unlike the diesel, part load operation is achieved by throttling the air flow. Thus as the throttle is gradually closed from full load and speed, the waste gate initially holds a constant pressure ratio and the operating point moves rapidly to the left. Thus the part throttle operating points all bunch up in the low-flow area of compressor operation. High compressor efficiency is required to keep inlet manifold temperature low over a wide flow range, to avoid knock. Figure 13.22 shows the full-load compressor match of the European Porsche 924 turbo.

13.9 Valve Timing

When sizing the turbocharger and waste gate system, a compromise must be accepted between the need for a small turbine to achieve boost at low engine speeds

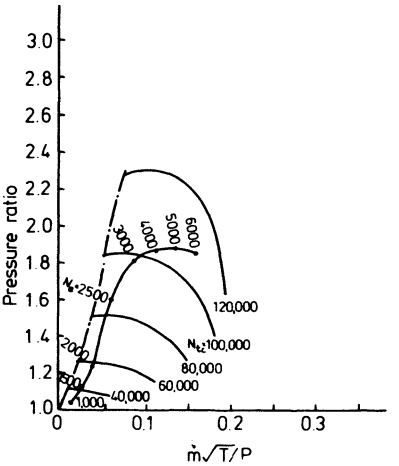

Figure 13.22 *Full-load air requirement of Porsche 924 [12]*

and the ratio of gas flow through turbine and waste gate, at high speeds. Use of a very small turbine results in a large by-pass flow to prevent excessively high exhaust manifold pressure, and it is then difficult to achieve the desired boost pressure and torque curve profiles. Thus, while efforts are made to match for good low-speed boost, it is difficult to achieve much boost pressure below 1500 rev/min. It is therefore desirable to select valve timing and lift to suit a lower operating engine speed than would normally be the case on a naturally aspirated engine. Thus valve timing should be selected for low-speed torque, and the turbocharger compensates for any resultant loss in high-speed performance.

Figure 13.23 compares valve lift diagrams for the naturally aspirated and turbo-

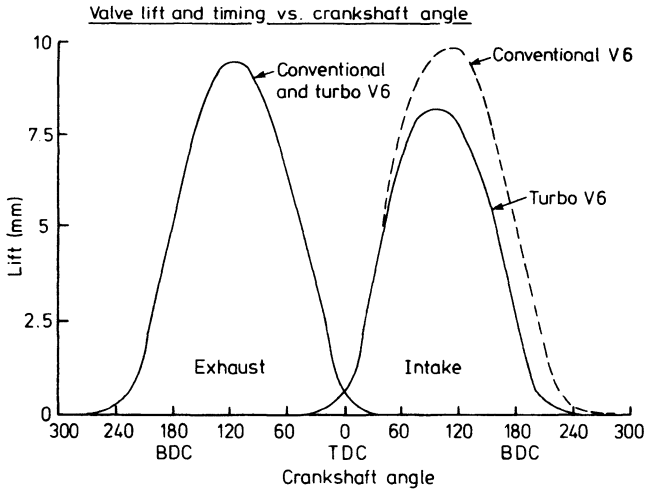

Figure 13.23 *Naturally aspirated and turbocharged Buick engine camshaft profiled [8]*

charged 3.8 litre Buick engines. No change is made to the exhaust valve lift or timing, to preserve good energy transfer to the turbine. However, inlet valve lift and opening period are reduced. The lower-lift shorter duration camshaft profile increases volumetric efficiency below 2400 rev/min and reduces it at higher speeds (that is, valve timing and lift are optimised at low speed). This results in higher torque at low speeds due to the camshaft alone (figure 13.24). Turbocharged versions of high-performance naturally aspirated engines require less valve overlap, not only to bias optimum volumetric efficiency to lower speeds, but to avoid mixture passing into the exhaust system under some engine conditions and reverse flow from exhaust to intake when the exhaust pressure exceeds the intake pressure. Thus, for example, valve overlap on the Porsche 911 was reduced from 100 to 82° when turbocharged.

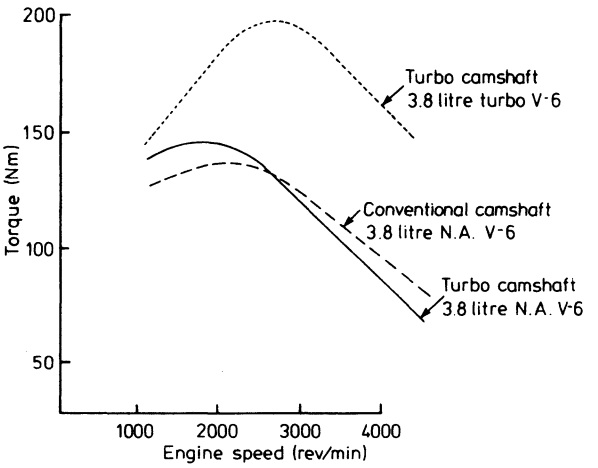

Figure 13.24 *Effect of camshaft change on torque, Buick engine [8]*

13.10 Engine Performance

A limited number of turbocharged passenger cars were manufactured by Buick and Oldsmobile in the United States in the early 1960s. [13] More recently, Audi, BMW, Porsche, Saab, GM and Ford have offered turbocharged cars to the public. The Audi, BMW, Porsche and Saab are high-performance versions of cars normally manufactured in naturally aspirated form. They have been made in limited numbers and sell at a substantial price premium, but are fitted with fuel-injection and similar equipment usually restricted to expensive, performance vehicles. In contrast, the GM Buick is not intended as a high-performance vehicle – it is an attempt to combine reasonable performance with good fuel economy, by using an engine considerably smaller than would normally be fitted to a car of its size, yet turbocharged to maintain the performance associated with the larger engine. Thus the turbocharged 3.8 litre V6 Buick engine gives the same acceleration as a 5.7 litre V8 engine when fitted in the same vehicle (figure 13.25) together

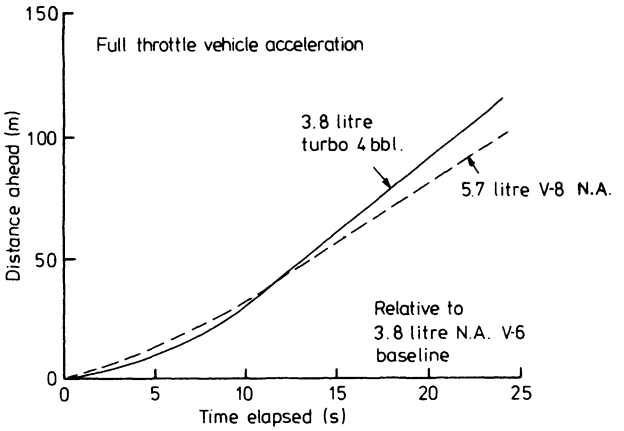

Figure 13.25 *1978 LeSabre Performance Comparison (5.7 litre naturally aspirated and 3.8 litre turbocharged) [8]*

with an engine weight reduction of 40 to 50 kg, and a fuel consumption saving of 5 per cent. [8] The power and torque increases are 59 and 43 per cent respectively (less with a two-barrel carburetter) with a maximum compressor pressure ratio of 1.6:1.

The more conventional knock-avoidance technique of reducing compression ratio has been used by Porsche (figure 13.26) for their 911 sports car. In this application the design of the waste gate and turbocharger match are such that the

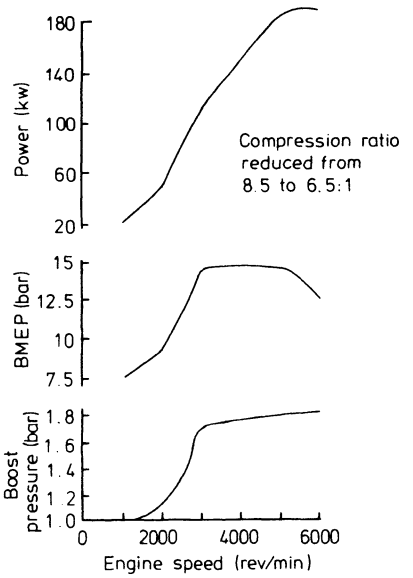

Figure 13.26 *Porsche 911 Turbo performance (waste gate controlled) [4]*

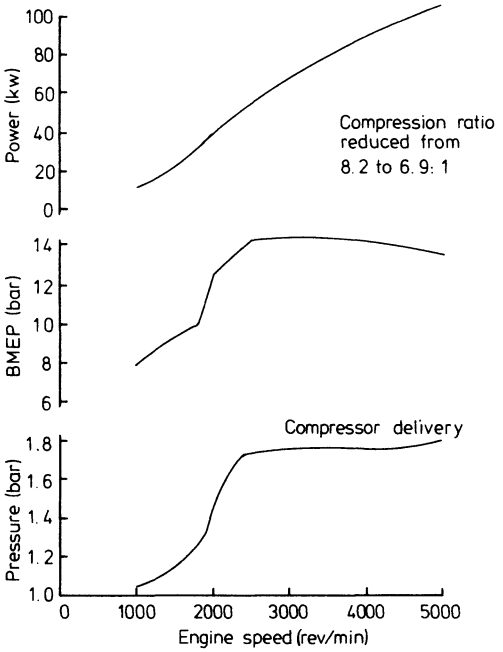

Figure 13.27 *Turbocharged Audi 100 performance, matched for a high-octane fuel (waste gas controlled) [6]*

boost pressure rises very rapidly above 2000 rev/min, but is then sharply controlled. This gives a rather abrupt change in the torque (BMEP) curve. A similar characteristic was obtained by Csallner and Spindler [6] on an Audi engine (figure 13.27). In contrast, the pressure-relief valve in the intake manifold used by BMW several years ago (figure 13.28), resulted in a more progressive rise in BMEP from low to medium engine speeds, but a rapid fall at high speed. The exhaust restrictor system used by Fuchs *et al.* [5] produced a similar characteristic (figure 13.29) but aimed

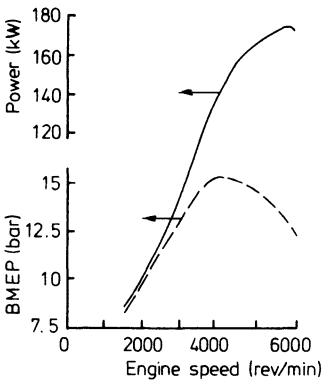

Figure 13.28 *BMW 2002 Turbo performance (relief valve controlled)*

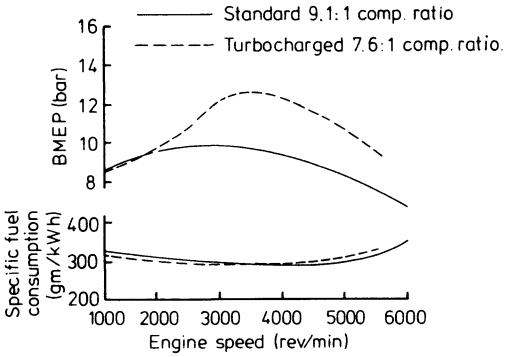

Figure 13.29 *Ford V6 turbocharged (exhaust restrictor controlled) [5]*

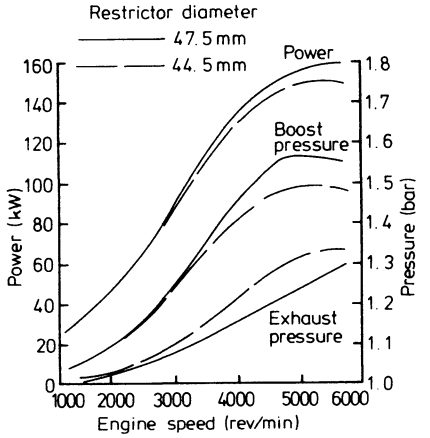

Figure 13.30 *Ford V6 turbocharged: the effect of exhaust manifold restriction on boost, exhaust pressure and power output [5]*

at a lower BMEP increase from the turbocharging system. Figure 13.30 shows the effect of varying the size of the exhaust restrictor on the turbine exit pressure. The smaller restrictor (44.5 mm diameter) increases back-pressure and reduces turbine work, leading to a reduction in boost pressure. Engine power output falls due to the combined influence of the lower boost and increased exhaust pumping work.

Most turbocharged car engines now use the exhaust waste gate boost control system, for the reasons given in section 13.8.7, with about 30 to 40 per cent of the mass flow by-passing the turbine at maximum speed and load. Likewise, most of these systems use the inlet manifold pressure, acting on a diaphragm to open and modulate the waste gate. An exception is the early 2 litre Saab engine on which the exhaust manifold pressure is used as a controlling medium. The objective is to use the continued rise in exhaust manifold pressure to open the waste gate

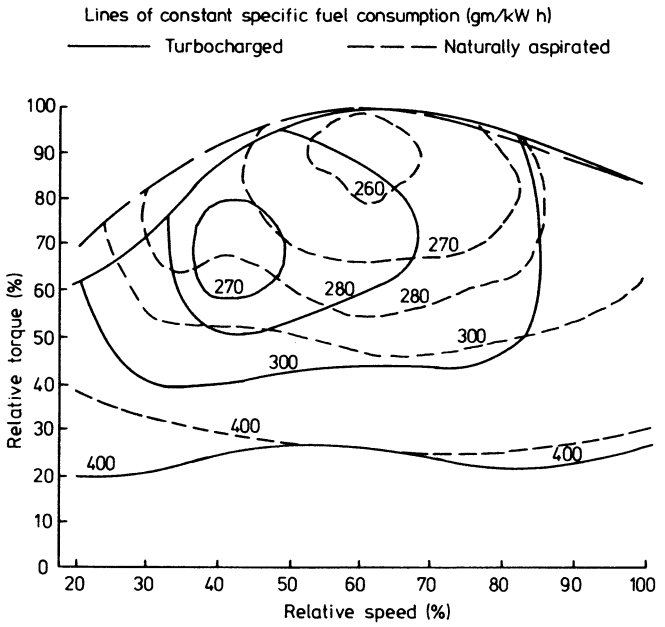

Figure 13.31 *Comparative specific fuel consumption of a turbocharged and naturally aspirated petrol engine scaled for the same maximum torque (adapted from Csallner and Spindler [6])*

valve further as engine speed rises, with a simple waste gate design. Thus boost pressure can fall gradually at very high engine speed, producing a reasonable torque curve shape. It is possible but more difficult to meet this requirement by careful design of the waste gate itself with inlet manifold pressure control.

Specific fuel consumption contours of the naturally aspirated and turbocharged Audi engine are compared in figure 13.31 in which data has been scaled to represent engines of different capacities, but the same maximum torque. In this case, the low compression ratio turbocharged engine exhibits a useful reduction in specific fuel consumption at low speed. The naturally aspirated engine is better at high speeds. Thus any benefit of one engine over the other will depend on the driving pattern of the vehicle when in service. Usually low-speed fuel consumption is more important since drivers rarely run their engines at high speeds for long periods of time.

Figures 13.32 and 13.33 illustrate how an improvement in fuel consumption increases as load is reduced on a turbocharged engine, and how this is reflected in steady speed vehicle operation. As important is the reduction in engine weight, relative to a naturally aspirated engine of the same power output, which has a strong influence on vehicle fuel economy when accelerating. Worthwile gains are possible if chassis weight is also reduced due to the requirement to carry a lighter engine.

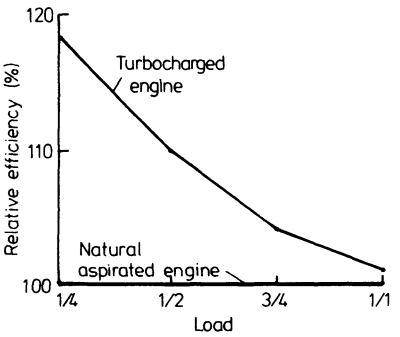

Figure 13.32 *Comparison of efficiency advantage of the turbocharged petrol engine with a naturally aspirated one of the same power, as a function of load [2]*

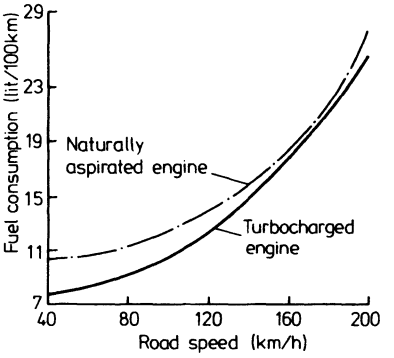

Figure 13.33 *Comparison of level road fuel consumption between a naturally aspirated petrol engine and a turbocharged version of the same power [2]*

13.11 Exhaust Emissions

Turbocharging can marginally reduce specific HC, CO and NO_x emissions from a petrol engine in certain, but not all, circumstances. HC and CO oxidation reactions are pressure, temperature and time sensitive. Evidence does suggest that the exhaust manifold and turbine partially act as a thermal reactor encouraging further oxidation. The benefit, however, will be small or non-existent in a badly designed system. [14]

NO_x is largely unaffected at low loads (figure 13.34) but can be significantly reduced at full throttle, probably due to the lower compression ratio. At low loads, the compression ratio effect will be offset by the wider throttle opening required to make up for the lower power output, since the turbocharger will only be idling.

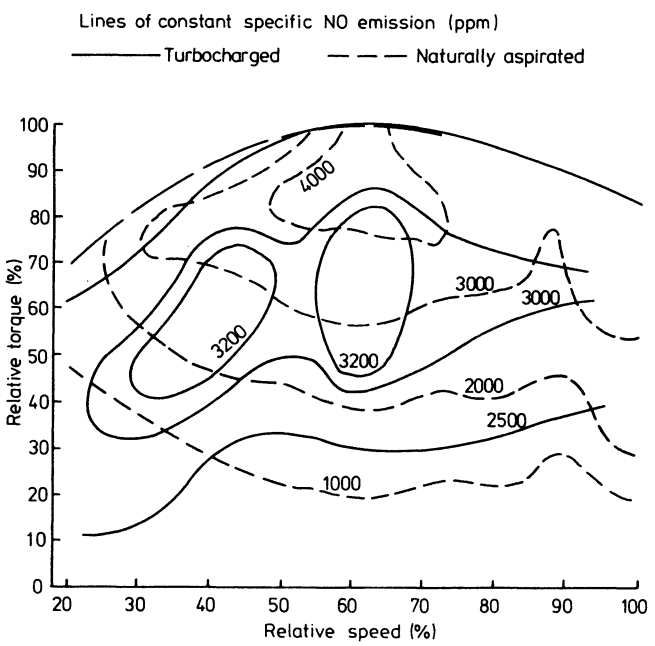

Figure 13.34 *Comparative specific NO emission of a turbocharged and naturally aspirated gasoline engine, scaled for the same maximum torque (adapted from Csallner and Spindler [6])*

Turbocharged petrol engines exhibit the same emissions sensitivity to air/fuel ratio (figure 13.35) as naturally aspirated engines, but the situation is compounded by resultant changes in turbine inlet temperature. Exhaust temperature will fall if the mixture is excessively weak or rich. If the waste gate is not open, turbocharger speed and hence boost pressure will therefore fall if the mixture is weakened. Thus the fall-off in power will be more rapid than that of a naturally aspirated engine. At rich mixtures, turbocharger speed will fall more slowly, hence the normal power gain with a mixture slightly richer than stoichiometric will remain.

Several attempts have been made to take advantage of the high exhaust manifold pressure of the turbocharged engine in a thermal oxidation reactor between engine and turbine. [15, 16] However, the gains are offset by the lack of pulse energy utilisation in reactor-type manifolds and consequent poor performance of the turbocharging system. If rich enough mixtures are used, however, significant oxidation of HC and CO can be combined with the low NO_x levels normally associated with rich mixtures, but at the expense of fuel consumption.

For low emission levels typical of those required in most of the United States in the late 1970s, NO_x emission was controlled by exhaust gas recirculation as on a naturally aspirated engine with a slightly fuel-rich mixture. An oxidation catalyst was used to control HC and CO, plus an air pump into the exhaust system

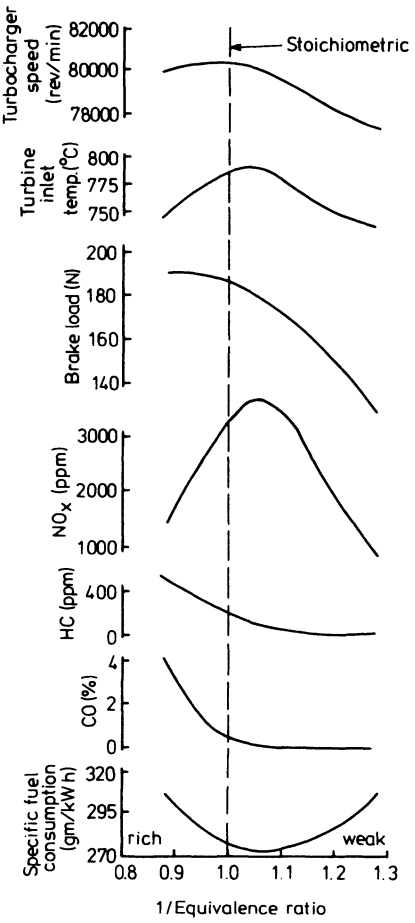

Figure 13.35 *The sensitivity of performance to change in air/fuel ratio of a turbocharged petrol engine [6]*

to obtain the necessary excess oxygen. To meet the more stringent 1980s legislation, three-way (HC, CO and NO_x) or dual catalyst systems are required. Thus exhaust treatment is similar to that of a naturally aspirated engine, but the high-pressure loss through the catalytic converter affects the selection of turbocharger match.

If a slightly rich mixture is used to control NO_x at full throttle, and an air pump is fitted to aid exhaust pipe oxidation of CO and HC, then the air injection can also be used to aid low-speed boost. By injecting air prior to the turbine, further reaction of the rich mixture increases turbine inlet temperature (and the mass flow rate rises), raising turbine work and therefore boost pressure (figure 13.36).

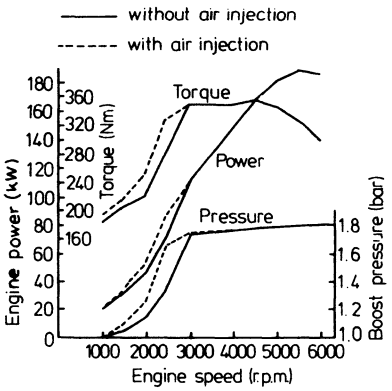

Figure 13.36 *The effect of secondary air injection (into the exhaust manifold) on turbocharged petrol engine performance [1]*

13.12 Racing Engines

Turbocharged petrol engines have been quite successful in the field of motor racing. In particular the prestigious US race, the Indianapolis 500, has been dominated by turbocharged engines for several years. The 2.8 litre engines produce up to 600 kW with fuel injection and an exhaust waste gate control system. However, the race conditions are far from typical of normal European practice. In particular, no limitations (in the past) have been placed on the fuel, allowing methanol and other knock-resisting additives to be used. Thus these engines have not been subjected to the low knock-limited boost pressures that normally limit turbocharged engine performance.

Other turbocharged petrol engines have raced successfully with normal octane fuels, for example, the 5 litre CAN-AM Porsche. The power output has been limited by engine reliability and fuel consumption, but over 700 kW has been recorded (figure 13.37). Significantly lower boost pressures, compared to normal values at Indianapolis, were used and therefore BMEP was much lower. Porsche have also raced turbocharged versions of their normal passenger cars, but without excessive boost pressures and using charge air cooling. In fact, it would seem essential to aftercool the air so that as high a boost pressure as possible may be used without inducing knock.

Currently turbocharged and intercooled 1.5 litre Formula 1 car engines are competing against 3 litre naturally aspirated engines, with some success.

13.13 Aircraft Engines

Turbocharged engines are well suited for operation at altitude. A normal naturally aspirated petrol engine will suffer a severe degradation of its performance at altitude due to the progressively reducing air density. The partial compensation of altitude effects make turbocharging an attractive proposition for light aircraft

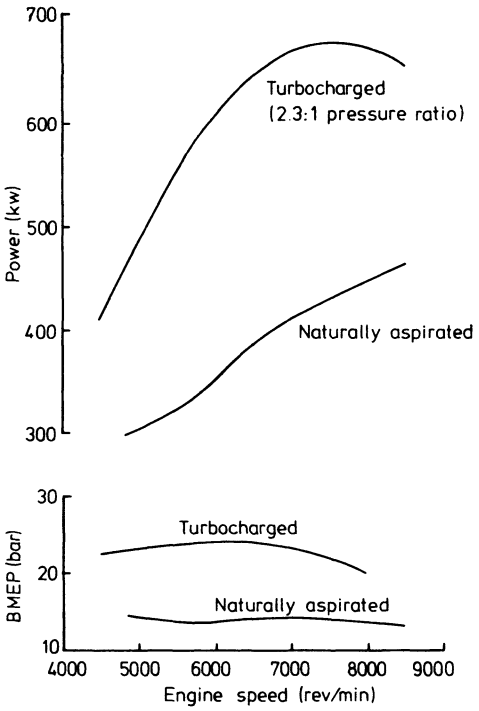

Figure 13.37 *Performance of 5 litre Porsche 917*

petrol engines. With a suitable design of a turbocharging system it is possible to maintain sea level engine performance up to quite high altitudes.

Consider a naturally aspirated engine that normally produces a certain power output at sea level. A turbocharging system with waste gate control may be fitted, such that the waste gate is fully open at sea level and the turbocharger generates little boost pressure. If the waste gate is controlled by the absolute intake manifold pressure, then the valve will gradually close at increasing altitude. In consequence, turbine power output will increase so that the compressor maintains the initial absolute inlet pressure at the cylinders with no loss of engine power output. Of course there is no reason why advantage should not be taken of the turbocharger to supercharge the engine up towards its knock-limited boost pressure at sea level, and it will then be this absolute inlet pressure that will be held at altitude. [17, 18]

The turbocharger will only maintain engine power up to the point at which the waste gate is fully closed. The altitude at which this occurs (the 'critical altitude') will depend on the engine, turbocharger and waste gate match. This will normally be governed by the initial choice of turbine size, the final limit being excess turbocharger speed at altitude. Above the critical altitude, engine power output will fall, although less rapidly than would be the case with a (larger) naturally aspirated engine developing the same power at that altitude (see section 10.9.1).

At altitudes above 6 to 7000 m it becomes essential to pressurise aircraft cabins for passenger comfort. Although separate mechanically driven Roots or centrifugal blowers may be used, it is feasible to bleed off compressed air from the turbocharger compressor, provided that the turbocharging system is matched for this duty. Details of bleed pressurisation systems are given by Cholvin [17] and Satchwell. [19]

13.14 Stratified Charge Engines

Although the diesel engine can be considered as a stratified charge engine, since its mixture during combustion is non-homogeneous, the term generally refers to special petrol engines. The special characteristic is that they do not use a homogeneous air/fuel mixture, but a mixture in which the air/fuel ratio varies in the combustion chamber. Some versions use a combustion chamber having two interconnected volumes like a pre-chamber diesel. A rich (homogeneous) mixture is supplied to the pre-chamber, and a weak mixture to the main chamber. Ignition of a mixture richer than stoichiometric takes place in the pre-chamber, a tongue of flame spreading into the main chamber burning the weaker mixture therein. These engines have been developed in the search for low NO_x emission power plant – typical is the Honda CVCC engine.

Somewhat closer in concept to the diesel engine are stratified charge spark-ignition engines using fuel injection direct into the cylinder. The best-known example is the Ford PROCO (figure 13.38). The principle is that a mixture strength close to stoichiometric is formed local to the spark plug area only. The remainder of the chamber contains progressively weaker mixture, air alone, or burnt combustion products. In addition to the benefit of low exhaust emissions common to all stratified charge engines, intake throttling is not required at part load, en-

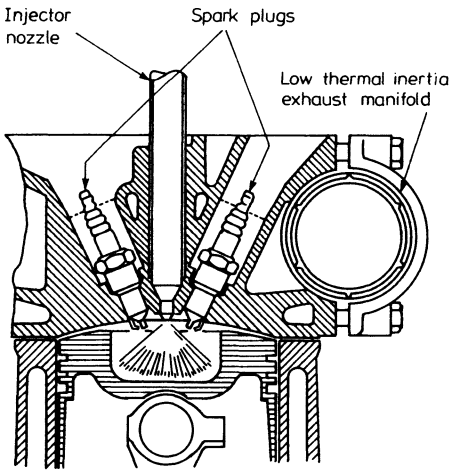

Figure 13.38 *Cross-section of a typical PROCO combustion chamber [20]*

abling better fuel consumption to be obtained. A further advantage of this latter class of engines is their tolerance to the use of fuel with diverse properties. The combination of direct fuel injection, spark ignition and progressive local burning as fuel is injected almost eliminates the problem associated with ignition delay (in the diesel engine) and combustion knock (in the petrol engine). It is the latter that is most significant in the present context because it removes the major limiting factor of the spark-ignition turbocharged petrol engine, by enabling higher boost pressure to be used.

The fuel-injected stratified charge engine may produce significantly less power than a petrol engine of equivalent displacement. This results from the basic air/fuel mixing process with localised combustion. To achieve the same power output a similar over-all mixture strength (at full load) would be required, but this is difficult to reconcile with good combustion, without a homogeneous mixture. Turbocharging has been used by Texaco, MAN and others to regain this power loss, and in some cases to generate a power advantage. However, the over-all cost of the engine, including fuel-injection system and turbocharger, is high.

13.15 Turbocharger Lag

The subject of transient response of turbocharged diesel engines is discussed in chapter 12. However, there are certain features of the turbocharged petrol engine that result in the lag being worse than that normally encountered on a diesel engine. Firstly, petrol engines are lighter and smoother, the latter enabling lighter flywheels to be used. As a result petrol engines are generally more responsive than diesel engines, and the delay of the turbocharger in increasing the air supply to the engine becomes more intrusive. Secondly, the petrol engine operates over a much wider mass flow range, from throttled low-speed idling to full-speed unthrottled. Thus air flow requirement can change very rapidly when the throttle is suddenly opened and the lag of the turbocharger is clearly noticed by the driver.

Although various extravagant claims are made from time to time regarding systems that 'eliminate' turbocharger lag, resort must be made to some additional energy input, if lag is to be eliminated. However, it can certainly be reduced by sensible design. The most important factors are turbocharger inertia, ignition timing, boost control system, the lengths and diameters of the inlet and exhaust systems and throttle position relative to the carburettor. For example, an engine with waste gate control allows a small (low-inertia) turbocharger to be fitted resulting in faster response than would occur with no waste gate and a larger turbocharger.

Passenger-car engines actually operate under unsteady conditions at most times. Only during steady cruising on motorways do engine conditions settle. Thus it is vitally important to match the turbocharger for transient conditions, which usually means fitting a turbine slightly smaller than that considered optimum when matching at steady speed.

Due to turbocharger lag, when the throttle is suddenly opened, the engine behaves as a naturally aspirated engine.

Figure 13.39 compares the steady speed torque of a 2.8 litre turbocharged engine, with the instantaneous torque developed while accelerating from a low

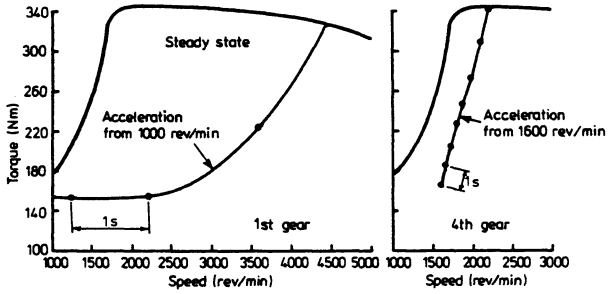

Figure 13.39 *Comparison of engine torque developed at steady state and during first and fourth gear wide open throttle accelerations [21]*

speed and load. In these tests the engine is driving an inertial load, simulating a vehicle, through a gearbox. In first gear, the torque developed is that of a naturally aspirated engine for at least 1 s, when accelerating from 1000 rev/min to 4500 rev/min. In fourth gear the initial lag is less serious, but the instantaneous torque developed remains substantially less than the potential steady speed torque.

The engine speed at which boost builds up on the steady state engine characteristic will influence response. For example, in the first gear acceleration shown in figure 13.39, the potential torque available with zero turbocharger lag is low. Figure 13.40 shows full throttle vehicle acceleration and the response of turbocharger boost pressure with turbochargers matched to develop full boost at steady speeds of 2050 (H) and 1740 rev/min (I). The response time to achieve maximum

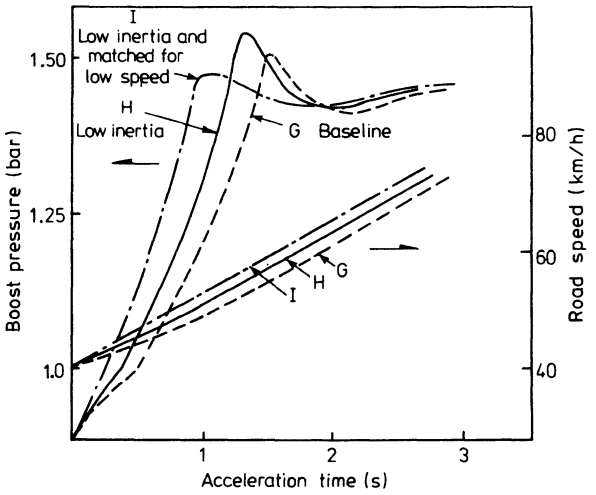

Figure 13.40 *Effects of torque characteristics and moment of inertia on vehicle acceleration [22]*

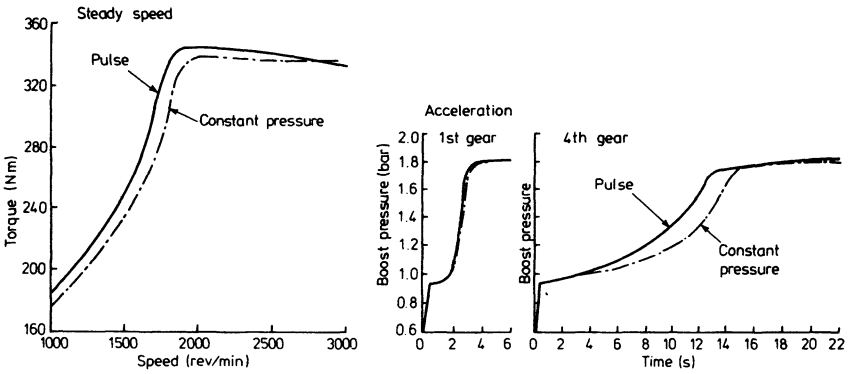

Figure 13.41 *Comparison of steady speed torque curve and acceleration with pulse and constant pressure turbocharging [21]*

boost pressure is reduced by 20 per cent with match I, and vehicle acceleration benefits accordingly. Also shown in figure 13.40 is the benefit of low turbocharger inertia, since the difference between matches H and G is 25 per cent lower inertia of turbocharger H.

Figure 13.41 shows the effect of pulse and semi-constant pressure turbocharging systems on the steady state torque curve and response. With proper pulse turbocharging, low-speed torque and response are better. Little difference is apparent in the first gear acceleration shown, since the engine response is too rapid for small differences to show, but in fourth gear response time is reduced by 14 per cent with the pulse system.

A turbocharged engine with high compression ratio and variable ignition timing will respond more rapidly than a low compression engine due to the effect

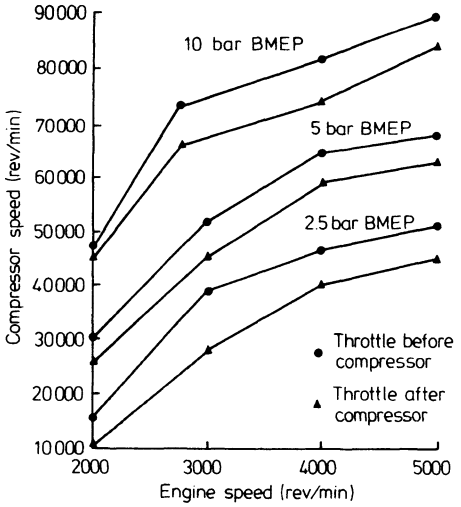

Figure 13.42 *Compressor speed at three loads, with throttle placed before or behind the compressor [21]*

of compression ratio and timing on power output. Optimum ignition advance is available in the absence of boost pressure.

Engine response is also better with the throttle placed before the compressor rather than after. Figure 13.42 shows that the low density of the air in the compressor, with the throttle before the compressor, moves the operating point to the right on the compressor map, towards higher compressor speeds. This results in a 5000 to 8000 rev/min higher turbocharger speed for the same engine speed and load. Since the final (full throttle) turbocharger speed at the end of an acceleration will be almost the same regardless of throttle position, the turbocharger speed change required will be less with the throttle before the compressor. This noticeably improves response, provided that manifold volume between throttle and inlet valves is small.

Thus good response is associated with a high engine compression ratio, throttle before compressor, waste gate or variable geometry, low-inertia pulse turbocharger system, having short pipe lengths on inlet and exhaust. Short inlet pipe length is particularly important if a carburettor is used, prior to the compressor, to keep the fuel-wetted surfaces to a minimum.

References

1. H. Mezger, Turbocharging engines for racing and passenger cars, *SAE 780718* (1978)
2. H. Hiereth and G. Withalm, Some special features of the turbocharged gasoline engine, *SAE 790207* (1979)
3. W. Spindler, Matching a turbocharger to a passenger car petrol engine, Paper C56/78, Turbocharging and Turbochargers Conference. Inst.Mech. Engrs (London, 1978)
4. H. Mezger, Abgasturbo-Aufladung an Rennfahrzeug- und Sensenfahrzeug-Motoren, Open lecture, Tech. Akad. Wuppertal (January, 1976)
5. E.R.R. Fuchs, K.G. Parker and B.T. Pritchard Lovell, Turbocharging the 3 litre, V6 Ford Essex engine, *Proc. Inst. Mech. Engrs,* **188**, No. 5/74 (1974)
6. P. Csallner and W. Spindler, Aufgeladener Ottomotor, Bericht Nr. 145-379, zum Forschungsvorhaben No. 170, Institut fur Kraftfahrtechnik, Forderwesen und Agrortechnik, W. German (October 1975)
7. H. H. Dertian, G.W. Holiday and G.W. Sandburn, Turbocharging Ford's 2.3 liter spark ignition engine, *SAE 790312* (1979)
8. T.F. Wallace, Buick's turbocharged V-6 powertrain for 1978, *SAE 780413* (1978)
9. K.F. Kaiser, C.R. Sarle, B.R. Owen, Installation and design problems associated with the automotive turbocharger, *SAE 790313* (1979)
10. K.D. Emmenthal, G. Hagemann and W.H. Hucho, Turbocharging small displacement spark ignition engines for improved fuel economy, *SAE 790311* (1979)
11. Z. Baazaari, Control systems for turbocharged petrol engines. Imperial College, Dept. of Mechanical Engineering (1974)
12. H. Dorsch and J. Weber, Abgasturbo-aufladung für den Porsche 924 Turbo, *MTZ,* **40**, No. 3 (1979) pp. 107-11
13. R.E. Thoreson and J.O. Brafford, The Corvair turbocharged engine, *SAE 531A* (1962)

14. J.F. Schweikart and J.H. Johnson, A turbocharged spark-ignition engine with low emissions and improved fuel economy, *SAE 730633* (1973)
15. S.J. Goddard, B.C. Jasper and D.C. McWhannell, A turbocharged spark-ignition engine with thermal reactor, performance and emissions characteristics, Paper C58/78, Turbocharging and Turbochargers Conference, Inst. Mech. Engrs (London, 1978)
16. P.J. Kern and O.B. Koropey, Effects of exhaust manifold configuration on a turbocharged engine employing charge stratification, *SAE 770047* (1977)
17. R.L. Cholvin, Turbocharging aircraft engine and cabin, *SAE 650380* (1966)
18. D.H. Gollings, Development of a new generation of simplified turbocharger systems, *SAE 771013* (1977)
19. D.L. Satchwell, Performance characteristics of aircraft with turbo-supercharged engine and cabin, *SAE 680226* (1968)
20. A.J. Scussel, A.O. Simko and W.R. Wade, The Ford PROCO engine update, *SAE 780699* (1978)
21. H. Heireth and G. Withalm, Das Instationarverhalten des aufgeladeners Ottomotors, 18th FISITA Congress, Hamburg (1980)
22. T. Watanable, S. Machida, Y. Sumi and S. Nakazama, A study of the performance improvement for turbocharged engines, 18th FISITA Congress, Hamburg (1980)

An additional textbook on practical aspects of turbocharging petrol engines is Hugh MacInnes, *Turbochargers* (H.P. Books Tucson, Ariz, 1976)

14

Diesel Engine Exhaust Emissions and Noise

14.1 Introduction

The upsurge of interest in environmental quality during the 1970s has resulted in much existing and proposed legislation for diesel exhaust emissions and noise. The bulk of this legislation is aimed at vehicles, but stationary power sources are not immune. The movement towards current legislation had two separate sources. First came general public hostility to the black smoke emitted from a substantial number of diesel engined trucks in the United Kingdom and Europe, followed by complaints directed at all noisy transportation means (aircraft, diesel trucks, cars and motorcycles). Meanwhile, in the United States the public nuisance of the Los Angeles 'smog' prompted the start of a major series of environmental quality laws. Although the number of diesel engined vehicles is increasing in the United States, the total proportion of vehicles so equipped (relative to petrol engines) remains low compared with that in Europe. Thus it was the petrol engine rather than the diesel engine that was originally singled out for criticism.

In the United Kingdom, legislation was originally aimed at smoke and noise, while that in the United States was directed towards limiting gaseous emissions. At first, when the formation mechanism of Los Angeles smog was not completely understood, US legislation limited the emission of carbon monoxide (CO) and unburnt hydrocarbons (HC) but the oxides of nitrogen (NO and NO_2, cumulatively called NO_x) were soon added to the list. With petrol engine emission limits established, interest turned to the diesel engine, principally that used in road transport. CO, HC and NO_x limits were established together with a smoke limit. More recently interest has been directed towards reducing the odour of the exhaust gas, other gaseous and particulate constituents and the emission of oxides of sulphur (SO_x) from the exhausts of industrial diesel engines.

Here the primary concern is with the effect of turbocharging on gaseous and particulate emissions, plus engine noise. To do this we must first look at the formation of these various pollutants.

14.2 Combustion

Unlike petrol, diesel fuel is a less volatile (higher boiling point) distillate of crude

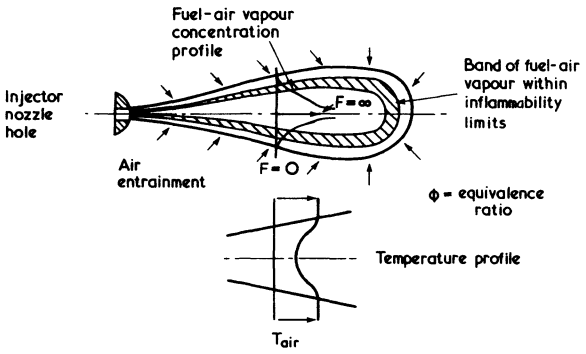

Figure 14.1 *Schematic of a fuel spray in quiescent air, prior to ignition*

oil and consequently does not readily evaporate at normal ambient temperatures. Thus gaseous emission from the diesel engine involves crankcase fumes and combustion products but not evaporative emissions from the fuel tank. Crankcase fumes may easily be recycled to the intake manifold for burning hence only combustion products are of interest.

Figures 14.1 and 14.2 are diagrammatic representations of a fuel spray (injected into quiescent and swirling air with wall impingement). The central core of the spray contains liquid fuel droplets and vapour. Air is entrained as the cross-sectional area of the spray increases (this must happen from conservation of mass laws). This air will be warmer than the injected fuel due to compression heating and, together with heat transfer from the surroundings, will help to evaporate the fuel droplets. The enthalpy of evaporation is supplied by the air surrounding the droplets, so this air will be cooled by evaporation. Thus the droplet will not ignite spontaneously the moment evaporation begins. Even if the vapour were hot enough for ignition, sufficient air (oxygen) must be entrained to generate a favourable air/fuel mixture ratio for combustion to proceed at a

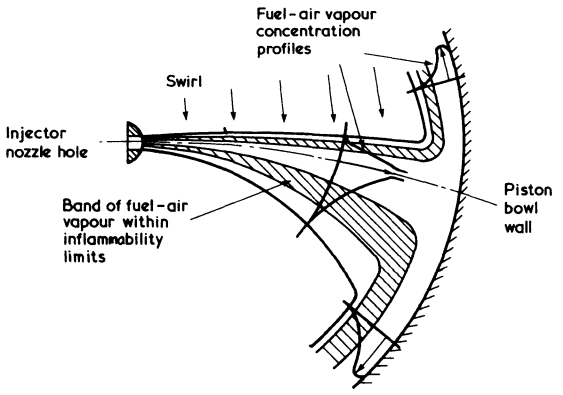

Figure 14.2 *Schematic of a fuel spray with wall impingement in swirling air prior to ignition*

noticeable rate. Thus we may imagine the fuel spray as a core of droplets and fuel vapour surrounded by an area comprising wholly evaporated droplets with significant air around them. Further from the centre of the spray, evaporation will be complete and an air/fuel vapour mixture will exist.

In a swirling air stream (figure 14.2), the light vapour–air cloud furthest from the centre of the spray will be swept round with the bulk air motion. The main core of the fuel spray, very fuel-rich but largely in the gaseous phase, will have sufficient momentum in the radial direction to be largely unaffected by swirl. Thus although the central core of the fuel spray is not substantially deflected, a large cloud of air/fuel vapour will be formed on the downstream (swirl) side. By this means swirl significantly increases air entrainment in the over-all fuel spray. In most small engines the (predominantly vapour) central core of the spray will hit the combustion chamber wall before combustion starts. The wall will usually be sufficiently warm to avoid condensation (except when the engine is cold), although its temperature will be much lower than the bulk gas temperature. Evidence is divided on how much fuel 'bounces' off the wall and how much spreads along the wall primarily, but not completely, in the direction of swirl. Certainly a significant amount of fuel forms into a 'wall-jet' in automotive size direct-injection diesels. This wall-jet (figure 14.2) consists largely of fuel on the wall, with more air entrainment further away from the wall. Again due to the conservation of momentum, the increase in cross-sectional area of the spray when the wall-jet is formed and develops, results in more air entrainment, relative to the main jet.

Thus, before combustion starts, the fuel spray may consist of a vapour core (of 'infinite fuel/air ratio'), extending right to the wall and possibly along its surface. The spray boundary will be pure air (fuel/air ratio = 0), and a discrete area just inside this boundary will be too weak to burn significantly whatever the temperature. The fuel/air ratio will become richer towards the spray core, passing through the stoichiometric value towards the centre. Ignition will start where the fuel has completely evaporated, the fuel/air ratio is close to stoichiometric and the temperature is sufficiently high for self-ignition. Quite a large part of the fuel spray may satisfy the first two conditions before any part satisfies the third. When ignition starts heat transfer to the adjacent area of the spray will increase rapidly, thus combustion will rapidly cover a major part of the spray. [1] It is this rapid combustion, following the delay period between the start of injection and ignition, that is characteristic of diesel combustion. Once this 'prepared' (or premixed with air before ignition) fuel has burnt, combustion slows down (figure 14.3).

The rate at which combustion proceeds during the latter part of combustion will be determined by many factors, but with the rate of local air entrainment dominating. Since this fuel is being sprayed into a chamber containing burning fuel, the temperature will be high and it will rapidly evaporate. The high temperature will also be favourable for ignition, provided that the local air/fuel ratio is reasonable. It will be the air/fuel mixing process that controls the rate of combustion, and this will be governed by swirl and turbulence. In addition some fuel deposited earlier on the chamber wall will be drawn off by subsequent air movement and will burn, the rate being controlled by air entrainment but opposed by the cooling effect of the walls. Generally, the second phase of burning

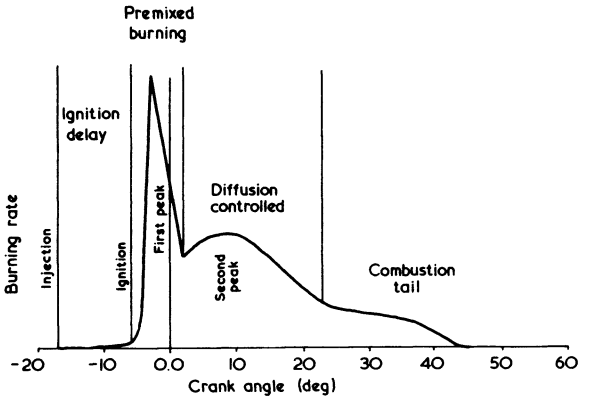

Figure 14.3 *Heat release rate diagram: diesel engines*

will largely be controlled by air entrainment and may loosely be called the diffusion burning period.

Towards the end of combustion, the cylinder pressure will be falling (and, to a lesser extent, the temperature also) as the piston moves down the bore. The combustion rate will slow down due to the temperature and pressure dependence of chemical kinetic effects as the chemical reactions slow down, so that the reaction rates rather than the air/fuel mixing process dominate.

To summarise, combustion may be loosely considered to consist of the delay period, governed by air/fuel mixing, diffusion, local turbulence and heat transfer, plus chemical kinetics and evaporation, followed by rapid pre-mixed burning, then a diffusion burning phase followed by a small amount of rate-controlled burning in the expansion stroke. It must be established where, and how, the pollutants are formed in these processes.

14.3 Formation of Pollutants

Unburnt Hydrocarbons

Some unburnt or partially burnt hydrocarbons (HC) are always present in the diesel engine exhaust. The amount, in terms of energy content is negligibly small, but their presence is objectionable due to the odour of some species, their contribution to the photochemical smog that first led to emission legislation, and potential toxic or carcinogenic effects. However, unburnt hydrocarbons should not be found in the products of combustion of lean mixtures if liquid fuel has been injected, properly mixed, heated and burnt. The oxidation reactions of hydrocarbons in a homogeneous mixture with air near stoichiometric proportions are among the fastest known. Chemical equilibrium calculations imply that only immeasurable quantities of HC gas can exist under these conditions at high temperature. The fact that HCs are emitted implies that they were not successfully ignited in the first place. The emissions usually consist of some partially decom-

posed fuel molecules, some recombined intermediate compounds and some HC from the lubricating oil (the latter being a small proportion). It is interesting to note that the recombined molecules often have a different structure from those of the original fuel.

There are several possible sources of unburnt HC in the diesel combustion process. First, some vapourised fuel at the edge of the spray is mixed with increasing quantities of air such that it is too weak to burn when the temperature becomes high enough for ignition. Greeves *et al.* [2] suggest that this is the major source of the HC emission. Secondly some HC could remain from the very rich region in the core of the fuel spray (although some recombination between hydrocarbon radicals and intermediate compounds may occur) but only a very small amount of HC, late in the injection process, will be involved. In a small high-swirl engine, a substantial quantity of fuel may impinge on the wall of the combustion chamber. This fuel should evaporate, but a very thin layer may be quenched and hence will not fully react. Further from the wall, HC vapour will burn if gas with sufficient oxygen is sweeping past it. The swirling air motion and that created by the piston moving down the bore, causes gases to rush out of the central area of the combustion chamber to the area above the piston lands, enabling most of this fuel to mix and to burn. Figure 14.4 shows a time history of HC concentration in the centre of a fuel spray in a quiescent chamber (obtained by a sampling probe). This shows how partially oxidised fuel is burnt up by subsequent combustion.

Towards the end of the injection process, when the injector is closing, the fuel spray will be weak resulting in little penetration of oxygen rich areas and poor atomisation. In addition, since cylinder pressure and temperature are falling, the oxidation reactions may be slow and incomplete, but active air motion and

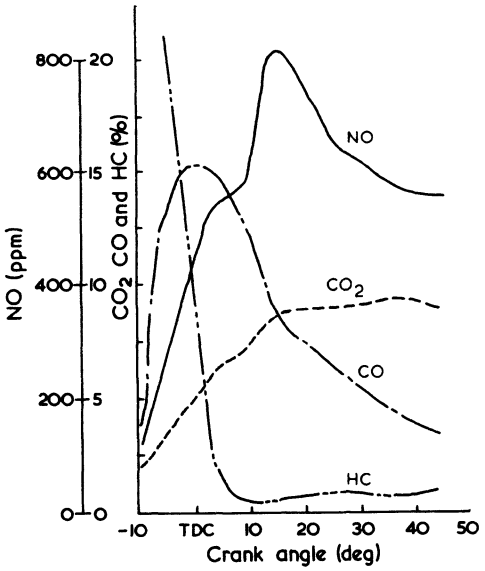

Figure 14.4 *Gaseous composition in the centre of the fuel spray [3]*

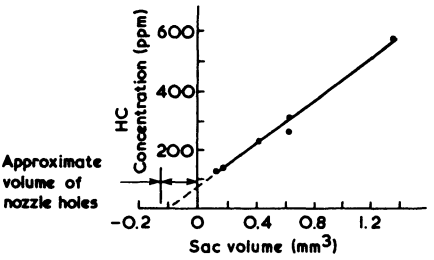

Figure 14.5 *Hydrocarbon concentration as a function of injector sac volume [2]*

surrounding combustion should prevent substantial HC from remaining unreacted. Any after-injection (fuel injection late in the cycle due to significant pressure waves in the fuel line) will cause HC emission due to the above reasons, and must be avoided at all running conditions.

Finally, a major source of HC emissions that tends to remain when a well-optimised combustion system with generally low HC output is developed, results from fuel being drawn out of the injector sac volume (between the needle seat and injector holes) after the injector has closed. This fuel has little chance of being fully atomised or mixed with oxygen and remains partially unburnt. Reduced injector sac volume is the solution to this problem (figure 14.5). In terms of magnitude, it is after-injection, sac volume, the weak areas at the periphery of the spray and cold walls that are the major sources of HC emission.

Carbon Monoxide

Carbon monoxide is an intermediate product in the combustion of hydrocarbon fuels. If sufficient oxygen is available, oxidation from CO to CO_2 will occur, but the reaction may be incomplete due to a short residence time or a low gas temperature. In certain areas of the combustion chamber it is quite likely that sufficient oxygen will not be available, the local mixture strength being quite rich (the fuel spray core and areas of wall impingement). Unless these areas receive oxygen later in the cycle, but before the temperature has dropped substantially, CO will be formed and remain unoxidised. Although CO may be formed in other areas during combustion reactions, the temperature and oxygen availability (due to over-all lean mixture strength of the diesel) will be high enough for complete oxidation to CO_2 to occur (figure 14.4). Fortunately, due to oxygen availability, the total quantity of CO formed is substantially less than that of petrol engines so that diesel engines easily meet current legislative levels.

Oxides of Nitrogen

Nitric oxide (NO) is formed during combustion due to the co-existence of the nitrogen and oxygen in air at very high temperatures. When additional oxygen is available the reaction will proceed to NO_2 but little NO_2 is actually formed in

diesel engines. Several simple reactions have been proposed for NO formation, the most widely accepted being the Zeldovich chain reaction

$$O_2 \rightarrow 2O$$
$$O + N_2 \rightarrow NO + N$$
$$N + O_2 \rightarrow NO + O$$
$$N + OH \rightarrow NO + H$$

The reaction is activated by atomic oxygen formed by dissociation of oxygen at the high temperatures encountered during combustion. It follows that the NO concentration is a function of local oxygen concentration and temperature, but the reaction rates are significant only at high temperature. Even in highly turbocharged diesel engines, the compression temperature is not sufficiently high for significant NO to be formed prior to combustion.

NO can be formed in all regions of the spray, but the temperature and local oxygen concentration dependence will result in a major variation of NO concentration throughout the combustion chamber. The time aspect of NO reaction rates is important. Calculations show that nitrogen in areas heated to a sufficiently high temperature for reaction to NO to begin, but late in the combustion process, will not exist at high temperature long enough for an equilibrium concentration to be formed. Thus local areas of nitrogen with high oxygen availability, exposed to high temperatures for the longest period of time, will form the principle NO during post-flame reactions. Henein [4] postulates that the amount of NO formed in the slightly lean regions round the fuel spray could be quite substantial due to local oxygen availability, the high temperature that must be reached, and the fact that these are the first areas to burn. However, Nightingale's experimental data [3] does not support this proposal. A major amount of NO could be formed in the central core of the spray since its temperature will become very high, but this will be subject to oxygen availability. Unfortunately, as the gas temperature decreases during the expansion stroke, the NO concentration does not fall to that predicted by chemical equilibrium calculations. The decomposition of NO during the expansion stroke is very slow due to reducing temperature, thus the high concentrations formed during combustion are virtually frozen in.

Smoke

Two quite different classes of smoke emission are emitted from diesel engines. Under cold starting, idling and possibly low-load conditions with low compression ratio engines, a cloud of vapour often referred to as blue-white smoke is emitted. This results mainly from fuel and lubricating oil being emitted without being completely burnt. The problem disappears as load is increased, but is a serious problem on highly rated turbocharged engines with low compression ratios (chapter 11) due to the combination of cold cylinder walls, low compression temperature and pressure, and over-penetration of the fuel spray.

Soot, or black smoke emitted during normal operation of a warm engine is a separate problem. Black smoke is emitted at all engine loads, but the amount is

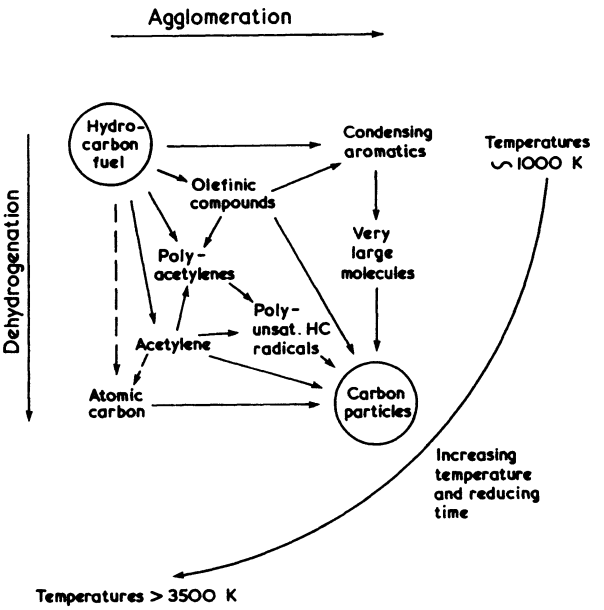

Figure 14.6 *Simplified carbon formulation scheme [5]*

usually low at weak fuel/air ratios (low loads). Normally, even when the smoke emission is very bad, the percentage of the total fuel input remaining unburnt is small. For example, a smoke reading of 5 Bosch units (approximately 72 Hartridge units) can occur with 99 per cent complete combustion. [5] Thus black smoke is not simply an incomplete combustion phenomenon.

The mechanism of soot formation is complex and not fully understood but Khan [6] and Broome and Khan [5] have proposed possible methods. Essentially the process can be divided into three phases: nucleation or the formation of precursors, the growth of these nuclei into soot particles and their coagulation into larger particles. Figure 14.6 shows a simplified scheme of reactions leading to the formation of soot nuclei.

In the diesel engine, temperatures are high yet the time available for soot formation is short, hence fast reactions at high temperature are most relevant. Thus initial decomposition or splitting of the fuel to an intermediate product of acetylene is a likely path. Very heavy but unstable hydrocarbon radicals appear to be an important link in the chain. The particles grow by the addition of poly-acetylenes and other hydrocarbons and by coagulation.

The final amount of smoke emitted by the engine will be determined by soot formation minus its rate of combustion and gasification. The burning up of soot formed during combustion will be largely governed by local oxygen availability and temperature late in the combustion process.

In the engine, fuel that is unmixed prior to the start of combustion (that is, that injected late in the central core of the spray and any on the walls) is likely to suffer the combined effects of lack of oxygen and high temperature later in

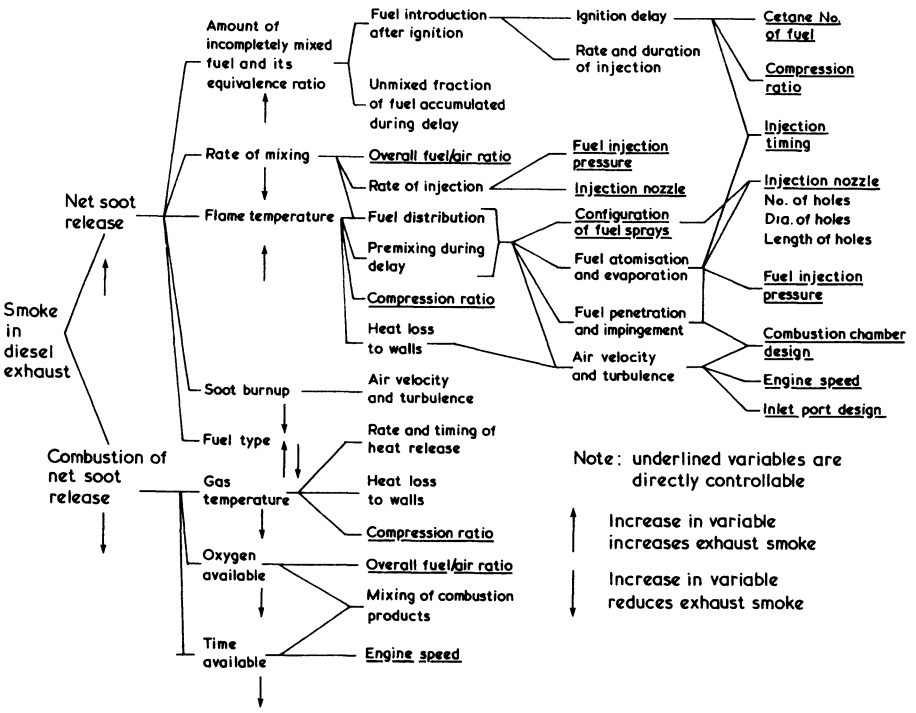

Figure 14.7 *Variables affecting diesel smoke [5]*

the cycle. However, it is the fuel injected after combustion has started that is least likely to receive sufficient oxygen and hence most exhaust pipe soot will result from the second phase of burning (the 'diffusion burning' phase). Any soot formed during the initial rapid combustion period is likely to be burnt up, oxygen availability being high. The exception will be soot formed on the combustion chamber walls hence this is likely to be a second source of soot formation in high-speed direct-injection engihes. In larger quiescent chamber engines, combustion takes place largely within the fuel-spray envelope, hence significant soot can be formed even at quite modest air/fuel ratios, due to a low rate of air entrainment within the spray. Figure 14.7 illustrates the effect of various parameters on smoke formation in direct-injection engines.

Particulates

The above discussion has concerned visual smoke emission, but smoke particles are carriers of a variety of organic compounds, some of which may be injurious to health. For example, benzo(a)pyrene (BaP) is absorbed on diesel particulates and may be carcinogenic. Although carbon and organics form the bulk of diesel particulate emission, traces of metals are also found.

14.4 Emissions from Naturally Aspirated Engines

In order to discuss the effect of turbocharging on exhaust emissions it is first necessary to analyse the pattern of emissions from naturally aspirated engines. Although this pattern varies greatly from one type of engine to another, figure 14.8 is reasonably typical of small automotive direct-injection and swirl-type pre-chamber engines with no emission-control features. The emissions of NO, HC and CO are plotted over the complete (smoke-limited) performance range, for engines optimised for performance, not emissions.

Since load is increased by raising the quantity of fuel injected, variation in almost all aspects of combustion occurs at different loads. At idling, or light load operation, unburnt hydrocarbon emission can result from residual fuel in the injector sac and slow elimination reactions in weak areas around the spray. At

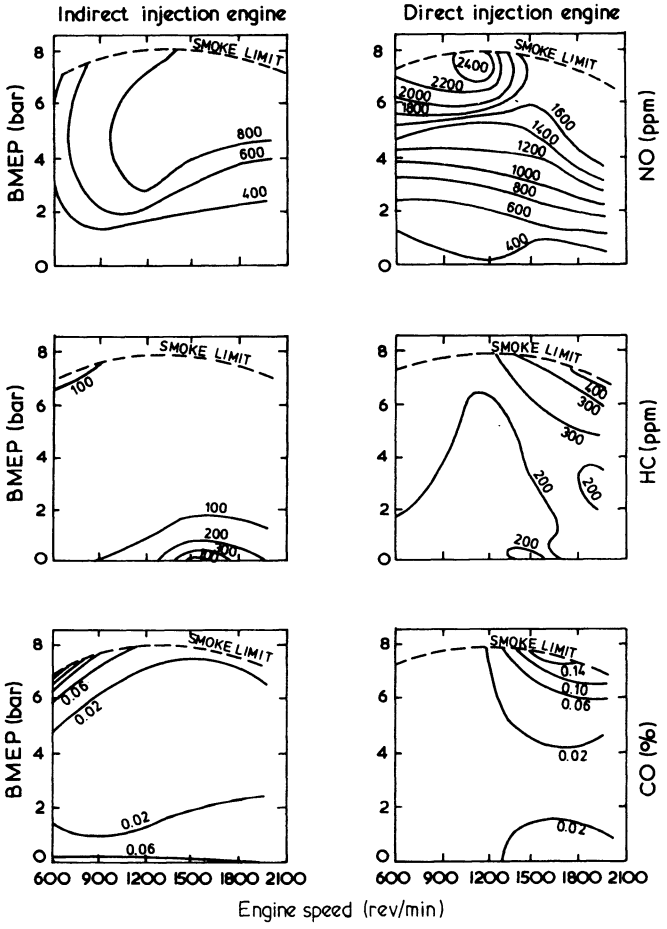

Figure 14.8 *Typical exhaust emission maps from direct and indirect (swirl chamber) injection engines [7]*

part load more fuel will be deposited on the walls and a large quantity of fuel exists in the central core of the spray. However, since the temperature in these regions will become quite high and local oxygen concentration is good, oxidation reactions will reduce the actual emission of HC. The same logic applies at full load when the oxidation reactions are promoted by the higher temperature but opposed by lower oxygen concentration, the former effect dominating. The result is a reduction in HC concentration with load in direct injection engines.

The indirect-injection engine performs differently, tending to emit less unburnt HC over most of its working range with a smaller dependence in load. Fuel is injected into a small pre-chamber which therefore contains a rich mixture. This mixture expands and burns through the connecting passage into the main chamber where the HC and CO are oxidised. Although hydrocarbon emissions from indirect-injection engines will always be lower than those of direct-injection engines, the emission trends at varying load and speed may be optimised by varying fuel injection timing (figure 14.9).

The CO emissions (figure 14.8) show that very little is produced relative to conventional petrol engines, hence reduction of this pollutant is not yet required. Generally, however, the CO emission that does occur is only significant at full load (that is, close to the smoke limit) due to partial combustion in areas of rich mixture. Since current diesel CO emissions are not yet considered a problem, they will not be considered further.

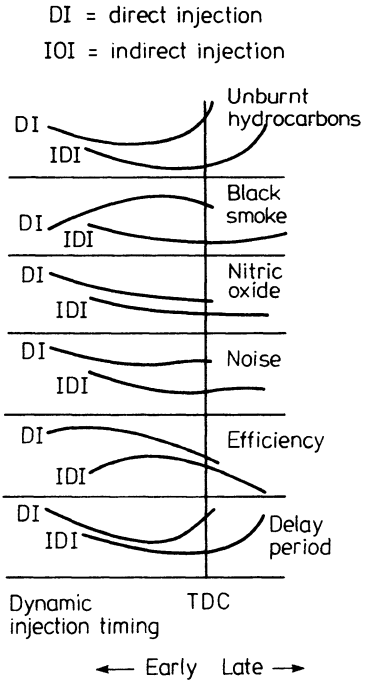

Figure 14.9 *The effect of injection timing on efficiency and exhaust emissions for direct-injection and indirect-injection diesel engines (CA V)*

Diesel engines produce quite high levels of NO_x and this is the principal gaseous emission that must be reduced. NO formation is related to local temperature, oxygen concentration and residence time. The NO concentration is greatest at high load due to very high gas temperatures encountered outweighing the effects of a richer mixture. Again the indirect injection engine exhibits far lower levels of NO_x emission, probably due to a combination of the rich mixture in the prechamber, high heat losses and late combustion in the main chamber all keeping peak temperatures down.

Exhaust smoke levels remain a major problem for the diesel engine manufacturer. In Europe the maximum fuel/air ratio is adjusted to keep smoke emission to socially accepted or legislative levels. Thus smoke limits power output from the engine. In North America weaker full-load fuel/air ratios are more common. Aldehyde and exhaust odour are directly related to unburnt hydrocarbon emission. [8]

14.5 The Effect of Turbocharging

Turbocharging affects exhaust emissions through its influence on the combustion process. The primary controlling mechanism is through changes in the pressure and temperature of the air trapped in the cylinder. It may also influence the swirl level in direct-injection engines, although this should be reoptimised. Implicit in the reoptimisation is a change in the fuel/air ratio at maximum load. The ratio may well be weaker than that used on a naturally aspirated engine to reduce the thermal loading and exhaust emissions. An additional factor is important when emissions are assessed on a specific power basis, rather than directly as a concentration. Since the IMEP will increase when turbocharging, without a corresponding rise in frictional losses, the brake power output will increase proportionately more than the indicated power output. This will reduce the brake specific emission figure for the same pollutant concentration.

Turbocharging, without aftercooling, will result in a higher charge temperature and consequently reduces the ignition delay period at high engine load and speed. Thus the rapid burn that follows the delay period is less severe due to the smaller quantity of fuel injected into the cylinder up to the moment of ignition (figure 14.10). It has been established that the primary sources of HC emission are the sac volume and areas around the fuel spray that have become too weak to burn prior to ignition. Ignition delay is shortened by turbocharging (except at low loads), hence the quantity of fuel accumulated in these weak areas is reduced and with it, hydrocarbon and aldehyde emission. An additional benefit at high loads is the promotion of oxidation reactions by higher charge temperature and the weaker maximum fuel/air ratio. Furthermore, there is some evidence that oxidation reactions continue in the very hot exhaust manifold and turbine of a turbocharged engine. Over-all, worth-while hydrocarbon emission reduction is possible (figure 14.11). Aldehydes (oxygenated hydrocarbons such as acrolein, C_3H_4O, and formaldehyde, HCHO) and odour reduce with hydrocarbons. However, at low loads, boost is virtually absent and therefore ignition delay will equal that of a naturally aspirated engine, or be even longer if the compression ratio has been reduced substantially. Thus little low-load HC reduction is achieved.

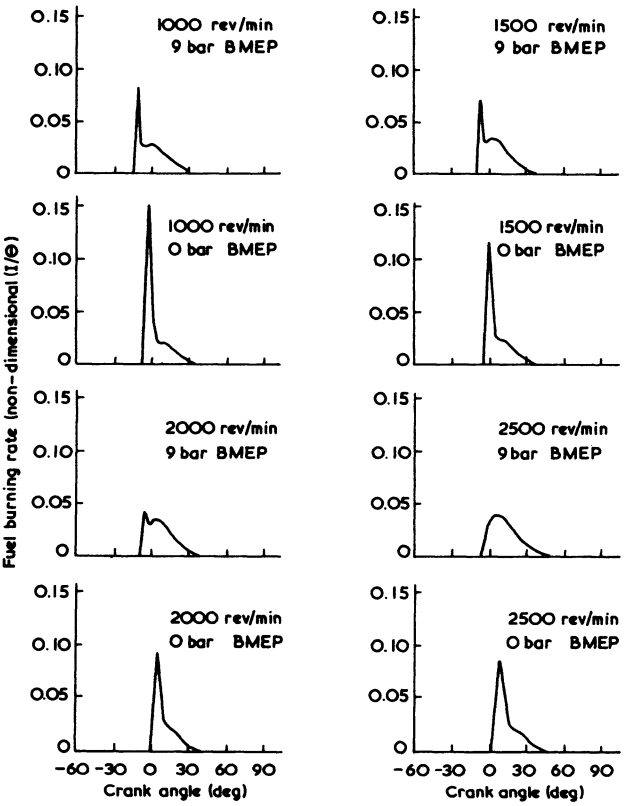

Figure 14.10 *Variation of fuel burning rate with load and speed for a turbocharged non-intercooled engine*

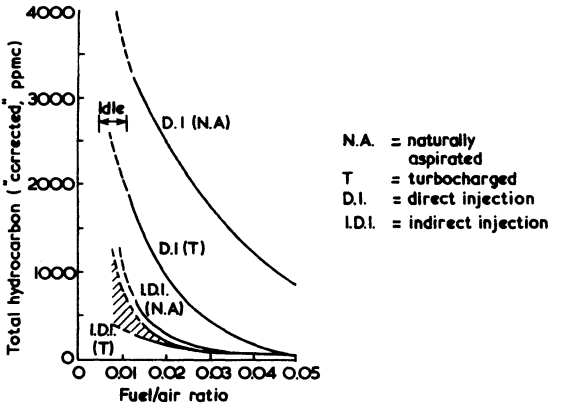

Figure 14.11 *The effect of air/fuel ratio on hydrocarbon emissions [9]*

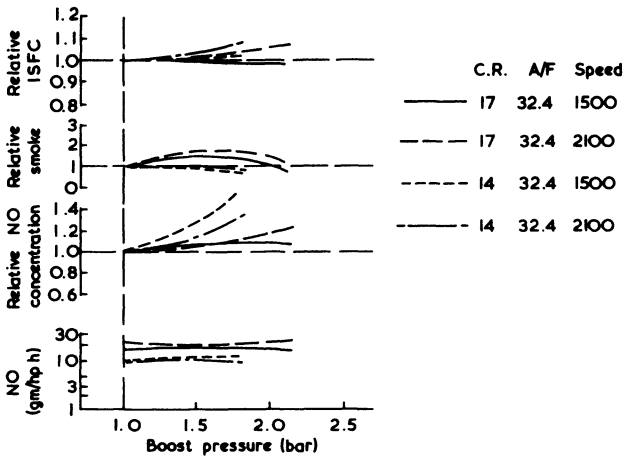

Figure 14.12 *The effect of boost pressure on emissions and economy [10]*

Turbocharging reduces CO emission due to high combustion temperature and weaker fuel/air ratios.

NO formation is governed by local temperature, local oxygen availability, residence time and, to a lesser extent, pressure. Turbocharging effects charge air temperature and pressure and in consequence, ignition delay, combustion rate and the over-all air/fuel ratio.

The most important of these effects is temperature, since the NO formation mechanism is very temperature sensitive. Turbocharging raises temperature and therefore increases NO formation. However, since the designer has more freedom to change the air/fuel ratio and injection timing on a turbocharged engine, this is not the complete story. To study the effects of all the controlling parameters mentioned, it is simpler at first to isolate the effect of each of them, even though it may not be possible to vary them independently on an engine, nor will their effects be cumulative.

Consider pressure first. Figure 14.12 shows that increasing the boost pressure raises the NO concentration, at a constant charge air temperature and air/fuel ratio. This is not surprising, since the reaction rates are pressure, as well as temperature-sensitive. However, since power output rises as additional fuel is injected to maintain a constant air/fuel ratio, the brake specific NO emission is relatively constant. As expected, raising inlet air temperature, at constant pressure and air/fuel ratio, increases NO concentration and brake specific emission (figure 14.13, note logarithmic scale), since power output reduces slightly.

Consider next the effect of air/fuel ratio. Increasing air/fuel ratio has two effects: oxygen availability increases and combustion temperature decreases due to the energy absorbed by the extra air. The effect of air/fuel ratio on NO formation through reducing combustion temperature exceeds the opposing effect of increasing oxygen availability since local fuel/air ratio changes little in the spray. Thus NO formation decreases as air/fuel ratio is increased (weakened), at

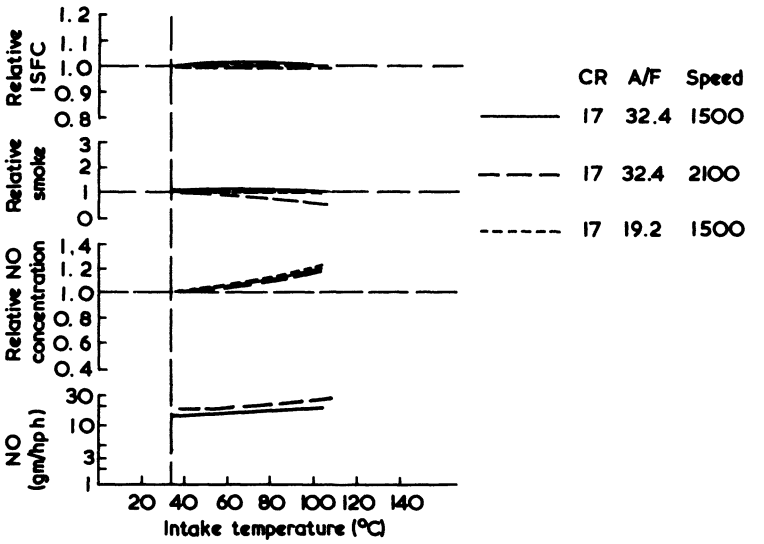

Figure 14.13 *The effect of inlet air temperature on emissions and economy [10]*

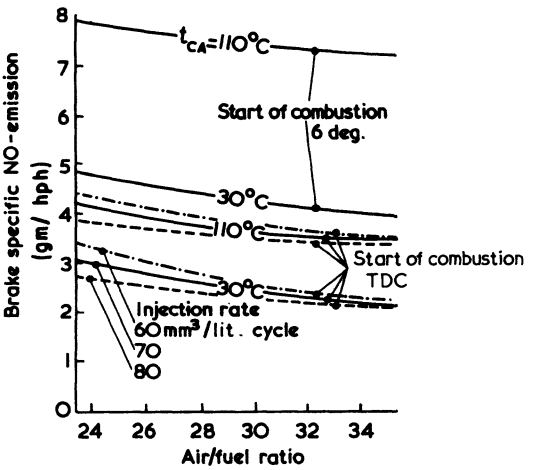

Figure 14.14 *The effect of charge air cooling on brake specific NO emission [11]*

a constant inlet air temperature. Figure 14.14 shows this effect at various constant values of air inlet temperature, injection timing (start of combustion) and injection rate.

The combined effects of pressure, temperature and air/fuel ratio may first be considered on an engine that is turbocharged to increase air/fuel ratio, not power output (a limiting case, no change in fuelling). An increase in temperature from 30 to 110 °C (figure 14.14) would accompany turbocharging to a boost pressure ratio of 2.0.1 (figure 9.3). The charge air density increase would be 1.5:1 (figure

9.5), increasing air/fuel ratio by 50 per cent. Figure 14.14 shows that the temperature rise due to turbocharging will have a much greater effect in raising brake specific NO than the benefit of the weaker fuel/air ratio, particularly at normal injection timing. At retarded injection timing the two opposing effects tend to cancel and indeed, only a small change in NO occurs at retarded timing, with a normal injection rate. Except in these special circumstances, increasing boost to reduce fuel/air ratio at a constant power output will significantly raise NO emission, due to the dominating effect of the accompanying inlet air temperature rise.

The other limiting case, turbocharging at constant air/fuel ratio to raise power output, increases brake specific NO emission by a greater amount.

14.6 Charge Air Cooling

Charge air cooling (chapter 9) may be used to increase inlet air density, air flow and power output, or to reduce air temperature and thermal loading if fuelling is not increased. In the latter case, NO will be reduced by the combined effects of reduced air temperature directly and the effect of a weaker fuel/air ratio on the combustion temperature. Thus charge air cooling can substantially reduce the NO emission from a turbocharged engine, if the rating of the engine remains unchanged. Relative to a naturally aspirated engine at the same rating, the large increase in air/fuel ratio will be enough to offset the effect of incomplete intercooling in many cases. Thus NO emission from the turbocharged and intercooled engine will be less than that from the naturally aspirated engine, provided that intercooling is reasonably effective. Smoke will obviously also be reduced, due to the weak fuel/air ratio. However, this is a highly artificial situation.

Turbocharging with charge air cooling is an expensive way of reducing NO emission, even though the reduction may be by up to 50 per cent. Invariably some increase in fuelling will be required to increase power output, for the system to be cost effective. Figure 14.15 shows the effect of charge air cooling to

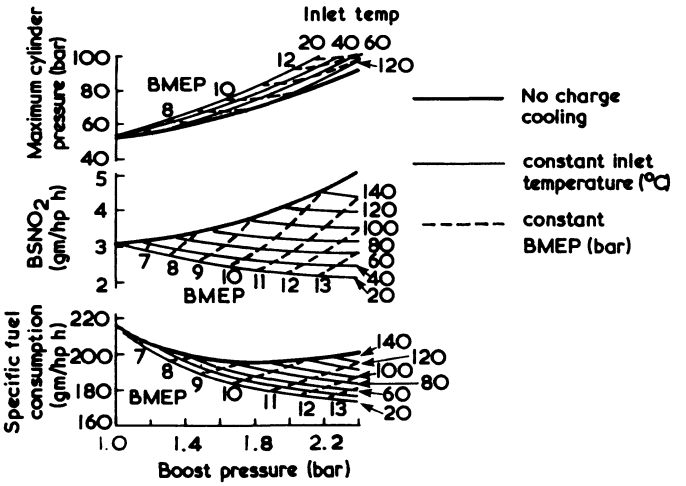

Figure 14.15 *The effect of charge cooling on emissions [12]*

different inlet temperatures on maximum cylinder pressure, brake specific NO and fuel consumption, at different levels of boost pressure and BMEP. As expected, with no charge cooling, NO increases with boost pressure if fuelling, and hence BMEP, is increased. Charge cooling will reverse this trend, provided that the cooler is effective enough to reduce the inlet air temperature below 80°C. Thus charge cooling can be used to raise power output without a corre sponding increase in NO emission, or to raise power output and reduce NO emission at the same time (on a brake specific basis), dependent on intercooler effectiveness and the temperature of the coolant. Clearly ambient air is a more attractive coolant than the cooling water of the engine, in respect of reducing NO emission.

In figure 14.16, HC + NO_x emissions are plotted against boost temperature at two engine speeds, from zero to full load. The HC emission is small with respect to the NO_x and may be discounted. The figure shows that charge cooling is more effective in reducing NO emission at high speed and load, when the boost temperature would otherwise be highest. At lower speeds and loads, the benefit is small. An intercooler of moderate effectiveness will reduce air temperature to

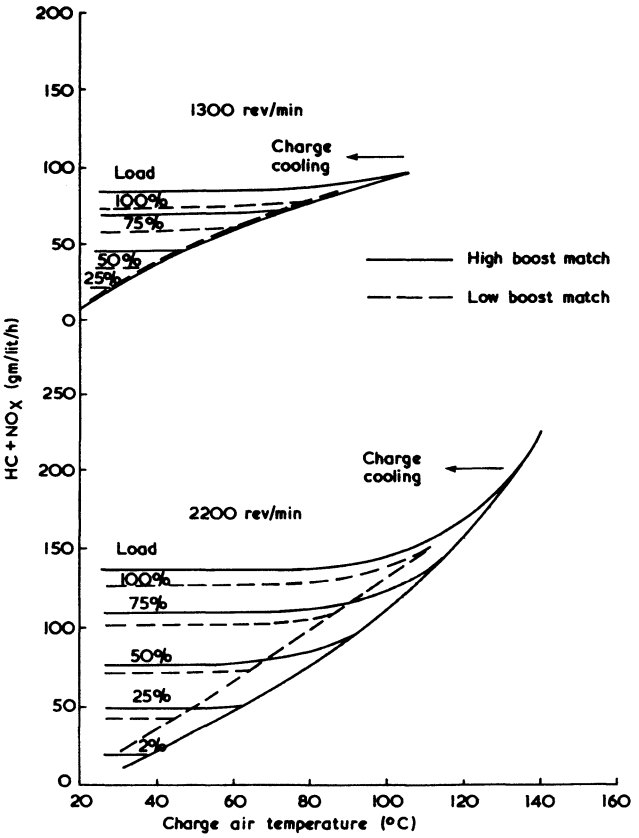

Figure 14.16 *The effect of charge air cooling on NO_x [11]*

80 °C with ambient air as the cooling medium. Further reduction of temperature will not be cost effective in terms of reducing NO emission. At low engine speeds, air flow reduces and the intercooler will become more effective, which is an aid to reducing low-speed smoke. Also shown in figure 14.16 are NO emissions at two levels of boost pressure, but the same fuelling. As expected the high-boost engine benefits more from charge cooling. However the increase in boost has raised NO emission even at the same inlet air temperature. No amount of charge cooling is enough to offset this trend.

The reduced temperature of charge cooling increases ignition delay from the short values associated with turbocharging alone. Thus the quantity of fuel too weak to burn at the edges of the fuel spray increases. This, together with the effect of reduced temperature on the oxidation reactions, increases the concentration of HC at high load. However, when the HC is expressed as a brake specific value, the increase in power output offsets this effect. At low speed and load the intercooler can over-cool, leading to excessively long ignition delay periods and, with a low compression ratio, poor combustion and excessive HC emissions.

14.7 Turbocharging with Retarded Injection

Retarding the timing of fuel injection and hence combustion is the simplest method of reducing the emission of NO (figure 14.17). The technique will shorten the ignition delay period since injection occurs closer to TDC with a correspondingly higher air temperature and pressure. In addition, since the major part of the combustion process takes place during expansion, further delay results in lower over-all temperatures and hence reduced NO formation. The technique can be combined with turbocharging and charge cooling to achieve very low brake specific NO levels, the turbocharger more than making up for power loss due to retarded injection. Figure 14.17 shows typical results of timing adjustment on direct and indirect (pre-chamber) engines in naturally aspirated, turbocharged and turbocharged and aftercooled form.

Consider first the brake specific NO_x emission. At standard timing (21° BTDC naturally aspirated, 18° turbocharged) the turbocharged version of the direct-injection engine emits slightly less NO than the naturally aspirated engine (due to later injection), while charge cooling is very effective in reducing NO further. At the same injection timing, the turbocharged engine has the highest $BSNO_x$ as expected, but this is not a normal situation. The same trend is followed as timing is retarded with progressively reducing brake specific NO emission. The penalty to be paid in specific fuel consumption becomes significant at very retarded timings. Late combustion means a shorter effective expansion stroke hence lower efficiency. Clearly the penalty of 8° retarding, for example, is unacceptable fuel consumption and a high smoke level. The unburnt hydrocarbon emission of the direct-injection engine is also increasing with retarded timing although it remains quite low on turbocharged engines. CO emission also increases but the level remains well below that considered objectionable in current legislation.

The conclusion is that if a turbocharged engine can be retarded mildly (5°) to achieve very low NO emission, without a smoke problem, the fuel consumption

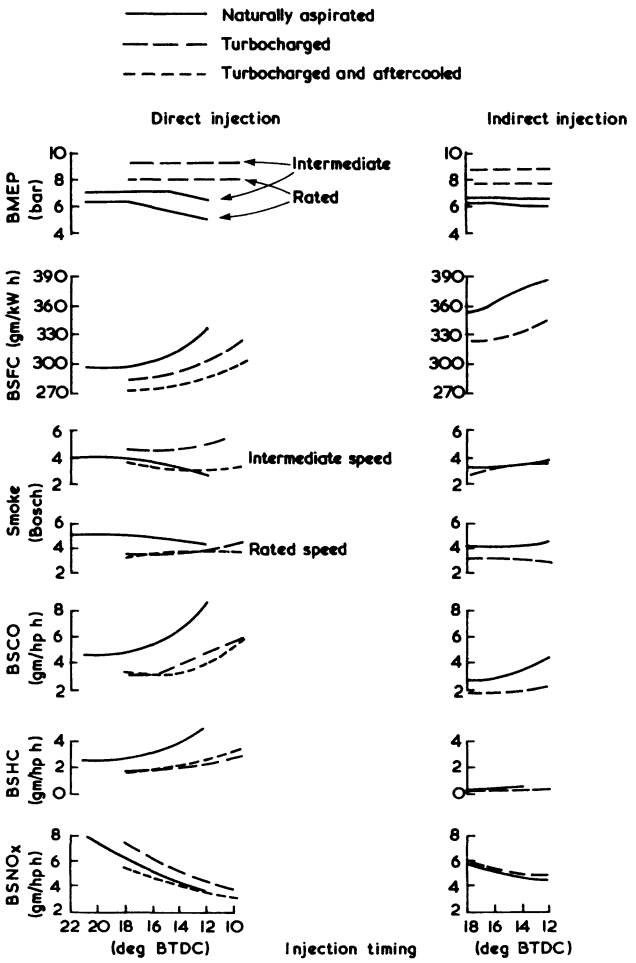

Figure 14.17 *The effect of retarded timing on emissions and performance of turbocharged engines (13 mode cycle unless stated) [13]*

penalty is not sufficient to eliminate its advantage over a naturally aspirated engine with normal timing. Furthermore, unlike the naturally aspirated engine with retarded timing, the turbocharger may be rematched to avoid derating. Less benefit is evident on the pre-chamber engine, but this has substantially lower emissions in its normal form. A somewhat greater over-all reduction in emissions could be obtained by using retarded, but more flexible timing (varying injection timing with engine speed and load).

Thus turbocharging may be used to offset the power and fuel consumption penalty of the naturally aspirated engine, when retarded for low NO emissions. Turbocharging improves the trade-off between NO, specific fuel consumption and exhaust smoke with retarded timings. Figure 14.18 illustrates this trade-off,

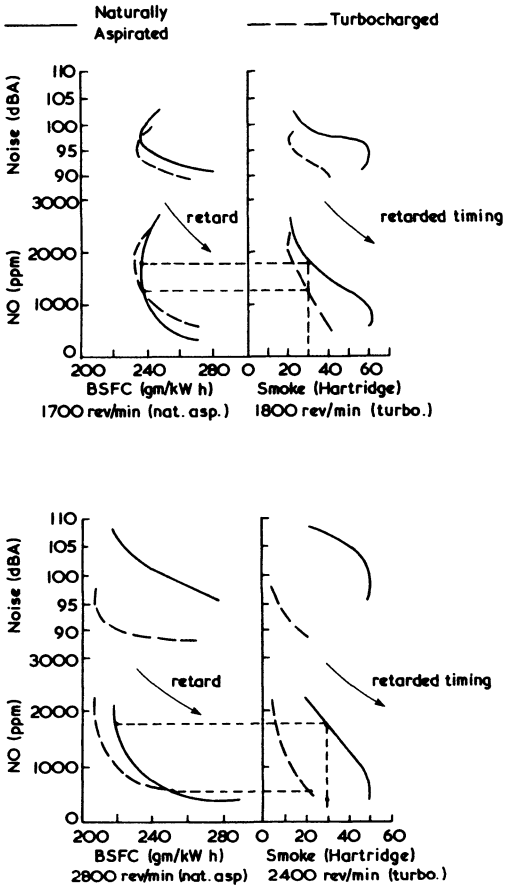

Figure 14.18 *The effect of turbocharging on the NO, specific fuel consumption, smoke and noise trade-off, with retarded timing [14]*

comparing average results from naturally aspirated engines at 8 bar maximum BMEP (21:1 air/fuel ratio) and turbocharged versions at 9.7 bar BMEP (25:1 air/fuel ratio). At the intermediate speed (1700 to 1800 rev/min) the NO against smoke trade-off improves with turbocharging but at maximum speeds benefits in the NO against smoke trade-off are greater. For a smoke limit of 30 Hartridge shown, the turbocharged engine can run further retarded with a substantial reduction in NO.

Whereas charge cooling and retarding injection both reduce NO through reducing combustion temperatures, their combined effects are not totally cumulative. Since the NO formation reactions are very temperature sensitive, additional temperature reduction achieved by combining these methods becomes progressively less effective. This can be seen in figure 14.14 where delaying combustion by 6° to TDC reduces the difference between NO emission at the two charge air temperatures of 110 and 30 °C.

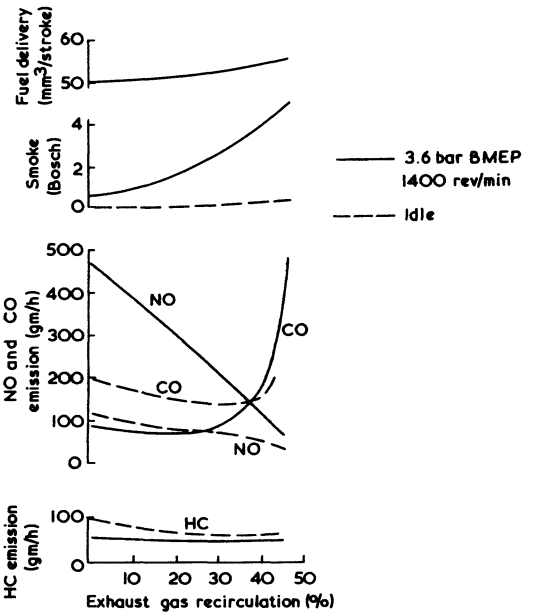

Figure 14.19 *The effect of exhaust gas recirculation on diesel emissions (naturally aspirated) [13]*

14.8 Turbocharging with Exhaust Gas Recirculation

Various other methods of reducing exhaust emission from diesel engines have been proposed. Exhaust gas recirculation is widely used on petrol engines. Figure 14.19 shows the effect of recirculating some exhaust gas on a naturally aspirated direct-injection diesel engine. The exhaust gas acts as an inert diluent, keeping peak temperature down by absorbing energy as it is heated from combustion. Clearly exhaust gas recirculation is very effective in reducing the emission of NO without increasing HC and CO emission. A substantial quantity (up to 30 per cent) may be recirculated with little increase in indicated specific fuel consumption but smoke increases and eventually CO also increases substantially with high exhaust gas recirculation rates. Thus exhaust gas recirculation cannot be used at full load, and the percentage of gas recirculated must vary with load. The smoke problem is aggravated by the need to increase fuelling to maintain BMEP with high rates of recirculation. Since smoke is a problem at the low-speed end of the operating range, exhaust gas recirculation can be used up to higher loads at higher speeds. It can be applied to turbocharged engines as well as naturally aspirated engines. However, fouling of the compressor and charge cooler by recirculated soot is a major problem, influencing the choice of position of the recirculation pipe and valve.

Exhaust gas recirculation from turbine exit to compressor intake may require a pressure depression butterfly valve at the air intake, to create the required pressure difference. If exhaust gas recirculation is taken from the exhaust mani-

fold before the turbine, it can be routed to intake or exit of the compressor. The exhaust gas will be hotter than if taken from after the turbine, but sufficient pressure is available. The advantage of recirculating into the inlet manifold at compressor exit is that it avoids build-up of oily sooty deposits otherwise found in the compressor. [15] However, the flow through the exhaust gas recirculation line will reduce the turbocharger speed at part load, which is undesirable from the viewpoint of subsequent engine acceleration.

Unfortunately exhaust gas recirculation increases particulate emission so the use of this technique depends on the allowable emissions of both. Figure 14.20 shows the performance and emissions of an engine in naturally aspirated and

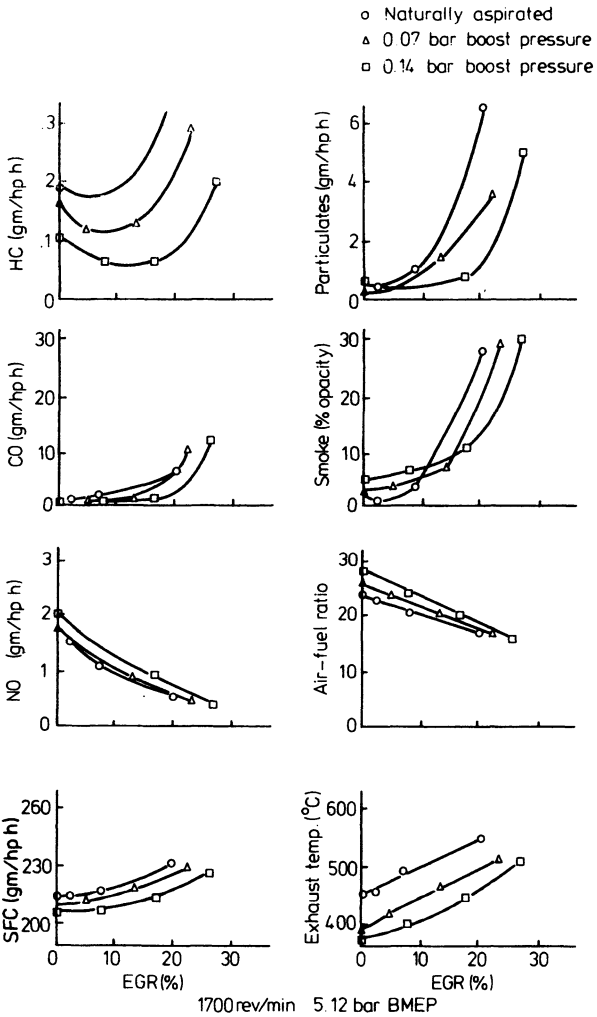

Figure 14.20 *Effect of turbocharging and exhaust gas recirculation on emissions and fuel consumption of swirl chamber diesel engine [16]*

turbocharged form, with exhaust gas recirculation. Increasing exhaust gas recirculation reduces NO_x emission whether naturally aspirated or midly turbocharged. However, turbocharging allows the exhaust gas recirculation rate to be increased for a specified HC, CO, smoke or particulate level. For example, for an exhaust particulate level of 1 g/hp h, the exhaust gas recirculation limit is 10 per cent in naturally aspirated form and 20 per cent with turbocharging.

14.9 Turbocharging with High Injection Rates

Increased injection rates are used to delay the onset of smoke as injection timing is retarded for low NO emission. Whether by changes in plunger size, cam profile, nozzle holes or injection pressure, increased injection rates result in more rapid early combustion. This is confirmed by the need to retard timing for minimum fuel consumption. Exhaust smoke becomes less sensitive to retarded timing as the air/fuel mixing rate increases. This is not surprising, since higher injection rates result in the accumulation of more fuel in the chamber prior to ignition. Thus more fuel is involved in the pre-mixed early stage of combustion and less remains for the smokey diffusion burning phase. In addition, more vigorous turbulent diffusion burning is an aid to burning up smoke.

It follows from the above that NO is likely to increase with higher injection rates, but fortunately the increase is small relative to the reduction achievable with retarded timing. Thus increased injection rates combined with retarded timing enable NO to be reduced without excessive smoke emission and little fuel consumption penalty. Figure 14.21 shows the NO, specific fuel consumption and smoke trade-offs for a turbocharged engine at different injection timings, rated and intermediate speed, with standard and increased injection pressure. The increase in injection rate resulting from the higher injection pressure, reduces smoke (at the intermediate speed) and allows injection to be retarded further reducing NO emission.

14.10 Other Methods of Pollutant Reduction

Water injection (in the inlet manifold or in emulsion with the fuel) is a powerful method of reducing NO emission, but its action is complex. Certainly it reduces temperature during combustion. Photographic evidence shows marked changes in the combustion process. However, practical problems have restricted its adoption.

Catalytic converters are widely used to oxidise CO and HC, and reduce NO emission on petrol engines. However, the very weak and cool exhaust gas of the diesel engine is a less favourable environment for catalysts, although virtually complete elimination of diesel hydrocarbon emission is possible.

14.11 Diesel Engine Noise

There are numerous sources of noise emission from diesel engines that combine

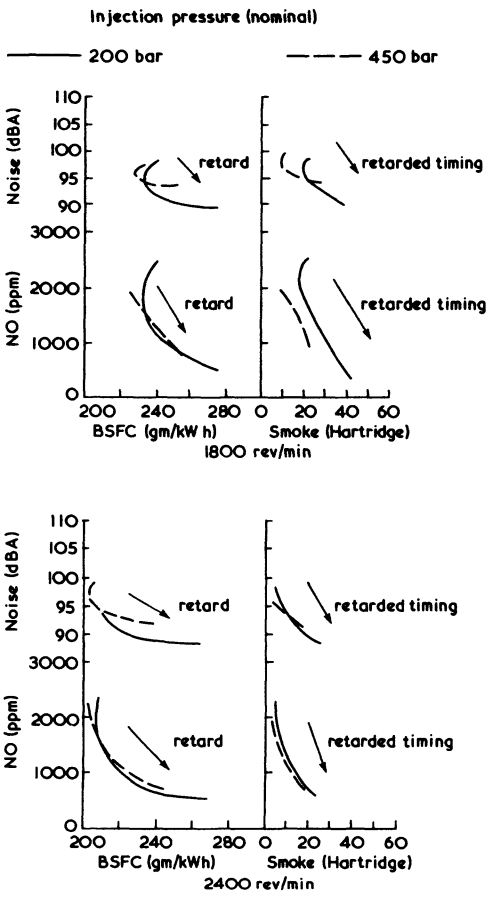

Figure 14.21 *The effect of increased injection rate on the NO, specific fuel consumption, and smoke trade-off with retarded timing (turbo-charged engine) [14]*

to produce the over-all noise pattern. The main noise sources are the exhaust and intake system due to the generation of large-amplitude pressure waves. However, these sources can generally be silenced. The remaining noise is emitted by vibrating surfaces. To reduce engine noise these surfaces must either be damped and/or the forces that excite the vibrations must be removed or attentuated. One such force is derived from the rapid rise in cylinder pressure (caused by rapid initial burning) at the start of combustion (figure 14.10) acting on the piston cylinder head and wall. The impact of this pressure rise is transmitted through the piston and connecting rod, then big end and main bearings to the engine structure which vibrates, generating noise. Other noise sources are caused by mechanical impacts, the most common being due to piston slap. timing gear rattle, the fuel injection system (injector closure), valve gear closure, etc.

Piston slap is the result of the piston moving (or tilting) from side to side in

the bore due to changes of inertia and gas pressure forces during the engine cycle. Timing gear rattle results from the sudden take-up of clearances between gear teeth due to the cyclic torque requirement of the camshaft and fuel injection pump. At particular engine speeds, a resonance may develop in the gear train causing excessive noise.

However, although turbocharging may have some influence on the above factors, the major influences are via combustion pressure rise generated noise, the engine intake and exhaust systems, noise radiated direct from the body of the turbocharger itself and piston slap.

A detailed analysis of engine noise is beyond the scope of this book. Priede [17] has presented a review of the subject, in detail. It is assumed that the reader is familiar with basic noise theory, and only information necessary to understand the effect of turbocharging on engine noise will be presented herein.

14.12 Air Inlet Noise

Air inlet system noise is generated by the action of the opening and closing of the inlet valves. The resultant air motion in the inlet manifold creates a pressure wave system that is heard as noise from the inlet. A second noise-generation mechanism is turbulence at the valve, this being a source of higher-frequency noise. The imposition of a compressor in the intake system of a turbocharged engine tends to damp down the heavy pulsations due to the intake process through the valves. This reduces low-frequency noise. However, the turbocharger compressor will generate high-frequency noise due to the high rotational speed and the blade passing frequency. It follows that the intake noise spectrum from a turbocharged engine is rather different from that of a naturally aspirated engine with reduced low-frequency noise, but greater noise at high frequency. Figure 14.22 illustrates this, the noise oscillogram being a high-frequency signal with no

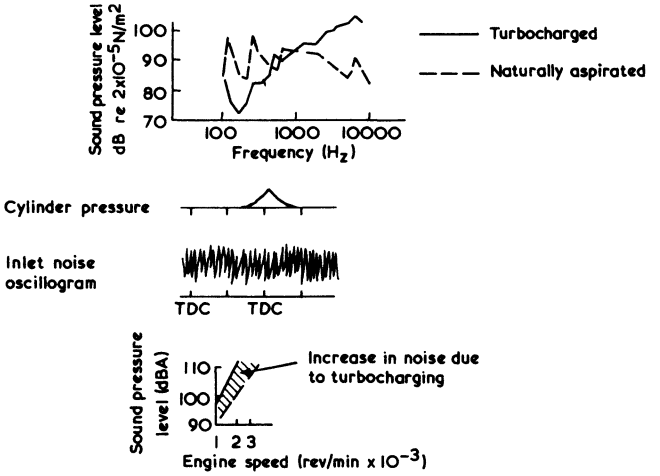

Figure 14.22 *The effect of turbocharging on inlet air noise [18]*

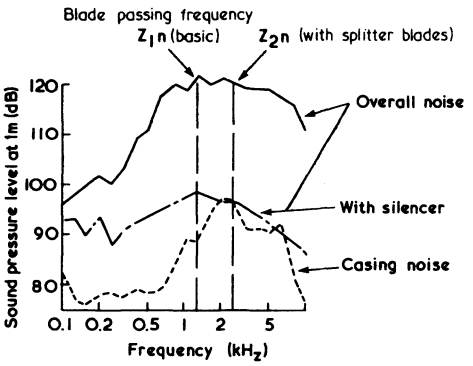

Figure 14.23 *Turbocharger noise and its reduction with inlet silencers [19]*

apparent dependence on the moment of inlet valve opening or closing, nor the instant of combustion. The increase in high-frequency noise results in a higher over-all noise level, particularly at high engine speeds when the turbocharger is rotating fast. Fortunately, this high-frequency noise is usually easier to attenuate through the silencer and/or intake filter. Figure 14.23 illustrates the effect of intake sound damping on over-all turbocharger noise from a MAN turbocharger. Note that intake noise dominates the over-all noise emission from the turbocharger, the noise from the casing alone being substantially less than the unsilenced intake.

Figure 14.24 shows the over-all noise spectrums measured by Hempel from three different sizes of turbochargers, one designed for slow two-stroke marine engines (Z576), others suitable for medium-speed four-stroke engines (NR20 and 34). All three have 18 compressor blades, 9 being splitter blades, starting part way through the impeller (see chapter 3). Although the maximum noise level occurs around the blade passing frequencies, a significant contribution to the over-all noise level can occur on either side of this maximum. Note that the use of splitter blades results in a lower peak noise than that generated by a normal type of 14-bladed compressor of the same size as the NR20.

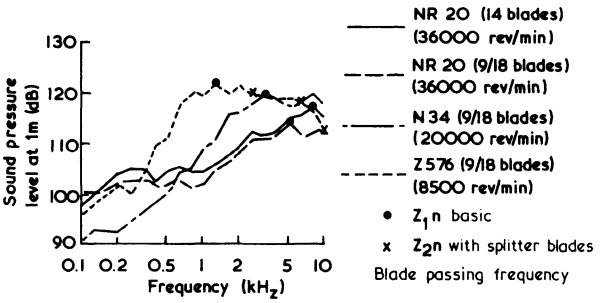

Figure 14.24 *Over-all noise spectrum from various turbochargers [19]*

Noise increases with rotational speed of the turbocharger hence the trend towards higher pressure ratios must be accompanied by increased efforts to attenuate noise. Two-stage turbocharging is attractive in this respect since the rotational speed of each unit is low and total noise emission is less than that of a single-stage unit at the same over-all pressure ratio.

In addition to the inlet noise from the compressor, and that radiated from the body of the turbocharger, noise is emitted from the compressor delivery, through the inlet manifold. This noise path can become significant at high pressure ratios but can be reduced by fitting absorbent panels (fitted with mineral wool, for example) to line the delivery path from compressor outlet to charge cooler inlet.

Rotary displacement compressors, (for example, Roots blowers), used for scavenging automotive two-stroke engines, are notorious as noise sources. Their intake noise can vary from 100 to 150 dB(A) over their working range and is often the predominant noise source on this type of engine.

14.13 Exhaust Noise

The exhaust noise from diesel engines is generated by the sudden expansion of combustion products from the cylinder into the exhaust manifold when the exhaust valve opens, and turbulence generated at the valve. The successive exhaust processes from the various cylinders set up a dynamic pressure wave system in the exhaust manifold. This is similar to that in the intake system except that the amplitude of the pressure waves is greater due to the high cylinder pressure at the point of exhaust valve opening. Figure 14.25 shows sound spectra from

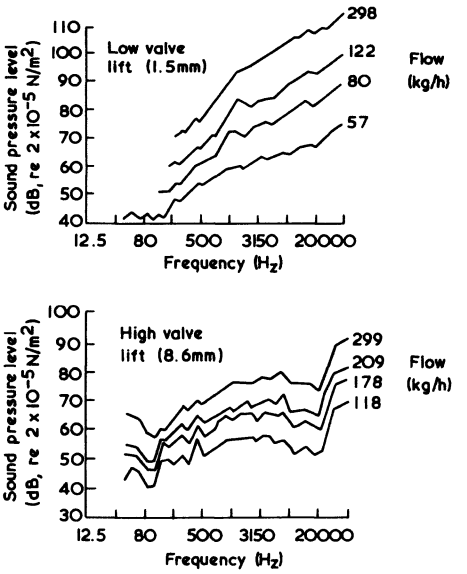

Figure 14.25 *Steady flow noise characteristics of a poppet valve [20]*

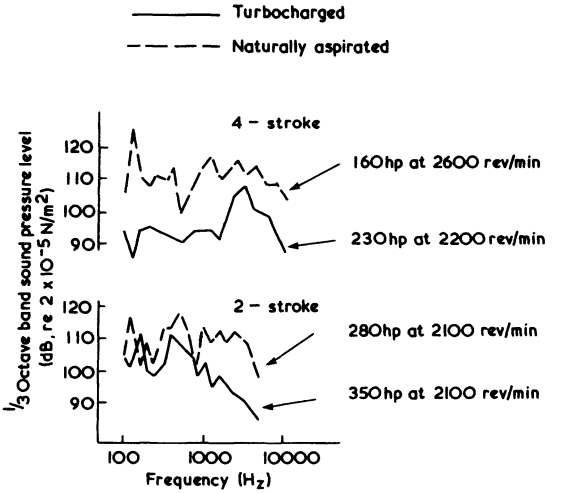

Figure 14.26 *The effect of turbocharging on noise from an unsilenced exhaust [18]*

steady flow tests on an exhaust valve at low and high lifts (with no turbocharger and an open exhaust). This illustrates the major contribution of turbulence-generated high-frequency noise, even though flow is subsonic except when valve lift is low and the mass flow rate high. Exhaust pulse frequency noise (low frequency) is less significant.

The use of a turbocharger substantially changes the exhaust noise of a diesel engine. By extracting energy from the exhaust gas through an expansion process, the amplitude of the pressure waves in the exhaust pipe is drastically reduced. Although the pressure diagram at the exit from the turbocharger will usually exhibit some flow unsteadiness, the variation is small if an exhaust pipe of large diameter with no major restriction, is fitted. Anderton and Duggal [18] have measured typical noise spectra from the exhaust of an unsilenced diesel engine (figure 14.26) in naturally aspirated and turbocharged forms. The over-all noise reduction at the rated engine speed is 8 to 10 dBA.

Since the noise emission is governed by the exhaust process from the cylinder, particularly the cylinder pressure at EVO, exhaust noise will be dependent on engine load, being greatest at full load. Although the turbocharger will substantially reduce exhaust noise and ease the problem of silencing, load dependence will still be apparent. The effect of the turbine blade passing frequency is not as apparent on the noise pattern as that usually exhibited in the intake system. Unsteady exhaust flow effects dominate.

14.14 Combustion-generated Noise

It has been stated that the rapid pressure rise during combustion results in the transmission of a force through to the engine structure resulting in vibration and

noise emission. It is this source of diesel engine noise that is usually dominant and, unfortunately, most difficult to reduce.

During the compression and combustion periods, the high cylinder pressure acts unidirectionally on the piston, connecting rod, crankshaft assembly. This force causes running clearances to be taken up, in the vertical (cylinder) direction. This force does not change direction when its magnitude is high, but the rapid change in magnitude sets up a vibrating system. The gas pressure excites the top part of the engine, such as the cylinder head, whereas the lower part of the structure reacts to the combined effects of gas pressure and the inertia force from moving parts. Each engine component deflects according to the time history of the exciting gas pressure force, but superimposed on this are vibrations at the natural frequency of the component part.

The mechanism of combustion-generated noise is shown in figure 14.27. The cylinder pressure diagram (A) is a pressure–time diagram. For noise analysis it is more conventient to convert this into a cylinder pressure level–frequency diagram (B), by Fourier analysis (the cylinder pressure diagram may be considered

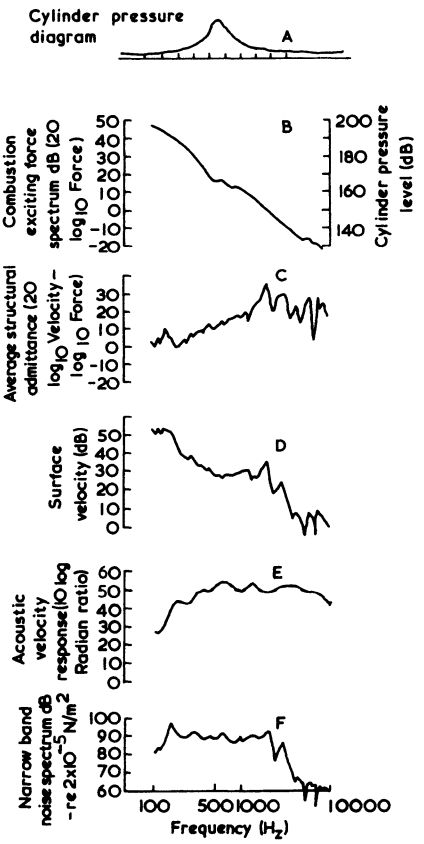

Figure 14.27 *Development of diesel combustion-generated noise [21]*

as an amalgamation of parts of pressure waves of different frequencies, whose pressure level varies with frequency). The low-frequency part of the diagram is usually a very wide peak centred around the frequency of the basic engine cycle, the magnitude being governed by peak pressure. In the middle part of the spectrum (500 to 3000 Hz), which acoustically is the more important part of the diagram, the slope is governed by the rapid pressure rise following the start of combustion. The high-frequency section is governed by small oscillations in the cylinder pressure diagram during combustion, which are believed to vary randomly from cycle to cycle.

The reaction of the engine to an exciting force (structural admittance) is shown as curve C, illustrating that the engine is more susceptible to the medium and high-frequency forces. Combining the exciting force (B) with the structural admittance (C), the amplitude of the engine surface velocity fluctuations resulting is shown as a function of frequency in D. The relationship between surface velocity and actual noise emission is governed by the generation of acoustic waves by the vibrating surface (acoustic velocity response E), which again is more susceptible to medium and high-frequency excitation. Hence the resultant narrow band noise spectrum shown in F is finally developed.

The human ear is more highly tuned to some frequencies than others, thus although the audible range extends from 20 to 2000 Hz, the lower end of this range is substantially attentuated. The 'A' rating noise scale (dBA) weighs the higher end of this frequency range more than any other frequencies and results in the dominant frequency band lying in the centre of the range shown in figure 14.27.

As a rough guide to the noise levels of diesel engines, Priede and his co-workers have correlated results from many conventional engines. The correlation is based on the assumption that the slope of the exciting force spectrum (figure 14.27B) is linear in the important frequency range. The average slope of this line for a range of engines [22] was found to be 30 dB/decade for naturally aspirated four 4-stroke diesels and 40 dB/decade for turbocharged four-stroke diesels. The effect of engine speed variation is to displace the force spectrum higher with increasing speed. The final correlation was also dependent on the bore of the cylinders.

(a) For four-stroke naturally aspirated engines

$$\text{dBA} = 30 \log_{10} N + 50 \log_{10} B - 515 \tag{14.1}$$

(b) For four-stroke turbocharged diesel engines

$$\text{dBA} = 40 \log_{10} N + 50 \log_{10} B - 87.8 \tag{14.2}$$

where

N = rated engine speed (rev/min)
B = cylinder bore (cm)
dBA = over-all noise level (1 m from side of engine)

Thus for a typical 14 cm bore engine with a rated speed of 2100 rev/min, these correlations give

105.5 dBA naturally aspirated
103.3 dBA turbocharged

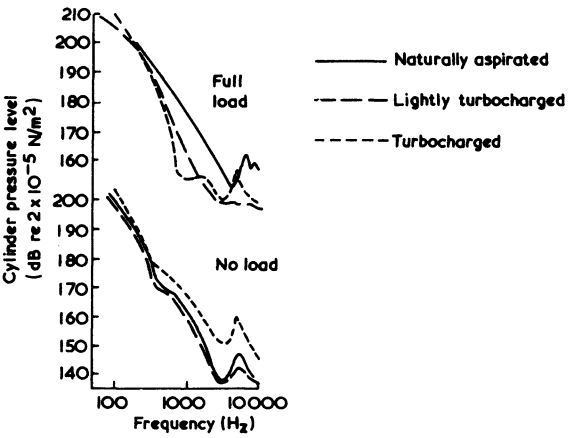

Figure 14.28 *The effect of turbocharging on the cylinder pressure spectra at rated speed [18]*

It must be emphasised that this is a wholly empirical correlation based on tests of standard engines. It will not be appropriate for low-noise engines, but it does illustrate the trend in noise variation with engine size (bore) and speed. This is useful, since it enables an estimated noise comparison to be made between a turbocharged engine and a naturally aspirated engine producing the same power due to an increase in bore size and/or speed to be made. Clearly the turbocharged engine should be significantly quieter.

The mechanism that results in the lower noise level of the turbocharged engine may be seen in figure 14.28. Consider the exciting force spectrum due to cylinder pressure of a six-cylinder four-stroke engine. Due to turbocharging the cylinder pressure is greater, hence the amplitude of the low-frequency exciting force is high. However, due to the normal reduction in the ignition delay period with turbocharging (itself due to the increase in temperature and pressure of the air compressed in the cylinders) the rate of pressure rise following ignition is less severe. Thus the amplitude of the higher-frequency components (around 1000 Hz) is reduced. Thus turbocharging increases low-frequency noise but reduces noise in the important frequency range. The effect of the increase in exciting forces at low frequency is masked by the lower response of the engine structure at low frequencies and the low-frequency noise attenuation of the human ear.

The over-all noise emission from the turbocharged engine will depend on how much mechanical noise is also present. This may increase with turbocharging. However, typical over-all reductions due to turbocharging are 3 to 6 dBA. Combustion noise dominated the results from the naturally aspirated engines in figure 14.26, but mechanical noise was significantly loud to exert an influence on the over-all noise level when turbocharged. If the mechanical noise could have been reduced, Anderton and Duggal [18] predicted the noise reduction due to turbocharging to be much greater (figure 14.29). These results were obtained at rated speed and load. At lower speeds and load, when the boost pressure is lower,

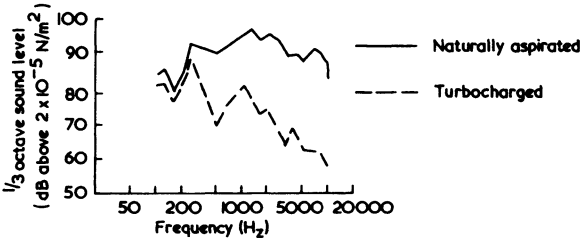

Figure 14.29 *Predicted combustion-generated noise alone [18]*

the difference between naturally aspirated and turbocharged engines is significantly less since the reduction in ignition delay is smaller. At no load (figure 14.28, lower) the beneficial effects of reduced ignition delay are absent and the turbocharged engine is as noisy or noisier than a naturally aspirated engine. This is important in urban driving conditions, where the noise problem is most severe, since the engine will be idling or at low load for long periods of time. [23]

When accelerating, the engine will experience a full load quantity of injected fuel but the boost pressure and temperature are low due to turbocharger lag. Ignition delay will be long and combustion-generated noise will be greater than that developed by the engine when running steadily at full load, especially at the start of acceleration. This is shown by Watanabe *et al.*, [24] figure 14.30.

Indirect-injection diesel engines, at full load, are quieter than direct-injection engines, due to shorter ignition delay, but the noise reduction from turbocharging is smaller. Spark-ignition combustion systems are substantially quieter. Figure 14.31 compares full-load over-all noise levels for a range of engine types and sizes.

The fact that engine noise increases substantially with speed (equations 14.1 and 14.2) means that reducing rated speed is a powerful noise-reduction tool. When combined with turbocharging, to regain power lost due to the lower speed, the result is a considerable improvement. The lower diagram of figure 14.18 indi-

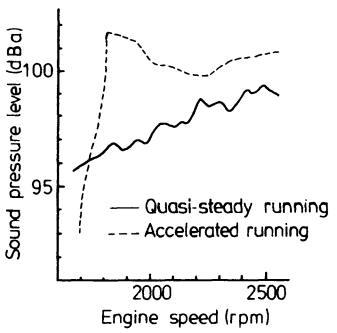

Figure 14.30 *Engine noise when accelerating and running steadily, turbocharged [24]*

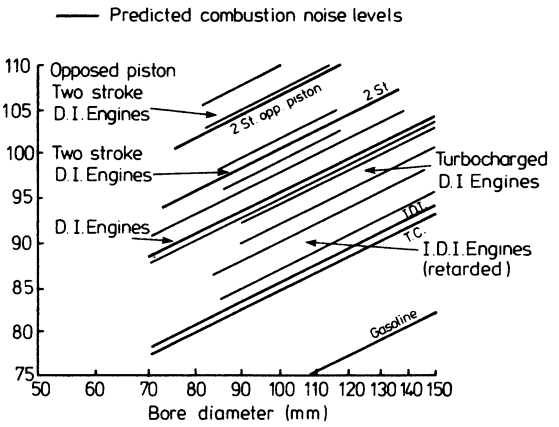

Figure 14.31 *Measured and predicted over-all noise against bore size for engines in the various groups at 2000 rev/min [25]*

cates the substantial gain in the noise, smoke, fuel consumption trade-off when comparing a turbocharged engine derated to 2400 rev/min relative to the naturally aspirated version, rated at 2800 rev/min.

14.15 Mechanical Noise

Mechanical noise is due to clearances between parts, such as bearings and the piston and liner, that are taken up by movement during engine operation. Impacts in the crankshaft bearings have been shown to be the major cause of mechanical noise in petrol engines operating at high speed. [26] Diesel engines usually require greater piston-to-liner clearances than petrol engines and are subjected to higher maximum cylinder pressure. Figure 14.32 shows the change in direction of the piston sideways force as the piston moves past TDC. The sideways force is

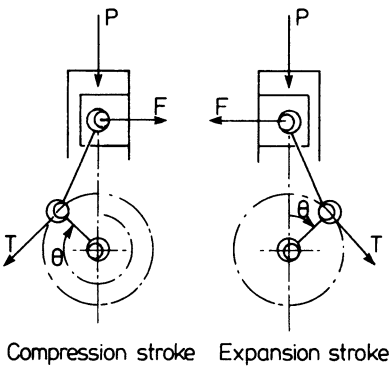

Figure 14.32 *Piston impact forces due to change of direction at TDC [27]*

proportional to cylinder pressure, and causes the piston to move across the bore and impact the liner, a noise-generating mechanism. Due to high cylinder pressure the mechanical noise from diesel engines is usually dominated by piston slap (its impact on the liner), rather than crankshaft bearing impacts. [27]

Piston slap forces are greatest when the piston moves sideways under a large pressure, namely at TDC. Since turbocharging increases the maximum cylinder pressure (it is rare that the compression ratio is lowered enough to offset the effect of high boost entirely, relative to a naturally aspirated engine), it will increase mechanical noise. Since piston slap forces are also a function of engine speed, [27] this effect will be most apparent on small high-speed diesel engines.

References

1. M. Meguerdichian and N. Watson, Predication of mixture formation and heat release in diesel engines, *SAE 780225* (1978)
2. G. Greeves, I.M. Khan, C.H.T. Wang and I. Fenne, Origins of hydrocarbon emissions from diesel engines, *SAE 770259* (1977)
3. D. Nightingale, A fundamental investigation into the problem of NO formation in diesel engines, *SAE 750848* (1975)
4. N.A. Henein, Analysis of pollutant formation and control and fuel economy in diesel engines, *Prog. Energy Combust. Sci.*, **1** (1976) pp. 165-207
5. D. Broome and I.M. Khan, The mechanism of soot release from combustion of hydrocarbon fuels with particular reference to the diesel engine, *Proc. Inst. Mech. Engrs*, Paper C140/71 (1971)
6. I.M. Kahn, Formation and combustion of carbon in a diesel engine, *Proc. Inst. Mech. Engr*, **184**, Pt.3J (1969/70)
7. P.M. Torpey, M.J. Whitehead and M. Wright, Experiments in the control of diesel emissions, *Proc. Inst. Mech. Engrs*, Air pollution control in transport engines, Paper C124/71 (1971)
8. S.W. Savery, R.A. Matula and T. Asmus, Progress in diesel odour research, *SAE 740213* (1974)
9. J.M. Perez and E.W. Landen, Exhaust emission characteristics of precombustion chamber engine, *SAE 680421* (1968)
10. R.P. Wilson, E.B. Muir and F.A. Pellicciotti, Emissions study of a single cylinder diesel engine, *SAE 740123* (1974)
11. H. Hardenberg and G. Fraenkle, The effect of charge air cooling on exhaust emissions and power output of turbocharged diesel engines, Paper C71/78, Turbocharging and Turbochargers Conference, *Inst. Mech. Engrs* (London, 1978)
12. E. Schreiber and R. Cichocki, Der Entwicklungsstand schadstaffarmer Fahrzeug-Dieselmotoren, *Auto-tech. Z.*, 77, No. 3 (1975)
13. R. Pischinger and W. Cartellieri, Combustion system parameters and their effect on diessel engine exhaust emission, *SAE 720756* (1972)
14. M.F. Russel and H.C. Grigg, Diesel engine fuel economy, emission and noise, Land Transport Engines, *Proc. Inst. Mech. Engrs* (January, 1977)
15. C.C.J. French and D.A. Pike, Diesel engined, light duty vehicles for an emission controlled environment, *SAE 790761* (1979)
16. W.R. Wade, Light-duty NO_x-HC-Particulate trade-off studies, *SAE 800335*, *Diesel Combustion and Emissions, SP86* (1980)
17. T. Priede, In search of origins of engine noise, *SAE 800534* (1980)

18. D. Anderton and V.K. Duggal, Effect of turbocharging on diesel engine noise, emissions and performance, *SAE 756797* (1975)
19. R.E. Wolfgang Hempel, Does turbocharging increase diesel engine noise? – Observations on the generation, emission and reduction of diesel engine noise, *SAE 680406* (1968)
20. T.J. Williams and J.B. Cox, The influence of exhaust poppet valve gas flow on reciprocating engine noise, *Proc. Inst. Mech. Engrs*, **189**, No. 45/75 (1975)
21. D. Anderton and J. Baker, Influence of operating cycle on noise of diesel engines, *SAE 730241* (1973)
22. C.M.P. Chan and D. Anderton, The correlation of machine structure surface vibration and radiated noise, Internoise 72 Proceedings, Washington DC (1972)
23. G.J. Hawksley and D. Anderton, Studies into combustion and noise in turbocharged engines, Paper C72/78, Turbocharging and Turbochargers Conference, *Inst. Mech. Engrs* (London, 1978)
24. Y. Watenabe H. Fujisaki and T. Tsuda, D.I. diesel engine becomes noisier at acceleration – the transient noise characteristics of diesel engine, *SAE 790269, SAE Diesel Engine Noise Conference, SP80* (February 1979)
25. D. Anderton, Relation between combustion system and engine noise, *SAE 790270, SAE Diesel Engine Noise Conference, SP80* (February 1979)
26. J.A. Raaf and E.C. Grover, A primary noise generation mechanism in petrol engines, *Proc. Inst. Mech. Engrs*, paper C320 (1973)
27. N. Lalor, E.C. Grover and T. Priede, Engine noise due to mechanical impacts at pistons and bearings, *SAE 800402* (1980)

15

Modelling

15.1 Introduction

The procedure of matching the turbocharger to a new design or an uprated engine can be time-consuming and laborious. If the engine in question is a large industrial prototype it will also be very expensive. It follows that if an analytical method is available for calculating performance with different turbocharger matches, then actual engine testing may begin with a turbocharger close to the optimum match. Development time, and hence cost, is reduced.

This type of model can be put to much wider use. For example, in the planning stages of a new engine, a suitable model may be used to estimate performance at different boost pressures and to calculate the resultant mechanical and thermal stresses. In this way the swept volume needed to produce the required power output with reliability may be calculated. Suitable programs can also be used to optimise valve timing, to compare performance with pulse or constant pressure turbocharging, to design the exhaust manifolds for the optimum use of exhaust pulse energy and to estimate performance at altitude.

The models that are available range from semi-empirical matching calculations to comprehensive analysis of the fluid and thermodynamic processes that take place in an engine. The usefulness, accuracy and running costs of these computer models vary tremendously. Generally the manufacturer of a mass-produced small engine may find it much cheaper to adopt a 'trial and error' type of procedure during test development of an engine. This is never the case with a very large, and therefore expensive, engine. However, in both cases, the first prototype represents a substantial investment. Major changes in the light of development experience are extremely costly in time and money. In consequence it is more important for the manufacturer of a large engine to get the design right at the first prototype stage. In contrast, however, the cost of improvements made after production has started, will be greater for the mass producer. Both types of manufacturer will find analytical models useful. The difference is that the manufacturer of large engines will find them essential and will benefit most from the more comprehensive models.

15.2 Simple Matching Calculation Techniques

Simple semi-empirical models may be used to start the turbocharger matching

process. The objective is to establish a sensible choice of turbocharger assembly for initial test bed work. The ability to do this competently will reduce development time.

It will be easier to predict the performance of a constant pressure turbocharging system than the pulse system. Simple methods are based on the constant pressure model, but are frequently used for pulse turbocharged engines by introducing empirical factors to account for the utilisation of pulse energy.

With constant pressure turbocharging (from equation 6.1) the compressor-turbine energy balance is

$$[(P_2/P_1)^{(\gamma_a-1)/\gamma_a} - 1]\, T_1 c_{p_a} = [1 - (P_4/P_3)^{(\gamma_e-1)/\gamma_e}]\, T_3 c_{p_e} \times (1 + \dot{m}_f/\dot{m}_a)\, \eta_c \eta_t \eta_{mech} \qquad (15.1)$$

where subscripts 1, 2, 3 and 4 denote compressor inlet, exit, turbine inlet and exit respectively. This equation may be linked to experimental engine test results for the purpose of turbocharger matching.

Usually a desired compressor pressure ratio will first be estimated. A suitable combination of turbocharger components required to achieve that boost pressure at the specified engine speed and fuelling is required. The calculation will be iterative, since several estimates of certain parameters are required. A typical procedure for a four-stroke engine might be as follows.

(1) Estimate the pressure ratio of the compressor (P_2/P_1).

(2) Assume a realistic value of compressor efficiency (η_c), calculate the inlet manifold temperature (T_2) and hence density, using the perfect gas law ($\rho_2 = P_2/RT_2$).

(3) Assume a realistic value for the volumetric efficiency (η_{vol}, figure 15.1) of the engine (based on inlet manifold density) and calculate the air flow rate ($\dot{m}_a = (N/2)\rho\, V_{sw}\, \eta_{vol}$).

(4) Assume a realistic minimum air/fuel ratio for the type of diesel engine involved (for example, 25:1), and hence estimate the temperature rise ($T_3 - T_2$) across the engine (figure 15.2). Calculate the turbine inlet temperature (T_3).

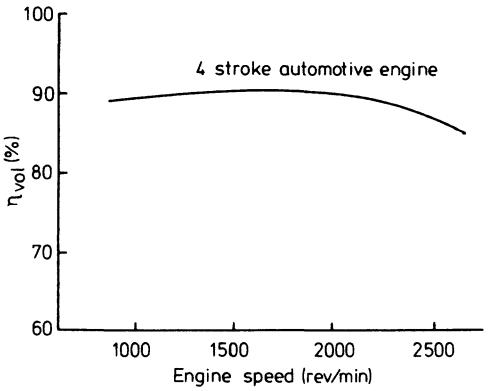

Figure 15.1 *Volumetric efficiency curve*

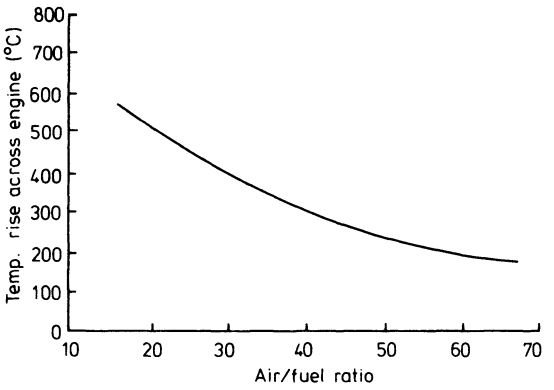

Figure 15.2 *Temperature rise across the engine*

(5) Estimate the turbine efficiency (η_t), or the over-all efficiency of the turbocharger, from manufacturers' data or previous experience with similar machines (chapters 4 and 5). The turbine efficiency term will usually include the mechanical efficiency. Calculate the turbine inlet pressure (P_3) from the energy balance (equation 15.1), assuming an exhaust pressure (P_4) slightly above atmospheric.

(6) Check that the pressure drop between the inlet and exhaust manifold ($P_2 - P_3$) is adequate for good scavenging or minimum pumping work during the gas exchange period.

(7) Calculate the mass flow parameter for the turbine ($\dot{m}_e\sqrt{(T_3)}/P_3$, where $\dot{m}_e = \dot{m}_a + \dot{m}_f$). Choose a turbine build whose swallowing capacity curve (figure 15.3) passes through (or close to) the point defined by the calculated values of expansion ratio (P_3/P_4) and mass flow parameter ($\dot{m}_e\sqrt{(T_3)}/P_3$).

(8) Calculate the mass flow parameter of the compressor ($\dot{m}_a\sqrt{(T_1)}/P_1$). Choose a compressor build such that the values of compression ratio and mass

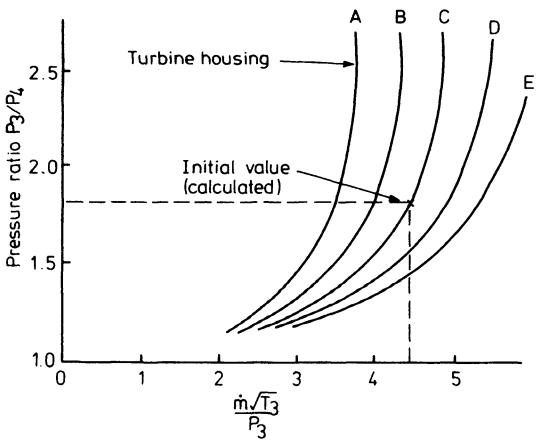

Figure 15.3 *Turbine 'swallowing capacity' curve*

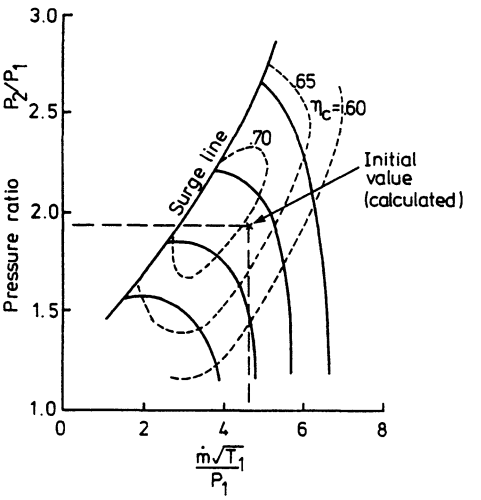

Figure 15.4 *Compressor characteristic*

flow parameter fix a point in the required area of the map (figure 15.4), taking account of efficiency and surge margin.

(9) Check that the product of compressor and turbine efficiencies at the operating point is compatible with that assumed. Adjust and recalculate if necessary.

Since many assumptions have been made in the above procedure, it follows that the answer will be an approximation. Many firms use their own variants of the procedure in an effort to improve accuracy or purely for their own convenience. Some techniques for improving the simple matching calculation rely heavily on a sufficient fund of experimental data under various engine conditions. These, and other techniques, will be discussed later.

Although the basic matching calculation outlined above is based on the assumption of constant pressure turbocharging, it can, with care, be extended to include pulse turbocharging. A quasi-steady state simulation is used, based on mean values of the fluctuating turbine inlet temperature and pressure. Thus the temperature rise term will be a mean of that actually occurring on a pulse turbocharged engine.

Several errors are introduced by this approach. Firstly, the turbine approach velocity will be ignored, which can cause significant errors in the mass flow rate and turbine energy calcualtion. Secondly, the calculated turbine mass flow parameter and pressure ratio will be based on time-averaged values of pressure, temperature and mass flow rate, rather than an average of $\dot{m}\sqrt{(T_3)}/P_3$ and mass flow averaged pressure ratio. The total error involved will depend on the amplitude and shape of the pressure fluctuations, the number of cylinders connected to each branch of the exhaust manifold, gas velocities, etc. Wallace and Cave [1] have used the method and claim little error. However, it is common to use a 'correcting factor', based on experimental data, to modify the turbine efficiency to produce an 'apparent pulse turbine efficiency'. [2] This apparent turbine

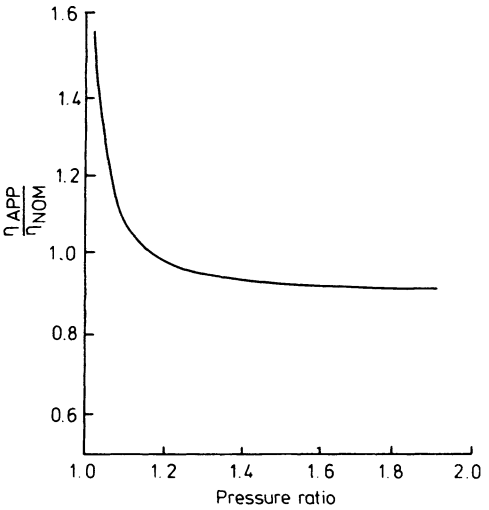

Figure 15.5 *Ratio of apparent turbine efficiency (under pulse conditions) to steady flow value*

efficiency may vary with speed and load, since the amplitude of the pressure fluctuations will not be constant (figure 15.5). The fact that the apparent efficiency exceeds 100 per cent at low speed is an indication that the energy available at the turbine with pulse turbocharging greatly exceeds that obtained with a constant pressure system under these conditions.

The numerical value of the apparent pulse turbine efficiency will naturally vary from one engine to another, since the cumulative effects of several parameters are hidden within it (particularly variation of pulse amplitude and frequency).

Improvements to the basic model largely consist of methods of improving the way certain parameters are used in the calculation. For example, the principal weakness of using the volumetric efficiency concept is that it becomes rather meaningless on engines which have significant scavenge air flow. The effectiveness of scavenging will depend on the instantaneous pressure difference between inlet and exhaust pipes during the valve overlap period, hence the 'volumetric efficiency' will be effected by the flow area of the valves and turbine. If sufficient data is available (sometimes from tests with simulated turbocharging), experimental air flow rates may be used directly (figure 15.6).

The temperature rise term $(T_3 - T_2)$ will show some variation with factors other than air/fuel ratio, such as the amount of scavenge air. This can be shown experimentally by plotting the temperature rise against boost pressure (or boost/exhaust pressure) for various air/fuel ratios (figure 15.7).

Simple matching methods may usefully be extended to estimate the power output of proposed engine designs or existing designs in uprated form. The fuel flow and boost pressure (P_2) are commonly used as linking factors to BMEP (figure 15.8), via experimental data from similar engines. If data of this type is

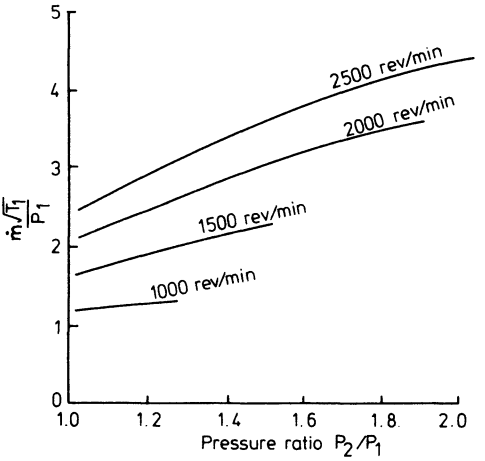

Figure 15.6 *Engine air flow rate curve*

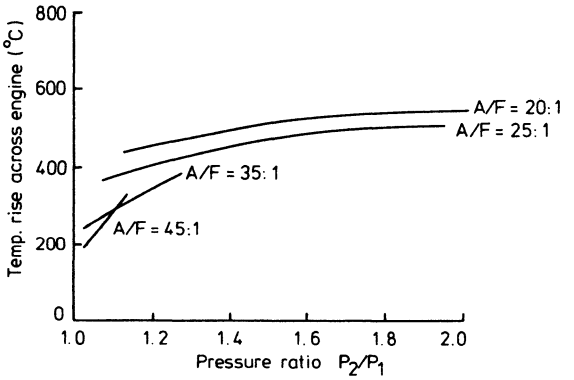

Figure 15.7 *Temperature rise across engine as a function of air/fuel ratio and compressor pressure ratio*

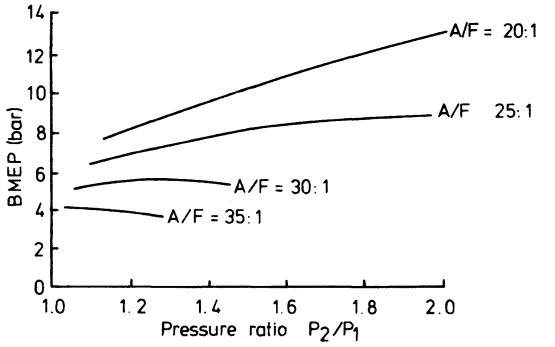

Figure 15.8 *BMEP as a function of air/fuel ratio and compressor pressure ratio*

not available, an alternative is to use the simple air standard (limited pressure) diesel cycle analysis. [1] The efficiency of this cycle is shown as a function of compression ratio and 'air/fuel' ratio in figure 15.9. Since this is an ideal closed thermodynamic cycle, the indicated power output will exceed that obtained in practice. This may be modified by a 'diagram efficiency' term relating actual to ideal indicated performance (figure 15.10). To evaluate the actual power output, the frictional and pumping losses must be estimated and subtracted (see section 15.11).

The methods outlined above must be modified for those two-stroke engines without positive displacement scavenge pumps or four-stroke engines with wide

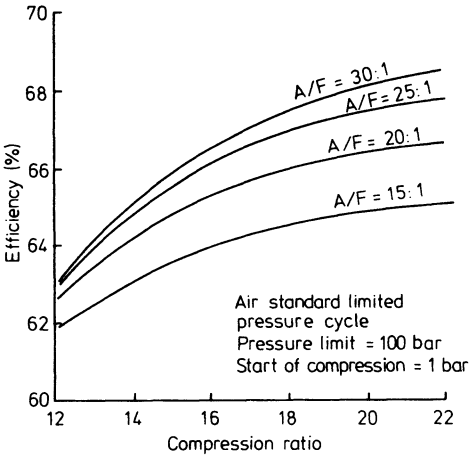

Figure 15.9 *Efficiency of the air standard limited pressure diesel cycle*

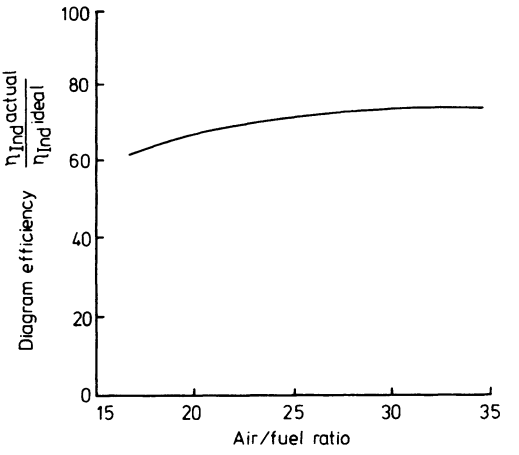

Figure 15.10 *Diagram efficiency: the ratio of actual to ideal indicated cycle efficiencies*

valve overlap. The air flow through two-stroke engines will be governed by the pressure ratio between inlet and exhaust manifolds. Thus, for air flow calculations, the engine can be considered as a flow restriction, or orifice.

The air mass flow rate is calculated from orifice flow theory for compressible (equation 15.2) or incompressible flow if the pressure difference is very small (equation 15.3).

$$\dot{m} = Cd\,A\sqrt{\{[2\gamma/(\gamma-1)]P_2\rho_2\,[(P_3/P_2)^{2/\gamma} - (P_3/P_2)^{(\gamma+1)/\gamma}]\}} \qquad (15.2)$$

(compressible flow) or

$$\dot{m} = Cd\,A\sqrt{[2\rho_2(P_2 - P_3)]} \qquad (15.3)$$

(incompressible flow)

An appropriate geometric flow area (A) is not easy to define, since the flow situation is analogous to two orifices in series, having time-variant flow areas. An arbitrary but commonly used datum area is the nominal total piston area (a discharge coefficient of unity therefore has no physical meaning). Figure 15.11 shows typical experimental data for the discharge coefficient (Cd). Alternatively, experimental air flow data can be plotted directly, against inlet/exhaust pressure ratio.

The air flow characteristics of four-stroke engines with large valve overlap are dependent on speed in the normal way, and inlet/exhaust pressure ratio during the scavenge period. The air flow can therefore be divided into two components: trapped (in the cylinders, speed dependent) and scavenge flow. The volumetric efficiency presentation (figure 15.1) can be used for the trapped component, while the two-stroke type orifice model (figure 15.11) is appropriate for the scavenge component.

Jenny [3] proposed a simple approximate method of establishing the effective flow area for scavenge flow during valve overlap on four-stroke engines. Figure 15.12 shows the effective valve area versus time diagrams for exhaust and inlet valves during overlap. The effective area of these two orifices placed in series is

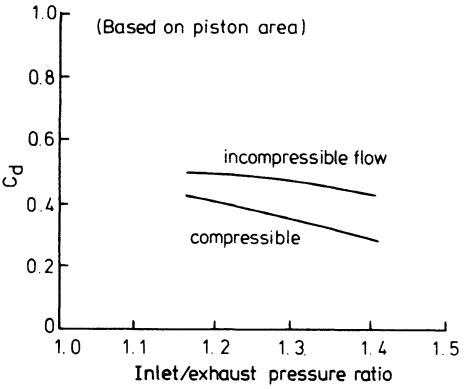

Figure 15.11 *Overall valve/port discharge coefficient for an opposed piston two-stroke engine*

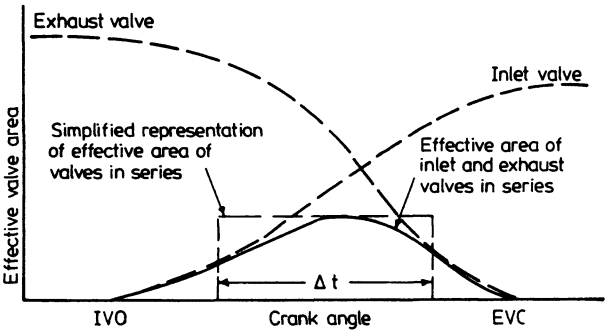

Figure 15.12 *Effective valve area during valve overlap period [3]*

also shown. Jenny proposed using a constant scavenge flow area, of magnitude equal to the maximum effective area of the two valves in series, but whose opening duration was shorter than the complete valve overlap period. This duration is calculated to produce the same integral under the area-time diagram as the two valves in series. The method has the merit of simplicity in use.

15.3 Quasi-steady Methods

The major limitation of the simple methods described above is the heavy reliance on a large fund of accurate engine data, over a wide range of operation. More sophisticated computer-based models are now widely used as a more accurate and informative alternative. These models follow the fluid mechanic and thermodynamic processes to which the air and fuel entering the engine are subjected. They are more fundamental and, as a result, more complex.

Unfortunately, since the turbocharged diesel engine is such a complex device, numerous approximations and simplifications must be made to achieve a solution. Some of these simplifications are introduced due to a lack of knowledge, but others result from the practical limits of computer storage and computing cost. It follows that accuracy must be weighed against complexity and cost, and one predictive program may not be ideal for differing applications. Two models will be described here, although variants will be mentioned. These models differ in only one important respect yet, as will be seen, this introduces a considerable difference in computing time and cost.

The major factor that governs the complexity of the processes occurring in the internal combustion engine is that all processes are unsteady (time variant). The simple models described previously average the effects of unsteady flow in the (experimental) input data. In a more sophisticated model, unsteady phenomenon must be modelled realistically. This is achieved by assuming quasi-steady flow (that is, that at any instant, the flow behaves in the same manner as if the flow were steady). Usually the calculation proceeds in a series of very short time steps (for example, 1 ° crank angle), it being assumed that the rate of change of relevant parameters (such as mass) remains constant for that time step only.

The error introduced by this assumption is difficult to estimate, but may be divided into two components. The first is a function of the size of the time step. Clearly the shorter the step the less the numerical error. The effect of the step size error may be evaluated, and the step size reduced if necessary. The second error is inherent in the basic assumption of quasi-steady flow, and cannot easily be determined; fortunately it does not usually introduce a major error.

Before considering details of quasi-steady performance and matching programs, it is helpful to consider the potential uses to which the program may be put. Since a detailed study of the fluid mechanics and thermodynamics is involved, the comprehensive nature of the model enables investigations other than purely matching calculations to be performed. Examples are:

(1) to investigate major design options (for example, the choice between pulse and constant pressure turbocharging, single or two-stage systems at high BMEP);
(2) to optimise aspects of design via parametric studies (for example, valve timing or exhaust manifold design with the pulse system);
(3) to predict cylinder pressure for component stress calculations;
(4) to predict component temperatures and hence thermal loading.

The over-all performance prediction program may be broken down into certain component parts (or models of specific processes) for simplicity. These component parts are shown diagrammatically in figure 15.13; they include

(1) turbocharger compressor
(2) charge cooler, if fitted
(3) inlet manifold or air chest
(4) inlet valve or port
(5) cylinders
(6) exhaust valve or port
(7) exhaust manifold system
(8) turbocharger turbine.

In addition models must be developed for certain processes, namely

(9) combustion
(10) heat transfer from the hot gases to walls
(11) property relationships for the working gas
(12) power loss to friction, auxiliaries, etc.

The basis of the model is to consider the multi-cylinder engine as a series of thermodynamic control volumes, linked by mass or work transfer. These control volumes are

(1) compressor
(2) inlet manifold
(3) cylinders
(4) exhaust manifolds
(5) turbine or turbine sectors.

As in all thermodynamic analyses, heat, work and mass transfers across the boundaries of these control volumes must be calculated.

(1) The compressor is bounded by mass flows at the inlet and outlet, plus work transfer from the turbine. Heat transfer is generally neglected.

(2) The inlet manifold is bounded by the mass flows supplied by the compressor and withdrawn by the cylinders when the inlet valves are open. Heat transfer to or from the walls is usually neglected, but a charge cooler model can be added.

(3) The cylinders are bounded by air flow from the inlet manifold and the flow of exhaust gases to the exhaust system, when the relevant valves are open. A flow of fuel issues from the injector intermittently. Work is transferred to or from the piston. Heat is transferred to the piston and combustion chamber walls. Heat is also released by combustion of the fuel.

(4) The exhaust manifolds are bounded by flow through the exhaust valves when they are open, and through the relevant sector of the turbocharger turbine. Heat is exchanged through the walls, to the surroundings.

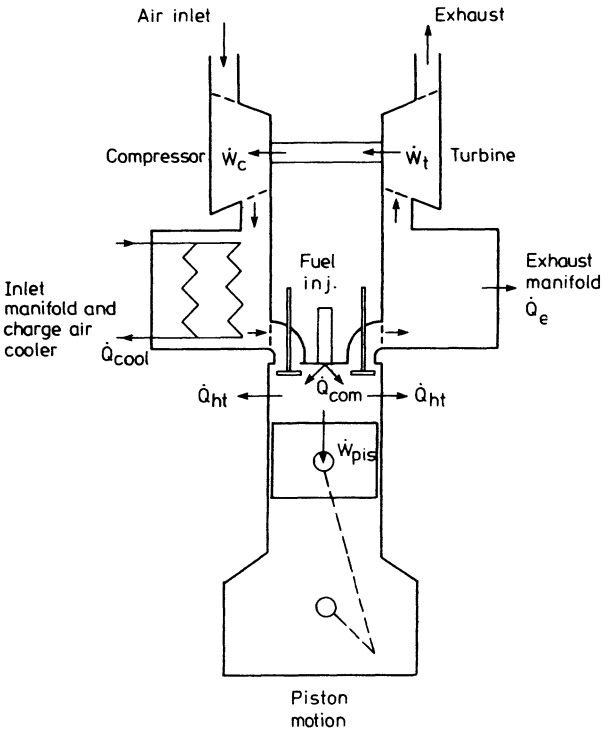

W_c	Compressor work
W_t	Turbine work
Q_{cool}	Heat rejected to charge air cooler
Q_{ht}	Heat rejected to cylinder walls
Q_{com}	Heat released by combustion
W_{pis}	Piston work
Q_e	Heat rejected from exhaust manifold

Figure 15.13 *Schematic of turbocharged engine system*

(5) The turbocharger turbine is bounded by flow through each sector from the exhaust manifolds and out into the exhaust pipe. Work is transferred to the compressor. Heat is transferred to the surroundings from the turbine casing surface and via the lubricating oil system. Some work is done overcoming friction in the turbocharger bearings.

The engine simulation calculates the relevant work, heat and mass transfers by applying the appropriate equations for the conservation of energy and mass. The systems are treated as quasi-steady open thermodynamic systems. The model described in the following sections is that due to Marzouk, [4] for steady speed and transient operation, which itself is a development of that by Borman, [5] McAulay *et al.* [6] and Streit and Borman. [7]

15.4 The Energy Equation

The control volume that is most complex to describe analytically is that of a cylinder. Processes involved are mass transfer in and out of the valves, plus fuel injection, heat transfer from the gas to the piston, cylinder liner, valves and head, heat released by combustion of the fuel, and work transfer through piston motion. By writing a general energy equation to include all of these processes, the same basis may be used for other control volumes (the manifolds) simply by putting inappropriate terms to zero.

The energy equation for an open thermodynamic system may be written (neglecting potential energy terms) as

$$\frac{dU}{dt} = \frac{dQ}{dt} - \frac{dW}{dt} + \sum_j \frac{dH_{0j}}{dt}$$

where subscript j denotes different entries to the control volume, or

$$\frac{d(mu)}{dt} = \sum_{sf} \frac{dQ_{sf}}{dt} - P\frac{dV}{dt} + \sum_j h_{0j}\frac{dm_j}{dt} \tag{15.4}$$

where subscript sf denotes surfaces with different rates of heat transfer. h_{0j} is the specific stagnation enthalpy of mass entering or leaving the system. By expressing the energy of air and combustion products as absolute values, [8] it is not necessary to include the heat released by combustion as a separate term, since this will be included in the energy terms above.

Differentiating the left-hand side of equation 15.4 gives

$$m\frac{du}{dt} + u\frac{dm}{dt} = -P\frac{dV}{dt} + \sum_{sf}\frac{dQ_{sf}}{dt} + \sum_j h_{0j}\frac{dm_j}{dt} \tag{15.5}$$

The internal energy of the gas in the cylinder will be a function of position and the local values of pressure, temperature and air/fuel ratio. A major simplifying assumption is made at this stage, namely that the contents of the control volume are homogeneous (that is, uniform in space). This may be a reasonable assumption for the manifolds, and the cylinder during the compression stroke, but is obviously not true during combustion. The error introduced by this

assumption is discussed in section 15.6. If the effects of chemical dissociation are neglected, then the internal energy will reduce to a function of temperature and air/fuel (or equivalence) ratio only. Thus $u = u\ (T, F)$ and the first term in equation 15.5 becomes

$$m \frac{du}{dt} = m \left[\frac{\partial u}{\partial T} \frac{dT}{dt} + \frac{\partial u}{\partial F} \frac{dF}{dt} \right]$$

Thus equation 15.5 may be written as

$$m \frac{\partial u}{\partial T} \frac{dT}{dt} + m \frac{\partial u}{\partial F} \frac{dF}{dt} + u \frac{dm}{dt} = - \frac{mRT}{V} \frac{dV}{dt} + \sum_{sf} \frac{dQ_{sf}}{dt} + \sum_{j} h_{oj} \frac{dm_j}{dt}$$

assuming that the gases involved behave as perfect gases ($PV = mRT$), or

$$\frac{dT}{dt} = \left[- \frac{RT}{V} \frac{dV}{dt} + \left(\sum_{sf} \frac{dQ_{sf}}{dt} + \sum_{j} h_{oj} \frac{dm_j}{dt} - u \frac{dm}{dt} \right) \frac{1}{m} - \frac{\partial u}{\partial F} \frac{dF}{dt} \right] / \frac{\partial u}{\partial T} \tag{15.6}$$

(A more complex equation results if dissociation is not neglected. [4, 5])

Equation 15.6 is the basic form of the energy equation that may be applied to each control volume, together with the following equation for conservation of mass

$$\frac{dm}{dt} = \sum_{j} \frac{dm_j}{dt} \tag{15.7}$$

Note that if the instantaneous volume of each control volume is known, together with the mass (from equation 15.7) and temperature (from equation 15.6), then the pressure may be calculated from the perfect gas law. The application of equation 15.6 to various components of the engine is presented in section 15.12.

To evaluate equation 15.6, the various terms on the right-hand side must be known. The rate of change of volume with time (dV/dt) will be zero for the

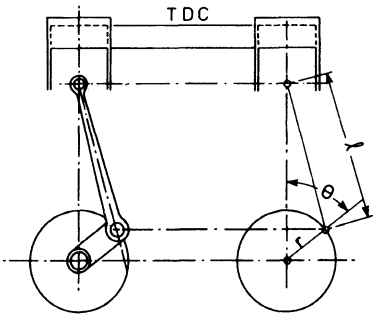

Figure 15.14 *Crank piston mechanism*

inlet and exhaust manifolds. For the cylinders it may be calculated from the geometry of the piston, crank and connecting rod (figure 15.14)

$$\frac{dV}{dt} = \frac{\pi B^2}{4}\left[r \sin\theta \frac{d\theta}{dt} + (1^2 - r^2 \sin^2\theta)^{-1/2} r^2 \sin\theta \cos\theta \frac{d\theta}{dt}\right] \quad (15.8)$$

where θ = crank angle displacement from TDC.

The evaluation of the next three terms in equation 15.6 (those involving heat, energy and mass transfer) is given in sections 15.6, 15.7 and 15.8. The rate of change of equivalence ratio with time ($\partial F/\partial t$) will depend on the current rate of fuel addition by injection, and the fuel content (in the form of combustion products) of gas entering or leaving the cylinder. If the quantity of fuel and air in the control volume is known at the start of the calculation, then the equivalence ratio at any subsequent time may be calculated from a knowledge of any subsequent fuel and air additions. Thus dF/dt is evaluated from knowledge of fuel and air flow rates (see section 15.12.2).

It remains to evaluate those terms concerning the properties of the gas (air and combustion products), heat transfer and combustion.

15.5 Gas Property Relationships

Tabulated data or algebraic expressions are required for the partial derivative of the internal energy (u) with respect to temperature and air/fuel ratio (and pressure, if dissociation is not to be neglected) and the gas constant (R). Relationships are required for air, combustion products and mixtures of the two. By deriving general algebraic expressions for combustion products in terms of air/fuel ratio, the properties of mixtures of air or combustion products may be evaluated by using the appropriate over-all value of air/fuel or equivalence ratio ($F = 0$ for pure air).

The assumption of a homogeneous mixture and equilibrium thermodynamic properties for the products of combustion is made. Clearly it would not be sensible to attempt to include non-equilibrium thermodynamics, once the gross assumption of homogeneity has been made. Rather than go through full thermodynamic combustion product calculations at each step, it is common to use algebraic expressions curve-fitted to the results of such calculations. Several approximate algebraic expressions are available, but probably the most useful are those of Krieger and Borman [9]

$$u = K_1(T) - K_2(T)\,F \text{ kJ/kg of original air} \quad (15.9)$$

where $K_1 = 0.692T + 39.17 \times 10^{-6}T^2 + 52.9 \times 10^{-9}\,T^3 - 228.62 \times 10^{-13}T^4 + 277.58 \times 10^{-17}T^5$

and $K_2 = 3049.39 - 5.7 \times 10^{-2}T - 9.5 \times 10^{-5}T^2 + 21.53 \times 10^{-9}T^3 - 200.26 \times 10^{-14}T^4$

and the gas constant (R) is given by

$$R = 0.287 + 0.02F \text{ kJ/kg K} \quad (15.10)$$

(per kg of original air).

These expressions were obtained by curve-fitting the equilibrium data of Newall and Starkman [10] for the combustion products of a hydrocarbon (C_nH_{2n}) and air. The stoichiometric fuel/air ratio is 0.0676 hence the above expressions must be divided by $(1 + 0.0676F)$ if the value of u or R is required per unit mass of combustion products. Modifications to the above expressions to account for pressure dependence at high temperatures are also given by Krieger and Borman. [9] For data relevant to richer than stoichiometric mixtures (including pressure effects) see Marzouk. [4] It is clearly a simple matter to differentiate equations 15.9 and 15.10 with respect to T and F as required by equation 15.6.

Some engine performance calculation programs calculate the equilibrium properties directly, but this usually increases computing time significantly with little benefit in accuracy.

15.6 Combustion

The combustion process is the most important aspect of any internal combustion engine. Unfortunately it is also the most complex and the least understood. A physical explanation of the combustion process was given in chapter 14. A complete mathematical model of combustion would require good models of the injection pump, fuel lines and injector nozzles, air motion in the cylinder (including spatial distribution, turbulence and variation with time), fuel atomisation, vapourisation, air/fuel mixing, chemical kinetics and pre-mixed and diffusion burning. A comprehensive model such as this has not yet been developed although it may not be beyond the scope of current knowledge. However, even if such a model were developed it would be too lengthy to justify inclusion in most turbocharged engine simulations.

Many attempts have been made to produce simplified combustion models (for example, Meguerdichian and Watson [11]) but these are not accurate enough to be used in all cases. An alternative semi-empirical approach is usually adopted.

An 'apparent' heat release or fuel burning rate may be calculated from experimental cylinder pressure diagrams. This is the reverse of the usual engine performance calculation in which a cylinder pressure diagram and hence work output is the goal. Thus the same assumptions and equations may be used, although the calculation process is different. Fortunately, it is simpler since only that portion of the cycle when the valves are closed need be considered. The term 'apparent' is used since the calculation is not exact because of the assumptions made and possible errors in the heat transfer and other models. However, apparent heat release or fuel burning rate diagrams can be extremely useful, provided that sufficient care is taken in measuring and recording the cylinder pressure diagram. [12, 13]

If an experimental apparent heat release rate is available, then this may be used in the turbocharged engine simulation as a wholly empirical replacement for a combustion model. The technique has the major advantage of simplicity and is therefore used almost universally. However, the heat release curve is valid only at the appropriate engine speed and load and only for the engine on which

the cylinder pressure diagram was measured. If the engine has already been run for the cylinder pressure diagram to be recorded, there is little point in trying to predict its performance! In practice, however, the technique is used to build up a set of heat release diagrams for a range of engine conditions and engine types. If these heat release diagrams are non-dimensionalised over the total quantity of heat released, then when calculating the performance of a new engine, or calculating conditions with a new turbocharger match and hence rating, a suitable diagram may be taken and scaled according to the appropriate quantity of fuel being injected.

When matching a turbocharger to an engine, for example, when uprating an existing design, some engine performance data will already be available, even if a heat release diagram is not. The usual procedure is then to derive the heat release diagram by a process of trial and error until the specific fuel consumption, maximum cylinder pressure and power output predicted match those measured at the previous engine rating. This diagram will then be scaled for the increased fuelling at the higher rating, enabling the effects of different turbine builds to be studied analytically.

The convenience of a turbocharger matching program can be greatly enhanced by building-in an algebraic expression for the heat release rate. [14] Since the actual rate will vary with speed, load, injection timing, engine type, etc., a simple empirical correlation is required whose 'constants' may be chosen to suit a particular engine and its circumstances. Probably the most widely used correlation is based on the Wiebe function. [15, 16] This is a simple algebraic formula, for the fuel burnt, as a fraction of the total fuel injected

$$FB = 1 - \exp\left[-K_2(t)^{(K_1+1)}\right] \tag{15.11}$$

or in differential form (fuel burning rate/total fuel injected)

$$FBR = K_2(K_1 + 1)\, t^{K_1} \exp\left[-K_2(t)^{(K_1+1)}\right] \tag{15.12}$$

where FB = fraction of fuel burnt/total injected per cycle per cylinder
FBR = non-dimensional fuel burning rate $[=\mathrm{d}(FB)/\mathrm{d}t]$
t = time from ignition, non-dimensionalised over the total time allowed for combustion $(=\Delta t/\Delta t_{\mathrm{com}})$
K_1 = shape factor for the curve
K_2 = combustion efficiency coefficient.

The non-dimensional fuel burning rate is related to the heat release rate by the calorific value of the fuel, if all fuel is burnt and dissociation is neglected (dissociation reduces heat release). K_2 is chosen such that all the fuel is burnt at the end of combustion (for example, $FB = 0.99899$ at $t = 1$ if $K_2 = 6.9$) if, as normal, this is indeed the case.

Shipinski *et al.* [16] and Woschni and Anisits [17] have attempted to fit the Wiebe function to combustion rate data obtained over a range of engine speeds and loads by deriving suitable expressions for K_1 and K_2.

Shipinski's results were obtained on a high-speed swirl-type direct-injection engine and included simulated turbocharged conditions, but he concluded that

the Wiebe function was insufficiently flexible to account for all the factors involved.

Woschni and Anisits [17] developed a Wiebe function correlation from test results relating to a larger industrial-type engine. The basis of their approach was not to define the heat release or fuel burning pattern directly, but rather to assume that a diagram was known at one condition and to define its change as conditions varied. Their value for K_2 was 6.9 (ensuring that combustion is 100 per cent complete at the end of the burning period). The change of shape factor (K_1) with running condition is given by the expression

$$K_1 = K_{1\,\mathrm{ref}} \left(\frac{ID_{\mathrm{ref}}}{ID}\right)^a \left(\frac{P_Z}{P_{Z\,\mathrm{ref}}} \times \frac{T_{Z\,\mathrm{ref}}}{T_Z}\right) \left(\frac{N_{\mathrm{ref}}}{N}\right)^b \tag{15.13}$$

where P_Z and T_Z = pressure and temperature at the beginning of compression
ID = ignition delay
a = empirical constant (0.5 suggested)
b = empirical constant (0.3 suggested).

The subscript ref is used to relate to datum conditions at which the heat release rate is known.The variation of ignition delay with running conditions can be calculated from well-established correlations (for example, Wolfer [18]). In addition, the variation of combustion duration with running conditions is required for the denominator of the dimensionless time function (t) in equation 15.11. Woschni and Anisits' data gives

$$\Delta t_{\mathrm{com}} = \Delta t_{\mathrm{com\,ref}} (F/F_{\mathrm{ref}})^{0.6} (N/N_{\mathrm{ref}})^{0.5} \tag{15.14}$$

Equations 15.12 and 15.13 may then be used to predict the heat release rate at other conditions.

Unlike Shipinski's correlation, Woschni and Anisits' does not require the fuel injection rate as data and is therefore simpler to use. However, the actual heat release shape defined by the Wiebe function differs markedly in character to that measured on most types of engine, and the range of operating conditions covered by equation 15.13 is limited.

The difference in character results from the use of a single parameter to define the shape of the heat release curve (K_1). Experimental data usually reveals a two-part characteristic, broadly relating to the pre-mixed and diffusion burning phases of diesel combustion. Watson *et al.* [14] suggested that a curve of this type would be produced by combining two functions, with a phase proportionality factor

$$FB = \beta f_1(t) + (1-\beta) f_2(t) \tag{15.15}$$

where $f_1(t)$ = 'pre-mixed' burning function
$f_2(t)$ = 'diffusion' burning function
β = phase proportionality factor of pre-mixed to total burning.

The phase proportionality factor (β) will largely be a function of ignition delay,

since the fuel injected during this period governs the internal 'pre-mixed' burning phase. Thus

$$\beta = 1 - aF^b/ID^c$$

where ID = ignition delay (ms). Correlation with data from turbocharged truck engines gives the following range of values for a, b and c

$$\begin{aligned} 0.8 &< a < 0.95 \\ 0.25 &< b < 0.45 \\ 0.25 &< c < 0.50 \end{aligned}$$

The diffusion burning function $[f_2(t)]$ is based on the Wiebe function, but $f_1(t)$ is an additional term

$$\left.\begin{aligned} f_1(t) &= 1 - (1 - t^{K_1})^{K_2} \\ f_2(t) &= 1 - \exp(-K_3 t^{K_4}) \end{aligned}\right\} \qquad (15.16)$$

With sufficiently large values of K_2 the differential of the first function will generate a typically spikey initial rate of burning whose integral has the required value of unity. Correlation with data from a typical truck engine mentioned above, suggests the following values for the constants K_1 to K_4

$$\begin{aligned} K_1 &= 2.0 + 1.25 \times 10^{-8} (ID \times N)^{2.4} \\ K_2 &= 5000 \\ K_3 &= 14.2/F^{0.644} \\ K_4 &= 0.79 K_3^{0.25} \end{aligned}$$

Combustion duration (Δt_{com}) is an arbitrary period in which combustion must be completed. The actual point at which combustion ceases has little real significance since the rate decays exponentially to almost zero long before combustion truly stops. A value of $\Delta t_{com} = 125°$ was used above.

The ignition delay may be computed by a Wolfer [18] or similar formula. Marzouk [4] and Watson and Marzouk [19] have used the method in conjunction with a simple injection delay formula (a function of the fuel line length) to enable the heat release rate to be calculated as a function of static injection timing, engine speed and quantity of fuel injected only. This type of expression may be built in to a turbocharged diesel engine simulation program, greatly increasing the ease with which it may be used for turbocharger matching calculations, etc. Although more complex than the Wiebe function, it has the major advantage of producing a more accurate shape for the heat release curve (figure 15.15).

Whitehouse and Way [20] have presented an alternative empirical model, based on elementary combustion principles. Fuel is assumed to be prepared, ready for combustion, due to fuel air mixing, at a rate given by

$$FPR = K_1 (m_f)^{K_2} (m_{fu})^{1-K_2} (PP_{O_2})^{K_3} \qquad (15.17)$$

where K_1 to K_3 are empirical constants and PP_{O_2} is the partial pressure of

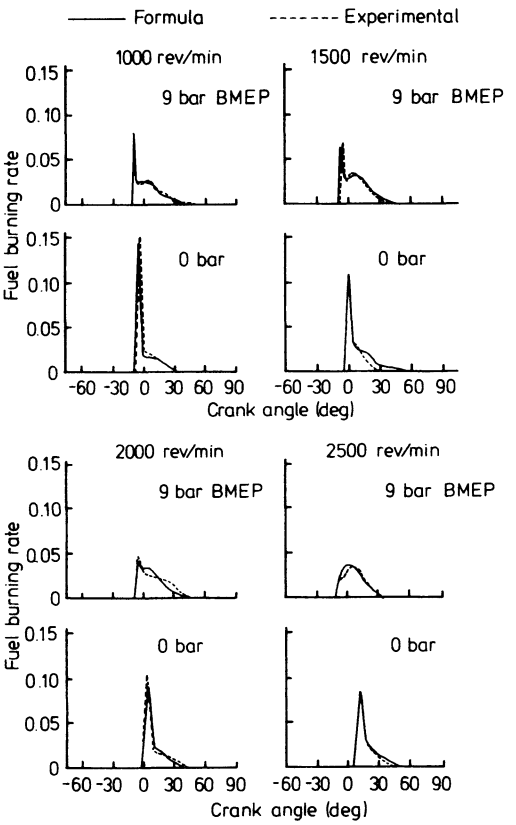

Figure 15.15 *Comparison of predicted and experimental fuel burning rate curves*

oxygen. A reaction rate equation is used to link the preparation rate to the burning rate, during the early 'pre-mixed' part of diesel combustion

$$FBR = \frac{K_4}{N} \times \frac{PP_{O_2}}{\sqrt{T}} e^{-K_5/T} \int (FP - FR)dt$$

where FP = fuel prepared
FR = fuel reacted.

During the diffusion burning phase, fuel is assumed to burn as rapidly as it is prepared (from equation 15.17), the reaction rate equation being dropped.

15.7 Heat Transfer

The prediction of energy loss due to heat transfer from the combustion chamber is, like combustion, an area where current knowledge is inadequate. Fortunately,

the effect of heat transfer, although important, is not as dominant as combustion, hence errors in modelling are not so serious. However, one of the uses to which designers might want to apply an engine simulation program is to predict component temperatures and resultant stresses. Naturally this will require a more accurate heat transfer model. Unfortunately virtually all the engine heat transfer models currently available can only be relied on to predict approximate values of component temperatures, unless they are coupled with a heavy reliance on some experimental data.

Heat is transferred from the gas in the cylinder, by convection at the cylinder wall, and by radiation from flame and luminous carbon particles. Heat entering the walls is conducted through to the coolant, whether water or air, with forced convection again playing a role at the metal-coolant interface.

Forced convective heat transfer at the gas-to-cylinder wall interface has a more important impact on total heat transfer than conduction through the wall or transfer from wall to coolant and therefore heat transfer models concentrate on the gas-to-wall interface. The heat transfer at this interface will depend on the temperature gradient in the boundary layer at the surface, and of course the surface area. Since the flow in the boundary layers cannot yet be calculated in diesel engines (except in the absence of combustion), empirical methods have been adopted. A convective (gas-to-wall) heat transfer coefficient (ht) is defined from the equation

$$\frac{\dot{Q}}{A} = ht(T_g - T_{sf}) \tag{15.18}$$

with subscripts g and sf denoting gas and combustion chamber wall surface respectively. Since the gas is assumed to be uniform and homogeneous throughout the cylinder, T_g is implicitly the bulk mean gas temperature. T_{sf} can be the local surface temperature on cylinder wall, head or piston, as appropriate. The problem is then to devise a method of calculating ht.

Dimensional analysis can be used to relate ht to gas conductivity (k), density (ρ), velocity (C), viscosity (μ), specific heat capacity (c_p) and a representative length (l). This shows that there is a fundamental relationship between the following three dimensionless parameters

Nu = Nusselt number = htl/k
Re = Reynolds number = $\rho Cl/\mu$
Pr = Prandtl number = $c_p \mu/k$

Fortunately the variation in Prandtl number is small, hence it can be omitted. Experiments with forced convective heat transfer have shown that

$$Nu = K_1(Re)^{K_2} \tag{15.19}$$

where K_1 and K_2 are constants, to a good approximation. Thus equation 15.19 relates the convective heat transfer coefficient (ht) to gas velocity, conductivity, density, viscosity and a characteristic length.

Many attempts have been made to apply equation 15.19 to internal combustion engines, and to determine constants K_1 and K_2 by experiment or trial

and error. Implicit in the engine model is the assumption that the cylinder contents behave as a homogeneous mixture of known composition. Thus the conductivity, density and viscosity can be calculated from the gas temperature, pressure and property data. The gas velocity should be that of the 'free stream', just outside the boundary layer on the appropriate surface, but this will not be known. The characteristic length is a length term that is also unknown in this application (in the classic case of forced convective heat transfer on a flat plate, it is the distance from the leading edge of the plate to the point of interest). Arbitrary but convenient definitions of velocity and length are adopted, such as the mean piston speed (C_{pis}) and cylinder bore (B).

Several heat transfer correlations incorporate a radiation term, in addition to the forced convection term described above. The radiation term is based on grey body radiation, thus

$$\frac{\dot{Q}}{A} = ht(T_g - T_{sf}) + \epsilon \sigma T_g^4 \tag{15.20}$$

where ϵ = emissivity

σ = Stephan-Boltzmann constant (56.7×10^{-12} kW/m^2 K^4).

Due to the difficulty of measuring instantaneous flame temperature and heat flux, it is difficult to determine how significant the contribution of radiation is to the over-all heat transferred. Estimates varied between 0 and 30 per cent and vary according to engine type.

Most recent correlations are based on equations 15.19 and 15.20. The most commonly used are those due to Annand, [21] Annand and Ma [22] and Woschni. [23] Annand uses mean piston speed and cylinder bore as characteristic gas velocity and length respectively, and therefore implies a relationship between piston speed and gas velocity in the cylinder. The form of this relationship is hidden in the empirical constants (K_1 and K_2) in equation 15.19. Annand added a radiation term, hence equation 15.20 becomes

$$\frac{\dot{Q}}{A} = K_1 \frac{k}{B} Re^{K_2}(T_g - T_{sf}) + K_3(T_g^4 - T_{sf}^4) \tag{15.21}$$

Suggested values of the constants are

K_1 = 0.25 to 0.8

K_2 = 0.7

$K_3 = 0.576\sigma$

For a petrol engine $K_3 = 0.0750\sigma$. During the intake, compression and exhaust processes, when the radiation term would be zero, $K_3 = 0$.

The large variation of parameter K_1 is confirmation that important parameters are being ignored and suggests that the implied relationship between piston speed and gas velocity is weak. To partially overcome this problem Annand and Ma [22] presented a more complex expression based on an energy mean value for the characteristic velocity and a time-lag term.

Woschni [23] developed another expression based on the forced convection power law but ignored radiation. He found a power of 0.8 to be more appropriate

$$Nu = 0.035(Re)^{0.8} \tag{15.22}$$

Quite correctly, Woschni argued that the significant Reynolds number is that of the local forced turbulent flow in the cylinder, but it is difficult to account for this correctly. He proposed an empirically based alternative in which the characteristic velocity term (in Re) is expressed as

$$C = K_4 C_{pis}$$

where K_4 is a 'constant' to be determined. To take account of the different gas velocities during scavenging and compression, the following value of the 'constant' was proposed

during scavenging, $K_4 = 6.18$

during compression, $K_4 = 2.28$

Woschni postulated that the effect of combustion on gas motion would be a function of the increase in cylinder pressure above the 'motored' pressure. During the combustion and expansion phases

$$C = 2.28\, C_{pis} + 3.24 \times 10^{-3} \left(\frac{V_{sw} T_{ref}}{P_{ref} V_{ref}}\right) (P - P_{mot})$$

where V_{sw} = swept volume

T_{ref}, P_{ref} and V_{ref} = temperature, pressure and cylinder volume at some reference condition (for example, inlet valve closure or the start of combustion), hence this term denotes the mass trapped in the cylinder

P-P_{mot} = cylinder pressure minus 'motored' cylinder pressure.

Woschni [23] used approximate algebraic expressions for gas viscosity and conductivity to simplify use of equation 15.22, which then becomes

$$ht = \frac{K_1 P^{0.8}}{B^{0.2} T^{0.53}} \left[K_2 C_{pis} + K_3 \frac{V_{sw} T_{ref}}{P_{ref} V_{ref}} (P - P_{mot})\right]^{0.8} \tag{15.23}$$

where $K_1 = 0.13$

$K_2 = 2.28$ (compression, combustion and expansion)

$K_2 = 6.18$ (scavenging period)

$K_3 = 0$ (compression and scavenging phases)

$K_3 = 3.24 \times 10^{-3}$ (for direct-injection engines)

$K_3 = 6.22 \times 10^{-3}$ (for pre-chamber engines).

A difficulty inherent in using Woschni's expression is that the 'motored' cylinder pressure must continue to be evaluated during combustion and expansion. This can be done by putting the fuel input to zero in the energy equation (equation 15.6) and computing motored conditions alongside firing conditions.

However, it is simpler and involves little error to assume isentropic compression and expansion with an appropriate index

$$\frac{P_{mot}}{P_{ref}} = \left(\frac{V_{ref}}{V}\right)^n$$

The index (n) may be evaluated from the pressure predicted during compression or a suitable mean value (for example, $n = 1.32$) may be chosen.

Woschni [24] has also suggested modifying equation 15.23 to take account of changes in swirl, which must effect gas velocity, using data from steady flow swirl test rigs

$$K_2 = 6.18 + 0.417C_{per}/C_{pis} \text{ (scavenging)}$$
$$K_2 = 2.28 + 0.308C_{per}/C_{pis} \text{ (compression, combustion and expansion)}$$

where C_{per} = peripheral gas velocity (m/s)
$= \pi BN_{an}/60$
N_{an} = swirl anemometer speed, $0.7B$ below cylinder head, steady flow tests.

Woschni's correlation has certain disadvantages. It is complex and Dent and Sulieman [25] have shown that it can over-estimate the combustion induced component and under-estimate the motored component, on high-speed engines. Hohenberg [26] has checked the correlation against measured instantaneous heat fluxes, confirming Dent's findings. Hohenberg presented a simplified form of equation 15.23, as follows

$$ht = \frac{K_1 P^{0.8}}{V_{sw}^{0.06} T^{0.4}} (C_{pis} + K_2)^{0.8} \tag{15.24}$$

where $K_1 = 130$
$K_2 = 1.4$

Equation 15.24 is applied to the piston area as defined below

$$A_{pis} = A\text{(piston crown)} + A^{0.3}\text{(piston top land)}$$

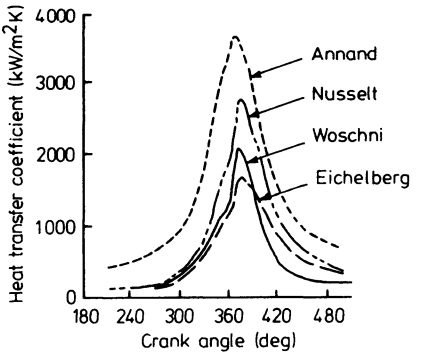

Figure 15.16 *Comparison of predicted heat transfer coefficients*

A comparison of some predicted instantaneous heat fluxes is given in figure 15.16, revealing a 2:1 variation. This partly reflects the use of base data from different types of engines. Equation 15.23 remains the most widely used. Other heat transfer correlations are discussed by Dent and Sulieman [25] Sitkie [27] and Kamel and Watson [28] (for indirect-injection engines).

Spatial variations in heat transfer rates are usually accounted for by assigning different wall temperatures to different areas of the combustion chamber surface based on practical experience. If these temperatures are to be calculated, a heat conduction model is required for the piston, valves, cylinder head and liner.

15.8 Flow through Valves and Ports

The solution to the energy equation (equation 15.6) requires knowledge of the instantaneous mass and energy flows through the valves or ports whenever they are open. With knowledge of the gas pressure, temperature and air/fuel ratio in each control volume the specific internal energy may be calculated from the gas property relationships. Hence knowledge of the instantaneous mass flow rate only is required. This will be a function of the pressure ratio across the valve (that is, between the control volumes on either side), the effective cross-sectional area of the valve throat, which will vary with crank angle, local geometrical effects, heat transfer, flow separation and other secondary flow effects.

It is generally assumed that the highly unsteady flow process through a valve or port may be analysed on a quasi-steady basis. This is a major simplification, and some doubts have been expressed as to the error involved. [29] Trengrouse *et al.* [30] have shown that significant errors can result from this assumption (with sharp-edged orifices) but that the error is greatest (up to 7 per cent) when the flow area is small. This is fortunate, since, during the analogous situation in an engine (low valve lift), the mass flow rate is a small proportion of the total. A further major simplifying assumption is to consider the flow to be one-dimensional. Again this is clearly not the case in practice, but some account of secondary flow effects is taken, by introducing an empirically based discharge coefficient into the results.

A simple one-dimensional model for flow through a valve or port using the analogy of an orifice, having an equivalent flow area (an area that produces the same flow rate under the same upstream and downstream pressures) is used. Applying the energy equation from upstream (station 1) to the valve throat (station 2) for isentropic steady flow, and assuming that the inlet velocity is negligible, gives

$$\frac{dm}{dt} = A_2 P_1 \sqrt{\left\{\left(\frac{2\gamma}{\gamma - 1}\right)\frac{1}{RT_1}\left[\left(\frac{P_2}{P_1}\right)^{2/\gamma} - \left(\frac{P_2}{P_1}\right)^{(\gamma+1)/\gamma}\right]\right\}} \qquad (15.25)$$

In practice, secondary flow effects, boundary layer separation, friction, etc., result in the mass flow rate being less than that calculated from equation 15.25 (figure 15.17).

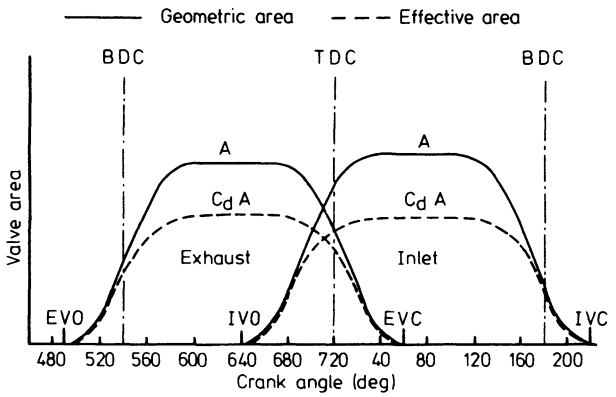

Figure 15.17 *Exhaust and inlet valve area against crank angle for a typical turbocharged four-stroke medium-speed diesel engine*

A discharge coefficient (Cd) is adopted to overcome this difficulty, hence

$$\frac{dm}{dt} = Cd\,A_2P_1\sqrt{\left\{\left(\frac{2\gamma}{\gamma-1}\right)\frac{1}{RT_1}\left[\left(\frac{P_2}{P_1}\right)^{2/\gamma}-\left(\frac{P_2}{P_1}\right)^{(\gamma+1)/\gamma}\right]\right\}} \quad (15.26)$$

Unfortunately the throat pressure (P_2) will not be known hence an assumption must be made to link P_2 to the downstream pressure (P_3). It is common to assume that no diffusion occurs between stations 2 and 3 due to the turbulent nature of the flow, hence $P_2 \approx P_3$. This is termed a constant (static) pressure model. Other models have been suggested. [31]

Flow through the valve may be considered in three distinct phases. For example, consider outflow through an exhaust valve. Initially the cylinder pressure will be high when the valve lift is low. The pressure ratio will be sufficient to choke the valve. When the flow is sonic, the flow will be independent of P_3, and the mass flow rate equation becomes

$$\frac{dm}{dt} = Cd\,A_2P_1\sqrt{\left[\frac{\gamma}{RT}\left(\frac{2}{\gamma+1}\right)^{(\gamma+1)/(\gamma-1)}\right]} \quad (15.27)$$

As the valve opens further and additional combustion products flow out, the cylinder pressure will reduce and the flow will become sub-sonic at the valve throat. The third phase, which will also be sub-sonic at the throat, will be the scavenge period, when inlet and exhaust valves are open. Equation 15.26, together with the assumption regarding P_2 and P_3, may be applied during the later two phases.

Thus the instantaneous mass flow through a valve or port may be calculated from a knowledge of the gas conditions in the adjacent control volumes (cylinder and manifold), plus the geometric valve area and discharge coefficient.

The valve area (figure 15.17) can be calculated from a knowledge of local geometry and the valve lift-crank angle diagram (itself derived from the camshaft profile and rocker ratio). Unfortunately no consistent definition of

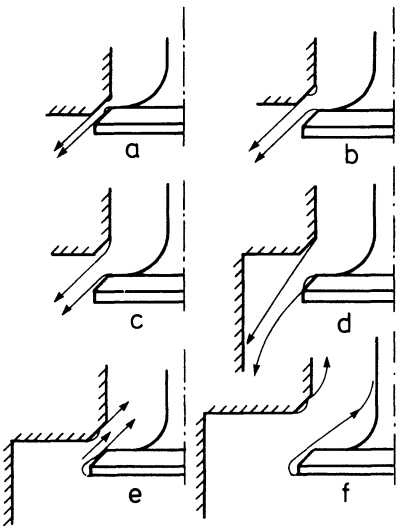

Figure 15.18 *Flow pattern for inflow and outflow through a poppet valve*

geometric valve area has been established. Consider the valve and port shown in figure 15.18. At high valve lifts, the governing area will be the surface of the cylinder formed between valve seat and valve head. At lower lifts, this surface will become the frustrum of a cone. At full lift, the port area may be the smallest part of the flow passage.

This lack of a consistent definition means that the values of discharge coefficient reported from various sources are not all directly comparable. The value of the discharge coefficient or effective area is established from steady flow tests at varying valve lifts and pressure ratios. [32] Woods and Khan [33, 34] have shown that the effective area ($Cd\,A_2$) is a function of valve lift and pressure ratio (figure 15.19), but that the effect of the latter is small and may be neglected.

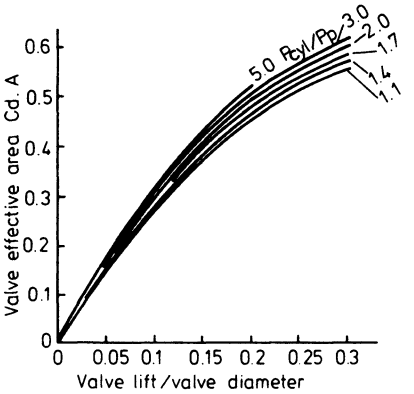

Figure 15.19 *Effective area variation with valve lift*

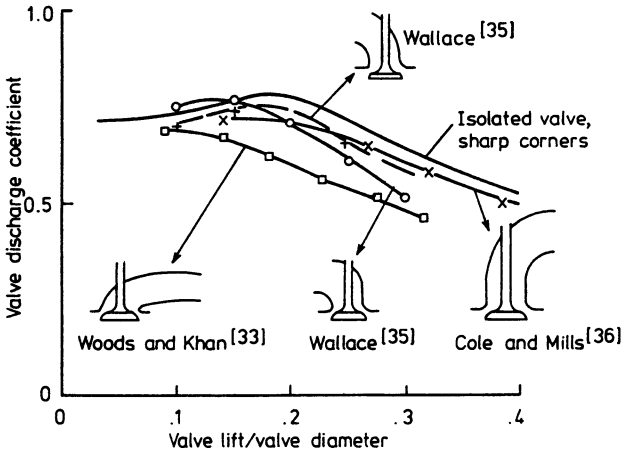

Figure 15.20 *The effect of exhaust port design on discharge coefficient [32]*

Since the pressure ratio is likely to be low when its influence is greatest (high lifts), it is reasonable to conduct steady flow tests at relatively low pressure ratios to achieve an average result.

Steady flow tests should be conducted on inlet and exhaust valves or ports, for normal and reverse flow situations. Often the discharge coefficient is of little direct interest since the designer is looking for maximum flow, and the simulation program user requires the effective area only. However, it is useful to adopt the discharge coefficient approach for comparative purposes. Frequently discharge coefficients for other similar valves may be used in the absence of better information. Figure 15.20 illustrates the variation in discharge coefficient with valve lift for a range of exhaust valve designs. The valves and passages are shown diagrammatically.

15.9 The Scavenging Process

During the scavenge period, air is entering the cylinder and exhaust products or a mixture of exhaust products and air are leaving. Some assumption regarding the state of the mixture in the cylinder and that leaving must be made.

Two extreme conditions may be considered. The first is displacement scavenging in which the combustion products are pushed out by incoming air with no mixing. This is the ideal process but cannot be realised in practice. At the other extreme is a complete by-pass, the fresh air by-passing the combustion products and passing out of the exhaust valve. Fortunately, it would be difficult to design a system as poor as this. A more practical case is that of complete mixing of fresh air and combustion products, the incoming air displacing some mixture. In practice, scavenging will usually be somewhere between the complete mixing and displacement models.

Good scavenging is critically important on a two-stroke engine. It is desirable,

but not critical on a four-stroke engine. It follows that an engine designer will take great care in designing his inlet ports and exhaust valves or ports to promote good scavenging in a two-stroke engine. The four-stroke engine designer will concentrate on achieving good volumetric efficiency and an efficient exhaust process. Besides, he has less scope to influence scavenging with the normal arrangement of inlet and exhaust valves in the cylinder head. Again, both designers will try to aid scavenging by arranging the turbocharging system to provide a favourable pressure drop between intake and exhaust during the period of valve overlap.

On engines with little valve overlap (automotive turbocharged four-stroke engines), little scavenging will occur. On others, such as large, constant speed, highly rated two-stroke engines, the choice of a scavenging model will be important. For four-stroke engines the complete mixing model has the advantage of being reasonably realistic, erring on the pessimistic side and being simple to program. Although the same model is frequently used for two-stroke engines, actual scavenging efficiency depends on engine design (figure 6.11) and the scavenging system. Metz *et al.* [37] have suggested a two-part model comprising part pure displacement and then complete mixing. The difficulty is to define the changeover point and clearly this will vary according to the effectiveness of the scavenging system on a particular engine. In addition, the discontinuity at the changeover point can cause numerical instability in the calculation process. Ideally, a knowledge of the changing scavenge conditions with time is required.

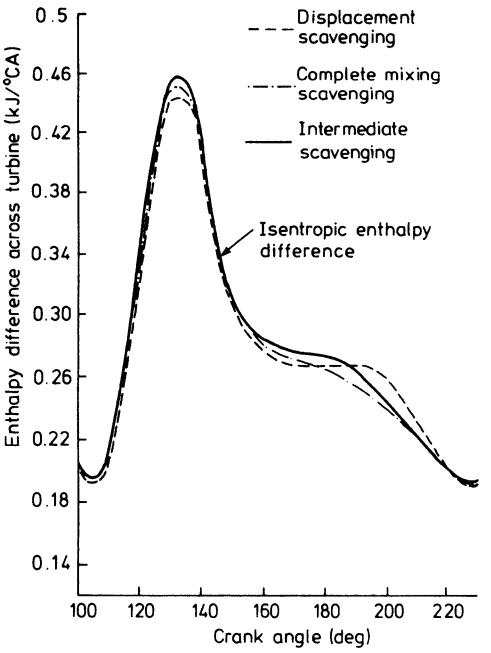

Figure 15.21 *Enthalpy difference across turbine for different scavenging methods [7]*

This is very difficult to do but has been attempted by Krieger, [38] Mayaski and Meyer [39] and Streit. [40] Moreover Streit showed that even though the predicted air delivery ratio was 18.3 per cent greater for the complete mixing model than for displacement scavenging, the energy available at the turbine was essentially the same (figure 15.21).

15.10 The Turbocharger

Either the complete turbocharger characteristics may be used as boundary conditions at the manifold 'control volumes', or the turbocharger may be simulated by a nozzle in the exhaust with the boost conditions being specified independently.

15.10.1 Simulated Turbocharging

Simulating the turbocharger by placing a nozzle (of effective area equal to the turbine in question) in the exhaust is a convenient, but major simplification. The same thermodynamic relationships as those derived for flow through the valves may then be applied. From the instantaneous values of pressure, temperature and gas composition, the instantaneous gas and energy flows may be calculated. The latter may be integrated over the engine cycle to obtain the turbine energy available per cycle.

A target boost pressure must also be specified, the equivalent temperature being calculated from this pressure and an approximate value of compressor isentropic efficiency and charge cooler effectiveness, if appropriate. The integrated value of energy required for charge compression may also be evaluated. The ratio of compression energy to expansion energy available at the turbine will be the over-all efficiency requirement of the equivalent turbocharger.

From a few trial runs with different 'turbine areas' (nozzles) a match will be established that results in a realistic value of equivalent turbocharger efficiency.

This technique has the advantage not only of simplicity of programming, but also minimum data requirements. Thus an approximate turbocharger match may be established with little detailed turbocharger information. Using the data from the simulated turbocharging exercise, a turbocharger compressor of suitable characteristics (freedom from surge, etc.) and a turbine of the correct flow area may be chosen. In many cases this will be sufficient information from the program, and actual engine trials will begin with that turbocharger build. Naturally, since the process is approximate, some changes may have to be made on the test bed before matching is complete.

Simulated turbocharging with an exhaust nozzle is a useful technique but one potential discrepancy must be considered. How well does a nozzle represent the flow characteristics of a turbine? Reasonably well is the answer, except in the case of a radial inflow turbine at high expansion ratios. The nozzle will choke when the expansion ratio reaches

$$\frac{P_{in}}{P_{out}} = \left(\frac{\gamma + 1}{2}\right)^{\gamma/(\gamma-1)} \tag{15.28}$$

If $\gamma \approx 1.3$, then the choked expansion ratio is 1.83. However, the vaneless radial inflow turbine does not choke completely even when the over-all pressure ratio is substantially greater than 1.83. These characteristics can be modelled by using two orifices in series.

The error introduced by the nozzle model may be reduced by using an actual turbine flow capacity curve as an alternative. The relevant data may be held in a matrix within the program, interpolating to find the effective mass flow parameter between data points, or an algebraic expression may be developed by curve fitting the data (see section 15.10.2).

15.10.2 Actual Turbocharging

Actual turbocharging may be modelled by using complete turbine and compressor characteristics, if these are available. Since instantaneous turbine performance is required, it is usual to treat the problem as quasi-steady flow (that is, the turbine performs under non-steady flow in the same manner as it would if those instantaneous flow conditions were steady). Evidence on the error introduced by this assumption, in radial [41, 42, 43, 44] and axial flow turbines [45, 46] is not wholly consistent. Some of these differences are due to the difficult instrumentation problem, varying pulse shapes and frequencies, etc. However, it is generally thought that the error will not exceed 5 per cent.

The turbine flow and efficiency characteristics may be stored in the computer, usually in matrix form, with interpolation being used in between data points. The swallowing capacity curve of the axial flow turbine may realistically

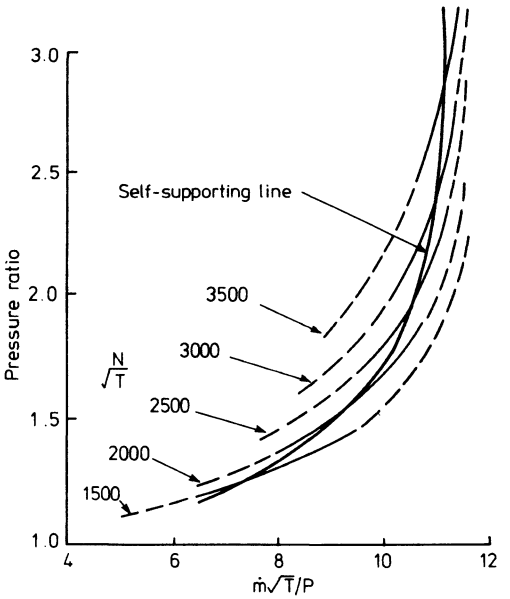

Figure 15.22 *Radial flow turbine mass flow characteristic*

be represented by a unique line, but the same is not true of the radial turbine. Rotational speed affects the characteristics through the influence of the centrifugal field (figure 15.22). However, the error introduced by the simplifying assumption of a single line is usually small. Usually the 'self-supporting' line (figure 15.22) is used, this being the operating line when turbine power balances compressor power under steady flow conditions. Turbine efficiency characteristics vary with turbine area, pressure ratio and/or speed (figure 15.23). Thus a complete matrix of efficiency curves (at various pressure ratios or turbocharger speeds) may have to be stored with correction for each turbine area. Much of this information may not be available, in which case predicted values (for example, by the Ainley-Mathieson technique discussed in chapter 5 for axial flow turbines) may have to be used. Regardless of whether measured or predicted turbine efficiencies are used, the values must be accurate otherwise a matching program will converge at an unrealistic boost pressure.

Further complications arise due to turbine windage and partial admission losses. Fortunately, unless the engine has a very unfavourable number of cylinders (chapter 7), windage periods will be short and the energy loss will be a small fraction of the total available. In this situation it may be adequate simply to assign an almost zero value to the turbocharger efficiency when the flow tends to zero. Ryti [47] has attempted to take proper account of windage losses, but if this is done, care has to be taken to avoid numerical instabilities due to the discontinuity in turbine power from positive to negative.

Partial admission losses may become significant when multi-entry turbines are used. Generally the turbine will be modelled as a series of smaller turbines (running at the same speed), each having the appropriate mass flow curve (that is, two turbines having half the flow area). Most partial admission data is obtained from tests with pure ventilation in the non-flow sectors. This is unlikely to occur for any significant period of time in a normal pulse turbocharging system, hence use of this data will over-estimate the efficiency loss. Full admission data will be more realistic if, for example, three cylinders are connected to a turbine entry. If the cylinder grouping results in less favourable turbine entry conditions, a partial admission loss coefficient may have to be used, reducing the turbine efficiency from full admission values by a few per cent.

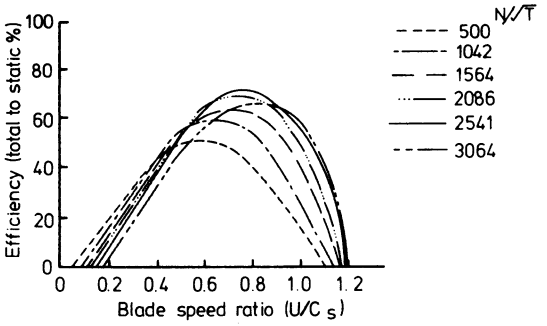

Figure 15.23 *Radial flow turbine efficiency curves*

Twin-entry vaneless radial flow turbines are usually divided meridionally, rather than circumferentially (figure 15.24). Flow through one sector has a considerable influence on the flow through the other. Thus representation of the flow characteristics as two separate 'half-turbines' causes errors, particularly at low engine speeds when pulse energy utilisation is important. Figure 15.25 shows that the equivalent isentropic area of each entry (the effective area that produces the required flow rate with density and velocity calculated via isentropic expansion to the exit pressure) is a function not only of the mean pressure ratio of the two entries, but also of the pressure ratio between the entries (P_1/P_2, figure 15.25).

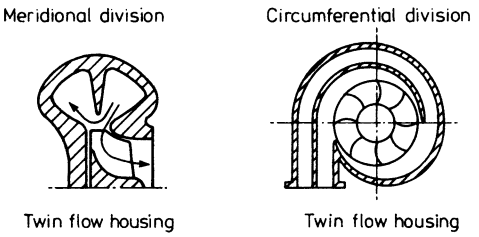

Figure 15.24 *Types of turbine housings (twin entry)*

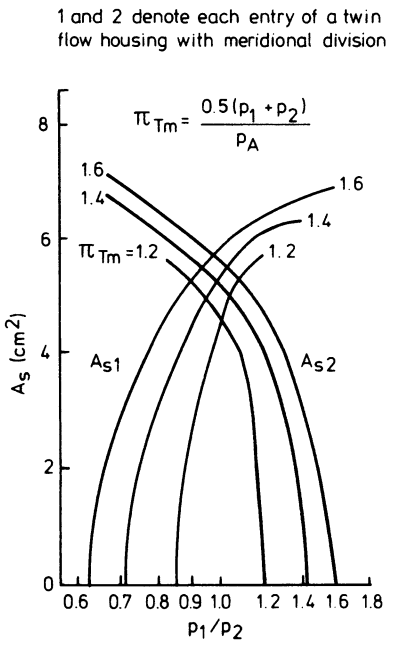

Figure 15.25 *Isentropic flow areas as a function of pressure ratio between turbine entries, with a twin-entry turbine [48]*

The compressor must also be represented by complete characteristics and these are usually more readily available. The data (pressure ratio, mass flow parameter, speed parameter and efficiency, at a series of points) can also be stored in matrix form, with linear interpolation between points.

With full compressor and turbine characteristics and a combustion model it is possible to produce a program that iterates until turbine and compressor powers balance, hence the program will find the turbocharger match automatically. [19] Error messages can be printed out if iteration results in the operating point moving into regions of compressor surge, choking, etc.

15.11 Engine Friction

Engine performance prediction programs generate the pressure-volume diagrams in the cylinder and enable indicated work and power output to be calculated. Since it is the brake power output at the flywheel that is of interest, the power required to overcome frictional losses in the engine and to drive the auxiliaries must be deducted. It is useful to have an analytical expression for these losses (usually lumped together under the heading of 'engine friction'), based on experimental or estimated data.

Most experimental test techniques include the work done by the piston during the intake and exhaust strokes (pumping work) and heat transfer losses directly in the measurement. The engine cycle analysis program will already take this work into account, so it must be calculated and subtracted from the test data. Potentially the best method of evaluating friction is to evaluate the indicated power output from an accurate cylinder pressure diagram and to subtract measured brake power output. However, this requires very careful and accurate measurement of the cylinder pressure diagram. [49] Alternatively, the engine can be motored electrically. Figure 15.26 shows the results of motoring tests on an engine as it is progressively dis-mantled. Values of frictional losses (expressed as frictional mean effective pressure) obtained from accurate cylinder pressure diagrams are included for comparison (dashed lines, 'IMEP meter').

Two simpler techniques are available for estimating frictional losses, the Willans line and 'Morse' tests, although both also include pumping losses. For the Willans line, the fuel consumption against BMEP line is extrapolated down to zero fuelling (figure 15.27), the resultant ordinate being the frictional mean effective pressure loss (FMEP or negative BMEP). However, error is introduced by the extrapolation, particularly since the line is slightly curved. The 'Morse' test is the equivalent of cutting the ignition to one cylinder of a petrol engine. The fuel to one cylinder is cut, and the engine load is adjusted so that the initial speed is regained. The load difference may be used to evaluate the frictional loss from

$$FL = (n - 1)LT_1 - nLT_2$$

where LT_1 and LT_2 = dynamometer loads (torques) normally running and with one cylinder cut

n = number of cylinders

FL = the frictional loss expressed in terms of engine load.

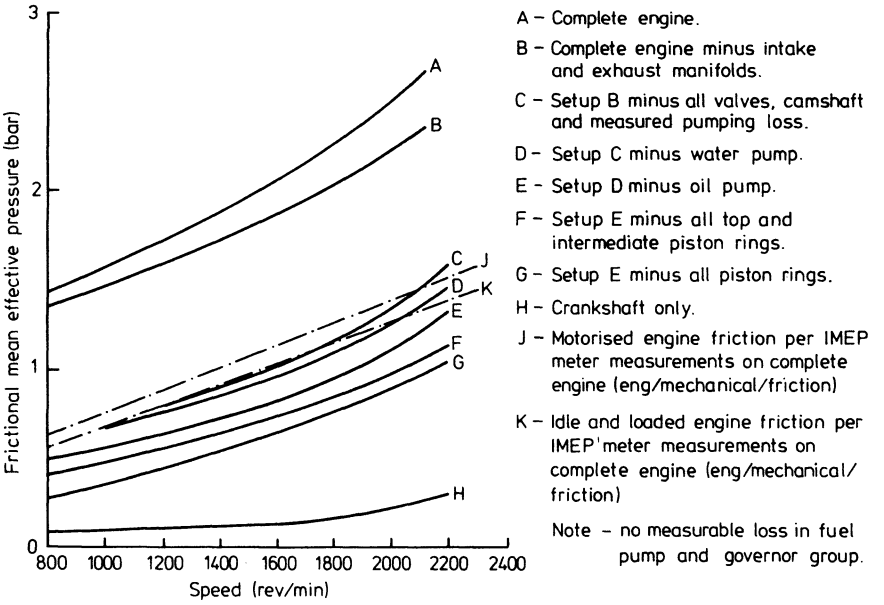

Figure 15.26 *Comparison of motored losses and FMEP evaluated from an accurate indicator diagram [49]*

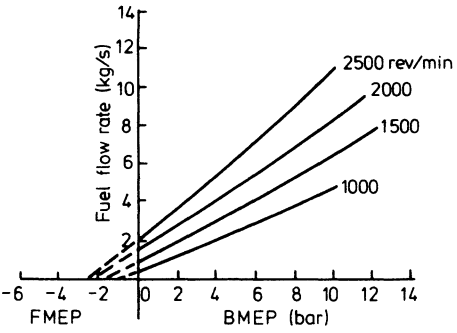

Figure 15.27 *Willans line test to estimate frictional losses*

Ideally, the fuel to each cylinder should be cut in turn, in case the work distribution between cylinders is not exactly equal. Furthermore, care must be taken to avoid influencing the fuel supply to all cylinders when one is cut out, if a common fuel pump is fitted. Only the cylinder pressure measurement method takes correct account on cylinder pressure forces on bearing surfaces.

Having measured the over-all 'frictional' losses, an algebraic correlation is required for computational purposes. Millington and Hartles [50] have corre-

lated the results of numerous motoring tests on naturally aspirated small engines into the formula

$$FMEP \text{ (motoring)} = (CR - 4)/14.5 + 0.475 \times 10^{-3} N + 3.95 \times 10^{-3} C_{pis}^2$$

For turbocharged engines, Chen and Flynn [51] recognised that the frictional losses will not only be dependant on engine speed (or mean piston speed) but also on the peak cylinder pressure, through its influence on bearing loads, etc. Their correlation takes the form

$$FMEP = 0.137 + 0.005P_{max} + 0.162C_{pis} \quad (15.29)$$

Values of the constants may be adjusted to suit particular engines.

15.12 Solution of the Energy Equation – Filling and Emptying' Models

15.12.1 Introduction

The basic energy and continuity of mass equations may be applied to the inlet manifold, cylinders and exhaust manifolds, although many of the terms may be zero for part or all of a cycle. Each manifold or cylinder will be a unique control volume being successively filled and emptied as mass passes through the engine – hence the term 'filling and emptying' model. Each control volume, $V(i)$, will be assigned a reference number (i), and the energy and continuity equations will be solved for each in turn. Thus the rate of change of temperature (equation 15.6), pressure, equivalence ratio and mass may be calculated at discrete points in the engine cycle.

The calculation proceeds in a series of time (or crank angle) steps. Thus if the values of T, V, F and m are known, defining the state of the gas in each control volume (manifolds and cylinders) at the start of a step, then the problem reduces to the following: given the state of the working medium in, for example, the cylinder, at instant 1, calculate the state at a moment later, instant 2, using an equation for the rate of change of state (for example, equation 15.6), with time or crank angle. Numerical integration of the equations for dT/dt, dm/dt and dF/dt is required. Pressure is a dependent variable which may then be calculated.

Most computer programs developed to simulate turbocharged diesel engines use Runge-Kutta or predictor-corrector numerical integration methods. Both are based on knowledge of the approximate shape of the curve (for example, dT/dt) over the step, from data at the initial point and the rate of change equation. For example, the predictor-corrector methods (figure 15.28) calculate a first estimate at instant 2 (point 2a) by the above method, then use data at instants 1 and 2 (that is, dT/dt at points 1 and 2, figure 15.28) to evaluate a second, more accurate value of dT/dt mean. The process may be repeated for several iterations to achieve mathematical convergence of the instant 2 value. Numerical instabilities may occur in most numerical methods if care is not taken. In an

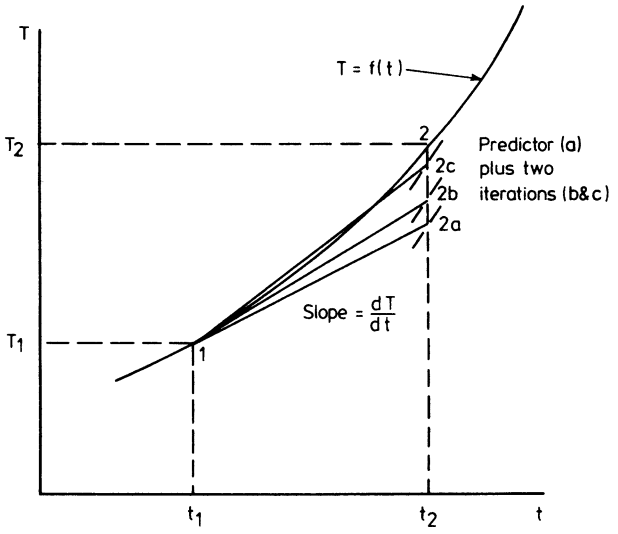

Figure 15.28 *Predictor-corrector method of numerical integration*

engine simulation program this is most likely to occur during the scavenging period (if this is large) due to the interconnection of several control volumes at similar pressures. The problem can best be avoided by adopting suitable numerical methods, using small step sizes (typically 1°) and 'weighting' successive iterations in mass flow (relaxation method). Iterative methods, such as the predictor-corrector, are generally faster and more stable than the Runge-Kutta and simpler techniques. [52]

At each step, new values of T, F and m are found and pressure calculated in each control volume. Thus the complete thermodynamic state in each cylinder and manifold is known throughout the cycle. Sufficient information is then available to calculate the work output per cycle (although this would normally be evaluated as the sum of the work increments calculated at each step) and hence indicated power output. Subtraction of frictional losses (section 15.11) results in brake power output. A very detailed account of the method is given by Watson and Janota. [53] A summary of the application of equation 15.6 to cylinder and manifolds is given below.

15.12.2 Application of Conservation Equations to Cylinders and Manifolds

The basis of the 'filling and emptying' model is to treat each cylinder and each manifold as a thermodynamic control volume. Equation 15.6 is an equation for the conservation of energy in a general control volume, and may be applied to cylinders and manifolds. This equation can be rewritten for any control volume

(i), on a crank angle (θ), rather than a time basis, as

$$\frac{dT(i)}{d\theta} = \left\{ \left[\sum_{sf} \frac{dQ_{sf(i)}}{d\theta} + \sum_{in} \left(\frac{dH_0(i)}{d\theta}\right)_{in} - \sum_{out} \left(\frac{dH_0(i)}{d\theta}\right)_{out} + \frac{dm_f}{d\theta} h_{for} - u(i) \frac{dm(i)}{d\theta} \right] \frac{1}{m(i)} - \frac{RT(i)}{V(i)} \frac{dV(i)}{d\theta} - \frac{\partial u(i)}{\partial F(i)} \frac{\partial F(i)}{\partial \theta} \right\} \Big/ \frac{\partial u(i)}{\partial T(i)} \quad (15.30)$$

where h_{for} = enthalpy of formation of the fuel (from its constituent elements).

For convenience, the enthalpy of inflowing and outflowing gases have been separated in equation 15.30. Furthermore, the enthalpy associated with the injection of a mass of fuel (dm_f) is shown calculated from the enthalpy of formation of the fuel from its constituent elements (used as the datum for the property expressions given in section 15.5).

In addition, equations for the conservation of mass, both air and fuel, are required. Considering total mass, (fuel plus air)

$$\frac{dm(i)}{d\theta} = \Sigma \left(\frac{dm(i)}{d\theta}\right)_j = \Sigma \left(\frac{dm(i)}{d\theta}\right)_{in} - \Sigma \left(\frac{dm(i)}{d\theta}\right)_{out} + \Sigma \left(\frac{dm_f}{d\theta}\right) \quad (15.31)$$

It is convenient to base a second specie conservation equation on the mass of burnt fuel. This, together with the total mass conservation equation (15.31), replaces the need for a separate conservation equation for air.

$$m(i) = m_a(i) + m_{fb}(i) \quad (15.32)$$

Since equation 15.30 incorporated the term $\partial F(i)/\partial\theta$, this must be evaluated.

$$F(i) = \frac{f(i)}{f_{sto}} = \frac{m_{fb}(i)}{m_a(i) f_{sto}} = \frac{m_{fb}(i)}{[m(i) - m_{fb}(i)] f_{sto}} \quad (15$$

Now

$$m_a(i) = \frac{m(i) m_a(i)}{m_a(i) + m_{fb}(i)} = \frac{m(i)}{[1 + (m_{fb}(i)/m_a(i))]} = \frac{m(i)}{1 + F(i) f_{sto}}$$

Putting $1 + F(i) f_{sto} = F1(i)$

$$m_a(i) = \frac{m(i)}{F1(i)}$$

Also

$$m_{fb}(i) = \frac{m(i)\, m_{fb}(i)}{m_a(i) + m_{fb}(i)} = \frac{m(i)\, m_{fb}(i)}{m_a(i)\,[(1 + (m_{fb}(i)/m}$$

that is

$$m_{fb}(i) = \frac{m(i) F(i) f_{sto}}{F1(i)}$$

Differentiating equation 15.33 gives

$$\frac{dF(i)}{d\theta} = \frac{1}{f_{sto}} \left\{ [m(i) - m_{fb}(i)] \frac{dm_{fb}(i)}{d\theta} - m_{fb}(i) \left[\frac{dm(i)}{d\theta} - \frac{dm_{fb}(i)}{d\theta} \right] \right\} \frac{1}{m_a^2(i)}$$

$$= \frac{1}{f_{sto} m_a(i)} \left(\frac{m(i)}{m_a(i)} \frac{dm_{fb}(i)}{d\theta} - \frac{m_{fb}(i)}{m_a(i)} \frac{dm(i)}{d\theta} \right)$$

that is

$$\frac{dF(i)}{d\theta} = \frac{F1(i)}{m(i)} \left(\frac{F1(i)}{f_{sto}} \frac{dm_{fb}(i)}{d\theta} - F(i) \frac{dm(i)}{d\theta} \right) \tag{15.35}$$

Equations 15.30, 15.31 and 15.35 are applied to each control volume in turn. Evaluation of $dT(i)/d\theta$, $dm(i)/d\theta$ and $dF(i)/d\theta$ enables new values of $T(i)$, $m(i)$ and $F(i)$ to be calculated at the end of a step. The perfect gas equation is then used to calculate $P(i)$, completing the solution for the step other than for storing data to be used later or printed out at the end of the cycle.

The solution of equations 15.30, 15.31 and 15.35 will be considered for cylinders, inlet and exhaust manifolds in turn. In all cases it is assumed that $T(i)$, $m(i)$, $F(i)$ and $P(i)$ are known at the beginning of a step. For the very first calculation step, these will be guessed values; for the remainder they will be known from the end of the previous step. For simplicity of presentation the control volume label 'i' will be omitted when a particular control volume is considered.

The Cylinder

The basic processes occurring in the cylinder can be divided into the following

Four-stroke	Two-stroke
(1) Closed cycle period	Closed cycle period
(2) Exhaust period	Blow-down period
(3) Valve overlap period	Scavenge period
(4) Inlet period	

These will be considered separately, and will be sub-divided according to flow direction as normal and reverse flow situations, and whether combustion is occurring.

(1) *Closed cycle period, from IVC to EVO*

a) Without combustion. During this period

$$\frac{dF}{d\theta} = 0 \; ; \; \frac{dm}{d\theta} = 0 \; ; \; \frac{dH_0}{d\theta_{\text{in or out}}} = 0 \; ; \; \frac{dm_{fb}}{d\theta} = 0$$

ıtion 15.30 becomes

$$\frac{dT}{\mathrm{i}\theta} = \left(\sum_{sf} \frac{dQ_{sf}}{d\theta} \times \frac{1}{m} - \frac{RT}{V} \frac{dV}{d\theta} \right) \Big/ \frac{\partial u}{\partial T}$$

The first term is evaluated from the heat transfer model (equation 15.20), summed for all cylinder surfaces, and knowledge of total mass in the cylinder (m). The second term is calculated from equation 15.8 and knowledge of cylinder gas temperature and volume at the start of the step. $\partial u/\partial T$ is calculated from the gas property relationship (equation 15.9) knowing temperature and equivalence ratio of the gas. Temperature at the end of the step may then be calculated, followed by pressure (from the perfect gas equation). Mass and equivalence ratio remain unchanged.

(b) With combustion. During this period

$$\frac{\mathrm{d}H_0}{\mathrm{d}\theta_{\text{in or out}}} = 0\,;\ \frac{\mathrm{d}m}{\mathrm{d}\theta} = \frac{\mathrm{d}m_\mathrm{f}}{\mathrm{d}\theta}$$

Fuel is assumed to be added to the cylinder contents and to burn instantaneously as it is added. The rate at which fuel is added and burnt ($\mathrm{d}m_{\mathrm{fb}}/\mathrm{d}\theta$) is calculated from the fuel burning rate model (*FBR*, equation 15.12 or 15.15). Equation 15.35 becomes

$$\frac{\mathrm{d}F}{\mathrm{d}\theta} = \frac{F1}{m}\left(\frac{F1}{f_{\text{sto}}}\frac{\mathrm{d}m_{\mathrm{fb}}}{\mathrm{d}\theta} - F\frac{\mathrm{d}m}{\mathrm{d}\theta}\right) = \frac{F1}{mf_{\text{sto}}}\frac{\mathrm{d}m_\mathrm{f}}{\mathrm{d}\theta}$$

and equation 15.30 becomes

$$\frac{\mathrm{d}T}{\mathrm{d}\theta} = \left\{\left[\sum_{\text{sf}}\frac{\mathrm{d}Q_{\text{sf}}}{\mathrm{d}\theta} + \frac{\mathrm{d}m_\mathrm{f}}{\mathrm{d}\theta}h_{\text{for}} - u\frac{\mathrm{d}m}{\mathrm{d}\theta}\right]\frac{1}{m} - \frac{RT}{V}\frac{\mathrm{d}V}{\mathrm{d}\theta} - \frac{\partial u}{\partial F}\frac{\partial F}{\partial \theta}\right\}\Big/\frac{\partial u}{\partial T}$$

The terms in this equation can be found from the heat transfer model ($\mathrm{d}Q/\mathrm{d}\theta$), the fuel burning rate model ($\mathrm{d}m_\mathrm{f}/\mathrm{d}\theta$), the piston-crank angle equation ($\mathrm{d}V/\mathrm{d}\theta$), the gas property relationships (u, $\partial u/\partial F$, $\partial u/\partial T$) and the above equation for $\partial F/\partial\theta$. Note that the gas property relationships and the enthalpy of formation term together take account of the energy released by combustion of fuel mass ($\mathrm{d}m_\mathrm{f}$).

(2) *Exhaust or blow-down period from EVO to IVO* During this period, combustion is assumed to be complete and gas at constant equivalence ratio flows into the exhaust manifold. However, a second flow condition of reverse flow from exhaust manifold to cylinder can occur instantaneously.

(a) Normal flow, cylinder to exhaust manifold, $P_{\text{cyl}} > P_{\text{p}}$. During this period

$$\frac{\mathrm{d}F}{\mathrm{d}\theta} = 0\,;\ \left(\frac{\mathrm{d}m}{\mathrm{d}\theta}\right)_{\text{in}} = 0\,;\ \left(\frac{\mathrm{d}H_0}{\mathrm{d}\theta}\right)_{\text{in}} = 0\,;\ \frac{\mathrm{d}m_\mathrm{f}}{\mathrm{d}\theta} = 0$$

Equation 15.31 becomes

$$\frac{\mathrm{d}m}{\mathrm{d}\theta} = \left(\frac{\mathrm{d}m}{\mathrm{d}\theta}\right)_{\text{out}}$$

and equation 15.30 becomes

$$\frac{\mathrm{d}T}{\mathrm{d}\theta} = \left\{\left[\sum_{\text{sf}}\frac{\mathrm{d}Q_{\text{sf}}}{\mathrm{d}\theta} - \left(\frac{\mathrm{d}H_0}{\mathrm{d}\theta}\right)_{\text{out}} - u\frac{\mathrm{d}m}{\mathrm{d}\theta}\right]\frac{1}{m} - \frac{RT}{V}\frac{\mathrm{d}V}{\mathrm{d}\theta}\right\}\Big/\frac{\partial u}{\partial T}$$

$(\mathrm{d}m/\mathrm{d}\theta)_{\text{out}}$ is evaluated from the valve flow model, equation 15.26 or 15.27,

depending whether the valve is choked or not. The pressure ratio at the exhaust valve is obtained from values of cylinder and exhaust manifold pressure at the beginning of the step. Valve area will be the area at the appropriate crank angle. dH_0 is evaluated from

$$\left(\frac{dH_0}{d\theta}\right)_{out} = h_0 \left(\frac{dm}{d\theta}\right)_{out}$$

where $h_0 = u + PV = u + RT$, u being calculated from the gas property equation 15.9 at the cylinder value of temperature and equivalence ratio.

(b) Reverse flow from exhaust manifold to cylinder, $P_p > P_{cyl}$. Equations 15.31 and 15.30 become, assuming no change in equivalence ratio between exhaust manifold and cylinder

$$\frac{dm}{d\theta} = \left(\frac{dm}{d\theta}\right)_{in}$$

and

$$\frac{dT}{d\theta} = \left\{ \left[\sum_{sf} \frac{dQ_{sf}}{d\theta} + \left(\frac{dH_0}{d\theta}\right)_{in} - u \frac{dm}{d\theta} \right] \frac{1}{m} - \frac{RT}{V} \frac{dV}{d\theta} \right\} \Big/ \frac{\partial u}{\partial T}$$

These equations are evaluated in the same manner as shown previously except that $(dm/d\theta)_{in}$ is calculated from reverse flow through the valve and h_0 is calculated using the exhaust manifold equivalence ratio and temperature.

(3) *Valve overlap or scavenge period, from IVO to EVC* During this period both valves or ports are open and normally air will flow from the inlet manifold into the cylinder, and a mixture of air and combustion products into the exhaust manifold. The scavenge model will determine the composition of cylinder contents and the gas flowing into the exhaust manifold. Account must be taken of possible reverse flow from exhaust manifold to cylinder and from cylinder to inlet manifold, during some crank-angle steps.

(a) Normal scavenging, $P_m > P_{cyl} > P_p$. During this period $dm_f/d\theta = 0$. If a complete mixing scavenge model (section 15.9) is used, then the flow into the cylinder may be assumed to be at inlet manifold equivalence ratio and the flow out of the cylinder at cylinder equivalence ratio. The treatment of the cylinder control volume as being of homogeneous composition automatically imposes a complete mixing model between the gas in the cylinder and that entering.

Equations 15.31, 15.35 and 15.30 become

$$\frac{dm}{d\theta} = \left(\frac{dm}{d\theta}\right)_{in} - \left(\frac{dm}{d\theta}\right)_{out}$$

$$\frac{dF}{d\theta} = \frac{F1}{m}\left[\frac{F1}{f_{sto}} \frac{dm_{fb}}{d\theta} - F \frac{dm}{d\theta}\right]$$

and

$$\frac{dT}{d\theta} = \left\{ \left[\sum_{sf} \frac{dQ_{sf}}{d\theta} + \left(\frac{dH_0}{d\theta}\right)_{in} - \left(\frac{dH_0}{d\theta}\right)_{out} - u \frac{dm}{d\theta} \right] \frac{1}{m} - \frac{RT}{V} \frac{dV}{d\theta} - \frac{\partial u}{\partial F} \frac{\partial F}{\partial \theta} \right\} \Big/ \frac{\partial u}{\partial T}$$

The mass flow rates are evaluated from the valve flow equation (15.26 or 15.27) and the stagnation enthalpies are calculated from the temperatures and equivalence ratios at the start of the step, for the inlet manifold (for $h_{0_{in}}$) and the cylinder ($h_{0_{out}}$). The mass flow rates of burnt fuel must be calculated from knowledge of total mass flow rate and equivalence ratio of the gas. Thus

$$\frac{dm_{fb}}{d\theta} = \left(\frac{dm_{fb}}{d\theta}\right)_{in} - \left(\frac{dm_{fb}}{d\theta}\right)_{out}$$

that is

$$\frac{dm_{fb}}{d\theta} = \frac{F_{in} f_{sto}}{Fl_{in}} \left(\frac{dm}{d\theta}\right)_{in} - \frac{F_{out} f_{sto}}{Fl_{out}} \left(\frac{dm}{d\theta}\right)_{out}$$

(b) Reverse flow into cylinder, $P_m > P_{cyl} < P_p$. During this period $dm_f/d\theta = 0$; $(dm/d\theta)_{out} = 0$; $(dm/d\theta)_{in}$ is the sum total of mass flows from inlet and exhaust manifolds, at the equivalence ratio of inlet and exhaust manifolds respectively. The appropriate simplified versions of equations 15.31, 15.35 and 15.30 will not be given, but are readily derived.

(c) Reverse flow into inlet manifold, $P_p > P_{cyl} > P_m$. During this period $dm_f/d\theta = 0$. Mass flow rates are calculated from exhaust manifold to cylinder, and from cylinder to inlet manifold, at the equivalence ratios of exhaust manifold, and cylinder respectively. The equations are the same as those given in section 3(a), except that the flow direction is reversed.

(4) *Inlet period, from EVC to IVC*

(a) Normal flow, inlet manifold to cylinder, $P_m > P_{cyl}$. During this period $dm_f/d\theta = 0$; $(dm/d\theta)_{out} = 0$. Equations 15.31, 15.35 and 15.30 become

$$\frac{dm}{d\theta} = \left(\frac{dm}{d\theta}\right)_{in}$$

$$\frac{dF}{d\theta} = \frac{Fl}{m}\left(\frac{Fl}{f_{sto}}\frac{dm_{fb}}{d\theta} - F\frac{dm}{d\theta}\right)$$

and

$$\frac{dT}{d\theta} = \left\{\left[\sum_{sf}\frac{dQ_{sf}}{d\theta} + \left(\frac{dH_0}{d\theta}\right)_{in} - u\frac{dm}{d\theta}\right]\frac{1}{m} - \frac{RT}{V}\frac{dV}{d\theta} - \frac{\partial u}{\partial F}\frac{\partial F}{\partial \theta}\right\}\Big/\frac{\partial u}{\partial T}$$

$dm_{fb}/d\theta$ must be calculated from knowledge of inlet manifold equivalence ratio. Normally this will be zero, but it could have a positive value due to previous reverse flow from any cylinder to the inlet manifold.

(b) Reverse flow, cylinder to inlet manifold, $P_{cyl} > P_m$. During this flow regime, the equivalence ratio in the cylinder will not change, hence $dF/d\theta = 0$; $dm_f/d\theta = 0$; $(dm/d\theta)_{in} = 0$. Equations 15.31 and 15.30 become

$$\frac{dm}{d\theta} = \left(\frac{dm}{d\theta}\right)_{out}$$

and

$$\frac{dT}{d\theta} = \left\{\left[\sum_{sf}\frac{dQ_{sf}}{d\theta} - \left(\frac{dH_0}{d\theta}\right)_{out} - u\frac{dm}{d\theta}\right]\frac{1}{m} - \frac{RT}{V}\frac{dV}{d\theta}\right\}\Big/\frac{\partial u}{\partial T}$$

The Inlet Manifold

Two flow regimes are likely to occur. Normal flow will be from the compressor to the inlet manifold and from inlet manifold to one or more cylinders, depending on how many have their inlet valve open during each crank-angle step. Reverse flow from any cylinder must also be considered, but reverse flow through the turbocharger compressor is unlikely to occur.

(a) Normal flow from compressor to cylinders, $P_m > P_{cyl}$. In this flow regime, air is being supplied from the compressor, hence inlet manifold equivalence ratio is constant and zero, unless some reverse flow from a cylinder has previously occurred. Taking this simpler case, $dF/d\theta = 0$; $dm_{fb}/d\theta = 0$; $dQ_{sf}/d\theta \approx 0$; $dV/d\theta = 0$. In practice, heat transfer to or from the inlet manifold is usually neglected due to the small gas to wall surface temperature difference. Thus equations 15.31 and 15.30 become

$$\frac{dm}{d\theta} = \left(\frac{dm}{d\theta}\right)_{in} - \sum_{out} \left(\frac{dm}{d\theta}\right)_{out}$$

and

$$\frac{dT}{d\theta} = \left\{ \left[\left(\frac{dH_0}{d\theta}\right)_{in} - \sum_{out} \left(\frac{dH_0}{d\theta}\right)_{out} - u \frac{dm}{d\theta} \right] \frac{1}{m} \right\} \Big/ \frac{\partial u}{\partial t}$$

The inlet mass flow rate, $(dm/d\theta)_{in}$, is calculated from the turbocharger compressor characteristic, as a function of turbocharger speed and pressure ratio (compressor inlet to inlet manifold). The outlet mass flow rates come from use of the valve flow equation at the inlet valves of appropriate cylinders.

(b) Reverse flow from any cylinder, $P_{cyl} > P_m$. If reverse flow occurs at any cylinder, then inlet manifold equivalence ratio will be affected. During this period $dm_{fb}/d\theta = 0$; $dQ_{sf}/d\theta \approx 0$; $dV/d\theta = 0$. The appropriate versions of equations 15.31, 15.35 and 15.30 can be derived but are not presented here.

The Exhaust Manifold

Two flow regimes can be identified: normal flow from cylinders to manifold and from manifold to turbine, and reverse flow at any cylinder. The possibility of reverse flow at the turbine is usually ignored. Heat transfer from gas to the exhaust manifold surface must be accounted for, unless the manifold is very well lagged. A number of empirical *Nu-Re* relationships for pipe flow are available for calculating the convective heat transfer coefficient and hence heat transfer (see, for example, Janota *et al.* [54]). The equivalence ratio in the exhaust manifold will not be constant if gas is entering from a cylinder during its scavenge or overlap period.

(a) Normal flow from cylinders and to turbine, $P_{cyl} > P_p$. During this period $dm_{fb}/d\theta = 0$; $dV/d\theta = 0$. Equations 15.31, 15.35 and 15.30 become

$$\frac{dm}{d\theta} = \sum \left(\frac{dm}{d\theta}\right)_{in} - \left(\frac{dm}{d\theta}\right)_{out}$$

$$\frac{dF}{d\theta} = \frac{F1}{m}\left[\frac{F1}{f_{sto}}\frac{dm_{fb}}{d\theta} - F\frac{dm}{d\theta}\right]$$

and

$$\frac{dT}{d\theta} = \left\{\left[\frac{dQ_{sf}}{d\theta} + \sum_{in}\left(\frac{dH_0}{d\theta}\right)_{in} - \left(\frac{dH_0}{d\theta}\right)_{out} - u\frac{dm}{d\theta}\right]\frac{1}{m} - \frac{\partial u}{\partial F}\frac{\partial F}{\partial \theta}\right\}\Big/\frac{\partial u}{\partial T}$$

The change in mass of burnt fuel (dm_{fb}) must be calculated from knowledge of the mass flows into the manifold from various cylinders and the equivalence ratio of each flow. Thus

$$\frac{dm_{fb}}{d\theta} = \Sigma\left(\frac{Ff_{sto}}{F1}\right)_{in}\left(\frac{dm}{d\theta}\right)_{in} - \left(\frac{Ff_{sto}}{F1}\right)_{out}\left(\frac{dm}{d\theta}\right)_{out}$$

The mass flow rate out of the manifold is calculated from the turbine flow characteristic (figure 15.22), from the turbine pressure ratio ($P_p/P_{\text{turbine exit}}$).

(b) Reverse flow into a cylinder, $P_p > P_{cyl}$. Equations 5.31, 5.35 and 5.30 become

$$\frac{dm}{d\theta} = \Sigma\left(\frac{dm}{d\theta}\right)_{in} - \Sigma\left(\frac{dm}{d\theta}\right)_{out}$$

$$\frac{dF}{d\theta} = \frac{F1}{m}\left[\frac{F1}{f_{sto}}\frac{dm_{fb}}{d\theta} - F\frac{dm}{d\theta}\right]$$

and

$$\frac{dT}{d\theta} = \left\{\left[\frac{dQ_{sf}}{d\theta} + \Sigma\left(\frac{dH_0}{d\theta}\right)_{in} - \Sigma\left(\frac{dH_0}{d\theta}\right)_{out} - u\frac{du}{d\theta}\right]\frac{1}{m} - \frac{\partial u}{\partial F}\frac{\partial F}{\partial \theta}\right\}\Big/\frac{\partial u}{\partial T}$$

Also

$$\frac{dm_{fb}}{d\theta} = \Sigma\left(\frac{Ff_{sto}}{F1}\right)_{in}\left(\frac{dm}{d\theta}\right)_{in} - \Sigma\left(\frac{Ff_{sto}}{F1}\right)_{out}\left(\frac{dm}{d\theta}\right)_{out}$$

15.12.3 Flow Diagram for a 'Filling and Emptying' Computer Program

Figure 15.29 is a flow diagram for a 'filling and emptying' computer program, in simplified form. Initially the data describing all geometric features of the engine is read in, together with data specifying the test condition, and initial estimates of pressure, temperature, equivalence ratio in each control volume (cylinders and manifolds). The starting crank angle is set and appropriate geometric parameters (cylinder volume and heat transfer area, valve areas) calculated. The instantaneous fuel burning rate is then calculated for all cylinders (it will be zero for many).

The program then enters a loop, skipping the next step on the very first crank-angle step. At any other step, the values of $dm/d\theta$, $dF/d\theta$ and $dT/d\theta$ from the end of the previous step, are used to 'predict' estimates of m, F and T at the end

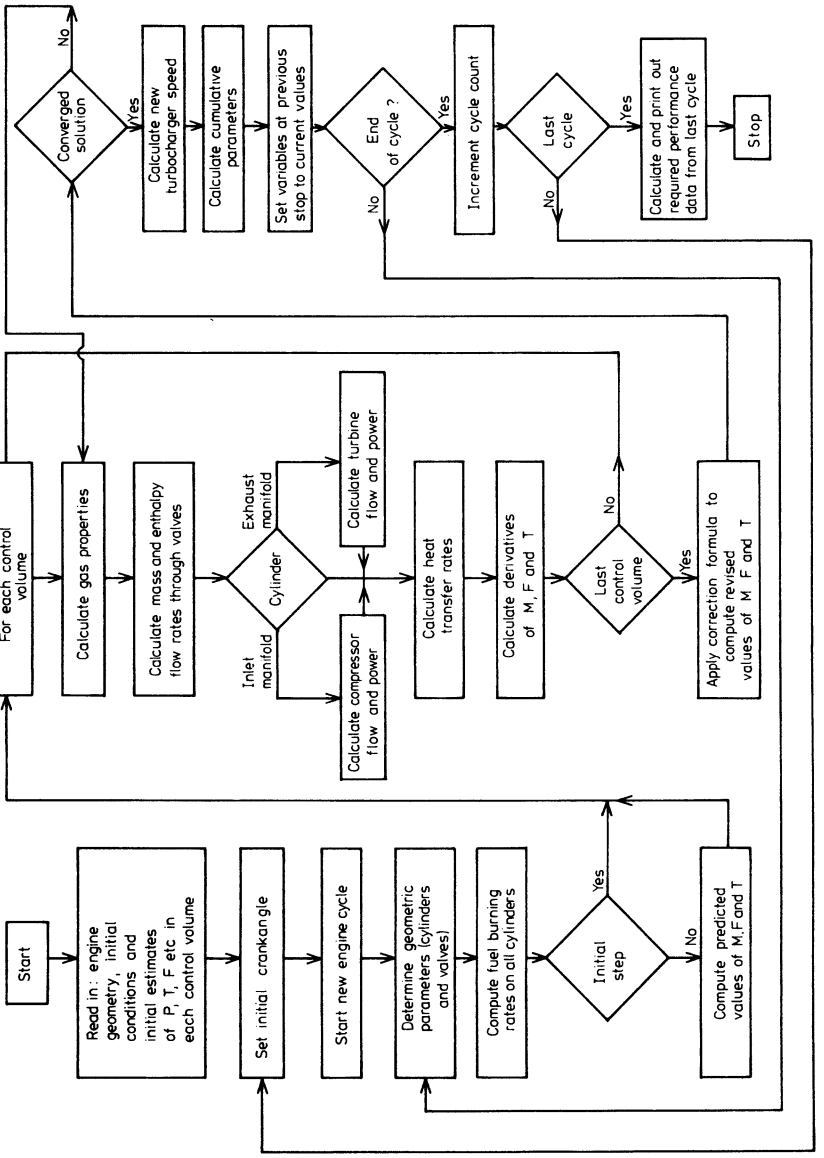

Figure 15.29 *Flow diagram for 'filling and emptying' model*

of the current step (figure 15.28), in each control volume. Pressure is calculated and F, T and P are used to calculate gas property relationships and mass and enthalpy flows through the valves, as required by equation 15.30, tailored to the appropriate control volume and flow situation. Compressor and turbine subroutines are used to calculate their respective mass flow rates. Heat transfer from each control volume is also calculated. Revised values of $dm/d\theta$, $dF/d\theta$ and $dT/d\theta$ are then used to 'correct' the initial estimate of m, F and T at the end of the step (figure 15.28), in each control volume. If the change in m, F or T is significant, the corrector loop will be repeated until convergence is achieved.

If a 'self-matching' program is used, then knowledge of the mass flow rate, energy flow rate and pressure ratio at the turbine and compressor are used together with the turbine and compressor characteristics to calculate a new turbocharger speed. This, together with the pressure ratio, will enable a new compressor mass flow rate to be calculated for the next step.

The calculation will proceed in small steps, for a complete engine cycle, with instantaneous and cumulative values of useful parameters (for example, cylinder pressure, piston work, mass flows) being stored for subsequent printing as output. Since initial starting values of P, T and F in each control volume were approximate, the cumulative values at the end of one cycle will not be accurate, and one or two more cycles may need to be calculated to ensure proper convergence and accuracy.

15.12.4 Application of Filling and Emptying Models

Filling and emptying models have been widely used for turbocharger matching, performance calculations, stress and thermal loading calculations, optimisation of exhaust manifold design, valve areas and timing optimisation and many other applications. Some examples are given below.

Figure 15.30 compares predicted and measured instantaneous pressures in the exhaust pipe of a single-cylinder engine. A nozzle has been used to simulate the turbine and each diagram relates to a different size of exhaust pipe between exhaust valve and nozzle. Very accurate prediction is shown with a small manifold, whose length is equal to its diameter (top diagram). If a larger manifold is fitted (of 2.35 times the volume of the previous case) the pressure diagrams are again accurately predicted, but if the larger volume is obtained by increasing pipe length and not diameter (middle diagram, chain-dotted line), then small pressure wave pulsations measured are not being predicted. Accuracy is least satisfactory with a very large volume manifold, formed by using a very long pipe (figure 15.30 bottom diagram: volume 10 times top diagram). The model accurately predicts the pressure diagram when the large manifold is as long as its diameter (solid line), but not when the diameter of the smallest manifold is retained and the pipe is made 23 times as long (chain-dotted line). It may be concluded that the filling and emptying model is capable of accurately predicting pressure pulsations in large or small manifolds, but not very long pipes.

The potential accuracy of a complete filling and emptying model is shown in figure 15.31, in terms of a truck engine performance. This calculation was made using the 'self-matching' type of program in which the boost pressure is predicted

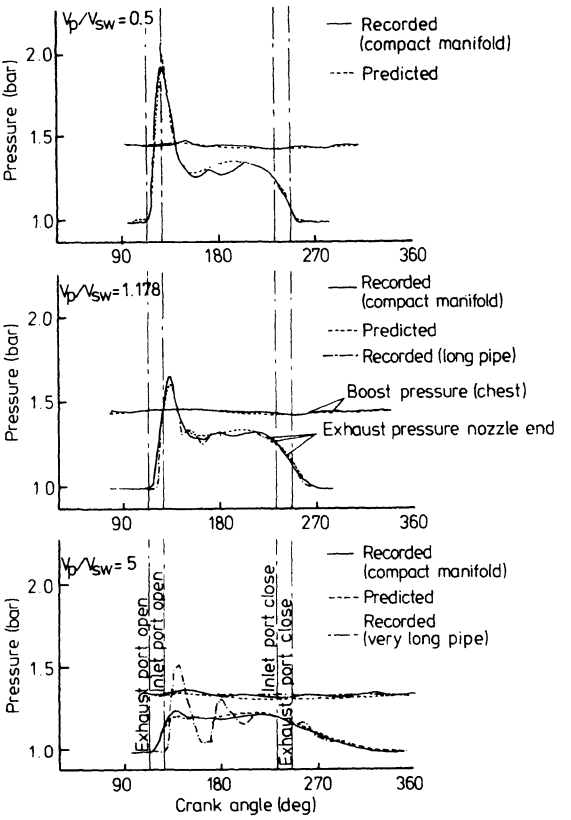

Figure 15.30 *Comparison of predicted and recorded transient pressures [54]*

from the turbocharger calculations and includes the combustion correlation described earlier.

An example of the use of the filling and emptying method is given in figure 15.32. Here the effect of changing valve timing and area is predicted on a very highly rated vehicle engine. At maximum engine speed the boost pressure is lower than the mean exhaust pressure, hence the pumping work is unfavourable. Figure 15.32 shows that increasing valve area and the period of valve opening both reduce pumping work during the exhaust period.

The filling and emptying model can be used not just to look at pressure differences across the valves, but to show instantaneous mass flow rates of air and combustion products through the valves. Figure 15.33 shows both the pressure and valve flow rate diagrams for the truck engine whose performance was predicted in figure 15.31. An engine of this type has little valve overlap and therefore no effective scavenge, but the pressure difference influences pumping work. Furthermore, reverse flow, such as that shown at the end of the inlet

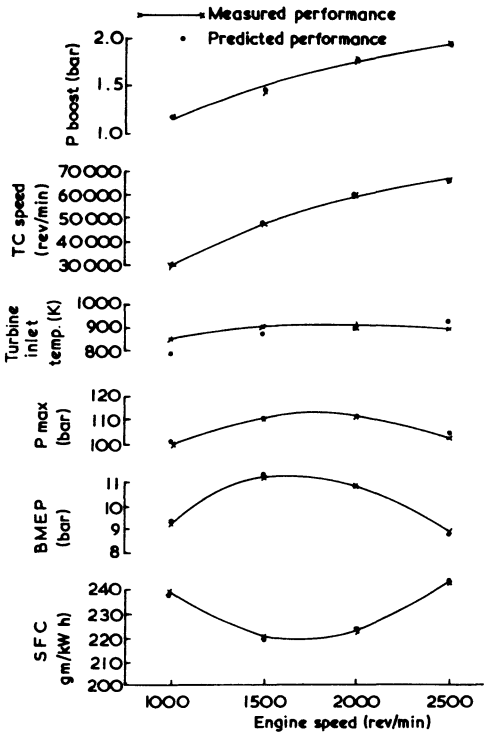

Figure 15.31 *Comparison of measured and predicted performance of a truck engine (filling and emptying method)*

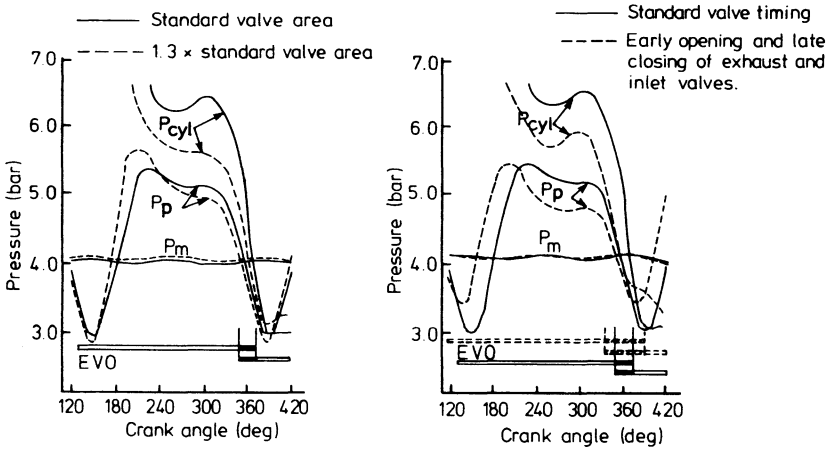

Figure 15.32 *The effect of valve area and timing on the gas exchange diagram (highly rated truck engine) [55]*

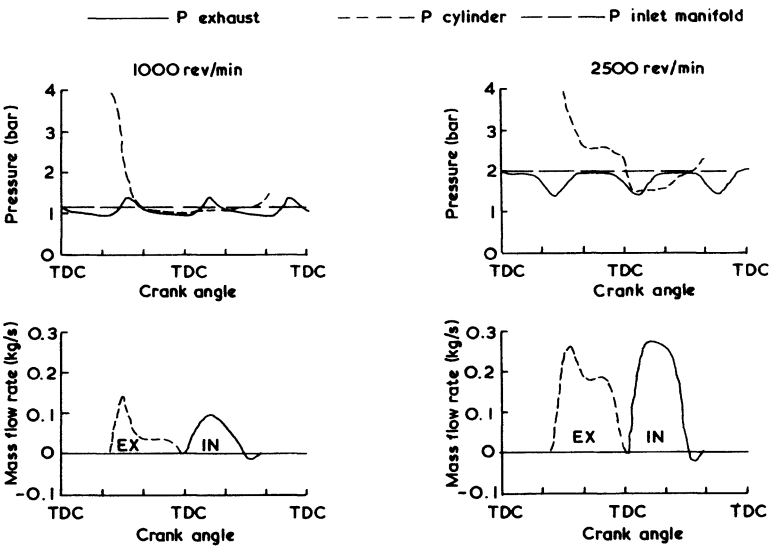

Figure 15.33 *Gas exchange and instantaneous valve gas flow rate diagrams for a truck engine (filling and emptying prediction)*

valve period in figure 15.33, can be detected and valve timing changed to optimise the gas exchange process.

Filling and emptying programs are frequently used for initial turbocharger matching studies for new engines or uprated versions of existing engines. Figure 15.34 shows the results of fine tuning of turbine area for a high-BMEP vehicle engine, required to operate over a wide speed range. The diagram shows that as turbine area is increased from the initial estimate (shown as a nominal area of 1), turbine speed and boost pressure fall, but specific fuel consumption and BMEP both improve due to a reduction in pumping work.

Figure 15.35 shows the predicted effect of reducing compression ratio of an engine, but increasing compression ratio of the turbocharger, for a highly rated medium-speed engine. For the same maximum cylinder pressure, the low-compression ratio engine (B, dashed line) has a 29.4 per cent greater IMEP, but a 7.1 per cent loss in indicated thermal efficiency. When expressed as a brake value, the efficiency of engine build B may exceed that of engine A, hence the technique of achieving high BMEP in this manner is attractive. The diagrams of integrated heat transfer show reduced values on the cylinder head and the piston but not the liner, due to the high cylinder temperature late in the expansion stroke when the liner has a large exposed surface area.

Filling and emptying programs have been used to derive several of the diagrams presented in earlier chapters, for example, figures 9.9, 9.10 and 9.11.

Stresses and bearing loads may be calculated from inertia forces and predicted cylinder pressure diagrams. More difficult to calculate are the component temperatures, due to the limitations of heat transfer models (section 15.7). However,

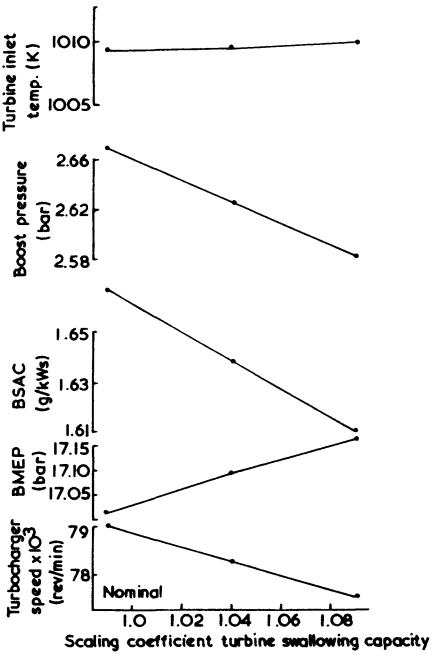

Figure 15.34 *Effects of varying turbine area on engine performance*

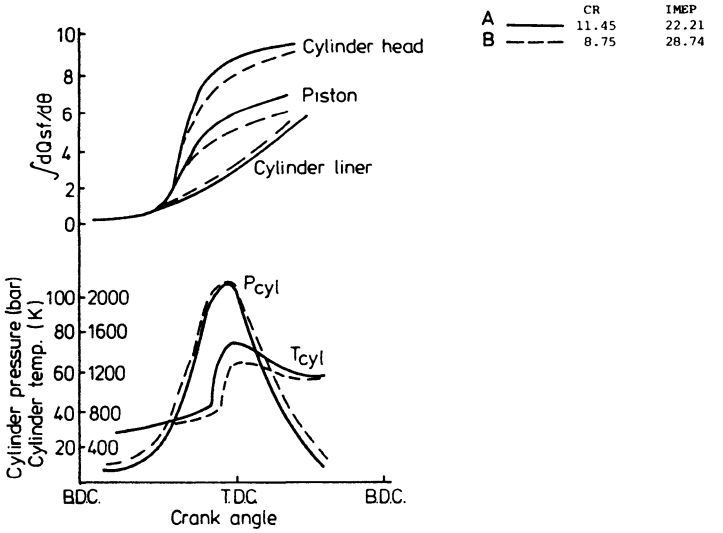

Figure 15.35 *Comparison between the reference cycle and a cycle with reduced compression ratio; influence of temperature and pressure on the heat transferred to the walls of the combustion chamber [56]*

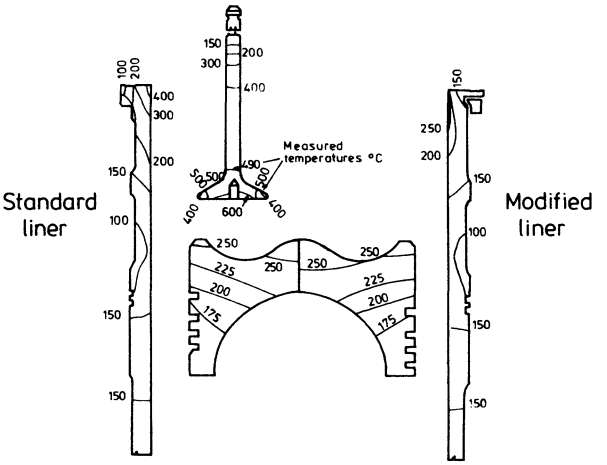

Figure 15.36 *Application of heat transfer and temperature calculation program showing valve temperatures and a design study of ring belt position and liner cooling for various medium speed engines [54]*

if some temperature measurements on similar engines are available, heat transfer correlations can be tailored to suit. These may then be used to predict component temperatures on other (broadly similar) engines or at other ratings. Figure 15.36 illustrates the results predicted when combining a performance calculation with a simple heat flux calculation procedure. Note the reduced top piston ring groove temperature predicted by lowering the groove and the major temperature reduction obtained by redesigning the cooling passage at the top flange of the liner.

15.13 The Method of Characteristics

The filling and emptying method of simulating a turbocharged diesel engine has one important disadvantage with respect to the pulse turbocharging system (chapter 7). By treating the exhaust manifolds as simple thermodynamic 'control volumes', the variation of gas state (for example, pressure and temperature) spatially along the manifold, is ignored. Yet the pulse turbocharging system relies on energy transfer in the form of a pressure wave, hence the instantaneous pressures at each end of the manifold, at any instant, must be different. The error introduced by neglecting this spatial difference and its consequences will depend on how long it takes for the pressure wave to travel the length of the manifold. If this time interval, expressed in terms of crank angular displacement, is very short, the error will be small. This will usually be the case with small, pulse turbocharged engines. However, with large engines the time interval may be long and a significant error will be introduced if pressure wave effects are ignored, particularly if the engine also runs at reasonably high speeds. As a very approximate rule it may be stated that if the pressure wave takes the equivalent

of 15 to 20° crank angle or less to travel the length of the manifold, reflect from the turbine and return to the valve, then the effect of ignoring the wave travel time will be negligible.

The time taken for a pressure wave to travel at sonic velocity a distance of $2l$ (where l is the length of the pipe or manifold) was given (equation 7.3) in terms of crank rotation, as

$$\Delta\theta = \frac{12lN}{\sqrt{\gamma RT}} \tag{15.36}$$

Equation 15.36 is plotted in figure 15.37, in terms of pressure wave reflection time (expressed as crank angle per unit manifold length), enabling a simple check to be made of the reflection time for any design.

From figure 15.37 it is clear that by neglecting pressure wave travel time, the filling and emptying method is introducing an error that will become significant on engines with long exhaust pipes that operate at high speeds. The effect of this error will be discussed later, but the pressure diagrams shown in figure 7.6 indicate the potential problem.

To account for pressure wave action in the exhaust (and if necessary, inlet) manifold, the equations for compressible, unsteady flow must be set up and solved. An essential, but not unreasonable, assumption is to restrict the analysis to one-dimensional flow. Although this may introduce errors if tapered pipes are used, this will rarely be a problem in practice. The 'method of characteristics' is a mathematical technique for solving hyperbolic partial differential equations such as those obtained for compressible flow. Engine simulation programs based on the method of characteristics apply the technique to analyse pressure wave action principally in the exhaust manifolds. There is no reason why treatment of

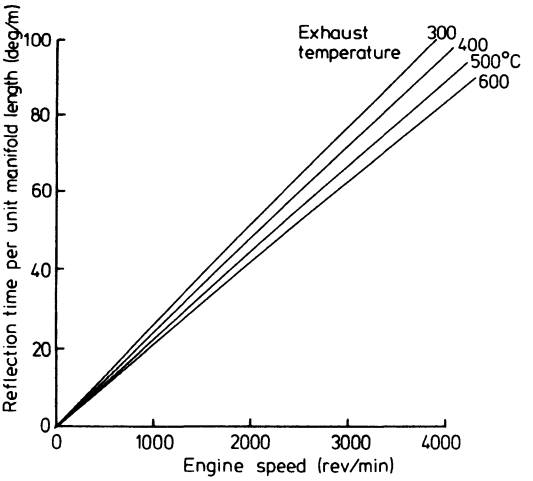

Figure 15.37 *Pressure wave reflection time (expressed in terms of crank angle per unit length of exhaust manifold)*

the remainder of the engine system (cylinders, valves, compressor, turbine and possibly intake manifold) should be any different from that adopted in filling and emtpying programs (sections 15.3 to 15.12).

Although the equations that represent the flow in the pipes may be solved by the method of characteristics, the flow itself is governed by what happens at the boundaries, at each end of the pipes. Thus the analysis must be coupled with the solution of the boundary conditions representing the exhaust valves, the turbine (or the nozzle that may simulate it) and junctions of various pipes. The analytical models presented in sections 15.8 (valves) and 15.10 (turbine) are sufficient for this purpose, but an additional model must be developed for a pipe junction. This will be presented later.

15.13.1 Isentropic Unsteady Flow in Pipes

Equations must be developed for unsteady, compressible, one-dimensional flow in pipes. For simplicity the analysis will initially be restricted to adiabatic, frictionless flow (hence isentropic) through pipes of constant cross-sectional area.

Consider the element of fluid (of volume $A\ dx$) shown in figure 15.38. The mass flow rate entering the element will be

$$\dot{m}_1 = \rho AC$$

The flow will vary along the pipe, hence the flow rate leaving the element will be

$$\dot{m}_2 = \rho AC + A\frac{\partial}{\partial x}(\rho C)dx$$

since A is constant. The flow will also vary with time, since it is unsteady. In time dt, the mass entering the element will be

$$m_1 = \dot{m}\ dt = \rho AC\ dt$$

and

$$m_2 = \left[\rho AC + A\frac{\partial}{\partial x}(\rho C)dx\right] dt$$

Thus the mass of fluid in the element will change (in time dt) by

$$\Delta m = m_1 - m_2 = -A\frac{\partial}{\partial x}(\rho C)dx\ dt \qquad (15.37)$$

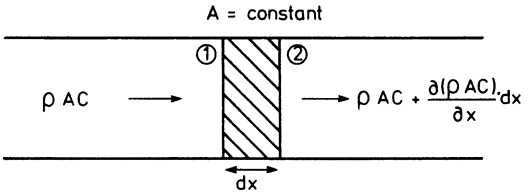

Figure 15.38 *Mass flow rate into and out of a fluid element in a pipe (constant cross-sectional area)*

The mass of the element may be expressed as the product of fluid density and its volume ($\rho A\ dx$). The former will vary with time, hence

$$\Delta m = m_{t_2} - m_{t_1} = \left(\rho + \frac{\partial \rho}{\partial t}\ dt\right) A\ dx - \rho A\ dx \tag{15.38}$$

Equations 15.37 and 15.38 give

$$A \frac{\partial \rho}{\partial t}\ dt\ dx + A \frac{\partial}{\partial x} (\rho C)\ dx\ dt = 0$$

which may be expanded to give

$$\frac{\partial \rho}{\partial t} + \rho \frac{\partial C}{\partial x} + C \frac{\partial \rho}{\partial x} = 0 \tag{15.39}$$

which is the general equation for continuity of mass for unsteady compressible flow in a duct with constant cross-section area.

Consider the forces acting on the element at an instant in time, as shown in figure 15.39. In the absence of external forces (that is, no wall friction, etc.) only pressure forces act. Thus the net force on the element F_x is given by

$$F_x = PA - \left(PA + A \frac{\partial P}{\partial x}\ dx\right)$$

that is

$$F_x = -\frac{A\ \partial P}{\partial x}\ dx$$

Newton's second law states that the net force will be equal to the rate of change of momentum, namely

$$A\ dx\ \rho \left(\frac{dC}{dt}\right)$$

where dC/dt is the total derivative of C with respect to time. Since $C = f(x, t)$

$$\frac{dC}{dt} = \frac{\partial C}{\partial x} \frac{dx}{dt} + \frac{\partial C}{\partial t} \frac{dt}{dt} = \frac{\partial C}{\partial x} \frac{dx}{dt} + \frac{\partial C}{\partial t} \tag{15.40}$$

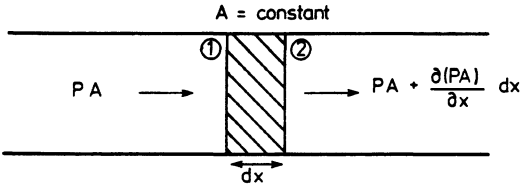

Figure 15.39 *Forces acting on a fluid element in a pipe (constant cross-sectional area)*

But $dx/dt = C$, therefore

$$\frac{dC}{dt} = C\frac{\partial C}{\partial x} + \frac{\partial C}{\partial t}$$

If second-order terms are ignored, the rate of change of momentum becomes

$$A\,dx\,(\rho)\left(C\frac{\partial C}{\partial x} + \frac{\partial C}{\partial t}\right)$$

Equating the net force (F) with the rate of change of momentum gives

$$-\frac{1}{\rho}\frac{\partial P}{\partial x} = C\frac{\partial C}{\partial x} + \frac{\partial C}{\partial t}$$

or

$$\frac{\partial C}{\partial t} + C\frac{\partial C}{\partial x} + \frac{1}{\rho}\frac{\partial P}{\partial x} = 0 \tag{15.41}$$

which is the general form of the momentum equation for one-dimensional unsteady, compressible flow, in the absence of body forces.

For a perfect gas

$$P = \rho RT \tag{15.42}$$

and the sonic velocity is given by

$$a^2 = \left(\frac{\partial P}{\partial \rho}\right)_s = \frac{\gamma P}{\rho} = \gamma RT \tag{15.43}$$

Differentiating equation 15.43 with respect to x gives

$$2a\frac{\partial a}{\partial x} = \frac{\gamma}{\rho^2}\left(\rho\frac{\partial P}{\partial x} - P\frac{\partial \rho}{\partial x}\right) = \frac{\gamma}{\rho^2}\left(\rho\frac{\partial P}{\partial \rho}\frac{\partial \rho}{dx} - P\frac{\partial \rho}{dx}\right)$$

$$= \frac{\gamma}{\rho^2}\left(\rho a^2\frac{\partial \rho}{\partial x} - P\frac{\partial \rho}{\partial x}\right)$$

(from equation 15.43)

$$= \frac{\gamma}{\rho}\left[a^2\frac{\partial \rho}{\partial x} - \frac{a^2}{\gamma}\frac{\partial \rho}{\partial x}\right]$$

Hence

$$\frac{\partial \rho}{\partial x} = \frac{2a\rho}{\gamma a^2\,[1 - 1/\gamma]}\left(\frac{\partial a}{\partial x}\right) = \frac{2\rho}{a(\gamma - 1)}\left(\frac{\partial a}{\partial x}\right) \tag{15.44}$$

Also

$$\frac{\partial \rho}{\partial t} = \frac{2\rho}{a(\gamma - 1)}\left(\frac{\partial a}{\partial t}\right) \tag{15.45}$$

and

$$\frac{\partial P}{\partial x} = \frac{2a\rho}{(\gamma - 1)}\left(\frac{\partial a}{\partial x}\right) \tag{15.46}$$

Using equations 15.44 and 15.45, the continuity equation 15.39 becomes

$$\frac{2\rho}{a(\gamma - 1)} \frac{\partial a}{\partial t} + \rho \frac{\partial C}{\partial x} + \frac{2\rho C}{a(\gamma - 1)} \frac{\partial a}{\partial x} = 0$$

therefore

$$\frac{\partial a}{\partial t} + \left(\frac{\gamma - 1}{2}\right) a \frac{\partial C}{\partial x} + C \frac{\partial a}{\partial x} = 0 \tag{15.47}$$

Using equation 15.46, the momentum equation 15.41 becomes

$$\frac{\partial C}{\partial t} + C \frac{\partial C}{\partial x} + \left(\frac{2a}{\gamma - 1}\right) \frac{\partial a}{\partial x} = 0 \tag{15.48}$$

Note that equations 15.47 and 15.48 are the continuity and momentum equations expressed in terms of the local fluid particle velocity (C) and the local sonic velocity (a) only. This is very relevant, since C is the exhaust gas velocity at any point in the pipe at any time, and the local sonic velocity is the propagating velocity of the pressure waves that are the essence of pulse turbocharging. The physical significance will be made clear shortly.

The method of characteristics is a mathematical technique used to simplify the solution of these equations. Firstly, equations 15.47 and 15.48 are combined in the following form. Equation 15.47 + $[(\gamma - 1)/2]$ x equation 15.48 gives

$$\left[\frac{\partial a}{\partial t} + (C + a) \frac{\partial a}{\partial x}\right] + \frac{\gamma - 1}{2} \left[\frac{\partial C}{\partial t} + (C + a) \frac{\partial C}{\partial x}\right] = 0 \tag{15.49}$$

Equation 15.47 - $[(\gamma - 1)/2]$ x equation 15.48 gives

$$\left[\frac{\partial a}{\partial t} + (C - a) \frac{\partial a}{\partial x}\right] - \frac{\gamma - 1}{2} \left[\frac{\partial C}{\partial t} + (C - a) \frac{\partial C}{\partial x}\right] = 0 \tag{15.50}$$

From equation 15.40

$$\frac{dC}{dt} = \frac{\partial C}{\partial t} + \frac{dx}{dt} \frac{\partial C}{\partial x} \tag{15.51}$$

and

$$\frac{da}{dt} = \frac{\partial a}{\partial t} + \frac{dx}{dt} \frac{\partial a}{\partial x} \tag{15.52}$$

Looking at the similarity between the expressions in brackets above, and the right-hand side of equations 15.51 and 15.52 it is evident that *if*

$$\frac{dx}{dt} = C + a \tag{15.53}$$

then equation 15.49 becomes

$$\frac{da}{dt} + \left(\frac{\gamma - 1}{2}\right) \frac{dC}{dt} = 0 \tag{15.54}$$

and, if

$$\frac{dx}{dt} = C - a \tag{15.55}$$

then equation 15.50 becomes

$$\frac{da}{dt} - \left(\frac{\gamma - 1}{2}\right)\frac{dC}{dt} = 0 \tag{15.56}$$

The significance of equations 15.53 and 15.55 becomes apparent when considering the motion of a pressure wave in the direction of the fluid motion and against it (figures 15.40 and 15.41). Since a weak pressure wave travels at sonic velocity relative to the surrounding medium, the absolute velocity of the pressure wave in figure 15.40 is $(C + a)$, while that in figure 15.41 is $(C - a)$. Thus $dx/dt = C + a$ and $dx/dt = C - a$ are the *position characteristics* of the pressure waves. They define pressure wave position (x) with time (t) where $dx/dt = C$ defines fluid particle position with time.

Equation 15.53 must be solved in conjunction with equation 15.54 and equation 15.55 in conjunction with equation 15.56. Thus equations 15.54 and 15.56 are the *compatibility conditions* accompanying the position characteristics.

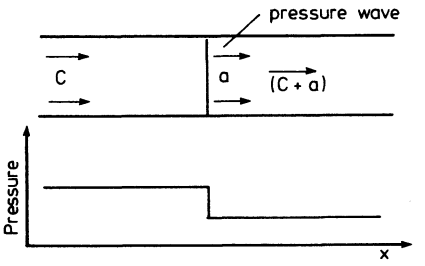

Figure 15.40 *A pressure wave travelling in the direction of fluid motion*

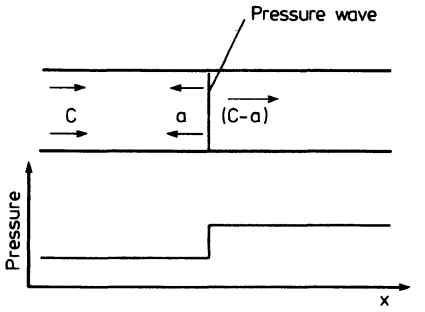

Figure 15.41 *A pressure wave travelling against the direction of fluid motion, relative to the fluid*

Solution of equations 15.53 to 15.56 enables the time and spatial variation of C and a to be found. Thus gas and pressure wave velocity will be known at any point in the exhaust pipe, at any time. Pressure, temperature and other parameters may then be calculated from the values of a and C.

Before attempting to solve equations 15.53 to 15.56 it is convenient to transform them into non-dimensional form, by introducing a reference sonic velocity (a_{ref}) (sonic velocity at a reference temperature), and a reference length l_{ref} (which will be related to a pipe length). Thus

$$a' = \frac{a}{a_{ref}};\ C' = \frac{C}{a_{ref}};\ x' = \frac{x}{l_{ref}};\ t' = \frac{t}{l_{ref}}\, a_{ref} \tag{15.57}$$

In terms of these non-dimensional parameters, the position characteristics become

$$(dx/dt)' = C' + a' \qquad \text{or} \qquad (dx/dt)' = C' - a' \tag{15.58}$$

and, with integration, the compatibility relationships become

$$\begin{aligned} a' + \left(\frac{\gamma-1}{2}\right) C' &= \text{constant} = \lambda \qquad \text{or} \\ a' - \left(\frac{\gamma-1}{2}\right) C' &= \text{constant} = \beta \end{aligned} \tag{15.59}$$

λ and β are called the Riemann parameters, and are therefore constant along the position characteristics.

By manipulating equations 15.59, the position characteristic gradients (equation 15.58) may be obtained in terms of the Riemann parameters λ and β. From equation 15.59

$$a' = \frac{\lambda+\beta}{2} \qquad \text{and} \qquad C' = \frac{\lambda-\beta}{\gamma-1} \tag{15.60}$$

hence

$$\left(\frac{dx}{dt}\right)' = C' + a' = \frac{\lambda-\beta}{\gamma-1} + \frac{\lambda+\beta}{2}$$

that is

$$\left(\frac{dx}{dt}\right)' = \lambda\left[\frac{\gamma+1}{2(\gamma-1)}\right] - \beta\left[\frac{3-\gamma}{2(\gamma-1)}\right] \qquad \text{for } (C' + a') \tag{15.61}$$

or

$$\left(\frac{dx}{dt}\right)' = \lambda\left[\frac{3-\gamma}{2(\gamma-1)}\right] - \beta\left[\frac{\gamma+1}{2(\gamma-1)}\right] \qquad \text{for } (C' - a') \tag{15.62}$$

The problem of solving the continuity and momentum equations for one-dimensional compressible, isentropic flow with pressure waves in a duct of constant cross-sectional area (equations 15.39 and 15.41) has been reduced to the solution of the four simpler differential equaitons (equations 15.59, 15.61 and 15.62).

These four equations are solved numerically, using a rectangular grid in the space (x', distance along the pipe) and time (t') directions, figure 15.42. Thus

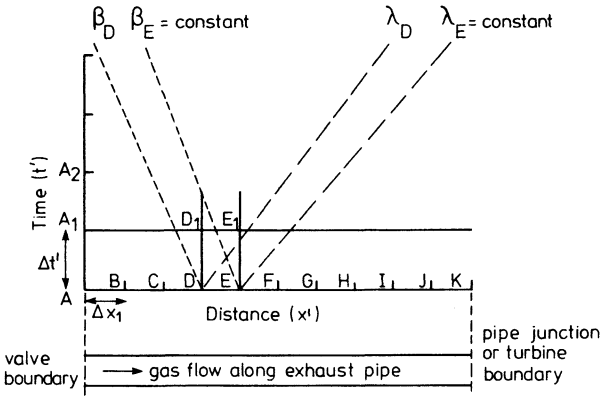

Figure 15.42 *Rectangular space-time grid superimposed on exhaust pipe (spatially fixed)*

the pipe length is divided into a number of sections or meshes, of equal length, with the vertical increments denoting time steps ($\Delta t'$). The mesh is a position diagram, fixed in time and space. A unique mesh is assigned to each pipe or section of pipe between junctions, in the exhaust manifold system.

If the values of the Riemann parameters (λ and β) can be found at all mesh points, then the values of a' and C' can be calculated from equations 15.60. The instantaneous gas temperature may be evaluated from the local sonic velocity (equation 15.43). Since the flow has been assumed to be adiabatic and frictionless

$$\frac{P}{\rho^{\gamma}} = \text{constant and } P \propto T^{\gamma/(\gamma-1)} \tag{15.63}$$

hence the local instantaneous gas pressure may also be determined, completing a full solution to the problem.

Lines of constant λ and β emanating from mesh points D and E are shown in figure 15.42. If it is assumed that values of λ and β are known at all mesh points at time $t' = t'_1$ (that is, at A, B, C etc.), then the problem is to calculate λ and β at the same mesh points, but at time $t'_2 = t'_1 + \Delta t'$.

An enlarged diagram around mesh D, E, E_1, D_1, is shown in figure 15.43. Since

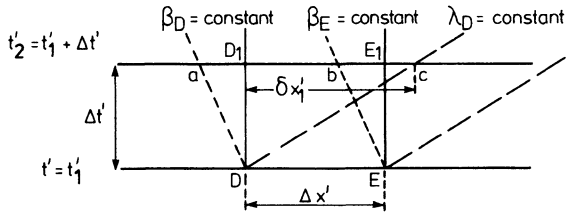

Figure 15.43 *Calculation of* λ *and* β *at time* $t'_2 = t'_1 + \Delta t'$

λ_D is known, and remains constant from point D to c, the displacement $\delta x'_1$, may be calculated from the direction condition (equation 15.61).

$$\left(\frac{dx}{dt}\right)'_1 = \left(\frac{\delta x}{\Delta t}\right)'_1 = \lambda_D \left[\frac{\gamma+1}{2(\gamma-1)}\right] - \beta_D \left[\frac{3-\gamma}{2(\gamma-1)}\right]$$

if the time step is specified. The positions at which all other lines of constant λ and β intersect the $t'_2 = t'_1 + \Delta t'$ line may be calculated in a similar way. Thus, for example, the values of β at points 'a' and 'b' can be calculated. It is then a simple matter to estimate the value of β at mesh point D_1 by linear interpolation. Clearly interpolation can be used to calculate the values of λ and β at all the mesh points for one time step after another.

It is instructive to review the physical interpretation of figure 15.43. Weak pressure waves travel at velocity $C+a$ or $C-a$ or, in non-dimensional from $C'+a'$ or $C'-a'$. They will travel along lines of slope given by equations 15.61 and 15.62, along which λ and β are constant. These are the dashed lines shown in figure 15.43. If a pressure wave existed at point D at time $t' = t'_1$, it would travel to point c in time $t'_2 = t'_1 + \Delta t'$. But in reality a pressure wave does not suddenly appear at point D. The rise and fall of pressure across the wave occupies some space along the pipe. If the mesh points (for example, D and E) are sufficiently close, they will represent points at different pressures on the same pressure wave (figure 15.44). These 'points' on the pressure wave will be moving as shown by the dashed lines of figure 15.43. After time $\Delta t'$, the new pressures at D and E may be calculated by the method outlined above (that is, from the new values of λ and β at D and E, through the new values of C', a' and t'). Thus by calculating the values of λ and β for all mesh points, for one time step after another, the movement of a pressure wave along the pipe (figure 15.45) can be calculated. At the same time, the fluid

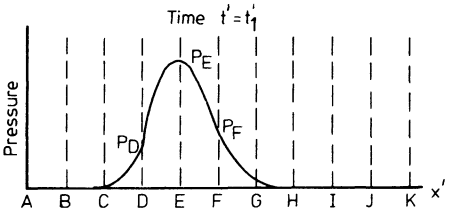

Figure 15.44 *Pressure diagram in a pipe at time* $t' = t'_1$

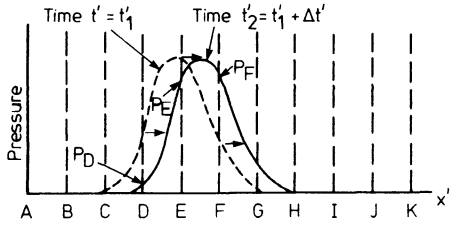

Figure 15.45 *Pressure diagram in a pipe at time* $t'_2 = t'_1 + \Delta t'$ *showing propagation of the pressure wave*

particle velocity (C) will also have been found. Naturally this will have been influenced by the passage of the pressure wave. The solution therefore appears complete, but three difficulties have not been mentioned. These concern the choice of mesh size, in the spatial and time directions, treatment of inflowing gas through a boundary, and the reflection of pressure waves at the boundaries. The choice of mesh size along the pipe is determined by the accuracy required in tracking the propagation of a pressure or temperature wave. This will be found by experience. Treatment of pipe 'end' effects (boundary conditions) is given in section 15.13.2. The time step (Δt) must be chosen such that the computational procedure remains stable, namely that

$$\frac{\Delta t'}{\Delta x'} < \frac{1}{a' + |C'|} \tag{15.64}$$

(see Benson *et al.* [57] for the derivation of equation (15.64).

15.13.2 Boundary Conditions at the Pipe Ends

At the pipe ends, the value of a λ or β characteristic leaving the pipe will be known. For example, the value of λ at the pipe end at time t'_2 (λ_{H_1} in figure 15.46) may be calculated from λ_G and λ_H even though point h does not really exist in the pipe. However, β_{H_1}, cannot be found, since its value depends on the inflow conditions through the boundary.

Consider the simplest boundary condition, a closed pipe end (for example, a closed exhaust valve) first. At a closed end, the gas velocity (C) will be zero. Equation 15.59 then becomes

$$\lambda = \beta \; (= a')$$

Thus a λ characteristic reaching a closed pipe end is reflected as a β characteristic, where

$$\lambda_{H_1} = \beta_{H_1} \tag{15.65}$$

that is, without change.

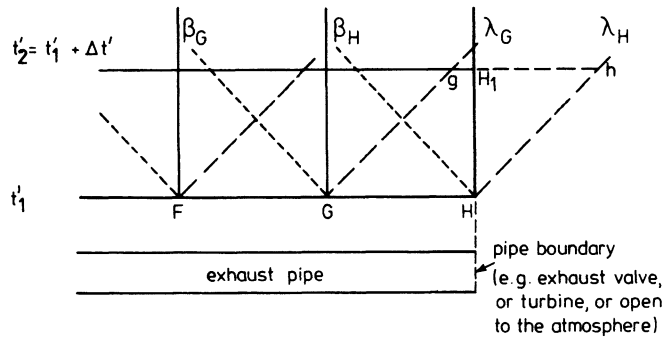

Figure 15.46 *Calculation of* λ *at a pipe boundary*

Consider next an open end. For example, point H, at the right-hand end of the pipe in figure 15.46, might be open to the atmosphere if the engine were naturally aspirated. λ_{H_1} could be calculated, but β_{H_1}, would depend on the conditions outside, which must be known. But, from equation 15. 60

$$\beta_H = 2a'_H - \lambda_H$$

Since

$$a' = \frac{a}{a_{ref}} = \left(\frac{\gamma RT}{\gamma RT_{ref}}\right)^{1/2} = \left(\frac{T}{T_{ref}}\right)^{1/2}$$

then, for isentropic flow

$$a' = \left(\frac{P}{P_{ref}}\right)^{(\gamma-1)/2\gamma} \tag{15.66}$$

Hence

$$\beta_H = 2\left(\frac{P_H}{P_{ref}}\right)^{(\gamma-1)/2\gamma} - \lambda_H \tag{15.67}$$

enabling β_H to be calculated, using an approximate value of P_H from its value at the beginning of the time step.

This is a simple example of subsonic outflow from a pipe. More important boundary conditions are flow through open or partially open valves or ports from the cylinder, flow through a turbine and through pipe junctions.

Just as equations 15.65 and 15.67 define the boundary conditions at closed and open pipe ends, so the equations for flow through valves and the turbine may be rewritten in terms of λ and β to become appropriate boundary conditions for these cases. [58, 34]

The pipe junction, however, is an additional boundary condition. A simple, widely used flow model at the junction is based on the approximation that the instantaneous pressures, at the ends of all pipes forming the junction, are equal. [59] If the gas flow separates at the junction, it is also assumed that at all pipes, thermodynamic states (temperature, density) are the same. Thus, for example, at a three-way pipe junction, with outflowing branches denoted by subscripts 2 and 3 (figure 15.47)

$$a'_1 = a'_2 = a'_3$$

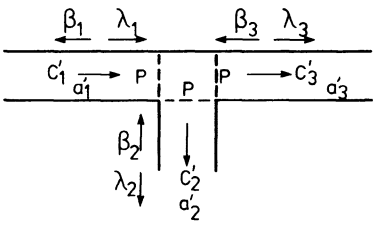

Figure 15.47 *Equal pressure assumption at a tee junction, separating flow*

From equations 15.60

$$\lambda_1 + \beta_1 = \lambda_2 + \beta_2 = \lambda_3 + \beta_3 \tag{15.68}$$

Conservation of mass gives

$$\rho_1 A_1 C_1 = \rho_2 A_2 C_2 + \rho_3 A_3 C_3$$

Introducing the Riemann variables from equations 15.60 and noting that the densities at the pipe ends must also be equal, since pressure and temperature are equal, gives

$$(\lambda_1 - \beta_1) A_1 = (\lambda_2 - \beta_2) A_2 + (\lambda_3 - \beta_3) A_3 \tag{15.69}$$

With the flow configuration shown (figure 15.47) values of β_1, λ_2 and λ_3 will be unknown, but can be found by solving equations 15.68 and 15.69. If two or more flow streams join at the junction, their thermodynamic states cannot be assumed to be equal. Equation 15.68 must therefore be replaced by a conservation of energy equation or some approximation on entropy in the merged flow pipe.

Pressure differences across the junction can be taken into account using experimental pressure loss data (Benson *et al.* [59] or Watson and Janota [60] for a pulse converter junction), with non-isentropic characteristic calculations in the pipes (section 15.13.3).

For the cylinder and turbine boundaries, the appropriate equations (given in sections 15.8 and 15.10) must be rewritten in terms of λ and β for a solution to be obtained.

15.13.3 Non-isentropic, Unsteady Flow in Pipes

The isentropic flow analysis presented in section 15.13.1 can reasonably be applied to the intake and exhaust pipe systems of internal combustion engines. However, the analysis is limited by the assumptions of constant pipe cross-sectional area,

TABLE 15.1 Characteristic equations for unsteady, isentropic flow in a pipe of constant cross-sectional area

λ characteristic

$$\lambda = \text{constant}$$

with the direction condition

$$\frac{dx'}{dt'} = C' + a' = \lambda \frac{(\gamma+1)}{2(\gamma-1)} - \beta \frac{(3-1)}{2(\gamma-1)}$$

β characteristic

$$\beta = \text{constant}$$

with the direction condition

$$\frac{dx'}{dt'} = C' - a' = \lambda \frac{(3-1)}{2(\gamma-1)} - \beta \frac{(\gamma+1)}{2(\gamma-1)}$$

no viscous friction between gas and pipe wall, and no heat transfer from the hot exhaust gas. These factors have some effect on energy transfer along the pipe, from cylinder to turbine, hence they should be taken into account. If this is done, then the assumption of constant entropy is abandoned and entropy gradients may exist, making the analysis more complex.

The corresponding set of equations to those of isentropic flow (table 15.1) are given in table 15.2. The principle difference is that the values of λ and β no longer remain constant along the characteristic lines defined by equations 15.T2

TABLE 15.2 Characteristic equations for unsteady non-isentropic flow in a pipe

λ characteristic

$$d\lambda = a'\frac{ds'}{s'} - \frac{(\gamma-1)}{2}\frac{a'C'}{A}\frac{dA}{dx'}\,dt' - \left(\frac{\gamma-1}{2}\right)\frac{2fl_{ref}}{D}$$

$$\times (C')^2\,\frac{C'}{|C'|}\left[1-(\gamma-1)\frac{C'}{a'}\right]dt' + \frac{(\gamma-1)^2}{2}\frac{\dot{Q}l_{ref}}{a_{ref}^3}\frac{1}{a'}\,dt' \qquad (15.T1)$$

with the direction condition

$$\frac{dx'}{dt'} = C' + a' \qquad (15.T2)$$

β characteristic

$$d\beta = a'\frac{ds'}{s'} - \left(\frac{\gamma-1}{2}\right)\frac{a'C'}{A}\frac{dA}{dx'}\,dt' + \left(\frac{\gamma-1}{2}\right)\frac{2fl_{ref}}{D}$$

$$\times (C')^2\,\frac{C'}{|C'|}\left[1+(\gamma-1)\frac{C'}{a'}\right]dt' + \frac{(\gamma-1)^2}{2}\frac{\dot{Q}l_{ref}}{a_{ref}^3}\frac{1}{a'}\,dt' \qquad (15.T3)$$

with the direction condition

$$\frac{dx'}{dt'} = C' - a' \qquad (15.T4)$$

Path line condition

$$ds' = \left(\frac{\gamma-1}{2}\right)\frac{s'}{(a')^2}\left[\frac{\dot{Q}l_{ref}}{a_{ref}^3} + \frac{2fl_{ref}}{D}\,|(C')^3|\right]dt' \qquad (15.T5)$$

with its direction condition

$$\frac{dx'}{dt'} = C' \qquad (15.T6)$$

Note: s' is a measure of entropy defined by

$$\frac{s'}{a'} = \left(\frac{P_{ref}}{P}\right)^{(\gamma-1)/2\gamma} \qquad (15.T7)$$

and 15.T4. Thus the variation of λ and β must be calculated during each time step, using equation 15.T1 and 15.T3. An entropy relationship (equation 15.T5) along a particle path line (equation 15.T6) is required to evaluate the first terms of equations 15.T1 and 15.T3. The method of calculation is otherwise similar to that used for isentropic flow. A detailed analysis is given by Benson *et al* [57] and Watson. [58]

15.13.4 Computer Program Structure

The structure of a filling and emptying program is based on the application of the energy equation to each control volume in turn, with the boundary conditions, plus heat and work transfer calculations, called up from sub-routines as and when required.

The models of in-cylinder conditions and flow through the valves will be the same when simulating an engine with pressure wave action in the exhaust (and possibly intake) manifolds. However, wave action calculations tend to dominate, particularly on multi-cylinder engines, hence the characteristic calculations govern program structure in this case.

Programs are usually organised around the pressure wave and mass flow calculation in the pipes. Thus the key to program structure will be setting up the characteristic grid (for λ and β) and the path line positions (non-isentropic flow only) in all pipes. Thus values of λ, β and s' (non-isentropic flow, table 15.2) will be stored in a two-dimensional matrix, the dimensions denoting a pipe number (for multiple pipe systems) and a grid point (or path line position) number. Each separate element of a complex exhaust pipe system must be set up as a unique pipe with each pipe end labelled to identify the appropriate boundary conditions. Thus, for a six-cylinder engine the pipe numbering system might appear as shown in figure 15.48. Ten separate pipes are involved (A to J), with six cylinder boundary calculations (pipe end numbers 1, 3, 5, 11, 13 and 17), four junction boundary calculations (pipe end numbers 2, 4, 7; 6, 8, 9; 12, 14, 15; 16, 18, 19), and two turbine boundary calculations (pipe end numbers 10, 20). The inlet system is not shown, but the numbering system could be extended to include all sections of the inlet manifold.

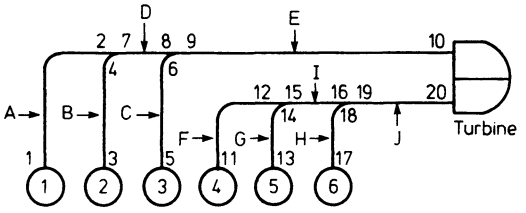

Pipes: numbers A – J

Pipe ends: Cylinder boundary 1, 3, 5, 11, 13, 17

Junction boundary (2, 4, 7) (6, 8, 9) (12, 14, 15) (16, 18, 19)

Turbine boundary (10, 20)

Figure 15.48 *Pipe numbering scheme for a six-cylinder engine*

The characteristic calculations will be enacted for each pipe in turn. Initial values of λ and β at each characteristic grid point, together with initial values of s' at each path line position (non-isentropic calculation), must be specified. These initial values will be guesses, since gas pressures, temperatures and velocities will not be known, but correct final values will be achieved by iterating the whole calculation over several engine cycles. Convergence is usually achieved in three or four cycles.

15.13.5 Application of Characteristic Calculations

On small engines it is unlikely that the method of characteristics will improve predictions significantly over those of a filling and emptying method, since pressure wave travel times are short. This may not be the case on a larger engine. Figure 15.49 compares calculated (from the method of characteristics) and experimental pressure diagrams for a large sixteen-cylinder, four-stroke engine. Here

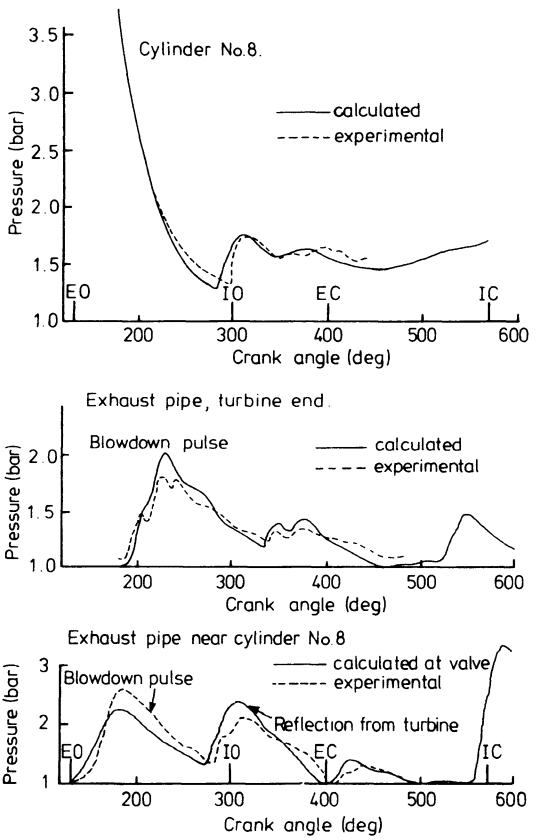

Figure 15.49 *Cylinder and exhaust pipe pressures, predicted and measured, from a sixteen-cylinder four-stroke engine [61]*

pressure wave travel time is important; this can be seen by following the blow-down exhaust pulse from cylinder 8. As the exhaust valve opens, the cylinder pressure drops and a pressure pulse is created in the adjacent exhaust pipe (figure 15.49, lower, the dashed line denoting measured exhaust pressure near to the exhaust valve in cylinder 8). This pressure pulse travels along the exhaust pipe and arrives at the turbine approximately 65 degrees (crank angle rotation) later (figure 15.49, centre). The reflected pressure wave arrives back at cylinder 8 about a further 65° later (figure 15.49, lower), at the beginning of the valve overlap period. Clearly this is undesirable, as is shown in the cylinder pressure diagram (figure 15.49, top). The reflected pressure wave has caused an increase in cylinder pressure, with subsequent deterioration in the scavenging process. The use of a characteristic analysis to predict the time lag of this pressure wave has cleary been very successful, since a filling and emptying program would predict identical diagrams at valve and turbine.

Figure 15.50 shows performance and pressure diagrams predicted for a Vee 8

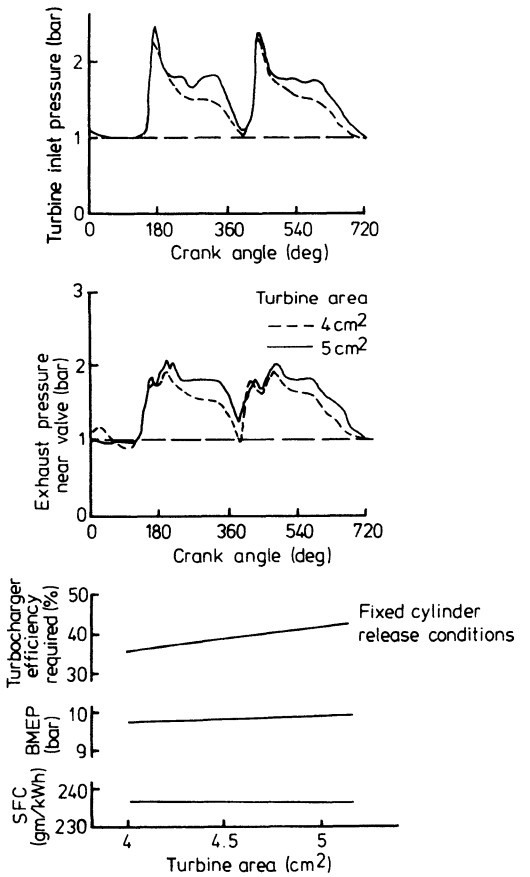

Figure 15.50 *The effect of turbine area on performance and exhaust pressure diagrams for a V8 engine*

turbocharged automotive four-stroke diesel engine with different turbine areas but a fixed boost pressure. The pressure diagrams relate to the turbine inlet and an exhaust port, with two cylinders (phased 270° apart) connected to a turbine inlet. Increasing turbine area reduces the amplitude of the pressure diagrams, particularly during the pumping period following blow-down. For fixed cylinder release conditions (that is, fixed boost, fuelling, etc.), specific fuel consumption and BMEP both improve due to a reduction in exhaust pumping work. However, the turbocharger efficiency required to achieve a match rises rapidly with increased turbine area. Comparison of figure 15.50 (lower) with expected turbocharger efficiencies enables the correct turbine housing to be selected, for the boost pressure assumed.

Following preliminary selection of the turbine, the optimum exhaust pipe diameter may be established. Figure 15.51 is a companion set of diagrams to figure

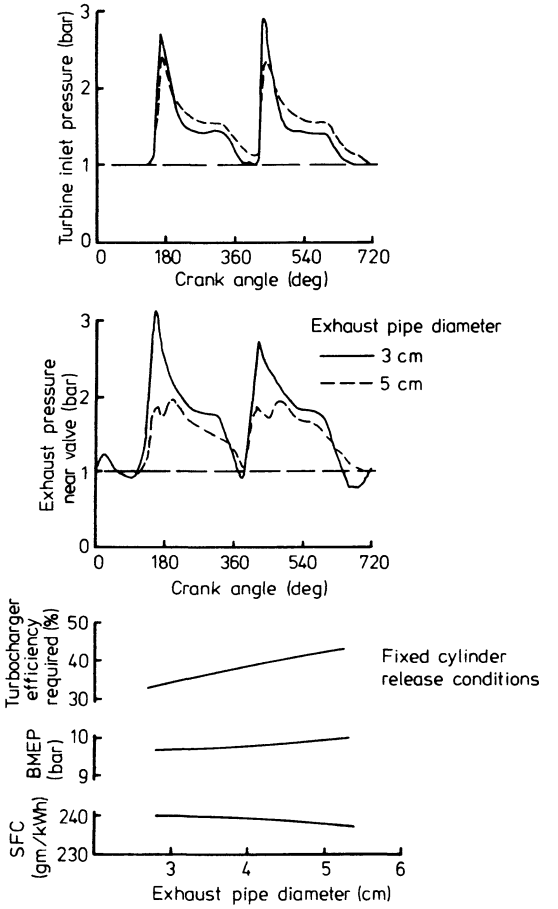

Figure 15.51 *The effect of exhaust pipe diameter on performance and exhaust pressure diagrams for a V8 engine*

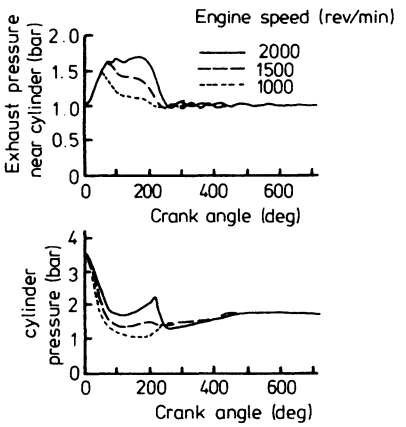

Figure 15.52 *The effect of engine speed on the exhaust process (0° CA = EVO) [62]*

15.50, but illustrating the effect of changing exhaust pipe diameter. Reducing diameter from 5 to 3 cm increases pressure pulse amplitude and hence the effectiveness of the pulse turbocharging system. Thus the over-all turbocharger efficiency required to achieve an energy balance is reduced from 41.5 to 34.5 per cent. However, a penalty results in specific fuel consumption and BMEP (1.5 per cent) due to the increased exhaust pumping work associated with high exhaust manifold pressure. Fixed cylinder release conditions have been assumed but, for a given turbocharger, boost would increase if the smaller manifold were used, offsetting the above mentioned penalties. Further substantial exhaust pipe diameter reduction is likely to lead to excessive gas frictional losses. With the 3 cm diameter pipe, the ratio of pipe cross-sectional area to exhaust valve geometric flow area at full lift is unity in this case.

Engine speed affects the exhaust pipe pressure history, since the time period of the exhaust process reduces at increasing speed. Thus at low speeds (figure 15.52, lower) the cylinder exhausts more readily and cylinder pressure falls more rapidly, on a crank-angle time scale. The increase in time available results in a lower exhaust pressure peak of the initial blow-down pulse than that occurring at higher speeds. Indeed, at high speed (2000 rev/min), the peak pressure occurring during the piston pumping phase of the exhaust process exceeds that predicted during blow-down. This results from the large quantity of gas remaining in the cylinder following the short blow-down period. Note that the cylinder pressure rises substantially as the piston nears TDC on the exhaust stroke. A change to more generous valve timing would reduce pumping work during this period.

15.14 Transient Response Models

The problem of poor transient performance of highly rated turbocharged diesel engines has been discussed in chapter 12, together with the effect of certain parameters on their response. It is very difficult to conduct accurate and re-

peatable transient tests, and even more difficult to isolate the effect of one parameter at a time during experimental tests. For example, many of the techniques outlined in chapter 12 for improving response call for a change in turbocharger match at the same time. This can rarely be done without changing the operating efficiency of the turbocharger over the appropriate part of its range (indeed, this may be one objective) and in some cases may result in an accompanying change in inertia (another objective). Transient response models avoid this difficulty and can be used to highlight and study the effect of dominant influencing parameters.

It will already be apparent that modelling the performance of the turbocharged diesel engine under nominally steady conditions is a complex task. Modelling transient performance will be yet more difficult. Relatively simple models are based on a linearising approach, and are generally an extension of the semi-empirical models described in section 15.2. More sophisticated, non-linear models are based on the assumption that since quasi-steady models follow the cyclic variation of events at a nominal steady engine speed, then it is logical to extend them for changing conditions.

15.14.1 Simple Transient Response Models

The model developed by Ledger and co-workers [63, 64] is typical. This is a simple extension of the model described in section 15.2 with the addition of sub-models for the dynamics of the engine and load, the turbocharger, governor and fuel pump. Thus the simple constant pressure turbocharging model is used, together with an 'apparent turbine efficiency' (figure 15.5) to take account of exhaust

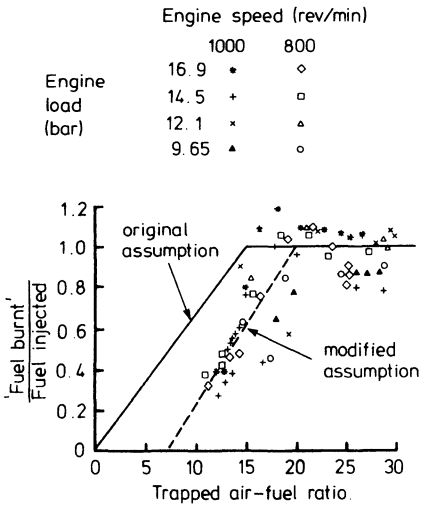

Figure 15.53 *'Incomplete combustion' at rich mixtures [64]*

pulse energy. An immediate problem that occurs is that the fuel/air ratio during many transient tests will exceed that for which steady state data is available. Thus extrapolation of figure 15.2 will be required. Even more of a problem is the link between BMEP (hence power) and fuel/air ratio (figure 15.8) at varying boost pressure and speed, when the fuel/air ratio is very rich. Ledger first made the assumption that not all of the fuel would burn at fuel/air ratios richer than stoichiometric, and that the ratio of fuel burnt to fuel injected would fall from 1 at the stoichiometric fuel/air ratio to 0 when no air was present (figure 15.53). Later, this assumption was modified to obtain closer agreement with experimental results (figure 15.53). The IMEP is calculated from experimental results, as a function of the quantity of 'fuel burnt' per cylinder per cycle (figure 15.54), extrapolated to rich mixtures. The resultant IMEP must then be adjusted to account for the effect of the quantity of air present on thermal efficiency (figure 15.55). The quantity of fuel injected is obtained from steady state fuel pump

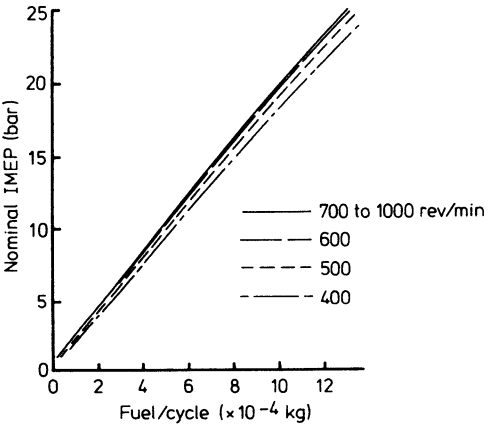

Figure 15.54 *Nominal IMEP as a function of fuel input [64]*

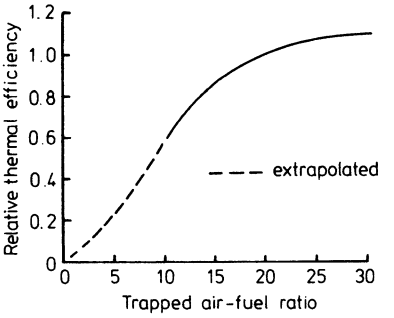

Figure 15.55 *Relative thermal efficiency at rich mixtures [64]*

delivery characteristics, as a function of rack position and speed. A simple second-order transfer function may be used to represent the governor dynamics namely

$$x = \frac{K_1}{K_2(K_3N^2 + K_4N + K_5)}y$$

where x = relative change in rack movement, from no load
y = relative change in speed, from a datum speed
N = speed
K_1 to K_5 = suitable constants, chosen from static and dynamic tests.

Instantaneous powers developed and absorbed by the turbine and compressor are evaluated from the appropriate characteristics, the difference being used to accelerate the turbocharger, since

$$TQ_t - TQ_c = I\left(\frac{d\omega}{dt}\right)_{tc}$$

where TQ = torque (instantaneous)
I = inertia
ω = rotational speed.

Similarly, surplus instantaneous power developed by the engine, over that required to run the engine and load at any speed, will be available to accelerate the engine. Instantaneously

$$TQ_e - TQ_l = (I_e + I_l)\left(\frac{d\omega}{dt}\right)_e$$

where subscripts e and l denote engine and load respectively.

Figure 15.56 shows a comparison of predicted and measured response to a very rapid, large load increase. Although the model predicts the correct trends, the results do not show good agreement, due to inaccuracies of the simple assumptions in the combustion model.

A similar model has been described by Bowns *et al.* [65] Greenhalgh and Tooth [66] and Egli [67] have used somewhat different, but equally simple models.

15.14.2 Advanced Models

Effectively the simple models use steady state experimental results that linearise performance characteristics; they take no account of the cyclic operating nature of the diesel engine. Watson and Marzouk [19] have extended a filling and emptying model to include transient operating conditions. Since the filling and emptying model assumes quasi-steady flow, but follows the unsteady gas and energy flows through the engine as they vary with time, no fundamental difficulties result from extending the solution to model transient conditions. However, some modifications must be made. The dynamics of engine, load, turbocharger and fuel pump governor must be incorporated. Furthermore, a combustion correlation of the type presented in section 15.6 must be used. The difficulty of using this type

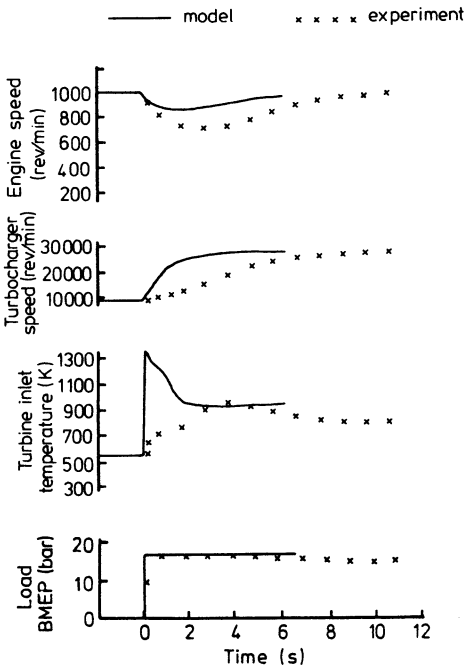

Figure 15.56 *Response to a 70 per cent load application [64]*

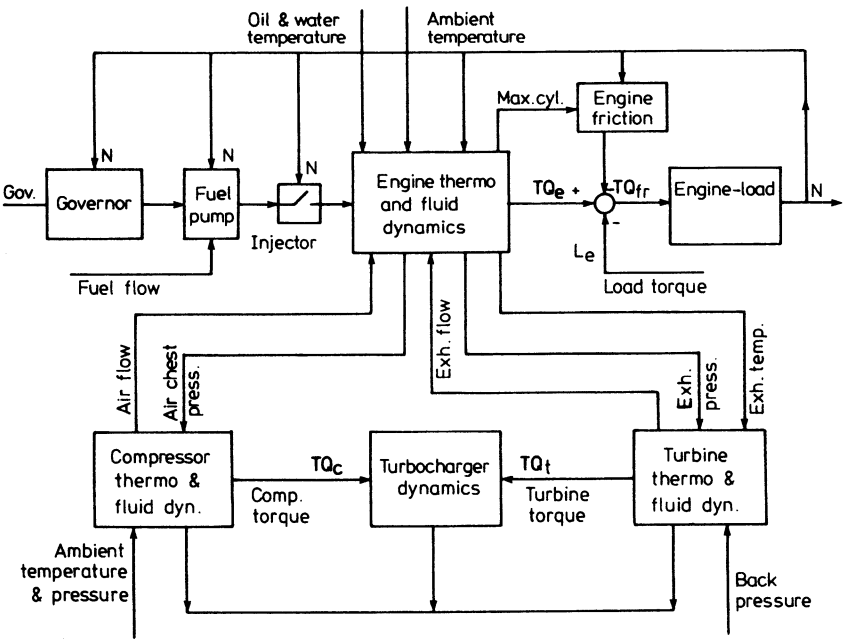

Figure 15.57 *Block diagram for a turbocharged diesel engine system*

of model with rich fuel/air mixtures is overcome by assuming that equilibrium thermodynamic property relations hold for rich as well as weak fuel/air mixtures (section 15.5). Thus incomplete combustion at fuel/air ratios richer than stoichiometric is automatically taken account of through the property relationships.

The basic control loop of a turbocharged diesel engine operating under transient conditions is shown in figure 15.57, including the interaction of the turbocharger and engine along gas paths. The basic thermodynamics and fluid dynamics of the engine may be treated in the same manner as a normal filling and emptying model, provided that rich fuel/air ratios are taken into account, as described above. However, a mathematical technique that does not rely on balancing energy and mass flow over the complete engine cycle must be adopted, since conditions at the end of a cycle will not equal those at the beginning. Watson and Marzouk [19] model conditions as an initial value problem, using a predictor-corrector solution.

Steady flow fuel pump delivery characteristics are used to specify fuelling as a

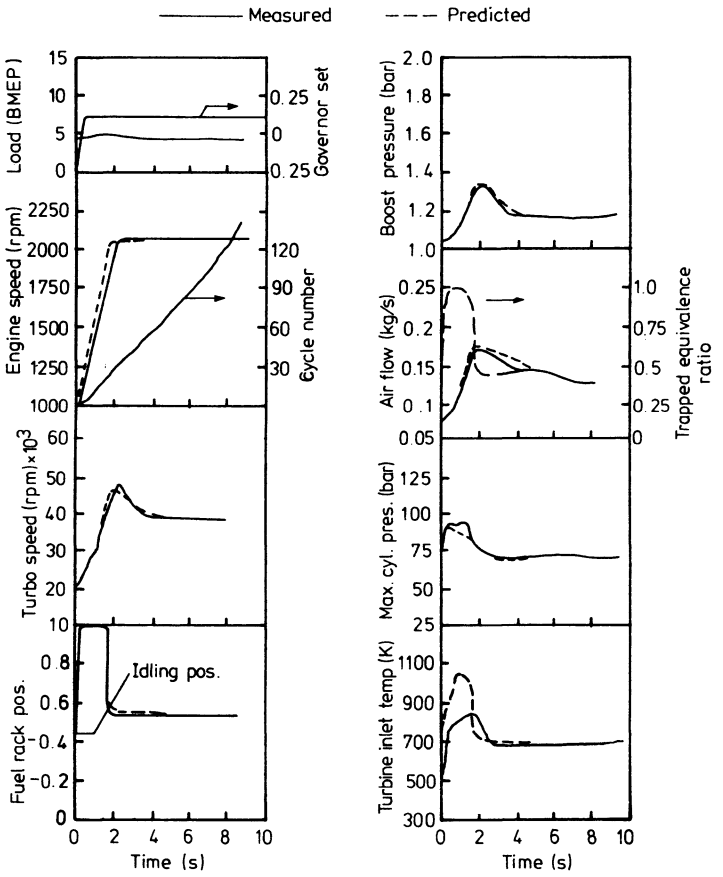

Figure 15.58 *Measured and predicted response to an increase in demand speed [19]*

function of fuel pump rack position and speed, the latter being evaluated from a second-order model of governor dynamic behaviour. The combination of fuel input and the trapped mass of fresh air (evaluated automatically in the filling and emptying program) provides the value of trapped equivalence ratio required for the combustion model (section 15.6). Full steady state turbine and compressor maps are used to evaluate the instantaneous surplus or deficit of energy so that the acceleration of deceleration of the turbocharger may be evaluated, knowing its inertia.

The IMEP is automatically calculated in the filling and emptying model and is translated into a brake value by subtracting predicted frictional losses (using Chen and Flynn's formula [51]). Knowledge of the inertia of engine and load, combined with the difference between the instantaneous torque produced by the engine, and that applied by the load, enable the acceleration of the engine and load to be calculated.

Figure 15.58 and 15.59 compare the predicted response with that measured

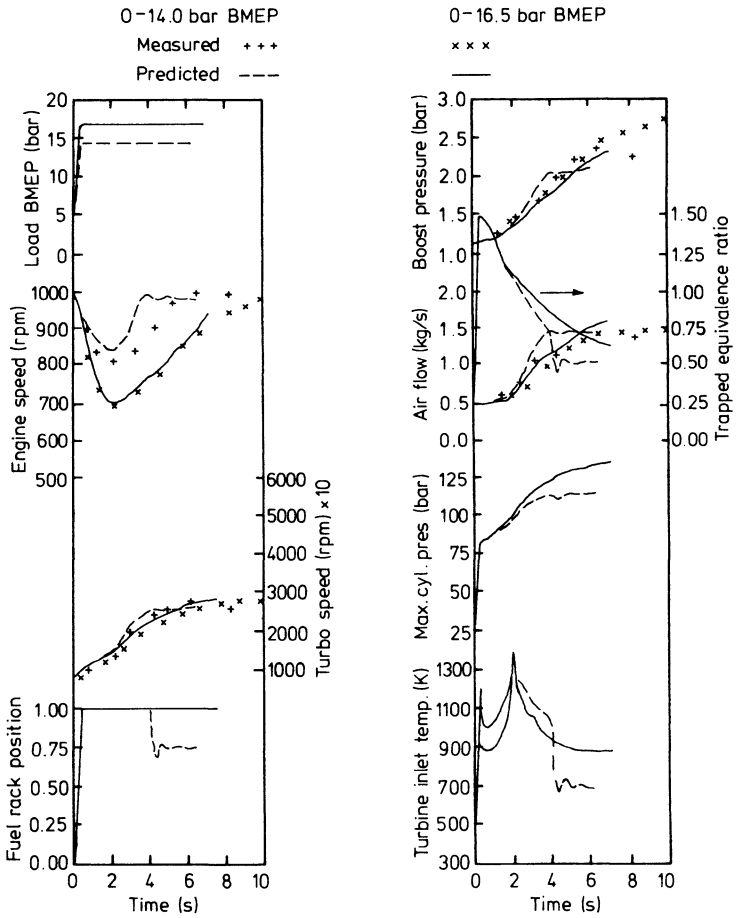

Figure 15.59 *Predicted and measured response of a medium-speed turbocharged diesel engine to two load levels [68]*

when a turbocharged automotive diesel engine accelerates and when a sudden large load is applied to a medium-speed engine.

The major advantage of the filling and emptying model over the simpler alternatives is that since it is more fundamental, it is also more versatile. Thus the effect of certain design changes can be established more readily (see chapter 12), and the model may be applied to other types of engine without the need to complete elaborate test programmes first, over a wide range of steady state conditions. The more elementary programs have the advantage of simplicity, but their heavy reliance on experimental data limits their use to a class of engines for which the data applies.

References

1. F.J. Wallace and P.R. Cave, Matching of high-output diesel engines with associated turbomachinery, *Proc. Inst. Mech. Engrs,* **187**, No. 48/73 (1973)
2. N.D. Whitehouse, A. Stotter and M.S. Janota, Effects of altitude, ambient temperature and turbocharger match on engine performance, *Proc. Inst. Mech. Engrs,* **178**, Pt. 1 (1963/4)
3. E. Jenny, The utilization of exhaust gas energy in the supercharging of the four-stroke diesel engine, *Brown Boveri Review,* **37** No. 11 (1950)
4. M. Marzouk, Simulation of turbocharged diesel engines under transient conditions, Ph.D thesis, University of London (Imperial College) (1976)
5. G.L. Borman, Mathematical simulation of internal combustion engine processes, Ph.D thesis, University of Wisconsin (1964)
6. K.J. McAulay, S.K. Chen, W. Tang, G.L. Borman, P.S. Myers and O.A. Uyehara, Development and evaluation of the simulation of the compression-ignition engine, *SAE 650451* (1965)
7. E.E. Streit and G.L. Borman, Mathematical simulation of a large turbocharged two-stroke diesel engine, *SAE 710176* (1971)
8. H.N. Powell, Applications of an enthalpy fuel/air ratio diagram to first-law combustion problems, *Trans. ASME,* **79** (1957)
9. R.B. Krieger and G.L. Borman, The computation of apparent heat release for internal combustion engines, *ASME paper 66-WA/DGP-4* (1966)
10. H.K. Newall and E.S. Starkman, Thermodynamic properties of octane and air for engine performance calculations, *SAE Progress in Technology Series,* vol. 7 (1964)
11. M. Megerdichian and N. Watson, Mixture preparation and heat release in diesel engines, *SAE 780225* (1978)
12. M. Marzouk and N. Watson, Some problems in diesel engine research with special reference to computer control and data acquisition, *Proc. Inst. Mech. Engrs,* **190**, No. 23/76 (1976)
13. W. Brown, Methods for evaluating requirements and errors in cylinder pressure measurement, *SAE 6700* (1967)
14. N. Watson, M. Marzouk and A.D. Pilley, A combustion correlation for diesel engine simulation, *SAE 800029, Diesel Combustion and Emissions* SP86 (February 1980)
15. I. Wiebe, Halbempirische Formel für die Verbrennungs-geschwindigkeit, Verlag de Akademic der Wissenschaften der VdSSR (Moscow, 1967)
16. J. Shipinski, O.A. Uyehara and P.S. Myers, Experimental correlation between rate of injection and rate of heat release in a diesel engine, *ASME paper 68-DGP-11* (1968)

17. G. Woschni and F. Anisits, Experimental investigation and mathematical presentation of rate of heat release in diesel engines dependent upon engine operating conditions, *SAE 740086* (1974)
18. H. Wolfer, Der Zundverzug im Dieselmotor, *VDI Forsch Hft.*, No. 392 (1938)
19. N. Watson and M. Marzouk, A non-linear digital simulation of turbocharged diesel engines under transient conditions, *SAE 770123* (1977)
20. N.D. Whitehouse and R.J.B. Way, A simple method for the calculation of heat release rates in diesel engines, based on fuel injection rate, *SAE 710134* (1971)
21. W.J.D. Annand, Heat transfer in the cylinders of reciprocating internal combustion engines, *Proc. Inst. Mech. Engrs*, **177**, No. 36 (1963)
22. W.J.D. Annand and T.H. Ma, Instantaneous heat transfer rates to the cylinder head surface of a small compression-ignition engine, *Proc. Inst. Mech. Engrs*, **185** (1971)
23. G. Woschni, A universally applicable equation for the instantaneous heat transfer coefficient in the internal combustion engine, *SAE 670931* (1967)
24. G. Woschni, Die Berechung der Wandverluste und der thermischen Belastung der Bauteile von Dieselmotoren, *MTZ*, **31**, No. 12 (1970)
25. J.C. Dent and S.J. Sulieman, Convective and radiative heat transfer in a high-swirl direct injection diesel engine, *SAE 770407* (1977)
26. G.F. Hohenberg, Advanced approaches for heat transfer calculations, *SAE 790825, Diesel Engine Thermal Loading*, SP449 (September 1979)
27. G. Sitkie, Heat transfer and thermal loading in internal combustion engines, Akademiai Kiado (Budapest, 1974)
28. M. Kamel and N. Watson, Heat transfer in the indirect injection diesel engine, *SAE 790826, Diesel Engine Thermal Loading* SP449 (September 1979)
29. L.J. Kastner, T.J. Williams and J.B. White, Poppet inlet valve characteristics and their influence on the induction process, *Proc. Inst. Mech. Engrs*, **178**, Pt. 1 (1963/4)
30. G.H. Trengrouse, B.W. Imrie and D.H. Male, Comparison of unsteady flow discharge coefficents for sharp edged orifices with steady flow values, *J.Mech.Engng.Sci.*, **8**, No. 3 (1966)
31. W.A. Woods, Steady flow tests on twin poppet valves, *Proc. Inst. Mech. Engrs*, **182**, Pt 3D (1967/8)
32. W.J.D. Annand and G.E. Roe, *Gas Flow in the Internal Combustion Engine* (Foulis, 1974)
33. W.A. Woods and S.R. Khan, An experimental study of flow through poppet valves, *Proc. Inst. Mech. Engrs*, **180**, Pt.3N (1965/6)
34. W.A. Woods and S.R. Khan, Discharge from a cylinder through a poppet valve to an exhaust pipe, *Proc. Inst. Mech. Engrs*, **182**, Pt.3H (1967/8)
35. W.B. Wallace, High output medium-speed diesel engine air and exhaust system losses, *Proc. Inst. Mech. Engrs*, **182**, Pt.3D (1967/8)
36. B.N. Cole and B. Mills, The theory of sudden enlargements applied to the poppet exhaust valve, *Proc. Inst. Mech. Engrs*, **1B**, No. 8 (1952/3)
37. J.R. Metz, A. Urben and A. Steiger, Contribution to investigation of the diesel cycle with the aid of digital computers, *Proc. Inst. Mech. Engrs*, **182**, Pt.3L (1967/8)
38. R.B. Kreiger, The simulation of a two-cycle, crankcase scavenged, spark-ignition engine on a digital computer and comparison of results with experimental data, Ph.D thesis, University of Wisconsin, (1968)

39. Y. Mayaski and W.E. Meyer, An analytical method for optimising the scavenging process of uniflow two-cycle diesel engines, *SAE 650447* (1965)
40. E.E. Streit, Mathematical simulation of a large, pulse turbocharger, two-stroke diesel engine, Ph.D thesis, University of Wisconsin, (1970)
41. F.J. Wallace and J.M. Adgey, Theoretical assessment of non-steady flow performance of inward radial flow turbines, *Proc. Inst. Mech. Engrs,* **182**, Pt.3H (1967/8)
42. F.J. Wallace, J.M. Adgey and G.P. Blair, Performance of inward radial flow turbines under non-steady flow conditions, *Proc. Inst. Mech. Engrs,* **184**, Pt.1 (1969/70)
43. R.S. Benson and K.H. Scrimshaw, An experimental investigation of non-steady flow in a radial gas turbine, *Proc. Inst. Mech. Engrs,* **180**, Pt.3J (1965/6)
44. T. Miyachita, T. Tomita and D. Ishikara, Performance of inward radial flow turbine under unsteady flow conditions, *IHI Engng. Rev.,* **7**, No. 1 (January 1974)
45. H.R.M. Craig *et al.,* An investigation of steady and unsteady flow through a Napier turboblower turbine under conditions of full and partial admission, *Proc. Inst. Mech. Engrs,* **183**, Pt.1 (1968/9)
46. H. Daneshyar *et al.,* A comparison of the perfomance of three model axial flow turbines tested under both steady and pulse flow conditions, *Proc. Inst. Mech. Engrs,* **184**, Pt.1 (1969/70)
47. M. Ryti, Ein Rechenprogram für den Ladungswechsel aufgeladener Dieselmotoren, *Brown Boveri Rev.,* **55** No. 8 (1968)
48. F. Pischinger and A. Wunsche, Characteristic behaviour of radial tubines and its influence on the turbocharging process, CIMAC (Tokyo, 1977)
49. W.L. Brown, The caterpillar IMEP meter and engine friction, *SAE 730150* (1973)
50. B.W. Millington and E.R. Hartles, Frictional losses in diesel engines, *SAE 680590* (1968)
51. S.K. Chen and P. Flynn, Development of a compression ignition research engine, *SAE 650733* (1965)
52. W.J.D. Annand, Choice of a computing procedure for digital computer synthesis of reciprocating engine cycles, *J. Mech. Engng. Sci.,* **10**, No. 3 (1968).
53. N. Watson and M.S. Janota, Matching and performance calculations, lectures E15 to E19, Short Course 79-1, Turbocharging the internal combustion engine, Fluid Dynamics Institute, Dartmouth College, New Hampshire, USA, and Imperial College, London (1979)
54. M.S. Janota, A.J. Hallam, E.K. Brock and S. G. Dexter, The prediction of diesel engine performance and combustion chamber component temperatures using digital computers, *Proc. Inst. Mech. Engrs,* **182**, Pt.3L (1967/8)
55. N. Watson, M. Marzouk and Z. Baazaari, Two-stage turbocharging for efficient, high-output, diesel engines, ASME paper No. 78-DGP-2, Energy Technology Conference, Houston, Texas (November 1978)
56. W. Glanzman, Calculation of diesel cycles with reduced compression ratio, *Brown Boveri Rev.,* No. 4 (1977)
57. R.S. Benson, R.D. Gard and D. Woollatt, A numerical solution of unsteady flow problems, *Int. J. Mech. Sci.,* **6** (1964)
58. N. Watson, Method of characteristics, lecture E20, Short Course 79/1, Turbocharging the internal combustion engine, Fluid Dynamics Institute, Dartmouth College, New Hampshire, USA, and Imperial College, London (1979)

59. R.S. Benson, W.A. Woods and D. Woollatt, Unsteady flow in simple branch systems, *Proc. Inst. Mech. Engrs,* **178**, Pt.3I(iii) (1963/4)
60. N. Watson and M.S. Janota, Non-steady flow in an exhaust system with a pulse converter junction, Paper 27, Conference on Internal Flows, University of Salford (1971)
61. R.S. Benson, A computer program for calculating the performance of an internal combustion engine exhaust system, *Proc. Inst. Mech. Engrs,* **182**, Pt.3L (1968)
62. J.D. Ledger, Computer aided design of the exhaust of a turbocharged diesel engine, On-Line Eurocomp, Interactive Systems, pp.171–186 (1975)
63. J. Ledger and S. Walmsley, Computer simulation of a turbocharged diesel engine operating under transient load conditions, *SAE 710177* (1971)
64. J.D. Ledger, R.S. Benson and N.D. Whitehouse, Dynamic modelling of a turbocharged diesel engine, *Proc. Inst. Mech. Engrs,* CP15/73 (1973)
65. D.E. Bowns, P.R. Cave, M.R.O. Hargreaves and F.J. Wallace, Transient characteristics of turbocharged diesel engines, *Proc. Inst. Mech. Engrs,* CP15/73 (1973)
66. R. Greenhalgh and P. Tooth, Application engineering techniques relating to high performance, medium speed, diesel engines, *Proc. CIMAC* (1975)
67. H. Egli, Transient torque responsiveness of turbocharged diesel engines for vehicles, Seminar, Technische Akademie, Wuppertal, Germany, (February, 1975)
68. M. Marzouk and N. Watson, Load acceptance of a turbocharged diesel engine, Paper C54/78 Turbocharging and Turbochargers Conference, *Inst. Mech. Engrs* (London, 1978)

Index